INDIAN AGRICULTURAL
RESEARCH INSTITUTE, NEW DELHI.

62479

I. A. R. I. 6.

MGIPC—S1—51 AR/57—3 4-58—5,000.

# PROCEEDINGS

OF THE

# ROYAL SOCIETY OF LONDON

# PROCEEDINGS

OF THE

# ROYAL SOCIETY OF LONDON

## SERIES A. MATHEMATICAL AND PHYSICAL SCIENCES

VOL 177

62479

Published by the Royal Society
Burlington House
Piccadilly
London, W.1

IARI

FIRST PRINTED IN GREAT BRITAIN FOR THE ROYAL SOCIETY AT THE
UNIVERSITY PRESS, CAMBRIDGE

REPRINTED IN GREAT BRITAIN BY OFFSET-LITHO BY BUTLER & TANNER LTD ,
FROME AND LONDON (1959)

# CONTENTS

## SERIES A VOL. 177

### No. A 968. 31 December 1940

PAGE

Anniversary address by Sir William Bragg, O.M., P.R.S. . . . 1

The apparent sizes of atoms in metallic crystals with special reference to aluminium and indium, and the electronic state of magnesium. By W. Hume-Rothery, F.R.S. and G. V. Raynor . . . . . 27

The characteristics of thermal diffusion. By S. Chapman, F.R.S. 38

Catalytic activity, crystal structure and adsorptive properties of evaporated metal films. By O. Beeck, A. E. Smith and A. Wheeler. (Plates 1–3) . . . . . . . . . . . . . . 62

On the mechanism of boundary lubrication. I. The action of long-chain polar compounds. By O. Beeck, J. W. Givens and A. E. Smith. (Plate 4) . . . . . . . . . . . . . . 90

On the mechanism of boundary lubrication II. Wear prevention by addition agents. By O. Beeck, J. W. Givens and E. C. Williams. (Plates 5, 6) . . . . . . . . . . . . . . 103

On the electromagnetic two-body problem. By J. L. Synge . . . 118

The structure of melamine, $C_3N_6H_6$. By I. E. Knaggs and K. Lonsdale. With a note on the optical properties of melamine. By R. G. Wood and G. Williams . . . . . . . . . . . . . 140

### No. A 969. 10 January 1941

The equilibrium diagram of the system silver-zinc. By K. W. Andrews, H. E. Davies, W. Hume-Rothery, F.R.S. and C. R. Oswin . . . 149

The magnetic and other properties of the free electrons in graphite. By N. Ganguli and K. S. Krishnan, F.R.S. . . . . . . . . 168

Radio echoes and cosmic ray showers. By P. M. S. Blackett, F.R.S. and A. C. B. Lovell . . . . . . . . . . . . 183

PAGE

The mobility of positive ions in their own gas. By R. J. Munson and A. M. Tyndall, F.R.S. . . . . . . . . . . 187

The mobility of alkali ions in gases. IV. Measurements in gaseous mixtures. By H. G. David and R. J. Munson . . . . . 192

The mobility of alkali ions in gases. V. Temperature measurements in the inert gases. By K. Hoselitz . . . . . . . . . . 200

The seasonal variations of cosmic-ray intensity and temperature of the atmosphere. By A. Duperier . . . . . . . . 204

A thermodynamical theory of the tensile strength of isotropic bodies. By R. Fürth . . . . . . . . . . . . 217

The derivation of mechanics from the law of gravitation in relativity theory. By G. L. Clark . . . . . . . . . . 227

The crystal structure of Rochelle salt (sodium potassium tartrate tetrahydrate $NaKC_4H_4O_6.4H_2O$). By C. A. Beevers and W. Hughes . 251

Application of the coincidence method for measurements of short life periods. By J. Rotblat . . . . . . . . . . 260

Molecular anisotropy of urea, $CO(NH_2)_2$, and of related compounds. By K. Lonsdale. (Plate 7) . . . . . . . . . . 272

No. A 970. 24 February 1941

The distribution of electricity in thundercloud, II. By Sir George Simpson, F.R.S. and G. D. Robinson . . . . . . . 281

Exchange effects in the theory of the continuous absorption of light. I. Ca and $Ca^+$. By D. R. Bates and H. S. W. Massey, F.R.S. . . 329

The polarization of electrons by double scattering. By H. S. W. Massey and C. B. O. Mohr . . . . . . . . . . . 341

$\beta$-ray spectra of light elements. By A. A. Townsend . . . . 357

Wind tunnel correction for a circular open jet tunnel with a reflexion plate. By B. Davison and L. Rosenhead . . . . . 366

An investigation of the disintegration of boron by slow neutrons. By R. S. Wilson . . . . . . . . . . . . . 382

PAGE

## No. A 971. 18 March 1941

A study of sensitized explosions. V. Some new experiments on the hydrogen-oxygen reaction sensitized by nitrogen peroxide. By F. S. Dainton and R. G. W. Norrish, F.R.S. . . . . . . 393

A study of sensitized explosions. VI. Experimental observations on the hydrogen-oxygen reaction sensitized by nitrosyl chloride. By F. S. Dainton and R. G. W. Norrish, F.R.S. . . . . . . 411

A study of sensitized explosions. VII. A chain-thermal theory of the reaction between hydrogen and oxygen sensitized by nitrogen peroxide or nitrosyl chloride. By F. S. Dainton and R. G. W. Norrish, F.R.S. . . . . . . . . . . . . . 421

Infra-red absorption spectra of some amino compounds. By L. Kellner 447

The vibrations and the molecular structure of urea and guanidonium. By L. Kellner . . . . . . . . . . . . . 456

Submarine seismic investigations. By E. C. Bullard and T. F. Gaskell . 476

The dissociation constants of the methylammonium ions and the basic strengths of the methylamines in water. By D. H. Everett and W. F. K. Wynne-Jones . . . . . . . . . . 499

Index . . . . . . . . . . . . . 517

# Address of the President Sir William Bragg, O.M., at the Anniversary Meeting, 30 November 1940

Many events conspire to make the past year notable in the history of our Society. Reference has been made to the majority of them in the Annual Report of Council, usefully supplemented by the Notes and Records which we continue to owe to our past Treasurer, Sir Henry Lyons. I do not propose to speak of them in detail, but on this occasion it does seem fitting to give further attention to one or two general matters of lasting interest.

One of these is personal. Fellows will have noted the long list of those whom we have lost, and the great names which the list contains. I have felt as I have been reading it that I have turned over the last leaves of a chapter that stands by itself. The present generation is quick to honour the names of J. J. Thomson and Oliver Lodge, but they cannot remember, as we older men can, the brilliant years when these men and their contemporaries were writing the chapter's first pages. What they wrote was eagerly read, their lectures were heard with rapt attention; they were the pioneers, and the scientists of that time, nearly half a century ago, streamed after them. All that is now a memory. The years have slipped away since their work was done, and we now look back on it and see it as a separate entity, a noble event in the history of science, and of British science in particular,

There is no vestige of sadness in such a retrospect, nor any trace of feeling that our pride must be founded only on what has passed. I am sure that all those who like myself can recall the long years, and compare those that have gone by with those that are still ours, will say happily and proudly that our young men of to-day are maintaining in full force the tradition that they have received. They are writing a new chapter; and it is a chapter of a novel importance because as they extend our record of the facts of Nature they find themselves compelled at the same time to consider a new problem, the relation of those facts to society and to the government of nations. Let me express my admiration of the willingness, vigour and ability with which the newer generation gets to work.

This same novelty is enlarging the range of work of our Society and is a second matter to which we are compelled to give serious attention. Our Fellows have constantly given their services to public interests; it has often been pointed out that they are to be found in association with almost every department of government. But this year new moves have been made which may, and I hope will, lead to developments of the highest importance. The Report contains a notice of the recent formation of a Scientific Advisory Committee over which Lord Hankey presides, with a reference which in effect directs it to consider the advances of science in their relation to national welfare. The Committee reports to the Cabinet through its chairman. A Committee of similar nature but lesser scope was set up a few months ago to consider the scientific aspects of the food policy of the Government: it consists of well-known authorities on nutrition, agriculture and economy, with myself as chairman. This Committee reports to Lord Privy Seal, and so to the Cabinet Food Policy Committee over which Lord Privy Seal presides. The significant feature of these committees is their close and direct association with the Cabinet, the central body that governs our nation. Hitherto scientists have been appointed man by man to various Government Departments so that they might act as useful items in departmental machinery. The new committees are not parts of any executive body and have no executive power of their own. They exist to make recommendations, which must of course be practical and take full account of difficulties of execution. But they are not hampered by traditions, nor by set habits; they have time and freedom to consider the whole field of scientific knowledge and its possible influence on practice. The Scientific Advisory Committee, the more important of the two, is particularly well fitted to watch all occasions and opportunities for the employment of science in the service of the nation, and also for the continuous encouragement of that employment. The President of the Society and the two principal Secretaries are in close touch with every branch of science; through the Fellows of the Society which they serve they have a unique view of scientific progress. The three Secretaries of the principal Research Councils of the Government, dealing with industry, agriculture and health, are in close touch with the chief national activities.

Thus a great opportunity is opened after long expectation; and the Royal Society is largely responsible for the development of that opportunity. We hope that no hindrances from without may interfere with the Society's task, and we are determined that there shall be no lack of energy from within.

We remember that it is science itself, not scientists, that we are trying to lift to the high places. In that respect our movement is not selfish. We do not claim that scientists shall be entrusted with authority because they are scientists: we do claim that authority shall be exercised in the light of a knowledge which grows continuously, and with continual effect on politics, on industry, and on thought itself. If at present the only way to bring this knowledge into use is to treat scientists as consultants, let us take that way. But we shall be taking the better way if in all ranks of the State, and especially in those that have authority and set an example, we can arouse a general appreciation of the position, and a constant understanding watchfulness on the increase of knowledge and the uses that are made of it and can be made. It cannot be said that the general aspect of the nation towards the increase of knowledge is satisfactory. Science has become an integral part of our educational system, yet the changes that have been made are often ridiculously like the casting of sacrifices to following wolves. Science is not a devouring monster, but a means of service; it is a knowledge, gained by an irresistible tendency of man to examine his surroundings. It may be rightly or wrongly used. There is a prime danger if those who are in the position to use it rightly shut their eyes to its presence and its power, like an army which relies on bows and arrows when its enemies know how to use machine guns.

It is not universally nor even sufficiently understood how important natural knowledge has become. It is true that in a vague way the nation is brought by the happenings of war to guess at the meaning of scientific research in every kind of enterprise. But still it would be difficult for most people to grasp the significance, much less the meaning of the description of a fact like this: that the R.A.F. could not carry out its operations without the knowledge resulting from the studies of cathode-rays and electrons made by our physicists, which is equivalent to saying that by this time we might well have lost the war. Similar cases of cause and consequence could be quoted in numbers; they happen to be found more readily in relation to the sciences that deal with inorganic materials than those that deal with organic processes, and the military demand for physicists has been great because they are wanted to put physical discoveries into practice. But this discrimination is only accidental and temporary, and in fact the whole range of science is equally concerned.

Since experimental science has assumed such a commanding influence on all our affairs, so that we run the risk of great perils if we take no account of it, and leave its uses to others, let us say less well disposed than ourselves, and, on the other hand, have opportunities of great benefit if we use it rightly, it becomes a first duty to direct our steps accordingly. Just as in former times schools and colleges were founded to train men for the service of Church and State, in ways which were appropriate to that high end, so now we have to see to it that the men are produced by our educational systems who can appreciate and act up to a new state of affairs. This can be done without jettisoning any of the fine instruction which has been a proud feature of our older systems.

I think that this is not essentially a matter of the rearrangement of school time tables, or the building of scientific laboratories, though such tactical methods must have their due consideration. This is a personal matter, as has been the case with every great human movement. We have not to force the use of new tools, but to encourage and develop a new appreciation and a new attitude. Our best method, as ever before, lies in our own actions. If we, in the continually increasing contacts of scientists with public affairs, can show that we have something of great value to contribute, and that we give it freely, placing our individual interests below those of a greater purpose; if we try to understand the motives and principles of those whom we meet who may not see our vision just as we may fail to appreciate theirs, then by so doing we have the best chance of bringing about the changes that we desire. It is the personal contact of the scientist, especially with those who are charged with duties to the nation, that is the moving force. That is where these new associations of science with government may mean so much, and shall mean it, if our devotion can achieve its purpose.

This afternoon I leave the Presidential chair. I have deeply appreciated the honour that has been paid to me by my election to it, and I want to thank with all my heart the officers of the Society, the members of Council, and the permanent officials who have helped me to fulfil its duties.

Charles Barrois (1848–1939) was elected a Foreign Member of our Society in 1913. He belonged to an industrial family in the north of France, and came to England as a young man to study English methods of manufacture. He became interested in geology, and particularly the geology of Great Britain and Ireland. His work in this field won him a doctor's degree at the Sorbonne. He completed investigations of high importance into the difficult geologies of Normandy, Brittany, northern France and Lorraine. He was head of the geological department of the University of Lille. He was well known in this country, especially to the geologists by whom he was held in great esteem. The Geological Society of London awarded him the Wollaston Medal in 1901.

Wilfred Trotter (1872–1939) was one of the most distinguished surgeons in this country. He was especially a master of the surgery of the brain and of the thyroid gland. He studied at University College and won the Gold Medal and University Scholarship in Surgery of the University of London in 1899. His outstanding skill and knowledge gave him a wide practice as a consultant. After being Consulting Surgeon to the King from 1928 to 1932 he became Sergeant Surgeon to the King in 1932 and held that office under three Sovereigns.

In 1934 Trotter gave up private practice in order to devote himself to work at University College Hospital and to the training of young men in the Medical School. He was a fine teacher. He added to his wide knowledge and his technical skill a precision of thought and a love of thoroughness which had a profound influence on his students.

Trotter took a great interest in qualities of the human mind as well as in the structure and functions of the human body. In 1915 he wrote in the *Sociological Review* on the herd instinct, and in later years he wrote on the mentality of nations at war. He studied the functions of nerves and the causes of pain.

Trotter was for many years a member of the Medical Research Council. He was elected to our Society in 1931, and twice served on our Council: on the latter occasion he acted as a Vice-President.

EDMUND NEVILLE NEVILL (1847–1940) was an able student of dynamical astronomy. He was especially interested in the perturbations of the moon due to the influence of the planets. In 1882 an observatory was built in Durban and he was appointed its first Director, arriving in Durban just in time to make observations of the transit of Venus on 6 December. He carried on the appropriate observational work, and at the same time pursued the theoretical researches which had established his reputation. Nevill was one of the original Fellows and a member of the first Council of the Institute of Chemistry. From 1888, until his retirement in 1912, he combined the post of Government Chemist and Official Assayer for Natal with that of Government Astronomer. He was elected a Fellow of the Royal Astronomical Society in 1873, and a Fellow of the Royal Society in 1908.

GILBERT MORGAN (1870–1940) was a great chemist. His skill, knowledge, versatility and energy were to no small degree responsible for the present sound position of British chemistry. In particular, he did much to promote the useful co-operation of laboratory and factory. Morgan was a student of Meldola when he was working on dyestuffs, and through his influence obtained a position as research chemist in the dyeing industry.

It is interesting that during a long research on the dihydroxynaphthalenes he prepared a representative of the substances afterwards known collectively as bakelite, but its future great usefulness was not then anticipated since it had no application in the production of artificial colours. In 1919 he was appointed to the Mason chair of Chemistry in Birmingham. His greatest work was begun when in 1925 he became the first Director of the Government Research Laboratory at Teddington. He made an unqualified success of the new enterprise. He designed its structure and organized its work: and the fact that so much useful knowledge has proceeded from it, especially in the last war months, is proof of his foresight and of the soundness of his management.

Morgan was a hard worker; he was kind and helpful to other workers, and a valuable counsellor in all chemical business. He was awarded the medal of the Society of Chemical Industry, of which he was President from 1932 to 1933. In 1915 he became a Fellow of the Royal Society. He was knighted in 1936.

John Henry Michell (1863–1940) made very important contributions to the subjects of elasticity and hydrodynamics. After an early education in Melbourne, Michell went to Cambridge. He was bracketed senior wrangler in the Mathematical Tripos in 1887, and was elected to a Fellowship at Trinity College. His work included the solution of a number of problems related to the behaviour of structures under stress. He discussed hydrodynamical problems also, and among other investigations he was responsible for that relating to the 'highest wave' in water.

He was for some years a lecturer in the University of Melbourne, and subsequently professor of mathematics. He retired in 1928. He was a hard worker, who kept up his devotion to his special subjects until the end of his life. He was an excellent teacher and writer. A former student of his, Professor Massey, writes that his modesty and good nature, combined with his remarkable intellectual qualities and willingness to assist in the smoothing out of difficulties, however trivial, endeared him to his students.

He became a Fellow of our Society in 1902.

Sydney John Hickson (1859–1940) was a distinguished zoologist devoted to the study of sedentary forms of life. In his early years at school he acquired a liking for the study of natural science, which after his first class in the Cambridge Tripos of 1881 led to his establishment in the laboratory of Michael Foster and F. M. Balfour. There he completed a classical research on 'The eye and optic tract of insects'. In 1882 he became demonstrator to Moseley at Oxford and in 1888 was a deputy professor there. He spent a year in zoological and anthropological studies in Celebes. For a few years he lectured at Cambridge and in 1894 was appointed to the Beyer professorship of zoology at Manchester. There he accomplished the great work of his life. While he pressed on with his zoological work, he also played a great part in the work of the University as a whole; he took a great part in the promotion of social life of the University, especially on the women's side. He was enthusiastic in the promotion of nature teaching in schools and in the development of school museums. He was a great figure in the educational world of Lancashire.

In 1926 he retired to Cambridge and, though he could now look back on a long life devoted to scientific work, he continued his zoological researches with even increased mastery, until he died in the early months of this year. In 1895 he was elected a Fellow of our Society.

ROOKES EVELYN BELL CROMPTON (1845–1940) was one of the most notable and honoured figures of electrical engineering, because on the one hand he was associated with its first lumbering efforts and on the other because he himself was the author of many of the advances which gave to it its present adaptability and enormous power. It was an extraordinary experience to meet in recent years this wonderful old man and to remember the variety of his experiences; they went so far back as service in the Crimean war, for which he held the medal and Sebastopol clasp. He was for some years after that at Harrow, which he left in 1860. He joined the Rifle Brigade when he was eighteen and served in India. He was seconded for special service as superintendent of the Government Steam Train Department. He backed his pioneering work on mechanical transport by his construction of 'The Blue Bell' which had an average speed of four miles an hour, but was followed by other 'Blue Bells' that moved somewhat faster. From 1878 he devoted himself to the new problems of electrical engineering, and was associated with other pioneers, John Hopkinson, Willans, Swan and others, in the first enterprises of a new industry. He lived to see the world-wide application of designs and conceptions with which he himself had been associated at the beginning of his long life. He was naturally elected on many occasions to the presidency of great engineering institutions. He was elected to our Society in 1933.

WALDEMAR CHRISTOFER BRØGGER (1851–1940) was a very distinguished geologist and mineralogist. His main work was concentrated on the rock formation and contents of the Oslo country and its fiords. So thoroughly did he describe this very rich district that it became a well-known field of study to which Brøgger himself often acted as guide. This work won for him the Murchison Medal of the Geological Society of London. From 1900 onwards he occupied the chair of mineralogy and geology at the University of Oslo. His enthusiasm for scientific research, his great ability in his own field, and his considerable administrative powers, gave him a leading place among Norwegian scientists. He has been described as one of the most prominent men of science whom Norway has ever produced. He was elected to a Foreign Membership of our Society in 1902.

The Earl of CRAWFORD AND BALCARRES (1871–1940) became a Fellow of our Society in 1924. So strong and able had been his support of all that the Society stands for that the Council gladly exercised on his behalf their right to elect a very limited number of persons on the ground that their election would be of signal benefit to the Society. Lord Crawford was educated at Eton and Magdalen College, Oxford. For some years he sat in the House of Commons; he served in the war of 1914–18 as private and as lieutenant. In 1916 he was recalled to England to take office as President of the Board of Agriculture and Fisheries, and subsequently held other offices in the Government. He was a member of the Cabinet in 1916 and 1922. He was Chancellor of the University of Manchester, a Trustee of the British Museum, of the National Gallery, of the National Portrait Gallery, and he was chairman of the Fine Art Commission. In all the duties which fell to him in these and other offices he took infinite pains to make his services effective. He drew largely on his extensive knowledge of archaeology, of the history of art, and of the humane studies in general. The nation has reason to be grateful to him for the good taste which has been displayed in many public activities, and we of the Society in particular for the warm support which he gave to the advancement of knowledge of every kind.

THOMAS HEATH (1861–1940) was, as Sir D'Arcy Thompson has described him in an understanding memoir, one of the most learned and industrious scholars of our time. He was one of the last to win double honours at Cambridge, where he took a first class in the Classical Tripos and was high in the list of Wranglers He entered the Treasury in 1884 and rose to be one of the two Permanent Secretaries.

All his leisure was spent on the subject of Greek mathematics, to which his studies at Cambridge supplied an apt introduction. He became a master in this field of knowledge. He wrote books, which are accepted as standards, on the work of Diophantus, Apolonius of Perga, Archimedes, Euclid and other Greek mathematicians. They are remarkable for their completeness and accuracy.

In addition to his public service at the Treasury and subsequently as Comptroller-General of the National Debt Office, he was one of the Cambridge Commissioners under the Universities of Oxford and Cambridge Act of 1923, and a member of the Royal Commission on Museums and Galleries from 1927 to 1929. He was elected to our Society in 1912, and served twice as a member of Council. He was knighted in 1909.

PATRICK LAIDLAW (1881–1940) is best known probably for his work on canine distemper, and on influenza. He was educated at the Leys School and St John's College, Cambridge, completed his medical course at Guy's Hospital and graduated in medicine in 1907. From 1909 to 1914 he was a member of the staff of the Wellcome Physiological Research Laboratories, and during that period carried out in conjunction with Dale a standard piece of research on histamine. He then joined the staff of Guy's Hospital as Lecturer on Pathology, but in 1922 returned to a research post at the National Institute for Medical Research.

Laidlaw's work with Dunkin on distemper led to the successful immunization of dogs, for which surely he will long be remembered with gratitude. It should further be remembered that this was a relatively early study of a virus disease from all aspects, including the means of producing immunity to the infection. The methods which Laidlaw evolved in the course of it played, accordingly, an important part in the astonishingly rapid developments which have since taken place in this field. Prominent, again, among these was the further discovery made by Laidlaw, with Andrewes and Smith, of a virus as the primary infective agent in epidemic influenza, which has opened entirely new lines of attack on that common enemy of mankind. He was counted to be one of the best of modern pathologists, whose contributions to knowledge spread also into physiology and biochemistry, and were only represented in part by what was published in his own name. His death at so early an age is a very serious loss.

Our Society elected him to its Fellowship in 1927, and recommended him for a Royal Medal in 1933. He was knighted in 1935.

HERBERT ALBERT LAURENS FISHER (1865–1940) was a distinguished scholar and statesman whom our Society was glad to elect as a Fellow under the Statute which allows the Society to invite to its membership persons who have rendered conspicuous service to the cause of science or are such that their election would be of signal benefit to the Society. When President of the Board of Education from 1916 to 1922 he instituted a number of reforms of the highest importance. Not all of them are in full application as yet, but he planned a road which our National Educational System has already entered and must continue to follow. Fisher's reputation as a writer will doubtless rest mainly on his famous *History of Europe*, but many other works of his show his great erudition and painstaking accuracy. Besides his term of public duty as a Cabinet Minister, Fisher spent some years as Vice-Chancellor of the University of Sheffield, and he was Warden of New College, Oxford from 1925 until his death. He was a Governor of the B.B.C., was a Trustee of the British Museum and filled many other important posts. He was given the O.M. in 1937; and joined our Society in 1920.

ALFRED CORT HADDON (1855–1940) was in his school-days intended for his father's firm of printers and type founders, but his interest in zoology was so compelling that he was in the end sent to Cambridge where he worked at zoology under F. M. Balfour. For a short time he served as a demonstrator in comparative anatomy, and then was appointed to the professorship of zoology in the Royal College of Science in Dublin. He became secretary of the Dredging Committee which worked off the south-west coast of Ireland. He was sent to Torres Straits in 1888. The year which he spent there roused those interests in anthropology which governed the work of the rest of his life. He was one of our first anthropologists, and not only that but also one of the leading pioneers of a new science. In 1900 he became a lecturer in physical anthropology. The importance then attached to the subject was measured by his salary of £50 a year. In 1898 the Cambridge Expedition to Torres Straits was formed with Haddon as leader. Though its preliminary purpose was the rescue of knowledge concerning the decaying culture of a primitive people, its main intention and its principal work was the study of the people's psychology, as a part of that social anthropology now become so important.

Haddon's own share in the work of the expedition led to his election to our Fellowship in 1899, and to a Readership in Ethnology at Cambridge. His subsequent life was devoted to the development and appreciation of his subject in many ways, by his collection illustrating the arts, tools and customs of primitive people, by his many writings and by his encouragement of anthropological enquiry in all fields, physical, social and technical.

AUGUSTUS EDWARD HOUGH LOVE (1863–1940) was famous for his researches and his writings on the elasticity of materials, and particularly for his studies in geodynamics. As a boy he was taught at the Wolverhampton Grammar School, from which he went as a sizar and subsequently a scholar to St John's College, Cambridge. He was second wrangler in 1885, and Smith's Prizeman in 1887. He was elected to a Fellowship at St John's in 1886, and became Sedleian Professor of Natural Philosophy in Oxford in 1899.

Love was an indefatigable worker who gave all his energies to the prosecution of the subjects in which he was so deeply interested, and of which he became an acknowledged master. His investigation of the forms of waves which may travel along the surface of the earth as it is constituted has been of great importance in the theory of earthquake movements. His *Mathematical Theory of Elasticity* is a standard work of the first class both in matter and in style. The same care and perfection appeared in his lectures. He contributed greatly to our knowledge of electromagnetic waves.

Love became a Fellow in 1894 and twice served on our Council. He was awarded a Royal Medal in 1909 and the Sylvester Medal in 1937. He received the de Morgan Medal in 1926 from the London Mathematical Society.

JOCELYN FIELD THORPE (1872–1940) was educated at King's College, London, at the Royal College of Science and at Heidelberg, where he studied organic chemistry under Victor Meyer. From 1895 to 1910 he was at Owens College, Manchester, with W. H. Perkin as research fellow and lecturer. For the next four years he worked at Sheffield as a Research Fellow of our Society. In 1914 he became professor of organic chemistry at the Imperial College.

Thorpe was a devoted student of organic chemistry. His researches were the foundation for some of the most important ideas and methods of to-day. More than that, he was, in his generosity and sympathy, a fine leader for the young men who came to work with him, and have helped on so many instances to place British chemistry in its present strong position. He laboured to draw chemical efforts together, and to make them effective in the national service. He served as chairman of many committees and societies: the Indian Chemical Services Committee, Safety in Mines Research Board, Explosives in Mines Committee, the Chemical Society, and the Institute of Chemistry, and he was an active member of the Chemical Defence Committee, the Dye-stuffs Development Committee, and other bodies. He edited the Supplement to Sir Edward Thorpe's *Dictionary of Applied Chemistry*, and has recently been engaged in the production of a new edition of it.

Thorpe became a Fellow of our Society in 1908; and was awarded the Davy Medal in 1922. He was knighted in 1939.

Arthur Harden (1865–1940) spent the greater part of his working life on the chemistry of the yeast cell and so made a material contribution to the new science of biochemistry. He studied at Owens College, Manchester, and at the University of Erlangen. He was a lecturer at Owens from 1888 until in 1897 he came to London to take charge of a section of the British Institute of Preventive Medicine, afterwards to become the Lister Institute. It was as head of the biochemical section of the Institute that he directed for thirty years a concerted attack upon bacterial enzymes, bacterial metabolism, and kindred subjects. He played also a valued part in extending our knowledge of the vitamins.

In 1929, for his work on alcoholic fermentation, Harden shared with von Euler the Nobel Prize in chemistry. As editor of the *Biochemical Journal* for twenty-five years he had a great influence on the development of biochemistry in Britain. In 1930 his contribution to the *System of Bacteriology* was a very able summary of a section of this subject.

Harden was knighted in 1936. He was elected to our Society in 1909 and was awarded the Davy Medal in 1935.

Alfred Fowler (1868–1940) won his way from local schools at Keighley in Yorkshire to the Royal College of Science in South Kensington, which he entered in 1882 with the aid of one of the exhibitions founded in the name of the Duke of Devonshire. He then became assistant to Sir Norman Lockyer, an association which was a main feature of his life. Their accurate and extensive work added largely to our knowledge of spectra. It must have been a source of great satisfaction to Fowler to watch the growing use of his spectral measurements as modern physics showed their full meaning, and the importance of their indications. In due time a demonstratorship in astrophysics was succeeded by an assistant professorship, and then by a professorship which he held from 1915 until in 1923 he became one of the first Yarrow professors of the Royal Society. To the end of his life he continued his researches on the spectroscopic side of astrophysics and won international reputation. He was elected to the Royal Society in 1910, was awarded a Royal Medal, and was the recipient of many foreign honours.

Fowler was a man of great charm. His colleagues, his friends and his students loved him for his continuous willingness to help and the warmth of his encouragement, and they admired him for the perfection of his work.

**Alfred Gibbs Bourne** (1859–1940) was a biologist of distinction whose chief services were given to Madras and the educational institutions of the Madras State. He was educated at University College and the Royal School of Mines, London. He was an assistant to Ray Lankester from 1879 to 1885; the last two years of this period was spent in research at the Zoological Station at Naples. In 1885 he was appointed to the chair of biology in Presidency College, Madras; he was Registrar of the University, Botanist to the Madras Government, Director of Public Instruction and held in succession a number of other important public posts. He was Director of the Institute of Science at Bangalore from 1915 to 1921. He wrote on a wide range of biological subjects and rendered valuable aid to Indian science. He was made K.C.I.E. in 1913. He was elected a Fellow in 1895.

**Oliver Joseph Lodge** (1851–1940) will be remembered for the highly important contributions which he made to the theory and the use of electric waves. His work in this field was done in the closing decades of last century, though for many subsequent years he was an active and influential leader in physical science.

Lodge was able to enter the University of London mainly as the result of unaided study, but having made his entry he was quick to develop his exceptional abilities. He had the advantage of doing experimental research under Frankland, Guthrie and Huxley. After he had filled various minor posts he became professor of physics in the University of Liverpool in 1881. In 1900 he became Principal of the University of Birmingham.

Lodge was first attracted to the study of electromagnetic waves by Maxwell's development of Faraday's researches. When Herz in 1885 first devised experiments which demonstrated the existence of these waves, Lodge at once took up the new line of research, examined the conditions for their emission and their receipt, and in particular showed the value of correct tuning. Modern radio transmission owes very much to his theoretical investigations and to his experimental skill. This is well known, and yet his name would be even more closely associated with the development of wireless if he had not given the greater attention to research. It is a very interesting fact that he persisted in giving the ether a reality which is now considered to be unnecessary; and if his views are no longer accepted, it is still true that his conceptions assisted himself in his work, and were of no little use to those who followed his lead. He was a magnificent lecturer; his matter and style were of the first order, and his expositions derived further force from his impressive personality.

He was a Fellow of our Society for fifty-three years. He was knighted in 1902.

CHARLES FREWEN JENKIN (1865–1940) was a distinguished engineer who made important contributions to our knowledge of the properties of materials, especially of such as are used in aeroplane construction. He was educated at Edinburgh and Cambridge. The first twenty years of his life were spent in mechanical engineering practice; he was at one time Assistant to Works Manager at the L.N.W.R. works at Crewe, and held other posts of like nature. In 1908 he became Professor of Engineering Science at Oxford, and held this post until 1929.

In 1920 the Aeronautical Research Committee published a 'Report on Materials of Construction' which was the result of many years' work by Jenkin and his assistants. The new emphasis on lightness of construction required a careful analysis of all that was known respecting the strength and form of materials and the purposes for which they were intended. Jenkin demonstrated the inadequacy of previous knowledge and directed enquiry into the channels that had become necessary. A vivid account of the position is given in his Presidential Address to a section of the British Association in 1920. He emphasized the need for studying the processes of 'fatigue', and the effects of surface cracks and other defects superficial and internal. He extended our knowledge of corrosion fatigue. He made a number of other interesting enquiries with matters of physical and engineering science, such as earth pressure, refrigeration, loud speakers, an 'Oxford Astrolabe' and so on. A man of great energy, and a keen student, he has given good service to engineering science. He was elected a Fellow in 1931.

The DUKE OF BEDFORD (1858–1940) was one of the main supporters in this country of zoological studies, by his writings, by his services to zoological enterprises and by his generous expenditure on behalf of zoological work. He formed a magnificent collection of animals at Woburn Park and studied very thoroughly the conditions of acclimatization in Britain of animals foreign to the country. He was President of the Zoological Society from 1899 to 1936 and was responsible for many of the great advances made by the Society during that period. He took a special interest in the Aquarium and in Whipsnade.

He served in the Grenadier Guards in Egypt in 1882 and was A.D.C. to Lord Dufferin when Viceroy of India. He served also in the regular army from 1914 to 1919. He was A.D.C. to King Edward VII and King George V. He was President, for a period, of University College Hospital, also of the Imperial Cancer Research Fund, and he was for some years a Trustee of the British Museum. Our Society elected him to its Fellowship in 1908, being anxious to show its deep appreciation of the benefits which zoological science had received at his hands.

**Joseph John Thomson** (1856–1940) was one of the greatest men of science of our time. He had the affection and esteem of the whole world of culture. When he died, a few weeks ago, testimonies of his personality and appreciation of his work appeared in every journal, and every scientist remembered that in some way or other he was in his debt.

The very number and fullness of the descriptions of the man and his work make it superfluous for me to relate the details of his life. We all are in fact well acquainted with them. As Fellows of the Royal Society of which he was a most distinguished member, we think gratefully of his services to those principles and purposes which are our essential care. He was entirely the type of man of whom our Society can most be proud. He was a great physicist, whose insight and perseverance revealed new modes of research, leading to some of the most wonderful advances of our time. He was an inspiring teacher. He gave fine service to his University, to his College, Trinity, of which since 1918 he had been Master, to our Society and, in many ways not always well known, to the national Government. It was all recognized. Numerous honours came to him from learned bodies in all parts of the world; he was awarded the Nobel Prize in Physics in 1906, he was knighted in 1908, and the King awarded him the Order of Merit in 1913.

He was our President from 1915 to 1920, and at many other times a member of our Council.

**Harold Carpenter** (1875–1940) had a world-wide reputation as a metallurgist, whose acknowledged position as a leader was due to the very great contributions he had made both to theory and to practice. At Oxford he was a scholar of Merton and obtained a first class in the Natural Science Honours Schools. He studied also at Leipzig, and was given the Ph.D. He was a research fellow and demonstrator at Owens College, Manchester, from 1898 to 1901, and professor of metallurgy at Manchester from 1906 to 1913. When the National Physical Laboratory was founded he was appointed to be head of the Chemical and Metallurgical Departments: the most important and fruitful years of his life were spent as professor of metallurgy in the Royal School of Mines.

Carpenter's chief work was concerned with the study of the formation and properties of alloys. He laid a foundation for this in a series of original and accurate researches. Perhaps the best known of his achievements is the method of producing single crystals of metals, by means of which it has been possible to throw a new light on the relation between structure and properties. These labours have fortunately coincided with, and to no small extent have been responsible for, the growth in the knowledge of alloy structure which has had a most important influence not only on metallurgical science but also on its application to British industry.

Carpenter was in turn President of all the great metallurgical institutions of Britain. He was frequently asked for advice by the Government and by industrial concerns. He was an excellent teacher. He has left behind him an abiding influence on metallurgical science.

Carpenter received many acknowledgements, British and foreign, of the esteem in which he was held. He became a Fellow of our Society in 1918, and was knighted in 1929.

CHARLES GABRIEL SELIGMAN (1873–1940) was educated at St Paul's School and St Thomas's Hospital, where he became house physician and director of the Clinical Research Laboratory. His first contact with anthropology was made when in 1898 he joined the Cambridge Expedition to the Torres Straits under Dr Haddon, of whom I have already spoken to-day. Although he went back to his medical research work when the expedition returned, and was appointed to direct the clinical laboratory at his old hospital, he had become so interested in ethnological study that he devoted to it the rest of his life. In 1904 he revisited New Guinea as a leader of the Daniels Ethnographic Expedition. In 1908 he went to Ceylon, accompanied by his wife, who also was an enthusiastic worker on the same lines, in order to gather knowledge about the Veddas. From 1909 onwards the two ethnologists were engaged with the concurrence of Government in the study of the peoples of the Sudan. All these researches were of the greatest importance to a new and growing subject. In 1910 Seligman was appointed lecturer in ethnology in the University of London, and in 1913 professor of that subject at the London School of Economics. He took a leading place in anthropological and ethnological societies and meetings in this country. His full and able descriptions of his observations and discoveries are standard works. He became a Fellow of our Society in 1919.

**Robert Abbott Hadfield** (1858–1940) was a great engineer and metallurgist. His skill, energy and directive power made the Hecla works one of the most important and distinctive of the steel works of modern times; his success was largely due to the devoted attention which he gave to scientific research into the processes of his industry. In 1875 he entered the laboratories of the works founded by his father: his attention was quickly drawn to the several attempts which had been and were then being made to add to the properties of manufactured steel by the addition of other substances, particularly manganese, and in 1882 he produced his famous 12% manganese steel, which was non-magnetic, became softer and tougher on quenching from high temperatures and was extremely resistant to abrasion. Later he was instrumental in developing the silicon and aluminium steels which have been of great use in the construction of electrical transformers and machinery.

Hadfield was thus successful in the development of great enterprises which have been of immense value to this country. He attached high importance to research, and was generous and persistent in its support. His liberality was exercised in many other ways. He was elected a Fellow of our Society in 1909 and was a frequent contributor, alone or in collaboration with others, to the Royal Society *Proceedings*. He was knighted in 1908, and received a baronetcy in 1917.

**Henry Head** (1861–1940) was a great neurologist who made important contributions to the knowledge of sensation, especially in relation to the skin and the spinal cord. He studied also the problems of aphasia. His work was original and led the way to much of the research of the present day.

Head was educated at Charterhouse and at Cambridge, where he was a scholar of Trinity College. He studied also at the German University of Prague and at the University of Halle. He worked for his medical degree at University College, London. He became a Fellow of our Society in 1899 and was knighted in 1927.

Taking his place worthily in succession to Ferrier, Jackson, Horsley and Gowers, great British neurologists and Fellows of this Society, Head gave most of his working years to the study of diseases, and particularly those of the nervous system, by the experimental method which he had learned as a physiologist. His enthusiasm led him to study on his own person the process of recovery from an experimentally inflicted nerve lesion, and he had a special gift for communicating his enthusiasm to others. During the last 20 years of his life a disease deprived him progressively of the power of movement, but left him to the end full of interest in research and in its further promotion. He was knighted in 1927.

**Vito Volterra** (1860–1940), who at the time of his death had been a Foreign Member of the Royal Society for thirty years, was one of the foremost mathematicians of the age. After graduating at Pisa and holding chairs in that University and in Turin, he was appointed in 1900 Professor of Mathematical Physics in the University of Rome, and later a Senator of the Kingdom, the Italian Government making use of his ability in the conduct of affairs in many missions to other countries. In the Senate during the years 1914–15, he was one of the strongest supporters of Italy's entry into the war on the side of the Allies.

In 1931, having refused the oath of allegiance then imposed on University Professors by the Fascist Government, he was deposed from his chair. His last years were spent chiefly in Paris.

He will be remembered in the history of mathematics as the creator of the theory of integral-equations 'of Volterra's type', the theory of functionals, and the theory of integro-differential equations, and as the greatest of the pioneers in the application of mathematics to biological problems, especially the fluctuations in the numbers of animal species living together. His contributions to mathematical physics, particularly to the theory of electricity, were also of the first importance; and it was most often from physical problems that he derived the first suggestions for his discoveries in pure mathematics.

**Arthur Neville Chamberlain** (1869–1940) was elected to our Society in 1938. The tributes to his life and work have been so many and so appreciative, being based on the universal admiration of himself and of his labours, and are still so fresh in our memories that it would be useless for me to add to them. I will say only that we have been proud to have his name on our roll, and that we remember with gratitude his support of learning, and his strivings that the world should be governed by reason and good will.

**Frederick Wallace Edwards** (1888–1940) was born at Fletton, Peterborough. From the Cambridge County School, where he early displayed a marked attraction to botany and zoology, Edwards entered Christ's College, Cambridge, and graduated in 1909; he took the degree of Sc.D. in 1931.

In 1910 he joined the staff of the Department of Zoology in the British Museum, as an assistant in the Entomological section. In 1937 he was promoted to be Deputy Keeper of the Department of Entomology which had been created in the interval. He was given charge of the mosquitos, the crane flies and the British collection of Diptera. Edwards flung himself wholeheartedly into his task and from the very first his published work showed a mastery of his subject and a great critical faculty.

In addition to his purely museum work, Edwards made two successful expeditions, the first to Patagonia, Chile and the Argentine which produced a far-reaching account of the Diptera of these regions. The second expedition was made from a desire to investigate the relationships existing between the faunas of the isolated high mountain groups of East Africa and was concentrated mainly on Mount Ruwenzori. The first results of this last expedition have also been published.

Edwards has described some 2000 new species, but his descriptions were only incidental to constructive taxonomic work on a large scale and his output of published work is represented by over 270 titles.

ERNEST WILLIAM MACBRIDE (1866–1940) was a very able zoologist who adhered strongly to the 'Lamarckian view of the inheritance of acquired characters'. He was educated at Queen's College, Belfast and St John's College, Cambridge, where he was a Foundation Scholar. He studied also at the Biological Station at Naples. At Cambridge he came under the influence of Adam Sedgwick, and was led to an extensive study of the embryology of the Echinodermata: in after years he contributed an important article on this subject to the *Cambridge Natural History*. He held the Strathcona chair of Zoology at McGill University from 1897 to 1909; from 1913 to 1934 he was Professor of Zoology at the Imperial College, London. He did useful public service in connexion with Fishery Research and other zoological enquiries; and wrote a number of important books and papers.

He became one of the leading authorities on embryology, to which his early work on the Echinodermata had introduced him. The strong views on Lamarckism were held with great vigour and much experimental work and argument were spent in the defence of his position against opposition. He became a Fellow of the Society in 1905.

## *Awards of Medals*, 1940

The **Copley Medal** has been awarded to Professor **Paul Langevin**.

Professor Langevin was one of the band of young pioneers who, in the closing years of the last century, were engaged in exploring the field which had been opened up by J. J. Thomson's discovery of the electron. He spent a year (1897–1898) at the Cavendish Laboratory, and his Paris Dr ès Sc. thesis (1902) is dedicated to J. J. Thomson. The thesis, a notable one, was entitled *Recherches sur les Gaz Ionisés*. It dealt mainly with the recombination and mobilities of ions, their coefficients and the relations between them. It is a standard work on this subject. In it he also devised and applied new and elegant methods of measuring these quantities which were an advance on all their predecessors and have not since been improved upon to any appreciable extent. Related to this, and coming later, were important contributions to the theory of the diffusion of gaseous ions and its relation to ionic mobilities.

Langevin's greatest achievement is the foundation of the electron theory of magnetism. The theories of paramagnetism and of diamagnetism are still very much as he made them and left them over thirty years ago.

There are few branches of contemporary physics which he has not illuminated and improved by his writings, and his work generally has the qualities of breadth, clearness, elegance and completeness which stamp the master.

He has had a great international influence. He has been a prominent figure at all the meetings of the conferences arranged by the Institut International de Physique Solvay since they started in 1911. On the death of Lorentz he was chosen to succeed him as President of the Institut.

He was awarded the Hughes Medal in 1915 and elected a Foreign Member of the Society in 1928.

The **Rumford Medal** is awarded to Professor **Karl Manne Georg Siegbahn**.

Professor Siegbahn, member of an old Swedish family, is, in the field of X-rays, what Rowland was in the field of ordinary optics sixty years ago. He has introduced high precision into X-ray measurements. For example, the most accurate wave-length measurements in 1913 were those of Moseley, with an accuracy of about 1 %. By a brilliant succession of improvements in methods, design, inventions and technique, Siegbahn by 1924 had improved this to 0·001 %, a factor of 1000.

Siegbahn is not only a great physicist, he is also a great engineer. He has made inventions and improvements in almost every useful type of apparatus connected with X-ray measurements, pumps, gratings, X-ray tubes, ruling machines, etc.

Among his many achievements are the determination of the structure of the *L* series of X-ray spectra, the discovery of the anomalous dispersion of X-rays (with Hjalmar), the accurate and direct measurement of the grating spaces of calcite and rock salt, and the selection rules for the frequencies of X-ray absorption edges. In conjunction with Larsson and Waller, he was the first to deviate X-rays with a prism. They developed this method till they could obtain by it measurements of refractive indices for X-rays which are of quite surprising accuracy.

In recent years he has been much occupied with the development and improvement of methods of measurement of 'ultra-soft' X-rays, the region between about 10 to 500 A, and with conspicuous success. This covers the gap between the ordinary X-ray region and the optical region of radiation.

He and his students have also been much interested in the values of the fundamental constants of physics and have made important contributions to our knowledge of them.

He has written a masterly book on the spectroscopy of X-rays. An extraordinarily large proportion of the information in it is due to the work of himself and his students. He has created an outstanding school at Uppsala and Stockholm, which now represents most of the physics of Sweden.

He was awarded the Hughes Medal in 1934.

A ROYAL MEDAL is awarded to Professor PATRICK MAYNARD STUART BLACKETT.

Professor Blackett is especially distinguished for his work on cosmic rays and the particles connected with them.

The early work which first brought his name into prominence was concerned with the disintegration of nitrogen by $\alpha$-particles; arising out of the experimental observations was the convincing proof that the disintegration process originated in the actual capture of the $\alpha$-particle by the nitrogen nucleus.

The demonstration of cosmic-ray showers was one of Blackett's early successes with direct Wilson chamber photographs, but perhaps his most spectacular discovery—made simultaneously by Anderson in America—was that, in a large cloud chamber controlled by the tripping of counters, tracks appeared which could only be explained as due to a new particle—

the positive electron. The importance of this discovery in the light of Dirac's theory was immediately realized by Blackett and his co-worker Occhialini, and important results have emerged.

Blackett also—in collaboration with Chadwick and Occhialini—extended the work on the positive electron, and it was soon found that there were sources other than cosmic rays. With the same collaboration Blackett was also instrumental in showing that quanta of sufficient energy could produce a pair of electrons and this production was related to the so-called nuclear absorption of $\gamma$-rays—a phenomenon previously known but until then unexplained.

Blackett has followed up his cosmic-ray work and has published a number of very interesting papers dealing with various aspects of these rays. He has measured their energy, inferring therefrom a cosmic-ray energy spectrum; he has observed, with an extraordinarily high degree of accuracy, the scattering and energy loss of cosmic-ray particles in their passage through metal plates and has discussed the nature of the penetrating component of Cosmic Rays. Two papers on this topic appeared in the *Proceedings of the Royal Society* for 1938.

Lastly, reference must not be omitted of Blackett's important experimental contributions to our knowledge of the heavy electron—the particle which seems destined to be of such importance in the understanding of the more familiar nuclear particles.

A ROYAL MEDAL is awarded to DR FRANCIS HUGH ADAM MARSHALL.

Dr Marshall's earlier research work (1903–1907) on the oestrous cycle, corpus luteum, and removal and grafting of ovaries laid the foundations for all the modern discoveries concerning the internal secretions of the sex organs.

The publication of his large text-book on the *Physiology of Reproduction*, in 1910, stimulated work on this subject throughout the world, not only on points of scientific interest but also in regard to the application to medicine and to questions of fertility and milk secretion in the domestic animals. He was engaged on a third edition of this book when war broke out. He is generally acknowledged to be the father of this subject, and but few papers on this branch of science to-day are published without some reference to his work.

Arising out of his research, and that of his pupils, the importance of the anterior pituitary as a source of internal secretions, affecting not only the sex organs but also other body functions, has been recognized, and has led the way to an enormous volume of research work in recent years throughout the world. It is one of the subjects in which the greatest advances have been made in recent years.

Recently, his research has been concentrated on the exteroceptive factors, such as light, ultra-violet irradiation and nerve stimuli, which affect the sex organs by way of their effects on the anterior pituitary. This work explains the physiological basis for the seasonal and other changes which occur in reproductive activity. He summarized this aspect of the subject in the 1936 Croonian Lecture on 'Sexual periodicity and the causes which determined it', beside adding new matter.

The DAVY MEDAL is awarded to Professor HAROLD CLAYTON UREY.

Professor Urey's first important piece of work consisted in carrying out extensive, accurate, spectroscopic measurements on diatomic and polyatomic molecules. This led him in 1931 to take up a detailed investigation on the abundance of natural isotopes of hydrogen, nitrogen and oxygen. During the next few years he succeeded in isolating deuterium and calculating the comparative thermodynamic properties of deuterium, hydrodeuterium and hydrogen. In 1934 he accomplished the first synthesis of deuteromethane.

Deuterium or 'labelled' hydrogen has proved of great value in investigating the mechanism of many organic and biologically important reactions, and its use has been the precursor of the modern general isotopic exchange reactions. A number of deutero derivatives have been prepared by Urey and his co-workers, and their entropies, vapour pressures and exchange equilibrium constants have been experimentally determined and compared with the theoretical values anticipated.

This isolation of deuterium from ordinary hydrogen and establishment of the thermodynamic, spectral and physico-chemical difference between it and pure hydrogen, as well as in the compounds containing deuterium and hydrogen, is a remarkably complete piece of work, for which Urey received the Nobel Prize.

More recently Urey has taken up the problem of the separation of the other important, naturally occurring isotopes· those of nitrogen, oxygen and carbon. He has examined their quantity distribution in nature and employed exchange methods for the enrichment of one species.

The DARWIN MEDAL is awarded to Professor JAMES PETER HILL.

Over a long series of years Professor Hill has carried out researches on the development of various mammals, particularly as regards the embryonic membranes and placenta, and added greatly to our knowledge of this subject. Many of his conclusions have clear evolutionary implications, as for example that marsupials are descended from oviparous ancestors with meroblastic ova. In his Croonian Lecture of 1932 Professor Hill summarized his researches on the embryology and embryonic membranes of the Primates. The views of primate evolution based on development which he then put forward are in accord with those of Elliot Smith founded on brain anatomy, and of W. K. Gregory on morphological and palaeontological evidence.

In collaboration with T. T. Flynn, Professor Hill has lately (1939) published the first part of extensive researches on the development of monotremes, both *Ornithorhynchus* and *Echidna*, which will be of great value in helping to assess the origin and relationships of these egg-laying mammals.

Professor Hill's research work is of first-class quality, being trustworthy and carried out with extreme care and the best techniques; it has never been scamped and is rich in original results over a wide field, most of the conclusions having a direct bearing on evolutionary questions.

Few living biologists have contributed more towards the solution of problems bearing on the interrelationships of the main groups of the Mammalia and on the phylogenetic history of the Primates, a subject with which Charles Darwin was so much concerned.

The SYLVESTER MEDAL *is* awarded *to* Professor GODFREY HAROLD HARDY.

G. H. Hardy is the author, or part author, of over 300 mathematical papers, two books, and several of the Cambridge Mathematical Tracts.

Much of his work has been directed to the building up of the technique of modern mathematical analysis, and the simplicity with which the routine aspects of new work can now be presented is due very largely to fundamental results established by him.

It is characteristic of much of his work that it has stimulated others and has proved to be the starting point of important developments. His work in collaboration with J. E. Littlewood on Tauberian theorems is an example. From an isolated classical result a subject was created which to-day would require a treatise for its exposition.

His most outstanding contributions to the advance of mathematical knowledge have been in the theory of the Riemann zeta-function and the theory of numbers. The achievement of which, it is believed, he himself is most justly proud is the invention of the 'circle method'. This is a technique of great beauty and generality which brings great refinement of mathematical analysis to bear on a wide class of unsolved problems in the theory of numbers.

No appreciation of the services of Hardy to the advance of mathematics would be complete which did not attempt to assess the value of his personal influence. Throughout his career he has been the driving force behind a vigorous group of younger research workers. A very considerable proportion of the pure mathematical research now being published in this country is traceable more or less directly to his interest and encouragement, or to the inspiration of his earlier work. His unstinted service during many years to the detailed work of the London Mathematical Society, and the freedom with which his experience and advice are available to all, have established him in a unique position in the regard of British mathematicians.

The HUGHES MEDAL is awarded to Professor ARTHUR HOLLY COMPTON.

Professor Compton has made a number of important contributions to physical science in the field of X-rays and elsewhere. Of late years he has been one of the leaders in the study of cosmic rays.

The experiments of Young and Fresnel early in the nineteenth century proved that light certainly had undulatory properties. But in the present century facts have been emerging, notably in connexion with photoelectric action, which are impossible to reconcile with the assumption that light can be described only as an electromagnetic wave of the classical type. These difficulties disappeared if light of frequency $\nu$ is assumed to be dynamically equivalent to a collection of particles of energy $h\nu$ ($h$ = Planck's constant).

It occurred to Compton that from this standpoint the interaction between radiation and free electrons is very simple, and in fact is the simplest interaction which radiation can undergo. Associated with the energy $h\nu$, according to the electromagnetic theory, there is momentum $h\nu/c$ ($c$ = velocity of light). The interaction is thus reduced to a very ancient problem, that of the encounter of two infinitesimal billiard balls with known energies and momenta. As the radiation moves with the velocity of light, in most cases the electron can be treated as if it were at rest. It is then obvious that in the collision the electron will acquire energy from the radiation and the conservation of momentum requires that if the electron moves off in a certain direction the radiation will travel in a certain other direction. But reduction of energy of a quantum of radiation means increase in wave-length, and this increase will be a predetermined function of the direction of the 'scattered' radiation and of the direction of motion of the 'recoil' electron.

He published these conclusions in 1922. In 1923 he established the change in wave-length, first qualitatively by Barkla's absorption coefficient methods and then quantitatively with the X-ray spectrometer. In the succeeding years he investigated the energies of the recoil electrons as a function of their direction of motion and showed that the correlation, predicted by the theory, between the direction and energy of the recoil electrons on the one hand and the direction and change of wave-length of the radiation on the other did in fact occur. This correlation is of fundamental importance in the general theory of the interaction of radiation with matter.

# The apparent sizes of atoms in metallic crystals with special reference to aluminium and indium, and the electronic state of magnesium

By William Hume-Rothery, F.R.S. and
Geoffrey Vincent Raynor

(*Received 4 September* 1940)

The interatomic distances in crystals of alloys cannot be accounted for by assigning a fixed atomic radius to each kind of atom, and the causes of this variation are discussed with special references to the Brillouin zone characteristics of different structures. According to the theory of Jones, the effect of an overlap across the side of a Brillouin zone is to compress the zone at right angles to the face concerned, and so to expand the crystal lattice in the same direction. This expansion is not a property of an atom which can be transferred to any of its alloys, but is a characteristic of a structure with sufficient electrons to produce an overlap. The lattice spacings of alloys of aluminium and indium with copper, silver, gold, and magnesium are examined, and the apparent sizes of the aluminium and indium atoms are discussed, and are shown to be in agreement with the theory. The previous suggestion, that in metallic aluminium the atoms exist in an incompletely ionized state, is improbable, and is no longer required in order to explain the facts. New experimental data for the lattice spacings of solid solutions of aluminium and indium are presented, and these show that, whilst the curves connecting the $a$ parameter with the composition are smooth and continuous, the corresponding curves for the $c$ parameter show an abrupt change in direction at about 0·75 atomic % of indium or aluminium. This is taken to imply that, although in metallic magnesium with two electrons per atom, the overlap of the first Brillouin zone is in the $a$ direction only, the structure is so near to the stage at which the c overlap sets in that the addition of less than one electron per hundred atoms causes the $c$ overlap to take place.

## I

It is well known that the interatomic distances in crystals of alloys cannot be accounted for by assigning a fixed atomic radius to each kind of atom, but that the apparent size of the atom depends on the nature and crystal structure of the particular alloy concerned. This variation in size has been ascribed to many factors, of which the following may be noted:

(*a*) *The effect of co-ordination number*. For ionic crystals, this effect is well understood, and a satisfactory theory exists. For the metals the position is less satisfactory, and, although the work of Goldschmidt (1928) suggests clearly that decreasing co-ordination number results in a contraction of the atomic radius, there are comparatively few cases in which the effect of co-ordination can be tested without the introduction of other complicating factors, some of which are described below.

(*b*) *Changes in the degree of ionization.* It is now accepted by many writers that the large interatomic distances in crystals of thallium (3·40 and 3·45 A) and lead (3·49 A) compared with that in the preceding element gold (2·88 A) are due to the great stability of the $Tl^+$ and $Pb^{++}$ ions, which results in these elements existing in forms resembling univalent and divalent, rather than trivalent and tetravalent elements respectively. The effect of this in connexion with the Brillouin zone theories of metals has not yet been discussed, and for some purposes it is considered as legitimate to regard all three valency electrons of, say, thallium as building up the zones, although, as regards cohesion, the underlying sub-group of two electrons is sufficiently developed to give rise to repulsion rather than to attraction, and to increase the interatomic distances. It has been suggested that the same phenomenon is the cause of the relatively large interatomic distances in indium and white tin. The fact that the interatomic distances in metallic aluminium are greater than those in many alloys has also been ascribed to the same phenomenon, but this explanation is very unsatisfactory, since the univalent $Al^+$ ion is very unstable. It is one of the objects of the present paper to present an alternative explanation.

(*c*) *Electrochemical effects.* In alloys of two metals, which differ widely in the electrochemical series, there is a tendency for the intermediate phases to acquire some of the characteristics of definite compounds, and a contraction in the interatomic distances is to be expected in both the intermediate phases, and the primary solid solutions.

(*d*) *Polarization and Van der Waals effects.* It has been suggested by Raynor (1938) that some of the departures from Vegard's Law in alloy systems are due to polarization and Van der Waals effects. These effects may be particularly important in alloys for which the interatomic distances are controlled mainly by the electron clouds of the ions ('full' metals).

It is the object of the present paper to suggest that, apart from the above factors, the apparent sizes of atoms in different structures are influenced by the Brillouin zone characteristics of the structure, and to illustrate this effect by some clear examples. For convenience we shall use the term 'normal atomic diameter' to denote the closest distance of approach of the atoms in the crystal of an element, and, where the structure is such that an atom has neighbours at slightly different distances, we shall refer to the atomic diameter in a particular direction. When a substitutional solid solution is formed in an element, there is usually a linear relation between lattice spacing or interatomic distance, and the composition in dilute solutions. If this straight line is extrapolated to 100 % of solute, the resulting interatomic distance may be called the apparent or extrapolated atomic diameter of the solute in the primary solid solution concerned. In the same way, for an intermediate phase of variable composition, if the lattice spacing-composition relation is linear, the straight line may be extrapolated to give the apparent or extrapolated atomic diameter of the two elements in the particular phase.

## II

The general method of representing conditions in a metal is to draw one curve (1) representing the energy of the lowest electronic state as a function of $r$, the distance between the atoms, and a second curve (2) showing the Fermi energy as a function of $r$. The interatomic distance in the metal is then given by the position of the minimum on the curve obtained by the summation of (1) and (2). The curve (1) is obtained by some method involving the wave-functions of the atoms, whilst the curve (2) is obtained from the simplified free-electron theory, or the more complete theories involving Brillouin zones. This method may be considered as one in which the interatomic distance is regarded as controlled by the sum of an atomic factor and an electronic factor, although the valency electrons are of course involved in the wave function of the atom. This concept applies to both 'full' and 'open' metals; in the latter the wave functions of the ions have almost vanished at the interatomic distances concerned, whilst, in the 'full' metals, the mutual penetration of the electron clouds of the ions is considerable, and the atomic factor involves the electrons of the outermost shell of the ion, as well as the valency electrons.

According to the theory of Jones (1934), the effect of an overlap across the side of a Brillouin zone is to compress the zone at right angles to the face concerned, and so to expand the crystal lattice in the same direction in real space. The work of Jones was concerned with hexagonal crystals in which the overlaps were different in different directions, but his equations (6) to (9) are quite general, and apply to any structure, so that in a cubic crystal where the zone overlaps are symmetrical, the effect will be to produce a uniform expansion of the lattice. This expansion is not a property of the atom which can be transferred to all of its alloys, but is a characteristic of a structure with sufficient electrons to produce an overlap. If, therefore, we consider an element $X$, whose crystal structure and valency are such that a Brillouin zone overlap occurs, the interatomic distances will be greater than those obtained by extrapolation of the values of the solid solution of $X$ in univalent elements, such as silver or copper, for which there is no overlap. The interatomic distances in the crystals of the element $X$ will also be greater than those in structures which correspond with a completely full Brillouin zone. Further, if the element $X$ enters into phases of variable composition with structures such that the Brillouin zone overlaps are not symmetrical (e.g. the close-packed hexagonal structure), the extrapolated values of the atomic diameter of $X$ will in general be different for the different directions of the crystal.

## III

Aluminium crystallizes in the face-centred cubic structure, and the curves of Mott and Jones (1937) show that, with three electrons per atom, there is a moderate overlap across the (200) planes. The interatomic distance in the crystal of the element, 2·857 A, should therefore be greater than the extrapolated atomic diameters of aluminium in solid solution in copper, silver and gold, and, as will be seen from table 1, this expectation is satisfied. Silver and gold have almost the same atomic diameter, and the fact that the extrapolated value for the AuAl$\alpha$ phase is smaller than that for the AgAl$\alpha$ phase may be ascribed to a combination of the electrochemical and polarization effects since both these are greater in the gold-aluminium alloys. The extrapolated values from the silver and gold $\alpha$-solid solutions are, however, larger than that from the copper $\alpha$-solid solution, and the reason for this may be as follows. The solid solution of aluminium in copper results in an expansion of the copper lattice, whereas the solid solution in silver causes a contraction of the lattice of silver. The first Brillouin zone of the face-centred cubic lattice always contains two electrons per atom. The effect of lattice expansion is to reduce the width of the band, and hence, if the $N(E)$ curves are drawn in the usual way, lattice expansion results in the $N(E)$ curve for the first zone becoming higher in the direction of the $N(E)$ axis, and shorter along the $E$ axis. Conversely, lattice contraction increases the width of the band, and the $N(E)$ curve for the first zone becomes longer in the direction of the $E$ axis, and shorter in the direction of the $N(E)$ axis. In dilute solutions of aluminium in copper, silver, or gold, the zone is only slightly more than half full, and the $N(E)$ curve does not differ greatly from the curve of the free electron theory. The above considerations, therefore, show that the addition of a given number of electrons in dilute solid solution will increase

$E_{\max}$ by a greater amount in the case of lattice contraction than for lattice expansion. The increase in pressure due to the addition of a given number of electrons will therefore be greater in the case of lattice contraction than for lattice expansion, and hence, other things being equal, the apparent size of the aluminium atom should be greater when it produces lattice contraction than when it causes lattice expansion. This is in agreement with the facts.

TABLE 1

| Alloy phase | Extrapolated atomic diameter of aluminium |
|---|---|
| CuAl$\alpha$ phase | 2·71 A |
| AgAl$\alpha$ phase | 2·799–2·808 A |
| AuAl$\alpha$ phase | 2·77 A |

The close-packed hexagonal phase in the system silver-aluminium also gives a clear indication of the effect of zone formation on the apparent atomic diameter. For this phase, the axial ratios vary with the composition, but are not far from those required by close-packed spheres. At the electron concentrations concerned, this indicates that the first Brillouin zone is overlapped in the $a$, but not in the $c$ direction. The values of the two distances of approach in this structure extrapolated to 100 % aluminium give the following values·

$$a \text{ parameter } (= \text{closest distance of approach in basal plane}) = 2{\cdot}934 \text{ A},$$

$$d \text{ or second distance of approach} = \sqrt{\left(\frac{a^2}{3}+\frac{c^2}{4}\right)} = 2{\cdot}695 \text{ A}.$$

The extrapolated value for the $a$ distance of approach is large in agreement with the fact that we are dealing with a direction involving a Brillouin zone overlap which, owing to the valency of aluminium, is increased by increasing aluminium content. The $d$ distance of approach involves both the $a$ and $c$ parameters and so is not simply related to the zone overlaps, but since $a$ is abnormally large, it is clear that the extrapolated value of $c$ must be abnormally small in order to give the low value of 2·695 A for the extrapolated $d$ value for aluminium. The extrapolated values for this structure are thus in complete agreement with expectation.

The $\delta$ phase, $Cu_9Al_4$, of the system copper-aluminium has a structure of the $\gamma$-brass type, and corresponds with an almost full zone. The Al-Al distance of approach in this phase is 2·77 A and is thus smaller than the normal atomic diameter, in agreement with our hypothesis.

The η phase, $Al_2Au$, of the system aluminium-gold, has a brilliant purple colour with the $CaF_2$ type of structure. This structure is usually associated with an electron/atom ratio of 8/3, which corresponds with a completely filled zone, and the properties of the compound $AuAl_2$ have led to the suggestion that, owing to the strong electrochemical factor, one of the electrons of the gold atom is removed from the *d* shell. If this is accepted,

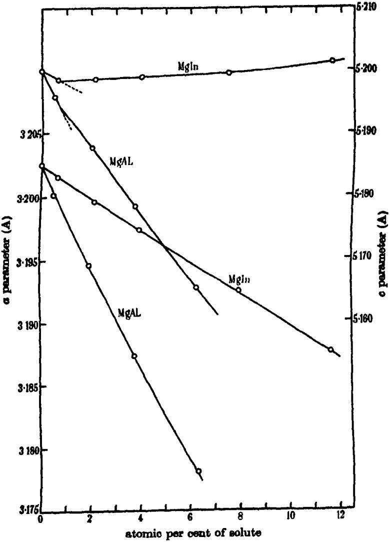

Figure 1

the compound $AuAl_2$ can be regarded as a full zone structure with a strong electrochemical factor, and the Au-Al interatomic distance should be smaller than that obtained from the normal atomic diameters (2·86 A). The actual Au-Al distance in $AuAl_2$ is only 2·59 A, and this low value is in agreement with expectation.

Magnesium has a close-packed hexagonal structure with axial ratio 1·6237. At two electrons per atom, this corresponds with Brillouin zone overlaps in the *a*, but not in the *c* direction. The lattice spacings of the solid solution of aluminium in magnesium have not previously been measured to the highest degree of accuracy. We have determined these lattice spacings accurately, using all the precautions described by Raynor (1940), and the results, which are shown in figure 1, are of great interest.

TABLE 2

| Alloy systems | At % solute | Lattice spacings | | Axial ratio |
|---|---|---|---|---|
| | | *a* | *c* | *c/a* |
| Pure Mg | — | 3 2025 (5) | 5·1999 (9) | 1·6237 |
| MgAl | 0·496 | 3·2001 (5) | 5·1957 (6) | 1·6236 |
| | 1·997 | 3·1945 (9) | 5·1876 (9) | 1·6239 |
| | 3·785 | 3·1873 (0) | 5·1784 (0) | 1·6247 |
| | 6·31 | 3·1780 (9) | 5·1653 (5) | 1·6253 |
| MgIn | 0·63 | 3 2015 (0) | 5·1982 (7) | 1·6237 |
| | 2·16 | 3·1995 (5) | 5·1983 (1) | 1·6247 |
| | 4·01 | 3·1973 (7) | 5·1989 (2) | 1·6260 |
| | 7·98 | 3·1924 (5) | 5·1995 (4) | 1·6287 |
| | 11·65 | 3 1875 (4) | 5·2013 (7) | 1·6325 |

The curve connecting the *a* lattice spacing with atomic percentage of aluminium is smooth and continuous, and the extrapolated atomic diameter of aluminium for the *a* distance of approach is 2·825–2·84 A. This is almost the same as the normal atomic diameter of aluminium (2·857 A), in agreement with the fact that both involve Brillouin zone overlaps. In contrast to this, the curve connecting the *c* lattice spacing with atomic percentage of aluminium, shows a change in direction at about 0·75 atomic % of aluminium, the first addition of aluminium producing a steeper fall in the *c* spacing than further additions. The change is slight, but is well outside the experimental error, and is of such a nature that the first small addition of aluminium lowers the axial ratio of magnesium, whilst further increase in the aluminium content produces an increase in the axial ratio (see table 1). We have also determined the lattice spacings of a very dilute solid solution of indium in magnesium, and these values, combined with the previous results of Raynor (1940), are also shown in figure 1, from which it will be seen that the curves for the $a$ and $c$ parameters of the solid solution of indium in magnesium have the same characteristics as those for the aluminium alloys. The curve for the $a$ parameter is smooth and continuous, whilst that for the $c$ parameter shows an abrupt change in direction at about 0·75 atomic % of indium.

The above results may be interpreted as showing that, although in metallic magnesium with two electrons per atom, the Brillouin zone overlap is in the $a$ direction only, the metal is so near to the stage at which the $c$ overlap sets in, that the addition of less than one electron per hundred atoms enables the overlap to occur in the $c$ direction, with the resulting alteration in the lattice spacing-composition relations. If this interpretation is correct, metallic magnesium exists in a state which is clearly of great theoretical interest.

We have already indicated (p. 31) that the second, or $d$, distance of approach in the close-packed hexagonal structure is not directly related to the Brillouin zone overlaps since it involves both the $a$ and $c$ spacings. It is of interest to note, however, that the extrapolated atomic diameter of aluminium for the $d$ distance of approach in solid solution in aluminium is 2·71 A before the $c$ overlap occurs, and 2·84 A afterwards.

In general, therefore, the apparent or extrapolated atomic diameters of aluminium are in good agreement with the Brillouin zone theories, and the assumption of incomplete ionization in metallic aluminium should be discarded.

## IV

Indium crystallizes in the face-centred tetragonal structure with axial ratio 1·077, so that the structure is very nearly that of a face-centred cube. This results in each atom having four neighbours at 3·24 A, and eight neighbours at 3·37 A; the atomic diameter for co-ordination number 12 would therefore be about 3·3 A. The Brillouin zone of the face-centred tetragonal structure with axial ratio slightly greater than unity is of the form shown in figure 2. This resembles the zone for the face-centred cube, but is compressed in the direction of the $c$-axis, this compression corresponding with the expansion of the unit cell in real space in the same direction. At three electrons per atom, the face-centred cubic structure involves overlaps across the $8A$ and $6B$ faces, and the effect of the compression of the zone in the tetragonal structure is to increase the overlap across the top and bottom $B$ faces, and to diminish that across the remaining $4B$ faces which may be distinguished by the symbol $B'$.

The interatomic distances in silver and gold are 2·88 A, and those in indium and thallium are 3·24, 3·37 A, and 3·40, 3·43 A respectively, so that the values for thallium are about 0·1 A greater than those for indium in spite of the fact that the atomic diameters of silver and gold are nearly equal. If we regard the values for thallium as the result of a very stable $Tl^+$ ion, those for indium suggest that the $In^+$ ion is not so stable, in agreement with the general chemistry of the elements. We shall adopt the point of view that in metallic indium, the normal Brillouin zone effects are superimposed upon the effect of incomplete ionization, with the result that the extrapolated atomic diameters of indium in alloys are not so simply related to those of metallic indium, as are the corresponding values for aluminium. Indium is also more electronegative than aluminium, with the result that the electrochemical factor is much greater in the magnesium-indium alloys.

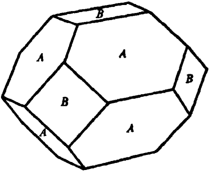

FIGURE 2

The lattice spacing relationships in the solid solutions of indium in magnesium have been described above, and the values for the extrapolated atomic diameters are as follows:

Extrapolated *a* value 3·089 A.
Extrapolated *d* value before the *c* overlap begins 3·07 A.
Extrapolated *d* value after the *c* overlap has set in 3·17 A.

These values agree with our general hypothesis, the extrapolated atomic value of indium being smallest in the case where there is no overlap.[*] The extrapolated atomic diameters for the directions in which overlaps are involved (3·09 and 3·17 A) are relatively much smaller than the values in metallic indium than are the corresponding values for aluminium, and this difference may be ascribed to the much greater electrochemical factor in the system magnesium-indium, and to the fact that, if our views are correct, metallic indium involves some tendency towards incomplete ionization, in the crystal of the element, whilst aluminium does not.

---

[*] As explained previously the *d* distance of approach involves both the *a* and *c* spacings, so that if the extrapolated value for the *a* spacing is 3·089 A, the *c* spacing must be small in order to give an extrapolated value of 3·07 A for the *d* distance.

The lattice spacings of solid solutions of indium in silver have been measured accurately by Owen and Roberts (1939), and by Hume-Rothery, Lewin, and Reynolds (1936), and the extrapolated atomic diameter is 3·07 A. This value confirms our hypothesis, since it is less than the normal atomic diameter in the element, and the difference is greater than in the case of aluminium in agreement with the concept of incomplete ionization.* The lattice spacings of the solid solution of indium in gold have only been measured roughly by Weibke and Hesse (1939) and the extrapolated atomic diameter of indium is 3·12 A and is thus again smaller than the normal atomic diameter.

The solid solution of indium in copper cannot be compared directly with those in silver and gold, since, in the copper alloy, the interatomic distances are influenced greatly by the electron cloud of the indium *ion*, which is larger than the ions of copper.† The extrapolated atomic diameter of indium from the CuIn$\alpha$-solid solution is 3·21 A, and is thus still smaller than the normal atomic diameter, although larger than the extrapolated values from the silver and gold solid solutions where the ions of indium are smaller than the solvent ions.

In general, therefore, the normal, and apparent or extrapolated atomic diameters of both aluminium and indium are in good agreement with the requirements of the Brillouin zone theories. All the examples considered are those in which aluminium or indium is the element of higher valency, so that extrapolation in the direction of increasing aluminium (or indium) content increases the zone overlap. The apparent atomic diameters obtained by extrapolation towards the element of lower valency will be influenced by the zone effects, but will clearly be less regular, since different effects may be in opposition. If, for example, an intermediate phase involves a zone overlap, this will make the lattice spacing high, but extrapolation in the direction of lower valency reduces the overlap, and so makes the lattice spacing decrease more rapidly than in the absence of an overlap, and so the resulting extrapolated atomic diameter involves two opposing effects. Irregularities in the lattice spacing-composition curves analogous to those shown in figure 1, may be expected for any phase in which change in composition produces a zone overlap, and it is clear that this effect emphasizes the necessity for detailed investigation if lattice spacing methods are used for the determination of phase-boundaries, since the bend in the curves would be readily overlooked if only a few alloys were examined.

---

* The value 3·07 A for the solid solution in silver, which involves no overlap, is the same as that for the extrapolated value for the *d* distance in the magnesium alloy which involves both the overlapped *a* spacing and the non-overlapped *c* spacing. This implies a contraction of the magnesium-solid solutions relatively to that of silver, and thus is due to the greater electrochemical factor in the magnesium alloys.

† This influence is shown clearly in the $\alpha$-solid solubility relations.

The authors must express their gratitude to Professor C. N. Hinshelwood, F.R.S., for laboratory accommodation, and many other facilities which have greatly assisted the present research. Grateful acknowledgement of financial assistance is made to the Council of the Royal Society, the British Non-Ferrous Metals Research Association, and the Curators of the Leigh Fund of the University of Oxford, and to the Imperial Chemical Industries Ltd., for the loan of apparatus. One of us (G. V. R.) thanks the Department of Scientific and Industrial Research for the award of a Senior Studentship.

## REFERENCES

Goldschmidt, V. M. 1928 *Z. phys. Chem.* **133**, 397.
Hume-Rothery, W., Lewin, G. F. and Reynolds, P. W. 1936 *Proc. Roy. Soc.* A, **157**, 167.
Jones, H. 1934 *Proc. Roy. Soc.* A, **147**, 400.
Mott, N. F. and Jones, H. 1937 *Proc. Roy. Soc.* A, **162**, 49.
Owen, E. A. and Roberts, E. W. 1939 *Phil. Mag.* (vii), **27**, 294.
Raynor, G. V. 1938 *Phil. Mag.* (vii), **26**, 152.
— 1940 *Proc. Roy. Soc.* A, **174**, 457.
Weibke, F. and Hesse, E. 1939 *Z. anorg. Chem.* **240**, 289.

# The characteristics of thermal diffusion

By S. Chapman, F.R.S.
*Imperial College, London*

(*Received* 26 *September* 1940)

When a gas mixture is contained in a vessel in which a steady temperature gradient is maintained, a concentration gradient is in general set up, whose amount is determined by the logarithm of the temperature ratio, and by $k_T$, the thermal diffusion ratio; the general theory of non-uniform gases gives successive approximations to $k_T$, and the first of these, $[k_T]_1$, is accurate within a few per cent. The paper discusses the dependence of $[k_T]_1$ on (*a*) the ratio of the molecular masses; (*b*) their concentration ratio ($c_1$ or $c_2$); (*c*) the two ratios of the molecular diameters, inferred from the coefficient of viscosity, to their joint diameter, inferred from the coefficient of diffusion; and (*d*) three parameters depending on the mode of interaction between the unlike molecules. When this interaction is according to the inverse-power law, the three parameters (*d*) are all expressible in terms of the mutual force index, and $[k_T]_1$ is a function of five independent variables. The general nature of its dependence on these variables is discussed, with particular reference to the end values (for $c_1$ or $c_2$ zero) of the thermal diffusion factor $\alpha$, given by $k_T/c_1c_2$; these end values involve fewer variables (less by two) than the general values, and their functional character can be represented graphically. It is shown that $k_T$ may be zero not only when $c_1$ or $c_2$ is zero, but also for at most one intermediate mixture ratio. Formulae for $[k_T]_1$ appropriate to various special cases are also given.

1. *Introduction.* This paper describes a systematic examination of the characteristics of thermal diffusion, particular aspects of which have been discussed previously by Enskog (1921) and myself (1917*a* and *b*, 1919, 1929), and more recently by Jones and Furry (1940), Brown (1940) and Jones (1940). The underlying theory, due to Enskog (1917, 1921), and myself (1916*a*, 1917*a*), is described also in my recent book with Cowling (1939); references to this book will be indicated by the initials MT. The present discussion has been undertaken because of the increased interest attaching to thermal diffusion since its application by Clusius and Dickel (1939), using a continuously convective method, to the separation of isotopes.

2. *The thermal diffusion coefficient* ($D_T$), *ratio* ($k_T$) *and factor* ($\alpha$). Of the two gases in a mixture, one will be numbered 1 and the other 2. Symbols for quantities relating solely to one or other constituent will be distinguished by the corresponding suffix 1 or 2; those relating jointly to both constituents will be distinguished by the suffixes 12 or 21, or sometimes by the single suffixes 1 or 2.

Let $n_1$, $n_2$ denote the number densities of the two constituents at any point, i.e. the numbers of molecules per unit volume. Their volume fractions or concentrations, $c_1$ and $c_2$, are given by

$$c_1 = n_1/(n_1+n_2), \quad c_2 = n_2/(n_1+n_2), \tag{2·1}$$

so that

$$c_1+c_2 = 1. \tag{2·2}$$

It is convenient to write

$$c = c_1-c_2, \tag{2·3}$$

so that

$$c_1 = \tfrac{1}{2}(1+c), \quad c_2 = \tfrac{1}{2}(1-c); \tag{2·4}$$

as $c_1$ ranges from 0 to 1, or $c_2$ from 1 to 0, $c$ ranges from $-1$ to 1.

Let $\mathbf{C}_1$ and $\mathbf{C}_2$ denote the mean molecular (vector) velocities of the two constituents at any point. In a non-uniform gas their difference $\mathbf{C}_1-\mathbf{C}_2$ is given by the equation of diffusion,

$$c_1c_2(\mathbf{C}_1-\mathbf{C}_2) = -D_{12}\mathbf{d}_{12}-(D_T/T)\,\mathrm{grad}\,T$$

(cf. MT, pp. 144, 244, 140), where, in the absence of external forces, and when the pressure is uniform,

$$\mathbf{d}_{12} = \mathrm{grad}\,c_1;$$

$T$ denotes the absolute temperature, $D_{12}$ the (ordinary) coefficient of diffusion, and $D_T$ the coefficient of thermal diffusion. When a constant temperature gradient is maintained, the gas tends to a steady state of no diffusion, in which there is a constant gradient of concentration given by

$$\mathrm{grad}\,c_1 = -k_T\,\mathrm{grad}\log_e T, \tag{2·5}$$

where $k_T = D_T/D_{12}$; $k_T$ is known as the thermal diffusion *ratio*.

The theory of non-uniform gases leads to successive approximations to such quantities as $D_{12}$, $D_T$, $k_T$ and the viscosity $\mu$; it is convenient to denote the $n$th approximation by the appropriate symbol (e.g. $D_{12}$ or $\mu$) enclosed within square brackets bearing the suffix $n$, i.e. $[\ldots]_n$. This paper is concerned almost wholly with the first approximation to $k_T$, which is correct within a few per cent.

The expression for $k_T$ contains the positive factor $c_1c_2$, and it is convenient to write

$$k_T = c_1c_2\alpha, \tag{2·6}$$

and to call $\alpha$ the thermal diffusion *factor*. If $\alpha$ were independent of the concentration, the graph of $k_T$ as a function of $c_1$ (or $c$) would be a parabola, with its vertex at $c_1 = c_2 = \frac{1}{2}$ or $c = 0$; at this point $k_T$ would have as its maximum value $\frac{1}{4}\alpha$. But in general $\alpha$ is a function of $c$, so that though

$k_T = 0$ at $c_1 = 0$ and $c_1 = 1$ (or $c = \pm 1$), its maximum in general does not occur at $c = 0$; we shall see, in fact, that $k_T$ may be zero also for some intermediate concentration (§16), in which case it will have both a (positive) maximum and a (negative) minimum. In the present paper the discussion relates mainly to $\alpha$, or rather to its first approximation $[\alpha]_1$; we first consider what factors, apart from $c_1$ or $c$, are involved in $[\alpha]_1$.

3. *The molecular mass ratio.* The ratio $k_T$ and the factor $\alpha$ of thermal diffusion involve the molecular masses $m_1$, $m_2$ only as ratios. It is convenient to write

$$M_1 = m_1/(m_1+m_2), \quad M_2 = m_2/(m_1+m_2),$$

$$M = (m \ -m_2)/(m_1+m_2) = M_1 - M_2, \tag{3·1}$$

so that $$M_1 + M_2 = 1, \quad M_1 = \tfrac{1}{2}(1+M), \quad M_2 = \tfrac{1}{2}(1-M). \tag{3·2}$$

The mass dependence of $\alpha$ will be indicated by expressing it as a function of $M$, the *proportionate* mass difference. When $m_1$ and $m_2$ are unequal, it is convenient to number the two gases so that $m_1 > m_2$, and therefore $M_1 > M_2$, or $M > 0$. Hence the range of $M$ to be considered is

$$0 \leqslant M \leqslant 1.$$

The values of $m_1/m_2$ corresponding to some values of $M$ are as follows:

| $M$ = | 0 | 0·1 | 0·2 | 0·3 | 0·4 | 0·5 | 0·6 | 0·7 | 0·8 | 0·9 | 1·0 |
|---|---|---|---|---|---|---|---|---|---|---|---|
| $m_1/m_2$ = | 1 | 1 22 | 1·5 | 1·86 | 2·33 | 3 | 4 | 5·67 | 9 | 19 | ∞ |

4. *The pure and mutual force laws.* The force between two molecules whose centres are at a distance $r$ apart is supposed to be a function of $r$ only, say $\phi_1(r)$, $\phi_2(r)$, or $\phi_{12}(r)$, according as the molecules are both of type 1, or both 2, or unlike (one 1 and one 2). These three functions determine what may be called the pure (1 or 2) and mutual (1, 2) force laws; they enter into the expression for $\alpha$ through the *ratios* of certain positive definite integrals $\omega^{(l)}(r)$, with suffix 1, 2 or 12 according to the type of force law involved. The integrals $\omega$ depend in general on the temperature $T$, but not on the molecular masses; they are related to the integrals $\Omega^{(l)}(r)$ of MT, pp. 157, 152, for the same $l$ and $r$, as follows:

$$\omega_{12} = M_1 M_2 (m_1+m_2)^{\frac{1}{2}} \Omega_{12}, \quad \omega_1 = (\tfrac{1}{2}m_1)^{\frac{1}{2}} \Omega_1, \quad \omega_2 = (\tfrac{1}{2}m_2)^{\frac{1}{2}} \Omega_2. \tag{4·1}$$

In $[\alpha]_1$ five such ratios are involved, namely,

$$A = \frac{\omega_{12}^{(2)}(2)}{5\omega_{12}^{(1)}(1)}, \quad B = \frac{5\omega_{12}^{(1)}(2) - \omega_{12}^{(1)}(3)}{5\omega_{12}^{(1)}(1)}, \quad C = \frac{2\omega_{12}^{(1)}(2)}{5\omega_{12}^{(1)}(1)}, \tag{4·2}$$

which depend only on $T$ and the mutual force law, and

$$x_{12} = \frac{\omega_{12}^{(2)}(2)}{\omega_1^{(2)}(2)}, \quad x_{21} = \frac{\omega_{12}^{(2)}(2)}{\omega_2^{(2)}(2)}, \tag{4·3}$$

each of which involves the mutual and one pure force law; $x_{12}$ and $x_{21}$ occur in the following expressions (MT, p. 253):

$$\frac{M_1 E}{[\mu_1]_1} = \frac{2A}{x_{12}(1-M)^{\frac{1}{2}}}, \quad \frac{M_2 E}{[\mu_2]_1} = \frac{2A}{x_{21}(1+M)^{\frac{1}{2}}}. \tag{4·4}$$

We may also note here the general expressions for $[\mu]_1$ and $[D_{12}]_1$; these involve $\omega$ or $\Omega$ directly, and not merely their ratios (MT, pp. 162, 165, 164):

$$[\mu_1]_1 = \frac{5kT}{8\Omega_1^{(2)}(2)}, \quad [D_{12}]_1 = \frac{3kT}{16(n_1+n_2)(m_1+m_2)M_1M_2\Omega_{12}^{(1)}(1)}. \tag{4·5}$$

Hence we may also express $x_{12}$ and $x_{21}$ in the form

$$\left.\begin{aligned} x_{12} &= \frac{6A[\mu_1]_1}{(1-M)^{\frac{1}{2}}(1+M)(n_1+n_2)(m_1+m_2)[D_{12}]_1}, \\ x_{21} &= \frac{6A[\mu_2]_1}{(1+M)^{\frac{1}{2}}(1-M)(n_1+n_2)(m_1+m_2)M_1M_2[D_{12}]_1}. \end{aligned}\right\} \tag{4·6}$$

For illustration, the values of $A$, $B$, $C$, $x_{12}$ and $x_{21}$ will be cited here for some specially simple force laws.

5. *Rigid elastic spherical molecules.* We first consider the case of molecules which are smooth rigid elastic spheres, of diameters $s_1$, $s_2$. Let

$$s_0 = \tfrac{1}{2}(s_1+s_2). \tag{5·1}$$

Then it is known (MT, p. 170) that

$$A = \tfrac{2}{5}, \quad B = \tfrac{3}{5}, \quad C = \tfrac{6}{5}, \quad 5(C-1) = 1, \tag{5·2}$$

and that

$$[\mu_1]_1 = \frac{5}{16s_1^2}\left(\frac{km_1T}{\pi}\right)^{\frac{1}{2}}, \quad [D_{12}]_1 = \frac{3}{8(n_1+n_2)s_{12}^2}\left(\frac{k(m_1+m_2)T}{2\pi m_1m_2}\right)^{\frac{1}{2}}, \tag{5·3}$$

where $s_{12} = s_0$.

Moreover, writing (in general)

$$\mu_1 = f_1[\mu_1]_1, \quad D_{12} = f_{12}[D_{12}]_1, \tag{5·4}$$

in the present case $f_1 = 1·016$, and $f_{12}$ is a factor which differs from unity by only a few per cent (it depends on $m_1/m_2$, $s_1/s_2$, $c$, and $T$).

By (4·6), (5·3), it follows that in the present case

$$x_{12} = s_0^2/s_1^2, \quad x_{21} = s_0^2/s_2^2. \tag{5·5}$$

6. *The molecular 'diameters'.* If any gas existed whose molecules were rigid elastic spheres, their diameters $s_1$ and $s_2$ could be obtained from experimental measures of $\mu_1$ and $\mu_2$ at any temperature, by means of (5·3). Similarly $s_{12}$ could be determined from experimental measures of $D_{12}$. The values obtained would of course be independent of the temperature at which the measures of $\mu$ and $D$ were made, and it would be found that $s_{12} = s_0$.

In actual gases the molecules are not rigid elastic spheres; the factors $f_1$, $f_2$ and $f_{12}$ in (5·4) must in general be functions of $T$; they will also, in general, be even more nearly equal to unity than in the case of rigid spherical molecules. If the values of these factors are either estimated, or treated as unity (which usually involves only a slight error), it is possible, from experimental measures of $\mu_1$, $\mu_2$ and $D_{12}$, to infer the corresponding values of $[\mu_1]_1$, $[\mu_2]_1$ and $[D_{12}]_1$, and from them, by means of (5·3), to determine quantities $s_1$, $s_2$ and $s_{12}$ which may be called the viscosity diameters and diffusion diameter respectively, or, more briefly, the 'diameters'. These 'diameters' represent certain mean values of the minimum distances between the centres of pairs of like or unlike molecules at collisions; hence, in general they depend on $T$ (decreasing as $T$ increases). Moreover, in general, $s_{12} \neq s_0$.

By means of equations (1), (2), (3), (5) of § 4, and (5·3), it follows that, in general,

$$x_{12} = \frac{5A}{2}\frac{s_{12}^2}{s_1^2}, \quad x_{21} = \frac{5A}{2}\frac{s_{12}^2}{s_2^2}; \tag{6·1}$$

these two equations reduce to (5·5) when the molecules are rigid elastic spheres.

Later we shall find it convenient to write

$$s = (s_1 - s_2)/(s_1 + s_2) = (s_1 - s_2)/2s_0, \tag{6·2}$$

so that

$$s_1/s_0 = 1 + s, \quad s_2/s_0 = 1 - s. \tag{6·3}$$

We also write

$$x = 5As_{12}^2/2s_0^2, \tag{6·4}$$

so that

$$x_{12} = x/(1+s)^2, \quad x_{21} = x/(1-s)^2. \tag{6·5}$$

In the case of rigid spherical molecules, by (5·5), $x = 1$.

7. *The inverse-power force law.* Another specially simple force law, called the inverse-power force law, is defined by

$$\phi(r) = \kappa r^{-\nu}, \tag{7·1}$$

with suffix 1, 2 or 12 added to $\phi$, $\kappa$ and $\nu$; $\kappa$ is called the force constant and $\nu$ the force index. If the pure and mutual force laws are all of this type, we have three force constants and three force indices. Rigid elastic spherical molecules may be considered as a special case of this force law, corresponding to $s = \kappa^{1/\nu}$, as $\nu \to \infty$, because then $\phi(r) = (s/r)^\nu$, which is zero if $r > s$, and $\infty$ if $r < s$, so that the molecules interact only when $r = s$.

In this case, as in § 5, $A$, $B$, $C$, which are as follows (MT, p. 172),

$$A = \frac{3\nu_{12}-5}{5(\nu_{12}-1)}\frac{A_2(\nu_{12})}{A_1(\nu_{12})}, \qquad B = \frac{(3\nu_{12}-5)(\nu_{12}+1)}{5(\nu_{12}-1)^2}, \tag{7·2}$$

$$C = \frac{2(3\nu_{12}-5)}{5(\nu_{12}-1)}, \qquad 5(C-1) = \frac{\nu_{12}-5}{\nu_{12}-1}, \tag{7·3}$$

are independent of $T$.

The viscosity diameters are given in terms of the force constant and index, and of $T$, by

$$s^2 = \tfrac{1}{2}\Gamma\left(4-\frac{2}{\nu-1}\right)A_2(\nu)\left(\frac{\kappa}{2kT}\right)^{2/(\nu-1)}, \tag{7·4}$$

with the suffix 1 or 2 added to $s$, $\nu$ and $\kappa$. The diffusion diameter is given by

$$s_{12}^2 = \Gamma\left(3-\frac{2}{\nu_{12}-1}\right)A_1(\nu_{12})\left(\frac{\kappa_{12}}{2kT}\right)^{2/(\nu_{12}-1)}. \tag{7·5}$$

Hence in this case $$x_{12} \propto T^{\tau_{12}}, \quad x_{21} \propto T^{\tau_{21}}, \tag{7·6}$$

where $$\tau_{12} = \frac{2(\nu_{12}-\nu_1)}{(\nu_{12}-1)(\nu_1-1)}, \quad \tau_{21} = \frac{2(\nu_{12}-\nu_2)}{(\nu_{12}-1)(\nu_2-1)}. \tag{7·7}$$

Thus unless the force indices $\nu_1$, $\nu_2$ and $\nu_{12}$ are all equal, $x_{12}$ and $x_{21}$ vary with $T$; their variation is in opposite senses if $\nu_{12}$ is intermediate between $\nu_1$ and $\nu_2$.

In the special case when $\nu_1 = \nu_2 = \nu_{12}$ ($= \nu$ say), $x_{12}$ and $x_{21}$ are independent of $T$, and are given by

$$x_{12} = (\kappa_{12}/\kappa_1)^{2/(\nu-1)}, \quad x_{21} = (\kappa_{12}/\kappa_2)^{2/(\nu-1)}. \tag{7·8}$$

8. *The numbers $A(\nu)$.* The factors $A_1(\nu)$, $A_2(\nu)$ involved in $A$ and $s$ in § 7 are pure numbers, functions of $\nu$ only; in the theory of non-uniform gases they occur in the form of definite integrals. The case $\nu = 3$ is specially simple, and involves only one numerical integration for each $A$, i.e. $A_1(3)$ and $A_2(3)$; in a former paper (1922) I have given values of $A_1(3)$ and $A_2(3)$ (or rather of $I_1 = 2\pi A_1$ and $I_2 = \pi A_2$), but on recalculating them recently I find that my values there given are in error by several per cent; I regret not having discovered this earlier, since it is only lately that these values have been used or quoted, as by Jones and Furry (1940) and Jones (1940).

My new values, which I have checked by making three separate calculations of them, using three different subdivisions of the range of integration, are*

$$A_1(3) = 0{\cdot}796, \quad A_2(3) = 1{\cdot}056. \tag{8·1}$$

The case $\nu = 2$, which is of importance for highly ionized gases, is also specially simple (MT, p. 177). In other cases, the calculation of $A(\nu)$ involves a series of numerical integrations to determine an auxiliary function $k$, and afterwards another integration for each $A(\nu)$, that is, $A_1$ and $A_2$; a convenient method of calculation, involving transformations of the integrals from their original form, was given in my 1922 paper.† Values of $k$ were given to five decimal places in my paper, for $\nu = 5, 7, 9, 11$ and $15$, and values of $I_1$ and $I_2$ were given to 4 decimal places; but as they were calculated by using Simpson's rule applied to ten intervals only, they may not be correct to more than 3 or 4 significant figures. An examination of the successive differences for my tabulated values of $k$ suggests that, except for $\nu = 5$, they may contain slight errors (this does not apply to the values of $k$ for $\nu = 5$, and the resulting values of $I_1(5)$ and $I_2(5)$ are probably correct at least to 0·1 %). Hassé and Cook (1929) recalculated the values for $\nu = 9$, and found

$$A_1(9) = 0{\cdot}3808, \quad A_2(9) = 0{\cdot}3303, \tag{8·2}$$

instead of my values 0·3820 and 0·3321. My values for $\nu = 7$, 11 and 15 may be in error by similar small amounts, but (except for $\nu = 3$, as indicated above) they are probably amply accurate enough for all practical applications of them.

The values of $A_2(\nu)$ and of $A$, $B$, and certain combinations of $A$ or $B$, or both, for the above values of $\nu$, are as follows:

TABLE 1

| $\nu$ | = | 3 | 5 | 7 | 9 | 11 | 15 | $\infty$ |
|---|---|---|---|---|---|---|---|---|
| $A_2(\nu)$ | = | 1·056 | 0·436 | 0·357 | 0·330 | 0·319 | 0·309 | $\frac{1}{3}$ |
| $A$ | = | 0·531 | 0·517 | 0·493 | 0·477 | 0·465 | 0·450 | $\frac{2}{5}$ |
| $B$ | = | 0·8 | 0·75 | 0·711 | 0·687 | 0·672 | 0·653 | $\frac{3}{5}$ |
| $5-4B$ | = | 1·8 | 2 | 2·156 | 2·25 | 2·312 | 2·388 | 2·6 |
| $H$ | = | 3·012 | 3·033 | 3 026 | 3·017 | 3·008 | 2·997 | 2·950 |
| $1/G$ | = | 0·532 | 0·526 | 0·489 | 0·466 | 0·449 | 0·429 | 0·364 |
| $J$ | = | 1·30 | 1·45 | 1·61 | 1·71 | 1·79 | 1·90 | 2·27 |

---

* R. C. Jones (1940) has recently pointed out that $A_1(\nu)$ and $A_2(\nu)$, for $\nu = 3$ only, *are equal to* $-B_1(\nu)$, $-B_2(\nu)$; *these are certain functions of* $\nu$ *that arise in connexion* with the Lennard-Jones molecular model (cf. MT, p. 186).

† Some misprints in this paper may be noted; in (2·3), after }, insert the index $-\frac{1}{2}$; on p. 2, in $I_2(2)$, for $(1+a_0^2)^{-1}$ read $-a_0^2(1+a_0^2)^{-1}$; on p. 3, line 5, for finite read infinite; for $k$ read $2k$ on p. 4, last line, and on p. 6 (twice); on p. 6 for $\phi$ read $2\phi$; on p. 7, line 5, for 16 read 15, and in (A 1) for $(n-1)/\mu$ read $2/\mu$.

9. *Experimental values of the 'diameters'.* In MT, p. 229, a list of values of $s_1$ is given for a number of simple gases, and on p. 252, a list of values of $s_{12}$ and of $\frac{1}{2}(s_1+s_2)$ for a few gas mixtures; all refer to $T = 0^\circ$ C. On p. 249 values of $\nu_1$, $\nu_2$ and $\nu_{12}$ are given for some gas mixtures; they are derived from the temperature variation of $\mu$ and $D_{12}$. Table 2, illustrating the discussion in §§ 6–8, is derived from these data (some of which are perhaps not very reliable); the gases in each pair are numbered so that $m_1 > m_2$.

We may note that in table 2 the values of $x_{12}$ and $x_{21}$ for two gas mixtures are both greater than unity, and for the other two, they lie on opposite sides of unity.

The values of $\tau$ are all small, showing that in these cases $x_{12}$ and $x_{21}$ do not vary greatly with $T$; for example, the largest value of $\tau$ in table 2, namely, 0·156, would correspond to an increase of $x_{12}$ by $4\frac{1}{2}$ % for a change of $T$ from 0° C to 100° C. It would be of interest to find gas pairs for which $\tau$ has more extreme values.

TABLE 2

|  | $O_2$-$H_2$ | $N_2O$-$CO_2$ | $CO_2$-$H_2$ | $O_2$-$N_2$ |
|---|---|---|---|---|
| $10^8 s_1$ | 3·62 | 4·66 | 4·63 | 3·62 |
| $10^8 s_2$ | 2·73 | 4·63 | 2·73 | 3·76 |
| $10^8 s_{12}$ | 2·94 | 4·30 | 3·30 | 3·45 |
| $\nu_1$ | 7 6 | 6·2 | 5·6 | 7·6 |
| $\nu_2$ | 11·3 | 5·6 | 11·3 | 8·8 |
| $\nu_{12}$ | 8·8 | 4·6 | 9·3 | 7·9 |
| $A$ | 0·478 | 0·520 | 0·475 | 0·486 |
| $x_{12}$ | 0·79 | 1·11 | 0·60 | 1·11 |
| $x_{21}$ | 1·38 | 1·12 | 1·73 | 1·02 |
| $\tau_{12}$ | 0·035 | −0·131 | 0·156 | 0·012 |
| $\tau_{21}$ | −0·074 | −0·084 | −0·084 | −0·035 |
| $M$ | 0·88 | 0·0002 | 0·91 | 0·067 |
| $x$ | 1·03 | 1·05 | 0·95 | 1·06 |
| $s$ | 0·14 | 0·003 | 0·26 | −0·02 |

10. *The general first approximation to $\alpha$.* The formula for $[k_T]_1$ given in MT, p. 253, is equivalent to the following formula for $[\alpha]_1$:

$$[\alpha]_1 = 5(C-1)g, \tag{10·1}$$

where

$$g = \frac{c_1 S_1 - c_2 S_2}{c_1^2 Q_1 + c_1 c_2 Q_{12} + c_2^2 Q_2}. \tag{10·2}$$

(In MT, $c_1$ and $c_2$ are denoted by $n_{10}$ and $n_{20}$, and $n_{12}$, $n_{21}$ denote $c_1/c_2$, $c_2/c_1$.)

The factor $5(C-1)$ occurs in all the approximations to $\alpha$, and therefore in $\alpha$ itself; it is independent of the concentration and the mass ratio, and depends only on the mutual force law and on $T$. When the mutual interaction is according to the inverse-power law, this factor is independent of $T$, and is positive if $\nu_{12} > 5$, negative if $\nu_{12} < 5$, and zero if $\nu_{12} = 5$ (§ 7); hence in the last case thermal diffusion does not occur at all. For other mutual force laws $5(C-1)$ may vanish at some particular temperature, but the inverse fifth-power force law is the only one for which it is always zero.

When the mutual interaction is according to the inverse-power law, the magnitude of $5(C-1)$ decreases from the value 1, when $\nu_{12} = \infty$ (that is, for rigid elastic spherical molecules), to 0 when $\nu_{12} = 5$, and increases again, numerically, to $-1$ when $\nu_{12} = 3$, and further to $-3$ when $\nu_{12} = 2$ (corresponding to ionized molecules and electrons). For most ordinary molecules, in so far as their mutual interaction approximates to the inverse-power law, $\nu_{12}$ lies between $\infty$ and about 4·5.

The complexity of the properties of $[k_T]_1$ or $[\alpha]_1$ depends mainly on the factor $g$; this is therefore the chief subject of the following discussion, which is illustrated by numerical examples referring to the inverse-power law of molecular interaction.

11. *The end and intermediate values of g.* The 'middle' and 'end' values of $g$, namely the value for an equal mixture ($c_1 = c_2 = \frac{1}{2}$, $c = 0$), and the limiting values as the mixture tends to the pure gas 1 ($c_1 = 1$, $c_2 = 0$) or the pure gas 2 ($c_2 = 1$, $c_1 = 0$), will be denoted by $g_0$, $g_1$ and $g_2$ respectively. The end values are given by

$$g_1 = S_1/Q_1; \quad g_2 = -S_2/Q_2. \tag{11·1}$$

The intermediate values can be expressed in terms of these, by substituting in (10·2) the values of $S_1$ and $S_2$ corresponding to (11·1), as follows:

$$g = \frac{c_1 Q_1 g_1 + c_2 Q_2 g_2}{c_1^2 Q_1 + c_1 c_2 Q_{12} + c_2^2 Q_2}. \tag{11·2}$$

This expression for $g$ is discussed in § 17.

12. *The factors S and Q.* Since we are concerned only with ratios of the factors $S$ and $Q$, the value of $g$ is unaltered if we multiply $S$ and $Q$ by any constant, the same for all: it is convenient to multiply the values given in MT (p. 253) by the factor $(1-M^2)^{\frac{1}{2}}/2A$; we thus obtain the following expressions:

$$\left.\begin{aligned} S_1 &= (1/2x_{12})(1+M)^{\frac{3}{2}}\{1-x_{12}S(M)\},\\ S_2 &= (1/2x_{21})(1-M)^{\frac{3}{2}}\{1-x_{21}S(-M)\},\end{aligned}\right\} \tag{12·1}$$

where $$S(M) = (1-M)^{\frac{3}{2}}(1-GM)/(1+M) \tag{12·2}$$

and $$G = 3/2A - 1 > 0; \tag{12·3}$$

also $$Q_1 = (1+M)^{\frac{1}{2}} q_1/x_{12}, \quad Q_2 = (1-M)^{\frac{1}{2}} q_2/x_{21}, \tag{12·4}$$

$$Q_{12} = 4A/x_{12}x_{21}+q_{12}, \tag{12·5}$$

where $q_1$, $q_2$, $q_{12}$ are functions of $M$, $A$ and $B$ given by

$$q_1 = 6M_2^2+(5-4B)\,M_1^2+8AM_1M_2 = H-(\tfrac{1}{2}+2B)\,M+(H-4A)\,M^2, \tag{12·6}$$

$$q_2 = 6M_1^2+(5-4B)\,M_2^2+8AM_1M_2 = H+(\tfrac{1}{2}+2B)\,M+(H-4A)\,M^2, \tag{12·7}$$

$$q_{12} = \tfrac{1}{2}(11-4B)\,\{JM^2(1-M^2)^{\frac{1}{2}}+(1-M^2)^{\frac{3}{2}}\}, \tag{12·8}$$

$$H = \tfrac{11}{4}-B+2A, \quad J = 3(5-4B)/A(11-4B). \tag{12·9}$$

In table 1 the values of $1/G$, $H$, $J$ and of $5-4B$ are given for various values of $\nu_{12}$.

13. *The functions $q_1$, $q_2$, $q_{12}$ and $S$.* If $5-4B>0$, $q_1$, $q_2$ and $q_{12}$ are positive for all relevant values of $M$; this condition is probably fulfilled for all physically suitable molecular models, and certainly is satisfied for the inverse-power mutual force law (cf. table 1). The function $q_2$ of $M$ is the same as the function $q_1$ with the variable $M$ replaced by $-M$.

When $M=0$, $q_1=q_2=H$, which would seem to be nearly independent of the mutual force law; at least it is nearly equal to 3 for all values of $\nu_{12}$ (table 1). When $M=1$ (or $M_1=1$, $M_2=0$), $q_1=5-4B$, $q_2=6$. Also

$$\frac{dq_1}{dM} = -(\tfrac{1}{2}+2B)+2(H-4A)\,M, \quad \frac{dq_2}{dM} = (\tfrac{1}{2}+2B)+2(H-4A)\,M,$$

so that $dq_2/dM$ is always positive, and $q_2$ steadily increases from $H$ to 6 as $M$ increases from 0 to 1.

The sign of $dq_1/dM$ is negative if $M<(\frac{1}{2}+2B)/2(H-4A)$; this upper limit exceeds 1 for $\nu_{12}=3$ (or 5), but for $\nu_{12}>7$ it is less than 1; in this case $q_1$ decreases from $H$ at $M=0$, to a minimum at $M=(\frac{1}{2}+2B)/2(H-4A)$, and then increases to $5-4B$ at $M=1$; otherwise it decreases steadily from $H$ to $5-4B$. The latter, its end value, depends considerably on $\nu_{12}$, being 2·6 for $\nu_{12}=\infty$, and 1·8 for $\nu_{12}=3$.

When $M=0$, $q_{12}=\frac{11}{2}-2B$; when $M=1$, $q_{12}=0$; at $M=0$, $dq_{12}/dM=0$; at $M=1$, $dq_{12}/dM=-\infty$; also $dq_{12}/dM=0$ at $M=M'$, where

$$M'^2 = (2J-3)/3(J-1),$$

provided that this value of $M'$ lies between 0 and 1, which is the case, for the inverse-power force law, if $\nu_{12}>6$; in this case $q_{12}$ increases from $M=0$ to $M'$, where it has a maximum value $(11-4B)\,J^{\frac{3}{2}}/3^{\frac{3}{2}}(J-1)^{\frac{1}{2}}$, from which it decreases steadily to 0 at $M=1$; if $J<1·5$, $q_{12}$ decreases steadily from its initial value $\frac{11}{2}-2B$ to 0 at $M=1$.

The functions $S(M)$ and $S(-M)$, for $0 < M < 1$, can be discussed by considering $S(M)$ for $-1 < M < 1$. The factor $1-GM$ steadily decreases from $1+G$ to $1-G$, as $M$ increases from $-1$ to $1$, and it changes sign from positive to negative values at $M = 1/G$. The remaining factor in $S$ steadily decreases from $\infty$ at $M = -1$ to $0$ at $M = 1$. Hence from $M = -1$ to $M = 1/G$, $S$ steadily decreases from $\infty$ to $0$, and it is negative from $M = 1/G$ to $M = 1$; it has a negative minimum within this range, and increases to $0$ at $M = 1$, where $dS/dM = 0$. This is illustrated by the following table, for $\nu_{12} = \infty$, $G = \frac{11}{4}$.

VALUES OF $S(M)$ AND $S(-M)$ FOR $\nu_{12} = \infty$, $G = \frac{11}{4}$

| | | | | | | | |
|---|---|---|---|---|---|---|---|
| $M$ | = | 0 | 0·2 | 0·4 | 0·6 | 0·8 | 1·0 |
| $S(M)$ | = | 1 | 0·269 | −0·033 | −0·103 | −0·060 | 0 |
| $S(-M)$ | = | 1 | 2·55 | 5·79 | 13·4 | 38·7 | $\infty$ |

14. *The parameters of $g$.* From (10·2) and § 12 it is clear that $g$ involves six parameters (in general independent), namely, $c$, $M$, the numbers $A$ and $B$ depending on the mutual force law, and the ratios $x_{12}$ and $x_{21}$ depending on the pure and mutual force laws. When the mutual force law is of the inverse-power type, the parameters are reduced to five, because $A$ and $B$ are known functions of the single parameter $\nu_{12}$.

The end-values of $g$ depend only on four parameters (or 3 when the mutual force law is of the inverse-power type), namely $A$, $B$, $M$ and either $x_{12}$ or $x_{21}$ (not both). We therefore first consider the characteristics of $g_1$ and $g_2$.

15. *The end values, $g_1$ and $g_2$.* By (11·1) and § 12,

$$g_1 = \frac{1+M}{2q_1}\{1-x_{12}\,S(M)\}, \quad g_2 = \frac{1-M}{2q_2}\{x_{21}\,S(-M)-1\}. \qquad (15{\cdot}1)$$

In these expressions the first factor involves $M$ (and $A$ and $B$) only, the second involves $M$ and $x_{12}$ or $x_{21}$.

It is convenient to represent the dependence of $g_1$ and $g_2$ on $M$ and $x_{12}$ or $x_{21}$ by means of a contour system of lines of constant $g_1$ or $g_2$, on a diagram whose abscissae are $M$ and whose ordinates are $x_{12}$ or $x_{21}$; since $-g_2$ is the same function of $-M$ and $x_{21}$ as $g_1$ is of $M$ and $x_{12}$, this can conveniently be done on a single diagram, as in figure 1, in which the right half (figure 1 *a*) refers to $g_1$, and the left half (figure 1 *b*) to $g_2$; the abscissae $M$ are measured outwards from the centre of the lower boundary, to right and to left. In the right half the ordinates represent $x_{12}$, in the left, $x_{21}$. The contour lines for $g_1$ and $g_2$ are continuous across the centre line which separates the $g_1$ and $g_2$

regions, but the sign of the contour value is reversed on crossing this line. Any point on the right half of figure 1 may be called a $g_1$ point, and any point on the left, a $g_2$ point. For convenience the scale of ordinates from 1 upwards is contracted, the distance from the $M$ axis to the scale point with ordinate $x$ being $2-1/x$.

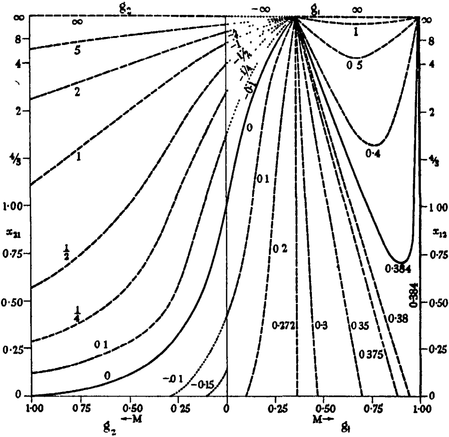

FIGURE 1. Contour lines of $g_1$ (right) and $g_2$ (left), as functions of $M$ and $x_{12}$ or $x_{21}$; the scale of ordinates is contracted from $x = 1$ upwards. The contours refer to a gas mixture composed of rigid spherical molecules ($\nu_{12} = \infty$).

The graph of $1/S(M)$ on the right, and $1/S(-M)$ on the left, is drawn as a full line, marked 0; its parts to the right and left of the centre line are the zero contours of $g_1$ and $g_2$, because along them $x_{12}S(M)$ and $x_{21}S(-M)$ are unity.

Let $P_1$ or $P_2$ denote any $g_1$ or $g_2$ point on figure 1, and let $P'_1$ or $P'_2$ denote the point at which the ordinate $NP_1$ or $NP_2$, extended upwards or downwards if necessary, meets the graph of $1/S(M)$ or $1/S(-M)$—including, in the $g_1$ diagram, the negative part (not shown) of the $1/S(M)$ graph. Then the second factor in the expression (15·1) for $g_1$ is equal to $1-NP_1/NP'_1$ or $P_1P'_1/NP'_1$, reckoning distances positive if upward; similarly the second factor in $g_2$ is represented by $NP_2/NP'_2-1$ or $P'_2P_2/NP'_2$. Since in each case the first factor in (15·1) is positive, $g_1$ is positive at points below and to the right of the $1/S(M)$ graph, and negative above and to the left; and $g_2$ is positive above and to the left of the $1/S(-M)$ graph, and negative below and to the right. The contour lines in the regions of negative $g_1$ or $g_2$ are drawn dotted, the others (except $g=0$ and one other $g_1$ line) are drawn as broken lines.

The first factor of $g_1$ is $(1+M)/2q_1$; for all values of $\nu_{12}$ ($>3$) it increases steadily with $M$, from $1/2H$ at $M=0$ to $1/(5-4B)$ at $M=1$, at which point its gradient is still positive. Along the right-hand lower boundary ($x_{12}=0$) of figure 1 *a*, this factor equals $g_1$, since the second factor is 1. For any other value of $x_{12}$, the second factor has a positive gradient ($=-x_{12}dS/dM$) with respect to $M$, up to the value of $M$ for which $S$ has its minimum (§ 13); at this point $1-x_{12}S$ has a maximum, and from this point it decreases to 1 at $M=1$, where its gradient with respect to $M$ is zero. Hence the variation of $g_1$ with $M$, for any sufficiently large value of $x_{12}$, must consist of a rise to a maximum, governed mainly by the second factor, and then a decline to a minimum and a subsequent increase to $M=1$ (because at $M=1$ the gradient with respect to $M$ depends only on the first factor, and is positive). For sufficiently small values of $x_{12}$, $g_1$ has neither the maximum nor the minimum, but steadily increases with $M$.

The $g_1$ contour system, as drawn with a contracted $x_{12}$ scale in figure 1 *a*, has two singular points on its upper boundary $x_{12}=\infty$, namely at $M=1/G$ and at $M=1$. The line $M=1/G$ is a $g_1$ contour line, because $S(1/G)=0$ (for $\nu_{12}=\infty$ the value of $g_1$ when $M=1/G$ is 0·272); this line meets the zero contour of $g_1$, namely the graph of $1/S(M)$, at $M=1/G$, $x_{12}=\infty$, which is therefore a singular point; $g_1$ takes all limiting values from $-\infty$ to $\infty$ as this point is approached from different directions; the line $x_{12}=\infty$ is the contour $g_1=-\infty$ from $M=0$ to $M=1/G$, and the contour $g_1=\infty$ from $M=1/G$ to $M=1$. The line $M=1$ in figure 1 *a* is part of the contour $g_1=1(5-4B)$ ($=0·384$ if $\nu_{12}=\infty$), since along this line $S(M)=0$ and

$$(1+M)/2q_1=1/(5-4B);$$

$g_1$ also takes the value $1/(5-4B)$ along a line joining the two points $M=1/G$ and $M=1$ on the line $x_{12}=\infty$ (this special contour is drawn as a full line).

Hence $M = 1$, $x_{12} = \infty$ is also a singular point. As this point is approached from the left, and from above the two-branched contour ($g_1 = 1/(5-4B)$), $g_1$ tends to values which range from $1/(5-4B)$ to $\infty$. If, however, the $x_{12}$ scale for $x_{12} > 1$ were not contracted, the contours which in figure 1 *a* are shown as meeting at the two singular points would be shown as asymptotically approaching the rectilinear contours $M = 1/G$ and $M = 1$.

The second factor in $g_2$ steadily increases from $x_{12} - 1$ at $M = 0$ to $\infty$ at $M = 1$; when $x_{21} = 0$ it is $-1$. The first factor decreases steadily from $1/2H$ at $M = 0$ to zero at $M = 1$. At $M = 1$ the product of the two factors is $2^{\frac{1}{2}}x_{21}/4A$, which increases steadily with $x_{21}$ from 0 to $\infty$. For $x_{21} < 1$, $g_2$ changes sign from negative to positive as $M$ increases from 0 to 1; for $x_{21} > 1$, it is always positive.

For any given mixture the values of $M$, $x_{12}$ and $x_{21}$ determine a point on each of the two contour diagrams for $g_1$ and $g_2$, drawn for the values of $A$ and $B$ appropriate to the mutual force law for the mixture. There may be some limitation, inherent in the constitution of actual gases, on the regions within which the $g_1$ and $g_2$ points on figures 1 *a*, *b* can lie; for example, if the molecules are rigid elastic spheres, the relation $s_{12} = \frac{1}{2}(s_1 + s_2)$ implies that $1/\sqrt{x_{12}} + 1/\sqrt{x_{21}} = 2$, so that when $x_{12}$ is given, $x_{21}$ is also known. Apart from any such relation, the only restriction on the $g_1$ and $g_2$ points is that they have the same abscissa $M$; hence it appears from figures 1 *a*, *b* that if $M < 1/G$, $g_1$ and $g_2$ may each be either positive, negative or zero; for $M > 1/G$, $g_1$ is positive, and $g_2$ may be positive, negative or zero. Hence, whatever the value of $M$, $g_1$ and $g_2$ may have the same or opposite signs; if $M < 1/G$, either or both may be zero; if $M > 1/G$, $g_2$ alone can be zero.

The points at which both $g_1$ and $g_2$ are zero form a linear sequence in a three-dimensional space in which the co-ordinates are $M$, $x_{12}$ and $x_{21}$; for each value of $M$ from 0 to $1/G$ there is one point at which $g_1 = g_2 = 0$, viz. the point whose $x_{12}$ and $x_{21}$ co-ordinates are given by the $1/S$ graphs in figures 1 *a*, *b*.

When the positions of the $g_1$ and $g_2$ points are restricted by some relation such as that for rigid elastic spherical molecules, these possibilities are diminished; for example, for such molecules only for one particular value of $M$ (which lies between 0 and $1/G$) is it possible for both $g_1$ and $g_2$ to be zero.

16. *Zero values of g*. If both $g_1$ and $g_2$ are zero, then by (11·2) $g$ is zero for all values of $C$; thus $[\alpha]_1$ can vanish for all values of $c$, not only through the vanishing of the factor $C-1$ in (10·1), but also through the vanishing of $g$. But the vanishing of $g$ for a given gas mixture will in general occur, if at all, only at a particular temperature, whereas $C-1$ vanishes whatever the

temperature, if the mutual force law is the inverse fifth-power law. Moreover, $C-1$ is a factor of $\alpha$ itself, and not merely of $[\alpha]_1$; if $g$ vanishes for all values of $c$, $\alpha$ is likely to be very small, but it will not vanish exactly.

If $g_1$ and $g_2$ have opposite signs, $g$ must vanish for some intermediate value of $c$; and $\alpha$ itself, and $k_T$, will in general vanish for this or some adjacent concentration-ratio. This may occur for $g_1$ negative and $g_2$ positive (case (i)) or vice versa (case (ii)). Case (i) can occur only if $M < 1/G$ and $x_{12} > 1$, and the greater the value of $M$ within this range, the larger must $x_{12}$ be for $g_1$ to be negative; $g_2$ will be positive provided that $x_{21}$ is not too small, i.e. it must correspond to points above the zero contour in figure 1 *b*. Case (ii) can occur for any value of $M$, and imposes no restriction on $x_{12}$ if $M > 1/G$, though for $M < 1/G$, $x_{12}$ must not be too large, as it must be below the zero contour in figure 1 *a*; $x_{21}$ must be less than or equal to a limit ($<1$) which decreases the larger the value of $M$.

The value of $c$ at which $g$ or $[\alpha]_1$ is zero may lie anywhere between $-1$ and 1; for example either of the end values, $g_1$ or $g_2$, may be zero, and the other not zero; if $g = 0$ for an intermediate value of $c$, the signs of $g_1$ and $g_2$ must be opposite, because $g$ cannot vanish for more than one value of $c$: this appears from (10·2), in which the denominator is positive, so that $g = 0$ only for the one value of $c$ given by $c_1/c_2 = S_2/S_1$.

Hence the graph of $k_T$ as a function of $c$ may take any of the forms shown in figure 2.

17. *The variation of* $[\alpha]_1$ *or* $g$ *with the concentration ratio.* When $A$ and $B$ are known, $g_1$ and $g_2$ are each functions of two variables only, whereas $g$ is a function of four variables, $M$, $x_{12}$, $x_{21}$ and $c$. It is not possible to give a simple graphical representation, such as was used for $g_1$ and $g_2$, of the dependence of $g$ on its independent variables, as this would require a 4-dimensional space. The discussion of $g$ will therefore centre mainly on the mode of variation of $g$ between its end values $g_1$ and $g_2$, which are determined, as has been seen in § 15, by $M$, $x_{12}$ and $x_{21}$; this variation will be supposed represented by a graph of $g$ as a function of $c$ from $c = -1$ ($c_1 = 0$, $c_2 = 1$) to $c = 1$ ($c_1 = 1$, $c_2 = 0$).

17*a*. The simplest variation of $g$ with $c$ corresponds to a rectilinear graph of $g$, or to $g = g_c$, where

$$g_c \equiv c_1 g_1 + c_2 g_2. \tag{17·1}$$

It is easy to show that the general equation (11·2) is equivalent to

$$g = g_c + c_1 c_2 g'/(c_1^2 Q_1 + c_1 c_2 Q_{12} + c_2^2 Q_2), \tag{17·2}$$

where

$$g' = (g_1 - g_2)(Q_1 - Q_2) + g_c(Q_1 - Q_{12} + Q_2). \tag{17·3}$$

Hence (17·1) corresponds to $g' = 0$. The first term in $g'$ is independent of $c$, the second is proportional to $g_c$; hence for $g$ to equal $g_c$ for all values of $c$, it is necessary that $Q_1 - Q_{12} + Q_2 = 0$ and either $g_1 - g_2 = 0$ or $Q_1 - Q_2 = 0$. The two latter equations are linear in $x_{12}$ and $x_{21}$, and may be regarded as defining ruled surfaces $S$ or $S'$ in a space whose coordinates are $M$, $x_{12}$ and $x_{21}$, the sections by planes $M =$ constant being straight lines, as shown in figure 3 for $M = 0, \frac{1}{2}, 1$. The equation $Q_1 - Q_{12} + Q_2 = 0$ is the equation of a surface $S''$ whose sections by the planes $M =$ constant are rectangular hyperbolae with their asymptotes parallel to the $x_{12}$ and $x_{21}$ axes, as shown in figure 3 for $M = 0, \frac{1}{2}, 1$. The sections of $S$ and $S''$ by the plane $M = 0$ have only one common point ($x_{12} = x_{21} = 1$, at which, however, $g_1 = g_2 = g = 0$); those by $M = \frac{1}{2}$ do not intersect (at least when $\nu_{12} = \infty$); those by $M = 1$ coincide, in the line $x_{21} = 4A/(5-4B)\sqrt{2}$, for which $g_1 = g_2 = g = 1/(5-4B)$.

FIGURE 2. Different forms of the graph of $k_T$ as a function of the concentration ratio.

In each plane $M =$ constant the surface $S''$ cuts the surface $S'$ in one point only. Hence the values of $M$, $x_{12}$ and $x_{21}$ corresponding to $g' = 0$, $g = g_c$, but for which $g_1 \neq g_2$, form a linear sequence in the $M$, $x_{12}$, $x_{21}$ space; as $M \to 1$, $x_{21} \to 4A/(5-4B)\sqrt{2}$, $x_{12} \to \infty$, and $g_1 - g_2 \to 0$ along this sequence.

17*b*. A less special case is that in which only $Q_1 - Q_{12} + Q_2 = 0$, corresponding to the doubly infinite set of $M$, $x_{12}$, $x_{21}$ points on the surface $S''$. In this case

$$g = \frac{c_1 Q_1 g_1 + c_2 Q_2 g_2}{c_1 Q_1 + c_2 Q_2}, \tag{17·4}$$

since, by (2·2),

$$c_1^2 Q_1 + c_1 c_2 Q_{12} + c_2^2 Q_2 = c_1 Q_1 + c_2 Q_2 - c_1 c_2 (Q_1 - Q_{12} + Q_2). \tag{17·5}$$

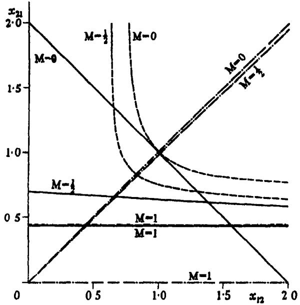

FIGURE 3. Sections of the surfaces $S$ (or $g_1 - g_2 = 0$; shown by full lines ——), $S'$ ($Q_1 - Q_2 = 0$; shown by chain lines —·—·), and $S''$ ($Q_1 - Q_{12} + Q_2 = 0$; shown by broken lines ------), by planes $M$ = constant.

In this case $g$ always lies between $g_1$ and $g_2$, because (17·4) implies that $g$ is the value of $g_c$ at that point on the straight line $g = g_c$, which divides this line in the ratio $c_2 Q_2 : c_1 Q_1$; since $Q_1$ and $Q_2$ are positive, this point is intermediate between the two ends.

In the present case, $g' = \frac{1}{2}(g_1 - g_2)(Q_1 - Q_2)$, and may be positive or negative, implying that the graph of $g$ may be either concave or convex as viewed from below. The parts of the surface $S''$ which correspond to the two alternatives can be inferred from figure 3; for in figure 3, for any value of $M$, $g_1 > g_2$ in the $x_{12}$, $x_{21}$ region *above* the line $g_1 = g_2$ for that value of $M$, $Q_1 > Q_2$ in the $x_{12}$, $x_{21}$ region *above* the line $Q_1 = Q_2$. Hence these two lines divide the $x_{12}$, $x_{21}$ plane, for that value of $M$, into four regions; $g' > 0$ in the upper and lower ones, and $g' < 0$ in the right and left-hand regions ($M = 1$ is a special case; the $x_{12}$, $x_{21}$ plane is divided into two regions only; $g' > 0$ in the upper, and $g' < 0$ in the lower region). The $S''$ section by the plane $M =$ constant may fall wholly in one region, as in the special case $M = 1$, for which (when $Q_1 - Q_{12} + Q_2 = 0$) $g' < 0$ for all values of $x_{12}$, and the $g$ curve is convex as viewed from below (cf. § 18); but it may fall partly in the region of $g' > 0$, and partly in the region $g' < 0$, as for example in the case $M = 0$, for which $g' > 0$ if $x_{21} > 1$, and $g' < 0$ if $x_{21} < 1$.

17*c*. In the two special cases thus far considered, $g'$ is either zero, or of one sign only, for all values of $c$; it is possible, however, for $g'$ to become zero and change sign for some value of $c$. This can occur for at most one value of $c$, because, by (17·2) and (17·3), $g'$ is a linear function of $c$, namely

$$g' = (g_1 - g_2)(Q_1 - Q_2) + \tfrac{1}{2}(g_1 + g_2)(Q_1 - Q_{12} + Q_2) + \tfrac{1}{2}c(g_1 - g_2)(Q_1 - Q_{12} + Q_2). \tag{17·6}$$

Hence, unless either $g_1 = g_2$ or $Q_1 - Q_{12} + Q_2 = 0$ (or both), the graph of $g'$ must cut the $c$ axis; it does so at the value of $c$ given by

$$c = -\frac{g_1 + g_2}{g_1 - g_2} - \frac{2(Q_1 - Q_2)}{Q_1 - Q_{12} + Q_2}. \tag{17·7}$$

This value is relevant to our discussion only if it lies between ± 1. The circumstances in which this condition is satisfied will not be discussed here; it will suffice to show that such solutions exist, by considering a simple special case. If $M = 0$, the solution of (17·7) is $c = 0$ for points lying on the line $x_{12} = x_{21}$, because along this line both $g_1 + g_2 = 0$ and $Q_1 - Q_2 = 0$ (the point $x_{12} = x_{21} = 1$, at which also $g_1 - g_2 = 0$, and $g = g_1 = g_2 = 0$, must be excepted).

17*d*. When the graph of $g$ crosses the straight line $g = g_c$, which it meets also at $c = \pm 1$, it must have a point of inflexion within this range. It may also have two stationary values, one a maximum and one a minimum; it cannot have more than two, because the condition $dg/dc = 0$ gives a quadratic equation in $c$; either or both of the roots of this equation may be outside the relevant range of $c$, $-1$ to $1$. These possibilities will not be discussed here in detail, but it may be noted that if $Q_1 - Q_{12} + Q_2 = 0$, both the roots are at infinity ($\pm\infty$). The equation $dg/dc = 0$ is that of a surface in the four dimensional space of the variables $M$, $x_{12}$, $x_{21}$ and $c$, which has a section by each plane $c =$ constant, this section being a three-dimensional surface in the space of $M$, $x_{12}$, $x_{21}$. These sectional surfaces certainly have some real portions in the range $0 < M < 1$, $x_{12} > 0$, $x_{21} > 0$; this is evident from consideration of the cases when $g_1 = g_2$, for except when $g' = 0$, the graph of $g$ must then necessarily have either a maximum or a minimum, and if the graph crosses the line $g = g_0$ ($= g_1 = g_2$ in this case) it will have both a maximum and a minimum. This simple example also illustrates the fact that the range of $g$ may exceed $g_1 \sim g_2$ (in this case $g_1 \sim g_2 = 0$, but the statement also has a range of validity when $g_1 \sim g_2 \neq 0$).

18. *Formulae for $g$ when $M = 1$.* We proceed to consider some formulae for $g$, or some numerical illustrations of $g$, in a few interesting special cases.

When $M \to 1$ (or $m_1/m_2 \to \infty$)

$$g \to \frac{1}{(5-4B)\,c_1 + 2A(c_2/x_{21})\sqrt{2}},$$

so that

$$g_1 \to \frac{1}{5-4B}, \quad g_2 \to \frac{x_{21}}{2A\sqrt{2}},$$

and the 'middle' value of $g$, for $c = 0$ or $c_1 = c_2 = \frac{1}{2}$, is given by

$$g_0 \to \frac{1}{\frac{5}{2} - 2B + (A/x_{21})\sqrt{2}}.$$

These formulae are readily established if, as $M \to 1$ or $M_2 \to 0$, $x_{12}$ and $x_{21}$ remain finite; with slightly more difficulty they may be proved even if $x_{12}$ or $x_{21}$ (or both) tends to zero or $\infty$ as $M_2 \to 0$.

Hence in the present special case $1/g$ is a positive linear function of $c$, and $g_0$ is the harmonic mean of $g_1$ and $g_2$; hence also the graph of $g$ as a function of $c$ is convex as viewed from below (that is, $g'$ is negative).

19. *Isotopic molecules of nearly equal mass.* When the pure and mutual force laws are identical, the two gas constituents will be called isotopic, whether or not they are of the same chemical constitution or of nearly the same mass. This condition is probably satisfied within narrow limits when the molecules are isotopic in the ordinary sense, being chemically identical but differing in that one or more atoms in them appear in different isotopic forms. Some gas mixtures of different chemical composition (e.g. $CO_2$ and $N_2O$, and $CO$ and $N_2$; cf. MT, p. 249) also appear to be approximately isotopic, or at least their pure force laws are nearly identical. The value of $M$ in isotopic mixtures is usually small, though not always (e.g. $H_2$ and $D_2$).

In isotopic mixtures there is no distinction between $\omega_1$, $\omega_2$ and $\omega_{12}$, for the same values of $l$ and $r$, so that, by (4·3),

$$x_{12} = 1, \quad x_{21} = 1. \tag{19·1}$$

In this case, if also $M$ is small, the formula for $g$ may be put in the approximate form (correct as far as the second power if $g$ is expanded in powers of $M$)

$$g = g_0(1-\gamma Mc), \tag{19·2}$$

where $g_0$ is the middle value of $g$ (for $c = 0$), and

$$g_0 = \frac{3(1+1/A)}{4H}M, \tag{19·3}$$

$$\gamma = \frac{3(1-\frac{1}{4}A)}{2(1+A)} - \frac{1+4B}{2H}. \tag{19·4}$$

Table 3 gives the values of $g_0/M$ and $\gamma$ for several values of $\nu_{12}$, when the mutual force law is of the inverse-power type. The last value of $g_0/M$, for $\nu_{12} = \infty$, corresponds to rigid elastic spheres, and is equal to 105/118.

TABLE 3. ISOTOPIC MOLECULES OF NEARLY EQUAL MASS

| $\nu$ | = | 3 | 5 | 7 | 9 | 11 | 15 | $\infty$ |
|---|---|---|---|---|---|---|---|---|
| $g_0/M$ | = | 0·718 | 0·726 | 0·750 | 0·768 | 0·785 | 0·806 | 0·890 |
| $\gamma$ | = | 0·025 | 0·074 | 0·120 | 0·152 | 0·171 | 0·199 | 0·281 |

A formula equivalent to (19·3) has been given by Jones and Furry (1940), together with a series of values of $(118/105)\,g_0/M$ (which is equal to 1 when $\nu_{12} = \infty$); allowing for the additional factor 118/105, their values correspond to those of $g_0/M$ in table 3, except for the correction to my earlier values of $A_1(3)$ and $A_2(3)$ (§ 8).

The approximate formula for $g_0/M$ given by (19·3–4) is of particular interest in that it enables $g$, $\alpha$ or $k_T$ to be estimated for any isotopic mixture of small mass difference $M$, when $\nu$ is known from the temperature variation of the viscosity of the gas; hence the following empirical approximate formula for $g_0/M$, appropriate for values of $\nu$ intermediate between those of table 3, may prove convenient:

$$g_0/M = 0·890 - 1·5/\nu + 4/\nu^2 - 3·15/\nu^3. \tag{19·5}$$

The variation of $g$ with the concentration ratio, when $M$ is small, is proportional to $M$ and to $c$; since $\gamma$ is positive, $g$ is greatest ($g_2$) when the lighter molecules predominate: $\gamma$ increases largely with $\nu$, the value for $\nu = \infty$ being more than 11 times as great as for $\nu = 3$. When $\nu = \infty$ and $M = \frac{1}{10}$, the whole change in $g$, from $c = -1$, to $c = 1$, is 5·6 % of $g_0$.

20. *The isotopic case when $M$ is not small.* When $m_1/m_2$ is neither nearly 1 nor very large, so that $M$ is neither 0 nor 1, $g$ must be calculated from the

general formula, subject to $x_{12} = x_{21} = 1$. Tables 4, 5 and 6 illustrate the dependence of $g_1$, $g_0$ and $g_2$ on $\nu$ and $M$ for isotopic mixtures.

These tables show that when $M$ is small $g$ does not vary much with $c$ (as is evident from (19·2)), nor with $\nu$; as $M$ rises towards 1, the variation with $\nu$ becomes greater, in opposite senses for $g_1$ and $g_2$. Up to about $M = \frac{1}{2}$

TABLE 4. VALUES OF $100g_1$ FOR ISOTOPIC MOLECULES
($x_{12} = x_{21} = x = 1$, $s = 0$)

| $\nu_{12} =$ | 3 | 5 | 7 | 9 | 11 | 15 | $\infty$ |
|---|---|---|---|---|---|---|---|
| $M = 0·1$ | 7 | 7 | 7 | 8 | 8 | 8 | 9 |
| 0·2 | 14 | 14 | 14 | 15 | 15 | 15 | 16 |
| 0·3 | 21 | 21 | 21 | 21 | 22 | 22 | 23 |
| 0·4 | 28 | 27 | 27 | 27 | 28 | 28 | 29 |
| 0·5 | 34 | 33 | 32 | 32 | 32 | 32 | 34 |
| 0·6 | 39 | 38 | 37 | 36 | 36 | 36 | 37 |
| 0·7 | 44 | 42 | 40 | 40 | 39 | 39 | 38 |
| 0·8 | 48 | 45 | 43 | 42 | 41 | 40 | 39 |
| 0·9 | 52 | 48 | 45 | 43 | 42 | 41 | 39 |
| 1·0 | 56 | 50 | 46 | 44 | 43 | 42 | 38 |

TABLE 5. VALUES OF $100g_0$ FOR ISOTOPIC MOLECULES
($x_{12} = x_{21} = 1$ or $x = 1$, $s = 0$)

| $\nu_{12} =$ | 3 | 5 | 7 | 9 | 11 | 15 | $\infty$ |
|---|---|---|---|---|---|---|---|
| $M = 0·1$ | 7 | 7 | 8 | 8 | 8 | 8 | 9 |
| 0·2 | 14 | 14 | 15 | 15 | 15 | 16 | 17 |
| 0·3 | 21 | 21 | 22 | 22 | 23 | 23 | 25 |
| 0·4 | 28 | 28 | 28 | 29 | 29 | 30 | 32 |
| 0·5 | 34 | 34 | 35 | 35 | 35 | 36 | 38 |
| 0·6 | 40 | 40 | 40 | 40 | 41 | 41 | 43 |
| 0·7 | 46 | 45 | 45 | 45 | 45 | 46 | 47 |
| 0·8 | 51 | 50 | 49 | 49 | 49 | 49 | 50 |
| 0·9 | 56 | 54 | 53 | 53 | 52 | 52 | 52 |
| 1·0 | 61 | 58 | 56 | 56 | 55 | 55 | 54 |

TABLE 6. VALUES OF $100g_2$ FOR ISOTOPIC MOLECULES
($x_{12} = x_{21} = x = 1$, $s = 0$)

| $\nu_{12} =$ | 3 | 5 | 7 | 9 | 11 | 15 | $\infty$ |
|---|---|---|---|---|---|---|---|
| $M = 0·1$ | 7 | 7 | 8 | 8 | 8 | 8 | 9 |
| 0·2 | 14 | 15 | 15 | 16 | 16 | 16 | 18 |
| 0·3 | 21 | 22 | 23 | 24 | 24 | 25 | 28 |
| 0·4 | 27 | 28 | 29 | 30 | 31 | 32 | 36 |
| 0·5 | 35 | 36 | 38 | 39 | 40 | 41 | 47 |
| 0·6 | 42 | 43 | 45 | 47 | 48 | 50 | 56 |
| 0·7 | 48 | 50 | 52 | 54 | 55 | 57 | 64 |
| 0·8 | 54 | 56 | 59 | 61 | 62 | 64 | 73 |
| 0·9 | 61 | 62 | 65 | 68 | 69 | 72 | 81 |
| 1·0 | 67 | 68 | 72 | 74 | 76 | 79 | 88 |

the value of $g/M$, for any $c$ or $\nu$, is nearly constant, though it decreases slowly as $M$ increases; at the same time the variation of $g$ with $c$ increases, in such a way that $g_1 < g_0 < g_2$. Moreover, $g_0 < \frac{1}{2}(g_1 + g_2)$, so that the graph of $g$ with respect to $c$ is convex towards the $c$ axis.

21. *Molecules of exactly equal mass:* $M = 0$. In considering the special case of molecules of exactly equal mass, we shall suppose the gases numbered 1 and 2 so that $s_1 > s_2$ or $x_{12} < x_{21}$. In this case

$$g_1 = \frac{1-x_{12}}{2H}, \quad g_2 = \frac{x_{21}-1}{2H}, \quad g_0 = \frac{x_{21}-x_{12}}{H(x_{12}+x_{21})+4A+2(H-2A)\,x_{12}x_{21}}. \tag{21·1}$$

Hence if $x_{12}$ and $x_{21}$ lie on opposite sides of unity, $g_1$ and $g_2$ have the same sign; if they lie on the same side, $g_1$ and $g_2$ have opposite signs.

In table 2, the only gas pair for which $M$ is nearly zero is $N_2O - CO_2$, for which $x_{12}$ and $x_{21}$ are nearly equal, and both are greater than 1; hence this mixture should illustrate the reversal of the sign of $g$ as $c$ varies, though $k_T$ will be very small for all values of $c$. For this gas, taking

$$\nu_{12} = 4{\cdot}6, \quad 5(C-1) = -\tfrac{1}{3};$$

the maximum value of $k_T$ will correspond to some value of $c$ between 0 and $-1$; for $c = -\frac{1}{2}$, the value of $g$ is approximately 0·01, that of $\alpha$ is approximately $-0{\cdot}001$, and that of $k_T$ is roughly $-0{\cdot}0003$; for $c = \frac{1}{2}$ it is approximately $+0{\cdot}0003$.

Another gas-mixture which might show the same reversal of sign of $k_T$ is $He - D_2$, for which, since $\nu_{12}$ is 11 or more, the factor $5(C-1)$ will be 0·6 or more; if $x_{12}$ and $x_{21}$ for this pair are of order 1·1, the maximum value of $k_T$ will be about 0·001.

21*a*. *The doubly special case* $M = 0$, $x = 1$. Probably when $M = 0$ the value of $x$ (§ 6) for most gas pairs will be nearly 1, unless the numbers of atoms in the molecules of the two constituents are very unequal. We therefore consider the special case $x = 1$ (always true if the molecules are rigid elastic spheres). We then have

$$g = \frac{s(1+\frac{1}{2}sc)}{H\{(1+sc)^2+\frac{1}{2}s^2(1-c^2)\}-2As^2(1-\frac{1}{2}s^2)(1-c^2)} \tag{21·2}$$

and

$$g_1 = \frac{s(1+\frac{1}{2}s)}{H(1+s)^2}, \quad g_2 = \frac{s(1-\frac{1}{2}s)}{H(1-s)^2}, \quad g_0 = \frac{s}{H(1+\frac{1}{2}s^2)-2As^2(1-\frac{1}{2}s^2)}. \tag{21·3}$$

Thus $g$ is proportional to $s$, the proportionate diameter-difference of the molecules, and is positive for all values of $c$ if $s > 0$.

When $s$ is small, (21·2) reduces approximately to

$$g = g_0(1-\tfrac{3}{2}sc), \quad g_0 = s/H \quad (M = 0,\ x = 1,\ s \text{ small}). \tag{21·4}$$

Since $H$ is approximately 3 for all values of $\nu_{12}$ from 3 to $\infty$, it follows that in this triply special case $g_0/s$ is nearly independent of $\nu_{12}$, and is approximately equal to $\frac{1}{3}$. Moreover, $g/s$ varies with the concentration ratio by a fraction $-\frac{3}{2}sc$, being greatest when the molecules of smaller diameter predominate ($c = -1$). As $c$ varies from $-1$ to 1, the percentage variation of $g/s$ is $300s$, or 15 % if $s = 1/20$.

When the diameters are very unequal, so that $s_1/s_2$ is large and $s = 1$, (21·2, 3) take the limiting forms

$$g = \frac{1+\frac{1}{2}c}{(\frac{1}{2}H-A)(1-c^2)+H(1+c)^2}, \tag{21·5}$$

$$g_1 = \frac{3}{8H}, \quad g_0 = \frac{1}{\frac{3}{2}H-A}, \quad g_2 = \frac{1}{2H(1-s)^2}, \tag{21·6}$$

so that $g_1$ and $g_0$ tend to different (finite) limits, and $g_2 \to \infty$.

When $s$ has values intermediate between 0 and 1 (and when $M = 0$, $x = 1$) the variation of $g$ may be illustrated as in table 7, for the case $\nu_{12} = 9$; for other values of $\nu_{12}$ the results are not very different.

TABLE 7. $M = 0$, $x = 1$, $\nu_{12} = 9$. WHEN $s = 0$, $g/s = 0·331$

| $s$ | | $\frac{1}{4}$ | $\frac{1}{2}$ | $\frac{3}{4}$ | 1 |
|---|---|---|---|---|---|
| $g_1$ | = | 0·060 | 0·092 | 0·111 | 0·124 |
| $g_0$ | = | 0·082 | 0·157 | 0·215 | 0·247 |
| $g_2$ | = | 0·129 | 0·497 | 2·48 | $\infty$ |

Hence $g_0/s$ decreases as $s$ increases, from 0·331 for $s = 0$, to 0·328, 0·314, 0·287 and 0·247 for $s = \frac{1}{4}, \frac{1}{2}, \frac{3}{4}, 1$. We may note also that $g_0 < \frac{1}{2}(g_1+g_2)$, so that the graph of $g$ as a function of $c$ is convex as viewed from below. The variation of $g$ with $c$ steadily increases with $s$.

21*b*. *The doubly special case $M = 0$, $s = 0$.* When the viscosity diameters of the pure constituents are equal, so that $s = 0$, and when also $M = 0$, $g$ is a function of $x$ only, given by

$$g = \frac{(1-x)c}{H\{x+1+(1-x)c^2\}-2A(x-1/x)(1-c^2)}, \tag{21·7}$$

$$g_1 = \frac{1-x}{2H} = -g_2, \quad g_0 = 0. \tag{21·8}$$

In this case $g$ is an odd function of $c$, proportional to $x-1$, which depends on $\nu_{12}$ and on the departure of the diffusion diameter $s_{12}$ from the mean viscosity diameter $s_0$. If $x-1$ is small, $g$ depends only slightly on $A$, as compared with $H$, and is therefore nearly independent of $\nu_{12}$.

When $1-x$ is small, (21·7) is approximately equivalent to

$$g = \frac{(1-x)c}{2H}\left\{1+\frac{(1-x)(1-c^2)(H-4A)}{2H}\right\}. \qquad (21\cdot9)$$

22. ***Mixtures of molecules that differ slightly in mass and interaction.*** When $M$, $s$ and $x-1$ are all small, the corresponding contributions to $g$ are approximately independent and additive, so that

$$g = \frac{3(1+1/A)}{4H}M(1-\gamma Mc)+\frac{s}{H}(1-\tfrac{3}{2}sc)$$
$$+\frac{(1-x)c}{2H}\left\{1+\frac{(1-x)(1-c^2)(H-4A)}{2H}\right\}. \qquad (22\cdot1)$$

Neglecting the terms in $M^2$, $s^2$ and $(1-x)^2$, this reduces to

$$g = \frac{3(1+1/A)}{4H}M+\frac{s}{H}+\frac{(1-x)c}{2H}; \qquad (22\cdot2)$$

here the first two terms are independent of $c$, and the third, which is proportional to $c$, has its greatest value when $c = \pm 1$. The maximum numerical magnitudes of the three terms are in the ratio

$$\frac{3}{2}\left(1+\frac{1}{A}\right):2:1;$$

$\frac{3}{2}(1+1/A)$ varies from 4·32 when $\nu_{12} = 3$ to 4·65 when $\nu_{12} = 9$ to $5\frac{1}{4}$ when $\nu_{12} = \infty$, so that the ratios are approximately 5 : 2 : 1. Thus a (small) difference of mass is more effective than a small difference of diameter, in promoting thermal diffusion, roughly in the ratio 5 : 2; a departure of $x$, which depends on the mutual diameter $s_{12}$, from the value 1 characteristic for rigid elastic spheres, is still less effective.

If $x = 1$ and $M$ and $s$ are of opposite signs, the contributions to $g_0$ due to the mass-difference and the diameter-difference may cancel one another, namely, if they bear to one another the inverse ratio $2:\frac{3}{2}(1+1/A)$. If $M/s$ has a slightly different value, $g$ will be small, though not zero. When $M$ and $s$ are not small (and also $x$ not nearly equal to 1) there is still a range of values of $M$ and $x$, $s$ (or $M$ and $x_{12}$ and $x_{21}$) for which $g_1$ and $g_2$ (and therefore all values of $g$) are zero, as shown in § 16.

23. It is hoped in a later paper to discuss the available experimental data for $k_T$, and to make suggestions for further experiments on thermal diffusion, in the light of the preceding discussion.

## References

Brown, H. 1940 *Phys. Rev.* **57**, **242**.
Chapman, S. 1916*a* *Phil. Trans.* **A**, **216**, **279**.
— 1916*b* *Proc. Roy. Soc.* **A**, **93**, **1**.
— 1917*a* *Phil. Trans.* **A**, **217**, **115**.
— 1917*b* *Phil. Mag.* **34**, **146**.
— 1919 *Phil. Mag.* **38**, **182**.
— 1922 *Mem. Manchr Lit. Phil. Soc.* **66**, **1**.
— 1929 *Phil. Mag.* **7**, **1**.
Chapman, S. and Cowling, T. G. 1939 *The mathematical theory of non-uniform gases.* Camb. Univ. Press.
Clusius, K. and Dickel, G. 1939 *Z. phys. Chem.* **44**, **397**.
Enskog, D. 1917 Dissertation, Upsala.
— 1921 *Ark. Mat. Astr. Fys.* **16**, **1**.
Furry, W. H., Jones, R. Clark and Onsager, L. 1939 *Phys. Rev.* **55**, **1083**.
Hassé, H. R. and Cook, W. R. 1929 *Proc. Roy. Soc.* **A**, **125**, **196**.
Jones, R. Clark. 1940 *Phys. Rev.* **58**, **111**.
Jones, R. Clark and Furry, W. H. 1940 *Phys. Rev.* **57**, **547L**.

---

# Catalytic activity, crystal structure and adsorptive properties of evaporated metal films

By Otto Beeck, A. E. Smith and Ahlborn Wheeler
*Shell Development Company, Emeryville, California*

(*Communicated by J. W. McBain, F.R.S.—Received* 4 *April* 1940)

[Plates 1–3]

Metal films of high and reproducible catalytic activity were obtained by condensation of their vapours on glass at any desired temperature. The catalytic activity was measured by the hydrogenation of ethylene. The crystal structure of these films was investigated by electron diffraction. By controlling the pressure of an inert gas (nitrogen, argon, etc.) during evaporation of the metals, unoriented and oriented films could be produced at will, and their catalytic activities were compared.

Completely oriented nickel films were obtained with an inert gas pressure of 1 mm., the (110) plane, the least dense of the planes, lying parallel to the backing and the two remaining axes showing random distribution. Iron films were oriented with their (111) plane parallel to the backing, again the least dense plane thus oriented.

Low-pressure adsorption of hydrogen at room temperature and of carbon monoxide at liquid-air temperature revealed that the oriented gas-evaporated nickel films have twice the available surface per gram of randomly oriented high-vacuum films but ten times the activity. The oriented films have therefore fivefold the activity of unoriented films. Oriented films of an available surface equal to unoriented but of fivefold activity could also be obtained in high vacuum by evaporation on to oriented films previously produced by evaporation in an inert gas.

The activity per unit weight of the films was constant, indicating ready accessibility to the interior of the film by the reacting gases.

Adsorption of hydrogen was found to be immeasurably fast in all cases.

Adsorption isotherms on nickel films were obtained for ethylene, carbon monoxide, nitrogen, hydrogen and oxygen; and the effect of catalyst poisoning by carbon monoxide and oxygen, as well as the effect of sintering, was studied. Loss of activity, decrease of hydrogen adsorption, and amount of poison were found to be proportional.

The most extensive studies were made on nickel films, but films of iron, cobalt, palladium, platinum and copper were also investigated, and with the exception of copper similar results were obtained. The enhanced activity of oriented films appears to be associated with the larger distances in the (110) plane of nickel or the (111) plane of iron.

The bearing of the results on the definition of active centres and on the general problem of adsorption is discussed.

## A. INTRODUCTION

The principal purpose of this investigation is to correlate catalytic activity and physical structure of catalysts. In order to achieve this objective it seemed desirable that the catalyst chosen for the study should be an element preferably not obtained from the oxide by reduction with hydrogen, that the catalyst should be obtained in the form of a flat film which would lend itself easily to investigation of its structure by electron diffraction, and that the catalysed reaction should have simple kinetics so that rates of reactions could be easily compared.

In addition to these requirements it seemed important to secure absolute reproducibility of results; this has been lacking in many catalytic investigations in the past.

After numerous orienting experiments with various catalytic materials in different forms of apparatus, suitable catalyst materials were found in the form of evaporated metal films of those elements which catalyse the hydrogenation of ethylene, a reaction found particularly suitable for the purpose. Metal films, both sputtered and evaporated, have been studied in the past from the standpoint of catalytic activity as well as from the standpoint of crystal structure,* although only a few attempts have been made to correlate activity and structure of such films.* The results reported in the literature in each of these fields are conflicting and often contradictory. Many of these discrepancies are readily explained from the standpoint of the results of this investigation.

---

* See, for instance, Ablesova and Roginsky (1935), where numerous references to earlier work on catalytic metal films are given. For recent observation of orientation in metal films see Kirchner (1932), Finch, Quarrell and Wilman (1935), Beeching (1936) and Nelson (1937).

## B. APPARATUS

*Reaction vessel.* The design of the reaction vessel was the outcome of careful study. Though essentially a static method was employed, it was found necessary to maintain a fast flow of the reacting gases past the catalyst in order to remove the reaction product and make the catalyst accessible for fresh reactants at all times. The vessel was therefore constructed in the form of a continuous circulatory flow system. Various forms were employed, one of which is shown in figure 1. The wide arm on the left side contains in its centre an approximate 10 cm. long constriction of about 1 cm. inside diameter. This constriction is surrounded by a jacket, and the thin-walled inner tube may be maintained at any desired temperature by pumping cooled or heated liquids through the jacket. Other forms of the vessel were totally or partly immersed into baths at the desired temperature. Figure 1 shows on the upper right side an all-glass turbine whose glass-enclosed soft iron rotor is driven by a rotating magnet from the outside. If the coils of this magnet are energized by A.C. or preferably by half-wave rectified A.C. of 60 cycles, the motor may be shut off after the rotor has been brought up to speed, and in the latter case (i.e. with half-wave rectifier A.C.) the turbine rotor will run at a constant speed of 30 rev./sec. which has been verified by means of a stroboscope.† With a well-built turbine a linear velocity of 2–3 m./sec. was obtained in the centre of the 1 cm. wide and 10 cm. long constriction. The catalyst was deposited on to the inside of this piece of tube by evaporation from an electrically heated hairpin-shaped wire. The wireholder was either sealed into the vessel or was set into position by means of a water-cooled ground joint. In figure 1 this is a double joint permitting the easy removal of the whole continuous flow system for cleaning purposes. The reaction rates were followed manometrically either by a mercury manometer directly or indirectly via a highly sensitive all-glass Bourdon gauge used as zero

---

* Bredig and Allolio (1927), Finch, Murison, Stuart and Thomson (1933) and Finch and Ikin (1934).

† The actual procedure in the latter case is as follows: Start the magnets rotating without energizing them, then energize with half-wave rectified arc. The rotor will turn slowly in *opposite* direction to the magnets. Then stop the rotation of the magnets and the rotor will come up to 30 rev./sec. with the magnets stationary.

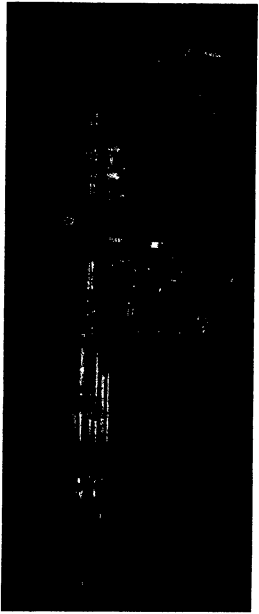

FIGURE 1

instrument. The latter procedure proved to be an unnecessary precaution, as most reaction rates were high as compared to the slow diffusion of mercury vapour from the gauge to the reaction vessel proper.

*Electron diffraction camera.* The electron diffraction camera was similar in design to that described in great detail by Germer (1935). The metal films for structure investigation were produced in a special glass apparatus under exactly the same conditions as the films used in the study of the chemical kinetics, the only modification being that the metal film could be produced on a flat water-cooled glass surface of 1–2 cm.$^2$ which could be removed as a separate unit and placed directly into the electron diffraction camera.

*Experimental procedure.* In order to obtain metal films of high activity and good reproducibility careful observance of the following procedure was found to be essential. Only extreme cleanliness and baking out of the reaction vessel proper under high vacuum for at least 2 hr. at or close to 500° C before each new metal deposition will secure the desired reproducibility. This point cannot be over-emphasized, and the failure of previous workers in the field to obtain active and reproducible films can be largely attributed to inadequate degassing of the apparatus. It is also necessary to free the filaments from occluded gases. This is best done by heating the filament just below the evaporation point for the last hour during the baking-out process.

After degassing of glass vessel and filament, the apparatus is allowed to cool and carefully purified gas is admitted if evaporation of the metal is to be carried out in a gas. During evaporation the glass wall upon which the evaporated metal is deposited is cooled to the desired temperature. The evaporation rate used was approximately 0·5 mg. of metal per min. After deposition of a film of desired thickness the apparatus is ready for measurement of the reaction rate. The catalyst is cooled or heated to the desired temperature, the circulation turbine is started, and a hydrogen-ethylene mixture is admitted. Initial pressures of 100–500 mm. were used most frequently, and, with a total volume of approximately 400 c.c., the pressure change may easily and accurately be followed by the mercury manometer. The velocity constants obtained were independent of initial pressure.

In order to standardize the experimental procedure as far as possible all reaction rates refer to the hydrogenation of ethylene and have been measured at 0° C unless otherwise indicated. The simplicity of the kinetics of this reaction has greatly facilitated the measurement and correlation of rate constants throughout this investigation. In all cases the reaction was of the first order with respect to hydrogen. However, in order to secure this result, especially for catalysts of high activity, it was necessary to use forced gas circulation by means of the turbine described above. Although the order of the reaction in a given run was independent of the ethylene pressure, an excess of ethylene lowers the reaction rate considerably in agreement with earlier work in this field. All rate measurements were therefore carried out with equi-molar mixtures of hydrogen and ethylene.

## C. Experimental results with nickel films

### *Activity measurements*

Figure 2 shows the usual logarithmic plot for first-order reactions, the curves (*a*)–(*f*) representing hydrogenation reactions of ethylene over evaporated nickel catalysts of various activities. The figure shows that the first-order law is well obeyed for slow as well as fast reactions. The slopes of similar curves were used throughout this work for evaluation of the velocity constants. Keeping the temperature at which the reaction rates are measured constant (0° C) three main factors affect the activity of the evaporated catalysts: (*a*) the film thickness, (*b*) the pressure of inert gas in which the film is evaporated, and (*c*) the temperature of the glass surface on to which the metal vapour is condensed. In figure 3 are plotted velocity constants (multiplied by 100/2·303 for convenience) against the weight * of

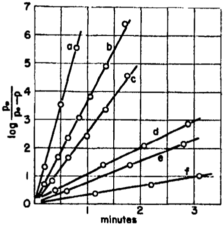

FIGURE 2. Logarithmic plot showing first-order reactions on various catalysts.

---

* For the given apparent surface of about 30 cm.², the films contain 212 atom layers per mg. (taken along the [100] axis).

the nickel films in mg./30 cm.². The upper curve shows the activity of nickel films evaporated in 1 mm. of nitrogen and deposited on a glass surface at 23° C, and the lower curve shows the activity of nickel films deposited at the same temperature in high vacuum. The point, marked *A*, represents a nickel film from evaporation in 1 mm. of argon under otherwise equal conditions. The two curves show that the activity increases with film thickness and that the films evaporated in 1 mm. of nitrogen or argon have many-fold higher activity than those evaporated in high vacuum.

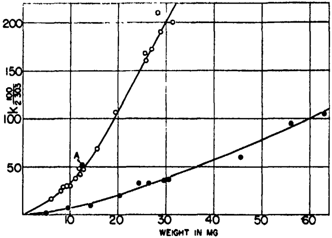

FIGURE 3. Activity of evaporated nickel films as a function of film weight (1 mg. ~ 212 atom layers). ○, evaporated in 1 mm. of nitrogen; ⊙, evaporated in 1 mm. of argon; ●, evaporated in high vacuum.

The extremely high activity of gas-evaporated films may best be judged from the fact that a nickel film of 29 mg. evaporated in nitrogen has a half time of less than 10 sec. for an equi-molar mixture of hydrogen and ethylene at atmospheric pressure. The increase of activity with film thickness (weight) is of great interest, since it suggests that the whole interior of the film partakes in the catalysis and must therefore be porous. It will be shown later that this is also borne out by measurements of adsorption and electrical conductivity. It may also be stated at this point that within the experimental limits no gas (nitrogen or argon) is adsorbed by the nickel film during evaporation. With the apparatus used one gas atom could have been detected for every 10,000 metal atoms evaporated.

The differences in height and shape of the two curves shown in figure 3 can only be due either to a difference in surface area or to a difference in intrinsic activity per unit area or both. To investigate these possibilities, surface areas were determined by gas adsorption measurements, and the crystal structure of the films was investigated by electron diffraction.

### *Adsorption measurements*

The adsorption measurements were carried out either directly in the same apparatus in which the reaction velocities were measured or in a tube of small volume in which the metal film was produced under conditions identical to those in the reaction chamber. With the latter apparatus dead space and glass surface could be reduced to a minimum. Pressure measurements were made by a McLeod gauge. The procedure was simply to allow the gases to expand from a known volume and known gas pressure into the catalyst chamber, the volume of which was likewise known. From the resulting over-all pressure the adsorption may be calculated.

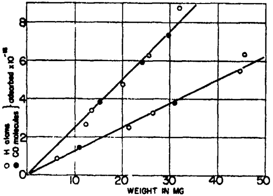

FIGURE 4. Adsorption of hydrogen and carbon monoxide on films evaporated in 1 mm. of nitrogen (upper curve) and in high vacuum (lower curve).

In figure 4 are shown results for adsorption measurements of hydrogen at room temperature and for carbon monoxide at −183° C on nickel films of various thickness evaporated in high vacuum and in 1 mm. of nitrogen. The residual gas pressure over the catalyst was in all cases close to 0·1 mm. The results are of interest in various ways. The striking fact that the number of hydrogen atoms adsorbed at 23° C is equal to the number of carbon monoxide molecules adsorbed at −183° C shows clearly that each available lattice space on the surface is occupied by a carbon monoxide molecule, whereas the same space is occupied by a hydrogen atom only. This result demonstrates convincingly the monomolecular nature of the carbon monoxide adsorption at −183° C as found by Emmett and Brunauer (1937) for synthetic ammonia catalysts. Of special interest, however, are two further results of the measurements presented in figure 4: (1) the surface of nickel films evaporated in 1 mm. of nitrogen is only twice as large as for the correspondingly high vacuum films, and (2) the surface of both film types increases linearly with the film thickness. On comparing these results with the activity curves of figure 3 it is seen that the activity differences of the two film types cannot be explained by differences in surface alone. It is to be noted that, although the area of the gas-evaporated films is only twice as large as that of the corresponding high-vacuum film, their activities differ by a very much greater factor, and that the adsorption shows a linear increase with film thickness, whereas the activities increase faster than linearly with the exception of gas-evaporated films heavier than 15 mg.

*Measurements of electrical conductivity*

The adsorption measurements were supplemented by measurements of the electrical conductivities of the two types of films. These measurements were made in the same apparatus. For this purpose the catalyst tube was equipped with two very thin platinum rings about 3 cm. apart from each other which were well 'worked' into the hot and soft glass surface so as to form two conductive rings. The catalyst films were simply evaporated across these rings in the usual manner, and the conductivity between the rings was measured via suitable sealed-in leads by a Leeds and Northrup Wheatstone Bridge. The results are shown in figure 5. The conductivity is given in ohm$^{-1}$ of a tube-shaped nickel film 2·7 cm. long and 1·2 cm. in radius as a function of the weight of the whole film, the thickness of which is 212 atom layers per 1 mg. of nickel. The conductivity of the high vacuum films (upper curve) is four times as high as the conductivity of the gas-evaporated films. The conductivity of both film types is linear with respect to film thickness with a small deviation for films lighter than 3 mg. This result is in perfect agreement

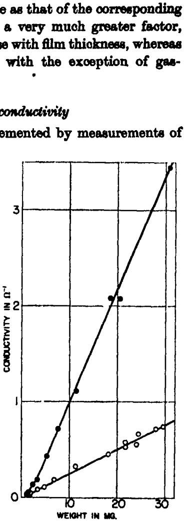

FIGURE 5. Electrical conductivity of nickel film in high vacuum (upper curve) and in 1 mm. of nitrogen (lower curve).

with the adsorption measurement, as both measurements show that the films are homogeneous throughout their thickness and that the films evaporated in 1 mm. of nitrogen are more porous than high-vacuum films. Calculation shows that the latter have about seven times the resistance of bulk nickel, while the gas-evaporated films possess twenty-eight times the resistance of bulk nickel.

Adsorption and conductivity measurements can explain any linear increase of the activity. They do not, however, explain the more than linear increases and especially not the large factor between the activities of gas and high-vacuum evaporated films shown in figure 3. These differences must therefore be due to differences in intrinsic activity per unit area of the two film types. A satisfactory and apparently complete explanation, however, has been found through the agency of electron diffraction studies of these films, leading to a new definition of active centres.

### *Electron diffraction studies*

As already mentioned, films of various thickness were evaporated on a special specimen holder under varied conditions identical with those obtaining in the catalytic vessel.

#### (*a*) *General results.*

Before discussing in more detail the variables affecting the structure of the films a number of electron diffraction pictures are shown in figure 6 (plate 1), each picture relating to a certain point (as indicated by arrows) on figure 3 which is here reproduced. The structural difference between the two film types is at once evident. The highly active films evaporated in 1 mm. of nitrogen or argon are highly oriented, whereas the films evaporated in high vacuum do not show any preferred orientation for thin films though a pronounced orientation was found for the heaviest films. Gas-evaporated films heavier than 15 mg. are practically completely oriented, and their activity increases linearly with the film thickness. This linear increase must therefore be due to the linear increase of active surface with film weight as shown in figure 4, the initial more than linear increase of activity for thinner films being due to the increase of degree of orientation with film thickness, until for films of about 15 mg. weight maximum effective orientation is obtained. The activity of the high vacuum-evaporated nickel films increases only slightly more than linearly with film thickness, and there seems to be no doubt that this is due to the tendency of these films to orient increasingly, though only slightly, with film thickness.

Therefore, in order to compare the activities of oriented and unoriented films quantitatively, some special experiments were carried out in an attempt to produce a number of high-vacuum films which would show no orientation. It was found that entirely non-oriented films of various thickness could be produced by evaporation in high vacuum on to a liquid-air cooled surface. Upon heating to 0° C, at which temperature the activity measurements were carried out, such films have a slightly larger surface than those evaporated on to a surface at room temperature, but the activity increases linearly with film thickness. This is shown in figure 7

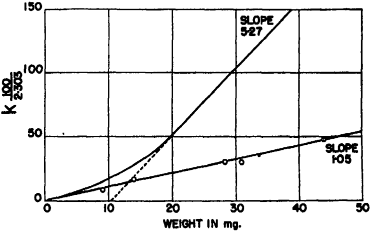

FIGURE 7. Activities of oriented and non-oriented nickel films reduced to the same adsorptive surface.

where all activities have been reduced to the surface of films evaporated in high vacuum at 23° C. The lower curve represents films which are entirely non-oriented, the upper curve represents the activity for gas-evaporated films. The ratio of the slopes of these two curves therefore represents the ratio of the activities of an oriented film and an unoriented film of equal surface. This ratio is very close to five.

(*b*) *Interpretation of diffraction patterns.*

The sharp ring patterns obtained with films evaporated in high vacuum were compared with transmission pictures of electrolytically prepared nickel foil, and both were found to have normal face-centred cubic lattice. Electron velocities were measured by calibration with transmission patterns of gold foils; in some cases the gold pattern was obtained simultaneously with the pattern of the film to be studied by allowing a fraction of the electron beam to be scattered by the gold foil. Within the maximum experimental error, which did not exceed 0·5 %, no deviations from the normal spacings in the nickel lattice were observed for either oriented or non-oriented films.

In the diffraction patterns of the oriented films the intensity maxima (spots or arcs) lie along well-defined layer lines, the distance of these lines corresponding to the (110) spacing. This, together with the correct position of the maxima as to azimuthal angle and radius, show a high degree orientation of the crystallites with their 110 planes lying parallel to the backing.

Though the diffraction patterns were obtained at nearly grazing incidence of the electron beam, the sharpness of the patterns and the lack of a marked displacement due to refraction show that the pattern must be mainly due to transmission through projecting crystals.

### *Catalytic activity, structure and adsorptive properties of 'double films'*

We shall designate as double films the strongly oriented films which were produced in high vacuum in the following manner. Initially a nickel film was evaporated on to the glass surface in 1 mm. of nitrogen so as to produce a strongly oriented film. Evaporation was then interrupted and the vessel was evacuated to high vacuum following which deposition was continued under a high vacuum until a film of desired thickness was produced on top of the oriented gas-evaporated film. In this way a strongly oriented high-vacuum film could be obtained as shown in figure 8 (plate 2), where a high-vacuum film of about 4200 atom layers was condensed on to a gas-deposited film of approximately equal thickness. This shows that the orientation induced by the oriented substrate is carried through relatively thick layers.

Such double films were investigated both for their adsorption properties and their catalytic activity. Curves $A$ and $B$ in figure 9 represent the adsorption properties of gas-evaporated and high vacuum-evaporated nickel films respectively (identical with figure 4). The points were obtained for double films. The upper number gives the amount of nickel in mg. evaporated in 1 mm. of nitrogen, the lower number the amount of nickel evaporated in high vacuum on to the first films. The parentheses indicate that the oriented high-vacuum film which is part of a double film has the same surface as the unoriented high-vacuum film.

Curves $A$ and $B$ in figure 10 represent the activities of the two types of film (identical with figure 3). The open circles are activities of double films, the upper number again giving the weight of the oriented gas-evaporated film, the lower number the weight of the oriented high-vacuum film. The parentheses ending at curve *B* indicate the activities expected for unoriented high-vacuum film. The parentheses ending at the open circle give the activities obtained for the oriented high-vacuum films. The respective activities may be compared directly, since the adsorption is equal for both high-vacuum films (figure 9). The activity increase will depend on the degree of orientation of the double films and on the degree of orientation of the high-vacuum films represented by curve *B* which, as we have seen, is gradually increasing with film thickness. Taking into account these facts, we again obtain the activity ratio of five to one for an oriented film to an unoriented film.

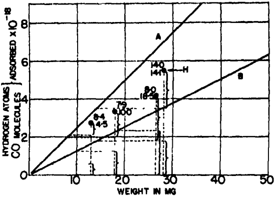

FIGURE 9. Adsorption on double films.

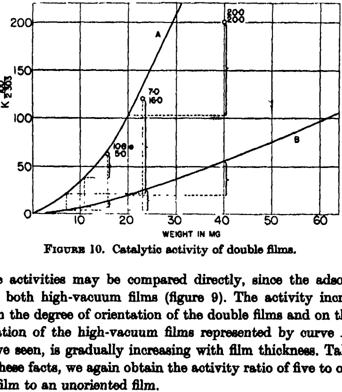

FIGURE 10. Catalytic activity of double films.

The black point in figure 10 represents a point of unusual high activity of an ordinary high-vacuum film. When investigated by electron diffraction, the pattern, figure 11, plate 2, was obtained. showing a fairly high degree of orientation which explains satisfactorily the high activity. Such unusual activities occurred occasionally after an apparatus had been in service for a long time. The only other detectable difference between such an apparatus and a newly made one was a strong fluorescence during a gas discharge of those glass parts on to which a nickel film had been often deposited. It seems possible that the glass surface is slowly transformed into a state of some unknown composition which induces the orientation. However, it seems more likely that the influence of surface impurities (water, oxygen) slowly disappears and that a single adsorbed gas layer may initiate the orientation. This view is supported by the following experiment with an apparatus which had occasionally shown these unusual activities. This apparatus was carefully baked out in high vacuum with liquid nitrogen traps in the pumping line close to the vessel. A deposited high-vacuum film showed no orientation. In the next experiment the procedure was the same, but shortly before deposition Apiezon grease vapour was intentionally admitted by removing for a short interval and then replacing a liquid nitrogen bath from a side arm containing some grease. The nickel film which was then deposited on the surface showed fairly good orientation. Evidently the layer of adsorbed grease (or gas from the grease) had induced the orientation.

For the sake of greater clearness we have discussed so far only high vacuum-evaporated films and films evaporated in 1 mm. of nitrogen or argon evaporated on to surfaces of room temperature which were previously baked out thoroughly. The effect of changing any of these factors will be discussed in the following paragraphs.

(c) *Gas pressure during evaporation.*

The gas pressure necessary to obtain complete orientation is not very critical and ranges from about 0·5–2 mm. of nitrogen or argon for nickel films. However, a gas pressure of $5 \times 10^{-2}$ mm. produces films of markedly less orientation and of about 30 % lower activity. If pressures higher than 2 mm. are used, orientation gradually disappears and films evaporated in 8–10 mm. show no orientation. The stronger general background and the broadening of the rings in the diffraction pattern show that the crystallites are much smaller in this case. Activities of these films were found to be comparable with those of oriented films. A more detailed investigation of this type of films is planned.

(*d*) *Baking-out temperature of the glass surface.*

As has been evident from figure 3 the thickness of the film influences the orientation so that a gas-evaporated film (1 mm.) has to be about 15 mg. of weight to be highly oriented. This is true for a film deposited at 23° on to a glass surface previously baked out at about 500° C. If the glass surface is not baked out, but only degassed by evacuation, the gas-evaporated film has to be much thicker in order to be well oriented, a film of about 15 mg. weight being practically unoriented. In figure 12 the catalytic activity relative to a film deposited on to a surface well degassed at 500° C is plotted against the baking-out temperature. A baking-out time of 1 hr. under high vacuum was chosen in this case. The activity of films deposited on a glass surface which had been merely degassed by evacuation at room temperature is in excellent agreement with the activity of a non-oriented film if we take into account that the gas-evaporated film has twice the surface of the high-vacuum film irrespective of its orientation.

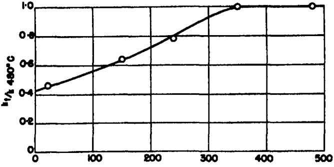

FIGURE 12. Catalytic activity of nickel films evaporated in 1 mm. of nitrogen as a function of the baking-out temperature of the supporting glass surface (given relatively to films baked out at 480° C).

### *Temperature of glass surface at time of deposition*

The influence of the temperature of the glass backing at the time of deposition of the metal film is especially marked at higher temperatures and affects equally strongly both oriented and unoriented films.

Strongly oriented gas-evaporated nickel films were still obtainable at 80° C, but a film deposited at 165° C was completely non-oriented. However, orientation loses importance at the higher temperatures, since the films lose their activity rapidly with increasing temperatures of sintering. Our main attention has therefore been given to the sintering process itself. Nickel films were prepared at 23° C and were then heated for 30 min. at the desired sintering temperature. The films were then cooled to 23 or 0° C respectively for standard adsorption and activity measurement. In figure 13 are plotted adsorption measurements and activity measurements (hydrogenation of ethylene) against sintering temperature. The ordinates of the points plotted are relative values based on the respective value for films deposited at 23° C. All values were reduced to a film weight of 14 mg./30 cm.². Of particular interest is the fact that the hydrogen adsorption decreases much more slowly with increasing sintering temperature than the activity. The percentage decrease in adsorption and activity for oriented and non-oriented films is very closely the same, though the oriented films are twice as porous and many times as active as the non-oriented films.

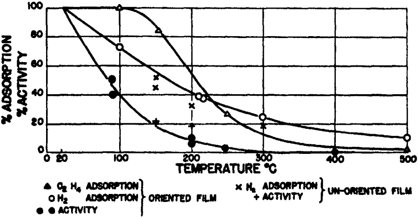

FIGURE 13. Adsorption and activity of sintered nickel films.

It is also of interest to note that the activity of a film is the same whether the film was deposited at 23° C and then heated to the sintering temperature or whether the film was evaporated at the sintering temperature. The black points in figure 13 were obtained by the latter method. It is difficult to say how much the observed sintering phenomena are due to structural changes of readily accessible parts of the interior surface and how much they are due to decreased pore size. These questions will be more fully discussed below. It should be mentioned that oriented films do not lose their orientation by heating, even for longer times, at 400 or 500° C, though it may be expected that the surface actually exposed to the gas may have changed in structure.

### *Adsorption isotherms*

In order to round out the general picture of the adsorption phenomena presented in this paper, adsorption isotherms were taken for a number of gases on nickel films. Isotherms were obtained for carbon monoxide at − 183 and at 23° C, for ethylene at 23° C, for nitrogen at − 183° C, for hydrogen at 23° C and for oxygen at 23° C. In all cases, except nitrogen, irreversible chemisorption was found, the adsorption taking place in a few seconds. No nitrogen is adsorbed at room temperature.

The isotherms are shown in figure 14 plotted in fractions of the surface which the gas covers at 0·1 mm. pressure. All isotherms are of the simple Langmuir type. As already reported in the case of hydrogen and carbon monoxide the adsorption of all gases increases linearly with film weight, and the adsorption on films evaporated in 1 mm. of nitrogen or argon is twice as great as on high vacuum-evaporated films. Curves of the type shown in figure 4 for hydrogen and carbon monoxide were obtained in all cases. With small deviations the following adsorption ratio relative to the carbon monoxide adsorption was found for the different gases on the same type of nickel surface:

| Gas | CO | $H_2$ | $N_2$ | $C_2H_4$ | $O_2$ |
|---|---|---|---|---|---|
| Ratio | 1 | 1/2 | 1/2 | 1/4 | 2 |

According to figure 4 the ratio 1/2 is very exact at 0·1 mm. pressure for carbon monoxide at − 183° C and hydrogen at 23° C. The carbon monoxide adsorption at 23° C is about 20 % less than at − 183° C, whereas the hydrogen adsorption at − 183° C is the same as at 23° C. The carbon monoxide isotherm is completely level until it drops steeply at very low pressure. The hydrogen isotherm at 23° C has a small slope, however, and drops sharply to only 80 % of its value at 0·1 mm. pressure. This 20 % may also be pumped off at 23° C, indicating that it concerns a different type of adsorption with a very much smaller heat of adsorption. In comparing, therefore, the carbon monoxide adsorption and hydrogen adsorption at 23° C, the points where the isotherms drop sharply should be chosen, and again we obtain the ratio 1/2. The van der Waals adsorption of nitrogen at − 183° C and 0·1 mm. pressure is almost exactly equal to the hydrogen adsorption at − 183° C (or 23° C) which probably means that the nitrogen molecules lie flat on the surface taking up two spaces of the nickel lattice, since the chemisorption of hydrogen is known to take place with a dissociation of the hydrogen molecules so that each hydrogen atom occupies one lattice space on the surface.

The ratio of the chemisorption of hydrogen and ethylene is very exactly 1/2, so that the ethylene molecule covers four spaces on the crystal lattice, presumably being adsorbed by the four hydrogen atoms. The adsorption of oxygen which was given above as being roughly twice the carbon monoxide adsorption is actually found to be somewhat larger. This, however, is probably due to diffusion of the oxygen into the interior of the

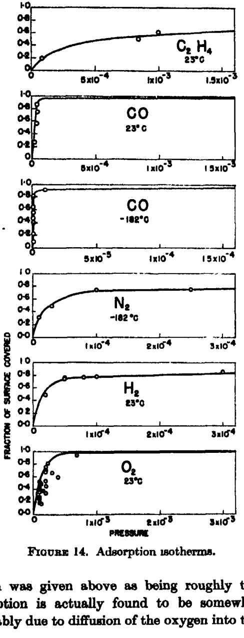

Figure 14. Adsorption isotherms.

lattice, evidence for which will be presented later. Nevertheless, a practically instantaneous adsorption of two molecules per lattice space on the surface takes place, and it must be assumed that the oxygen immediately penetrates the first layer to allow such a large amount to be adsorbed. A slow diffusion process into the interior continues afterwards, as a small amount of oxygen will be taken up over a long period. It will be shown below in connexion with some poisoning experiments that the oxygen adsorption layer will diffuse into the interior even if no additional oxygen is available from the gas phase. It should be mentioned that the oxygen used for the determination of the oxygen isotherms contained a small amount of nitrogen which undoubtedly caused the somewhat erratic behaviour at the lowest pressures.

### *Poisoning experiment*

Both carbon monoxide and oxygen poison the nickel catalysts for the hydrogenation reaction. This poisoning process has been studied in some detail and has given additional information on the catalytic and adsorption properties of the films. Since very fast chemisorption was observed for both oxygen and carbon monoxide, these poisons were not expected to be selective with respect to the lattice structure on the surface of the catalyst. Nevertheless, a curve was obtained as shown, drawn in full, in the upper part of figure 15. The open circles are experiments with carbon monoxide, the black with oxygen; they were made on oriented films. The crosses were found for carbon monoxide poisoning on an unoriented film. It may be added that whereas the total amount of carbon monoxide which the surfaces would adsorb was necessary to poison the surface completely, a rather smaller amount sufficed in case of oxygen (where, as we have seen, twice as many molecules as in the case of carbon monoxide were taken up anyhow). The fractions used in the case of oxygen are therefore taken relative to the amount which was found to poison the surface completely.

The curve obtained in figure 15 (upper part) for oriented film and the straight-line relationship (broken line) for the unoriented film may on first sight suggest that the oriented films of higher activity are poisoned somewhat selectively. However, if such were true, we should expect a much larger influence for small amounts of poison than shown in the figure where the maximum curvature occurs at the higher percentages of poison. We believe that the true explanation is as follows: From figure 3 it is seen that the integral activity of films deposited in 1 mm. of nitrogen increases rapidly with the film thickness, whereas the increase for the high-vacuum film is almost linear. If, now, the poisoning gas molecule is adsorbed where

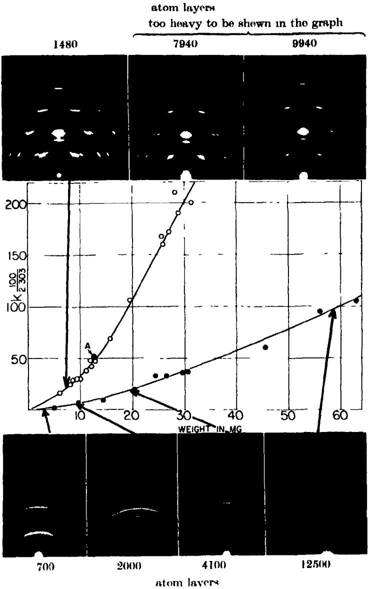

FIGURE 6. Electron diffraction patterns of evaporated nickel films. (Weight and activity indicated by arrows, the patterns above the figure correspond to the upper curve giving activities of films evaporated in 1 mm. of nitrogen, the lower patterns correspond to high-vacuum films. The oriented films of 7940 and 9940 atom layers are too heavy to be shown in the figure.)

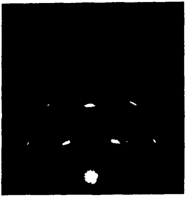

FIGURE 8. Orientation of high-vacuum layer in 'double film'.

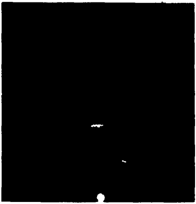

FIGURE 11. Orientation shown by high vacuum-evaporated nickel film of unusually high activity.

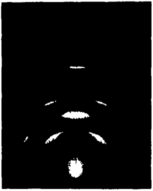

FIGURE 16. Electron diffraction pattern of iron film evaporated in 1 mm. of nitrogen showing (111) orientation parallel to the backing.

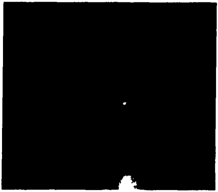

FIGURE 18. Electron diffraction pattern of palladium single-crystal film with its (100) plane parallel to the rocksalt cleavage plane (grazing incidence).

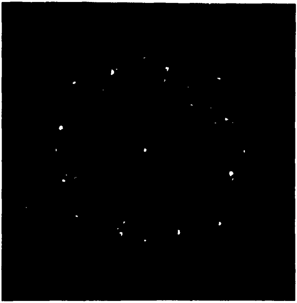

FIGURE 19 X-ray pattern of palladium single-crystal film (20,000 atom layers thick) with rocksalt backing

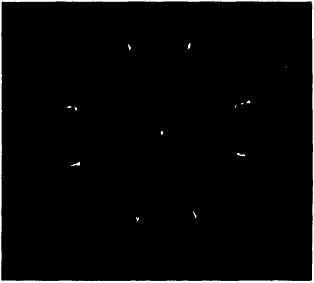

FIGURE 20 Same film as figure 19 (rocksalt dissolved)

it hits first we must expect that the upper more active part of the film is poisoned first leaving the lower less active part free. In computing from this standpoint the activity remaining, after poisoning, the straight-line relationship shown in the lower part of figure 15 is obtained.

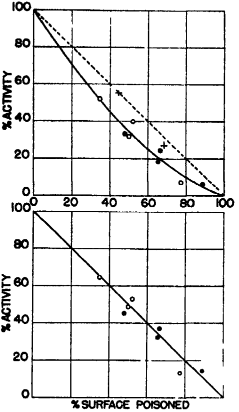

FIGURE 15 Poisoning curves, ○ carbon monoxide, ● oxygen (upper curves: uncorrected, lower curve corrected for changes in activity with film thickness)

Surfaces, poisoned by carbon monoxide or oxygen will still adsorb 20 % of the amount of hydrogen that a clean surface would have taken up. This amount is the same as is represented by the nearly level part of the hydrogen isotherm As in the case of hydrogen alone, this hydrogen can be pumped off from the carbon monoxide or oxygen adsorption layer. In agreement with observations of Benton and others (White and Benton 1931; Griffin 1939) on reduced nickel oxide catalysts the amount of hydrogen adsorbed is somewhat larger than expected if the surface is only partially covered with carbon monoxide. As we have seen from the poisoning curve such a partially covered surface will exist only at the more or less sharp boundary between the outer parts of the film which are totally covered and the inner part which is not covered at all. This could easily be the reason for the effect observed here being very much smaller than in Benton's experiments.

An observation of special interest is the fact that a film poisoned by oxygen for chemisorption of hydrogen and consequently for the ethylene hydrogenation will upon standing for half a day regain its power to chemisorb instantaneously the regular amount of hydrogen, the oxygen apparently having diffused into the interior of the crystal lattice. This enables one to explain the slow disappearance of hydrogen from the gas phase over an oxygen-poisoned nickel catalyst without the assumption of a slow reaction between hydrogen and oxygen at room temperature. These observations are particularly important from the standpoint of the slow activated adsorption of hydrogen reported so frequently in the literature and will be discussed in more detail below.

### *Results with other metal films*

Besides nickel films, which have been studied in greatest detail, all elements of the transition series in the eighth group of the periodic system seem to have the same properties. In particular, cobalt, iron, palladium and platinum were investigated. Of these, more detailed investigations were carried out with iron and palladium which will be published in later communications. From the standpoint of the present paper the following results are important: The elements of the same structure as nickel (face-centred cubic) respond to evaporation in a gas atmosphere with the same orientation found for nickel, i.e. the (110) plane parallel to the backing.

The body-centred iron, however, orients with the (111) plane parallel to the backing when evaporated in nitrogen or argon, as shown in figure 16, plate 2, the oriented films having higher activity than the unoriented films. The observations on iron are very helpful in explaining the orientation of the gas-evaporated films. This will be more fully discussed below.

It was found that copper films sinter immediately upon evaporation to such a degree that no measurable internal surface could be observed either by chemisorption or van der Waals's adsorption at $-183^\circ$ C. Blackish films were obtained by evaporating copper in nitrogen or argon on to a surface at $-183^\circ$ C. Upon warming, the gas was completely released and the film could be seen to acquire a more coppery appearance during this process. Only under one condition was a copper film of low though easily measurable activity obtained, that is when the film was evaporated in hydrogen on to a surface cooled to − 183° C. This film also retained some hydrogen upon warming, which evidently is the reason for its not sintering entirely. No oriented copper films could be made at room temperature, whereas oriented gold films could be obtained fairly easily. It seems that the metals of high atomic weight respond more easily to orientation by gas evaporation. This is also borne out by palladium and platinum which orient more easily than nickel, cobalt and iron; the data, however, are still incomplete with respect to this last point.

## D. DISCUSSION

### *Gas-induced orientation*

Unless we deal with natural cleavage planes it seems impossible to make a definite statement as to the actual array of atoms in the boundaries of a crystal. The fact that it has been possible to produce nickel films, the crystallites of which are oriented with their (110) planes parallel to the backing, would not in itself definitely answer this question if it were not for the additional fact that this orientation can be induced by a gas from which further deductions can be made. If orientation is produced by the gas it seems likely that the oriented planes obtained are also exposed to the gas.* The mechanism by which gases such as nitrogen or argon induce the orientation is as yet not fully understood, and it is planned to investigate this question more carefully from the experimental standpoint before attempting an explanation.

It seems likely that an adsorbed gas layer could induce the orientation by forcing the metal atoms into positions corresponding to the plane of least density (which is also the plane of highest surface energy) within the structure of the crystal lattice. In the case of nickel as shown in figure 17 the (110) plane is in fact the plane of least density. In the case of iron, orientation of the (111) plane parallel to the backing was obtained (see figure 16, plate 2), and this plane happens to be the one of least density in the body-centred iron lattice.

However, the inducing effect of argon or nitrogen could scarcely be of this type, since neither of the gases shows, nor is expected to show, any adsorption at room temperature and 1 mm. pressure. It can be shown easily that the time an argon molecule would have to stay on the surface in order to cover the surface with argon molecules at 1 mm. pressure is roughly $10^{-5}$ sec., which is a time many orders of magnitude greater than might reasonably be expected, even if the accommodation coefficients were unity. It seems therefore that the effect of these gases on the orientation is a purely kinetic one either through dissipation of condensation energy at the surface, i.e. by affecting the freshly formed surface itself, or through an effect on the energy distribution of the metal atoms before they reach the surface. The larger porosity of gas-evaporated film can also be explained from the standpoint of faster energy dissipation of the energy of condensation. In most of our experiments condensation took place at a rate $10^5$ times less than that of the gas collisions with the surface.

---

* Differences in contact potential or photo-electric emission will be the most direct proof of this question since theoretically the work function is expected to be different for different crystal planes. Such experiments are planned. In agreement with these expectations Paul A. Anderson has just reported (1939) a contact potential of 0·12 ± 0·01 V between an oriented (100) silver film (deposited on rocksalt) (Brück 1936) and an unoriented film deposited on glass.

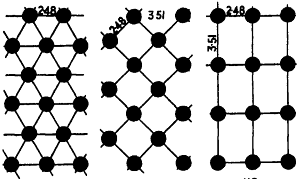

111 100 110

FIGURE 17. The simple crystal planes of nickel.

### *Accessibility of catalyst interior*

The increase of catalytic activity with the mass of the film is of great interest and shows that even for reactions which are completed in fractions of a minute the innermost layers of the catalyst participate in the reaction to the full extent of their inherent activity. This was quite clearly brought out by the poisoning experiments. The total interior surface of an oriented nickel film of for instance 50 mg. weight was found to be very close to 10,000 cm.$^2$, whereas the apparent surface is only 30 cm.$^2$. Let us, for the purpose of simplification, assume that the film is composed of cylindrical canals whose diameters just touch. If then the weight of the film is 50 mg., the interior surface 10,000 cm.$^2$, and the apparent surface 30 cm.$^2$, it can be easily shown that the film will have $4{\cdot}4 \times 10^{11}$ canals with a radius of $4{\cdot}2 \times 10^{-6}$ cm. and a length of $8{\cdot}7 \times 10^{-4}$ cm. It may be shown now that the innermost portion of such a film can partake in the reaction to nearly the fullest extent on the basis of simple kinetics only. From the known reaction rate we can calculate that at ½ atm. in an equal molar mixture of hydrogen and ethylene, 40 mol. of ethylene will be hydrogenated per second per single lattice space. According to figure 4 there are $12{\cdot}5 \times 10^{18}$ lattice spaces available in the film under consideration. The film will therefore hydrogenate $5 \times 10^{20}$ ethylene mol. or $8{\cdot}25 \times 10^{-4}$ g.mol./sec. This amount has to be carried into the interior through $4{\cdot}4 \times 10^{11}$ canals of $8{\cdot}4 \times 10^{-6}$ cm. diameter and of average length of $4{\cdot}35 \times 10^{-4}$ cm. Though the diameter of the canals and the mean free path of the molecules at ½ atm. of equimolar gas mixture are of the same order of magnitude, it can be shown that the gas flow through the canals is essentially of molecule nature, and that Knudsen's law (1909) for molecular flow will hold very closely. In calculating by this law the average pressure difference necessary between the outside and the interior of the film in order to supply $5 \times 10^{20}$ hydrogen mol. per sec., and the same amount of ethylene molecules, we find an average partial pressure difference of about 0·5 mm. for hydrogen and about 2 mm. for ethylene. The maximum pressure differences between the outside and the most inner parts of the film will therefore be 1 and 4 mm. for hydrogen and ethylene respectively which is roughly 0·5 and 2 % of the partial pressure of ½ atm. of each of the gases.

Since the reaction is first order with respect to hydrogen and since a slightly lower partial pressure of ethylene will increase rather than decrease the reaction rate, we may conclude that within the experimental error and under the simplifying assumption of straight canals the observed activity of the catalyst interior is satisfactorily explained from the standpoint of simple kinetics.

The same may be said for the apparently instantaneous adsorption of most of the gases studied. If the adsorption is irreversible or if the time for which a molecule is adsorbed is very long compared with the time necessary to cover the interior surface, we may use a formula derived by Clausing (1930) for this very problem of non-stationary molecular flow into a canal. According to this approximate formula the time $t$ necessary to cover the surface of the canal with molecules is

$$t = \frac{3L^2}{8fr^2N},$$

where $L$ is the length and $r$ the radius of the canal, $f$ the surface taken up by an adsorbed molecule, and $N$ the number of molecules which collide from the gas phase per second with the unit area of the wall.

To cover the interior surface of our film with hydrogen atoms, $6 \cdot 25 \times 10^{18}$ hydrogen molecules are needed which with a stationary pressure outside the film of 0·5 mm. will be supplied according to Clausing's formula in about $10^{-3}$ sec. For ethylene molecules, which cover four lattice spaces each, the time required would be twice as long. The time required to build up the gas pressure in the interior of the film to the pressure outside the film may be easily calculated and is negligibly small as compared to the time required to supply the molecules for the adsorbed layer.

It should be mentioned that during the reaction the ethane molecules formed will leave the interior of the film by setting up a pressure difference which is, of course, close to that of ethylene but in the opposite direction. When, however, the ethane molecules leave the film it can be readily shown that diffusion alone is not able to provide for their transport away from the film and that artificial agitation is necessary, a fact which has been amply verified by experiment, and which has necessitated the use of a circulation turbine.

We hope to take up the problem of gas diffusion into our films in greater detail after measurements of their density have been made.

### *Orientation and catalytic activity*

The evidence which has been presented, showing that nickel films with (110) orientation possess five times the activity of unoriented films, brings up at once the very interesting question as to the actual seat of activity. The developments of the last few years leave investigators divided into two camps: adherents to the active centre theory propounding the non-uniformity of catalytic surfaces and believers in the uniformity of catalytic surfaces. There seems to be no doubt that surfaces of predominantly uniform activity exist; yet it must be remembered that certain experimental procedures may indicate such uniformity where none really exists. The poisoning experiments of this investigation, for instance, could be interpreted as proving uniform activity if it were not for the fact that the poisons used appear to be definitely non-selective. The correlation between activity and orientation (and to some extent also the sintering experiments) show that the surfaces are in reality not uniform. Even if we assume that oriented films are uniformly active because (110) planes only are exposed to the reacting gases we are forced to conclude that the crystallites of unoriented films either expose to the reacting gases other planes which are less active or that they expose a small fraction of active (110) planes together with a large fraction of planes which are less active or entirely inactive. The active centres or "active regions" would in this case coincide with a homogeneous, definite crystal lattice rather than with extra-lattice atoms or related atomic arrangements which put the emphasis on crystal or field distortions.

The (110) plane of nickel contains the distances $a = 3{\cdot}51$ A and $a/\sqrt{2} = 2{\cdot}48$ A (see figure 17). Although the distance 3·51 A occurs also in the (100) plane it is not only less frequent in this plane but the adsorption of a hydrogen molecule by adiabatic expansion of its two atoms to the distance 3·51 A is made less probable in the (100) plane on account of repulsion and exchange forces exerted by the two neighbouring atoms. This has been discussed by Okamoto, Horiuti and Hirota (1936), who have calculated activation energies of the hydrogen adsorption for pairs of adjacent metal atoms in the three main crystal planes of nickel and have come to the conclusion that the activation energy is lowest for the (110) plane. Their calculations are based on Sherman and Eyring's (1932) quantum mechanical treatment of the hydrogen adsorption on a pair of carbon atoms which showed that a most favourable carbon-carbon distance exists (about 3·6 A) for which the activation energy of adsorption is a minimum.

It is, however, difficult to decide from our experimental evidence whether the process of adsorption, reaction or evaporation is faster on the (110) plane and is thus able to account for the observed difference in reaction rate. We have seen that the chemisorption of hydrogen is practically instantaneous on both oriented and unoriented films, indicating that the activation energy is very low in both cases and that the proper spacing is possibly of less importance from this standpoint than it may be from the standpoint of the reaction itself especially in the light of recent investigations by Farkas (1940), which indicate that the two hydrogen atoms are added to the double bond simultaneously. Even then the adsorption of hydrogen can still remain the slow and rate-determining process as suggested by the kinetics of the hydrogenation reaction and more directly by recent work of Twigg and Rideal (1939) and Farkas (1938).

Work is under way to investigate more specifically the relative activity of the different crystal planes. This may be done indirectly by seeking small differences in the activation energy of the hydrogenation reaction which has been found in agreement with earlier work to be about 10 kcal. If the reaction proceeds on different planes with different activation energies such a difference in activation energy should be observable though the difference will be small. If, on the other hand, the reaction proceeds on the (110) plane predominantly, and if this plane is simply five times less abundant in the unoriented film, no difference in activation energy is expected. Measurement of the heat of adsorption would also be very desirable in this connexion. A more direct way is also being attempted. Single crystal films of palladium which show (100) planes parallel to the backing have been successfully obtained by evaporating palladium on to rocksalt cleavage planes. Figure 18 (plate 2) shows an electron diffraction pattern obtained by grazing incidence of the beam from a film several thousand atoms thick which was obtained by evaporating palladium on to a rocksalt cleavage plane at about 350° C. Figure 19 (plate 3) shows an X-ray pattern of another film (20,000 atoms thick) still on its rocksalt base, the beam being normal to the film. Figure 20 (plate 3) shows the X-ray pattern of the film itself after the rocksalt was dissolved. It is seen that the palladium single crystal film is rather strained. A fuller discussion of these films will be given in a later communication when the catalytic experiments have progressed further.*

From the standpoint of the theory of crystal growth, Stransky (1921) has pointed out that there is a fundamental difference between ionic crystals and homopolar crystals. Whereas the former grow from sharp corners and edges, the planes filling up subsequently, the latter grow from the centre of the planes and leave, instead of edges and corners, surfaces of higher specific surface energy, possibly (110) planes or possibly planes of even higher indices which will serve as active regions. These surfaces will have a small area, corresponding to their high surface energy unless they are forcibly produced as in our case by evaporation in a gas.

### *Bearing of the results on the general problem of adsorption*

The results of adsorption measurement are of particular interest from the standpoint of the work of Roberts (1935). Roberts has developed a direct method of measuring the adsorption of certain gases on a bare tungsten surface by using the change of the accommodation coefficient of neon on a bare surface and a surface covered with an adsorbed film. He found that chemisorption of hydrogen, for instance, takes place very rapidly at extremely low pressures ($10^{-4}$ to $10^{-5}$ mm.) and even at very low temperature (79° K), and he has rightly pointed out that this behaviour is not in agreement with the conception of activated adsorption which is generally assumed to govern this adsorption phenomenon. The present work corroborates these views for surfaces more than a million times greater than those of Roberts. Furthermore, these surfaces are typical hydrogenation catalysts for which the application of Roberts's findings on tungsten has been repeatedly questioned in the literature. Roberts has already pointed out that if the term 'chemisorption' be reserved for an irreversible adsorption as observed by him and in the present work, it must be stressed that this adsorption is not synonymous with activated adsorption, though many cases of activated adsorption may also be chemisorption. Roberts has also expressed the suspicion that activated adsorption of hydrogen, as observed on reduced metal oxide catalysts, very likely may be an effect of residual oxygen which by slow reaction with hydrogen simulates a slow adsorption. Even this assumption is not fully necessary, as we have been able to show that a freshly adsorbed layer of oxygen on nickel will prevent immediate hydrogen adsorption but, upon standing for half a day in high vacuum, will have diffused into the metal interior far enough to allow the adsorption of a complete hydrogen layer. Furthermore, Roberts has shown that a diatomic gas like hydrogen when admitted to the tungsten surface will leave about 8 % of the lattice spaces empty. This again is in agreement with our observation according to which about 20 % of the hydrogen adsorbed at 0·1 mm. and room temperature may be readily pumped off. It seems likely that comparatively loosely bound molecules of hydrogen are adsorbed on the empty single spaces which would account for at least 16 % of the total amount adsorbed. In this case, also, the measurements of heats of adsorption which we have planned are very desirable.

---

* These experiments were carried out in the latter part of 1938. Independently S. Fordham and R. G. Khalsa (1939) have reported the same method of obtaining palladium single crystals. Earlier literature is to be found in their paper.

Mr F. Rust has collaborated during the earlier stages of this work and Mr W. A. Cole has assisted with the adsorption measurements during later stages. Grateful acknowledgement is made to the directors of the Shell Development Company for permission to publish this work and especially to Dr E. C. Williams for his continued interest in its progress.

## REFERENCES

Ablesova, K. and Roginsky, S. 1935 *Z. phys. Chem.* **174**, 449.
Anderson, P. A. 1939 *Phys. Rev* **56**, 850.
Beeching, R. 1936 *Phil. Mag.* **22**, 938.
Bredig, G. and Allolio, R. 1927 *Z. phys. Chem.* **126**, 41.
Brück, L. 1936 *Ann. Phys., Lpz.*, **26**, 233.
Clausing, P. 1930 *Ann. Phys., Lpz.*, (v) **7**, 520.
Emmett, P. H. and Brunauer, S. 1937 *J. Amer. Chem. Soc.* **59**, 310.
Farkas, A. 1939 *Trans. Faraday Soc.* **35**, 906.
Farkas, A. and L. 1938 *J. Amer. Chem. Soc.* **60**, 22.

Finch, G. I. and Ikin, A. W. 1934 *Proc. Roy. Soc.* A, **145**, **551**.
Finch, G. I., Murison, C. A., Stuart, N. and Thomson, G. P. 1933 *Proc. Roy. Soc.* A, **141**, **414**.
Finch, G. I., Quarrell, A. G. and Wilman, H. 1935 *Trans. Faraday Soc.* **31**, **1050**.
Fordham, S. and Khalsa, R. G. 1939 *J. Chem. Soc.* p. **406**.
Germer, H. L. 1935 *Rev. Sci. Instrum.* **6**, **138**.
Griffin, C. W. 1939 *J. Amer. Chem. Soc.* **61**, **270**.
Kirchner, F. 1932 *Z. Phys.* **76**, **576**.
Knudsen, M. 1909 *Ann. Phys., Lpz.*, (IV) **28**, **75**.
Nelson, R. H. 1937 *J. Chem. Phys.* **5**, **252**.
Okamoto, G., Horiuti, T. and Hirota, K. 1936 *Sci. Pap. Inst. Phys. Chem. Res., Tokyo*, **29**, **223**.
Roberts, J. K. 1935 *Proc. Roy. Soc.* A, **152**, **445**.
Sherman, A. and Eyring, H. 1932 *J. Amer. Chem. Soc.* **54**, **2661**.
Stransky, I. 1921 *J. Phys. Chem.* B, **11**, **342**.
Twigg, G. H. and Rideal, E. K. 1939 *Proc. Roy. Soc.* A, **171**, **944**.
White, T. A. and Benton, A. F. 1931 *J. Phys. Chem.* **35**, **1784**.

---

# On the mechanism of boundary lubrication

## I. The action of long-chain polar compounds

BY OTTO BEECK, J. W. GIVENS AND A. E. SMITH

(*Communicated by J. W. McBain, F.R.S.—Received* 4 *April* 1940)

[Plate 4]

The effect of long-chain polar compounds on the coefficient of kinetic friction under boundary conditions has been studied using the Boerlage four-ball friction apparatus in various modifications. With steel balls of the highest grade, coefficients of friction for a great number of lubricants were measured as a function of the relative velocity of the rubbing surfaces.

The structure of thin films of these lubricants rubbed on polished mild steel surfaces was investigated by electron diffraction.

It was found that lubricants showing little or no surface orientation had a constant coefficient of friction of about 0·1 over the available velocity range from 0 to 1 cm./sec. With oils which showed high surface orientation imparted by addition of long-chain polar compounds, a sudden decrease of the coefficient of the friction was observed at various velocities of the sliding surfaces, depending upon the compound used. Investigation of a great number of compounds gave a direct correlation of this effect with molecular orientation: those compounds causing the effect to occur at the lowest velocities were found to be most highly oriented with their carbon chains most nearly perpendicular to the surface. Since such a change of the coefficient of friction can only be explained by the wedging of oil under the surface (oil drag), the effect was termed the 'wedging effect' leading to a type of lubrication which may be called 'quasi-hydrodynamic'.

By measuring the electrical resistance between the sliding surfaces it was found that the regions of sudden decrease of the coefficient of friction correspond to a change from metallic contact to extremely high resistance.

The investigation shows that long-chain polar compounds act primarily by inducing the 'wedging effect' and not by giving a direct protection to the surface.

## 1. INTRODUCTION

Since the early formulation of the law of Amontons (1699) numerous studies of kinetic friction under boundary conditions have been made, but it is only lately that the work of Langmuir (1934) on frictional properties of built-up films on solids, the electron diffraction work of Murison (1934) and, in particular, the recent work of Bowden and collaborators (1934–1939) on the discontinuous nature of sliding friction and their investigation of contact areas and of the mechanism of polish, have materially advanced our understanding of the phenomenon of sliding friction.

In the presence of a lubricant boundary lubrication (sometimes also called 'non-viscous' or 'thin film' lubrication) occurs under high pressures and low-sliding velocities, and is characterized by coefficients of friction which are practically independent of viscosity and sliding velocity. It has long been known, however, that different oils have different coefficients of friction under boundary conditions, and that oil-soluble compounds having long carbon chains and polar groups at one end are especially effective in reducing the coefficient of boundary friction when they are added to highly refined mineral oil (white oil).

It has also been generally expected that any material that would reduce the coefficient of boundary friction would also reduce the rate of wear, and a great deal of work has been done on a variety of friction machines in the hope of finding some compounds that would reduce friction to an extraordinary degree. But, owing to widely varying designs of the machines, the results of the different investigators cannot be correlated. This greatly adds to the difficulties in interpreting the results in terms of simple physical concepts.

It seemed clear at the outset that the reduction of friction produced by long-chain polar compounds must be due to their adsorption on the rubbing surfaces, but there appeared to be considerable speculation as to the nature of the adsorbed films and the mechanism of their action. It is this ignorance which has led to vague and confusing terms like 'oiliness' and 'film strength' which, undoubtedly, will disappear as our knowledge of the properties of oils and of liquids in general increases.*

Moreover, it is now quite certain that so-called 'oiliness compounds' which lower the coefficient of friction under boundary conditions do not necessarily lower the rate of wear, but, on the contrary, often increase the rate of wear.

In order to elucidate more completely the mechanism of boundary lubrication and especially the action of long-chain polar compounds, the structure of adsorbed oil films was studied by electron diffraction and their coefficients of friction were studied as a function of the sliding velocity. These observations have shown a new frictional effect, not previously reported in the literature, which may be directly correlated with the orientation of the adsorbed lubricant film.

## 2. APPARATUS AND EXPERIMENTAL TECHNIQUE

### (a) *Electron diffraction experiments*

The electron diffraction camera used in this work was similar in design to that described in detail by Germer (1935). The reflexion method was used, and nearly all the surface films were produced on highly polished mild steel plates by dipping the plates into the lubricant and rubbing with lens paper until all excess lubricant was completely removed. Most substances examined were pure long-chain polar compounds or other pure addition agents of which the majority were solids at room temperature and had to be applied to the steel plate at temperatures slightly above their melting point. However, several lubricant-like petroleum fractions and solutions of addition agents in white oil were also studied.

### (b) *Measurements of coefficients of friction*

The principal apparatus chosen for the study and analysis of sliding friction was the four-ball top developed in its original form by Boerlage and Blok (1937) on the four-ball principle which was used previously by the same authors in their four-ball apparatus for testing extreme pressure lubricants. This apparatus, in which a single ball rotates under variable loads on a support formed by three similar balls clamped together in an oil cup (see figure 1), is particularly adaptable to measurements of coefficients of friction at low-sliding velocities of 0–1 cm./sec. and high pressures of a few thousand kg. per cm.$^2$ or higher. Assuming that the coefficient of friction was constant over the small velocity range, Boerlage and Blok simply measured the time required for the frictional force to stop the top-like rotor attached to the upper ball, after the rotor was given definite initial angular velocity by a falling weight mechanism. In this case the coefficient of friction $f$ can be calculated by the formula:

---

* See also Givens (1939).

$$f = C(n/t^2),$$

where $n$ is the number of revolutions, $t$ the running time of the top and $C$ a constant depending on the weight and the moment of inertia of the rotor and the size of the balls.

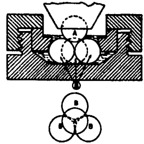

FIGURE 1. Four-ball bearing.

Preliminary experiments of the present investigation had shown, however, that the deceleration of the top was not always constant over the whole velocity range. A careful analysis of the motion of the rotor was made therefore by means of the revolving drum recorder which is shown together with the modified four-ball top in figure 2. The recorder served as a chronograph and received its impulses from a photo-electric cell, the illumination of which was interrupted by the motion of the rotor. The impulses were recorded by a stylus on waxed paper stretched on the outside of the drum. From these records the angular displacement was plotted against time; and from the plots instantaneous values for the velocity and deceleration were readily obtained by graphical differentiation. The

FIGURE 2. Boerlage four-ball top and photo-electric chronograph.

coefficients of friction were then calculated by equating the observed decelerating torque to the friction moment. The results were finally expressed in plotting coefficients of friction against velocities.

To supplement the four-ball top which allowed deceleration experiments only, an apparatus was used in which a highly polished steel cylinder was sliding on four supporting clamped balls as shown in figure 3. Discs were attached to the ends of the cylinder increasing its moment of inertia, and cords were wound in grooves on the periphery of the discs so that the rotation of the cylinder could be accelerated by weights hanging on the cords. The motion was again analysed by means of the chronograph and the coefficients of friction were calculated and related to the angular velocity as for the four-ball top.

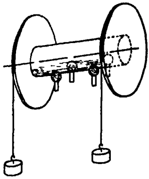
FIGURE 3. Acceleration apparatus.

### (c) *Measurement of electrical conductivity of oil films under boundary conditions*

The conductivity measurements of boundary films were carried out with the four-ball bearing. A motor-driven modification of the Boerlage four-ball top was used for this purpose. The apparatus is shown in figure 4. The rotor can be brought to any desired speed and is able to rotate freely after the driving mechanism is disengaged. For kinematic studies of boundary friction the rotor's deceleration is observed by means of a photo-electric chronograph that receives its light impulses via a decagonal mirror attached to the upper part of the rotor. The three lower balls were insulated and provided with separate contacts. The measuring current passed from one lower ball through the top ball and back to a second lower ball. The resistance measurements were made by means of an A.C. operated direct-reading electron-tube ohm meter of high sensitivity. The measuring potential was always kept below 0·1 V.

### (d) *Method of cleaning metal surface*

In these experiments cleanliness is of paramount importance in order to obtain reproducible results. Excessive oil is first removed with solvents. The balls, chuck, and all stationary parts near the friction elements are then boiled for 10 min. in a solution of 70 g. of potassium hydroxide in

1 litre of isopropyl alcohol. The parts are rinsed in distilled water and finally in boiling isopropyl alcohol. After the last rinsing the parts should not be touched by hand.

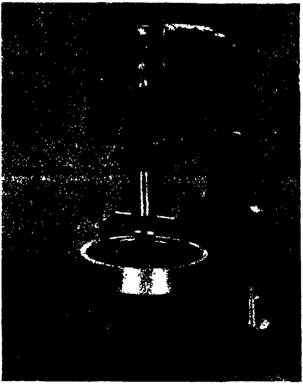

FIGURE 4. Modified four-ball top (serving also as wear apparatus).

## 3. EXPERIMENTAL RESULTS

Figures 5 and 6 show typical curves obtained with the four-ball top. These curves are to be read from higher to lower angular velocities since they represent deceleration experiments The curves show an effect which is entirely unexpected and new for boundary lubrication and which consists of a rapid decrease of the coefficient of frictions at the initial higher velocities. At certain critical and easily reproducible velocities the curves bend over sharply and the coefficients of friction become constant, that is, independent of velocity for the rest of the run. White oil* and ricinoleic acid do not show this effect. The other curves can be characterized by two constants. the steady value of the coefficient of friction and the critical velocity at which the coefficient of friction falls off rapidly. If the initial

---

* White mineral oil, U.S.P. Viscosity at 100° F, 349·3 S.U.S. Viscosity at 210° F, 51·6 S.U.S. Viscosity index, 65·0. Density at 60° F, 0·8876.

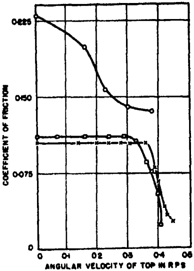

FIGURE 5. ○ white oil, □ white oil + 1% oleic acid, × U S.P. oleic acid.

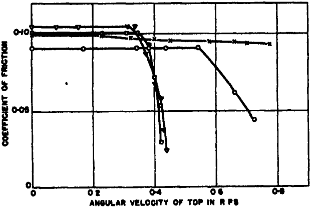

FIGURE 6 ○ castor oil, × ricinoleic acid, ▽ fatty acid fraction from castor oil; □ 1% stearic acid in ricinoleic acid.

velocity of the top is lowered beyond the critical velocity, the effect is not observed, if the top is started at much higher velocities, a rather unsteady state of rapid and irregular fluctuation of the coefficient of friction is observed. The measurements presented were started therefore at velocities only slightly higher than the critical velocity.

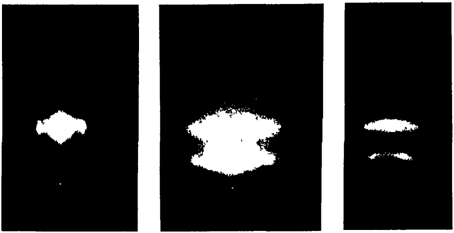

1 2 3

FIGURE 8. Electron diffraction photographs of lubricant films rubbed on polished mild steel. 1, tetratriacontane, 2, ethyl cerotate, 3, ferric stearate

In order to be certain that the observed effect was not a transient due to the rapid initial acceleration of the top, some experiments were made with the second friction apparatus described in section 2 (*b*) which allows slow acceleration. A typical curve obtained from this apparatus is shown in figure 7. Data were taken during both acceleration and deceleration. Although the low value of friction is obtained in this case by slow acceleration, the deceleration part of the curve is of striking similarity to the curves obtained by the four-ball top.

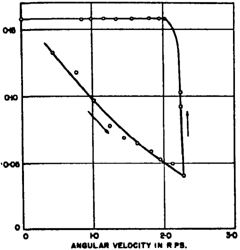

FIGURE 7.

From these results it appears likely that the observed effect of low coefficients of friction at higher velocities is produced by oil drag under the surface and that this wedging of oil is a property which is imparted to the oil by a certain surface activity. The *wedging effect* should occur, however, only if material is available to be wedged under the surface, and the effect should disappear if a well-rubbed thin film is used. It has already been contended by Langmuir (1934) and has lately been proven by Germer and Storks (1939) that such rubbed films consist essentially of a monolayer. Experiments with the four-ball top under these conditions do not show the decrease of the coefficient of friction at higher velocities under any circumstances. It is significant, however, that the steady state coefficient of boundary lubrications obtained with the oil flooding the balls is practically unaltered with rubbed boundary films. This is further proof that boundary conditions are actually prevailing at low velocities with the bulk of the lubricant present.

Furthermore, changing the viscosity of the white oil by blending it with non-polar pure polyisobutylene had little effect on the critical velocity and the steady state coefficient of friction. Blends containing 1% oleic acid and with their viscosities differing by a factor 100, show only about 10% change in the critical velocity and in the coefficient of pure boundary lubrication. These experiments show clearly that differences in bulk properties of the lubricant have only negligible effects on the wedging effect.

However, a study of the surface structure of the lubricant films revealed that all substances showing the wedging effect at low velocities exhibited a high degree of orientation of their surface films. White oil and ricinoleic acid which as shown in figures 5 and 6 do not exhibit the wedging effect, also do not show any orientation. A particularly extensive study was made in the case of ricinoleic acid with both rubbed and vapour-condensed films. In no case was orientation observed, although this fatty acid was undoubtedly adsorbed on the surface as the low coefficient of boundary friction (compared with white oil) shows. It is likely that these molecules, because of the hydroxyl group near the centre of the chain, are adsorbed lying flat in an irregular manner. White oil showed always high but very irregular coefficients of friction. It will be shown later that its critical velocity is about six times higher than that of a 1% solution of oleic acid in white oil.

All substances showing the wedging effect also showed orientation. The lowest critical velocities were observed with those long-chain polar compounds for which the electron diffraction experiments showed the highest degree of orientation, the carbon chains extending out from the surface either perpendicular or slightly inclined. Figure 8, plate 4, gives a few examples of the type of patterns obtained.

It seems to be unnecessary for the carbon chains to be anchored to the metal surface by polar groups in order to give rise to the wedging effect. Long-chain non-polar hydrocarbons like tetratriacontane are also able to induce the effect at room temperature. A rubbed film of this material shows a high degree of orientation with the chains perpendicular to the surface. The same is true for stearone, a long-chain ketone with the oxygen group in the centre. At higher temperatures, however, a marked difference between molecules with and without a polar group on one end was observed. The difference is most striking in electron diffraction experiments in which the specimen holder was heated during the experiment. At a temperature close to the melting point of stearone, all molecules adsorbed with their long chains perpendicular to the surface evaporated, leaving, however, some molecules on the surface which may have been impurities or stearone molecules which were adsorbed lying flat. In the case of tetratriacontane the same procedure led to a complete evaporation of the molecules at temperatures close to their melting point. The completeness of evaporation is indicated by the appearance of a clear diffraction pattern belonging to the iron backing. Most of the polar compounds are tenaciously adsorbed at still higher temperatures (about 200° C). In case of stearic acid, for instance, a fairly thick film was applied and gave a diffraction pattern of inclined bands with well-defined spots characteristic of oriented imperfect crystals. This film was heated slowly and a series of fifteen exposures was

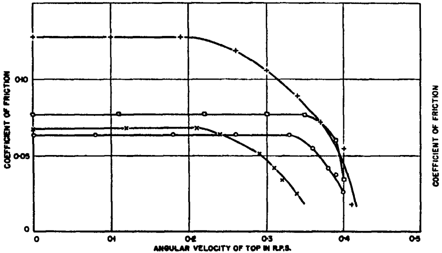

FIGURE 9. ○ tetratriacontane (80° C); × stearic acid (80° C); + octadecyl alcoho (130° C); □ methyl stearate (150° C).

taken over the temperature range of 26–180° C. As the temperature was increased the spot pattern faded and the pattern characteristic of adsorbed stearic acid molecules gradually appeared. The spot pattern had disappeared completely at 50° C, but the pattern of curved bands was still persistent at 110° C, although by that time the plate had been heated for 2 hr. in high vacuum. A further increase in temperature caused the bands to become fainter and more diffuse, and the ring pattern of the iron backing increased in intensity. There is an unmistakable correlation between these findings and the fact that at higher temperatures low critical velocities for the wedging effect are obtained only for compounds which are strongly adsorbed at these temperatures with their carbon chain extending out from the surface. Figure 9 shows the wedging effect for some pure compounds at elevated temperatures. The critical velocity for tetratriacontane would fall out of the range of these experiments for temperatures higher than 80° C.

In view of the abrupt drop in coefficient of friction in these experiments, it seemed possible that the critical velocities could be found through electrical resistance measurements. Method and apparatus have been described in section 2 (c). It was found that if the rotor was brought up to a high speed and was then disengaged from the driving motor the resistance was that of an open circuit (with the apparatus used 10,000 ohms or greater). As the speed became lower, the resistance decreased slowly until upon reaching about 250 ohms violent oscillation occurred for a moment after which the resistance suddenly fell to very low values. In identifying the speed of the rotor at which the oscillations occur with the critical velocity, satisfactory agreement is obtained with the methods using the graphical evaluation of the coefficient of friction. The comparison is shown in table 1.

TABLE 1. COMPARISON OF CRITICAL VELOCITIES DETERMINED BY THE ELECTRICAL AND GRAPHICAL METHODS FOR VARIOUS LUBRICANTS

| | Critical velocity R.P.S. | |
|---|---|---|
| Lubricant | Electrical | Graphical |
| White oil | 2·25 | * |
| Pennsylvania bright stock | 0·30 | 0 28 |
| White oil + 1% Pennsylvania bright stock | 0·53 | 0·36 |
| Motor oil S.A.E. 20 | 0·60 | 0·35 |
| Castor oil | 0·83 | 0·50 |
| Light Pennsylvania neutral | 0·90 | * |

* Critical velocity too great to measure on the four-ball top, > 0·60.

Data by the electrical method, showing the effect of various compounds in lowering the very high critical velocity of pure white oil, are shown in table 2.

TABLE 2. THE EFFECT OF VARIOUS POLAR COMPOUNDS IN LOWERING THE CRITICAL VELOCITY OF WHITE OIL. 1% SOLUTIONS

| Compound added to white oil | Critical velocity R.P.S. |
|---|---|
| None | 2·42 |
| Ethyl cerotate | 0·57 |
| Heptadecyl tetrahydronaphthyl ketone | 0·17 |
| Lauryl β-naphthyl ether | 1·13 |
| Trincinolein | 1·10 |
| Chlorinated ethyl oleate | 2·40 |
| Lauramide | 2·42 |

It should also be mentioned that all experiments were carried out with the same grade of highly polished steel balls. A certain degree of polish is necessary to induce the wedging effect. Rough surfaces will not show the effect at all, whereas polished surfaces which in addition have been run in with a chemical polishing agent like tricresyl phosphate (see Part II) showed the wedging effect even to the lowest measurable velocities of the rubbing surfaces.

## DISCUSSION

Earlier observations (Murison 1934, Clark, Sterrett and Lincoln 1936, and others) which had shown that many effective lubricants have oriented surface films had led to the widespread belief that such films acted themselves by protecting the surfaces and were behaving much like two carpets sliding over each other with their piles lying flat at the place of actual contact. The X-ray evidence even showed that in some cases the oriented layers were hundreds of molecules thick, although it appears quite certain that under severe conditions none but the first layer is bound to the substrate with forces strong enough to withstand the great shearing stresses to which such layers are submitted under sliding conditions.

The monomolecular layer, however, extends into space far less than the irregularities of even the best machined metal surfaces. Since such surfaces carry the load on isolated spots only, the actual pressures at these spots are so high that not even the first monomolecular layer can be expected to withstand the forces which prevail when the surfaces slide over each other. Furthermore, the high temperatures expected at the local points of contact will cause decomposition of the molecules caught under them, and the atoms of the polar groups (oxygen, etc.) will react with the metal and form a high melting corrosion product. It is clear that under these conditions the wedging effect will not operate. If, however, the surfaces are highly polished, that is if the load is distributed evenly over the apparent surface of contact, sliding can take place without immediate disruption of the surface film. Under these conditions the wedging effect will occur and it is evident that the full benefit of this effect can be expected only if the surfaces are initially brought into a high state of polish and are maintained in this state under operation. Most of the friction reducing polar compounds are themselves not able to produce or to maintain such a state and have therefore in most cases failed to be effective wear-prevention agents.

In Part II of this series addition agents will be discussed which have the ability to polish the metal surface and to maintain the polish. This class of compounds, which evidently is more important, acts through a mechanism totally different from the action of long-chain polar compounds, but it will be shown that the latter compounds, if introduced with polishing agents, are able to reduce wear by at least a factor of two.

It is a pleasure to acknowledge the interest of the directors of the Shell Development Company, especially of Dr E. C. Williams, in this work.

## REFERENCES

Amontons 1699 *Mém. Acad. Roy. Sci. Paris*, p. 206.
Boerlage and Blok 1937 *Engineering*, **144**, 1.
Bowden and Hughes 1937 *Proc. Roy. Soc.*, A, **160**, 575.
— — 1939 *Proc. Roy. Soc.* A, **172**, 263.
Bowden and Leben 1939 *Proc. Roy. Soc.* A, **169**, 371.
Bowden and Ridler 1936 *Proc. Roy. Soc.* A, **154**, 640.
Bowden and Tabor 1939 *Proc. Roy. Soc.* A, **169**, 391.
Clark, Sterrett and Lincoln 1936 *Industr. Engng. Chem.* **28**, 1318.
Germer 1935 *Rev. Sci. Instrum.* **6**, 138.
Germer and Storks 1939 *Phys. Rev.* **55**, 648.
Givens 1939 *Industr. Engng. Chem.* **31**, 1135.
Langmuir 1934 *J. Franklin Inst.* **218**, 143.
Murison 1934 *Phil. Mag.* **17**, 201.

# On the mechanism of boundary lubrication

## II. Wear prevention by addition agents

By Otto Beeck, J. W. Givens and E. C. Williams
*Shell Development Company, Emeryville, California*

(*Communicated by J. W. McBain, F.R.S.—Received* 4 *April* 1940)

[Plates 5, 6]

If two metal surfaces slide over each other in the presence of a lubricant and under high load, high pressures and temperatures prevail at those isolated spots which actually carry the load, leading to wear and possibly to breakdown.

The action of wear preventing agents under these conditions has been studied in detail and it has been found that such agents are effective through their chemical polishing action, by which the load becomes distributed over a larger surface and local pressures and temperatures are decreased. Especially effective are compounds containing phosphorus or other elements of group V of the periodic system. These have been found to form a metal phosphide or homolog on the surface which is able to alloy with the metal surface, lowering its melting point markedly, and by this action aiding greatly in maintaining a polish.

The wear experiments were carried out with a highly sensitive and accurate method which uses metal-plated steel balls as its sliding elements. Under the experimental conditions additions of 1·5 % triphenyl phosphine or triphenyl arsine in white oil gave wear prevention factors of 7·2 and 12·2 respectively (relative to pure white oil). A further addition of 1 % of a long chain polar compound is able to double the wear prevention factor obtained with the polishing agents and wear prevention factors as high as 17·6 have been observed. The specifically physical action of the long-chain polar compounds is discussed in the preceding paper.

### 1. Introduction

Engineering developments of the last ten years have called for lubrication under more and more severe conditions both with respect to temperature and pressure. These demands have been met, up to the present, by the purely empirical method of adding small amounts of certain chemicals to the oil in order to impart certain desired properties. One of the most important of these properties is the prevention of wear and in extreme cases of seizure and breakdown. Excessive wear, if truly mechanical, will in all cases eventually lead to seizure unless the welding of the surfaces is prevented by anti-welding agents, which of necessity are corrosive in order to create non-metallic bodies between the surfaces. Such remedy will prevent seizure but will add 'corrosive wear' to the mechanical wear after the latter has caused a sufficient temperature increase to bring about rapid corrosion. Anti-welding agents are often corrosive even at room temperature.

It has already been pointed out in Part I that under severe conditions of high pressure (which may be intentional as well as accidental) no truly fluid film of the lubricant will exist between the sliding surfaces, and the term of 'boundary lubrication' has been widely adopted for this condition. Boundary or non-hydrodynamic lubrication is, therefore, readily distinguished from fluid film or hydrodynamic lubrication, which takes place under maintenance of an oil film of sufficient thickness that hydrodynamic properties such as viscosity are the sole characterizations necessary. Under these conditions no frictional wear takes place. From the scientific standpoint boundary lubrication is a very elusive and complicated problem, and it is apparently for this reason that practical investigators have tried, almost at random, thousands of compounds for imparting to a given oil properties which, under boundary conditions, would prevent wear of the sliding surfaces. Almost as many positive claims have been made for wear-preventing compounds, although no clear understanding of the mechanism has been achieved in any of these cases.

Although sliding friction and mechanical wear are logically closely connected, *no significant correlation is found between the coefficients of friction and wear with various oils with and without addition agents.* Under moderate conditions the coefficient of boundary friction varies but little with pressure, temperature, and material of both the lubricant and the surfaces. The reason for this lies in the fact that wear takes place momentarily at isolated spots, which are small compared to the whole surface, and that, although these isolated spots must exhibit a higher coefficient of friction at the moment of abrasion, the resulting change for the whole system is too small to affect the over-all coefficient of friction unless refinements of the type of Bowden's 'stick-slip' method are used.

Wear is, however, an accumulative effect and, therefore, its measurement is always possible even if the rate of wear is very low. The present investigation is based on wear measurements of great accuracy and simplicity. The conceptions arrived at and the mechanism presented will be deduced and elucidated step by step. From the basic conception of a *temperature selective chemical polishing agent* we will proceed to a *eutectic theory of polish and wear prevention*, and shall finally show that the use of long-chain polar compounds in conjunction with chemical polishing agents is highly effective, although long-chain polar compounds alone are of comparatively little value from the standpoint of wear prevention.

The mechanism by which long-chain polar compounds help to prevent wear on highly polished surfaces has been discussed in Part I (preceding this paper) in detail from the standpoint of the coefficient of friction and surface film orientation.

Among the many wear-preventing agents mentioned in the literature tricresyl phosphate is very effective and has been widely used. It is for this reason that a detailed study of its action was made the starting-point of this investigation, which finally has led to a mechanism of wear prevention in no way limited to this material, but including several large groups of compounds.

## 2. APPARATUS

For the wear measurements the motor-driven modification of the Boerlage four-ball apparatus (Boerlage and Blok 1937) was used, which is described in detail in Part I, section 2 (*b*), (*c*).

Wear measurements may be made either by measuring the wear spot diameters on the stationary lower balls or by actual measurement of the quantity of abraded iron in the oil. The former method is not very accurate and applicable only if time is allowed for sufficient material to be abraded, so that the roughness of the surface has little influence on the measurements. But even then the unavoidable change in pressure and pressure distribution over the wear spot makes correlation of the measurements difficult. A third method which proved extremely sensitive and reproducible consisted in electrolytically plating the steel balls with a very even thin layer of the metal to be investigated, and to run the plated balls in the wear apparatus until the track on the upper rotating ball was worn through to the steel. The time elapsed could be measured very accurately and was found to be reproducible within 1%.

A few experiments were carried out by pressing a metal rod or block against a rotating steel disk.

## 3. WEAR EXPERIMENTS WITH TRICRESYL PHOSPHATE ON STEEL SURFACES

The experiments consisted in running the four-ball wear apparatus with ½ in. steel balls in solutions of tricresyl phosphate in white oil* for 2 hr.

---

* White Mineral Oil U.S.P.:

| | | |
|---|---|---|
| Viscosity at | 100° F | 349·3 S.U.S. |
| | 210° F | 51·6 S.U.S. |
| Viscosity index | | 65 |
| Density at | 60° F | 0·8876 |

at 14·4 kg. load and determining the wear-spot diameters and quantities of abraded iron. The data obtained are shown in figure 1.

These results show clearly that the measurement of wear-spot diameters is too insensitive for small amounts of wear. In this particular case there is not even a deviation beyond the experimental error from the theoretical diameter of the contact area of 0·0154 cm., which may be calculated from the elastic properties of the steel and the geometrical set-up of the four balls (Timoshenko 1934). The chemical method, however, shows the important result that there is an optimum concentration of about 1·5% of tricresyl phosphate for which the wear is a minimum under the given conditions. The numerical wear decrease is very considerable and, as seen in figure 1, the addition of 1·5% tricresyl phosphate to white oil causes a wear reduction to 20% of the original value. We may express this by simply stating that the new combination has a 'wear reduction factor' 5. This term will be used throughout this paper.

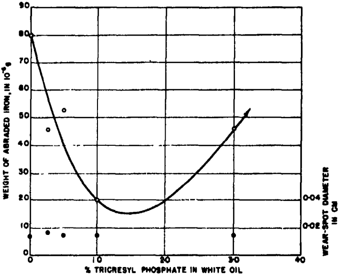

FIGURE 1

## 4. THE CONCEPT OF A TEMPERATURE SELECTIVE POLISHING AGENT AND ITS EXPERIMENTAL VERIFICATION

The finding of a pronounced wear minimum for the addition of tricresyl phosphate, together with the fact that pure tricresyl phosphate showed excessively high wear, suggested at once that this material acted by corrosive action rather than by protective action. It is well known that the most carefully machined metal parts have a microscopic roughness and that, if two such surfaces are pressed against each other, the load is not uniformly distributed over the entire area of geometrical contact, but is carried on a number of isolated points. Bowden and collaborators have verified this in a series of beautiful experiments, and have shown that for steel surfaces the actual area of contact may be less than one ten-thousandth of the apparent area. This varies, of course, with the pressure.

It is evident, then, that if such surfaces slide over each other, the enormous pressure at the isolated points of contact will produce excessively high temperatures (see also Bowden and Ridler (1936) and Blok (1937)) at local spots followed by welding and tear and general roughening of the surfaces leading to higher and higher temperatures of the bulk of the metal and ultimately to seizure and breakdown. It is evident, too, that under such conditions adsorbed layers of, for instance, long-chain polar molecules, cannot possibly give enough protection, since the high pressures and temperatures at the isolated spots will destroy such a film instantly. But it is clear, on the other hand, that if the load were distributed better over the apparent surface, less severe conditions of pressure and temperature would prevail. In other words, if the surfaces were highly polished and could be maintained at a high polish, wear would decrease or even disappear, since the thin layer of lubricant molecules will withstand more easily the lower pressure and temperature without breakdown.*

The same general considerations will also hold if the load is so high that plastic deformation occurs. The extreme case would be that in which through plastic deformation the actual surface of contact approaches the apparent surface of contact. This is, undoubtedly, the case in the experiments with copper- and gold-plated steel balls which will be described later. Although in these cases the load is carried from the beginning by a larger surface and the extreme pressures at local spots will not be so high, the surfaces of contact will still be irregular although they may conform better. If, therefore, a tangential force is applied (sliding conditions), local pressures much higher than the normal pressure will occur, and these pressures will only disappear after the sliding surfaces have been worn plane or at least conform perfectly in the direction of sliding.

---

* In fact, Witte (1935) has described a journal bearing, the babbit metal of which was sprayed on to the surface under a large centrifugal force. The babbit metal layer was only 0·1 mm. thick and was a perfect mirror surface. Such bearing showed surprisingly good properties in rigorous wear tests.

It was suspected, therefore, that tricresyl phosphate was helping to cause and to maintain a higher polish of the surface by preferentially corroding away the isolated spots, since these are, as we have seen, initially at the highest temperature. As soon as the high points are smoothed off, the load will be distributed over a much larger surface, and consequently the temperature will decrease which in turn will make tricresyl phosphate less effective.

In figure 2 are shown corrosion experiments which clearly support this view, and which completely explain the occurrence of the wear minimum in figure 1 by simultaneous corrosion and polishing action. At low concentrations the lack of polish causes mechanical wear, and at high concentration corrosive wear becomes predominant; in between is the region of temperature selective chemical polishing action.

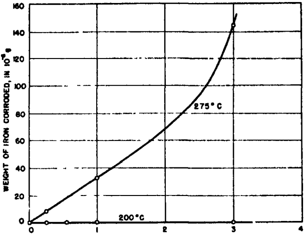

Figure 2. Corrosion of steel balls by solutions of tricresyl phosphate in white mineral oil.

The importance both of temperature and of truly chemical action has been demonstrated separately and conclusively with two further series of experiments.

The first series was carried out by pressing a weighted steel pin (2 mm. in diameter) against a flat rotating horizontal steel disk. The load applied was 10·3 kg. and the sliding velocity was 794 cm./sec. In these experiments the disk was kept running for 2 hr. with a continuous flow of oil over its surface. An oil with and without 1·5% tricresyl phosphate was used. The results are shown in figure 3 (plate 5). The pin that was lubricated with oil containing tricresyl phosphate was highly polished on part of its cross-section (it evidently had been sliding on this part only) and the original carefully machined shape was unaffected. The pin which had been lubricated with the straight oil only was peened over at its end to a clearly visible mushroom-like shape. In both cases the actual wear could not be detected by weighing the pins. However, in the case without tricresyl phosphate, the temperature must have been raised high enough to cause plastic flow of the mild-steel pin. The extraordinary roughness of this surface shows that this flow did occur in crystalline boundaries rather than in the crystallites themselves, showing that plastic flow in itself is not able to produce a polish. This proves conclusively that, in case of the addition agent, the temperature stayed very much lower because of better distribution of the load over the surface.

The second series of experiments was designed to verify the correctness of the assumption of a chemical action without which no polish and, subsequently, no wear prevention could be obtained, if this concept is right. These experiments were made in the four-ball wear apparatus with gold-plated steel balls by the method described above. Since tricresyl phosphate cannot react with gold under the experimental conditions, it should have no influence on the time required to wear the gold plate through. The two photomicrographs in figure 4 (plate 6) show the appearance of the wear track of the upper rotating ball after the underlying steel surface had just broken through. The time required was 97 min. Both experiments were made with the same set of balls, which were merely shifted in their holders to use new surfaces. Thus equal thickness was guaranteed in both experiments. These experiments prove, therefore, conclusively that tricresyl phosphate is effective by its *chemical* action. Likewise, the appearance of a tungsten pin pressed against the rotating steel disk was not influenced by tricresyl phosphate in agreement with the fact that tungsten was not even attacked in boiling tricresyl phosphate.

For completeness it should be mentioned that steel balls when heated for a few minutes in tricresyl phosphate or its solution in white oil become coated with a smooth uniform film that often shows bright interference colours. Observations on these films have shown that they are probably formed through catalytic action of traces of phosphoric acid at the metal surface, and that they consist of resinous material incapable of resisting any greater shearing stress. Their presence is merely incidental and without influence on the mechanism of wear prevention.

### 5. COMPARATIVE RATES OF WEAR WITH TRICRESYL PHOSPHATE, DIBENZYL DISULPHIDE, AND LONG-CHAIN POLAR COMPOUNDS

The great sensitivity and reproducibility of the method employed with gold-plated steel balls made it desirable to use this method whenever possible. Platings of almost all metals could be obtained, but their mechanical properties were not always suitable. Excellent platings were obtained with copper and, since experiments with this material have led to a satisfactory generalization of the mechanism of wear prevention presented, most of the following experiments were carried out with copper-plated balls in the four-ball apparatus. All experiments were made with reference to runs with white oil on each set of balls, and could easily be compared. Our wear-reduction factor became then simply the ratio of the time for the copper plate to be worn through with the oil containing the addition agent to the time for the same plate to be worn through with white oil alone. The time for the plate to wear through without addition agents was usually from 30 to 50 min. with a load of 2·2 kg. running at 120 r.p.m. and using $\frac{1}{4}$ in. balls.

A comparison of the wear-reduction factor for five specially chosen compounds is given in table 1. It is seen that the wear reduction factor for tricresyl phosphate on copper is close to the factor five found for steel. The optimum wear-prevention factor of dibenzyl disulphide,* however, is only 2·5, indicating that the particular type of corrosion is of great importance and requires further study. Long-chain polar compounds* are relatively ineffective under the same conditions, and it seems that oleic acid and stearone are superior to copper oleate by their corrosiveness towards copper at the high temperatures of the actual points of contact.

It was observed that the wear track was particularly bright and highly polished after running with tricresyl phosphate, but in all other cases was relatively dull and streaked.

### 6. THE EUTECTIC THEORY

In studying the comparative chemistry of sulphur and phosphorus, one is immediately struck by the alloy-like character of the metal phosphides. Their compositions are somewhat indefinite and are not determined by the valence of the metal. The compositions of the sulphides, on the other hand, are strictly determined by valence.

---

* Dibenzyl disulphide (see also figure 5) and the long-chain polar compounds do not show a pronounced wear minimum, their effect being independent of concentration over a wide range from a few tenths of one per cent to several per cent.

The literature also shows that in the equilibrium diagrams of iron, copper, and nickel with phosphorus sharp eutectics at rather low concentrations of phosphorus are to be found. In the case of iron, the eutectic mixture contains 10·2% phosphorus and has a melting-point of 1020° C, 515° below that of iron. The solid phases present are Fe and $Fe_3P$. In the iron-carbon-phosphorus system there is a ternary eutectic at 952° C having the composition 10% phosphorus, 3·5% carbon, and 86·5% iron. In the case of copper, the eutectic mixture contains 8·27% phosphorus and melts at 707° C, 376° below that of copper. The solid phases present are Cu and $Cu_3P$.

It is further known that heating together phosphates or phosphoric acid, a metal, such as iron or copper, and carbon gives the metal phosphide as the principal product. This was verified by refluxing iron powder with tricresyl phosphate and identifying the iron phosphide formed by its rapid decomposition by dilute acid accompanied by copious evolution of phosphine.

TABLE 1. COMPARATIVE RATES OF WEAR FOR SOLUTIONS OF TRICRESYL PHOSPHATE, DIBENZYL DISULPHIDE, AND LONG-CHAIN POLAR COMPOUNDS IN WHITE OIL. WEARING OF COPPER-PLATED BALLS ON THE FOUR-BALL WEAR APPARATUS

2·2 kg. load. 120 r.p.m.

| No. | Material added to white oil | Wear reduction factor |
|---|---|---|
| 1 | 1·5% tricresyl phosphate | 5·4 |
| 2 | 1·5% dibenzyl disulphide | 2·5 |
| 3 | 1·0% oleic acid | 1·4 |
| 4 | Stearone (saturated solution) | 1·4 |
| 5 | 1·0% copper oleate | 1·1 |

From these facts, the occurrence of an effect peculiar to phosphorus and not to sulphur can be deduced. This is the formation, by corrosive action and subsequent reduction by carbon, of a metal phosphide. The phosphide, being metallic in nature, alloys with the metal surface, lowering its melting-point markedly, and aiding greatly in maintaining a polish (Bowden and Hughes 1937). The lowering of the melting-point was easily demonstrated by heating a phosphide-coated copper surface until the melting of the surface was easily seen. A similar reduction of the melting-point by sulphur or chlorine on an iron or copper surface is not possible.

In view of this new picture of the action of tricresyl phosphate it is evident that there is no reason for using phosphorus in the form of phosphates; instead, it might be better to use it as a phosphide, thus eliminating the step involving the reduction from phosphate to phosphide. It also should be possible by aid of existing phase equilibrium data to propose other elements for addition agents (see also table 5).

Such a selection has been made and experiments with oil-soluble substances containing such elements are presented in table 2. In most cases 1·5% of the material was added to white oil, and it is shown in figure 5 that this is in fact approximately the concentration to obtain minimum wear not only for tricresyl phosphate but also for the two most effective substances, triphenyl phosphine and triphenyl arsine. The following points are of particular interest:

TABLE 2. COMPARATIVE RATES OF WEAR FOR SOLUTIONS OF VARIOUS COMPOUNDS IN WHITE OIL. WEARING OF COPPER-PLATED BALLS ON THE FOUR-BALL WEAR APPARATUS

2 2 kg. load. 120 r.p.m.

| Material added to white oil | Wear reduction factor |
|---|---|
| 1·5% triphenyl phosphine | 7·2 |
| 1·5% triphenyl arsine | 12·2 |
| 1·5% triphenyl arsenite | 9·0 |
| 1·5% triphenyl stibine | 3·0 |
| 1·2% tetrabenzyl silicon | 3·2 |
| 1·5% tetraphenyl silicon (130° C) | 1·5 |
| 1·5% triphenyl phosphine sulphide | 1·0 |
| Saturated triphenyl methoxy phosphorus dichloride | 6·8 |
| Phosphonitrilic chloride $(PNCl_2)_3$ | 7·3 |

(1) Triphenyl phosphine is more effective than tricresyl phosphate. (The respective wear-reduction factors are 7·2 and 5·4.)

(2) Triphenyl arsine is better than any other compound investigated.

(3) A chemical disturbance may completely nullify the polishing action as is shown by the result with triphenyl phosphine sulphide. Evidently a non-corrosive, non-eutectic-forming reaction takes place with this addition agent.

The wear preventing action shown by triphenyl phosphine and triphenyl arsine indicates the predominating influence of the alloy formation. In this case the possibility of corrosion by strong acid is very remote. Since the elements are already in their lowest valences, alloy formation proceeds directly. This shows that the form in which an element, capable of reducing wear according to the mechanism described above, is used, is not of great importance as long as it is able to react with the surface in the desired way.

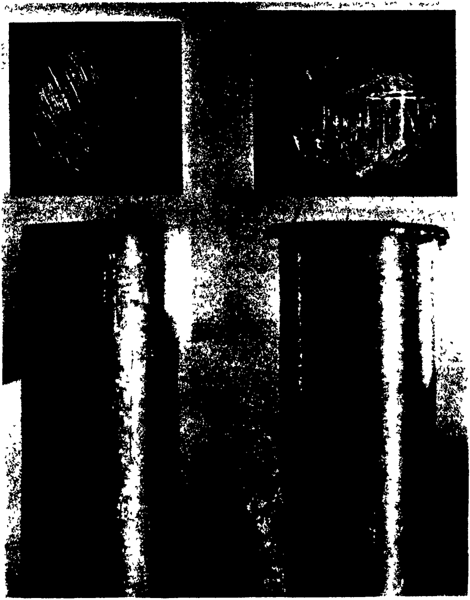

FIGURE 3. Steel pins sliding on rotating steel disk. Left: lubricated with white oil + 1.5% tricresyl phosphate. Right: lubricated with white oil only.

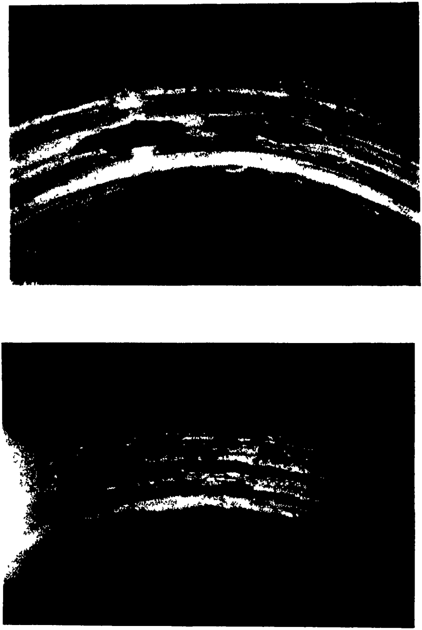

FIGURE 4. Wear tracks of gold-plated steel balls Upper track. lubricated with white oil + 1·5% tricresyl phosphate. Lower track: lubricated with white oil only.

The last two compounds in the table do not contradict the proposed mechanism although they contain chlorine. It is known that both are very stable toward hydrolysis with the liberation of hydrochloric acid. The phosphonitrilic chloride polymer is also stable with respect to thermal decomposition. The triphenyl methoxy phosphorus dichloride decomposes on heating, but the products obtained are not well known.

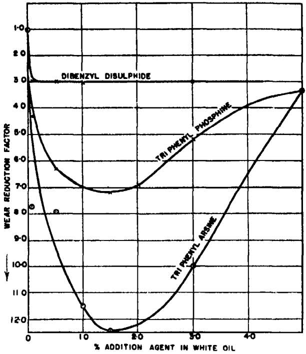

FIGURE 5

According to the theory an entirely different behaviour should be expected for tin. Here the tin phosphide, which is easily formed, alloys with tin to form a compound of higher melting-point than tin. This should raise the temperature of the sliding surfaces and inhibit the polishing effect. The wear should be large. In fact, a tin block pressed against the rotating steel disk wore approximately four times as fast with 1·5% tricresyl phosphate in white oil than with white oil alone.

This is probably the reason for the ineffectiveness of tricresyl phosphate with bronze balls containing tin, while the wear of brass balls containing zinc was effectively reduced.

This also shows that it is not possible to speak precisely of wear preventing addition agents without specifying the metals for which they are suitable.

### 7. LONG-CHAIN POLAR COMPOUNDS IN COMBINATION WITH CHEMICAL POLISHING AGENTS

The complete isolation of boundary lubrication is not always easy, since any sliding mechanism in motion seems to show fluid film lubrication to some degree. This fluid film lubrication, however, completely disappears for surfaces sliding under high pressure at very low velocities. A careful study has been made in these laboratories (see Part I, preceding this paper) of the relations between friction, sliding velocity, lubricant, and nature of the surface. It was found that the transition from boundary lubrication to a state of 'quasi-hydrodynamic' lubrication could be induced or promoted by the addition of certain polar compounds. The 'wedging effect' of these compounds consists of the easy formation of exceptionally thick lubricant films under high pressures and relatively low sliding speeds. The state of quasi-hydrodynamic lubrication is characterized by low coefficients of friction approaching those of hydrodynamic lubrication. The effect is most marked on highly polished surfaces. This suggested that the chemical polishing agents might produce surfaces on which long-chain polar compounds would show a high activity and would reduce wear still further. The following experiments have verified this view beyond expectation.

TABLE 3. RATES OF WEAR FOR COMBINATIONS OF CHEMICAL POLISHING AGENTS WITH LONG-CHAIN POLAR COMPOUNDS. WEARING OF COPPER-PLATED BALLS IN THE FOUR-BALL WEAR APPARATUS

2·2 kg. load. 120 r.p.m.

| Material added to white oil | Wear reduction factor |
|---|---|
| 1·5% tricresyl phosphate + 1·0% oleic acid | 10·3 |
| 1·5% tricresyl phosphate + 1·0% copper oleate | 10·3 |
| 1·5% tricresyl phosphate + stearone (saturated solution) | 8·6 |
| 1·5% tricresyl phosphate + 1·0% mesityl heptadecyl ketone | 10·4 |
| 1·5% triphenyl phosphine + 1% tristearin | 14·2 |
| 1·5% triphenyl arsine + 1·0% oleic acid | 2·4 |
| 1·5% triphenyl arsine + 1·0% mesityl heptadecyl ketone | 17·6 |
| 1·5% triphenyl arsenite + 1% mesityl heptadecyl ketone | 7·2 |
| 1·5% dibenzyl disulphide + 1·0% mesityl heptadecyl ketone | 3·4 |
| 1·5% dibenzyl disulphide + 1·0% oleic acid | 2·2 |

Table 3 shows wear-reduction factors for various chemical polishing agents in combination with long-chain polar compounds, including also some unfavourable combinations.

The effect of polar compounds in combination with tricresyl phosphate and triphenyl phosphine is most striking. The combinations are about twenty times as effective as the polar compound alone and twice as effective as either polishing agent alone. In the case of triphenyl arsine, the addition of 1% of mesityl heptadecyl ketone increased the wear-prevention factor from 12·2 to 17·6.

In the cases where dibenzyl disulphide was used, the polar compounds are of little effect which shows independently that this compound exerts only a mild polishing action.

## 8. UNFAVOURABLE COMBINATIONS

Table 3 shows that the combination of triphenyl arsine and oleic acid is very unfavourable while the combination of tricresyl phosphate and oleic acid is very effective. It seems difficult at this stage to explain these facts satisfactorily. We must remember, however, that compounds of the type of triphenyl phosphine or triphenyl arsine oxidize easily and that the oxidation products are relatively oil-insoluble in contrast to the readily oil-soluble tricresyl phosphate. It seems possible, therefore, that a reaction between oleic acid and triphenyl arsine or phosphine at the sliding surfaces renders the metals unavailable for the phosphide or arsenide formations, although this effect may also be produced by a preferential strong adsorption of oleic acid on the surface. In the case of tricresyl phosphate, however, small amounts of phosphoric acid may be formed at the higher temperature between the sliding surfaces and the phosphoric acid may be able to replace the oleic acid, thus permitting the surface alloy to form. But there may be still other possibilities of explaining the observed fact. In general, strong oxidizing materials containing oxygen, sulphur or the halogens are detrimental to the action of chemical polishing agents, as shown in table 4.

## 9. TABLES TO AID IN THE SYSTEMATIC SEARCH FOR CHEMICAL POLISHING AGENTS

A survey was made of binary systems involving metals and semi-metallic elements that have the properties required by the mechanism outlined in this report. The data given were taken largely from the *International Critical Tables*, exceptions being noted. The systems are classified with

TABLE 4. COMBINATIONS OF COMPOUNDS UNFAVOURABLE TO WEAR PREVENTION. COPPER PLATE WEAR TESTS. SOLVENT: WHITE MINERAL OIL

| Chemical polishing agent 1·5% by wt. | Added compound 1% by wt. | Wear reduction factor |
|---|---|---|
| Tricresyl phosphate | None | 5·4 |
| | Chlorinated cracked wax | 2·4 |
| | α-Bromo stearic acid | 0·9 |
| | Oleic acid and dibenzyl disulphide | 2·4 |
| | Benzoyl peroxide | 1·8 |
| Triphenyl phosphine | None | 7·2 |
| | Castor oil | 6·0 |
| | Fatty acids from castor oil | 6·0 |
| | α-Bromo stearic acid | 1·8 |
| | Oleic acid | 6·0 |
| Triphenyl arsine | None | 12·2 |
| | Stearic acid | 4·3 |
| | Oleic acid | 2·4 |
| | Fatty acids from castor oil | 4·3 |

respect to the semi-metallic element. The information tabulated consists of the melting-point lowering due to the eutectic, its ultimate composition, and the solid phases present. The data are given in table 5.

With the exception of boron, the elements known to have the desired properties belong to groups IV and V of the periodic system.

The data for systems with phosphorus are somewhat meagre, but one may expect by analogy that phosphorus will probably be similar in behaviour to arsenic and antimony. Little is known of the wear preventing properties of the group IV elements.

## 10. CONCLUDING REMARKS

In view of the fact that earlier investigators have tested large numbers of substances added in small proportions to mineral oil without being able to put forward a common characteristic as the cause of their behaviour, it is not at all surprising that the present investigation has revealed rather complex relations between the chemical and the physical aspects of boundary lubrication. However, the successful segregation of addition agents into chemical polishing agents and wedging materials at once makes these relations much clearer. The vague terms 'oiliness' and 'film strength' have lost their significance. A distinct differentiation between wear preventing agents and agents for extreme conditions is now possible. A wear prevention agent reduces pressure and temperature through better distribution of the load over the apparent surface. If the resulting minimum

TABLE 5. MELTING-POINT LOWERINGS, EUTECTIC COMPOSITION, AND SOLID PHASES IN EUTECTIC MIXTURE FOR BINARY SYSTEMS OF METAL AND SEMI-METALLIC ELEMENTS

| Semi-metallic element | Metal | Melting-point lowering, °C | Eutectic composition | Solid phases in eutectic mixture |
|---|---|---|---|---|
| Systems containing As | Ag | 423 | 20% As | Ag, As |
| | Au | 400 | 27% As | Au, ? |
| | Co | 584 | 30% As | Co, $Co_5As_2$ |
| | Cu | 395 | 21% As | Cu, $Cu_3As$ |
| | Mn | 330 | 22% As | Mn, $Mn_2As$ |
| | Pt | 1152 | 1·3% As | Pt, $Pt_2As_3$ |
| | Fe | 700 | 30% As | (Fe, As), $Fe_2As$ |
| Systems containing Sb | Ag | 402 | 28% Sb | Ag, $Ag_3Sb$ |
| | Au | 695 | 25% Sb | Au, $AuSb_2$ |
| | Cu | 449 | 28% Sb | Cu, $Cu_3Sb_2$ |
| | Ni | 355 | 35% Sb | Ni, $Ni_4Sb$ |
| | Pt | 1001 | 23% Sb | Pt, $Pt_5Sb_2$ |
| | Fe | 533 | 50·5% Sb | Fe, $Fe_3Sb_2$ |
| | Co | 410 | 39% Sb | Co, CoSb |
| Systems containing P | Ni | 570 | 11% P | Ni, $Ni_3P$ |
| | Fe | 515 | 10·2% P | Fe, $Fe_3P$ |
| | Cu | 376 | 8·3% P | Cu, $Cu_3P$ |
| Systems containing Si | Ag | 133 | 1·8% Si | Ag, (Ag, Si) |
| | Au | 693 | 6% Si | Au, Si |
| | Co | 285 | 16% Si | Co, $Co_2Si$ |
| | Cu | 283 | 8·6% Si | — |
| | Ni | 295 | 10% Si | Ni, $Ni_3Si$ |
| | Fe | 330 | 20% Si | Fe, FeSi |
| Systems containing B | Ni | 310 | 0·4% B | Ni, $Ni_2B$ |
| | Fe | 370 | 3·5% B | Fe, $Fe_2B$ |
| „ „ Ti | Fe | 205 | 13% Ti | Fe, FeTi |
| „ „ Ge* | Cu | 433 | 35% Ge | — |
| „ „ Zr† | Fe | 205 | 16% Zr | Fe, $FeZr_2$ |

* Schwarz and Elstner (1934). † Vogel and Tonn (1931).

pressure is still too high for the maintenance of a stable oil film, metal to metal contact will take place in spite of the high polish. Since in this case the surface of actual contact is relatively very large, seizure and breakdown will follow very rapidly. An extreme pressure addition agent should, therefore, be corrosive in the sense of preventing any polishing action. This will be the case if the reaction product has anti-welding properties, i.e. if its melting-point is high and if it does not form low melting alloy with the metal below. This shows that good wear preventing agents can never be good extreme pressure agents, and conversely, agents capable of preventing seizure under extreme conditions will generally not be able to reduce wear. These deductions are in good agreement with the observed facts.

### References

Blok 1937 *2nd World Petroleum Congress.*
Boerlage and Blok 1937 *Engineering*, **144**, 1.
Bowden and Hughes 1937 *Proc. Roy. Soc.* A, **160**, 575.
Bowden and Ridler 1936 *Proc. Roy. Soc.* A, **154**, 640.
Schwarz and Elstner 1934 *Z. anorg. Chem.* **217**, 289.
Timoshenko 1934 *Theory of elasticity.* McGraw-Hill Book Co.
Vogel and Tom 1931 *Arch. Eisenhüttenw.* **5**, 387
Witte 1935 *Z. Ver. dtsch. Ing.* **79**, 98.

# On the electromagnetic two-body problem

By J. L. Synge

*Department of Applied Mathematics, University of Toronto*

(*Communicated by E. T. Whittaker, F.R.S.—Received* 11 *July* 1940)

The paper contains a direct attack on the electromagnetic two-body problem, based on the hypotheses (i) that the bodies are particles, (ii) that the fields are given by the retarded potential, (iii) that the force on a particle is the Lorentz ponderomotive force (without a radiation term). A method of successive approximation leading to an exact solution is outlined. General expressions are found for the rates of change of invariant quantities which are the constants of energy and angular momentum in the Kepler problem, and formulae are developed for the principal parts of these expressions in the case where the ratio of the masses of the two particles is small. This is applied in detail to the case where the orbit of the light particle is approximately circular. It is found that energy disappears from the motion, so that the orbital particle slowly spirals in, but the rate at which this occurs is much less than that given by the usual formula for radiation from an accelerated electron. Except in some final calculations, no assumption of small velocity is made, the sole basis of approximation being the smallness of the mass-ratio.

## 1. Introduction

The present paper is classical in the sense that it does not refer to quantum mechanics, but it is relativistic in the sense of the special theory. Its purpose is to investigate the motion of two charged particles under the following hypotheses:

(i) The particles are mathematical points with no size.

(ii) The electromagnetic field due to a moving charge is that given by the usual retarded potential (2·5).

(iii) A charged particle moves in accordance with the relativistic equations of motion (2·8) based on the Lorentz ponderomotive force (without a 'radiation term').

These hypotheses are logically consistent. Whatever their physical validity may be, they lead to a mathematically determinate motion corresponding to assigned initial conditions. It is perhaps necessary to insist on their logical consistency, because there appears to be an opinion that it is necessary to supplement the equations of motion with a radiation term, involving the rate of change of acceleration. The arguments in this connexion do not show any intrinsic inconsistency in the three hypotheses stated, but only an inconsistency between these hypotheses and the law of conservation of energy, assuming that the energy in the field may be represented by the usual form of energy-tensor.

It is hoped in a later paper to discuss this question of the conservation of energy with some care, in connexion with a modified definition of the energy-tensor which avoids any inconsistency between the three hypotheses stated above and the law of conservation. For the present my purpose is merely to insist on the intrinsic logical consistency of the above hypotheses, and to discuss the motion determined by them.

Darwin (1920) used these hypotheses, but assumed small velocities; he did not push his approximations beyond the order $(u/c)^2$, where $u$ is the velocity of a particle and $c$ the velocity of light. To this order, the motion does not degenerate, if the word 'degeneracy' may be used to imply that the particles spiral in to an ultimate collision.

Sommerfeld (1934) placed no restriction on velocities, but confined himself to the limit $m'/m \to 0$, where $m$, $m'$ are the masses of the particles. In fact, he investigated the Kepler problem, in which one particle (by virtue of its great mass) is regarded as fixed. In this case also the motion does not degenerate.

These being apparently the only previous investigations, it appeared desirable to push the approximations further in order to see whether degeneracy would appear. It does appear, at one stage beyond the approximation of Darwin, and at one stage beyond the approximation of Sommerfeld.

A general method of successive approximations is set up. A relativistically invariant energy is defined, and also a 4-vector of angular momentum;

general expressions for their rates of change are found. Then the argument becomes approximate, the basis of approximation being the smallness of the mass-ratio $m'/m$. Except at the very end of the paper, no assumption is made regarding smallness of velocities relative to the velocity of light.

Detailed calculations of degeneracy are confined to the case of nearly circular orbits. It is found that such orbits remain nearly circular, and explicit expressions are found for the rate of degeneracy. The final approximate equations (8·29), (8·30) and (8·35), will perhaps appear most interesting from a physical standpoint.

For discussions and criticisms during the writing of the paper, my thanks are due to Professor L. Infeld and Professor A. F. Stevenson.

## 2. NOTATION AND EQUATIONS OF MOTION

Space-time is regarded as flat. Latin suffixes have the range 1, 2, 3, 4, and Greek the range 1, 2, 3, with the usual summation convention. The space-time co-ordinates are $x_r$, with $x_4 = ict$, and the fundamental form is $dx_r dx_r$. This notation avoids the distinction between covariant and contravariant components; all suffixes are written as subscripts.

The scalar product of two vectors $V_r$, $W_r$ is written

$$(VW) = V_r W_r. \tag{2·1}$$

For a unit vector we have

$$(VV) = \pm 1, \tag{2·2}$$

according as it is space-like or time-like.

Quantities relating to one particle are left unaccented, and those relating to the other particle are accented. Thus:

$L, L'$ = world-lines,

$m, m'$ = proper masses,

$e, e'$ = charges in e.s.u.,

$x_r, x'_r$ = co-ordinates,

$\lambda_r, \lambda'_r$ = unit tangent vectors to world-lines,

$ds, ds'$ = elements of proper time,

$u_\alpha, u'_\alpha$ = velocities,

$$\gamma^{-2} = 1 - u^2/c^2, \quad \gamma'^{-2} = 1 - u'^2/c^2,$$

$$u^2 = u_\alpha u_\alpha, \quad u'^2 = u'_\alpha u'_\alpha.$$

We note that

$$\lambda_\alpha = \gamma u_\alpha/c, \quad \lambda_4 = i\gamma; \quad \lambda'_\alpha = \gamma' u'_\alpha/c, \quad \lambda'_4 = i\gamma'. \tag{2·3}$$

We put
$$\mu = \frac{m'}{m}, \quad k = -\frac{ee'}{m'c^2}, \tag{2·4}$$

$\mu$ being dimensionless and $k$ having the dimensions of a length. These two constants characterize any particular two-body problem, apart from initial conditions.

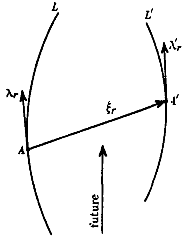

FIGURE 1

Consider a charge $e$ describing any curve $L$ in space time (figure 1). Let $A'$ be any event. Let $A$ be the intersection of $L$ with the null-cone drawn into the past from $A'$; let $\lambda_r$ be the unit tangent vector to $L$ at $A$, and let $\xi_r$ be the null-vector $AA'$. Then, by hypothesis (ii), the field at $A'$ due to $L$ is given by the potential 4-vector (Pauli 1920)

$$\phi_r = -\frac{e\lambda_r}{(\lambda\xi)}, \tag{2·5}$$

and the corresponding electromagnetic tensor is

$$F_{rs} = \frac{\partial\phi_s}{\partial x'_r} - \frac{\partial\phi_r}{\partial x'_s} = e(P_r\xi_s - P_s\xi_r), \tag{2·6}$$

where
$$P_r = -\frac{\lambda_r}{(\lambda\xi)^3}\left[1 + \left(\frac{d\lambda}{ds}\xi\right)\right] + \frac{1}{(\lambda\xi)^2}\frac{d\lambda_r}{ds}. \tag{2·7}$$

By hypothesis (iii), the world-line $L'$ of a charge $e'$, passing through $A'$, satisfies the equations of motion

$$m'\frac{d\lambda'_r}{ds'} = \frac{e'}{c^2}F_{rs}\lambda'_s, \tag{2·8}$$

or
$$\frac{d\lambda'_r}{ds'} = -k[P_r(\lambda'\xi) - \xi_r(\lambda'P)]. \tag{2·9}$$

If we regard $L$ as assigned, (2·9) is a set of ordinary differential equations for the determination of $L'$, and yields a definite curve $L'$ passing through an arbitrarily assigned event in an arbitrarily assigned direction.

If we interchange the roles of the two world-lines and regard $L'$ as assigned, we have with the notation of figure 2 the following equations of motion for $L$:

$$\frac{d\lambda_r}{ds} = -\mu k[P'_r(\lambda\xi') - \xi'_r(\lambda P')], \tag{2·10}$$

$P'_r$ being defined as in (2·7) with all letters accented.

We note that $\mu$, $k$ are now the only constants appearing in (2·9) and (2·10), $\mu$ being absent from (2·9).

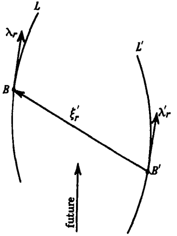

FIGURE 2

Although (2·9), (2·10) are formal equations of motion, they do not form an ordinary system on account of the retardations involved in drawing the null-vectors $\xi_r$, $\xi'_r$: they are in a sense difference equations, and this fact constitutes the great difficulty of the problem. Only when $L$ is given can (2·9) be regarded as ordinary equations of motion for $L'$, and only when $L'$ is given can (2·10) be regarded as ordinary equations of motion for $L$. But the fact that these equations can be so regarded under the stated conditions forms the basis of the method of successive approximations about to be described.

## 3. A METHOD OF SUCCESSIVE APPROXIMATIONS

Let us suppose $\mu < 1$. (The smaller $\mu$ is, the more rapid the convergence of the process to be described.) Let $A$, $A'$ be any two events in space-time, and let $(\lambda_r)_A$, $(\lambda'_r)_{A'}$ be time-like unit vectors arbitrarily assigned at these events (figure 3). Our purpose is to obtain world-lines $L$, $L'$ for the two particles, such that (2·9), (2·10) are satisfied and (as initial conditions) $L$ is to pass through $A$ with the direction $(\lambda_r)_A$ and $L'$ through $A'$ with the direction $(\lambda'_r)_{A'}$.

First, we put $\mu = 0$ and choose as basic approximation for $L$ the world-line $L_0$ which passes through $A$ in the direction $(\lambda_r)_A$ and satisfies (2·10) with the right-hand side replaced by zero. This means that $L_0$ is a geodesic (the world-line of an infinitely massive particle).

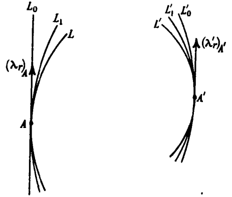

FIGURE 3

Secondly, we find $L'_0$ to pass through $A'$ with the direction $(\lambda'_r)_{A'}$ and to satisfy (2·9), in which the field is taken to be that due to $L_0$. This means that $L'_0$ is the orbit of the Kepler problem discussed by Sommerfeld (1934).

Thirdly, we find $L_1$ to pass through $A$ with the direction $(\lambda_r)_A$ and to satisfy (2·10) in which the field is taken to be that due to $L'_0$. And so on.

Thus we get a sequence of world-lines, each defined by ordinary differential equations, the unaccented passing through $A$ with the assigned direction $(\lambda_r)_A$ and the accented through $A'$ with the assigned direction $(\lambda'_r)_{A'}$, derived from one another according to the scheme

$$L_0 \rightarrow L'_0 \rightarrow L_1 \rightarrow L'_1 \rightarrow L_2 \rightarrow L'_2 \rightarrow \ldots. \tag{3·1}$$

To see how the convergence proceeds, we may indicate the order of the differences between the elements of $L_0$, $L_1$ at the same value of $s$, measured from $A$, by writing symbolically

$$L_1 - L_0 = 0(\mu); \tag{3·2}$$

this is evident from (2·10). Thus when we use (2·9) to determine $L'_1$, the field (due to $L_1$) will differ by $0(\mu)$ from that (due to $L_0$) used in (2·9) to determine $L'_0$. Hence

$$L'_1 - L'_0 = 0(\mu). \tag{3·3}$$

We may group $(L_0, L_0')$ as the zero approximation, and $(L_1, L_1')$ as the first approximation.

To compare the elements of $L_2$ and $L_1$, we have

$$\left.\begin{aligned} &\text{for } L_1\text{:} \quad \frac{d\lambda_r}{ds} = -\mu k(P_r'\xi_s' - P_s'\xi_r')_{L_0'}\lambda_s, \\ &\text{for } L_2\text{:} \quad \frac{d\lambda_r}{ds} = -\mu k(P_r'\xi_s' - P_s'\xi_r')_{L}\,\lambda_s, \end{aligned}\right\} \tag{3·4}$$

and the right-hand sides differ by $0(\mu^2)$. Hence symbolically

$$L_2 - L_1 = 0(\mu^2), \tag{3·5}$$

and similarly $$L_2' - L_1' = 0(\mu^2). \tag{3·6}$$

Generally $$L_n - L_{n-1} = 0(\mu^n), \quad L_n' - L_{n-1}' = 0(\mu^n). \tag{3·7}$$

Thus, if $\mu < 1$, there is good reason to suppose that the process is convergent, and that the curves

$$L = \lim_{n\to\infty} L_n, \quad L' = \lim_{n\to\infty} L_n' \tag{3·8}$$

exist and constitute a solution of (2·9), (2·10); if so, $L$ and $L'$ will be the required world-lines for the two-body problem, under the assigned initial conditions at the events $A$, $A'$.

## 4. THE RELATIVE ENERGY AND ITS RATE OF CHANGE

In this and the next section we give some formal developments, to be used later. The reasoning is exact, no approximations being used. $L$ and $L'$ (figure 4) are the world-lines of the two particles, satisfying the equations of motion.

Let $A$ be any event on $L$, $\xi_r$ the null-vector drawn into the future from $A$ to intersect $L'$ (at $A'$), and $\lambda_r, \lambda_r'$ the unit tangent vectors at $A$, $A'$ respectively. We define the *energy of $L'$ relative to $L$ at $A$* to be the invariant

$$E = -m'c^2\left[(\lambda\lambda') - \frac{k}{(\lambda\xi)}\right], \tag{4·1}$$

$k$ being defined as in (2·4).

To link $E$ with a well-known expression, we take for the moment axes in which the time-axis coincides with $\lambda_r$. Then

$$\lambda_\alpha = 0, \quad \lambda_4 = i; \qquad (\lambda\lambda') = -\gamma', \quad (\lambda\xi) = -r, \tag{4·2}$$

where $r$ is the spatial distance between $A$ and $A'$. Thus

$$E = m'\gamma'c^2 + \frac{ee'}{r}, \tag{4·3}$$

a familiar expression for energy.

Reverting to general axes, we now differentiate $E$ with respect to $s$, the arc-length of $L$. Denoting $d/ds$ by a dot, we obtain

$$\dot{E} = -m'c^2\left[(\dot{\lambda}\lambda') + (\lambda\dot{\lambda}') + \frac{k}{(\lambda\xi)^2}\{(\dot{\lambda}\xi) + (\lambda\dot{\xi})\}\right]. \tag{4·4}$$

Now, if $x_r$ are the co-ordinates of $A$ and $x'_r$ those of $A'$, we have

$$\xi_r = x'_r - x_r, \quad \dot{\xi}_r = \lambda'_r\dot{s}' - \lambda_r, \tag{4·5}$$

and hence, since

$$\xi_r\xi_r = 0, \quad \xi_r\dot{\xi}_r = 0, \tag{4·6}$$

we have

$$\dot{s}' = \frac{(\lambda\xi)}{(\lambda'\xi)}. \tag{4·7}$$

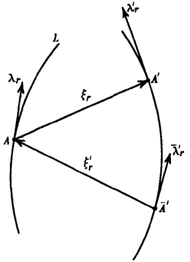

FIGURE 4

By (2·9)

$$\dot{\lambda}'_r = -k[P_r(\lambda'\xi) - \xi_r(\lambda'P)]\frac{(\lambda\xi)}{(\lambda'\xi)}, \quad (\lambda\dot{\lambda}') = -k[(\lambda P)(\lambda'\xi) - (\lambda\xi)(\lambda'P)]\frac{(\lambda\xi)}{(\lambda'\xi)}. \tag{4·8}$$

But since $(\lambda\lambda) = -1$, $(\lambda\dot{\lambda}) = 0$, we have by (2·7)

$$(\lambda P) = \frac{1}{(\lambda\xi)^3}[1 + (\dot{\lambda}\xi)], \quad (\lambda'P) = -\frac{(\lambda\lambda')}{(\lambda\xi)^3}[1 + (\dot{\lambda}\xi)] + \frac{(\dot{\lambda}\lambda')}{(\lambda\xi)^2}, \tag{4·9}$$

and hence

$$(\lambda\dot{\lambda}') = -k\left[\frac{1}{(\lambda\xi)^2}\{1 + (\dot{\lambda}\xi)\} + \frac{(\lambda\lambda')}{(\lambda\xi)(\lambda'\xi)}\{1 + (\dot{\lambda}\xi)\} - \frac{(\dot{\lambda}\lambda')}{(\lambda'\xi)}\right]. \tag{4·10}$$

Also, by (4·5) and (4·7) we have

$$(\lambda\dot{\xi}) = 1 + \frac{(\lambda\lambda')(\lambda\xi)}{(\lambda'\xi)}. \tag{4·11}$$

On substituting from (4·10) (4·11) in (4·4) we find that all terms cancel save those containing a derivative of $\lambda_n$, and we obtain the following result:

I. *In the two-body problem, the rate of change of the energy of $L'$ relative to $L$ is given (without approximation) by the formula*

$$\dot{E} = -Q_n \dot{\lambda}_n, \tag{4·12}$$

*where the dot signifies $d/ds$ and*

$$Q_n = m'c^2\left[\lambda'_n\left\{1+\frac{k}{(\lambda'\xi)}\right\} - \xi_n \frac{k(\lambda\lambda')}{(\lambda\xi)(\lambda'\xi)}\right]. \tag{4·13}$$

This result was suggested by the fact that in the Kepler problem $E$ is an integral of the motion. It may be interesting to note that for large $c$ we have approximately from (2·3), (4·13), (4·12)

$$\left.\begin{aligned} &\dot{\lambda}_\alpha = \frac{1}{c^2}\frac{du_\alpha}{dt}, \quad \dot{\lambda}_4 = \frac{iu}{c^2}\frac{du}{dt}, \\ &Q_\alpha = m'cu'_\alpha, \quad Q_4 = im'c^2, \\ &\frac{dE}{dt} = -m'u'_\alpha \frac{du_\alpha}{dt} + m'u\frac{du}{dt}. \end{aligned}\right\} \tag{4·14}$$

These formulae are not used later.

We shall now get rid of $\dot{\lambda}_n$ from (4·12). Returning to figure 4, let us draw the null-cone from $A$ into the past, cutting $L'$ at $\bar{A}'$. Let $\xi'_r$ be the null-vector $\bar{A}'A$, and let $\bar{\lambda}'_r$ be the unit tangent vector to $L'$ at $\bar{A}'$. Then, as in (2·10),

$$\dot{\lambda}_r = -\mu k[P'_r(\lambda\xi') - \xi'_r(\lambda P')], \tag{4·15}$$

where, as in (2·7),

$$P'_r = -\frac{\bar{\lambda}'_r}{(\bar{\lambda}'\xi')^3}\left[1+\left(\frac{d\bar{\lambda}'}{d\bar{s}'}\xi'\right)\right] + \frac{1}{(\bar{\lambda}'\xi')^2}\frac{d\bar{\lambda}'_r}{d\bar{s}'}. \tag{4·16}$$

Substituting from (4·15) in (4·12) we obtain this result:

II. *The rate of change of the energy of $L'$ relative to $L$ at $A$, is given (without approximation and without reference to the acceleration of $L$ at $A$) by the formula*

$$\dot{E} = \mu H, \tag{4·17}$$

*where*

$$H = m'c^2k\left[\begin{vmatrix} (\lambda\xi') & (\lambda'\xi') \\ (\lambda P') & (\lambda' P') \end{vmatrix} + \frac{k}{(\lambda\xi)(\lambda'\xi)}\begin{vmatrix} 0 & (\lambda'\lambda) & (\xi\lambda) \\ (\lambda\xi') & (\lambda'\xi') & (\xi\xi') \\ (\lambda P') & (\lambda' P') & (\xi P') \end{vmatrix}\right], \tag{4·18}$$

*and $P'_r$ is defined in* (4·16), *so that*

$$\left.\begin{aligned}(\lambda P') &= -\frac{(\lambda\bar{\lambda}')}{(\bar{\lambda}'\xi')^3}+\frac{1}{(\bar{\lambda}'\xi')^3}\begin{vmatrix}\left(\lambda\dfrac{d\bar{\lambda}'}{d\bar{s}'}\right) & \left(\xi'\dfrac{d\bar{\lambda}'}{d\bar{s}'}\right)\\ (\lambda\bar{\lambda}') & (\xi'\bar{\lambda}')\end{vmatrix},\\ (\lambda' P') &= -\frac{(\lambda'\bar{\lambda}')}{(\bar{\lambda}'\xi')^3}+\frac{1}{(\bar{\lambda}'\xi')^3}\begin{vmatrix}\left(\lambda'\dfrac{d\bar{\lambda}'}{d\bar{s}'}\right) & \left(\xi'\dfrac{d\bar{\lambda}'}{d\bar{s}'}\right)\\ (\lambda'\bar{\lambda}') & (\xi'\bar{\lambda}')\end{vmatrix},\\ (\xi P') &= -\frac{(\xi\bar{\lambda}')}{(\bar{\lambda}'\xi')^3}+\frac{1}{(\bar{\lambda}'\xi')^3}\begin{vmatrix}\left(\xi\dfrac{d\bar{\lambda}'}{d\bar{s}'}\right) & \left(\xi'\dfrac{d\bar{\lambda}'}{d\bar{s}'}\right)\\ (\xi\bar{\lambda}') & (\xi'\bar{\lambda}')\end{vmatrix}.\end{aligned}\right\} \tag{4·19}$$

### 5. THE RELATIVE ANGULAR MOMENTUM AND ITS RATE OF CHANGE

With the same construction as in figure 4, we define the *angular momentum of $L'$ relative to $L$ at $A$* to be the 4-vector

$$h_r = -im'c\,\epsilon_{rmns}\xi_m\lambda'_n\lambda_s, \tag{5·1}$$

where $\epsilon_{rmns}$ is the usual permutation symbol.

To give $h_r$ a physical meaning, we take for the moment axes in which the time-axis coincides with $\lambda_r$, so that (4·2) hold. Then we find

$$h_\alpha = m'\gamma'\epsilon_{\alpha\beta\gamma}\xi_\beta u'_\gamma, \quad h_4 = 0. \tag{5·2}$$

Since $\xi_\beta$ are the spatial co-ordinates of $A'$ relative to $A$, we see that $h_\alpha$ is the usual 3-vector of angular momentum, in relativistic form through the inclusion of $\gamma'$. This vector is conserved in the Kepler problem, and hence (as in the case of $E$) we expect to find for $\dot{h}_r$ an expression linear in $\dot{\lambda}_n$.

Reverting to general axes, we differentiate (5·1), obtaining

$$\dot{h}_r = -im'c\,\epsilon_{rmns}\xi_m(\dot{\lambda}'_n\lambda_s+\lambda'_n\dot{\lambda}_s); \tag{5·3}$$

the term with $\dot{\xi}_m$ disappears, since by (4·5) it is linear in $\lambda_m$, $\lambda'_m$. Substituting for $\dot{\lambda}'_n$ from (4·8) and (2·7) and dropping terms which vanish, we obtain

$$\begin{aligned}\epsilon_{rmns}\xi_m\dot{\lambda}'_n\lambda_s &= -k\epsilon_{rmns}\xi_m P_n\lambda_s(\lambda\xi)\\ &= -k\epsilon_{rmns}\xi_m\dot{\lambda}_n\lambda_s/(\lambda\xi).\end{aligned} \tag{5·4}$$

Substitution in (5·3) gives this result:

III. *In the two-body problem, the rate of change of the angular momentum of $L'$ relative to $L$ is given (without approximation) by the formula*

$$\dot{h}_r = R_{rn}\dot{\lambda}_n, \tag{5·5}$$

*where the dot signifies $d/ds$ and $R_{rn}$ is the skew-symmetric tensor*

$$R_{rn} = im'c\,\epsilon_{rmns}\xi_m\left[\lambda'_s + \frac{k}{(\lambda\xi)}\lambda_s\right]. \tag{5·6}$$

We note that
$$R_{rn}\lambda_n = h_r. \tag{5·7}$$

Thus if we take for the moment axes in which the time-axis coincides with $\lambda_r$, we have

$$iR_{\alpha 4} = h_\alpha. \tag{5·8}$$

Let us now convert (5·5) into a form analogous to (4·17), depending on the elements of $L'$ at $A'$ and $\bar{A}'$ (figure 4), and without reference to the acceleration of $L$ at $A$.

Any vector may be resolved into components along four selected vectors (not all contained in a 3-flat); thus we may write

$$\left.\begin{aligned} \xi'_r &= A\lambda_r + B\lambda'_r + C\xi_r + Dh_r, \\ P'_r &= A'\lambda_r + B'\lambda'_r + C'\xi_r + D'h_r. \end{aligned}\right\} \tag{5·9}$$

Since, by (5·1), $h_r$ is perpendicular to $\lambda_r$, $\lambda'_r$ and $\xi_r$, we obtain

$$\left.\begin{aligned} (h\xi') &= Dh^2, \qquad (hP') = D'h^2, \\ (\lambda\xi') &= A(\lambda\lambda) + B(\lambda\lambda') + C(\lambda\xi), \\ (\lambda'\xi') &= A(\lambda'\lambda) + B(\lambda'\lambda') + C(\lambda'\xi), \\ (\xi\xi') &= A(\xi\lambda) + B(\xi\lambda') + C(\xi\xi), \\ (\lambda P') &= A'(\lambda\lambda) + B'(\lambda\lambda') + C'(\lambda\xi), \\ (\lambda' P') &= A'(\lambda'\lambda) + B'(\lambda'\lambda') + C'(\lambda'\xi), \\ (\xi P') &= A'(\xi\lambda) + B'(\xi\lambda') + C'(\xi\xi). \end{aligned}\right\} \tag{5·10}$$

These equations may be solved for $A$, $B$, $C$, $A'$, $B'$, $C'$; we note in particular that

$$\left.\begin{aligned} (\lambda\xi')D' - (\lambda P')D &= h^{-2}\begin{vmatrix} (\lambda\xi') & (h\xi') \\ (\lambda P') & (hP') \end{vmatrix}, \\ (\lambda\xi')A' - (\lambda P')A &= -F/\Delta, \\ (\lambda\xi')B' - (\lambda P')B &= G/\Delta, \end{aligned}\right\} \tag{5·11}$$

where

$$\left.\begin{aligned}
F &= \begin{vmatrix} (\lambda\lambda') & (\lambda\xi) & 0 & 0 \\ (\lambda\lambda') & (\lambda\xi) & (\lambda\xi') & (\lambda P') \\ (\lambda'\lambda') & (\lambda'\xi) & (\lambda'\xi') & (\lambda'P') \\ (\xi\lambda') & (\xi\xi) & (\xi\xi') & (\xi P') \end{vmatrix}, \\
G &= \begin{vmatrix} (\lambda\lambda) & (\lambda\xi) & 0 & 0 \\ (\lambda\lambda) & (\lambda\xi) & (\lambda\xi') & (\lambda P') \\ (\lambda'\lambda) & (\lambda'\xi) & (\lambda'\xi') & (\lambda'P') \\ (\xi\lambda) & (\xi\xi) & (\xi\xi') & (\xi P') \end{vmatrix}, \\
\Delta &= \begin{vmatrix} (\lambda\lambda) & (\lambda\lambda') & (\lambda\xi) \\ (\lambda'\lambda) & (\lambda'\lambda') & (\lambda'\xi) \\ (\xi\lambda) & (\xi\lambda') & (\xi\xi) \end{vmatrix}.
\end{aligned}\right\} \qquad (5{\cdot}12)$$

When we substitute in (4·15) from (5·9), and then substitute (4·15) in (5·5), we obtain the following result:

IV. *The rate of change of the angular momentum of $L'$ relative to $L$ at $A$ is given (without approximation and without reference to the acceleration of $L$ at $A$) by the formula*

$$\begin{aligned} \dot{h}_r = \mu k h_r\left[F + G\frac{k}{(\lambda\xi)}\right]\Delta^{-1} \\ - im'c\mu k\epsilon_{rmns}\xi_m h_n\left[\lambda'_s + \frac{k}{(\lambda\xi)}\lambda_s\right]h^{-2}\begin{vmatrix} (\lambda\xi') & (h\xi') \\ (\lambda P') & (hP') \end{vmatrix}. \end{aligned} \qquad (5{\cdot}13)$$

## 6. FIRST-ORDER APPROXIMATIONS FOR THE RATES OF CHANGE OF RELATIVE ENERGY AND ANGULAR MOMENTUM

So far the results given have been exact. Let us now prepare for approximations.

We shall call world-lines $(L, L')$ *natural* if they satisfy the equations of motion (2·9), (2·10). Let $(L, L')$ be two world-lines, natural or unnatural. Let $A$ be a point on $L$, and $A'$ the point where $L'$ cuts the future null-cone drawn from $A$. Let $(\lambda_r)_A$, $(\lambda'_r)_{A'}$ be the unit tangent vectors at $A$ and $A'$. (The situation is as shown in figure 1, but now we do not necessarily think of the world-lines as natural.) The pair of points $A$, $A'$, with the associated unit vectors $(\lambda_r)_A$, $(\lambda'_r)_{A'}$, we shall call a *state* of the system. The complete world-lines $(L, L')$ may be regarded as a single infinity of states, each state corresponding to a definite point $A$ on $L$, and therefore to a definite value of the proper time $s$ of $L$.

If $(L, L')$ are natural, then (as seen in (3)) a single state determines the world-lines.

A state is determined by thirteen numbers as follows: the four co-ordinates $x_r$ of $A$ and the nine independent components of $\lambda_r$, $\xi_r$, $\lambda'_r$ (where $\xi_r = \overrightarrow{AA'}$), these vectors satisfying the identities

$$\lambda_r \lambda_r = -1, \quad \xi_r \xi_r = 0, \quad \lambda'_r \lambda'_r = -1. \tag{6·1}$$

The history (natural or unnatural) of two particles may be described by sixteen functions of $s$, the proper time of $L$:

$$x_r(s), \quad \lambda_r(s), \quad \xi_r(s), \quad \lambda'_r(s). \tag{6·2}$$

We shall refer to these sixteen functions as the *elements* of the motion. Of course six functions suffice to describe the motion of two particles; the sixteen functions in (6·2) are connected not only by the three identities (6·1), but also by the seven identities

$$\dot{x}_r = \lambda_r, \quad \lambda_r + \dot{\xi}_r = \theta \lambda'_r. \tag{6·3}$$

where $\theta(s)$ is undetermined.

Let us associate the constants $m$, $e$ with $L$ and the constants $m'$, $e'$ with $L'$. The invariant $E$ and the vector $h_r$ are defined as in (4·1) and (5·1) for any state. For any history $(L, L')$ they are functions of $s$, and so $\dot{E}$ and $\dot{h}_r$ exist, but the expressions given by (4·17) and (5·13) apply only to natural histories.

Let us now consider a system for which $\mu$ is small. We seek an approximate evaluation of the behaviour of $E$ and $h_r$ as functions of $s$ for a pair of natural world-lines $(L, L')$.

We see from (4·17), (5·13) that $\dot{E}$ and $\dot{h}_r$ are small of the order of $\mu$. We shall therefore only make an error of order $\mu^2$ if we substitute in the right-hand sides for the actual elements of $(L, L')$ the elements of other (unnatural) world-lines $(\Lambda, \Lambda')$ which differ from those of $(L, L')$ by quantities of order $\mu$.

We shall now show that the last term in (5·13) is $0(\mu^2)$, whether we use the elements of $(L, L')$ or those of $(\Lambda, \Lambda')$, differing by $0(\mu)$. In either case these elements differ from those of the zero approximation $(L_0, L'_0)$ only by $0(\mu)$, and hence it is only necessary to show that when we substitute the elements of $(L_0, L'_0)$ the last term in (5·13) vanishes rigorously. This is seen as follows.

In deriving (5·5) we used the fact that $L'$ was a natural motion in the field of $L$, but not that $L$ was a natural motion in the field of $L'$. Now $L'_0$ is a natural motion in the field of $L_0$, for which $\dot{\lambda}_n = 0$. Thus $h_r$ is a constant vector for $(L_0, L'_0)$, and so is perpendicular not only to $\lambda_r$, $\lambda'_r$, $\xi_r$, but also to $\bar{\lambda}'_r$ and to the null-vector drawn to $\bar{A}'$ from $L_0$, since $L_0$ is straight. But $\xi'_r$ is a linear combination of $\lambda_r$ and this last null-vector. Hence $(h\xi') = 0$. Also, by (4·16), $P'_r$ is a linear combination of $\bar{\lambda}'_r$ and $d\bar{\lambda}'_r/d\bar{s}'$, and the latter, being the acceleration of $L'_0$, is easily seen by application of (2·9) at $\bar{A}'$ to be a linear combination of $\lambda_r$ and $\xi'_r$. Hence $(hP') = 0$. Thus the last term in (5·13) vanishes when we substitute the elements of $(L_0, L'_0)$, and so the result is established.

We may now state the following result:

V. *When $\mu$ is small, the rates of change of $E$ and $h_r$ for natural world-lines $(L, L')$ are given by*

$$\dot{E} = \mu H + 0(\mu^2), \tag{6·4}$$

$$\dot{h}_r = \mu k h_r \left[ F + G \frac{k}{(\lambda\xi)} \right] \Delta^{-1} + 0(\mu^2), \tag{6·5}$$

*where $H$, $F$, $G$, $\Delta$ are formally as in* (4·18), (5·12), *but the right-hand sides of* (6·4), (6·5) *may be calculated for the elements of any pair of world-lines $(\Lambda, \Lambda')$ which differ from those of $(L, L')$ only by quantities of order $\mu$.*

We note that if the term $0(\mu^2)$ is omitted from (6·5), $\dot{h}_r$ are proportional to $h_r$; this shows that to this order of approximation the direction of $h_r$ in space-time is fixed. Hence we may say that the rate of change of the direction of $h_r$ is $0(\mu^2)$, and that the magnitude of this vector satisfies

$$\dot{h}/h = \mu k \left[ F + G \frac{k}{(\lambda\xi)} \right] \Delta^{-1} + 0(\mu^2) \quad (h^2 = h_r h_r). \tag{6·6}$$

We might now choose for $(\Lambda, \Lambda')$ the zero approximation $(L_0, L'_0)$ corresponding to $s = 0$. But if $(L_0, L'_0)$ is of general type, the computations are formidable, and indeed hopeless without the introduction of another approximation based on smallness of relative velocity. Since it is desirable to base the approximations entirely on the smallness of mass-ratio, this course will not be taken. Instead simplicity will be attained by confining attention to approximately circular orbits. Since the questions of approximation involved here are rather delicate, it will be necessary to make some preliminary statements regarding Kepler orbits.

## 7. RELATIVISTIC KEPLER ORBITS

Corresponding to any state in the two-body problem $(L, L')$, there exists a zero approximation $(L_0, L'_0)$, in which $L_0$ is a geodesic and $L'_0$ a world-line described in accordance with the equations of motion (2·9) in the field of $L_0$. Then $L'_0$ is a Kepler orbit. (No confusion is likely to arise from using the word 'orbit' indifferently in the three-dimensional sense and also in the four-dimensional sense.)

Let us take space-time axes so that $L_0$ is time-axis. The equations of motion (2·9) give for $L'_0$

$$m'\frac{d}{dt}(\gamma' u'_a) = \frac{ee'}{r^2} l_a, \tag{7·1}$$

where $l_a$ are the direction cosines of the radius vector $r$ drawn from the origin to the moving particle. From these equations we obtain

$$m'\gamma' c^2 + ee'/r = E, \quad m'\gamma' r^2 d\theta/dt = h, \tag{7·2}$$

where $\theta$ is the polar angle in the plane of the orbit, and $E$, $h$ are constants, being precisely the invariants $E$, $h$ of energy and angular momentum defined by the state of $(L, L')$ at which $(L_0, L'_0)$ is the zero approximation.

Defining $\rho = 1/r$, we easily obtain from (7·2) the following differential equation for the orbit:

$$\frac{h^2}{m'^2c^2}\left\{\left(\frac{d\rho}{d\theta}\right)^2 + \rho^2\right\} + 1 = \left(\frac{E - ee'\rho}{m'c^2}\right)^2. \tag{7·3}$$

The reciprocals $\rho_1$, $\rho_2$ of the apsidal distances $r_1$, $r_2$ are given by putting $d\rho/d\theta = 0$; they satisfy

$$\rho^2\left\{\left(\frac{h}{m'c}\right)^2 - \left(\frac{ee'}{m'c^2}\right)^2\right\} + 2\rho\frac{Eee'}{(m'c^2)^2} + 1 - \left(\frac{E}{m'c^2}\right)^2 = 0. \tag{7·4}$$

In general the orbit is not closed, and the word 'eccentricity' (in the ordinary sense) does not apply. But we may generalize the meaning of the word by defining the eccentricity of any orbit in which the radius vector oscillates between a minimum $r_2$ and a maximum $r_1$ to be

$$\epsilon = \frac{r_1 - r_2}{r_1 + r_2} = \frac{\rho_2 - \rho_1}{\rho_2 + \rho_1}, \tag{7·5}$$

where $\rho = 1/r$. When applied to a focal ellipse, this definition gives the usual eccentricity.

Putting
$$J = \frac{E}{m'c^2}, \quad K = -\frac{ee'}{hc}, \tag{7·6}$$

we have by (7·4)
$$\epsilon^2 = J^{-2} + K^{-2} - J^{-2}K^{-2}. \tag{7·7}$$

For a circular orbit it is necessary and sufficient that $\epsilon = 0$, or
$$J^2 + K^2 = 1. \tag{7·8}$$

Further, for a circular orbit of radius $r$ we have in addition to (7·2) the equation
$$m'\gamma' u'^2/r = -ee'/r^2, \tag{7·9}$$

so that
$$J = \gamma'^{-1}, \quad K = u'/c. \tag{7·10}$$

Just as energy and angular momentum determine the form of a Newtonian Kepler orbit, so do $J$ and $K$ determine the form of a relativistic Kepler orbit. There exists an orbit having arbitrarily assigned values of $J$ and $K$, provided that these values satisfy
$$0 < J < 1, \quad J^2 + K^2 \geqslant 1. \tag{7·11}$$

The orbit will be circular if, and only if, the sign of equality holds.

Let us now suppose that we are given a Kepler orbit $C$ which is nearly circular, in the sense that $\epsilon$ is small. Let $J$, $K$ be its constants. There exists a circular Kepler orbit with constants $J_0$, $K_0$ differing from $J$, $K$ only by quantities of the order of $\epsilon^2$. For example, we may obtain such an orbit by taking $J_0 = J$, $K_0 = (1 - J^2)^{\frac{1}{2}}$. If, further, we take the plane of $C_0$ nearly coincident with that of $C$, and take the positions on $C_0$ and $C$ at time $t = 0$ close to one another (the differences in both cases being of the order of $\epsilon^2$), the elements of $C_0$ and $C$ (in the sense of (6·2)) will differ only by quantities of the order of $\epsilon^2$.

Let us now return to the space-time viewpoint. Let $(L, L')$ be natural world-lines and $A$ a point on $L$. We define the eccentricity of $(L, L')$ at $A$ to be $\epsilon$, where $\epsilon^2$ is given by (7·7) and $J$, $K$ by (7·6), $E$ and $h$ being the invariants of $(L, L')$ at $A$. In fact, we define the eccentricity of $(L, L')$ to be the eccentricity of the zero approximation $(L_0, L_0')$, but when stated as above there is no need to refer to $(L_0, L_0')$ in the definition.

Let us suppose that the eccentricity of $(L, L')$ at $A$ is small of the order of $\mu^{\frac{1}{2}}$, so that $\epsilon^2 = 0(\mu)$. Then there exist world-lines $(\Lambda, \Lambda')$, with elements differing from those of $(L, L')$ only by $0(\mu)$, such that $\Lambda$ is a geodesic in space-time and $\Lambda'$ is a circular Kepler orbit, having $\Lambda$ for centre.

## 8. THE HISTORY OF A NEARLY CIRCULAR ORBIT

Let us suppose that at $A$ the natural world-lines have an eccentricity small of the order $\mu^{\frac{1}{2}}$, so that $\epsilon^2 = 0(\mu)$. Since $\dot{E}$, $\dot{h}$, are small of order $\mu$, the increments in $E$, $h$ in finite time are $0(\mu)$, and hence by (7·7) $\epsilon^2$ remains $0(\mu)$ for a finite time, starting from $A$.

Let $(\Lambda, \Lambda')$ give the circular Kepler orbit described at the end of § 7. Since the elements of $(\Lambda, \Lambda')$ differ from those of $(L, L')$ only by order $\mu$, it is permissible to use the elements of $(\Lambda, \Lambda')$ in the right-hand sides of (6·4), (6·5) or (6·6). These equations are invariant. Let us carry out our calculations for axes such that $\Lambda$ is time-axis.

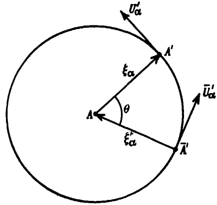

FIGURE 5

Figure 5 is a space-diagram, showing the circular orbit with centre at the fixed point $A$. $A'$ is any position of the moving particle, $\xi_\alpha$ the co-ordinates of $A'$ relative to $A$, and $u'_\alpha$ the velocity at $A'$. $\bar{A}'$ is the space-point corresponding to the event $\bar{A}'$ in figure 4, so that the time taken by light to travel along the broken line $\bar{A}'AA'$ is equal to the time taken by the particle to pass from $\bar{A}'$ to $A'$. Hence if $r$ is the radius of the orbit, we have

$$2r/c = r\theta/u', \quad \theta = 2u'/c, \tag{8·1}$$

where $\theta$ is the angle $\bar{A}'AA'$.

In accordance with the notation of figure 4, $\xi'_\alpha$ are the co-ordinates of $A$ relative to $\bar{A}'$.

We note the following values:

$$\lambda_\alpha = 0, \quad \lambda_4 = i; \quad \lambda'_\alpha = \gamma' u'_\alpha/c, \quad \lambda'_4 = i\gamma'; \quad \bar{\lambda}'_\alpha = \gamma' \bar{u}'_\alpha/c, \quad \bar{\lambda}'_4 = i\gamma';$$
$$\xi_4 = ir, \quad \xi'_4 = ir. \tag{8·2}$$

Hence, putting $\beta = u'/c$, we have

$$\left.\begin{aligned}(\lambda\lambda') &= (\lambda\bar{\lambda}') = -\gamma',\\ (\lambda\xi) &= (\lambda\xi') = -r,\\ (\lambda'\xi) &= (\bar{\lambda}'\xi') = -r\gamma',\\ (\lambda'\bar{\lambda}') &= -\gamma'^2(1-\beta^2\cos 2\beta),\\ (\lambda'\xi') &= (\bar{\lambda}'\xi) = -r\gamma'(1-\beta\sin 2\beta),\\ (\xi\xi') &= -r^2(1+\cos 2\beta).\end{aligned}\right\} \tag{8·3}$$

Also
$$\frac{d\bar{\lambda}'_\alpha}{d\bar{s}'} = \frac{\gamma'^2}{c^2}\frac{d\bar{u}'_\alpha}{dt}, \quad \frac{d\gamma'_4}{d\bar{s}'} = 0. \tag{8·4}$$

But from the equations of motion of $\Lambda'$

$$m'\gamma'\frac{d\bar{u}'_\alpha}{dt} = -\frac{ee'}{r^2}\frac{\xi'_\alpha}{r}, \tag{8·5}$$

and, by resolution along and perpendicular to the radius vector,

$$k/r = \gamma'\beta^2. \tag{8·6}$$

Hence
$$\frac{d\bar{\lambda}'_\alpha}{d\bar{s}'} = \frac{\gamma'^2}{r^2}\beta^2\xi'_\alpha, \tag{8·7}$$

and thus
$$\left.\begin{aligned}\left(\lambda\frac{d\bar{\lambda}'}{d\bar{s}'}\right) = 0, \quad \left(\lambda'\frac{d\bar{\lambda}'}{d\bar{s}'}\right) = \frac{\gamma'^2}{r}\beta^3\sin 2\beta,\\ \left(\xi\frac{d\bar{\lambda}'}{d\bar{s}'}\right) = -\gamma'^2\beta^2\cos 2\beta, \quad \left(\xi'\frac{d\bar{\lambda}'}{d\bar{s}'}\right) = \gamma'^2\beta^2.\end{aligned}\right\} \tag{8·8}$$

From (4·19) we obtain, remembering that $\gamma'^{-2} = 1-\beta^2$,

$$\left.\begin{aligned}(\lambda P') &= -\frac{1}{r^3},\\ (\lambda' P') &= \frac{\gamma'}{r^3}(-1+\beta^3\sin 2\beta+\beta^2\cos 2\beta),\\ (\xi P') &= \frac{1}{r^3}(-1+\beta\sin 2\beta-\beta^2\cos 2\beta).\end{aligned}\right\} \tag{8·9}$$

Thus we have from (6·4) the following result:

VI. *When the eccentricity of $(L, L')$ is small of order $\mu^{\frac{1}{2}}$ at $A$, the rate of change of the energy of $L'$ relative to $L$ is given (without any approximation based on smallness of velocity) by the formula*

$$\dot{E} = -\frac{m'c^2}{k}\mu\gamma'^2\beta^5\Phi(\beta) + 0(\mu^2), \tag{8·10}$$

where
$$\Phi(\beta) = 2\beta(1-\beta^2)\cos 2\beta - (1-3\beta^2+\beta^4)\sin 2\beta, \qquad (8{\cdot}11)$$
$$\beta = u'/c, \quad \gamma'^{-2} = 1-\beta^2, \quad \mu = m'/m, \quad k = -ee'/m'c^2.$$

*Here $u'$ is the velocity in the adjacent circular Kepler orbit $\Lambda'$, and* (8·10) *holds for a finite time after the event $A$.*

Let us now consider the rate of change of angular momentum, for which we have the formula (6·6). Substitution from (8·3) and (8·9) in (5·12) gives

$$\left.\begin{aligned} F &= \gamma'^2[\beta^2(2-\beta^2)\cos 2\beta - \beta(1-2\beta^2)\sin 2\beta], \\ G &= \gamma'[\beta^2\cos 2\beta - \beta(1-\beta^2)\sin 2\beta], \\ \Delta &= -\gamma'^2\beta^2 r^2, \\ k/(\lambda\xi) &= -\gamma'\beta^2. \end{aligned}\right\} \qquad (8{\cdot}12)$$

Hence we have this result:

VII. *When the eccentricity of $(L, L')$ is small of order $\mu^{\frac{1}{2}}$ at $A$, the rate of change of the magnitude of the angular momentum of $L'$ relative to $L$ is given (without any approximation based on smallness of velocity) by the formula*

$$\frac{\dot{h}}{h} = -\frac{\mu}{k}\gamma'^2\beta^3\Phi(\beta) + 0(\mu^2), \qquad (8{\cdot}13)$$

*where $\Phi(\beta)$ is given by* (8·11). *This formula holds for a finite time after the event $A$.*

Let us write $E'$, $h'$ for the energy and angular momentum in $(\Lambda, \Lambda')$. By (7·10)

$$\gamma' = J'^{-1}, \quad \beta = K', \qquad (8{\cdot}14)$$

whereas in (7·6)
$$J' = \frac{E'}{m'c^2}, \quad K' = -\frac{ee'}{h'c}. \qquad (8{\cdot}15)$$

We may substitute from (8·14) in the right-hand sides of (8·10), (8·13). But $J'$, $K'$ differ from $J$, $K$ for $(L, L')$ (as given by (7·6)) only by $0(\mu)$ in a finite time-interval from the event $A$. Thus, after substituting from (8·14), we may drop the accents from $J'$, $K'$, absorbing the differences in the terms $0(\mu^2)$.

Thus we obtain the following equations, valid during any finite time-interval measured from an instant $A$ at which $\epsilon^2 = 0(\mu)$:

$$\dot{J} = -\mu k^{-1}J^{-3}K^5\Phi(K) + 0(\mu^2), \qquad (8{\cdot}16)$$
$$\dot{K} = \mu k^{-1}J^{-2}K^4\Phi(K) + 0(\mu^2). \qquad (8{\cdot}17)$$

To investigate the rate of change of eccentricity, we have by (7·7)

$$\epsilon^2 = (J^2+K^2-1)\,J^{-2}K^{-2}. \qquad (8{\cdot}18)$$

By (8·16), (8·17) we have

$$\frac{d}{ds}(J^2+K^2-1) = O(\mu^2), \quad \dot{J} = O(\mu), \quad \dot{K} = O(\mu), \tag{8·19}$$

and also, since $\epsilon^2 = O(\mu)$, $\quad J^2+K^2-1 = O(\mu)$. (8·20)

Hence
$$\frac{d}{ds}(\epsilon^2) = O(\mu^2). \tag{8·21}$$

Let us now consider a large time-interval of order $\mu^{-1}$, extending from $s = 0$ to $s = \alpha/\mu$, where $\alpha$ is a finite constant. At $s = 0$ we suppose $\epsilon^2 = O(\mu)$. We divide the time-range into a large number of equal intervals $(0, s_1)$, $(s_1, s_2), \ldots, (s_{n-1}, s_n)$. In each of these intervals (8·16), (8·17), (8·21) hold, provided that at the beginning of the interval in question $\epsilon^2 = O(\mu)$. From (8·21) it is clear that these equations will hold through all the intervals, because the total increment in $\epsilon^2$ will only be $O(\mu)$.

Let us state this result:

VIII. *Starting from an instant at which the eccentricity of* $(L, L')$ *is small of order* $\mu^{\frac{1}{2}}$, *the equations* (8·16), (8·17) *for the rates of change of energy and angular momentum, and the equation* (8·21) *for the rate of change of eccentricity, are valid for a long interval of proper time on* $L$ *of order* $\mu^{-1}$. *Here* $J, K$, *are defined in terms of* $E, h$ *by* (7·6).

The fate of the system depends on the sign of $\Phi(K)$, where $K$ is approximately equal to $K'$, so that by (8·14) $0 < K < 1$. Now

$$\left.\begin{aligned} \Phi(K) &= 2K(1-K^2)\cos 2K - (1-3K^2+K^4)\sin 2K, \\ \Phi'(K) &= 2K\sin 2K - 2K^4\cos 2K; \end{aligned}\right\} \tag{8·22}$$

$\Phi'(K) = 0$ only if $\qquad \tan 2K/2K = \frac{1}{2}K^2$. (8·23)

For $0 < K \leqslant \pi/4$, the left-hand side exceeds unity, while the right-hand side is less than unity; for $\pi/4 < K < 1$, the two expressions have opposite signs. Hence $\Phi'(K)$ has one sign in the range, and it is positive, since for small $K$

$$\Phi(K) = \tfrac{4}{3}K^3, \tag{8·24}$$

approximately. Thus $\dot{J} < 0$, $\dot{K} > 0$, and so $E$ and $h$ both decrease steadily.

By virtue of (8·20) we may separate the variables in (8·16), (8·17), writing them in the form

$$\dot{J} = -\mu k^{-1}J^{-3}(1-J^2)^{\frac{5}{2}}\Phi[(1-J^2)^{\frac{1}{2}}] + O(\mu^2), \tag{8·25}$$

$$\dot{K} = \mu k^{-1}(1-K^2)^{-1}K^4\Phi(K) + O(\mu^2). \tag{8·26}$$

Let us now state our result in a form easy to understand physically:

IX. *When a particle, of charge $e'$ and small mass $m'$, rotates about a particle of charge $e$ and mass $m$ in an orbit which is initially approximately circular, the orbit remains approximately circular, and its radius shrinks at a rate which is small of the order of $m'/m$. The orbital velocity $u'$ increases at a rate given by*

$$\frac{d\beta}{dt} = \frac{m'}{m}\left(\frac{m'}{-ee'}\right)c^3\frac{\beta^4\Phi(\beta)}{1-\beta^2}, \tag{8·27}$$

*where $\beta = u'/c$ and $\Phi(\beta)$ is given by* (8·11); *the time taken to fall into the centre is large of the order $m/m'$, being in fact given by*

$$t \doteq \frac{m}{m'}\left(\frac{-ee'}{m'}\right)\frac{1}{c^3}\int_{\beta_0}^{1}\frac{(1-\beta^2)\,d\beta}{\beta^4\Phi(\beta)}, \tag{8·28}$$

*$\beta_0$ being the initial value of $\beta$. These results are independent of any approximation based on smallness of $\beta$.*

*When $\beta$ is small, we have approximately for the rates of change of energy and velocity*

$$\frac{dE}{dt} = -\frac{4}{3}\frac{m'}{m}\left(\frac{m'^2}{-ee'}\right)\frac{u'^8}{c^3}, \tag{8·29}$$

$$\frac{du'}{dt} = \frac{4}{3}\frac{m'}{m}\left(\frac{m'}{-ee'}\right)\frac{u'^7}{c^3}, \tag{8·30}$$

*where the energy $E$ is* $$E = m'\gamma'c^2 + ee'/r, \tag{8·31}$$

*or (since the orbit is circular)* $$E = m'c^2/\gamma'. \tag{8·32}$$

We may also express $dE/dt$ in terms of the acceleration of the moving charge. We have approximately by (7·9)

$$\frac{1}{r} = -\frac{m'u'^2}{ee'}, \tag{8·33}$$

and hence the acceleration in the approximately circular orbit is

$$f' = \frac{u'^2}{r} = -\frac{m'u'^4}{ee'}, \quad u'^4 = -ee'f'/m'. \tag{8·34}$$

Substitution for $u'$ in (8·29) gives

$$\frac{dE}{dt} = -\frac{4}{3}\frac{m'}{m}(-ee')\frac{f'^2}{c^3}. \tag{8·35}$$

Starting from the equations of motion with the radiation term (Dirac 1938)

$$m'\dot{\lambda}'_r = \frac{e'}{c^2}F_{rs}\lambda'_s - \frac{2}{3}\frac{e'^2}{c^2}(\ddot{\lambda}'_r - \lambda'_r\dot{\lambda}'_s\dot{\lambda}'_s), \tag{8·36}$$

instead of (2·8), and taking as basis of approximation the smallness of velocities relative to $c$, P. R. Wallace has calculated in his thesis an approximate value for $dE/dt$ by a different method. No restriction being placed on the ratio of the masses, but the orbits being approximately circular, he finds as principal part

$$\begin{aligned}\frac{dE}{dt} &= -\frac{2}{3}\left(e' - e\frac{m'}{m}\right)^2\frac{f'^2}{c^3}\\ &= -\frac{2}{3}e'^2\frac{f'^2}{c^3} - \frac{4}{3}\frac{m'}{m}(-ee')\frac{f'^2}{c^3} - \frac{2}{3}\left(\frac{m'}{m}\right)^2 e^2\frac{f'^2}{c^3}.\end{aligned} \tag{8·37}$$

Here the first term agrees with the outflow of energy at infinity given by the Larmor formula, while the second term agrees with (8·35). If we let $m'/m \to 0$, we get the Larmor formula

$$\frac{dE}{dt} = -\frac{2}{3}e'^2\frac{f'^2}{c^3}. \tag{8·38}$$

Thus while the acceptance of the equations (2·8), without the radiation term, does not give a stable two-body system, we do at least obtain a rate of disappearance of energy considerably less (1/925 in the case of the hydrogen atom) than that given by the equations (8·36), with the radiation term.

## REFERENCES

Darwin, C. G. 1920 *Phil. Mag.* **39**, 537.
Dirac, P. A. M. 1938 *Proc. Roy. Soc.* A, **167**, 148–168.
Pauli, W. 1920 *Encyklopädie d. math. Wissenschaften*, **19**, 645.
Sommerfeld, A. 1934 *Atomic Structure and Spectral Lines*, p. 251. London: Methuen and Co.

# The structure of melamine, $C_3N_6H_6$

BY I. ELLIE KNAGGS, PH.D. AND KATHLEEN LONSDALE, D.SC.

### WITH A NOTE ON THE OPTICAL PROPERTIES OF MELAMINE

BY R. G. WOOD, M.SC. AND G. WILLIAMS, M.SC.

(*Communicated by Sir William Bragg, P.R.S.—Received 5 September* 1940)

Magnetic and X-ray measurements on crystalline melamine, $C_3N_6H_6$, indicate that the molecular formula is of the amide type, based on the cyanuric ring, but that weak hydrogen bridges exist between the $NH_2$ groups of one molecule and the ring nitrogens of others, so that the substance may also tend to behave as an imide. The density is 1·571, the space group $P\,2_1/a$, and there are four molecules in the unit cell. An approximate structure is given. New optical data confirm that this structure is of a layer type, in which respect it is similar to all other cyanuric ring compounds so far examined.

Melamine, $C_3N_6H_6$, is a ring compound whose structural formula (Sidgwick 1937, p. 371) is generally given as (I) although an imide formula (II) has also been considered possible (Beilstein 1938). It does not melt, but sublimes on careful heating (Heilbron 1936). It is a weak base (Franklin 1922), and in the solid state it can add three hydrochloric acid molecules, but does this so slowly that Barnett (1930) has suggested that neither the amide nor the imide formula is satisfactory, although under the influence of hydrochloric acid solid melamine must slowly change to one or the other structure. He puts forward a third formula (III) which, however, would involve very considerable straining of the valency bonds and has little to recommend it to chemists.

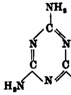
(I)

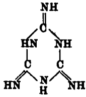
(II)

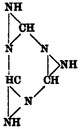
(III)

Melamine crystallizes from water in monoclinic prismatic prisms on the basal planes {001} and with side faces {110} and sometimes {011}.

Heydrich (1910) gives the crystallographic data $a:b:c = 1{\cdot}4121:1:0{\cdot}9728$, $\beta = 112^\circ\ 16'$, which are confirmed by X-ray measurement. The dimensions of the unit cell are as follows: $a = 10{\cdot}54$ A, $b = 7{\cdot}48$ A, $c = 7{\cdot}28$ A. The measured density is 1·571 g./c.c. at 20°/4°, and there are thus four molecules per cell. The space group is $P\,2_1/a$.

The crystals have been optically examined by Heydrich (1910) but a simple microscopic test soon shows that his published data cannot be correct. Detailed optical measurements given in the accompanying note by R. G. Wood and G. Williams show that the crystals must have a layer structure, since the birefringence is strongly negative. The acute bisectrix is nearly normal to the (201) plane.

The magnetic anisotropy of a single large crystal weighing 0·0393 g. has been measured at 20° C in a field of some 7000 G. The minimum susceptibility was measured on a number of small crystals by the Rabi-Krishnan method, using as suspension liquid a diluted Toulet solution saturated with melamine and containing an adjustable amount of nickel chloride.

$$\chi_1-\chi_2 = 19{\cdot}55, \quad \chi_3-\chi_2 = 17{\cdot}85, \quad \chi_1-\chi_3 = 1{\cdot}6\times10^{-6}$$

$$\chi_1\ (\text{measured}) = -58{\cdot}1\times10^{-6}.$$

Hence

$$\chi_2 = -77{\cdot}6_5\times10^{-6},$$

$$\chi_3 = -59{\cdot}8\times10^{-6}\ (\text{along } b \text{ axis}),$$

$$\psi\ (\text{angle } \chi_1 : c \text{ taken positive in obtuse } \beta) = -25^\circ{\cdot}0.$$

The structure, therefore, is magnetically almost uniaxial, with $\chi_2$ as the unique axis. If the molecule itself is uniaxial, as seems very probable from its formula, then the direction of minimum numerical susceptibility $\chi_1$ will be the line in which the plane of the molecule intersects the (010) plane (Lonsdale and Krishnan 1936) and the value of $\chi_1$ will be the susceptibility of the molecule in its own plane. Denoting the molecule susceptibilities by $K_1 = K_2$ (in plane of atoms) and $K_3$ (normal to plane of atoms)

$$\begin{aligned}\Delta K &= K_1-K_3 = 3K_1-(K_1+K_2+K_3)\\ &= 3\chi_1-(\chi_1+\chi_2+\chi_3) = (\chi_1-\chi_2)+(\chi_1-\chi_3)\\ &= 21{\cdot}1_5\times10^{-6}.\end{aligned}$$

The molecular anisotropy of cyanuric triazide, $C_3N_3(N_3)_3$, is $21{\cdot}9\times10^{-6}$ (Lonsdale 1937). This indicates that the predominant formula of melamine is that based on the cyanuric ring (I). Form (II), containing three

$\mathrm{HN}\rangle\mathrm{C{=}NH}$ groups, would probably only have at most an anisotropy of about three times that of $CO_2$ (Krishnan, Guha and Banerjee 1933) or COOH (Lonsdale 1939), namely, $15 \times 10^{-6}$; while the anisotropy of form (III) would be quite small, probably having $K_3$ numerically less than $K_1$ and $K_2$, since no double bonds are present.

The direction cosines of the normal $N$ to the molecular plane can be estimated from the magnetic data, relative to the $a$, $b$, $c'$ axes. The results, which depend on the assumption that $K_1 = K_2$, and are therefore only approximate, are

$$\alpha_N = 48^\circ\!\cdot\!8, \quad \beta_N = 74^\circ\!\cdot\!0, \quad \gamma_N = 45^\circ\!\cdot\!5.$$

The direction of $K_3$ (that is, $N$) is 16° out of the (010) plane and is nearly equally inclined to $a$ and to $c'$. The molecules therefore lie closely parallel to the (201) planes and the structure is definitely of the layer type, as indicated by the optical data.

This conclusion is strongly confirmed by the X-ray investigation. It is found that the (201) planes, spacing 3·4 A, give reflexions of outstanding intensity, so that the molecules must be not only parallel to, but nearly in, the (201) planes. This fact helps us to eliminate many of the possible structures consistent with an arrangement of four molecules in the $P\,2_1/a$ space group.

The magnetic data give only the orientation of the normal to the molecular plane; they cannot indicate the orientation of the molecule in its own plane. The intensities of X-ray reflexion show, however, well-marked maxima for some of the high-index planes. In particular the (060) (170) (270) (071) (208) $(80\bar{7})$ and $(100\bar{6})$ planes have structure factors considerably larger than the average value for the observed reflexions, indicating that all the atoms lie in or near these planes. We already know that the molecules are nearly perpendicular to the (010) planes. The only way of explaining the strong (060) reflexion is to presume that the (010) plane intersects the molecule in a line nearly parallel to a $\mathrm{N} \ldots \mathrm{C{-}NH_2}$ axis. The projection of two molecules *normal* to the (010) planes will then be approximately as shown in figure 1, while that of the structure *on* the (010) planes will be somewhat as shown in figure 2.

The detailed analysis of the structure is not yet complete, but estimates of the intermolecular distances are possible from purely spatial considerations and it is found that the $NH_2 \ldots N$ distance is approximately 3 A and therefore comparable with the $NH_2 \ldots O$ distance of 2·97 A in urea (Wyckoff and Corey 1934). In the latter case it is highly probable that there is a hydrogen bridge from the amide group to the oxygen atom of another molecule, the structure being of a typically polar type. Although the power of association of a hydrogen attached to a nitrogen atom is probably small (Sidgwick 1937, Introduction, p. 19), it is possible not only for a hydrogen atom to form a bridge between nitrogen and oxygen, as in urea, but also between nitrogen and nitrogen as in associated ammonia and also in metal-free phthalocyanine. It appears to be very probable that such a

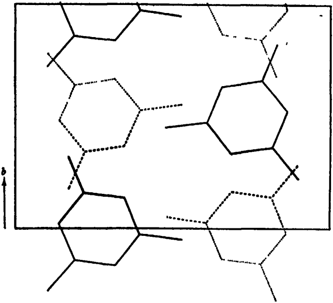

FIGURE 1. Projection on (201). (Inclination and position of molecules not exact.)

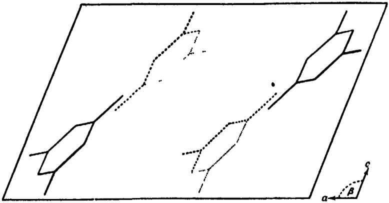

FIGURE 2. Projection on (010).

weak bridge also occurs in melamine, and this may account for the fact that solid melamine does not behave exclusively like an amide but appears to partake to a small degree of the nature of an imide structure also.

It is noteworthy that all the cyanuric compounds so far examined possess layer structures. This has been proved for cyanuric triazide (Knaggs 1935), cyanuric trichloride (Lonsdale 1936), cyanuric acid (Wiebenga and Moerman 1938) and cyanuric acid dihydrate (Lonsdale, unpublished optical and magnetic measurements), as well as for melamine. The occurrence of layer structures among benzene derivatives is relatively infrequent.

Our thanks are due to the Managers of the Royal Institution for laboratory facilities.

### REFERENCES

Barnett 1930 *J. Phys. Chem.* **34**, 1497.
Beilstein 1938 *Handbuch der Organische Chemie*, 4th ed. **26**, 245; supp. p. 74.
Franklin 1922 *J. Amer. Chem. Soc.* **44**, 504.
Heilbron 1936 *Dictionary of Organic Compounds*, **2**, 543.
Heydrich 1910 *Z. Kristallogr.* **48**, 279.
Knaggs 1935 *Proc. Roy. Soc.* A, **150**, 576.
Krishnan, Guha and Banerjee 1933 *Phil. Trans.* A, **231**, 235.
Lonsdale 1936 *Z. Kristallogr.* **95**, 471.
— 1937 *Proc. Roy. Soc.* A, **159**, 149.
— 1939 *Proc. Roy. Soc.* A, **171**, 541.
Lonsdale and Krishnan 1936 *Proc. Roy. Soc.* A, **156**, 603.
Sidgwick 1937 *Organic Chemistry of Nitrogen*, ed. by Taylor and Baker. Oxford: Clarendon Press.
Wiebenga and Moerman 1938 *Z. Kristallogr.* **99**, 217.
Wyckoff and Corey 1934 *Z. Kristallogr.* **89**, 462.

# Note on the optical properties of melamine

By R. G. Wood, M.Sc. and G. Williams, M.Sc.

The optical properties of melamine have been investigated by the method described by Wood and Ayliffe (1936) in which the crystal is immersed in a series of liquids of known refractive index and examined under a polarizing microscope. For this purpose the crystal is mounted on a microscope stage-goniometer in such a way that it can be rotated about the $\beta$-axis of the indicatrix. If $\theta$ denotes the angle through which the crystal has been turned from the position in which the $\alpha$-axis is parallel to the stage, then the refractive index $\mu$ for light vibrating *perpendicular* to the axis of rotation is given by

$$\frac{1}{\mu^2} = \frac{1}{\gamma^2} + \left(\frac{1}{\alpha^2} - \frac{1}{\gamma^2}\right) \cos^2 \theta.$$

The refractive index for light vibrating *parallel* to the axis of rotation is $\beta$ and is independent of $\theta$.

In order to determine the principal refractive indices the match position (defined by $\theta$) is found for each liquid of known refractive index in the series, and then $1/\mu^2$ is plotted against $\cos^2\theta$. From the equation above it is evident that the graph will be a straight line and that the points corresponding to $\theta = 0°$ and $\theta = 90°$ will give $\alpha$ and $\gamma$ respectively. The intermediate index $\beta$ is best found by immersing the crystal in a liquid of refractive index as near $\beta$ as possible (a slight discrepancy makes a negligible difference in the result) and measuring the optic axial angle $2V$. By putting $\theta = V$ the value of $\beta$ can be deduced from the graph, for in the above equation $\mu = \beta$ when $\theta = V$. (If the crystal has positive birefringence, i.e. the axis $\gamma$ is the acute bisectrix, then $2V$ must be taken as the *acute* angle between the optic axes. If the birefringence is negative, $2V$ must be taken as the *obtuse* angle.)

The orientation of the indicatrix relative to the crystallographic axes is easily found if the position of a known face in the zone parallel to $\beta$ is determined relative to $\alpha$, and a method of achieving this has been given by Wood and Ayliffe (1935).

The crystals of melamine which were available were extremely small and they were therefore very difficult to mount sufficiently firmly and accurately in the proper orientation. Eventually, however, measurements were made on two different specimens. The results are combined in the graph of $1/\mu^2$ against $\cos^2\theta$ (figure 3), the points obtained from the two specimens being distinguished by rings and dots respectively. The optic axial angle was measured with the crystal immersed in a liquid of refractive index 1·84 which was very near $\beta$. The numerical results are as follows:

$$2V = 151° \, 22' \quad \text{(birefringence negative)},$$

$$\alpha = 1{\cdot}487, \quad \beta = 1{\cdot}846, \quad \gamma = 1{\cdot}879, \quad \text{(for sodium light)}.$$

The orientation of the indicatrix was determined by making use of the face (001) and is defined by the angle $\hat{\alpha a} = 45° \, 45'$. This orientation is illustrated in figure 4 which also shows the positions of the optic axes

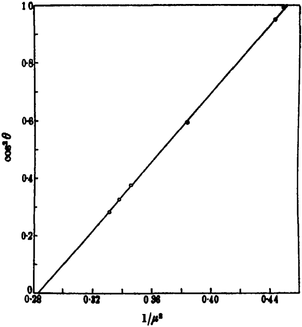

FIGURE 3. Graph of $1/\mu^2$ against $\cos^2\theta$.

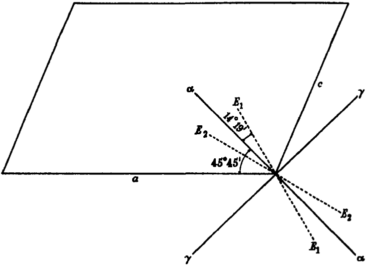

FIGURE 4. Orientation of indicatrix in melamine.

$E_1$ and $E_2$. The approximate limits of error are ± 0·002 in the refractive indices, ± 10′ in the optic axial angle ($2V$) and ± 1° in the angle defining the orientation.

The values of $\alpha$ and $\gamma$ agree with those found by Heydrich (1910), but the value of $\beta$ and the orientation of the indicatrix are entirely different. It would appear probable that Heydrich made some error in cutting the section he used for determining $\beta$.

### REFERENCES

Heydrich 1910 *Z. Kristallogr.* **48**, 279.
Wood and Ayliffe 1935 *J. Sci. Instrum.* **12**, 299.
— — 1936 *Phil. Mag.* **21**, 321.

# The equilibrium diagram of the system silver-zinc

By K. W. Andrews, H. E. Davies, W. Hume-Rothery, F.R.S. and C. R. Oswin

(*Received* 3 *August* 1940)

The equilibrium diagram of the system silver-zinc has been investigated by thermal, microscopic, and X-ray methods. This has enabled the following points to be established:

(1) The depression of the freezing-point of silver by zinc is slightly greater than that produced by equal atomic percentages of indium. This does not confirm the hypothesis of whole-number liquidus factors previously suggested by Hume-Rothery, Mabbott and Channell-Evans (1934).

(2) The solidus and liquidus curves for the $\beta$-phase do not coincide at 50 atomic % of zinc as was proposed by B. G. Petrenko (1929). The freezing range of the equiatomic alloy is approximately 3½°.

(3) The determination of phase boundaries by X-ray methods with quenched filings is unreliable for this class of alloy, and its limitations are discussed.

## I. Introduction

The equilibrium diagram of the system silver-zinc has attracted great attention since the liquidus curve was first investigated by Heycock and Neville (1897). The main form of the diagram was established by Carpenter and Whiteley (1913), and the general conclusions of the earlier work are summarized by M. Hansen (1936), whose diagram is shown in the full lines in figure 1. B. G. Petrenko (1929) concluded that the liquidus and solidus curves for the $\beta$-phase coincided at 50 atomic % of zinc, so that the equiatomic alloy froze at constant temperature. More recently, Owen and Edmunds (1938), using X-ray methods with quenched filings, have proposed considerable changes in the phase boundaries; these are shown in dotted lines in figure 1, and in some places are in conflict with the results of Heycock and Neville. The system is of interest because, as was shown by Hume-Rothery, Mabbott and Channel-Evans (1934),* the depression of the freezing-point of silver produced by addition of zinc was, to within the limits of accuracy then available, that to be expected for a trivalent element, a fact which led to the concept of whole-number liquidus factors. The system is also of general importance, since zinc contracts the lattice spacing of silver by an amount almost equal to the lattice expansion produced by an equal atomic percentage of cadmium. An examination of the equilibrium diagrams of the systems silver-zinc and silver-cadmium thus enables us to compare the relative effects of lattice contraction and expansion. In view of the discrepancies between the results of previous investigators, and the general interest of these alloys, we have made a very detailed examination of the whole system. The present paper describes the general results of this work, whilst the full details have been deposited with the Royal Society.*

---

* This paper will be referred to as H.-R., M. and C.-E.

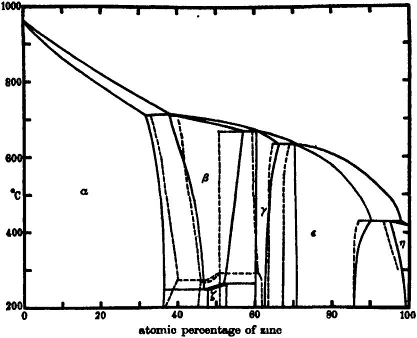

FIGURE 1

## II. EXPERIMENTAL DETAILS

The silver used in the present work was assay silver grain from Messrs Johnson Matthey and Co., Ltd. The zinc used for the cooling curve work was Crown Special Zinc of 99·995 % purity, kindly presented by the National Smelting Co., Ltd., of Avonmouth. For the alloys prepared for phase-boundary determinations, use was made of two brands of spectroscopically pure zinc presented by the New Jersey Zinc Corporation of

---

* Additional copies of the details have been deposited in the Radcliffe Science Library of the University of Oxford, and with the British Non-Ferrous Metals Research Association, and the Institute of Metals.

U.S.A., and by the National Smelting Co., Ltd., of Avonmouth; the authors must express their extreme gratitude to these two firms for their generosity.

For the determination of the liquidus curves, alloys were melted in quantities of 100–150 g. in graphite crucibles. For alloys melting above 700° C a sodium-chloride/potassium-chloride flux was used, together with a layer of small pieces of charcoal, whilst for the alloys of low melting-point a covering of powdered charcoal alone was employed. The cooling curves were taken in the manner described by Hume-Rothery and Reynolds (1937), and all the precautions taken by these authors were followed. The composition of the melts at the moment of freezing were determined by two methods. In one of these, a small sample was removed by suction through a silica tube when the melt was slightly above the expected liquidus point, and the change in composition owing to the volatilization of zinc between the time of extraction and that of freezing was allowed for. In the second method, the crucible was removed from the furnace immediately the arrest was established, and was allowed to cool in air, after which the whole ingot was dissolved for analysis. In alloys for which the liquidus and solidus curves are close together (e.g. the $\beta$-liquidus curve) the two methods gave results in close agreement, but, when the alloys had a greater freezing range, the extraction method was found to give liquidus points which were higher by amounts of the order 0·5–2·5° C than those obtained by the analysis of the whole ingot. This phenomenon was similar to that found by Hume-Rothery and Reynolds for silver-tin alloys, the probable explanation being that, as the suction tube is raised, a small drop of semi-liquid alloy falls back into the melt, so that the composition of the extracted sample is no longer that of the melt as a whole. The method involving the analysis of the whole ingot is therefore more accurate, since the volatilization of zinc during rapid cooling was negligible.

The solidus curves of the $\eta$, $\epsilon$ and $\gamma$ phases were determined by the usual method of quenching, followed by microscopic examination. In all cases the specimens were first made homogeneous by a preliminary annealing treatment, and were then heated at the required temperature for a period of at least 30 min., during which the temperature was controlled by hand to within $\pm 0{\cdot}5°$ C of the required value. For the $\beta$-solidus curve, this method was unsatisfactory, since the frequent decomposition of the $\beta$ phase on quenching made it difficult to detect the first traces of chilled liquid. A heating curve method was therefore adopted, using a cylindrical specimen enclosed in an evacuated silica tube, as described by Hume-Rothery and Raynor (1937). With a rate of heating of the order 1° C per min., the thermal arrests were sharp, and there was no tendency to obtain arrests at too high temperatures owing to a time lag between the thermocouple and the alloy. It was, however, essential to test the ingot most scrupulously for segregation, since any variation in composition results in the alloy melting at too low a temperature. Experiment showed that the loss of zinc during an actual heating curve in a sealed tube was negligible, and the policy adopted was therefore to cut a second specimen from the part of the ingot adjacent to that used for the heating curve specimen, and to give this duplicate specimen exactly the same preliminary heat treatment as that of the heating curve specimen. The inside and outside of the duplicate specimen were then analysed, and, if any marked difference was found, the ingot was rejected. Where the differences in composition were a few tenths of an atomic per cent, the value with the higher zinc content was taken, since the zinc-rich portion would melt first. This procedure does not guard against the danger of longitudinal segregation, but this was not serious for the $\alpha$- and $\beta$-alloys, although for the $\gamma$- and $\epsilon$-alloys, segregation effects were much greater, and only the quenching method was possible. For the $\alpha$ phase, both the heating curve and the quenching methods were used, and the results were in good agreement, and, since the dangers from segregation are greater for the $\alpha$ than for the $\beta$ phase alloys, the points for the $\beta$ phase may be accepted with confidence.

The solid solubility curves for the different phases were determined by the usual methods of annealing, quenching, and microscopic examination. The general methods have already been described by H.-R., M. and C.-E. (1934) and by Hume-Rothery and Raynor (1937), and Foster temperature controllers were again used for controlling the temperature. For the majority of alloys, the most suitable etching reagent was found to be a mixture of sulphuric and chromic acids, the strength of which required careful adjustment according to the class of alloy.

In cases where the high-temperature X-ray camera was used to determine phase boundaries, the general methods of Hume-Rothery and Reynolds (1937) and Hume-Rothery and Raynor (1939) were used. Annealing of the X-ray specimens was carried out in the high-temperature camera, the temperature of which was controlled by a Foster potentiometric regulator. The chief source of error found was that, in sealing off the silica capillary containing the filings, accidental heating of some of the filings might occur, and cause local volatilization of zinc, with the production of a specimen of uneven composition. The policy adopted was to analyse the actual X-ray specimens after the experiment, with the rejection of the filings near the extreme tip of the specimen. The lump from which the filings were prepared was also analysed, and if any marked difference between the two analyses was found, the experiment was rejected.

The analyses of the alloys were carried out by Messrs Johnson Matthey and Co., Ltd., and the author's thanks are due to Mr A. R. Powell for his constant help in this connexion. For the cooling curve ingots, both zinc and silver were determined. For the alloys used in the determinations of the solidus and solid solubility curves, the critical alloys in the immediate vicinity of the phase boundaries were analysed, the analyses being carried out on the actual specimens used for the microscopic examinations. Both sides of the specimens, and sometimes an additional cross-section were examined before the specimens were dissolved for analysis. In general the specimens were analysed by determining silver only, but a large number of alloys were analysed for both silver and zinc as a check on the purity. The analyses were highly satisfactory, and no indication of any contamination was found.

## III. THE LIQUIDUS CURVE

The results of the cooling curve experiments are shown in figures 2–4, and are in table 1 of the collected tables deposited with the Royal Society. The liquidus points of Heycock and Neville (1897) were published in a series of tables, of which those for the silver-rich alloys contained a value for the freezing-point of silver, these freezing-points varying by 2 or 3° C. If, as in the paper of H.-R., M. and C.-E., it is assumed that these variations are due to an error in the pyrometer, which remained constant throughout the particular series, the figures can be corrected to the standard silver point of 960·5° C. If, however, the variation is due partly or wholly to oxidation of the silver, this procedure is incorrect, since zinc acts as a deoxidizer. In view of this uncertainty, we have in figures 2–4 shown these results of Heycock and Neville by means of vertical lines, the lower ends of which give the freezing-points recorded in the original paper, and the upper ends, the same points corrected to a silver point of 960·5° C.

Examination of figures 2–4 shows that our liquidus results are in extremely good agreement with those of Heycock and Neville, and the liquidus curve may be regarded as established to a high degree of accuracy. The curve divides itself into five parts corresponding with the crystallization of the $\alpha$, $\beta$, $\gamma$, $\epsilon$ and $\eta$ phases. The temperatures of the four peritectic horizontals are as follows:

$\alpha + \text{liquid} \rightleftharpoons \beta$ 709·8° C, $\gamma + \text{liquid} \rightleftharpoons \epsilon$ 631·2° C,
$\beta + \text{liquid} \rightleftharpoons \gamma$ 660·6° C, $\epsilon + \text{liquid} \rightleftharpoons \eta$ 430·7° C.

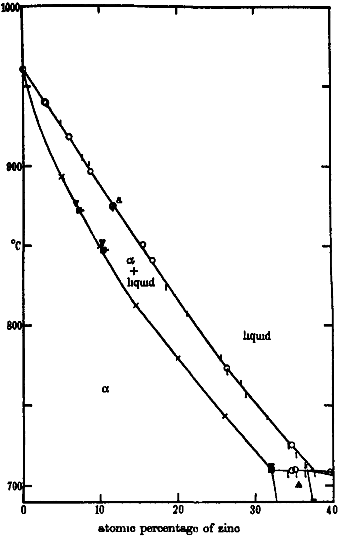

○ Liquidus points by analysis of whole ingot.
| Liquidus points from Heycock and Neville with and without correction.
× Heating curve arrests.
▼ Partly liquid alloys. ■ Homogeneous alloys. ▲ Two-phase alloys.
■- Alloys shown thus were recorded as containing possible traces of chilled liquid.

There are two independent determinations in the present work at the point marked *a*.

In this figure all points from the present work refer to specimens or ingots which were actually analysed.

FIGURE 2

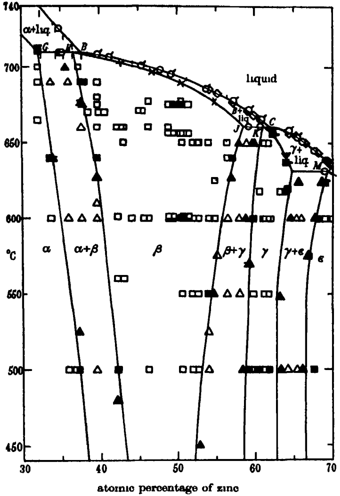

σ Liquidus points by extraction method.
○ Liquidus points by analysis of whole ingot.
| ◇ Liquidus points of Heycock and Neville.
× Heating curves arrests. ▼▽ Partly liquid alloys.
■ Alloys containing possible traces of chilled liquid
■□ Homogeneous alloys. ▲ △ Two-phase alloys.
▲ Two-phase alloys with trace of second phase.
The shaded points refer to the actual specimens which were analysed.

FIGURE 3

The arrest due to the $\beta$ + liquid $\rightleftharpoons \gamma$ reaction is only given by alloys in a narrow range of composition, indicating that the liquidus and solidus are very close together. This is in agreement with the diagrams of the earlier

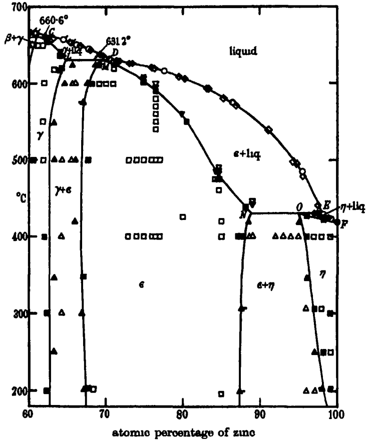

σ Liquidus points by extraction method.
○ Liquidus points by analysis of whole ingot.
◇ Liquidus points from Heycock and Neville.
■ □ Homogeneous alloys.
▲ △ Two-phase alloys.
▼ ▽ Partly liquid alloys.

The shaded points refer to the specimens which were actually analysed after annealing at the temperature concerned.

Figure 4

workers, but in contradiction with the phase boundaries proposed by Owen and Edmunds, which would require the arrest to be shown by all alloys between 51 and 62 atomic % zinc. The present liquidus curve gives the composition of the *liquid* phase at the $\alpha$ + liquid $\rightleftharpoons \beta$ peritectic horizontal as 37·5 atomic % of zinc, and is thus in conflict with the results of Owen and Edmunds, who give the composition of the *solid* $\beta$ phase at this point as 40·0 atomic % zinc, this composition lying in totally liquid region, according to the results of both Heycock and Neville, and of the present work.

## IV. THE $\alpha$ PHASE

The $\alpha$-solidus curve as determined by the quenching, and heating curve method is shown in figure 2, and is in places as much as 10° C lower than the values given in the collected tables of H.-R., M. and C.-E. Reference to the original tables shows that all but two of the temperature brackets of H.-R., M. and C.-E. could be reconciled with the present data, but one point was definitely incorrect, and it is this which accounts for the incorrect solidus curve drawn by H.-R., M. and C.-E.

The $\alpha$-solid solubility limit at the 709·8° C peritectic horizontal was determined as 32·1 atomic % of zinc. This value was accurately established by means of alloy 32·06* which consisted of homogeneous $\alpha$ after quenching from 710·5° C, but contained clear traces of chilled liquid after quenching from 712·5° C. The whole of the high-temperature portions of the $\alpha/\alpha+\beta$ boundary determined in the present work lies slightly to the silver-rich side of that proposed by Owen and Edmunds, and this cannot be ascribed to insufficient annealing, since the times of annealing in the present work were very much the greater. The microstructures of these alloys were quite clear, and since the actual specimens were analysed, we can only conclude that the boundary given by Owen and Edmunds is incorrect, a possible explanation of this discrepancy is given later (p. 158).

With falling temperature, the solubility of zinc in silver increases, as in the typical $\alpha/\beta$ brass type of equilibrium, until a maximum of 40·2 is reached at 258° C (point $P$). The value obtained by Owen and Edmunds for this point was 40·0 atomic % zinc. Below 258° C the solubility of zinc in silver diminishes comparatively rapidly, and at 200° C it is only 36·7 atomic %. This decrease in solubility is due to the fact that below 258° C, the $\alpha$ phase is in equilibrium not with the $\beta$, but with the $\zeta$ phase which has a complicated hexagonal structure. For this part of the diagram, the $\alpha/\alpha+\zeta$ boundary was determined by annealing alloys which had previously been made homogeneous by a long treatment at 300° C. Precipitation of the $\zeta$ phase took place slowly, and it is probably this fact which accounts for our finding a greater decrease in solubility of zinc in silver than Owen and Edmunds, since our final annealing treatment varied from 37 days at 250° C to 52 days at 202° C, whereas the maximum time given in the table of Owen and Edmunds is 76 hr.

---

* For convenience an alloy containing $x$ atomic % of zinc will be described as alloy $x$.

## V. THE $\beta$ PHASE

The $\beta$ phase limits are shown in figures 3 and 5, and it is for this phase that our results at high temperatures differ most widely from those of Owen and Edmunds. For the composition of the $\beta$ phase at the 709·8° C peritectic horizontal, we obtain the value 36·0 atomic % zinc, as compared with the value 40·0 atomic % zinc given by Owen and Edmunds, and for the whole of the high temperature region, our results give the $\alpha+\beta/\beta$ boundary as lying considerably to the silver-rich side of that of Owen and Edmunds, although below 500° C the two investigations are in reasonable agreement. These differences are probably due to decomposition of the $\beta$ phase on quenching, since microscopic examination showed that on quenching from temperatures above 500° C, it was impossible to prevent decomposition of the $\beta$ phase, even though small specimens were quenched in iced brine. Fortunately, the structure of the decomposed $\beta$ phase was so fine that no difficulty was experienced in distinguishing between alloys quenched from the $\alpha+\beta$, and $\beta$ regions, and so the $\alpha+\beta/\beta$ phase boundary could be accurately determined; photomicrographs of these alloys have been deposited with the Royal Society. Below 500° C no visible decomposition of the $\beta$ phase could be observed. This does not, of course, prove the absence of submicroscopic decomposition, or mass transformation to a new structure, but it is at least significant that below 500° C the X-ray and microscopic methods give results differing by less than 1 atomic %. Decomposition of the $\beta$ phase during quenching occurs by precipitation of the $\alpha$ phase, so that if Owen and Edmunds's specimen were affected by decomposition, this might account for an apparent shift of the $\alpha+\beta/\beta$ boundary in the zinc-rich direction, and also possibly for a similar error in the $\alpha/\alpha+\beta$ boundary. For, on account of the slope of the solubility curve, any decomposition of the $\beta$ phase during cooling will presumably result in the precipitation of $\alpha$ phase of increasing zinc content, and although this may not be sufficient to produce fuzzy lines, the centres of darkening of the lines may be shifted slightly, in the direction corresponding with increasing zinc content.

The results of the heating curve experiments for the determination of the $\beta$ solidus curve are shown in figure 3. The freezing range of the $\beta$ phase is always small, and the solidus curve confirms the general type of diagram of the older investigations.

For the $\beta/\beta+\gamma$ boundary, Owen and Edmunds gave an almost vertical line at 50·7–50·9 atomic % zinc, whereas our own results indicate that the boundary curves from 50·0 atomic % of zinc at 274° C, to 58·6 atomic % of zinc at the 660·6° C peritectic horizontal, in agreement with the evidence of the liquidus and solidus determinations. The difference between this conclusion and that of Owen and Edmunds is undoubtedly connected with changes of the $\beta$ phase on quenching, since our results show that, between 45 and 48 atomic % of zinc, the alloys can be quenched without any apparent decomposition,* but that when the zinc content exceeds about 50 atomic % of zinc, the character of the alloys changes entirely. By quenching in iced brine, alloys in the range 50–55 atomic % zinc can be obtained which show large crystals of $\beta$ with little or no sign of decomposition. Quenching of the same alloys in ice and water produces a number of indefinite structures, some of which apparently contain three phases, whilst quenching in hot water gives rise to structures with clear decomposition. Alloys in the region 52–58 atomic % of zinc always underwent decomposition on quenching, with the formation of structures similar to those found in alloys from the corresponding parts of the $\beta$ phase areas in other systems (Cu-Zn, Cu-Ga). There was also a general tendency for the $\beta$ phase to decompose more readily in alloys quenched from the two-phase $(\beta+\gamma)$ area than in those quenched from the homogeneous $\beta$ region. Photographs of some of the decomposed structures have been deposited with the Royal Society, and fortunately, at the higher temperatures, these decomposed structures were sufficiently fine to be distinguished from those of alloys which contained the $\gamma$ phase as a genuine equilibrium constituent at the temperature of quenching, and in this way the $\beta/\beta+\gamma$ boundary was readily determined down to 450° C, but below this temperature further difficulties were encountered, owing to the stability of some of the decomposed structures. If, for example, an alloy which at 300° C was in the $(\beta+\gamma)$ region was first made homogeneous by annealing at 650° C, and then quenched, the 'decomposed' structure of the quenched alloy was sometimes so stable that prolonged annealing was necessary to obtain equilibrium at 300° C. To overcome this difficulty, the alloys were first made homogeneous by annealing at 600 or 650° C, and were then slowly cooled to successive temperatures, and then quenched. Under these conditions the $\gamma$ phase precipitated clearly, usually in the grain boundaries, and a period of 5 days at the final temperature was sufficient to ensure precipitation, and thus to obtain the $\beta/\beta+\gamma$ boundary.

---

* A mass decomposition to an ordered structure is of course not disproved.

The $\beta/\beta+\gamma$ phase boundary determined by microscopic methods clearly resembles that of the older diagrams, but it was thought advisable to obtain additional confirmation by X-ray methods. For this purpose, alloys 51·7 and 54·4 were annealed in lump form at 500° C, and quenched, after which X-ray specimens were prepared in silica capillaries, and films taken after annealing in the camera for 21 hr. at 500° C. The film from alloy* 54·4 showed lines due to both $\beta$ and $\gamma$ phases, whilst that from alloy 51·7 showed $\beta$ lines only. The $\gamma$ phase is characterized by a strong diffraction line near to the (211) line of the $\beta$ phase, and this forms a sensitive test for the presence of the $\gamma$ phase. These results agree with the microscopic evidence which was further confirmed by a photograph of alloy 53·9 which showed $\beta$ phase lines only at 600° C. A sample of alloy 56·0 was similarly treated at 640° C, and photographed after 6 hr. annealing in the camera, and the film showed a faint $\gamma$ line although, according to the microscopic work, the alloy at this temperature should consist of the $\beta$ phase only. Using another specimen of the same alloy with a longer time of annealing in the camera the $\gamma$ line became fainter, suggesting that true equilibrium had not been reached. Finally, filings of the same alloy were prepared in nitrogen, using the apparatus of Hume-Rothery and Raynor (1939), and films were taken after annealing the specimen in the camera for 23, 47 and 94 hr. respectively. These films showed lines due to the $\beta$ phase alone. The temperature of the camera was then reduced by steps of 20° C, and films were taken after annealing for periods of about 22 hr. at each temperature.† The films at 560 and 580° C showed clear $\gamma$ lines. These films were not suitable for lattice spacing measurements, since, in contrast to the films taken at 500° C, the high-angle lines were very faint, and the general scattering considerable. The low-angle lines were, however, quite clear, and the whole series of films was therefore examined in the region of the (211) $\beta$ phase line by means of a Hilger photoelectric microphotometer, and the photometer curves showed a definite indication of a faint $\gamma$ line in the 600° C film, but not in the films at 620 and 640° C. The analysis of the specimen gave the value 55·7 atomic % zinc, and the method therefore gives the $\beta/\beta+\gamma$ phase boundary for this alloy as lying between 600 and 620° C in complete agreement with the value 615° C obtained for the curve given by the microscopic work. Further, the marked increase in the intensity of the $\gamma$ line as the temperature fell below 600° C clearly supports the phase boundary of the type shown in figure 3, and is not what would be expected from an almost vertical boundary. The microscopic and high temperature X-ray results are thus in complete agreement.

---

* The compositions are here the compositions of the actual filings at the conclusion of the experiment.

† In these experiments the camera was loaded with the specimen at the high temperatures, and the camera was never cooled.

## VI. THE $\zeta$ PHASE

The $\alpha+\zeta/\zeta$, and $\zeta/\zeta+\gamma$ phase boundaries were determined by microscopic methods, and the results which are shown in figure 5, indicate that, at the lower temperatures, the $\zeta$ phase extends over a range of composition which is considerably greater than previously had been imagined. The times of annealing were extended to as much as 52 days at 200° C, and it is probably this which accounts for the discovery of the wider range of solid solubility.

The $\beta\rightleftharpoons\zeta$ transformation was studied by X-ray methods, since the work of previous investigators showed that, although the transformation extended over a comparatively short range of temperature, the arrest points on heating and cooling curves might differ by as much as 20–40° C. In the present work the alloys in the homogeneous $\zeta$ region were given two different annealing treatments in lump form, (*a*) a preliminary high-temperature treatment followed by 25 days at 230–250° C, in order to obtain the alloy in thorough equilibrium in the $\zeta$ region, and (*b*) an annealing treatment at 600–650° C, followed by quenching in cold water. Filings were then prepared, and annealed for 5–6 hr. at different temperatures, in the high-temperature X-ray camera, after which an exposure was made, and the camera was allowed to cool to room temperature, and was then heated to another temperature, and a further exposure made. This procedure will be called the 'normal method', and, during the preliminary anneal in the camera, the temperature was controlled to within $\pm 1{\cdot}5^\circ$ C of the desired temperature by automatic control, whilst during the actual exposure, the temperature was controlled by hand to $\pm 0{\cdot}5^\circ$ C. The lump-annealing treatments (*a*) and (*b*) gave equally sharp lines for the $\zeta$ phase, showing that the period of 5–8 hr. was sufficient for the quenched alloy to reach equilibrium in the homogeneous $\zeta$ region, although in the two-phase region much longer times were required. Using the normal method, the results were reproducible in the sense that if, for example, a particular alloy was found to be in the $\zeta$ region at 260° C, and in the $\beta$ region at 265° C, a subsequent exposure at 260° C again gave $\zeta$ phase lines only, showing that, on using the normal method, the effect of heating into the $\beta$ region was destroyed by the subsequent annealing in the $\zeta$ region. In this way films were obtained showing $\beta$ or $\zeta$ lines, whilst at some intermediate temperatures $(\beta+\zeta)$ lines were obtained. The effect of extending the annealing period from 5 to 28 hr. was studied for one alloy in the $(\beta+\zeta)$ region, and only slightly increased the relative intensity of $\beta$ lines, suggesting that the normal method gave results very near to those of true equilibrium. When, however, alloys were heated in the X-ray camera to 350° and 400° C, and then cooled rapidly to fixed temperatures, and annealed for 5 hr., the transformation from the $\beta$ to the $\zeta$ phase took place at temperatures as much as 10° C lower than those given by the normal method. An alloy heated a few degrees above the transformation temperature, and then slowly cooled over a period of several days, transformed at a temperature about 5° C lower than that indicated by the normal method, and the proportion of the $\zeta$ phase increased considerably with time of annealing. These differences may be connected with the development of short-range order in the $\beta$ phase at low temperatures, since, although superlattice lines are not shown, many facts* suggest that ordered structures of some kind are present, and the magnitude of the effects resemble those found by Sykes and Jones (1939) for the CuPd transformation. The procedure adopted was to draw the most probable curve through the points obtained by the normal method, and then to lower this curve by 3° C in order to allow for the difference between results obtained on heating up or cooling down. This adjusted curve is shown in figure 5, and, in view of the narrowness of the two-phase region, further progress is impossible until the X-ray camera can be controlled to within a fraction of a degree over a long period. The temperature of the $\beta+\gamma=\zeta$ transformation is based on the results for an alloy containing 50·0 atomic % of zinc, which is just at the boundary of the $\beta$ phase, and this was confirmed by additional experiments which showed that with two-phase alloys this transformation exhibited little or no hysteresis. The temperature of the $\alpha+\zeta\rightleftharpoons\beta$ transformation was determined by means of two-phase alloys annealed in lump form at 250° C, and then treated by the normal method. Additional experiments, in which the specimen was first heated above the transformation temperature and then cooled down by small steps, gave a result 5° lower than that from the normal method, and the line in figure 5 is therefore drawn 3° C lower than that given by the normal method. Full details of the experiments made to test these effects have been deposited with the Royal Society (table 11).

---

* The suggestion of ordered structures of some kind are (1) the sudden change in the stability of the $\beta$ phase when the zinc content exceeds 50 atomic %, (2) the ready formation of long-range order on quenching, (3) the fact that the $\beta$ phase at low temperatures extends up to but not beyond 50 atomic % of zinc.

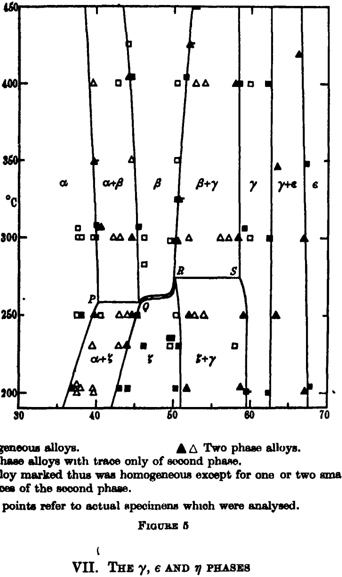

■ □ Homogeneous alloys. ▲ △ Two phase alloys.

▲ Two phase alloys with trace only of second phase.

■ The alloy marked thus was homogeneous except for one or two small regions showing traces of the second phase.

The shaded points refer to actual specimens which were analysed.

FIGURE 5

## VII. THE $\gamma$, $\epsilon$ AND $\eta$ PHASES

The solid solubility limits of the $\gamma$, $\epsilon$ and $\eta$ phases are shown in figures 3–6, and are in tables 6–10 of the collected tables. Between 500 and 600° C our results for the $\beta+\gamma/\gamma$ boundary are in good agreement with those of

Owen and Edmunds, but above 600° C we place this boundary further to the zinc-rich side, and for the limiting value at the peritectic horizontal (point *K*) we obtain 61·4 ± 0·3 atomic % zinc as compared with Owen and Edmunds's value of 59·5 atomic %. We think that the present values are

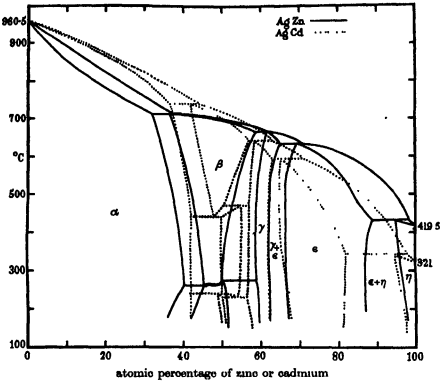

FIGURE 6

the more probable, since both alloys 59·77 and 60·00 contained appreciable quantities of the $\beta$ phase after annealing for 6 days at 650° C. Between 500 and 300° C we place the $\beta+\gamma/\gamma$ boundary to the silver-rich side of that of Owen and Edmunds, and we confirm their observation that the $\gamma$ phase area narrows below the temperature of the $\beta \rightleftharpoons \zeta$ transformation. For the $\gamma/\gamma+\epsilon$ boundary, our results are in good agreement with those of Owen and Edmunds at high temperatures, but at the lower temperatures our results show that the $\gamma$ phase becomes more restricted on the zinc-rich side than was previously supposed. We think that this may be due to the fact that, whilst both series of investigations gave satisfactorily long preliminary annealing temperatures, the final annealing temperatures were very much longer in the present work, and this longer anneal may have enabled precipitations to occur.

For the $\epsilon$ phase[*] our phase boundaries are in general agreement with those of Owen and Edmunds, except that the present $\epsilon/\epsilon+\eta$ boundary lies slightly more to the zinc-rich side, the difference at the higher temperatures being of the order 1 to 2 atomic %.

The microscopic methods do not distinguish between the different modifications of zinc, and we have therefore adopted the policy of Hansen, and denoted the zinc-rich phase by the symbol $\eta$. At the 430·7° C peritectic horizontal we place the maximum solubility of silver in solid zinc as 5·0 atomic %. This is considerably smaller than the value 6·2 atomic % given by Owen and Edmunds, but in good agreement with the value 5·3 atomic % given in the International Critical Tables as the most probable value given by the older work. The smaller solubility indicated by the microscopic methods is not likely to be due to insufficient annealing, since, in our work, alloy 96·07 became homogeneous after 10 days at 400° C, whilst alloy 95·04 still contained traces of the $\epsilon$ phase after 10 days at 400° C followed by 10 days at 419° C. At the lower temperatures the $\epsilon+\eta/\eta$ boundary was determined by the annealing of specimens previously made homogeneous by annealing for 10 days at 400° C; the final annealing treatments were extended to 81 days at 203° C, since a period of 29 days was found to be insufficient to ensure precipitation.

## VIII. DISCUSSION

The present accurate determination of the equilibrium diagram of the system silver-zinc establishes certain points which may be briefly discussed.

(*a*) The liquidus curve of the $\alpha$-solid solution of zinc in silver is slightly but definitely lower than the corresponding curve in the system silver-indium which was accurately determined by Hume-Rothery and Reynolds (1937). The hypothesis of whole number liquidus factors is therefore not confirmed.

(*b*) The suggestion of B. G. Petrenko (1929) that the $\beta$-liquidus and solidus curves coincide at 50 atomic % of zinc is not confirmed. The freezing range is slight, but is about $3\frac{1}{2}$° C at the equiatomic composition.

(*c*) A comparison of the equilibrium diagrams of the system silver-zinc and silver-cadmium is made in figure 5.* The $\alpha$ solid solution is more restricted in the system silver-zinc, whilst the $\beta$ solid solution is very much larger. The ordered $\beta'$ (body-centred cube, caesium chloride structure) phase which is present as a stable constituent of the system silver-cadmium, is not a stable constituent in the system silver-zinc. The fact that some alloys in the $\beta$ phase area in the system silver-zinc pass into the ordered state on quenching, suggests that the free energy of the ordered form is very nearly but not quite low enough to make the ordered structure a stable constituent. The remarkable change in the stability on quenching of the $\beta$ phase when the zinc content exceeds 50 atomic %, suggests clearly that a short-range order, not revealed by the present X-ray methods, is present.

---

[*] In the work of Owen and Edmunds this phase is called $\theta$, but we have preferred the symbol $\epsilon$ used by Hansen (1936) since it agrees with the terminology suggested by Bradley (1937).

The liquidus curves of the $\beta$, $\gamma$ and $\epsilon$ phases of the system silver-zinc show a marked flattening on the silver-rich side in agreement with the conclusion of Hume-Rothery, Reynolds, and Raynor (1940) that increasing electrochemical factors give liquidus curves which tend to resemble those of definite compounds.

(*d*) If the present results are accepted, it is clear that the X-ray methods with quenched filings are unreliable for this class of alloy, and that if any suggestion of decomposition is found, other methods must be used, not merely for the phase which is decomposing (e.g. the $\alpha+\beta/\beta$ and $\beta/\beta+\gamma$ boundaries), but also for the phase in equilibrium with the decomposing phase (e.g. the $\alpha+\beta/\beta$ boundary). It is also clear that the use of quenched filings does not enable the phase boundaries to be determined accurately with short periods of annealing at the lower temperatures, since the longer times of annealing in the present work have given results which differ from those of Owen and Edmunds in the way to be expected if short annealing did not give true equilibrium. The conclusion may be drawn that for the accurate determination of phase boundaries in alloys of elements of which reasonable quantities are available, the classical methods are more suitable and reliable except in special cases such as superlattice formation, or failure to distinguish between phases by etching, etc. High temperature X-ray methods offer many possibilities, but the analysis of the actual specimens appear to be essential, and for this a microchemical technique is required.

---

* This is taken from the review by Hansen (1936), and the $\alpha$-solid solubility curve from the work of H.-R., M. and C.-E. We have not used the data of Owen, Rogers and Guthrie (1939), since these authors mention difficulties in preventing decomposition during the quenching of these alloys, and in view of the present results, the classical methods of Durrant and others appear more reliable.

The authors must express their gratitude to Professor C. N. Hinshelwood, F.R.S., for laboratory accommodation and many other facilities which have greatly encouraged the present research. Grateful acknowledgement of financial assistance is made to the Council and Government Grant Committee of the Royal Society, the British Non-Ferrous Metals Research Association, and the Trustees of the Leigh Fund of the University of Oxford, and also to the Imperial Chemical Industries Ltd. for the loan of apparatus.

## REFERENCES

Bradley, A. J. 1937 *Monthly J. Inst. Met.* **4**, **222**.
Carpenter, H. C. H. and Whiteley, W. 1913 *Int. Z Metallogr.* **3**, **145**.
Hansen, M. 1936 *Der Aufbau der Zweistoff legierungen.* Berlin: Julius Springer.
Heycock, C. T. and Neville, F. H. 1897 *J. Chem. Soc.* **71**, **407**.
Hume-Rothery, W., Mabbott, G. W. and Channel-Evans, K. M. 1934 *Phil. Trans.* A, **233**, **1**.
Hume-Rothery, W. and Raynor, G. V. 1937 *J. Inst. Met.* **61**, **205**.
— — 1939 *J. Inst. Met.* **65**, **379**.
Hume-Rothery, W. and Reynolds, P. W. 1937 *Proc. Roy. Soc.* A, **160**, **282**.
— — 1938 *Proc. Roy. Soc.* A, **167**, **25**.
Hume-Rothery, W., Reynolds, P. W. and Raynor, G. V. 1940 *J. Inst. Met.* **66**, (**6**), **191**.
Jones, F. W. and Sykes, C. 1939 *J. Inst. Met.* **65**, **419**.
Owen, E. A. and Edmunds, I. G. 1935 *J. Inst. Met.* **57**, **297**.
— — 1938 *J. Inst. Met.* **63**, **265**, **279**.
Owen, E. A. and Pickup, L. 1933 *Proc. Roy. Soc.* A, **140**, **344**.
Owen, E. A., Rogers, J. and Guthrie, J. C. 1939 *J. Inst. Met.* **65**, **457**.
Petrenko, B. G. 1929 *Z. anorg. Chem.* **184**, **369**.

# The magnetic and other properties of the free electrons in graphite

By N. Ganguli and K. S. Krishnan, F.R.S.

*Indian Association for the Cultivation of Science, Calcutta*

(*Received* 16 *August* 1940)

1. Graphite crystals have a large free-electron diamagnetism, which is directed almost wholly along the hexagonal axis. Over the whole range of temperature over which measurements have been made, namely, from 90 to 1270° K, this free-electron diamagnetism of graphite per carbon atom is found to be equal to the Landau diamagnetism per electron of a free-electron gas obeying Fermi-Dirac statistics and having a degeneracy temperature of 520° K.

2. From this experimental result it is concluded (*a*) that the number of free or mobile electrons in graphite is just one per carbon atom; (*b*) that the effective mass of these electrons for motion in the basal plane is just their actual mass, showing that the movements in this plane are completely free and uninfluenced by the lattice field; (*c*) that on the other hand their effective mass for motion along the normal to the basal plane is enormous, about $190^2$ times the actual mass, which indicates that the mobile electrons belonging to any given basal layer of carbon atoms are tightly bound to the layer, though, according to (*b*), they can migrate quite freely over the whole of the layer; (*d*) that this tight binding accounts for the observed low degeneracy temperature of the electron gas in the crystal.

3. The electron gas in graphite thus conforms to a simple model which is easily amenable to theoretical treatment, and it has a low degeneracy temperature which is conveniently accessible for experimenting. It therefore forms a suitable medium for studying the properties of an electron gas.

4 The conclusions stated in 2 are in accord with the quantal views of the electronic structure of graphite, and also with its Brillouin zones. There is one zone which can just accommodate three electrons per atom, and the energy discontinuities at all of its boundary surfaces are large. There is a bigger zone which can just accommodate all the four valency electrons, but the energy discontinuities at those of its faces that are perpendicular to the basal plane are very small.

## 1. Introduction

As is well known, graphite crystals exhibit an abnormal diamagnetism, directed almost wholly along the hexagonal axis of the crystal, and having a large temperature coefficient. This diamagnetism is evidently due to the presence of 'free' electrons in the crystal, and a detailed study of the diamagnetism should enable us to obtain at least some of the general characteristics of these free electrons. In the present paper is given a discussion of the diamagnetism of graphite from this point of view, and it is found that the magnetic data indeed reveal all the main features of the free electron gas in the crystal. For example, it is found that the number of free electrons is just one per carbon atom, that under the influence of the lattice field the movements of these electrons along the normal to the basal plane are severely restrained, whereas their movements in the basal plane remain almost completely free, and lastly, that as a result of the restraint imposed on the movements along the former direction, and the peculiar structure of the Brillouin zones of the crystal, the degeneracy temperature of the electron gas becomes very low indeed, sufficiently low to be easily accessible for experimenting in the laboratory.

This simple picture of the free electron gas in graphite revealed by the magnetic data naturally makes graphite a very suitable medium for studying in general the properties of an electron gas. An account of some of these studies will be given in Part II.

## 2. THE MAGNETIC PROPERTIES OF A FREE-ELECTRON GAS

It was discovered by Landau (1930) that an electron gas should have, besides its spin-paramagnetism, an appreciable diamagnetism also, superposed on it, due to the quantized orbital motions of the electrons in the magnetic field. For a *free*-electron gas both the diamagnetic and the paramagnetic susceptibilities are easily calculated. Neglecting terms that are dependent on the magnetic field, the diamagnetic susceptibility per unit volume of the gas is given by the expression (see Stoner 1935)

$$K_d = -\frac{n\mu^2}{3kT}\frac{F'(\eta)}{F(\eta)}, \tag{1}$$

where $n$ is the number of electrons per unit volume, $\mu$ is the Bohr magneton,

$$F(\eta) = \int_0^\infty \frac{x^{\frac{1}{2}}\,dx}{e^{x-\eta}+1}, \tag{2}$$

$$\begin{aligned} F'(\eta) &= \frac{\partial}{\partial\eta}F(\eta), \\ &= \frac{1}{2}\int_0^\infty \frac{x^{-\frac{1}{2}}\,dx}{e^{x-\eta}+1}, \end{aligned} \tag{3}$$

$$\eta = \zeta/kT, \tag{4}$$

$\zeta$ being the thermodynamic potential per electron. $k$ and $T$ have their usual significance.

The numerical values of $F(\eta)$ and $F'(\eta)$ for different values of $\eta$ can be obtained from the tables for Fermi-Dirac integrals given by McDougall and Stoner (1938).

To the same approximation, the paramagnetic susceptibility per unit volume is given by

$$K_p = \frac{n\mu^2}{kT}\frac{F'(\eta)}{F(\eta)}, \tag{5}$$

which is just three times the diamagnetic susceptibility.

The resultant susceptibility, namely, $K = K_p + K_d$, will therefore be paramagnetic.

Let us define the degeneracy temperature $T_0$ of the gas by the usual expression

$$T_0 = \zeta_0/k \tag{6}$$

$$= \frac{h^2}{2mk}\left(\frac{3n}{8\pi}\right)^{\frac{2}{3}}, \tag{7}$$

where $\zeta_0$ is the value of $\zeta$ at the absolute zero of temperature, or the maximum kinetic energy of an electron in the gas when it is completely degenerate. At very high temperatures, $T \gg T_0$, $F'/F$ tends to reach asymptotically the value 1, and the two susceptibilities will then conform to the Curie laws

$$K_d = -\frac{n\mu^2}{3kT} \quad \text{and} \quad K_p = \frac{n\mu^2}{kT}, \tag{8}$$

respectively. At very low temperatures, $T \ll T_0$, the expressions for the two susceptibilities will reduce to the temperature-independent values

$$K_d = -\frac{n\mu^2}{2kT_0} \quad \text{and} \quad K_p = \frac{3n\mu^2}{2kT_0}. \tag{9}$$

## 3. EFFECT OF THE LATTICE FIELD

When the electrons are not quite free, but are under the influence of the lattice field, as the conduction electrons in any actual metal are, the expressions for the two susceptibilities, particularly for the diamagnetic susceptibility, will naturally be complicated. But in the special case, which is of practical interest, when the surfaces of constant energy of these electrons in $k$-space* may be represented by the family of similar ellipsoids,

$$E = \frac{h^2}{2m}(\alpha_1 k_x^2 + \alpha_2 k_y^2 + \alpha_3 k_z^2), \tag{10}$$

the two susceptibilities can be evaluated easily (see Mott and Jones 1936, chap. VI, § 6.2). We shall take the number of electrons per unit volume of this gas also to be $n$, and denote the various quantities relating to this gas by the same letters as for the free-electron gas, but with the subscript $g$ attached to them.

The degeneracy temperature $T_{0g}$ of this gas can be shown to be related to that of a free-electron gas of the same density by the equation

$$T_{0g} = T_0(\alpha_1\alpha_2\alpha_3)^{\frac{1}{3}}. \tag{11}$$

The effect of the lattice field is thus to increase the degeneracy temperature by a factor $(\alpha_1\alpha_2\alpha_3)^{\frac{1}{3}}$. Its effect on the paramagnetism of the electron gas, given by expression (5), will therefore be to increase the argument in the functions $F'$ and $F$ from $\eta$ to $\eta_g$, where

$$\eta_g = \eta(\alpha_1\alpha_2\alpha_3)^{\frac{1}{3}} = \frac{\zeta}{kT}(\alpha_1\alpha_2\alpha_3)^{\frac{1}{3}}. \tag{12}$$

At high temperatures, $T \gg T_{0g}$, the paramagnetic susceptibility will thus be the same as for a free-electron gas of the same density, namely,

$$K_{pg} = \frac{n\mu^2}{kT}. \tag{13}$$

At low temperatures, $T \ll T_{0g}$, when the gas is completely degenerate,

$$K_{pg} = \frac{3n\mu^2}{2kT_{0g}} \tag{14}$$

$$= \frac{3n\mu^2}{2kT}(\alpha_1\alpha_2\alpha_3)^{-\frac{1}{3}}, \tag{15}$$

as compared with the value

$$K_p = \frac{3n\mu^2}{2kT_0}$$

for a free-electron gas of the same density.

Considering next the effect of the lattice field on the diamagnetism of these electrons, we may notice here that the effect is two-fold. The first is due to the increase in the degeneracy temperature, by the factor $(\alpha_1\alpha_2\alpha_3)^{\frac{1}{3}}$, and will be similar to the effect of the lattice field on the paramagnetism of the gas. The second is more direct and arises from the fact that the kinetic energies of the electrons conform to equations of the type (10), which shows that the electrons behave as though their 'effective masses' were $m/\alpha_i (i = 1, 2, 3)$, instead of $m$. This will be so in the equations of motion of the electrons in the magnetic field also. Taking the direction of the magnetic field to be along the $z$-axis of the energy ellipsoid, the equations of motion of the electrons in the $xy$-plane will thus differ from the equations for free electrons in having an effective magnetic moment $\mu_g = \mu(\alpha_1\alpha_2)^{\frac{1}{2}}$, in the place of $\mu$ for the free electrons. The diamagnetic susceptibility along the $z$-axis will therefore be given by

---

* $k$ is here taken to be equal to $1/\lambda$, where $\lambda$ is the electronic wave-length.

$$K_{dg} = -\frac{n\mu_g^2}{3kT}\frac{F'(\eta_g)}{F(\eta_g)}$$

$$= -\frac{n\mu^2}{3kT}\frac{F'(\eta_g)}{F(\eta_g)}\alpha_1\alpha_2, \tag{16}$$

where $\eta_g$ has the value (12). Hence at high temperatures, $T \gg T_{0g}$,

$$K_{dg} = -\frac{n\mu^2}{3kT}\alpha_1\alpha_2, \tag{17}$$

and at low temperatures, $T \ll T_{0g}$,

$$K_{dg} = -\frac{n\mu^2}{2kT_{0g}}\alpha_1\alpha_2 \tag{18}$$

$$= -\frac{n\mu^2}{2kT_0}\left(\frac{\alpha_1^2\alpha_2^2}{\alpha_3}\right)^{\frac{1}{3}}. \tag{19}$$

On comparing (17) with (13), and similarly (18) with (14), it will be seen that the ratio of the diamagnetic to the paramagnetic susceptibility is no longer equal to $\frac{1}{3}$, but is equal to $\frac{1}{3}\alpha_1\alpha_2$. When $\frac{1}{3}\alpha_1\alpha_2$ is very large, the paramagnetic part of the susceptibility will become relatively insignificant.

## 4. GRAPHITE A SUITABLE CRYSTAL FOR STUDYING THE PROPERTIES OF AN ELECTRON GAS

The conditions obtaining in the crystal of graphite, as we shall see presently, are exceptionally favourable for verifying some of the results given in the previous section. Graphite, as is well known, is a hexagonal crystal, with a perfect basal cleavage. The carbon atoms in it are arranged in layers parallel to the basal plane, the atoms in each layer forming a regular hexagonal network. The distance of separation between adjacent layers is 3·40 A, which is much larger than the distance between adjacent atoms in the same layer, namely, 1·42 A, which shows that the binding between adjacent layers is extremely loose, and is probably of the van der Waals type.

The diamagnetic properties of this crystal have been studied by us in detail in some recent papers (1934, 1937, 1939). The specific susceptibility per g. of the crystal perpendicular to the hexagonal axis, $\chi_{\perp}$, is about $-0{\cdot}5 \times 10^{-6}$, which is nearly that of diamond. On the other hand, the susceptibility along the hexagonal axis, $\chi_{\parallel}$, is numerically very large, and it varies much with temperature. At room temperature $\chi_{\parallel}$ is about $-21{\cdot}5 \times 10^{-6}$ per g., and is thus more than 40 times $\chi_{\perp}$.

The abnormal part of the susceptibility of graphite, which we may take as equal to $\chi_{\parallel} - \chi_{\perp}$, and which we shall denote by $\chi_e$, appears to be the contribution from the free or the mobile electrons in graphite. We shall assume that it is so, and further that an explanation can be found for the absence of a paramagnetic contribution from these electrons. The experimental finding that $\chi_e$ is directed wholly along the normal to the basal plane then indicates that the mobility of these electrons is practically confined to the basal plane. Adopting the language of the Bloch theory this would mean, in view of the layered structure of graphite, that the mobile electrons belonging to any given layer of carbon atoms, parallel to the basal plane, are tightly bound to the layer, the probability of their migrations to the adjacent layers being very small. This is indeed to be expected from the large separation, which we referred to just now, between adjacent layers, and the looseness of the binding between them.

Though the mobile electrons belonging to any given basal layer are tightly bound to the layer, the magnetic data require, as we found just now, that there should be large movements of these electrons in the plane of the layer. The magnetic data further require, as we shall find in § 6, that these movements in the basal plane should be *completely* free, i.e. quite uninfluenced by the lattice field.

We thus have in graphite a particularly simple model of an electron gas, the electrons behaving in their movements in the basal plane as though they were completely free, and in their movements perpendicular to the plane as though they were tightly bound. Moreover, as we shall again find in § 6, the number of mobile electrons is just one per carbon atom, and this finding further enhances the simplicity of the model.

Now the observed large temperature variation of $\chi_e$ shows that the electron gas in graphite should have, in spite of its large density, a low degeneracy temperature. This result, as we shall show in § 8, is a consequence of the tight binding of the electrons along the hexagonal axis, and the peculiar structure of the Brillouin zones of the crystal.

The electron gas in graphite, conforming as it does to a simple model which is amenable to easy theoretical treatment, and having a low degeneracy temperature which is conveniently accessible in the laboratory, offers a very suitable medium for studying the magnetic and other properties of an electron gas.

## 5. THE MAGNETIC DATA FOR GRAPHITE

Detailed measurements of the temperature variation of the diamagnetic anisotropy of graphite, namely, $\chi_\parallel - \chi_\perp$, denoted by $\chi_e$, from the temperature of liquid oxygen to about 1270° K, were given by us in a previous paper (1939). These data need some supplementing. In the first place there was a gap between 90 and 130° K in the low temperature measurements, since we used a liquid bath of light petroleum ether for maintaining steady temperatures in the cryostat, and the liquid became too viscous for use below about 130° K. The only temperature lower than this, at which measurements were made, was that of liquid oxygen itself. The region included between these two temperatures is rather important, since $\chi_\parallel - \chi_\perp$ is almost independent of temperature at 90°, while at 130° it has a large temperature coefficient. We have now made measurements in this region, with a new type of cryostat* in which the use of a liquid bath for maintaining steady temperatures is eliminated altogether.

Secondly, the high temperature measurements were made previously inside a furnace from which oxygen from air could not be wholly excluded. There was consequently a slight oxidation of the graphite crystal at high temperatures. Immediately after each magnetic measurement, the crystal was quickly cooled and its mass determined; this was taken to be the mass of the crystal when the measurement at the high temperature was made This would make the numerical values of $\chi_\parallel - \chi_\perp$ reported before for the highest temperatures slightly too high. We have now repeated these measurements in an air-tight furnace in an atmosphere of nitrogen, and under these conditions there was no detectable change in the crystal even at the highest temperatures. These new values of $\chi_\parallel - \chi_\perp$ are found to differ only slightly from the old values, and both the sets of values are included in the present paper.

---

* We wish to express here our thanks to Mr Akshayananda Bose for designing the cryostat. A detailed description of the apparatus will be published by him elsewhere.

## 6. Discussion of the magnetic data

Plotting the values of $\chi_{\parallel}-\chi_{\perp}=\chi_e$ per gram of graphite against the reciprocal of the temperature, we find (see figure 1) that at high temperatures the susceptibility tends to reach asymptotically the value

$$\chi_e = -0{\cdot}010/T,$$

and at low temperatures it tends to reach the temperature-independent value

$$\chi_e = -30\times 10^{-6},$$

and the curve in general resembles closely the theoretical susceptibility curve for a free-electron gas whose energy distribution conforms to Fermi-Dirac statistics.

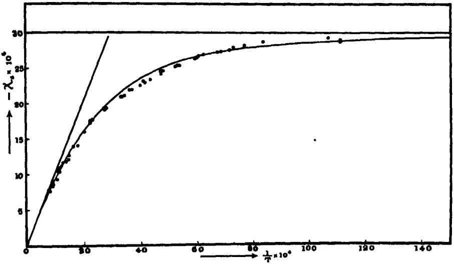

FIGURE 1

On more detailed examination of the curve we find that the high temperature values, namely, $\chi_e = -0{\cdot}010/T$, conform closely to the formula

$$A\chi_e = -\frac{0{\cdot}12}{T} = -\frac{N\mu^2}{3kT}, \tag{20}$$

where $A$ is the atomic weight of carbon and $N$ is the Avogadro number.*

---

* We may mention here that the volume susceptibility $K$ and the specific susceptibility $\chi$ are connected by the relation

$$K/n = A\chi/N. \tag{20a}$$

Similarly the temperature-independent value of $\chi_e$ at low temperatures conforms to the formula

$$A\chi_e = -360 \times 10^{-6} = -\frac{N\mu^2}{2kT_{0g}}, \tag{21}$$

where $T_{0g}$ has the value 520° K. At all temperatures, in the range investigated, the curve is found to fit well with the formula

$$A\chi_e = -\frac{N\mu^2}{3kT}\frac{F'(\eta)}{F(\eta)}, \tag{22}$$

in which the value of $\eta$ is the same as for a free-electron gas whose degeneracy temperature is 520° K. In other words, *the observed electronic susceptibility of graphite per carbon atom is the same as the Landau susceptibility per electron of a free-electron gas having a degeneracy temperature of* 520° K. The curve drawn in figure 1 is indeed the *theoretical* curve calculated on this basis, and the straight line passing through the origin represents the line

$$A\chi_e = -\frac{N\mu^2}{3kT},$$

which the theoretical curve tends to reach at high temperatures. It will be seen that the experimental values, represented by the circles, lie close to the curve.

This experimental finding may be taken to indicate that *the number of mobile electrons in graphite is just one per carbon atom, and that the movements of these electrons in the basal plane are completely free and uninfluenced by the lattice field.* From the point of view adopted in § 3, these conclusions may be expressed in the following form: first, that $\nu$, the number of free electrons per carbon atom, is equal to unity, and secondly, that $\alpha_1$ and $\alpha_2$, which determine the freedom of movements of these electrons in the basal plane, are also equal to unity.

It should be mentioned immediately that these conclusions do not follow *uniquely* from the magnetic data. On comparing the experimental relations (20) and (21) with the theoretical relations (17) and (18) respectively, and in view of (20*a*), one can see that the experimental data merely require that

$$\nu\alpha_1\alpha_2 = 1. \tag{23}$$

The obvious conclusion that we drew from the magnetic data in the previous paragraph, namely, that

$$\nu = 1 \quad \text{and} \quad \alpha_1 = \alpha_2 = 1, \tag{24}$$

is only a particular solution. This solution, however, appears from other considerations to be the most probable one. For example, it fits well with the modern quantal views regarding the electronic structure of aromatic molecules in general, and of graphite in particular—indeed each layer of carbon atoms in graphite may be regarded as a giant aromatic molecule—according to which one electron per carbon atom is free to migrate from atom to atom over the whole condensed network. Incidentally such a migration is also the solution for the sixty-year-old controversy regarding the location of the extra bonds in the benzene ring—the bonds are not localized at all! (Ingold 1938).

## 7. SURFACES OF CONSTANT ENERGY IN $k$-SPACE APPROXIMATELY A SET OF COAXIAL CYLINDERS

For a free-electron gas containing as many electrons per c.c. as there are carbon atoms per c.c. of graphite, one can easily calculate the degeneracy temperature, with the help of equation (7), and it is found to be about 98,000° K. Now the observed degeneracy temperature of the electron gas in graphite, namely 520° K, is $\frac{1}{190}$ of this value. From the magnetic data it was deduced in the previous section that the number of free electrons in graphite, namely $\nu$ per atom, is given by the relation $\nu\alpha_1\alpha_2 = 1$. For this density of electrons, remembering that the effect of the lattice field is to increase the degeneracy temperature by a factor $(\alpha_1\alpha_2\alpha_3)^{\frac{1}{3}}$ (see (11)), we obtain

$$T_{0g} = 520^\circ = 98{,}000^\circ \times \nu^{\frac{2}{3}} \times (\alpha_1\alpha_2\alpha_3)^{\frac{1}{3}}, \quad \text{or} \quad \alpha_1\alpha_2/\alpha_3 = 190^3, \tag{25}$$

which indicates a very high eccentricity for the ellipsoidal surfaces of constant energy in the $k$-space. Indeed the eccentricity is so large that one may regard these surfaces as a set of coaxial cylinders, with their common axis along the '$c$' axis of the crystal.

Now the 'effective mass' of an electron is $1/\alpha_i$ times the actual mass, where $\alpha_1$ has the value $\alpha_1$ or $\alpha_2$ for motion in the basal plane, and the value $\alpha_3$ for motion perpendicular to the plane. The very large value of $\alpha_1\alpha_2/\alpha_3$ obtained in (25) indicates that the effective mass for motion perpendicular to the plane is enormous, as indeed it should be, because of the tight-binding of the mobile electrons to their respective layers. The effective mass for motion in the basal plane will be much smaller, and if we adopt the conclusion provisionally accepted in the previous section, namely $\alpha_1 = \alpha_2 = 1$, it will be just the actual mass.

## 8. BRILLOUIN ZONES OF GRAPHITE

We shall next consider these results in relation to the Brillouin zones in the crystal. The unit cell of graphite has the dimensions

$$a = 2{\cdot}46, \quad c = 6{\cdot}79\,\text{A},$$

and it contains four atoms of carbon. The structure factors for the various crystallographic planes are given in table 1 (see Mott and Jones 1936, p. 163).

TABLE 1

| Plane | $\{1\bar{1}0, 0\}$ | $\{2\bar{2}0, 0\}$ | $\{2\bar{1}\bar{1}, 0\}$ | $\{000, 1\}$ | $\{000, 2\}$ |
|---|---|---|---|---|---|
| $S$ | 1 | 1 | 4 | 0 | 4 |

The energy discontinuities across $\{000, 2\}$, and across $\{2\bar{1}\bar{1}, 0\}$ are the strongest. Let us consider the Brillouin zone in $k$-space ($k$ is taken to be equal to $1/\lambda$, as before) bounded by these sets of planes. It will be a flat hexagonal prism of the second order, with its axis along '$c$'. The height of the prism will be $2/c$, and its cross section, by the basal plane, will be a regular hexagon of side $2/(\sqrt{3}a)$ (see figure 2, the inner hexagon). The volume of this Brillouin zone in the $k$-space will be $4\sqrt{3}/(a^2c)$. Since each unit volume in the $k$-space will correspond to two electrons per unit volume of graphite, and since the atomic volume of carbon in the crystal is $\sqrt{3}a^2c/8$, it can be readily seen that the above Brillouin zone can contain just three electrons per carbon atom.* The energy discontinuities at all the faces of the zone are large, and hence these three electrons in each carbon atom may be regarded as forming a closed group.

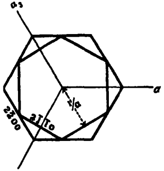

FIGURE 2

---

* The Brillouin zone described by Mott and Jones on p. 163 of their book is really this three-electron zone.

There is a bigger zone which can just accommodate all the four valency electrons of the carbon atom, namely, the one bounded by $\{000, 2\}$ and $\{2\bar{2}0, 0\}$. This zone also is a flat hexagonal prism, of the same height as before, but of the first order, whose cross-section is a hexagon of side $4/(3a)$ (the outer hexagon in figure 2). But the energy discontinuities across $\{2\bar{2}0, 0\}$, as will be clear from the values given in table 1, are small.

We mentioned just now that the three electrons per carbon atom that can be accommodated in the smaller Brillouin zone, whose bounding faces are all surfaces of large energy discontinuity, may be regarded as forming a closed group. The remaining electrons, namely one per carbon atom, may occupy any of the outer zones. Using reduced wave numbers, it can be easily seen that there is much overlapping of these zones into one another, and on this account the maximum kinetic energy of the electrons will be much smaller than it would be otherwise. Further, in view of the small value of $\alpha_3$ (which is only $1/190^3$ of $\alpha_1\alpha_2$), the electrons will take up all the permitted values of $k_z$ in the zones under consideration right up to the boundary surface parallel to the basal plane. For the same reason, neither $k_x$ nor $k_y$ will reach high values; in other words, along the $x$ and $y$ directions the zones will be 'nearly empty'. In terms of the Brillouin zones, one thus gets a natural explanation why in spite of the large density of free electrons in graphite, namely one per atom, the degeneracy temperature is so low, and also why for motion in the basal plane (i.e. in the $xy$-plane) the electrons behave as if they were completely free, whereas for motion along the normal to the plane (i.e. along the $z$-axis) they behave as if they were tightly bound.

## 9. AN ALTERNATIVE VIEW OF THE FREE-ELECTRON DIAMAGNETISM OF GRAPHITE

We have seen that a particularly simple solution of the experimental finding that $\nu\alpha_1\alpha_2 = 1$ is to put

$$\nu = 1 \quad \text{and} \quad \alpha_1 = \alpha_2 = 1,$$

and that this solution receives much support from general structural considerations, and also from a consideration of the Brillouin zones. Assuming, for the sake of argument, that this solution is not acceptable, the only other permissible solution seems to be to regard the larger Brillouin zone, which can accommodate all the four valency electrons, as the proper zone, and to attribute the diamagnetism to the few electrons that may overlap into the next zone. $\nu$ will then represent the number of such overlap electrons per atom, and will be much less than unity. The surfaces of constant energy in the $k$-space in the region immediately outside any pair of parallel surfaces $\{2\bar{2}0, 0\}$ bounding the Brillouin zone may still be represented by ellipsoids of the type (10), the origin of the coordinate system being now taken at the surface. Taking the $z$-axis as before along the '$c$' axis of the crystal, and the $x$-axis along the normal to the surfaces of energy discontinuity under consideration, it can be shown (see Mott and Jones 1936, p. 84) that both $\alpha_2$ and $\alpha_3$ should be of the order of unity, whereas $\alpha_1$ should be very large; indeed the larger it is, the smaller is the energy discontinuity. The relation $\alpha_1\alpha_2/\alpha_3 = 190^3$ deduced from the observed degeneracy temperature of the electron gas in graphite will then give for $\alpha_1$ the value

$$\alpha_1 \sim 190^3.$$

Such a large value of $\alpha_1$ indicates an extremely small energy discontinuity at the surface, of the order of $10^{-4}$ or $10^{-5}$ electron volt, and this will be the case at all the $\{2\bar{2}0, 0\}$ faces of the four-electron Brillouin zone. We may then legitimately disregard these discontinuities altogether, regard the one electron per carbon atom that cannot be accommodated in the smaller Brillouin zone to be effectively free, and shift the origin of the coordinate system to the beginning of the one-electron zone. We will then have

$$\nu = 1, \quad \alpha_1 = \alpha_2 = 1, \quad \alpha_3 = 1/190^3.$$

This is precisely the first alternative view, which we had adopted.

In other words, in order to explain, on the second alternative view, the experimental finding that the number of electrons overlapping beyond the four-electron Brillouin zone bears a definite relation to the $\alpha$'s in the basal plane—the relation being $\nu\alpha_1\alpha_2 = 1$—the energy discontinuities across the $\{2\bar{2}0, 0\}$ planes have to be negligibly small. The existence of the discontinuities can then be ignored altogether, in which case the second alternative view reduces itself to the first. This is very gratifying.

## 10. ABSENCE OF SPIN-PARAMAGNETISM

Now we have to explain why the spin-paramagnetism of the free-electrons, which normally should have predominated over their diamagnetism, is practically absent. According to the second alternative view proposed in the preceding section, this is merely a consequence of the large value of $\alpha_1\alpha_2/3$, which, as we noticed in § 3, represents the ratio of the diamagnetic to the paramagnetic susceptibility. But we have already preferred, on other grounds, the first alternative. The absence of paramagnetism has then to be explained in the following manner. Each permitted energy level of the electron gas can accommodate, according to Pauli's exclusion principle, two electrons, with opposing spin moments. Under the conditions usually obtaining in an electron gas all the lower energy levels will be so occupied by electron pairs, but some of the higher energy levels, near about $\zeta_0 = kT_{0g}$, will be occupied by single electrons, and the higher the temperature the larger will be the number of such energy levels occupied by single electrons. In graphite, in order to explain the absence of paramagnetism, we have to assume that *all* the occupied energy levels are occupied each by a pair of electrons, and none of the levels by single electrons. This will be the case if there is some coupling between the opposite spin moments, and the energy of coupling is large in comparison with $kT$ even at the higher temperatures of our measurement, and therefore large in comparison with $kT_{0g}$ also. Such a pairing of the electron spins is indeed contemplated in the quantal theory of the mobile electrons in aromatic molecules.

In spite of such a coupling—which will result in an energy level being either occupied by an electron pair or not occupied at all—if the occupied energy levels are so closely spaced that they may be regarded as almost continuous (this condition is satisfied ordinarily), the energy distribution will be practically the same as when the spin-spin coupling is absent. The coupling will not therefore affect the diamagnetism of the electron gas, and the temperature variation of the diamagnetism will still be in accordance with the statistics of Fermi and Dirac, as is actually observed.

At sufficiently high temperatures, however, we should expect the paramagnetism to become more and more important relatively to the Landau diamagnetism of the electrons, and ultimately to predominate over the latter in the ratio of 3 : 1.

Thus in addition to the observed degeneracy temperature of 520° K, which when multiplied by $k$ represents the maximum kinetic energy which an electron in the gas will have at very low temperatures, there must be another characteristic temperature $T_s$ for the electron gas in graphite, much higher than 520° K, such that $kT_s$ will represent the energy of dissociation of the components of a pair of electrons with opposite spins The temperature $T_s$ will be somewhat analogous to the Curie temperature of a ferromagnetic body.

## 11 THE LANDAU DIAMAGNETISM AND THE FERMI-DIRAC ENERGY DISTRIBUTION OF THE ELECTRON GAS

Treating the abnomal diamagnetism of graphite as the Landau diamagnetism of its electron gas, we found that the various results deduced from the magnetic data are just what we should expect from other and independent considerations. Arguing conversely, we may regard the observed magnetic data for graphite, especially at very high and very low temperatures, at which the magnetic behaviour is particularly simple, as providing an experimental demonstration of Landau's value for the diamagnetism of an electron gas. The region that we have studied extends from the completely degenerate to the almost completely non-degenerate state; and includes in particular the region of transition from the one to the other. The close agreement between the theoretical curve plotted in figure 1, calculated on the basis that the energy distribution of the electrons is in accordance with Fermi-Dirac statistics, and the experimental values may therefore be regarded as verifying experimentally the Fermi-Dirac distribution over the whole range from temperatures very much lower than the degeneracy temperature to temperatures much higher than the latter. This is very gratifying, since ordinarily it is only the degenerate state that is accessible for experimenting, whereas for verifying the Fermi-Dirac distribution, it is the transition region between the degenerate and the non-degenerate states that is most interesting.

In conclusion we wish to express our thanks to Dr D. N. Wadia, Government Mineralogist at Ceylon, for his kind present of some of the graphite crystals with which the measurements described in this paper were made.

## REFERENCES

Ganguli, N. 1936 *Phil. Mag.* **21**, 355.
Ingold, C. K. 1938 *Proc Roy. Soc.* A, **169**, 149.
Krishnan, K. S. 1934 *Nature, Lond.*, **133**, 174.
Krishnan, K. S. and Ganguli, N. 1937 *Nature, Lond.*, **139**, 155.
—— —— 1939 *Z. Kristallogr.* A, **100**, 530.
Landau, L. 1930 *Z Phys.* **64**, 629
McDougall, J. and Stoner, E. C. 1938 *Phil. Trans.* A, **237**, 67.
Mott, N. F. and Jones, H. 1936 *The theory of the properties of metals and alloys.* Oxford Univ. Press.
Stoner, E. C. 1935 *Proc. Roy. Soc.* A, **152**, 672.

# Radio echoes and cosmic ray showers

By P. M. S. Blackett, F.R.S., and A. C. B. Lovell

(*Received* 22 *October* 1940)

It is suggested that the origin of some of the transient ionic clouds, generally assumed to be responsible for the low level sporadic radio reflexions, may be due to large cosmic ray showers.

It is shown that cascade cosmic ray showers of sufficient energy to produce some of these radio reflexions certainly exist, but there is insufficient published evidence to decide whether any of the echoes already observed are actually due to such showers. More conclusive evidence could be obtained from the frequency-size distribution of the radio echoes observed from a horizontal or vertically directed beam.

## 1. Introduction

The anomalous 'scattering' of radio waves into the normal skip zone was reported by Eckersley in 1929 and subsequently by many other workers. Though the majority of these echoes appear to originate in the *E* layer (Appleton, Naismith and Ingram 1937), the work of Watson Watt, Wilkins and Bowen (1937), Appleton and Piddington (1938), Colwell and Friend (1936, 1939) and others have proved the existence of reflexions from levels as low as 10 km. Little definite is known of the magnitude or frequency of these low level sporadics, but the work of Appleton and Piddington (1938) suggests reflexion coefficients of the order of $2 \times 10^{-5}$ to $10^{-4}$, while the frequency of occurrence appears to be of the order of several per minute both day and night.*

It is generally assumed that these sporadic reflexions in *E* regions must be due to transient ionic clouds, but a variety of opinions has been expressed as regards both the nature and origin of the tropospheric scattering centres. Suggestions have been made that they may be caused by solar activity, aurora phenomena, thunderstorms, meteorites and water vapour discontinuities. The object of this note is to draw attention to the possibility that some of these reflexions, particularly those at low levels, may be due to the ionization produced by large cosmic ray showers. It will be shown that the detection of these showers by modern high power pulse transmitters, such as are nowadays used in ionospheric and tropospheric investigations, should certainly be possible.

---

* Eckersley (1940) found one per 30,000 km.$^2$/sec. in the *E* layer, and a composite plate in the paper of Watson Watt *et al.* (1937) shows the frequency of occurrence of the low level sporadics to be about ten times as great.

## 2. COMPARISON OF ENERGIES

A cosmic ray shower of high energy produces a long narrow cylinder of ionization traversing the whole atmosphere. Consider a shower at a distance $R$ from a powerful radio transmitter with a wave-length $\lambda$ large compared with the diameter of the column of ionization. Diffraction theory shows that the amplitude of the reflected wave at the transmitter will be approximately equal to that which would be produced by a point cluster of $n$ ions, where $n$ is the number of ions contained in a column, whose length $L$ is that of the first Fresnel zone, that is, where

$$L = \sqrt{\lambda R}.$$

From the cascade theory of showers, it can be calculated that the maximum number of electronic ions produced per centimetre of air at a pressure $p$, expressed as a fraction of an atmosphere, by an incident electron of energy $E$, is roughly given by

$$n = \tfrac{1}{2} 10^{-7} pE. \tag{1}$$

Thus the number of electrons in the equivalent point cluster is

$$N = nL = \tfrac{1}{2} 10^{-7} pE \sqrt{\lambda R} \tag{2}$$

If the reflexion coefficient $\rho$ is defined as the ratio of the reflected amplitude to that incident on the cluster, then a point cluster of $N$ electrons at a distance $R$ from the sender will have a reflexion coefficient

$$\rho = \frac{Nr}{R}, \tag{3}$$

where $r = \frac{e^2}{mc^2} = 2\cdot 8 \times 10^{-13}$ cm.

Considering (2) and (3) we obtain for the reflexion coefficient of a shower of energy $E$ at a distance $R$,

$$\rho = \tfrac{1}{2} 10^{-7} pEr \sqrt{\frac{\lambda}{R}} \tag{4}$$

For instance, putting $\rho = 2 \times 10^{-5}$, $p = 1$, $\lambda = 50$ m., $R = 10$ km. we get $E = 2 \times 10^{16}$ eV. Now showers of nearly this energy have already been observed directly by Auger and his collaborators (1939), Jánossy and Lovell (1938), Lovell and Wilson (1939) and others. We conclude therefore that cascade cosmic ray showers certainly exist of sufficient energy to produce measurable radio reflexions.

## 3. FREQUENCY-SIZE DISTRIBUTION

Whether some of those reflexions already observed are from such cosmic ray showers is difficult to decide without more evidence than appears to be available at present of the frequencies of the echoes. The frequency-size distribution of the echoes from cosmic ray showers will depend on the energy spectrum of the incident rays. Consider first, the reflexion of a nearly horizontally directed radio wave by a nearly vertical shower. If, as is probable, the number of rays with energy above $E$, falling on unit area from a nearly vertical direction is roughly of the form

$$G(E) = \alpha E^{-2}, \tag{5}$$

then the number of rays of energy greater than $E$ which fall within a distance $R$ and $\overline{R+dR}$ from the sender, will be equal to

$$v\,dR = 2\pi \frac{\alpha}{E^2} R\,dR. \tag{6}$$

Substituting $E$ from (4) we get

$$v\,dR = \frac{\pi}{2} 10^{-14} \alpha p^2 r^2 \lambda \frac{dR}{\rho^2}. \tag{7}$$

We see therefore that the number of echoes between ranges $R$ and $\overline{R+dR}$ with reflexion coefficients greater than $\rho$ is inversely proportional to $\rho^2$, but is independent of the range $R$. If the observed echoes from a horizontally directed radio beam are found to obey this relation, it will be strong evidence that the echoes are from showers.

From the work of Auger (1939), it can be calculated that

$$G(E) \simeq 1{\cdot}6 \times 10^{-9}/\text{cm.}^2/\text{min.} \quad \text{for} \quad E = 10^{15}\,\text{eV},$$

whence $\alpha \simeq 1{\cdot}6 \times 10^{21}/\text{ergs}^2/\text{cm.}^2/\text{min.}^{-1}$. Taking again $p = 1$, $\lambda = 50$ m., we find

$$v\,dR = 10^{-14}\,dR/\rho^2. \tag{8}$$

The number of echoes with reflexion coefficients greater than $10^{-4}$ observable over a range $\delta R = 10$ km. should therefore be about one per minute. The observed echoes appear to occur with a frequency of this order of magnitude.

If we now consider a radio transmitter giving a directed beam vertically instead of horizontally, then it is clear that it will be the horizontal showers which give echoes. To take into account the decrease of pressure upwards we can write $p = e^{-\beta R}$ in (7). The frequency of the echoes will therefore fall off exponentially with $R$, in contrast to the case of a horizontally directed beam, which is shown above to give a frequency independent of $R$.

Numerical calculation shows that the observed $E$ level sporadics are much too frequent to be explained in this way, and therefore are probably to be attributed to some other cause than cosmic ray showers.

With any normal radio transmitter, radiating in all directions, the frequency-size distribution will be too complicated to allow an easy test of the theory.

## 4. Duration of the echoes

The duration of an echo will be the lifetime of the free electronic ions, and this is governed mainly by the rate of attachment to molecules. Thus the duration of the echoes will be roughly inversely proportional to the pressure, and will have a value of $10^{-5}$ to $10^{-6}$ sec. at ground level and of the order of a second at 100 km. Thus, though the amplitude of an echo will decrease with the pressure, its duration will increase in the same proportion, leaving the product of amplitude and duration unchanged. It is possible that some types of receiving apparatus may not detect the very short echoes from low levels as easily as the smaller but longer echoes from greater altitudes. This might give an apparent maximum frequency of detectable echoes at a considerable altitude.

## 5. Conclusion

If the suggestion put forward here, that radio echoes should be detectable from cosmic ray showers, is substantiated by experiment, a new and powerful technique will be available for cosmic ray research, especially for the investigation of the energy spectrum at very high energies.

## References

Appleton, Naismith and Ingram 1937 *Phil. Trans.* A, **236**, 254.
Appleton and Piddington 1938 *Proc. Roy. Soc.* **164**, 467.
Auger 1939 *Rev. Mod. Phys.* **11**, 288.
Colwell and Friend 1936 *Phys. Rev.* **50**, 632.
— — 1939 *Proc. Instn Rubber Engrs*, **27**, 626.
Eckersley 1929 *J. Instn Elect. Engrs*, **67**, 992
— 1940 *J. Instn Elect Engrs*, **86**, 548.
Jánossy and Lovell 1938 *Nature, Lond.*, **142**, 716.
Lovell and Wilson 1939 *Nature, Lond.*, **144**, 863.
Watson Watt, Wilkins and Bowen 1937 *Proc. Roy. Soc.* A, **161**, 181.

# The mobility of positive ions in their own gas

By R. J. Munson, Ph.D., and A. M. Tyndall, D.Sc., F.R.S.
*H. H. Wills Physical Laboratory, University of Bristol*

(*Received* 9 *September* 1940)

Values for the mobility of positive ions of neon in neon, argon in argon, krypton in krypton and xenon in xenon have been obtained in pure gas. It is possible to deduce the mobility of an ion of the same mass as the gas atom from the known values for alkali ions in the gas on the assumption that the same mass relationship holds. In each case the observed value is considerably less, the ratio of the two being of the order of 0·60–0·75. This result may be attributed to the phenomenon of electron exchange in the case of ions in their own gas which does not arise with alkali ions.

The variation of mobility with field $E$ and pressure $p$ has been studied. In Kr and Xe there is a marked fall of mobility with increase of $E/p$, at higher values the velocity of the ion increasing in a linear manner with increase of $(E/p)^{\frac{1}{2}}$.

In 1931 Tyndall and Powell determined the mobility of positive ions of helium in very pure helium. The clustered ions, due to gross impurity, with which all the early mobility measurements were carried out, could be fairly easily eliminated, but the authors showed that when small traces of impurity were present secondary processes in the path of the point discharge, from which the ions were derived, produced other types of ion to an extent out of proportion to the concentration of the impurity.

They tried also to make similar measurements on ions in their own gas using neon, argon and krypton, but the results were never published because of their indefinite nature. Owing no doubt to residual impurity more than one group of ions was obtained, neon and argon giving two and krypton several groups. Attempts to purify the gas still further by electrodeless discharge in situ altered the relative abundances of the groups and sometimes added others, leaving the results still ambiguous (Tyndall and Powell 1931). Helium has an advantage over these gases in that a charcoal-liquid oxygen trap can be inserted between the measuring tube and the last stopcock. The gas can thus be led through the trap and kept in connexion with it during measurements. For the other gases the charcoal must be removed, so that the gas is more liable to contamination. For this reason they turned their attention to the alkali ions which, owing to the low ionization potential of alkali atoms and the absence of electrons and metastable atoms from the discharge, do not demand so high a criterion of purity.

Later, Mitchell and Ridler (1934) were able to make nitrogen pure enough to determine the mobility of $N_2^+$ in $N_2$ (2·67). Similarly, Mitchell (Tyndall 1938) found a value for $H_2^+$ in $H_2$ (14·7).

Recently the technique of the gas purification has been improved, notably (Munson and Tyndall 1939) by the introduction of mercury traps instead of stopcocks requiring tap grease in the gas plant. In view of the present use of discharge tubes containing inert gases, a reinvestigation was therefore made in 1939, the results of which are here recorded.

The apparatus was the same as that employed in recent work on alkali ions except that the source of ions was a platinum wire rounded in the blowpipe to a sphere of about 0·5 mm. diameter and placed a few millimetres from a perforated platinum plate, through which positive ions were dragged to the first shutter of the mobility apparatus. The holes in the platinum plate were staggered with respect to those in the shutters in order to prevent radiation from the corona from reaching the electrometer plate and causing a background of current at all frequencies due to photoelectric emission. With Xe, $CO_2$ slush had to be substituted for liquid oxygen on the traps. Mercury vapour at least was thus excluded.

## RESULTS

In view of the data obtained for alkali ions on the variation of mobility with field $E$ and pressure $p$, values for $Ne^+$ in Ne, $A^+$ in A, $Kr^+$ in Kr and $Xe^+$ in Xe have been obtained at various values of $E/p$. These are shown graphically in figure 1 *a*, *b*. The graph for neon is of a type similar to those obtained by Hershey (1939) for potassium ions in various gases. The argon graph over a more extended range of $E/p$ might possibly have assumed a similar form, but the use of higher values of $E/p$ was prevented because of the incidence of glow discharge throughout the tube. The results for Kr and Xe are very striking. If the mobility is constant at low values of $E/p$ it is only so over a very limited range, after which it falls off rapidly. To emphasize the contrast between this and the behaviour of an alkali ion, results for $Cs^+$ in Xe are also included in the graph.

In the collected results in table 1 for the mobility $k_0$ at $E/p = 0$, obtained by extrapolation, the last figure in the values for Kr and Xe must be regarded as somewhat uncertain, as may be seen from the form of the graphs themselves which are drawn on the assumption that the mobility tends to a constant value at very low $E/p$. The earlier result of Tyndall and Powell for He is included in the table for completeness. In column three the mobility $k_A$ for the alkali ion having the same electronic configuration as the gas atom is also given for comparison. It will be seen that in all cases the ion of the gas itself has a lower mobility than that of the corresponding alkali ion. Full data are available for all the alkalis in these gases from which graphs representing the variation in a given gas of the mobility of a monatomic ion with its mass may be drawn. From these we may deduce the value of the mobility of an ion of the gas itself, it if be assumed that its mass is the determining factor. The values are given as $k_M$ in column 4; the helium value must be regarded as very doubtful due to the extent of extrapolation required. The ratios $k_0/k_M$ are recorded in column 5.

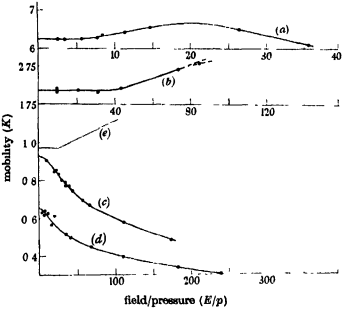

*a*, Ne$^+$ in Ne; *b*, A$^+$ in A, *c*, Kr$^+$ in Kr; *d* Xe$^+$ in Xe; *e* Cs$^+$ in Xe

FIGURE 1

TABLE 1

| Gas | $k_0$ | $k_A$ | $k_M$ | $k_0/k_M$ |
|---|---|---|---|---|
| Helium | 21·4 | 25·6 (Li) | 28·8 | 0·74 |
| Neon | 6·23 | 8·70 (Na) | 8·93 | 0·70 |
| Argon | 1·93 | 2·81 (K) | 2·77 | 0 70 |
| Krypton | 0·94 | 1·57 (Rb) | 1·58 | 0·60 |
| Xenon | 0·65 | 0·97 (Cs) | 0·98 | 0·66 |

As has been pointed out (e.g. Tyndall 1938), the law of force between an alkali ion and a gas atom differs in one fundamental respect from that between an ion of the same gas as the atom. In the former case, owing to the relatively low ionization potential of the alkali atoms, exchange forces are absent. In the latter case the probability of electron exchange between the two colliding bodies is a maximum. Now the statistical effect of electron exchange is equivalent to an increase in the number of collisions between ion and atom. Consequently one would expect the mobility of an ion in its own gas to be less than that which would be deduced from the consideration of mass alone. The ratios given in column 5 ranging between 0·60 and 0·74 may thus be regarded as a measure of the effect of electron exchange. A similar result was found by Mitchell and Ridler for $N_2^+$ in $N_2$, but in this

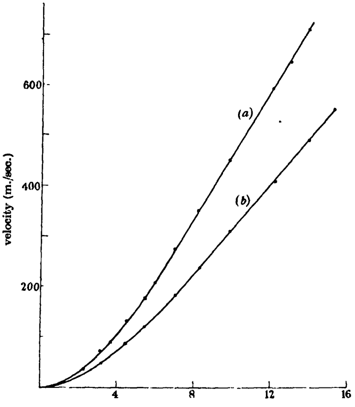

*a*, $Kr^+$ in Kr; *b*, $Xe^+$ in Xe

FIGURE 2

case the ratio was higher (0·925). Without a wave mechanical treatment of the mobility problem it is not possible to say whether this difference in order of magnitude is connected with the diatomic nature of both ion and molecule in nitrogen.

By making the arbitrary assumption that the velocity distribution remains Maxwellian at all values of $E/p$ Hershey has extended Langevin's theory to show that the relation between mobility and $E/p$ is of the general type found by him for $K^+$ ions in various gases and now by the writers for $Ne^+$ in neon. It would appear that any classical model leads one to the conclusion that provided $E/p$ is sufficiently great the *velocity* of an ion in the field should vary linearly with $(E/p)^{\frac{1}{2}}$. In figure 2 the results for krypton and xenon are shown with velocity plotted against $(E/p)^{\frac{1}{2}}$. It will be seen that above about $E/p = 36$ for Kr and 50 for Xe this linear relationship is obtained.

## REFERENCES

Hershey 1939 *Phys. Rev.* **56**, 908.
Mitchell and Ridler 1934 *Proc. Roy. Soc.* A, **146**, 911.
Munson and Tyndall 1939 *Proc. Roy. Soc.* A, **172**, 28
Tyndall 1938 *The mobility of positive ions in gases*, p. 53. Cambridge Univ. Press.
Tyndall and Powell 1931 *Proc Roy. Soc.* A, **134**, 125

# The mobility of alkali ions in gases
## IV. Measurements in gaseous mixtures

By H. G. David, B.Sc., and R. J. Munson, Ph.D.
*H. H. Wills Physical Laboratory, University of Bristol*

(*Communicated by A. M. Tyndall, F.R.S.—Received* 9 *September* 1940)

The mobilities of some of the alkali ions have been measured in binary mixtures of the inert gases. Blanc's relation that the reciprocal of the mobility is a linear function of the concentration of one of the constituents is accurately obeyed in all cases except for $Li^+$ in He-Xe mixtures, where the maximum deviation is 4%.

With clustered $Li^+$ ions in mixtures of water vapour and an inert gas deviations from this simple relation are observed and increase in magnitude progressively with the density of the gas. These deviations, due to the polar nature of the water molecule, can be explained by assuming a gradual increase in the size of the clustered ion with increase in the percentage of water vapour.

The first measurements of the mobility of ions in mixed gases were made by Blanc (1908) with mixtures of carbon dioxide and air, and carbon dioxide and hydrogen. He found in each case that the reciprocal of the mobility was a linear function of the concentration of the constituents for both positive and negative ions. Similar experiments by Przibram (1912), Wellish (1909), Loeb and collaborators (1928) with various mixtures showed that in some cases the reciprocal relation held whilst in others it did not.

This earlier work, in which the ions were loaded with clusters of impurity molecules, does not provide an entirely satisfactory test of this relation or of any of the others proposed owing to the uncertainty in the nature of these clusters. In this paper the problem is re-examined at 20° C using (*a*) alkali ions and pure inert gases in which no clusters are formed on the ions and (*b*) clustered alkali ions in mixtures of an inert gas and water vapour in all proportions.

### Inert gas mixtures

Blanc's relation would appear to follow directly from momentum considerations if (*a*) the ratio of the field $E$ to the pressure $p$ is small, (*b*) $p$ is sufficiently low that the effect of three-body collisions may be neglected and (*c*) the nature of the ion does not change with gas composition. Conditions (*a*) and (*b*) were satisfied in all the experiments described herein. With regard to (*c*) the experiments of Munson and Hoselitz (1939) on alkali ions in pure inert gases show that above a given critical temperature no attachment of gas atoms to an alkali ion takes place. Reference must however be made to the results of Loeb and his collaborators for ions in hydrogen mixed with various polar gases (Loeb 1926, 1928) in which a marked divergence from Blanc's relation was found. Taking ammonia in hydrogen as an example, Loeb suggested that the divergence from the relation was due to the high dielectric constant of ammonia which gives rise to a local concentration of ammonia molecules in the neighbourhood of the ion, so that the measured mobility corresponds to that for an ammonia concentration greater than the average. But Langevin treated the case of an ion moving in a gas, the molecules of which acquire induced dipoles in the field of the ion and showed that the mobility is inversely proportional to the pressure of the gas, in agreement with experiment. In other words, this effect is already allowed for. One would not expect that this conclusion would be upset by the presence of another gas relatively unpolarizable unless condition (*b*) is violated. Consequently in the case of mixtures of the inert gases the mobilities should obey Blanc's relation.

Experiments were made with $Li^+$ and $K^+$ ions in A-Xe mixtures and $Cs^+$ and $Li^+$ ions in He-Xe mixtures. The apparatus and experimental methods of Part I (Munson and Tyndall 1939) were employed and the mobilities measured over a considerable range of fields and pressures. This paper, however, only deals with those at low values of $E/p$. $p$ ranged from 3 to 12 mm., so that the mean intramolecular distance was of the order of $10^3$ atomic radii.

The results are shown in figures 1 and 2. It will be seen that the linear relation holds quite accurately in three of the four graphs, the only exception being a small deviation in the case of $Li^+$ in He-Xe In this case a graph drawn through the experimental points would have a small curvature so that at intermediate concentrations it would be slightly above the theoretical straight line shown in the figure. The deviation is of the order of 4 % at 20 % Xe, which we regard as beyond the limits of experimental error The reason for the deviation in this one case is not clear. It has previously been shown that even at room temperature a $Li^+$ ion can unite with two Xe atoms to form a stable molecular ion so that two groups of ions, one clustered and the other unclustered, appear in the mobility analysis; but as it was always possible to distinguish between the two groups the values for the monatomic $Li^+$ ions are not affected. An experimental argument against the view that the deviation is due to a local concentration of the more highly polarizable Xe atoms in the neighbourhood of the ion is that the deviation is not shown in the case of the more slowly moving ion $Cs^+$. It might alternatively be suggested that $Li^+$ spends a fraction of its life attached to a Xe atom, but this is not borne out by the fact that in pure xenon its mobility in common with the other alkalis is given by the mass relationship $k\alpha(1 + m/M)^{\frac{1}{2}}$, where $m$ is the mass of the gas atom and $M$ the mass of the alkali atom.

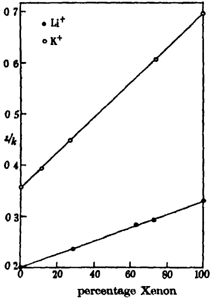

FIGURE 1

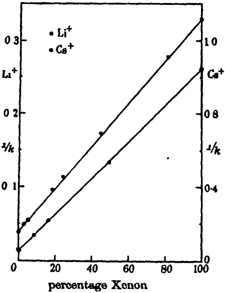

FIGURE 2

## WATER VAPOUR-INERT GAS MIXTURES

The experimental technique detailed in Part I (Munson and Tyndall 1939) was followed in these experiments. By making measurements in each mixture over a wide range of values of $E$ and extrapolating to $E = 0$ the mobility of an ion was deduced under conditions in which its attached cluster of water molecules was in thermodynamical equilibrium with its surroundings. All the mobility data given below refer to clustered ions in this state. The total pressures of the mixtures which were used ranged between about 2 and 7 mm.

An extensive series of measurements was made with the clustered ions of lithium and figure 3 shows the results obtained with binary mixtures of water vapour with helium, argon, krypton and xenon. The reciprocal of mobility is plotted against percentage of water vapour and a smooth curve drawn through the experimental points for each gas. The points at low percentages and at 100 % were taken from the data given in Parts I and III (Munson 1939) of this paper. It should be emphasized that no attempt has been made in figure 3 to represent the rise in mobility which must occur at extremely low concentrations of water as the percentage tends to zero and the ion becomes unclustered.

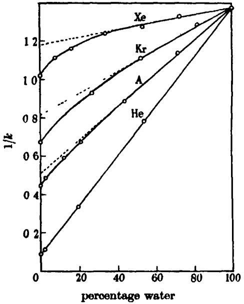

FIGURE 3

It will be seen that in $H_2O$-He mixtures Blanc's relation is accurately obeyed, but that in mixtures with the other gases the deviations are considerable and increase progressively through the series. The observed mobility is less than that calculated from the reciprocal law, the difference reaching a maximum in each case at about 30 % $H_2O$, where for A it is 4 %, for Kr 7 % and for Xe 9 %.

Some measurements were also made with the clustered ions of caesium in mixtures of water vapour with helium and with argon. The results for the He mixtures are shown in figure 4, the point at 100 % $H_2O$ being omitted in order to illustrate more effectively the deviation from Blanc's relation at small percentages. For the purpose of comparison the graph for lithium is also included. The results for the argon water mixtures are given in figure 5 the curve for the $Li^+$ cluster being included for the same reason.

In all cases in which a deviation from Blanc's relation is observed it is similar in character to that found by Loeb and his collaborators with polar molecules in hydrogen. Though Langevin's treatment of mobility does not consider the case of permanent dipoles, we are not convinced that any change in the law of force between an ion and a gas atom which permanent dipoles would require is able to explain these deviations. We turn, therefore, to an explanation in terms of actual attachment.

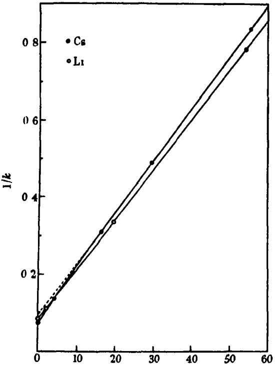

FIGURE 4

Consider an alkali ion in an inert gas containing a small amount of water vapour. In the equilibrium state the average number of water molecules attached to the ion will depend on the concentrations of both water vapour and inert gas. The mean size of the cluster will increase when the concentration of water is increased; but also, since the bombardment of the cluster by inert gas atoms tends only towards its disintegration, a decrease in the concentration of the inert gas will have a similar effect on the cluster size. If the total pressure of the mixture is kept constant, as was approximately true in these experiments, the equilibrium size of the cluster will increase as the percentage of water vapour is raised, qualitative considerations suggesting that the growth will be rapid until a monomolecular shell has formed around the ion. Any water molecule in a second layer would have a comparatively short life of attachment owing to the much smaller energy which would be necessary to detach it from the cluster. But as the water vapour pressure is further increased the frequency of these brief attachments will increase and since their effect will be equivalent to an increase in the mean size of the cluster, it may be anticipated that the early rapid growth will be followed by a further and much slower growth until finally the medium consists entirely of water vapour. It is clear that the initial growth rate will depend on the binding energy of the ion and water molecule and will therefore be much more rapid with a small ion like $Li^+$ than with a large ion like $Cs^+$.

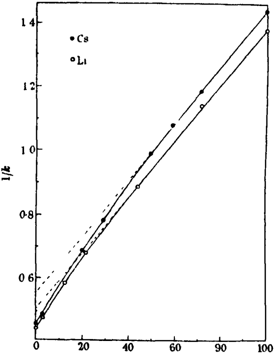

FIGURE 5

In view of these changes in the mass and size of the ion with change in water vapour concentration it is not to be expected in general that Blanc's relation should hold.

In figure 6 let the point $A$ represent the observed mobility of a clustered ion in an inert gas containing a small trace of water vapour and the point $B$ that in pure water vapour. If the average number of molecules in the cluster at $A$ is $n_1$ and at $B$ is $n_2$ then the mobilities of clustered ions which have constant water contents of $n_1$ and $n_2$ molecules will be represented by two straight lines $AA'$ and $BB'$. If the cluster grows between $A$ and $B$ in the manner outlined above we may expect the experimental graph to be of the form shown by the full line.

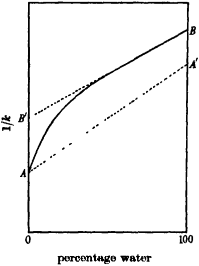

FIGURE 6

Returning to figure 3 it will be observed that in the case of Xe the experimental points at the higher water percentages lie approximately on a straight line and that the whole graph is similar in form to the curve in figure 6. On the assumption that the number of molecules in the cluster is constant at these higher percentages the point corresponding to $B'$ in figure 6 can be obtained by extrapolation of this straight section to zero concentration as indicated by the dotted line in figure 3. From this value of 0·84 for the mobility one can deduce an upper limit to the mass of the cluster by the method described in Part I of this paper. The value obtained corresponds to a cluster of 14 water molecules round the $Li^+$ ion. For such a large ion, however, the simple mass relationship $k\alpha(1+m/M)^{\frac{1}{2}}$ does not hold and the magnitude of the deviation varies rapidly with the 'diameter' of the ion. Without any knowledge of the change in the effective cross-section of the ion with change in the number of water molecules attached to it any estimation of the number from the observed mobility must therefore be regarded as highly speculative and the most one can say is that it is almost certainly less than 10 for $Li^+$.

The results on mixtures of water vapour with krypton and argon are still less open to quantitative treatment but are not in disagreement with this conclusion.

The graphs in figure 3 appear to show that the changes in the mass and size of the ion as the water vapour concentration in the mixture is increased have a negligible effect in helium in which Blanc's relation holds, but that their effect increases with increase in mass of the gas atom. This would follow from the form of the mass factor if the main effect of further loading was due to the consequent increase in the mass of the ion. But in view of the accompanying changes in size it is doubtful whether this furnishes a full explanation.

Finally the graphs in figures 4 and 5 give support to the view expressed above regarding the influence of the size of an ion upon the growth of its equilibrium cluster with small and increasing percentages of water. In the case of helium water vapour mixtures the graph for the $Cs^+$ cluster is curved below 16 % $H_2O$ but above this point is sensibly straight. The interesting feature of this curve is that it crosses the graph for the $Li^+$ cluster at about 5 % $H_2O$, whereas the straight line through the points at the higher percentages does not. This suggests that the $Cs^+$ cluster is still growing appreciably long after the $Li^+$ cluster has practically ceased to grow The results for the argon water vapour mixtures are not so convincing, since the graphs for both clustered ions are curved at low percentages, but the extent of the curvature is slightly greater for caesium than for lithium.

## REFERENCES

Blanc 1908 *C.R. Acad. Sci., Paris*, **147**, 39.
Loeb 1926 *Proc. Nat. Acad. Sci., Wash.*, **12**, 35.
-- 1928 *Phys Rev.* **32**, 81.
Munson 1939 *Proc. Roy. Soc.* A, **172**, 51.
Munson and Hoselitz 1939 *Proc. Roy. Soc.* A, **172**, 43.
Munson and Tyndall 1939 *Proc. Roy. Soc.* A, **172**, 28.
Przibram 1912 *Phys Z.* **13**, 845.
Wellish 1909 *Proc. Roy. Soc.* A, **82**, 500.

# The mobility of alkali ions in gases
## V. Temperature measurements in the inert gases

By K. Hoselitz

*H. H. Wills Physical Laboratory, University of Bristol*

(*Communicated by A. M. Tyndall, F.R.S.—Received* 9 *September* 1940)

The variation with temperature of the mobility of $Li^+$ ions in helium, $K^+$ ions in argon, $Rb^+$ ions in krypton and $Cs^+$ ions in xenon has been measured over a considerable range of temperature. Comparison of the results with existing classical theories suggests that the approximate agreement found by Pearce over a similar range of temperature for $Cs^+$ and $Na^+$ in He does not hold in general. A quantum mechanical treatment for each individual case seems to be required and for this purpose the experimental data here recorded should be of value.

In view of the value of information on the variation of the mobility of a gaseous ion in the theoretical development of the subject, data were obtained by Tyndall and Pearce (1935) for $He^+$ in He, $N_2^+$ in $N_2$ and by Pearce (1936) for $Na^+$ and $Cs^+$ in He.

The present paper describes the extension of the experiments to ions and atoms of similar electronic structure, i.e. $Li^+$ in He, $K^+$ in A, $Rb^+$ in Kr and $Cs^+$ in Xe.

The method employed was that used in the previous work and the apparatus and procedure was similar to that used by Pearce. The only important changes were that ion glass sources were used and precautions to exclude gas impurity increased (Munson and Tyndall 1939).

The experiments were made over as wide a range of temperature as possible. The lower limit was set by the nature of the gas and the cold jacket temperatures conveniently available. Thus helium was investigated down to liquid hydrogen temperature, but xenon could not be used below solid $CO_2$ temperature because its saturation pressure is then too low. The upper limit was set by unsteadiness in the electrometer behaviour due to strain set up in the insulating distance pieces or by the electrical condition through the hot pyrex glass.

All the values, with one exception ($K^+$ in A at 460° K), were determined by several runs at various values of field $E$ and pressure $p$, the value finally quoted being given by extrapolation to $E/p = 0$.

## RESULTS

The results are collected in table 1 in which $k_p$ is the mobility at constant (normal) pressure and $k_\rho$ at constant density. Thus $k_\rho = k_p\, 291/T$.

TABLE 1

| | $Li^+$ in He | | $K^+$ in A | | $Rb^+$ in Kr | | $Cs^+$ in Xe | |
|---|---|---|---|---|---|---|---|---|
| $T°$ K | $k_p$ | $k_\rho$ | $k_p$ | $k_\rho$ | $k_p$ | $k_\rho$ | $k_p$ | $k_\rho$ |
| 20·5* | 1·41 | 20·0* | — | — | — | — | — | — |
| 78 | 5·86 | 21·8 | 0·35 | 1·30 | — | — | — | — |
| 90 | 6·85 | 22·2 | 0·47 | 1·52 | 0·364 | 1·15 | — | — |
| 195 | 16·0 | 23·9 | 1·565 | 2·34 | 1·05 | 1·57 | 0·684 | 1·02 |
| 273 | — | — | — | — | 1·48 | 1·575 | 0·943 | 1·005 |
| 291 | 25·8 | 25·8 | 2·81 | 2·81 | 1·58 | 1·58 | 1·01 | 1·01 |
| 370 | — | — | — | — | 2·25 | 1·59 | 1·285 | 1·01 |
| 389 | 37·2 | 27·8 | — | — | — | — | — | — |
| 400 | — | — | 4·225 | 3·07 | — | — | — | — |
| 450 | — | — | — | — | — | — | 1·59 | 1·03 |
| 455 | — | — | — | | 2·57 | 1·64 | — | — |
| 460 | — | — | 4·67 | 2·95 | — | — | — | — |
| 483 | 48·5 | 29·2 | — | — | — | — | — | — |

* See p. 202.

The values of $k_\rho$ are also shown graphically in figure 1 for convenience on a logarithmic scale. In figure 1 *a* full lines give $Li^+$ in He together with the previous experimental results of Pearce (1936) for $Na^+$ and $Cs^+$ in He. For reasons given later, the $Cs^+$ graph is repeated with a different origin in the upper half of figure 1 *a*, and the scale omitted. Figure 1 *b* gives the results in the other gases. It will be noted that in Pearce's result for $Cs^+$ in He $k_\rho$ passed through a maximum within the experimental range of temperature. If a corresponding maximum occurs for $Cs^+$ in Xe it must be very flat because no change in $k_\rho$ was detectable within the range of temperature available, 195–450° K. The mobility of $Rb^+$ in Kr at constant density also appears to reach a constant value as the temperature is raised. Except for the highest point in the $K^+$ in argon graph the values for both $K^+$ in A and $Li^+$ in He are still rising even at the highest temperatures The highest point for $K^+$ in A could not be checked, owing to great electrometer unsteadiness, whereas the other points were repeated several times. The suggested maximum in this graph is therefore doubtful. At the temperature of liquid hydrogen any error in assuming that the mean temperature of the gas is the same as that of the bath is magnified five times. The lowest point for $Li^+$ in He is therefore, if anything, somewhat too high. Indeed there is some evidence that the gas temperature there exceeded that of the bath by 1·3°. If so the value of $k_\rho$ at the lowest temperature should be 18·8 instead of 20·0.

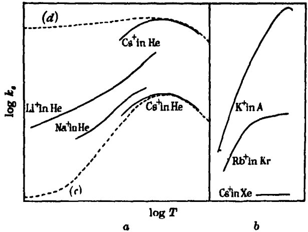

FIGURE 1. Full lines, experimental. Dotted lines, (c) centres of force model, (d) elastic sphere model

## DISCUSSION

Theoretically it should be possible to develop a general wave mechanical treatment of the mobility problem in terms of known laws of force; but it would be very laborious. Since electron exchange does not take place between an alkali ion and an inert gas atom it has previously been suggested that in such cases one might not go seriously wrong by substituting a classical model. There are two such models available: (a) Langevin's theory in which ions and atoms are assumed to be elastic spheres, the atoms being polarized in the field of the ion, and (b) Hassé and Cook's theory in which the elastic spheres are replaced by point centres of attractive and repulsive force each varying by an inverse power law with distance. For mathematical convenience the powers were assumed to be 5 and 9 respectively.

Clearly Langevin's model is relatively crude but it is interesting to note that at room temperature it gives absolute values for the mobility of all the alkali ions in all the inert gases agreeing with the experimental results to within the order of 5 % (Tyndall 1938). One objection to Hassé and Cook's model is that a model of this character applied to collisions between neutral atoms can only be fitted to experiment by using a power of repulsive field higher than 9, the power used varying from case to case (Lennard-Jones 1931). Also the use of a single term to the power of 5 for the attractive field is not justified. Another objection is that in a wave mechanical treatment the repulsive field follows an exponential law with distance and thus an inverse power law for the repulsive field cannot be correct. The reaction between atom and ion when they are within close range may consequently be very different from that given by the classical model.

At the same time in the absence of a general wave mechanical analysis one would expect on general grounds a better agreement with experiment by replacing the concept of elastic spheres by point centres of forces provided the most suitable power law could be found. For this reason Pearce compared his experimental results on the temperature variation for $Na^+$ and $Cs^+$ in He with the two theories and showed that they bracketed his results in such a way as to suggest that by using a power law of repulsion higher than 9, say 13, a better agreement could be reached. It is therefore natural to make a similar comparison with the new results recorded above.

Pearce (1936) plotted the values of certain parameters and attempted to fit the graph so obtained to the experimental graph of $\log k_p$ with $\log T$ by keeping the corresponding pairs of axes parallel and shifting the point of origin of one of the graphs until the best possible fit is obtained. If the fit is good then the values of the arbitrary constants in the theoretical expression can be deduced from the intercepts of the axes. If the fit is only fair the deviation suggests the direction in which modification in the theories are required. In figure 1 the two dotted graphs (*c*) Langevin, (*d*) Hassé and Cook, are taken from Pearce's paper and fitted in this way to his results for $Cs^+$ in He. It was the way in which the theoretical curves bracket his results that led him to suggest that a power of repulsive force higher than 9 might give a much better fit.

But when one applies the same process to the results of this paper shown in the other graphs in the figure, it is fairly obvious even by eye that no appreciable portion of the theoretical graphs (*c*) and (*d*) can be fitted to the experimental results by shifting them by movements parallel to the axes. It is true that $Li^+$ in He, though giving no certain fit anywhere, falls with the other ions in He within the bracketing scheme, but the graphs for $K^+$ in A, $Cs^+$ in Xe and $Rb^+$ in Kr are quite different in shape and slope and clearly cannot be reconciled with the theoretical graphs. These results make it clear that the partial success of the classical model in He is not obtained in other cases. Moreover, the fact that, on comparing the various results, the deviations from the theoretical graphs are so widely different in character strongly suggests that each case must be treated separately and cannot be expressed in such simple terms as those on which the classical models are based. A quantum mechanical treatment for each individual case seems to be required and it is hoped that the experimental data here recorded may ultimately be of use in this connexion.

The writer wishes to express his indebtedness to the University of Bristol for a research grant and to Professor Tyndall for valuable discussions and help during the course of the work, and to Mr H. G. David who took the measurements on lithium ions in helium.

### REFERENCES

Hassé and Cook 1931 *Phil. Mag.* **12**, 554.
Langevin 1905 *Ann. Chim. Phys* **5**, 245.
Lennard-Jones 1931 *Proc. Phys. Soc.* **43**, 461.
Munson and Tyndall 1939 *Proc. Roy. Soc.* A, **172**, 28.
Pearce 1936 *Proc. Roy. Soc.* A, **155**, 490.
Tyndall 1938 *The mobility of positive ions in gases*. Cambridge Univ. Press.
Tyndall and Pearce 1935 *Proc. Roy. Soc.* A, **149**, 426.

---

# The seasonal variations of cosmic-ray intensity and temperature of the atmosphere

BY A. DUPERIER, Sc.D.

(*Communicated by P. M. S. Blackett, F.R.S.—Received* 4 *March* 1940 —*Revised* 18 *October* 1940)

A careful examination of the upper atmospheric data for Europe and the United States indicates that the mean temperature of the upper atmosphere in spring differs from that in summer more than from that in winter. The magnitude of the second difference as defined by (1) depends on the height of the atmosphere which is considered and is a maximum at a height of about 6 km. and changes sign at heights above 12 km. (figure 1).

This lag in the warming of the atmosphere in spring is found to be paralleled by a lag in the diminution of intensity of the cosmic-rays.

A similar phenomenon is found in autumn. The cooling of the atmosphere as a whole is found to be less between summer and autumn than between autumn and winter, though the effect is markedly less definite than in spring.

The cosmic-ray variations are found to be correlated more closely with the mean temperature of the atmosphere up to 16 km. than with the temperature near the ground This provides additional support for the theory of Blackett that the temperature variation of penetrating cosmic-rays is related to the instability of the mesotron.

The temperature coefficient of the cosmic-rays as deduced from the seasonal data is found to be 0 18 %/° C, and this is in rough agreement with the prediction of the theory.

## 1. INTRODUCTION

It is known that the cosmic-rays intensity, as observed in various parts of the world, shows an annual variation inverse to that of the temperature near the ground. Blackett (1938) has attempted to relate this temperature effect with the instability of the mesotrons which form the main part of the penetrating component, and has thus explained the decrease of cosmic-rays intensity as being the consequence of the greater distance which the mesotrons have to travel to reach the sea-level in a warm atmosphere owing to its greater extension upwards.

In order to test this theory, Blackett pointed out that the observed intensity variations should be correlated with the mean temperature of the atmosphere up to the height where the penetrating component is supposed to be formed, rather than with the temperature near the ground as has been done hitherto.

The main difficulty of carrying out this lies in the fact that we have not at our disposal many observations of the temperature of the free atmosphere at those localities where the cosmic-ray observations have been carried out. However, if we abandon at present the possibility of correlating the monthly values and confine ourselves to the seasonal variations, it is found possible to correlate the cosmic-ray observations at a few stations with the meteorological observations at similar geographical positions. On the other hand, in many cases only the seasonal temperatures of the free atmosphere have been published, while the cosmic-ray data must generally be deduced from diagrams showing the monthly changes.

The majority of upper atmospheric observations have been made in Europe between latitude 40° N (Madrid) and 60° N (Pawloswk) and in the United States between 33° N (Dallas) and 47° N (Ellendale). For this reason, we have confined our study to the cosmic-ray observations which are listed in § 3.

## 2. THE SEASONAL TEMPERATURE CHANGE OF THE FREE ATMOSPHERE

It is well known that the difference of mean temperature near the ground between winter and spring is less than the difference between spring and summer. Here the seasons are defined as usual, i.e. winter is defined as December, January, February, etc.

The upper atmospheric data for Europe compiled by Wagner (1931) in the *Handbuch der Klimatologie* show that the difference is still greater in the upper atmosphere than near the ground. If $T_W$, $T_{Sp}$, $T_{Su}$, $T_A$ are the temperatures of the atmosphere in winter, spring, summer, autumn respectively, then we can call the quantities

$$\Delta T_1 = (T_{\mathrm{Su}} - T_{\mathrm{Sp.}}) - (T_{\mathrm{Sp.}} - T_{\mathrm{W.}}), \quad \Delta T_2 = (T_{\mathrm{A.}} - T_{\mathrm{W.}}) - (T_{\mathrm{Su.}} - T_{\mathrm{A.}}), \quad (1)$$

the second differences of the seasonal temperature for spring and autumn respectively.

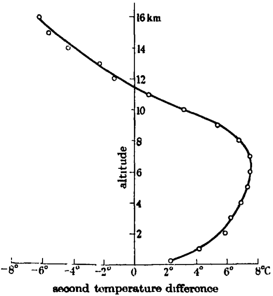

FIGURE 1. Variation of spring second temperature difference of free atmosphere with height.

Figure 1 shows $\Delta T_1$ for Europe plotted against the height from the ground. This figure shows that up to a height of about 11 km. the increase of temperature of the atmosphere in Europe between spring and summer is greater than that between winter and spring, but that at greater heights the difference becomes reversed. The maximum value of the second temperature difference occurs between 6 and 7 km.

We can summarize these results for Europe by saying (*a*) that the temperature of the troposphere in spring is nearer to its temperature in winter, but that (*b*) the temperature of the stratosphere in spring is nearer to its temperature in summer.

Lennahan (1938) has shown that in the United States the result (*a*) is true. It appears, however, from Lennahan's results, that the levels at which the maximum and zero values of the second temperature difference occur are about 10 and 15 km., that is, appreciably higher than in Europe.

The same type of phenomenon occurs in autumn. Here the temperature difference between summer and autumn is less than that between autumn and winter. However, the difference is not so great as in spring and the phenomenon is clearly more complicated.

The characteristics of the rise and fall of seasonal atmospheric temperatures in the first 7 or 10 km. are no doubt due to the fact that the air nearest the ground becomes warmed or cooled more rapidly than the air at greater heights with the advance of spring or autumn respectively, and also to the fact that the temperature mean lapse rates in the lower layers are greater in summer than in winter. From 7 km. upwards the air in spring becomes more and more rapidly warmed as the height increases On the other hand, the same upper atmosphere data show that the average annual amplitude of the monthly means of temperature first decreases rapidly in the first 2 or 3 km. then increases very slightly, and finally starts to decrease again at the height of 7 km., where the second difference of the seasonal temperature reaches its maximum. It is possible that this latter effect of the annual amplitude and the more rapid warming of the air, which together determine the change of the second difference at 7 km , may be connected with the ozone content of the atmosphere, which is known to become appreciable in the upper troposphere and to have a maximum early in spring at the latitudes we are here considering.

In spite of the change of sign of the second temperature difference at great altitudes, the *mean* temperature of the atmosphere up to 16 km. in spring is nearer to that in winter than to that in summer, and this difference is clearly greater here than near the ground.

## 3. THE CORRELATION BETWEEN THE SEASONAL VARIATIONS OF COSMIC-RAY INTENSITY AND TEMPERATURE OF THE ATMOSPHERE

In our study we have utilized the following observations of cosmic-rays:

TABLE 1

| Locality | Latitude | Observer |
|---|---|---|
| Amsterdam | 52°·4 N | Clay and Bruins (1939) |
| Pacific Ocean | 48°·5 N–33°·1 S | Compton and Turner (1937) |
| Hafelekar (near Innsbruck) | 47° 3 N | Demmelmair (1937) |
| Cheltenham (U.S.) | 38°·7 N | Gill (1939) |
| Potsdam | 52°·4 N | Miczaika (1939) |
| Capetown | 34° S | Schonland, Delatizky and Gaskell (1937) |

In all these investigations the ionization chamber with which the measurements were made was sufficiently shielded, e.g. by 10 cm. or more of lead, to cut out the soft radiation.

We will first consider the conclusion to be derived by averaging all the above observations.

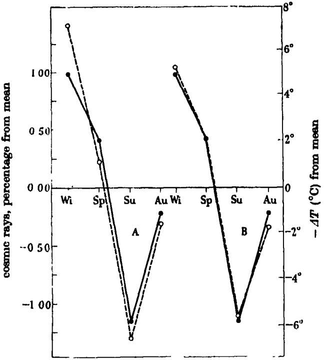

FIGURE 2 Correlation of temperature change of atmosphere and cosmic-ray intensity in shielded chamber. A, temperature near ground, B, mean temperature up to 16 km.

The full curve of figure 2 A gives the mean variation of penetrating cosmic-ray intensity with the seasons as deduced from the six series of observations of table 1 The same curve is repeated in figure 2 B. We have included the observations made in Capetown because it is probable that at this latitude the mean temperature of the upper atmosphere does not differ very appreciably from that of the corresponding northern latitude, in spite of the different distribution of lands and seas in the two hemispheres.

The dotted curve of figure 2 gives the mean temperature *near the ground* for the four seasons, expressed as a difference from the annual mean. Figure 2 B gives the mean temperature *up to* 16 *km.*, which is calculated by averaging over the separate mean temperatures ascribed to the different stations under consideration. In both the cases the sign of the temperature is reversed in order to bring out clearly the correlation between the two phenomena.

The cosmic-ray intensity is certainly correlated better with the mean temperature of the atmosphere up to 16 km. than with the temperature near the ground. The lag in the warming of the atmosphere in spring is clearly very well paralleled by an equivalent lag in the decrease in intensity of the cosmic-rays.

In order to test the significance of such a correlation with so few pairs of data, we will make use of Fisher's method of calculating the probability, $P$, that the observed correlation should arise by random sampling from uncorrelated observations. We therefore calculate the correlation coefficients, $r_{c,g}$, $r_{c,a}$, between the seasonal average changes of the cosmic-ray intensity and the changes of temperature (*a*) near the ground and (*b*) of the free air up to 16 km.

We obtain the following values:

$$\begin{array}{cc} (a) & (b) \\ r_{c,g} = -0{\cdot}983 & r_{c,a} = -0{\cdot}996 \\ P = 2\,\% & P < 0{\cdot}4\,\% \end{array}$$

Although both the coefficient and its significance are greater in the second case, one would consider the difference as being not entirely convincing. However, as the correlation between the two temperature changes is also very great ($+0{\cdot}98$), it is permissible to calculate the partial correlation coefficients $r'$, e.g. the correlations between the cosmic-ray intensity and one of the two temperature changes when the other is supposed constant. We find

$$r'_{c,g} = -0{\cdot}12, \quad r'_{c,a} = -0{\cdot}89.$$

It therefore seems that it is the average temperature of the free atmosphere that determines the temperature effect of cosmic-ray rather than the temperature near the ground. The recent study of Loughridge and Gast (1939) concerning the changes in cosmic-rays intensity at the fronts separating different air masses leads to the same view.

If the mean temperature of the atmosphere up to some other height than 16 km. is evaluated, e.g. up to 10 or to 20 km., the correlation with cosmic-ray intensity is found to be appreciably worse. Though of course the comparison is not very sensitive to the height, this result does support roughly the assumption made by Euler and Heisenberg (1938) that the mesotrons are formed at about the maximum of the transition curve for vertical rays. This is also in agreement with the results recently obtained by Dymond

(1939) and showing that the intensity of vertically directed mesotrons rises to a maximum at about the same height.

Table 2 gives the value of the temperature coefficient, $\alpha$, of the total cosmic-ray intensity for the six localities of table 1, as deduced by the various observers. Each value is an average over a period of a year or more.

TABLE 2

| Locality | Temperature coefficient %/° C |
|---|---|
| Amsterdam | −0·21 |
| Capetown | −0·12 |
| Cheltenham | −0·15 ± 0·02 |
| Hafelekar | −0·08 |
| Potsdam | −0·15 |
| Pacific Ocean | −0·18 ± 0·01 |
| Mean | −0·15 |

Table 3 gives the *seasonal* values of $\alpha$ as deduced from the results contained in figure 2A and B, for all six localities taken together.

TABLE 3

|  | From (*a*) with the temperature near the ground %/° C | From (*b*) with the temperature of the upper atmosphere up to 16 km. %/° C |
|---|---|---|
| Winter | −0·14 | −0·19 |
| Spring | −0·37 | −0·19 |
| Summer | −0·18 | −0·21 |
| Autumn | −0·14 | −0·13 |
| Mean | −0·21 + 0·08 | −0·18 + 0·025 |

The greater regularity of the values in the second column shows in another way the better correlation of the penetrating cosmic-ray variations with those of the temperature of the atmosphere up to 16 km.

The mean value of −0·18 %/° C is quite consistent with the observed mean life-time of the mesotron. A recent survey of the evidence as to the life-time of the mesotron has been given by Rossi (1939).

In addition to the data of table 1, with fully shielded ionization chambers, some data with partially shielded chambers have been given by Clay and Bruins, Demmelmair, Miczaika and Schonland, Delatizky and Gaskell. Such data included some part of the soft radiation as well as the hard.

The full curves of figure 3 A and B give the mean results of these observations. The dotted curve of figure 3 A gives the mean temperature near the ground and that of figure 3 B the mean temperature up to 16 km. expressed as before. It is more difficult in this case to say which temperature is the more suitable. The correlation coefficient appears to be greater with the temperature near the ground than with the mean to 16 km., but its significance is slight. Probably the cosmic-ray results with partially shielded chambers are subject to the influence of radon, and the amount of this present in the lower atmosphere may depend on the temperature of the soil. According to the measurement of Zupancic (1934) the exhalation of radon during the day is about 1·5 times as much as during the night, having a minimum in January and a maximum in June.

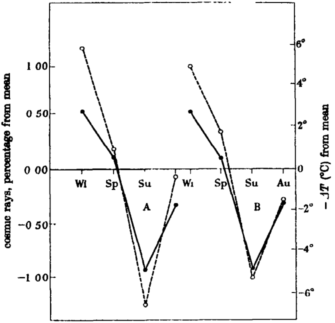

FIGURE 3. Correlation of temperature change of atmosphere and cosmic-ray intensity in partially shielded chambers. A, temperature near ground; B, mean temperature up to 16 km.

### 4. NOTES ON THE DATA OF TABLE 1

The results of Compton and Turner (1937) cover a wide range of latitude, but use has here been made only of those results which refer to geomagnetic latitudes between 42·5 and 52°·5 N. Compton and Turner defined the seasons as

| Winter | Spring | Summer | Autumn |
|---|---|---|---|
| 8 Nov.–18 Jan. | 17 Mar.–20 May | 22 May–5 Aug. | 18 Aug.–24 Oct. |

In our analysis, correction has been made for this fact to bring these results into agreement with the usual definition.

The mean variation of cosmic-ray intensity with the seasons as obtained by Compton and Turner shows a much better correlation with the mean temperature of the atmosphere up to 16 km. than with the temperature near the ground, both temperatures being expressed as a difference from the annual mean.

A similar result is shown by the observations of Clay and Bruins (1939), using the upper atmospheric data deduced from sounding balloon observations made in Lindenberg, Kew and Trappes, and by the observations of Miczaika, (1939) using those of Lindenberg. Since Lindenberg is near Potsdam and since the monthly values are available, we will for comparison give the annual variation as represented in figure 4.

It is shown that the monthly data, like the seasonal data, indicate the better correlation with the temperature of the atmosphere.

On the Hafelekar at a height of 2·3 km. the seasonal variations of the upper atmospheric temperature, as deduced from meteorological data obtained in Munich and Vienna, are very similar to those of the temperature near the ground, so that the two correlations with the penetrating cosmic-ray observations of Demmelmair (1937) are very similar.

On the contrary, the observations of Gill (1939) in Cheltenham (U.S.A.) show a better correlation with the temperature near the ground than with that of the upper atmosphere, as deduced from sounding balloon observations made *in other localities of the United States* However, the decrease of intensity of the cosmic-rays from winter to spring appears excessive in relation even to the corresponding increase in temperature of the ground. Further, a careful examination of the meteorological results up to heights of 5 or 6 km. obtained by kites and aeroplanes (appearing in Lennahan's work already quoted), and corresponding to stations *very near and around Cheltenham*, indicates that in those regions the lag in the warming of the atmosphere in spring is practically constant and smaller than the normal for the United States.

Now, if the regions near Cheltenham obey the apparently general law of a quicker warming in spring above a certain height, the mean upper atmospheric temperature above Cheltenham in spring would be nearer the mean temperature in summer than the mean temperature in winter. As a consequence, even in this case which appeared at first sight to be an exception, the correlation of the cosmic-ray intensity with the mean upper atmospheric temperature would be still better than with the mean temperature near the ground. If this argument is correct, the observations of cosmic-rays would have served to foretell the general trend of the mean temperature of the atmosphere up to a height extending several kilometres into the stratosphere.

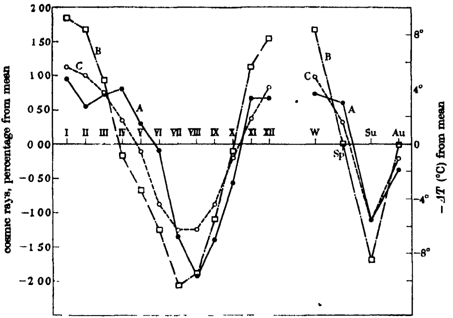

FIGURE 4. Correlation of temperature change at Lindenberg with cosmic ray intensity at Potsdam. A, cosmic ray intensity, B, temperature near ground; C, mean temperature up to 16 km.

Because of lack of sufficient upper atmospheric data in latitudes of the southern hemisphere similar to that of Capetown, it is not possible to say whether the results of Schonland, Delatizky and Gaskell (1937) would correlate better with the temperature near the ground, or that up to 16 km.

For the same reason we cannot use the observations of Gill (1939) in Christchurch (43°·5 S). In addition, in this case the observations cover only nine consecutive months omitting the summer period.

Again, the observations at Teoloyucan (19°·8 N) and at Huencayo (12°·1 S) lie outside the range of latitudes for which the meteorological data are sufficient to allow us to know the seasonal characteristics of the upper air. The comparatively low value of the temperature coefficient near the equator, found by Gill at Teoloyucan, is in agreement with Blackett's (1938) theory, but unfortunately insufficient upper atmospheric data exist to make a detailed comparison possible.

## NOTES ADDED LATER

After this work was completed several other papers concerning the temperature effect of cosmic-rays have been published.

The correlation made by Beardsley (1940) between the cosmic-ray intensity at Cheltenham and the upper air pressures and temperatures, as observed by radio-sonde balloons sent up nearly every day during the period covered by the observations, shows that the changes in air temperature up to a height of 10 km. follow quite closely those near the ground, but that at greater heights the changes are widely different This result seems to be in agreement with the discussion given above in § 4 of the special condition apparently existing near Cheltenham.

Beardsley finds that up to 10 km. the correlations between cosmic-ray intensity and air temperature are not appreciably different from that based on ground temperature, and that this correlation is negative and very close to unity. Above 10 km. the observed correlation decreases but changes sign as the height increases. This would mean that the temperature averaged over a height of 15 km. would be less closely correlated with the cosmic-ray intensity.

On the other hand, Beardsley's results also show that changes in pressure at the height of 5 km. are closely correlated with the cosmic-ray changes and, what is more remarkable, remain so correlated up to 15 km. As the height change $dz$ corresponding to a pressure change $dp$ depends on $p$ (that is, $dz = -gdp/RTp$), those results would not give support to the interpretation based on the instability of the mesotron. The reason for this lack of accord might be that it is not generally possible to eliminate for observations extending over a period of only one year influences on air pressure other than temperature. For such a short period of observations consideration to the different types of weather should be given.

Hess (1940) by analysis of the observations of the cosmic-ray ionization on the Hafelekar during five years has found a seasonal variation with an amplitude of +0·9 %. He finds, however, by correlation with the ground temperature, that the temperature coefficient of cosmic radiation shows a very marked seasonal change from −0·12 %/° C in winter to −0·055 %/° C in summer.

The reason for this variation in the temperature coefficient may be due to the use of the ground temperature for the correlation instead of the mean atmosphere temperature. For the departures of the monthly ground temperature from the annual mean at Hafelekar seem to be smaller in winter than in summer, compared with the similar departures for the average temperature of the upper air up to 15 km. As we have not at our disposal upper atmospheric data over Hafelekar, use can be made of the upper data at Munich and Vienna for comparison. Table 4 gives the monthly departures from the annual mean of the temperature near the ground, as observed at Hafelekar during the period 1936–7, and from the average air temperature up to 15 km. as deduced from sounding balloon data at Munich and Vienna. These two departures are represented by $\Delta T_g$, $\Delta T_a$ respectively in the table.

TABLE 4

| | Jan. | Feb. | Mar. | Apr. | May | June |
|---|---|---|---|---|---|---|
| $\Delta T_g$ | −5·02 | −6·12 | −6·62 | −1·52 | +2·63 | +5 08 |
| $\Delta T_a$ | −6 35 | −4·25 | −4·25 | −2·60 | +1·30 | +4 45 |
| | July | Aug. | Sept. | Oct. | Nov. | Dec. |
| $\Delta T_g$ | +7·98 | +7·48 | +5·08 | −2·82 | −2 42 | −3 82 |
| $\Delta T_a$ | +6·25 | +6 20 | +4·55 | +2·10 | −1 45 | −5 95 |

We see from the table that for the six months from October to March taken together $\Delta T_g/\Delta T_a = 0{\cdot}79$, and for April to September $\Delta T_g/\Delta T_a = 1{\cdot}23$. Thus Hess's factor 2 between the temperature coefficients for winter and summer would have been reduced to 1·29 if the atmosphere temperatures had been used.

Finally, Nishina, Sekido, Simamura and Arakawa (1940) have studied the effect of air masses, particularly of cyclones, on the intensity of cosmic-rays in Japan. They find that the passage of a warm air mass tends to decrease the cosmic-ray intensity and that of a cold air mass to increase it. A similar decrease is found when they consider the approach and passage of a warm front, but no effect appears at all at the passage of a cold front. As this latter result is, as the authors point out, in conflict with that of Longhridge and Gast (1939) for cold fronts, one is led to recognize the necessity for a more detailed knowledge of the variation from region to region of the various weather types.

I wish to express my gratitude to the Society for the Protection of Science and Learning for making this work possible by a generous grant. Also to Professor P. M. S. Blackett for giving me facilities to carry out the work at Manchester University and for his interest in its progress and for many helpful discussions.

## References

Beardsley 1940 *Phys. Rev.* **57**, 336.
Blackett 1938 *Phys. Rev.* **54**, 973.
Clay and Bruins 1939 *Physica*, **6**, 628.
Compton and Turner 1937 *Phys Rev.* **52**, 799.
Demmelmair 1937 *S.B. Akad. Wiss. Wien*, **146**, 643.
Dymond 1939 *Nature, Lond.*, **144**, 782.
Euler and Heisenberg 1938 *Ergebn. exakt. Naturw.* **17**.
Gill 1939 *Phys. Rev.* **55**, 429.
Hess 1940 *Phys. Rev.* **57**, 781.
Lennahan 1938 *Mon. Weath. Rev.*, Supp. no. 38.
Longhridge and Gast 1939 *Phys. Rev.* **56**, 1169.
Miczaika 1939 *Z. Phys.* **113**, 161.
Nishina, Sekido, Simamura and Arakawa 1940*a* *Nature, Lond.*, **145**, 703.
— — — — 1940*b* *Phys. Rev* **57**, 663, 1050.
Rossi 1939 *Rev. Mod. Phys.* **11**, 297.
Schonland, Delatizky and Gaskell 1937 *Terr. Mag. Atmos. Elect.* **42**, 137.
Wagner 1931 *Handbuch der Klimatologie*, **1**, F I.
Zupancic 1934 *Terr. Mag. Atmos. Elect.* **39**, 33.

# A thermodynamical theory of the tensile strength of isotropic bodies

By R. Fürth, *Edinburgh*

(*Communicated by M. Born, F.R.S.—Received* 24 *April* 1940—
*Revised* 21 *June* 1940)

By thermodynamic considerations a new formula connecting the tensile strength of an isotropic body with its melting energy and Poisson's elastic constant is developed and found in good agreement with experiments.

## 1. Problem of the paper

It is well known that attempts to calculate the tensile strength of crystals by means of the lattice theory have failed as yet: the tensile strength, calculated in this way, is about one hundred times larger than the actual value of this quantity, determined by experiments (Born 1923, Zwicky 1923). Recently M. Born and myself (1940) tried a more rigorous treatment of this problem by formulating the stability conditions of a cubic crystal, under a certain stress in the direction of one of the axes, for any small homogeneous deformation. One gets a number of inequalities which must all be satisfied if the lattice is to be stable. If the stress is increased, a certain critical value will be reached at which at least one of the stability conditions will break down. This critical value of the stress is supposed to be the tensile strength. But the numerical calculations on the basis of this theory for a faced-centred lattice, under a special assumption about the forces between the atoms, give a result not essentially different from the former ones. Breaking should take place when a relative increase of length of about 25 % is reached, whereas the experimental value is about 0·3 %, so that the theoretical value of the tensile strength is about 80 times larger than the experimental value For the tensile strength $F$ one gets approximately $0{\cdot}3S\rho$, where $S$ is the sublimation energy per unit of mass and $\rho$ the density. This result is also incorrect The values of the tensile strength calculated in this way are far too large.

The lack of success of the former attempts to calculate the tensile strength from a pure atomistic theory has long ago led many physicists (see Schmidt and Boas 1935, p. 284) to believe that the usual experiments do not give the real values of the tensile strength, because of the imperfections of the real crystals, such as small holes and cracks, which could considerably diminish their strength. Several attempts have been made (Schmidt and Boas 1935, p. 271) to perform the experiments under such conditions as to compensate for these defects. But the results of these experiments are not very convincing, and the whole conception of the 'apparent' and the 'real' strength is very unsatisfactory and improbable.

In a recent paper M. Born (1939) has developed a theory of the melting of crystals based upon principles very similar to those which are used for the treatment of the breaking of crystals mentioned above. He calculates the density of free energy of the crystal at a certain temperature and a certain uniform pressure over which an arbitrary small deformation is superposed. From this the conditions for the stability of the lattice for such deformations can easily be derived, and it is postulated that melting should take place when at least one of these conditions is violated. The results of this theory are in good agreement with the experimental facts, as regards the absolute value of the melting temperature and its dependence on the pressure. This suggests the existence of a close relation between the phenomena of melting and breaking. According to Born's theory, melting is nothing else than a breaking due to the action of the heat movement of the atoms; or putting it the other way round, breaking is nothing else than melting enforced by the action of the external forces. So it might further be suggested that the tensile strength should rather be connected with the heat of melting than the heat of sublimation per unit of volume, as predicted by the lattice theory. And indeed, comparing the experimental values, one can see immediately that they are of the same order of magnitude. This fact was the starting point for the following considerations which have led, as will be shown, to a formula relating the tensile strength of an isotropic body with the heat of melting per unit of volume, in good agreement with the experiments.

## 2. METHOD OF THERMODYNAMICAL TREATMENT

In order to simplify the main idea of the thermodynamical treatment of the problem as far as possible, consider an ideal homogeneous and isotropic material, completely elastic and with no plasticity. Let an arbitrarily shaped piece of this material of volume $V$ be stressed by outside forces. If these forces are increased gradually, a stage will be reached at last where cracks or holes are formed inside the body so that breaking will follow immediately. Let $V+\delta V$ be the volume of the body just before this stage has been reached, and let $u+\delta u$ be the potential energy per unit volume. When the holes or cracks have been formed, the matter outside the holes must again take the original density and the original volume $V$ (since it has been supposed that breaking follows immediately, i.e. that the strain vanishes), and the energy density will reduce to $u$. Let $u_0$ be the energy density inside the holes. The conservation of energy requires that the equation

$$(V+\delta V)\,(u+\delta u) = Vu+\delta V-u_0 \tag{1}$$

must be satisfied. As $s = u_0 - u$ obviously is the energy of sublimation per unit volume, and as this quantity is large compared with $\delta u$, (1) can be rewritten as follows:

$$U = V\,\delta u = \delta V\,s, \tag{2}$$

where $U$ is the potential energy of the elastic forces, accumulated in the whole body just before it is broken. Equation (2) means that this breaking should occur if the energy $U$ is sufficient to 'sublimate' the matter in a volume $\delta V$. On the other hand, the maximum stress $F$ will be of the order of magnitude $U/\delta V$; thus, from (2) it follows that ($\rho$ density, $S$ heat of sublimation per unit mass)

$$F \sim s = S\rho, \tag{3}$$

which expresses that the breaking strength should be of the order of magnitude $s$, the sublimation energy per unit volume, and corresponds therefore with the result of the rigorous treatment on the basis of the lattice theory, mentioned in § 1.

The reason for the incorrectness of the relation (3) is clear. Actually, the matter in the volume $\delta V$ will 'melt' long before it could be sublimated, namely, when the energy $U$ has reached the value $\delta V q$, where $q$ is the melting energy per unit of volume. Indeed, when this stage is reached, the matter inside $\delta V$ must loose its rigidity completely, i.e. the body behaves exactly as if this volume consisted of holes or cracks, and therefore breaking will take place. Hence, the relations (2) and (3) have to be replaced by

$$U = V\,\delta u = \delta V\,q \tag{2'}$$

and

$$F \sim q = Q\rho, \tag{3'}$$

where $Q$ is the melting energy per unit of mass. Equation (3′) is identical with the suggestion expressed in § 1, and is in agreement with the experimental facts.

### 3. DERIVATION OF A FORMULA FOR THE TENSILE STRENGTH

Having laid down in § 2 the general idea of the thermodynamical treatment of this problem, the actual calculation of the tensile strength of the supposed ideal material can now be begun. Consider a rod of length $l$ of such a material, stressed by a force $X$ per unit cross-section. Let Young's modulus be denoted by $E$ and Poisson's constant by $\mu$. Then $l$ will be increased by $\delta l$ according to

$$\frac{\delta l}{l}=\frac{X}{E}, \tag{4}$$

and the volume $V$ by $\delta V$, according to

$$\frac{\delta V}{V}=\frac{\delta l}{l}(1-2\mu)=\frac{X}{E}(1-2\mu). \tag{5}$$

The increase of potential energy will be

$$U=V\frac{X^2}{2E}. \tag{6}$$

Inserting from (5) and (6) into the fundamental equation (2′), we get immediately the critical value of the stress $X$, i.e. the tensile strength $F$.

$$F=2Q\rho(1-2\mu). \tag{7}$$

Although the formula (7) is in far better agreement with the experiments (as will be shown later) than any other theoretical formula for $F$ given before, it cannot be correct. The reason is, that in the foregoing calculation we have not accounted for the potential energy accumulated in the device which is used for the production of the stress, e.g. a spring or a weight. The situation is analogous to that in the thermodynamics of equilibrium between two states. Here, if the volume of the system under consideration is kept constant, the equilibrium is maintained if the free energy in the two states is equal. But if the volume is not constant during the transition so that work is done by the outside forces, this equilibrium condition has to be replaced by another condition accounting for this work. If, for example, the pressure is kept constant, the work done by the outside forces equals $p.\Delta V$, where $\Delta V$ is the change of volume by the transition from one state to the other, and accounting for this work one has to replace the free energy by the 'thermodynamic potential' in the equilibrium condition. In our case the problem how to formulate the equilibrium condition correctly is even more complicated, because after the rupture a part of the potential energy of the breaking device will certainly be transformed into the kinetic energy of the movement of the pieces and the rest of the energy possibly might have been used for the breaking itself.

The best way to overcome these difficulties is to invent a suitable mechanism which automatically avoids the broken pieces being moved, and which therefore allows for the exact energy balance. It is clear that the broken pieces can be stopped from moving only if certain forces are exerted on them. In order to make the final state after the rupture a real thermodynamic equilibrium, these forces must further have the form of a uniform pressure. If a model can be constructed which satisfies all these conditions, the energy balance can be made without difficulty, and one can be sure that the relation for the breaking strength derived from this particular model can be applied generally, just as a thermodynamic formula, derived by considering a special model, can be applied in any other case.

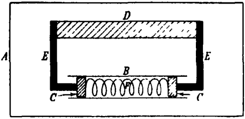

FIGURE 1

The following model fulfils all that is required It consists of a closed box $A$ (see figure 1) with absolutely rigid walls, and a cylinder $B$ of the same kind in which the two pistons $C$ can be moved. The pistons are connected with the rod $D$ by absolutely rigid pieces $E$, and they are pressed apart by the spring $F$, so that the rod is stressed. The whole space between the box and the cylinder is filled with an incompressible liquid in which the pressure is zero when the stress equals $F$. By passing this value the rod will break and immediately afterwards the pistons will exert the pressure $F$ on the liquid, and therefore the same pressure $F$ will also act on the pieces of $D$. At the same time their very slight motion will be stopped at once, and the kinetic energy of the system during the whole process will be negligibly small.

Now the potential energy of the rod before the rupture is, just as before, given by equation (6). But after the breaking the rod is compressed by the same pressure $F$, giving rise to a potential energy

$$U' = V\frac{\kappa F^2}{2}, \tag{8}$$

where $\kappa$ is the compressibility. This quantity is connected with $E$ and $\mu$ by the relation

$$\kappa = \frac{3(1-2\mu)}{E}; \tag{9}$$

thus (8) takes the form $$U' = V\frac{3(1-2\mu)}{2E}F^2. \tag{10}$$

The energy disposable for the process of melting equals $U-U'$ plus the work $A$ done by the slight movement of the pistons after the rupture, which is equal to the pressure $F$ times the whole change of volume of the rod material. Since the volume of the pieces under the pressure $F$ is equal to

$$V' = V+\delta V' = V(1-\kappa F) = V\left[1-\frac{3(1-2\mu)}{E}F\right], \tag{11}$$

one gets from (5) (with $X = F$) and (11),

$$A = F(\delta V-\delta V') = \frac{4VF^2(1-2\mu)}{E}. \tag{12}$$

Hence, from (6), (10), (12),

$$U-U'+A = V\frac{F^2}{E}(3-5\mu). \tag{13}$$

According to what has been said before, the expression (13) is to be used in equation (2′) instead of $U$. Thus using (5′) we get instead of (7),

$$F = Q\rho\frac{1-2\mu}{3-5\mu}, \tag{14}$$

which differs from (7) only by the factor $\frac{1}{2(3-5\mu)}$.

## 4. DISCUSSIONS OF EXPERIMENTAL CONDITIONS

To check the theoretical relations (7) or (14) with the experimental data, one has to be very careful since these relations apply directly only to the supposed idealized material. Real materials differ from these ideal ones in several important points.

(1) No real material is completely homogeneous. There is first the inhomogeneity due to the complex atomic structure of the crystal-lattice of a chemical compound. It can be avoided by only considering pure elements. There is further the inhomogeneity due to the imperfections of the real lattices They will be most prominent in polycrystalline materials, but even single crystals are never free from imperfections due to wrong

positions of a few atoms or empty places in the lattice. Since any such imperfection of the material will undoubtedly diminish its strength (as has been mentioned in § 1), one would expect the breaking strength of single crystals to be much larger than that of polycrystals But experimental facts are to the contrary. I shall give the explanation of this fact a little later, but it is quite obvious from the facts alone that we should be wrong in using the values of the tensile strength obtained by experiments with single crystals for checking the theoretical formulae, and that the values obtained for polycrystalline samples must be used.

(2) A further cause of inhomogeneity is the heat movement of the atoms, which gives rise to local fluctuations of density It is clear that this phenomenon must have an effect similar to that of structural imperfections, diminishing therefore the strength of the material with increasing temperature. Experiments indeed show a strong dependence of tensile strength on the temperature in this sense. For checking the theory one must therefore use the values of the tensile strength for zero temperature where thermal fluctuations vanish. This also follows from a purely phenomenological point of view by the fact that no account has been taken of thermal expansion in the present theory.

(3) There is no real isotropic material. In order to check the theory one must therefore choose substances at least behaving like isotropic ones. Metals in the usual polycrystalline form which have not been worked satisfy this and the former conditions and are therefore suitable for our purpose.

(4) This theory supposes an ideal, completely elastic material, i.e. a material behaving like an elastic system up to the breaking point. Actually every solid submitted to the action of a stress will undergo a plastic deformation long before the breaking stress is reached. This is a consequence of the 'slip' movement along certain planes in the interior of the crystals. In a perfect single crystal, uniformly stressed precisely in the direction of one of the axes, no slip could occur by reasons of symmetry. Such conditions, however, are never realized, and therefore the slip movement begins almost suddenly on passing a certain critical stress. During the subsequent large non-elastic deformation of the sample the stress can be increased within relatively narrow limits only, until the rupture takes place. The measured tensile strength of a single crystal will therefore be considerably smaller than the strength to be expected by theoretical considerations which make no account of the slip motion.

In a sample with a polycrystalline structure slip movement will take place in a large number of crystallites at different times and therefore the region of elastic deformation goes over continuously into the region of plastic deformation. Accordingly the stress increases uniformly with the deformation up to the maximum value, where the 'creep' of the sample begins which is followed by the rupture. Each single slip motion goes only for a very short distance, and its result is not a strong disturbance of the structure as in the case of a single crystal but, on the contrary, the formation of better contact between neighbouring crystallites, and therefore an increase in strength almost to the value expected for a material without imperfections.

It is true that a sample of a material which undergoes a large plastic deformation during the process of stretching will not work in a model mechanism such as proposed in § 3. But since the deformation of the rod does not appear in the resulting formulae (7) and (14), which contain only the maximum stress $F$, these relations can properly be used for the real material, provided only that the measured maximum stress is sufficiently close to the ideal tensile strength, which seems to be very likely for the foregoing reasons.

## 5. COMPARISON BETWEEN THEORY AND EXPERIMENTS

The discussion of § 4 shows the right way to test the theory: the values of the tensile strength of pure polycrystalline and unworked metals, measured at very low temperatures, must be compared with the values calculated from the measured quantities $Q$, $\rho$ and $\mu$ of these substances by means of one of the formulae (7) or (14).

Actually no measurements of tensile strength have been made as yet at very low temperatures, but for a number of substances the dependence of $F$ on $T$ is fairly well known over a range of temperatures so as to make possible an extrapolation of $F$ to zero temperature with an accuracy sufficient for the present purpose. The figures for Al, Cu, Fe, Ni, Pb, Sn, Zn were taken from a table in Landolt-Börnstein (1927) and a table in the *Handbuch der Physik* (1928) based on the observations of different authors. Figure 2 shows how the extrapolation was made graphically. No reliable figures were available for Ag, Au and Pt. But a comparison of the values of tensile strength for cold stretched and annealed metals (*Handbuch der Physik* 1928) shows that the increase of strength due to the former treatment of the metals is almost the same as the increase due to the cooling, which is very plausible indeed. It therefore seems permissible to use the figures given for cold stretched samples of the three metals mentioned above, given in a table in the *Handbuch der Physik*.

The values of $F$ for ten of the most common metals determined in the way just explained are given in the second column of table 1. Considering the inexactness of the experimental methods, the large influence of mechanical and thermal treatment of the samples on their strength, and the uncertainty of the extrapolation, the possible error of these values is certainly considerable. The uncertainty which must be attributed to them can hardly be less than about 30 %.

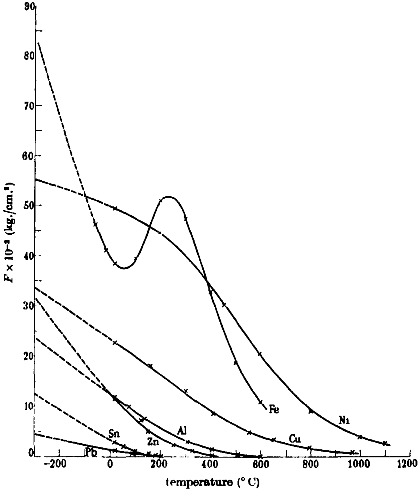

FIGURE 2

The 3rd, 4th, and 5th columns of the table contain the values of $Q$, $\rho$, and $\mu$ for the ten metals, also taken from the Landolt-Börnstein tables. The uncertainty in these figures can be neglected in comparison with the uncertainty of the $F$'s. The 6th column gives the values of $2Q\rho(1-2\mu)/F$, which, according to equation (7), should be equal to unity, and the 7th column the values of the quantity $Q\rho(1-2\mu)/F(3-5\mu)$ which should equal unity if the relation (14) is correct. In calculating the values of these two columns one must not forget to measure $F$ and $Q\rho$, which have the same dimensions, in the same units, i.e. using the figures given in the table one has to multiply by a factor $\dfrac{1\text{ cal./cm.}^3}{100\text{ kg./cm.}^2} = \dfrac{4{\cdot}2\times 10^7}{9{\cdot}8\times 10^7} = 0{\cdot}43$.

TABLE 1

| Element | $F.10^{-2}$ kg./cm.$^2$ | $Q$ cal./gr. | $\rho$ | $\mu$ | $\dfrac{2Q\rho(1-2\mu)}{F}$ | $\dfrac{Q\rho(1-2\mu)}{F(3-5\mu)}$ | $\dfrac{Q\rho}{4F}$ |
|---|---|---|---|---|---|---|---|
| Ag | 29 | 25 | 10·5 | 0·38 | 1·9 | 0·85 | 0·95 |
| Al | 23 | 90 | 2·7 | 0·345 | 2·8 | 1·1 | 1·1 |
| Au | 27 | 16 | 19·3 | 0·42 | 1·6 | 0·89 | 1·2 |
| Cu | 32 | 50 | 8·9 | 0·35 | 3·6 | 1·4 | 1·5 |
| Fe | 80 | 66 | 7·8 | 0·28 | 2·4 | 0·75 | 0·7 |
| Ni | 55 | 63 | 8·8 | 0·31 | 3·3 | 1·2 | 1·05 |
| Pb | 4 | 6 | 11·3 | 0·445 | 1·6 | 1·03 | 1·8 |
| Pt | 34 | 27 | 21·4 | 0·385 | 3·4 | 1·6 | 1·8 |
| Sn | 12 | 14 | 7·3 | 0·33 | 2·5 | 1·08 | 0·9 |
| Zn | 30 | 26 | 7·1 | 0·33 | 1·8 | 0·66 | 0·65 |

Looking at the figures in the 6th column of the table it is obvious that formula (7) cannot be correct, as has been presumed in § 3. The values are spread over a rather large range and the average is 2·5 instead of 1. The figures in the 7th column, however, show the correctness of the rigorous equation (14). The average of all the values is 1·056 and the mean deviation of the single values from the average is 0·275 or about 27 %. Thus the spread of the single values is not larger than is to be expected because of the uncertainty of the $F$'s. The mean error of the average value is $0{\cdot}275/\sqrt{10} = 0{\cdot}085$; the deviation of the average from the theoretical value 1 is therefore within the experimental error

Since the values of the $\mu$'s are all in the vicinity of $\frac{1}{3}$, one could suggest that a formula of the form

$$F = Q\rho\lambda \tag{15}$$

with a constant $\lambda$ would be as suitable as the formula (14). It can be shown, however, that this is not the case. Inserting the value $\frac{1}{3}$ for $\mu$ into (14), one gets $\lambda = \frac{1}{4}$. In the 8th column of the table the values of $Q\rho/4F$ are inserted. They have the average 1·16 which also is close to 1, but the spread of the single values is much greater than the spread of the values in the 7th column, and plotted against $\mu$ they show a strong and distinct dependence on $\mu$, whereas the values of the 7th column show no dependence on $\mu$. This fact strongly suggests that our consideration is correct and that equation (14) gives the real values of the tensile strength at low temperatures for isotropic substances.

I have to thank Professor Born for his interest in this investigation and for many valuable discussions.

## References

Anon. 1928 *Handbuch der Physik*, 6, 626, 627. Berlin
Born, M. 1923 *Atomtheorie des festen Zustandes*. Berlin.
— 1939 *J. Chem. Phys.* 7, 591.
Born, M. and Fürth, R. 1940 *Proc Camb. Phil. Soc.* 36, 454.
Landolt-Bornstein 1927 *Phys.-Chem. Tabellen*, Erg. I, p 53.
Schmidt, E and Boas, W. 1935 *Kristallplastizität*. Berlin.
Zwicky, F. 1923 *Z. Phys.* 24, 131.

---

# The derivation of mechanics from the law of gravitation in relativity theory

By G. L. Clark, Ph.D.

(*Communicated by Sir Arthur Eddington, F.R.S. –Received* 17 *July* 1940)

The paper gives a general review of an investigation on some problems on motion in the relativity theory. We begin by discussing the motion of a single particle in a weak gravitational field and obtain both the linear and angular equations of motion; this is followed by brief accounts of the problem of two bodies and that of a rotating rod. In each case considered the equations of motion arise as conditions of integrability of the relativity equations for empty space. Only one of these problems has previously been treated by this method, this being the case of two bodies not connected by a material tension. However, this investigation, which was carried out by Einstein, Infeld and Hoffmann, introduces difficult ideas relating to the use of certain spatial surface integrals; in the present paper we avoid the use of these integrals

An essential feature of the work is that we take a first-order solution for the particular problem considered and substitute this solution in the quadratic terms of $G_{\mu\nu}$, and then build up a second-order solution. This method can be employed when we discuss the interior of matter; and, as an example, we conclude the paper by investigating the case of a rotating mass of liquid of constant density.

## 1. INTRODUCTION

In general relativity theory a 'particle' is represented by a singularity in the field $g_{\mu\nu}$. The singularity is a line in four dimensions, namely, the world-line of the particle. If we arbitrarily specify a set of curves in a co-ordinate system in four dimensions, it is in general impossible to determine a field $g_{\mu\nu}$ with these curves as singularities and satisfying the law of gravitation for empty space $G_{\mu\nu} = 0$ elsewhere. Thus the gravitational equations impose a restriction on the possible courses of the particles. It has been recognized that these restrictions are the source of the ordinary laws of mechanics, that is to say, the laws of mechanics, which in Newtonian theory are additional conditions to be satisfied by the possible motions of a system, are in relativity theory implicit in and directly derivable from the law of gravitation.

Although the general principle is clear, the actual derivation of the ordinary laws of mechanics (linear and angular equations of motion, etc.) in this way is highly complicated. The most far-reaching discussion is that of Einstein, Infeld and Hoffmann (1938). They show that for two-dimensional spatial surfaces containing singularities certain surface integral conditions are valid which determine the motion. In the present paper we show how this and allied problems can be investigated without introducing the difficult ideas associated with the surface integral method. By either method the calculations involved are very tedious; we therefore give a general review, rather than a detailed account, of the theory, and we omit as far as possible the long expressions which arise in the course of the work.

We set
$$g_{\mu\nu} = \eta_{\mu\nu} + h_{\mu\nu},$$
where the $\eta_{\mu\nu}$ are the Galilean values of $g_{\mu\nu}$, and the $h_{\mu\nu}$ are small. It is convenient to write
$$G_{\mu\nu} = -\tfrac{1}{2}M'_{\mu\nu} + L_{\mu\nu},$$
where $-\frac{1}{2}M_{\mu\nu}$ denotes the terms linear in $h_{\mu\nu}$, and $L_{\mu\nu}$ the non-linear terms. We start with the $h_{\mu\nu}$ given by the well-known first-order solution for a particle with a specified position, and add terms chosen so that, retaining the square of a velocity, no terms of the form $mv^s$ or $mv^r v^s$ appear in $M_{\mu\nu}$. We find that $M_{\mu\nu}$ does not then vanish unless we impose the condition $d^2x_1^s/dt^2 = 0$. This solution therefore represents the motion of the particle under no extraneous force.

Now consider a given gravitational field $h'_{\mu\nu}$ satisfying the equations for empty space, the values of $h'_{\mu\nu}$ and its ordinary derivatives at the singularity are denoted by $\bar{h}_{\mu\nu}, \bar{h}_{\mu\nu|\tau}, \ldots$. It is well known that the motion of a particle of negligible mass placed in the field is along a geodesic, and if we suppose that the given field is weak and the velocity of the particle is small the actual motion is given by the approximate equation

$$\frac{d^2x_1^s}{dt^2} = -\tfrac{1}{2}\bar{h}_{44|s} + v^r\bar{h}_{4s|r} - v^r\bar{h}_{4r|s} + \tfrac{1}{2}\bar{h}_{44|4}v^s + v^r\bar{h}_{rs|4} + \bar{h}_{4s|4}. \tag{1·1}$$

Our first task is to show (§ 4) how this result can be derived directly from the equations for empty space. We put

$$h_{\mu\nu} = h'_{\mu\nu} + h^{(1)}_{\mu\nu},$$

where $h^{(1)}_{\mu\nu}$ are the terms representing an isolated particle. Substituting in the expressions for $L_{\mu\nu}$ gives three types of terms. The quadratic terms in $h'_{\mu\nu}$ do not concern us, as we start from the assumption that the given field satisfies the conditions for empty space; nor need we calculate the quadratic terms in $h^{(1)}_{\mu\nu}$, since $m$ is taken to be very small. We only consider, therefore, the cross-terms which we note are of the order $m\bar{h}$. We assume a general form containing a large number of parameters for the cross-terms. We then find that it is impossible to satisfy the equations for empty space unless we impose the condition (1·1); and although a number of arbitrary parameters remain in the solution, this condition is unique.

We then proceed to discuss angular motion; we set

$$h_{\mu\nu} = h'_{\mu\nu} + h''_{\mu\nu},$$

where $\quad h'_{44} = U, \quad h'_{mn} = U\delta_{mn}, \quad h'_{4n} = 0 \quad (m, n = 1, 2, 3)$

and $\quad h''_{44} = A\left(\frac{3x^{1^2}}{r^5} - \frac{1}{r^3}\right) + B\left(\frac{3x^{2^2}}{r^5} - \frac{1}{r^3}\right) + C\left(\frac{3x^{3^2}}{r^5} - \frac{1}{r^3}\right).$

The quantity $U$ is a Newtonian potential, and at the singularity we denote the values of $U$, $U_{|s}$, $U_{|rs}$ by $\bar{U}$, $\bar{U}_{|s}$, $\bar{U}_{|rs}$, .... We write down a general form for $h''_{\mu\nu}$, and then we substitute the first-order solution in the expression for $L_{\mu\nu}$ and pick out the cross-terms $A\bar{U}_{|rs}$. It is found that in order to satisfy $G_{\mu\nu} = 0$, terms containing parameters $\varpi_s$ must be introduced into the solution such that

$$\varpi_1 = \tfrac{1}{2}(B-C)\,\bar{U}_{|23}, \text{ etc} \tag{1·2}$$

We readily show that the expressions on the right-hand side of (1·2) are simply the components of the couple due to the given field acting on the body, and so the conditions (1·2) are the angular equations of motion. This leads to the consideration of the actual derivation of Euler's equations.

The method is then applied to the problem of two bodies not connected by material tension, and also to the problem of a rotating rod or to the case of two bodies connected by a string. When we proceed to discuss the interior of a continuous distribution of matter, similar methods can be used to calculate the values of the energy-tensor $T_{\mu\nu}$. As an example we conclude the paper by referring to the case of a rotating mass of liquid of constant density.

Except in the last problem, the method in all cases consists in finding equations which are *conditions of integrability* of the equations $G_{\mu\nu} = 0$ in empty space in the circumstances relating to the problem considered.

## 2. *Approximate values of the Einstein tensor $G_{\mu\nu}$*

Following the authors quoted above, we use the convention that Latin indices take only the spatial values 1, 2, 3, while Greek indices refer to both space and time, running over the values 1, 2, 3, 4. We denote the ordinary derivative of a quantity by means of a line followed by the appropriate suffix, as

$$\frac{\partial g_{\mu\nu}}{\partial x_\sigma} \to g_{\mu\nu|\sigma}, \quad \frac{\partial^2 g_{\mu\nu}}{\partial x_\sigma \partial x_\rho} \to g_{\mu\nu|\sigma\rho}.$$

The expressions for $G_{\mu\nu}$ are then

$$G_{\mu\nu} = -\tfrac{1}{2}M_{\mu\nu} + L_{\mu\nu}, \tag{2·1}$$

where $-\frac{1}{2}M_{\mu\nu}$ represents the linear and $L_{\mu\nu}$ the non-linear terms. We have

$$\left.\begin{aligned} M_{44} &= h_{44|ss} - 2h_{4s|s4} + h_{ll|44}, \\ M_{4n} &= h_{4n|ss} - h_{4s|sn} + h_{ll|n4} - h_{ns|s4}, \\ M_{mn} &= h_{mn|ss} - h_{ms|sn} - h_{ns|sm} + h_{ll|mn} - h_{mn|44} + h_{4m|n4} + h_{4n|m4} - h_{44|mn}. \end{aligned}\right\} \tag{2·2}$$

In general the $h_{\mu\nu}$ will be small relative to unity, and if we neglect the cubes of $h_{\mu\nu}$ we can determine the values of $L_{\mu\nu}$ without much difficulty; for example, we find

$$\begin{aligned} L_{44} = {} & h_{rs}h_{4s|4r} - \tfrac{1}{2}h_{rs}h_{44|rs} + h_{rs|r}h_{4s|4} - \tfrac{1}{2}h_{rs|r}h_{44|s} - \tfrac{1}{2}h_{rs}h_{rs|44} - \tfrac{1}{2}h_{4r|r}h_{44|4} \\ & - \tfrac{1}{4}h_{rs|4}h_{rs|4} + \tfrac{1}{2}h_{4s|r}h_{4r|s} - \tfrac{1}{2}h_{4r|s}h_{4r|s} + \tfrac{1}{4}h_{44|s}h_{44|s} - \tfrac{1}{2}h_{4r|4}h_{ss|r} \\ & + \tfrac{1}{4}h_{44|r}h_{ss|r} + \tfrac{1}{4}h_{44|4}h_{ss|4}. \end{aligned} \tag{2·3}$$

It is convenient to rewrite the equation $G_{\mu\nu} = 0$ in the form

$$M_{\mu\nu} - 2L_{\mu\nu} = 0. \tag{2·4}$$

For the greater part of the paper we shall be investigating the conditions to be satisfied in order that this equation can be integrated.

## THE LINEAR AND ANGULAR EQUATIONS OF MOTION

### 3. *The case of a single particle*

We begin our investigation of the solutions of (2·4) by taking as the first approximation to $h_{44}$

$$h^{(1)}_{44} = -\frac{2m}{r},$$

where
$$r^2 = (x^s - x^s_1)(x^s - x^s_1).$$

For convenience I shall take the particle (co-ordinates $x^s_1$) to be at the origin, and we can then write $x^s$ for $x^s - x^s_1$. We write $v^m$ for $dx^m_1/dt$. Neglecting terms in $v^s$ we see that $M^{(1)}_{mn} = 0$ is satisfied by

$$h^{(1)}_{mn} = \frac{mA\delta_{mn}}{r} - m(A+2)\frac{x^m x^n}{r^3},$$

where $A$ is arbitrary. We want to find a solution retaining the square of the velocity. We assume for trial that the additional terms are of the general form

$$h^{(1)}_{44} = m\alpha_3 \frac{v^s v^s}{r} + m\alpha_4 \frac{x^r x^s}{r^3} v^r v^s,$$

$$h^{(1)}_{4n} = m\alpha_1 \frac{v^n}{r} + m\alpha_2 \frac{x^n x^s}{r^3} v^s,$$

$$h^{(1)}_{mn} = m\alpha_5 \frac{v^m v^n}{r} + m\alpha_6 \frac{v^s v^s}{r}\delta_{mn} + m\alpha_7\left(\frac{x^n x^s}{r^3} v^m v^s + \frac{x^m x^s}{r^3} v^n v^s\right)$$
$$+ m\alpha_8 \frac{x^r x^s}{r^3} v^r v^s \delta_{mn} + m\alpha_9 \frac{x^m x^n}{r^3} v^s v^s + m\alpha_{10} \frac{x^m x^n x^s x^r}{r^5} v^r v^s,$$

containing disposable constants $\alpha_i$. The solution values of the $\alpha_i$ will not be unique, because the solution can be given different forms by transformations of the co-ordinate system which leave the vectors at the origin unaltered. Having calculated the $M^{(1)}_{\mu\nu}$ corresponding to the above $h^{(1)}_{\mu\nu}$, we find that it is possible to make the part of $M^{(1)}_{\mu\nu}$ which does not involve the acceleration vanish by imposing certain relations between the $\alpha_i$; and $M^{(1)}_{\mu\nu}$ then reduces to

$$\left.\begin{aligned} M^{(1)}_{44} &= m\frac{x^s}{r^3}\frac{d^2x_1^s}{dt^2}(4\alpha_1+2A-10),\\ M^{(1)}_{mn} &= m\left(\frac{x^n}{r^3}\frac{d^2x_1^m}{dt^2}+\frac{x^m}{r^3}\frac{d^2x_1^n}{dt^2}\right)(2-A-2\alpha_1)+m\frac{x^s}{r^3}\frac{d^2x_1^s}{dt^2}(8-A-2\alpha_1)\,\delta_{mn}\\ &\qquad +3m\frac{x^m x^n x^s}{r^5}\frac{d^2x_1^s}{dt^2}(A-6+2\alpha_1),\end{aligned}\right\} \tag{3·1}$$

and $M^{(1)}_{4n}$ is of the order $mv^s\dfrac{d^2x_1^s}{dt^2}$.

Thus the condition $M_{\mu\nu} = 0$ requires

$$\frac{d^2x_1^s}{dt^2} = 0 \quad (s = 1, 2, 3).$$

The physical interpretation of this section is quite trivial, namely, the singularity represents a particle moving with constant acceleration. We next introduce a weak gravitational field $h'_{\mu\nu}$.

### 4. *Particle in a gravitational field*

We now suppose that there are additional terms $h'_{\mu\nu}$ which satisfy the equations for empty space. In the neighbourhood of the particle

$$h'_{\mu\nu} = \bar{h}_{\mu\nu}+x^s\bar{h}_{\mu\nu|s}+\tfrac{1}{2}x^s x^r\bar{h}_{\mu\nu|rs}+\ldots,$$

where $\bar{h}_{\mu\nu}$, $\bar{h}_{\mu\nu|s}$, ... are the values of $h'_{\mu\nu}$, $h'_{\mu\nu|s}$, ... calculated at the singularity. The total field will be given by

$$h_{\mu\nu} = h'_{\mu\nu}+h^{(1)}_{\mu\nu}+h^{(2)}_{\mu\nu},$$

where $h^{(2)}_{\mu\nu}$ denotes the terms of order $m\bar{h}_{\mu\nu}$. For the present we neglect the squares of $\bar{h}_{\mu\nu}$ and the squares of a velocity in $2L_{\mu\nu}$. The contributions to $M_{\mu\nu}$ from the terms $h^{(2)}_{\mu\nu}$ are denoted by $M^{(2)}_{\mu\nu}$, thus

$$M^{(2)}_{44} = h^{(2)}_{44|ss}-2h^{(2)}_{4s|4s}+h^{(2)}_{ss|44}.$$

The equations $G_{\mu\nu} = 0$ can then be written

$$M^{(1)}_{\mu\nu}+M^{(2)}_{\mu\nu}-2L_{\mu\nu} = 0. \tag{4·1}$$

We add a term $2L^*_{\mu\nu}$ such that it is possible to solve the equations

$$M^{(2)}_{\mu\nu}-2L_{\mu\nu}+2L^*_{\mu\nu} = 0. \tag{4·2}$$

The equation (4·1) then becomes

$$M^{(1)}_{\mu\nu} - 2L^*_{\mu\nu} = 0. \tag{4·3}$$

In order that (4·3) can be satisfied, it is evident from (3·1) that the most general form $2L^*_{\mu\nu}$ can take is

$$\left.\begin{aligned} 2L^*_{44} &= m\frac{x^s}{r^3}(4\alpha_1 + 2A - 10)\,P^s, \\ 2L^*_{mn} &= m\left(\frac{x^n}{r^3}P^m + \frac{x^m}{r^3}P^n\right)(2 - A - 2\alpha_1) + m\delta_{mn}\frac{x^s}{r^3}P^s(8 - A - 2\alpha_1) \\ &\qquad + 3m\frac{x^m x^n x^s}{r^5}P^s(A - 6 + 2\alpha_1), \end{aligned}\right\} \tag{4·4}$$

where $$P^s = p_1\bar{h}_{44|s} + p_2\bar{h}_{44|4} + p_3 v^r\bar{h}_{4r|s} + p_4 v^s\bar{h}_{4r|r} + p_5 v^r\bar{h}_{4s|r} + \ldots, \tag{4·5}$$

the $p_s$ being disposable constants. By (3·1) the condition (4·3) requires

$$\frac{d^2x^s_1}{dt^2} = p_1\bar{h}_{44|s} + p_2\bar{h}_{44|4} + p_3 v^r\bar{h}_{4r|s} + p_4 v^s\bar{h}_{4r|r} + p_5 v^r\bar{h}_{4s|r} + \ldots. \tag{4·6}$$

We assume a fairly general solution $h^{(2)}_{\mu\nu}$, and substituting in (4·2) gives a set of linear equations. The condition that these equations are consistent requires that $P^s$ shall be unique: thus the 'equations of motion' (4·6) are unique although the solution $h^{(2)}_{\mu\nu}$ is not. The coefficients in (4·6) can be determined, and we find that it reduces to the equation of a geodesic, namely,

$$\frac{d^2x^s_1}{dt^2} = -\tfrac{1}{2}\bar{h}_{44|s} + v^r\bar{h}_{4s|r} - v^r\bar{h}_{4r|s} + \tfrac{1}{2}\bar{h}_{44|4}v^s + v^r\bar{h}_{rs|4} + \bar{h}_{4s|4}. \tag{4·7}$$

On account of the length of the calculations we shall content ourselves with obtaining the result $p_1 = -\frac{1}{2}$ The relevant terms in $2L_{\mu\nu}$ are

$$\begin{aligned} 2L_{44} &= (A+5)\,m\frac{x^s}{r^3}\bar{h}_{44|s}, \\ 2L_{mn} &= \left(-\frac{A}{2} - 4\right)m\frac{x^s}{r^3}\bar{h}_{44|s}\delta_{mn} + 3\left(3 + \frac{A}{2}\right)m\frac{x^m x^n x^s}{r^5}\bar{h}_{44|s} \\ &\qquad - (\tfrac{1}{2}A + 1)\,m\left(\frac{x^m}{r^3}\bar{h}_{44|n} + \frac{x^n}{r^3}\bar{h}_{44|m}\right) \end{aligned}$$

Assuming the general solution

$$\begin{aligned} h^{(2)}_{44} &= \lambda_1 m\frac{x^s}{r}\bar{h}_{44|s}, \\ h^{(2)}_{mn} &= \lambda_2\delta_{mn}m\frac{x^s}{r}\bar{h}_{44|s} + \lambda_3 m\left(\frac{x^n}{r}\bar{h}_{44|m} + \frac{x^m}{r}\bar{h}_{44|n}\right) + \lambda_4 m\frac{x^m x^n x^s}{r^3}\bar{h}_{44|s}, \\ P^s &= p_1\bar{h}_{44|s}, \end{aligned}$$

we find

$$M^{(3)}_{44} - 2L_{44} + 2L^*_{44} = \{-2\lambda_1 - A - 5 + (4\alpha_1 + 2A - 10)\,p_1\}\,m\frac{x^s}{r^3}\bar{h}_{44|s},$$

$$\begin{aligned} M^{(3)}_{mn} - 2L_{mn} + 2L^*_{mn} \\ &= \{\lambda_1 - \lambda_2 - \lambda_4 + 1 + \tfrac{1}{2}A + (2 - A - 2\alpha_1)\,p_1\}\,m\left(\frac{x^n}{r^3}\bar{h}_{44|m} + \frac{\dot{x}^m}{r^3}\bar{h}_{44|n}\right) \\ &\quad + \{\lambda_1 - 3\lambda_2 - 3\lambda_4 + 4 + \tfrac{1}{2}A + (8 - A - 2\alpha_1)\,p_1\}\,\delta_{mn}\,m\frac{x^s}{r^3}\bar{h}_{44|s} \\ &\quad - 3m\{\lambda_1 - \lambda_2 - \lambda_4 + 3 + \tfrac{1}{2}A + (6 - A - 2\alpha_1)\,p_1\}\frac{x^m x^n x^s}{r^5}\bar{h}_{44|s}. \end{aligned}$$

Equating the coefficients to zero, we deduce the necessary condition $p_1 = -\frac{1}{2}$.

Two deductions from (4·7) may be noted:

(*a*) *Newtonian potential.* The equations for empty space are satisfied by $h'_{44} = -2V$, $h'_{mn} = -2V\delta_{mn}$, where $V$ is independent of time and satisfies $V_{|ss} = 0$. The equations of motion (4·6) are then simply

$$\frac{d^2x^s_1}{dt^2} = V_{|s}.$$

We may interpret the above solution as representing a particle at $x^s_1$ moving under the influence of a Newtonian potential $V$. In particular we notice that if $h'_{44} = -2m_2/r_2$, where $r^2_2 = (x^s - x^s_2)(x^s - x^s_2)$, then $m_2$ is the gravitational mass of a particle situated at $x^s_2$. In a similar manner it is clear that the constant $m_1$ occurring in $h^{(1)}_{44}$ is the gravitational mass of the body at $x^s_1$.

(*b*) *Rotating axes.* If we use rotating axes the additional terms give, on neglecting $\omega^2_s$, the well-known equations

$$\frac{d^2x^1_1}{dt^2} = V_{|s} + (\omega_2 v^3 - \omega_3 v^2), \text{ etc.}$$

The above outline shows in a very elementary manner how the equations of motion arise in the relativity theory. To obtain the equations of motion we have only considered the terms $\bar{h}_{\mu\nu}$, $\bar{h}_{\mu\nu|s}$, $\bar{h}_{\mu\nu|4}$. It will be noticed that further terms occur such as $\bar{h}_{\mu\nu|rs}$, $\bar{h}_{\mu\nu|s4}$, $\bar{h}_{\mu\nu|44}$ in the expression $2L_{\mu\nu}$. It is found, however, that the solution containing these terms can be found without difficulty, and no additional conditions of integrability are imposed.

### 5. *The angular equations*

The analysis given above may be taken to cover the case of a non-spherical body—the solution being valid at distances large compared with the dimensions of the body but nevertheless still fairly close to the body. We now continue the discussion to the next approximation as regards the dimensions of the body, the purpose being to show how the angular equations of motion arise in the theory.

We suppose the body is moving in a static Newtonian potential field $-\frac{1}{2}U$; we denote the values of $U$, $U_{|m}$, $U_{|mn}$, ... evaluated at the body by $\overline{U}$, $\overline{U}_{|m}$, $\overline{U}_{|mn}$, .... This field will be due to the sum of a number of particles $P_s$, at distances $R_s$ from the body under consideration. For the sake of definiteness we suppose that terms of order $-4$ in $R_s$ can be neglected, that is, we neglect the quantities $\overline{U}_{|mnp}$, $\overline{U}_{|mnpq}$, .... Consequently in the neighbourhood of the body

$$U = \overline{U} + x^s\overline{U}_{|s} + \tfrac{1}{2}x^s x^r \overline{U}_{|sr} + \dots,$$

$$U_{|m} = \overline{U}_{|m} + x^s\overline{U}_{|ms} + \dots,$$

$$U_{|mn} = \overline{U}_{|mn} + \dots.$$

Now consider for the moment the potential $V$ due to the body. If $a$ is the maximum linear dimension of the body, at distances $r$ from the body for which $(a/r)^3$ may be neglected, $-2V$ takes the form

$$-\frac{2m}{r} + A\left(\frac{3x^{1^2}}{r^5} - \frac{1}{r^3}\right) + B\left(\frac{3x^{2^2}}{r^5} - \frac{1}{r^3}\right) + C\left(\frac{3x^{3^2}}{r^5} - \frac{1}{r^3}\right),$$

where $A$, $B$, $C$ are the principal moments of inertia, the origin being at the centre of gravity and the axes oriented in a suitable manner.

In view of the above considerations we take as the value of $h_{44}^{(1)}$,

$$h_{44}^{(1)} = U - \frac{2m}{r} + A\left(\frac{3x^{1^2}}{r^5} - \frac{1}{r^3}\right) + B\left(\frac{3x^{2^2}}{r^5} - \frac{1}{r^3}\right) + C\left(\frac{3x^{3^2}}{r^5} - \frac{1}{r^3}\right),$$

and build up a solution of the equations $G_{\mu\nu} = 0$. We suppose that $U$ satisfies $U_{|ss} = 0$, $U_{|4} = 0$, and quantities $\overline{U}_{|mnp}$ are neglected The quadratic terms $2L_{\mu\nu}$ are expressed as the sum of three terms

$$2L_{\mu\nu} = 2\overline{U}\,L'_{\mu\nu} + 2\overline{U}_{|s}\,L''_{\mu\nu,s} + 2\overline{U}_{|rs}\,L'''_{\mu\nu,rs}.$$

Each type of term can be discussed separately. In order to integrate the second type, we require the condition

$$\frac{d^2x_1^s}{dt^2} + \tfrac{1}{2}\overline{U}_{|s} = 0. \tag{5·1}$$

To solve for the third type we have to introduce quantities $\varpi_1$, $\varpi_2$, $\varpi_3$ such that

$$\left.\begin{aligned}\varpi_{1|4} &= \dot{\varpi}_1 = \tfrac{1}{2}(B-C)\,\overline{U}_{|23},\\ \varpi_{2|4} &= \dot{\varpi}_2 = \tfrac{1}{2}(C-A)\,\overline{U}_{|31},\\ \varpi_{3|4} &= \dot{\varpi}_3 = \tfrac{1}{2}(A-B)\,\overline{U}_{|12}.\end{aligned}\right\} \tag{5·2}$$

The conditions (5·1) determine the linear motion, and (5·2) are the angular equations of motion.

The terms arising from $-2m/r$ have been investigated in § 4; we need therefore only consider the terms involving $A$, $B$ and $C$. We take, as the first approximation,

$$h^{(1)}_{44} = h'_{44} + h''_{44}, \tag{5·3}$$

where
$$h'_{44} = U, \quad h''_{44} = A\left(\frac{3x^{1^2}}{r^5} - \frac{1}{r^3}\right),$$

$U$ being independent of $x^4$ and satisfying $U_{|ss} = 0$. If the velocity and acceleration of the body are neglected the value of $h^{(1)}_{mn}$ satisfying the equations $M^{(1)}_{44} = 0$ and $M^{(1)}_{mn} = 0$, is readily seen to be

$$h^{(1)}_{mn} = h'_{mn} + h''_{mn}, \tag{5·4}$$

where $\quad h'_{mn} = U\delta_{mn},$

$$\begin{aligned}h''_{mn} = A\Bigg\{&\frac{a_1}{r^3}\delta_{mn} + a_2\frac{x^{1^2}}{r^5}\delta_{mn} + a_3\frac{x^m x^n}{r^5} + a_4\frac{x^{1^2}x^m x^n}{r^7}\\ &+ a_5(x^m\delta_{n1} + x^n\delta_{m1})\frac{x^1}{r^5} + a_6\frac{\delta_{m1}\delta_{n1}}{r^3}\Bigg\},\end{aligned}$$

provided that

$$a_3 = -3a_1 - 3, \quad 2a_2 = 2a_5 + 3a_6 + 6, \quad 2a_4 = -10a_5 - 15a_6. \tag{5·5}$$

The corresponding terms in $B$ and $C$ can be written down by a suitable interchange of $x^1$, $x^2$, $x^3$.

## 6. *The terms in* $\overline{U}_{|rs}$

The expressions $2L_{44}$ and $2L_{mn}$ have the values

$$2L_{44} = -\overline{U}_{|rs}h''_{rs} + \overline{U}_{|sr}x^r(\tfrac{3}{4}h''_{44|s} + \tfrac{1}{2}h''_{ll|s} - h''_{rs|r}), \tag{6·1}$$

$$\begin{aligned}2L_{mn} = {}&\overline{U}_{|sr}x^r[h''_{ms|n} + h''_{ns|m} - 2h''_{mn|s} + \delta_{mn}(\tfrac{1}{2}h''_{ll|s} - h''_{rs|r} - \tfrac{1}{2}h''_{44|s})]\\ &+ \tfrac{1}{2}\overline{U}_{|sr}x^s x^r(h''_{ms|sn} + h''_{ns|sm} - h''_{ll|mn} - h_{mn|ss} - h_{44|mn})\\ &+ \overline{U}_{|ns}x^s(h''_{mr|r} - h''_{ll|m}) + \overline{U}_{|ms}x^s(h''_{nr|r} - h''_{ll|n}) - \delta_{mn}\overline{U}_{|sr}h''_{rs}\\ &+ \overline{U}_{|ms}h''_{ns} + \overline{U}_{|ns}h''_{ms} - \overline{U}_{|mn}(h''_{ll} + h''_{44}).\end{aligned} \tag{6·2}$$

On substituting the value for $h''_{\mu\nu}$, (6·1) becomes

$$2L_{44} = A\bar{U}_{|rs}\left\{\frac{x^s x^r}{r^5}\left(\tfrac{9}{2} - 3a_1 - 3a_3 - a_5 - \tfrac{3}{2}a_6\right) + \frac{x^1 x^r}{r^5}\delta_{1s}(9 + a_2 + a_4 + 3a_6)\right.$$
$$\left. + \frac{x^{1^2} x^s x^r}{r^7}\left(-\tfrac{45}{2} - \tfrac{5}{2}a_2 - \tfrac{5}{2}a_4\right) - a_6\frac{\delta_{1s}\delta_{1r}}{r^3}\right\}. \qquad (6·3)$$

The solution of $M_{44} - 2L_{44} = 0$ is then

$$h_{44} = A\bar{U}_{|rs}\left\{\alpha\frac{x^r x^s}{r^3} + \beta\frac{x^1 x^r}{r^3}\delta_{1s} + \epsilon\frac{x^{1^2} x^s x^r}{r^5} + \gamma\frac{\delta_{1s}\delta_{1r}}{r}\right\}, \qquad (6·4)$$

where $\gamma$ is arbitrary, and

$$\beta = -\tfrac{1}{2}a_6, \quad \alpha = -1 - \tfrac{1}{2}a_1, \quad \epsilon = \tfrac{3}{2} - \tfrac{1}{2}a_5 - \tfrac{3}{4}a_6,$$

on using the relations (5·5). We then find

$$h_{44|mn} + 2L_{mn} = A\bar{U}_{|rs}\left\{E_1\frac{x^r x^s}{r^5}\delta_{1m}\delta_{1n} + E_2\delta_{ms}\delta_{nr}\frac{x^{1^2}}{r^5} + E_3(x^n\delta_{1m} + x^m\delta_{1n})\frac{x^1 x^r x^s}{r^7}\right.$$
$$+ E_4\frac{x^r x^s}{r^5}\delta_{mn} + E_5\frac{x^m x^n x^r x^s}{r^7} + E_6\frac{x^{1^2} x^r x^s}{r^7}\delta_{mn} + E_7\frac{x^{1^2} x^m x^n x^r x^s}{r^9}$$
$$+ E_8\frac{x^1 x^r}{r^5}\delta_{1s}\delta_{mn} + E_9(x^m\delta_{ns} + x^n\delta_{ms})\frac{x^r}{r^5} + E_{10}(\delta_{ns}\delta_{m1} + \delta_{ms}\delta_{n1})\frac{x^1 x^r}{r^5}$$
$$+ E_{11}(x^n\delta_{ms} + x^m\delta_{ns})\frac{x^{1^2} x^r}{r^7} + E_{12}\frac{x^1 x^m x^n x^r}{r^7}\delta_{1s} + E_{13}\frac{\delta_{ns}\delta_{mr}}{r^3}$$
$$+ E_{14}(\delta_{1m}\delta_{nr} + \delta_{1n}\delta_{mr})\frac{\delta_{1s}}{r^3} + E_{15}\frac{\delta_{mn}\delta_{1s}\delta_{1r}}{r^3} + E_{16}\frac{x^m x^n}{r^5}\delta_{1s}\delta_{1r}$$
$$\left. + E_{17}\frac{x^r}{r^5}(x^m\delta_{n1} + x^n\delta_{m1})\delta_{1s} + E_{18}\frac{x^1}{r^5}(x^m\delta_{nr} + x^n\delta_{mr})\delta_{1s}\right\}, \qquad (6·5)$$

where the $E_k$ are known constants We assume a solution of the same form as (6·5) except for a factor $1/r^2$, namely,

$$h_{mn} = A\bar{U}_{|rs}\left\{p_1\frac{x^r x^s}{r^3}\delta_{m1}\delta_{n1} + p_2\frac{x^{1^2}}{r^3}\delta_{ms}\delta_{nr} + \ldots + p_{18}\frac{x^1}{r^3}(x^m\delta_{nr} + x^n\delta_{mr})\delta_{1s}\right\}$$

It is found that by suitably choosing the $p_k$ a solution can be obtained such that

$$M_{mn} - 2L_{mn} = 3A\bar{U}_{|rs}\left(-\delta_{1s}\delta_{1n}\frac{x^m x^r}{r^5} - \delta_{1s}\delta_{1m}\frac{x^n x^r}{r^5} + \delta_{1s}\delta_{nr}\frac{x^1 x^m}{r^5} + \delta_{1s}\delta_{mr}\frac{x^1 x^n}{r^5}\right)$$
$$= 3A\left\{\bar{U}_{|12}\left[\frac{x^1}{r^5}(x^m\delta_{n2} + x^n\delta_{m2}) - \frac{x^2}{r^5}(x^m\delta_{n1} + x^n\delta_{m1})\right]\right.$$
$$\left. + \bar{U}_{|13}\left[\frac{x^1}{r^5}(x^m\delta_{n3} + x^n\delta_{m3}) - \frac{x^3}{r^5}(x^m\delta_{n1} + x^n\delta_{m1})\right]\right\}.$$

The terms in $B$ and $C$ can be written down by a suitable interchange of $x^1, x^2, x^3$. It is evident that the solution is such that

$$\begin{aligned} M_{mn}-2L_{mn} = 3\Big\{&(B-C)\bar{U}_{|23}\left[\frac{x^2}{r^5}(x^m\delta_{n3}+x^n\delta_{m3})-\frac{x^3}{r^5}(x^m\delta_{n2}+x^n\delta_{m2})\right] \\ &+(C-A)\bar{U}_{|13}\left[\frac{x^3}{r^5}(x^m\delta_{n1}+x^n\delta_{m1})-\frac{x^1}{r^5}(x^m\delta_{n3}+x^n\delta_{m3})\right] \\ &+(A-B)\bar{U}_{|12}\left[\frac{x^1}{r^5}(x^m\delta_{n2}+x^n\delta_{m2})-\frac{x^2}{r^5}(x^m\delta_{n1}+x^n\delta_{m1})\right]\Big\}. \qquad (6{\cdot}6)\end{aligned}$$

Since $-\tfrac{1}{2}U$ is the potential of the external field, the components of the force at any point are $-\tfrac{1}{2}U_s$. In the neighbourhood of the body

$$-\tfrac{1}{2}U_s = -\tfrac{1}{2}\bar{U}_{|s}-\tfrac{1}{2}x^r\bar{U}_{|rs},$$

and accordingly the component of the couple about the $x_3$-axis is

$$\begin{aligned} N &= \int(x^1U_{|2}-x^2U_{|1})\,dV \\ &= \int\tfrac{1}{2}\bar{U}_{|12}(x^{2^2}-x^{1^2})\,dV \\ &= +\tfrac{1}{2}(A-B)\,\bar{U}_{|12}.\end{aligned}$$

Further terms can be introduced into (6·6) by taking the quantity

$$h_{4n} = 2\left\{\delta_{n1}\left(\varpi_2\frac{x^3}{r^3}-\varpi_3\frac{x^2}{r^3}\right)+\delta_{n2}\left(\varpi_3\frac{x^1}{r^3}-\varpi_1\frac{x^3}{r^3}\right)+\delta_{n3}\left(\varpi_1\frac{x^2}{r^3}-\varpi_2\frac{x^1}{r^3}\right)\right\}, \qquad (6{\cdot}7)$$

which we notice satisfies $h_{4s|s} = 0$. The new value of $M_{mn}-2L_{mn}$ is then

$$\begin{aligned} 6\Big\{&[\dot{\varpi}_1-L]\left[\frac{x^3}{r^3}(x^m\delta_{n2}+x^n\delta_{m2})-\frac{x^2}{r^3}(x^n\delta_{m3}+x^m\delta_{n3})\right] \\ &+[\dot{\varpi}_2-M]\left[\frac{x^1}{r^5}(x^m\delta_{n3}+x^n\delta_{m3})-\frac{x^3}{r^5}(x^n\delta_{m1}+x^m\delta_{n1})\right] \\ &+[\dot{\varpi}_3-N]\left[\frac{x^2}{r^5}(x^m\delta_{n1}+x^n\delta_{m1})-\frac{x^1}{r^5}(x^n\delta_{m2}+x^m\delta_{n2})\right]\Big\},\end{aligned}$$

where $(L, M, N)$ are the components of the couple about the axes. The conditions for integrability are therefore

$$\dot{\varpi}_1 = L, \quad \dot{\varpi}_2 = M, \quad \dot{\varpi}_3 = N. \qquad (6{\cdot}8)$$

These conditions are the angular equations of motion and are usually written

$$\frac{d}{dt}(A\omega - H\omega_2 - G\omega_3) = L, \text{ etc.}$$

In general the quantities $A$, $B$, $C$, $F$, $G$, $H$ are not constants but are continually changing in consequence of the rotation. Our calculation refers to the instant at which the products of inertia $F$, $G$, $H$ are zero.

### 7. *Euler's equations*

The field, to a first approximation, of a number of isolated particles is

$$h_{44} = V, \quad h_{mn} = V\delta_{mn}, \quad \text{where} \quad V = -\Sigma_i \frac{2m_i}{r_i}. \tag{7·1}$$

At great distances from the system we can write

$$\frac{1}{r_i} = \frac{1}{r} + \frac{x_s x_{1s}}{r^3} - \frac{1}{2}\frac{x_{is} x_{is}}{r^3} + \frac{3}{2}\frac{(x_{is} x_s)^2}{r^5}$$

We suppose the particles are rotating about the centre of gravity. Summing over all the particles gives

$$V = -\frac{2m}{r} + \bar{A}\left(\frac{3{x^1}^2}{r^5} - \frac{1}{r^3}\right) + \bar{B}\left(\frac{3{x^2}^2}{r^5} - \frac{1}{r^3}\right)$$
$$+ \bar{C}\left(\frac{3{x^3}^2}{r^5} - \frac{1}{r^3}\right) - 6\bar{F}\frac{x^2 x^3}{r^5} - 6\bar{G}\frac{x^3 x^1}{r^5} - 6\bar{H}\frac{x^1 x^2}{r^5}, \tag{7·2}$$

where $\bar{A}$, $\bar{B}$, $\bar{C}$, $\bar{F}$, $\bar{G}$, $\bar{H}$ can be expressed in terms of the moments of inertia referred to axes fixed in the body. In fact, if $\omega_s$, $\dot{\omega}_s$ are the components of the angular velocity and angular acceleration of the moving set of axes about axes fixed in space and instantaneously coinciding with them, then the direction cosines of the moving system at a later instant are given by

$$\left.\begin{aligned}
&l_1 = 1 - \tfrac{1}{2}(\omega_2^2 + \omega_3^2)\,t^2, && m_1 = \omega_3 t + \tfrac{1}{2}\dot{\omega}_3 t^2 + \tfrac{1}{2}\omega_1\omega_2 t^2,\\
&l_2 = -\omega_3 t - \tfrac{1}{2}\dot{\omega}_3 t^2 + \tfrac{1}{2}\omega_1\omega_2 t^2, && m_2 = 1 - \tfrac{1}{2}(\omega_1^2 + \omega_3^2)\,t^2,\\
&l_3 = \omega_2 t + \tfrac{1}{2}\dot{\omega}_2 t^2 + \tfrac{1}{2}\omega_3\omega_1 t^2, && m_3 = -\omega_1 t - \tfrac{1}{2}\dot{\omega}_1 t^2 + \tfrac{1}{2}\omega_2\omega_3 t^2.\\
&\qquad n_1 = -\omega_2 t - \tfrac{1}{2}\dot{\omega}_2 t^2 + \tfrac{1}{2}\omega_3\omega_1 t^2, &&\\
&\qquad n_2 = \omega_1 t + \tfrac{1}{2}\dot{\omega}_1 t^2 + \tfrac{1}{2}\omega_3\omega_2 t^2, &&\\
&\qquad n_3 = 1 - \tfrac{1}{2}(\omega_1^2 + \omega_2^2)\,t^2. &&
\end{aligned}\right\} \tag{7·3}$$

With the aid of these results we find

$$\left.\begin{aligned}\bar{A} &= A+(C-A)\omega_2^2t^2+(B-A)\omega_3^2t^2,\\ \bar{F} &= (C-B)\omega_1t+\tfrac{1}{2}(C-B)\dot{\omega}_1t^2+\tfrac{1}{2}(2A-B-C)\omega_2\omega_3t^2, \text{ etc.}\end{aligned}\right\} \tag{7·4}$$

I have found that starting from

$$h_{44} = V, \quad h_{mn} = V\delta_{mn}$$

alone, no equation of motion is obtained on building up a second-order solution; but if we also consider the terms derived from

$$h_{4n} = 4\Sigma_i \frac{m_i v_i^n}{r_i},$$

then additional terms appear in the first approximation to $h_{4n}$; these terms are of the form (6·7), where

$$\left.\begin{aligned}\varpi_1 &= A(\omega_1+\dot{\omega}_1t)-(B-C)\omega_2\omega_3t,\\ \varpi_2 &= B(\omega_2+\dot{\omega}_2t)-(C-A)\omega_3\omega_1t,\\ \varpi_3 &= C(\omega_3+\omega_3t)-(A-B)\omega_1\omega_2t.\end{aligned}\right\} \tag{7·5}$$

Inserting these values of $\varpi_k$ in (6·8), we obtain Euler's equations

$$\left.\begin{aligned}A\dot{\omega}_1-(B-C)\omega_2\omega_3 &= L,\\ B\dot{\omega}_2-(C-A)\omega_3\omega_1 &= M,\\ C\dot{\omega}_3-(A-B)\omega_1\omega_2 &= N\end{aligned}\right\} \tag{7·6}$$

### THE PROBLEM OF TWO BODIES*

8. We now introduce quantities $\gamma_{\mu\nu}$, $\Lambda'_{\mu\nu}$ defined by

$$\gamma_{\mu\nu} = h_{\mu\nu}-\tfrac{1}{2}\eta_{\mu\nu}\eta^{\sigma\rho}h_{\sigma\rho}, \quad \Lambda'_{\mu\nu} = L_{\mu\nu}-\tfrac{1}{2}\eta_{\mu\nu}\eta^{\sigma\rho}L_{\sigma\rho},$$

where $\eta_{\mu\nu}$ are the Galilean values of $g_{\mu\nu}$. If the $\gamma_{\mu\nu}$ satisfy the conditions

$$\gamma_{4s|s}-\gamma_{44|4} = 0, \tag{8·1}$$

$$\gamma_{ms|s} = 0, \tag{8·2}$$

the equations $G_{\mu\nu} = 0$ become

$$\gamma_{\mu\nu|ss} = 2\Lambda_{\mu\nu}, \tag{8·3}$$

---

* I quote freely, with slight changes in notation, from the paper by Einstein *et al.* (1938).

where the values of the $\Lambda_{\mu\nu}$ are given by

$$2\Lambda_{44} = 2\Lambda'_{44},$$

$$2\Lambda_{4n} = 2\Lambda'_{4n},$$

$$2\Lambda_{mn} = 2\Lambda'_{mn} - \gamma_{4m|4n} - \gamma_{4n|4m} + \delta_{mn}\gamma_{44|44} + \gamma_{mn|44}.$$

Our two-body problem consists in taking the quantity

$$\gamma^{(1)}_{44} = -\frac{4m_1}{r_1} - \frac{4m_2}{r_2}$$

and trying to build up a solution satisfying (8·1), (8·2) and (8·3). Owing to difficulty in dealing with the interaction terms, we are restricted to a solution which is only valid in the neighbourhood of one of the particles. We find that our solution satisfies the equations

$$\gamma_{\mu\nu|ss} = 2\Lambda_{\mu\nu}, \quad \gamma_{4s|s} - \gamma_{44|4} = 0$$

But

$$\gamma_{ms|s} = -c_1^{(m)}/r_1,$$

where

$$c_1^{(k} = 4m_1\left[\frac{d^2x_1^k}{dt^2} + m_2\frac{(x_1^k - x_2^k)}{r^3} - 4m_2^2\frac{(x_1^k - x_2^k)}{r^4} - 4m_2\frac{(x_1^s - x_2^s)}{r^3}v_1^k v_1^s\right.$$

$$+ m_2\frac{x_1^k - x_2^k}{r^3}\left(v_1^s v_1^s + 2v_2^s v_2^s - \tfrac{3}{2}\epsilon_2^2 - \frac{5m_1}{r}\right) - 3m_2\epsilon_2\frac{(v_1^k - v_2^k)}{r^2}$$

$$\left. + 4m_2\left\{\frac{(x_1^s - x_2^s)}{r^3}v_2^k - \frac{(x_1^k - x_2^k)}{r^3}v_2^s\right\}v_1^s\right],$$

$r$ being a distance between the singularities and $r\epsilon_2 = (x_2^s - x_1^s)v_2^s$ The condition $c_1^{(k)} = 0$ therefore gives us the equations of motion of the first singularity. The equations of motion for the other particle are obtained by replacing $m_1$, $m_2$, $x_1^s$, $x_2^s$ by $m_2$, $m_1$, $x_2^s$, $x_1^s$.

## 9. *The first and second approximations*

We shall write

$$(a)\quad -\frac{2m_1}{r_1} = \psi, \quad -\frac{2m_2}{r_2} = \chi, \qquad (b)\quad \phi = \psi + \chi.$$

Substituting our initial value

$$\gamma^{(1)}_{44} = -\frac{4m_1}{r_1} - \frac{4m_2}{r_2}$$

in (8·1) we obtain

$$\gamma^{(1)}_{4s|s} = -4m_1\frac{(x^s-x^s_1)}{r_1^3}v^s_1 - 4m_2\frac{(x^s-x^s_2)}{r_2^3}v^s_2$$

$$= \left(4m_1\frac{v^s_1}{r_1} + 4m_2\frac{v^s_2}{r_2}\right)_{|s}.$$

Integration gives $$\gamma^{(1)}_{4s} = 4m_1\frac{v^s_1}{r_1} + 4m_2\frac{v^s_2}{r_2}.$$

We take $\gamma^{(1)}_{mn} = 0$. Substituting $\gamma^{(1)}_{\mu\nu}$ in the expression for $2\Lambda_{\mu\nu}$ we obtain

$$2\Lambda^{(2)}_{44} = -\tfrac{3}{2}\phi_{|s}\phi_{|s},$$

$$2\Lambda^{(2)}_{4n} = \phi_{|s}\gamma^{(1)}_{4s|n} - \phi_{|sn}\gamma^{(1)}_{4s} - 3\phi_{|4}\phi_{|n},$$

$$2\Lambda^{(2)}_{mn} = -\gamma^{(1)}_{4m|4n} - \gamma^{(1)}_{4n|4m} + 2\delta_{mn}\phi_{|44} - 2\phi\phi_{|mn} - \phi_{|m}\phi_{|n} + \tfrac{3}{2}\delta_{mn}\phi_{|s}\phi_{|s}.$$

The solution $\gamma^{(2)}_{mn} = \gamma'_{mn} + \gamma''_{mn}$ of $\gamma^{(2)}_{mn|ss} = 2\Lambda^{(2)}_{mn}$ can only be found in the neighbourhood of one of the singularities. The part of the solution not containing interaction terms is

$$\gamma'_{mn} = \left\{-\frac{2m_1}{r_1}[(x^n-x^n_1)v^m_1 + (x^m-x^m_1)v^n_1 - \delta_{mn}(x^s-x^s_1)v^s_1]\right\}_{|4}$$
$$+\left\{-\frac{2m_2}{r_2}[(x^n-x^n_2)v^m_2 + (x^m-x^m_2)v^n_2 - \delta_{mn}(x^s-x^s_2)v^s_2]\right\}_{|4}$$
$$+7m_1^2\frac{(x^m-x^m_1)(x^n-x^n_1)}{r_1^4} + 7m_2^2\frac{(x^m-x^m_2)(x^n-x^n_2)}{r_2^4}.$$

The interaction terms of order 0 and $-1$ in $r_1$ are

$$\gamma''_{mn} = -m_1\frac{(x^m-x^m_1)(x^n-x^n_1)(x^s-x^s_1)}{r_1^3}\bar{\chi}_{|s} - 2m_1\delta_{mn}\frac{(x^s-x^s_1)}{r_1}\bar{\chi}_{|s}$$
$$-2m_1\frac{(x^m-x^m_1)(x^n-x^n_1)}{r_1^3}\bar{\chi} - \frac{2m_1}{r_1}\alpha_{mn},$$

where $\bar{\chi}$, $\bar{\chi}_{|s}$ are the values of $\chi$, $\chi_{|s}$ evaluated at $x^s_1$, and $\alpha_{mn}$ is a function of time. We have

$$\gamma'_{ms|s} = -\frac{4m_1}{r_1}\frac{d^2x^m_1}{dt^2} - 4m_1\frac{(x^s-x^s_1)}{r_1^3}v^s_1v^m_1,$$

$$\gamma''_{ms|s} = -\frac{2m_1}{r_1}\bar{\chi}_{|m} - 2m_1\frac{(x^s-x^s_1)}{r_1^3}\bar{\chi}.$$

Hence $$\gamma^{(2)}_{ms|s} = \gamma'_{ms|s} + \gamma''_{ms|s}$$
$$= -\frac{4m_1}{r_1}\left(\frac{d^2x^m_1}{dt^2} + \tfrac{1}{2}\bar{\chi}_{|m}\right) + 2m_1\left(\frac{x^s-x^s_1}{r^3}\right)(\alpha_{ms} - 2v^s_1v^m_1 - \bar{\chi}).$$

The condition $\gamma^{(2)}_{ms|s} = 0$ requires

$$c_1^{\prime(m)} = 4m_1\left(\frac{d^2x_1^m}{dt^2} + \tfrac{1}{2}\overline{\chi}_m\right) = 0, \tag{9·1}$$

$$\alpha_{ms} = 2v_1^s v_1^m + \delta_{ms}\overline{\chi}. \tag{9·2}$$

The equation
$$\gamma^{(2)}_{44|ss} = 2\Lambda^{(2)}_{44} \tag{9·3}$$

has the solution
$$\gamma^{(2)}_{44} = -\tfrac{3}{4}\phi\phi - \frac{2m_1}{r_1}\alpha_{44} - \frac{2m_2}{r_2}\beta_{44}, \tag{9·4}$$

where $\alpha_{44}$, $\beta_{44}$ are functions of time. The solution $\gamma^{(2)}_{4n} = \gamma'_{4n} + \gamma''_{4n}$ of $\gamma^{(2)}_{4n|ss} = 2\Lambda^{(2)}_{4n}$ can only be found in a series valid in the neighbourhood of one of the singularities. The part of the solution not containing interaction terms is (including only relevant terms for the expression $c_1^{(m)}$)

$$\gamma'_{4n} = -7m_1^2\frac{(x^n - x_1^n)(x^s - x_1^s)}{r_1^4}v_1^s + \frac{3m_1^2 v_1^n}{r_1^2}. \tag{9·5}$$

The interaction terms of order 0 and $-1$ in $r_1$ are

$$\begin{aligned}\gamma''_{4n} = {} & \frac{2m_1}{r^3}(x^n - x_1^n)(x^s - x_1^s)\overline{\chi}v_2^s + \frac{m_1}{r_1^3}(x^n - x_1^n)(x^s - x_1^s)(x^r - x_1^r)\overline{\chi}_{|r}v_2^s \\ & + 3m_1\frac{(x^s - x_1^s)}{r_1}\overline{\chi}_{|n}v_2^s + 2m_1(x^n - x_1^n)v_1^s\overline{\chi}_{|s} - m_1\frac{(x^s - x_1^s)}{r_1}\overline{\chi}_{|s}v_2^n \\ & - 3m_1\frac{(x^s - x_1^s)}{r_1}v_1^s\overline{\chi}_{|n} - 2m_1\frac{(x^n - x_1^n)}{r_1}\overline{\chi}_{|s}v_2^s - \frac{2m_1}{r_1}\alpha_{4n},\end{aligned} \tag{9·6}$$

where $\alpha_{4n}$ is a function of time.

The terms of order $-2$ and $-1$ in $r_1$ in $\gamma^{(2)}_{44|4}$ and $\gamma^{(2)}_{4s|s}$ are respectively

$$\begin{aligned}\gamma^{(2)}_{44|4} = {} & \frac{m_1}{r_1}(3\overline{\chi}_{|4} - 2\alpha_{44|4} - 3v_1^s\overline{\chi}_{|s}) + m_1\frac{(x^s - x_1^s)}{r_1^3}(3v_1^s\overline{\chi} - 2v_1^s\alpha_{44}) \\ & + 3m_1\frac{(x^s - x_1^s)(x^r - x_1^r)}{r_1^3}v_1^r\overline{\chi}_{|s},\end{aligned}$$

$$\begin{aligned}\gamma^{(2)}_{4s|s} = {} & \frac{2m_1}{r_1^3}(x^s - x_1^s)(\alpha_{4s} + \overline{\chi}v_2^s) + \frac{m_1}{r_1}(-v_1^s\overline{\chi}_{|s} - 2\overline{\chi}_{|s}v_2^s) \\ & + 3m_1\frac{(x^s - x_1^s)(x^r - x_1^r)}{r_1^3}v_1^r\overline{\chi}_{|s}.\end{aligned}$$

The condition (8·1) requires therefore

$$\alpha_{4s} + v_1^s\alpha_{44} = \tfrac{3}{2}v_1^s\overline{\chi} - \overline{\chi}v_2^s. \tag{9·7}$$

$$\alpha_{44|4} = -v_1^s\overline{\chi}_{|s} - \tfrac{1}{2}\overline{\chi}_{|s}v_2^s. \tag{9·8}$$

Using (9·1) the condition (9·8) may be written

$$\alpha_{44|4} = (v_1^s v_1^s + \tfrac{1}{2}\overline{\chi})_{|4},$$

and hence

$$\alpha_{44} = v_1^s v_1^s + \tfrac{1}{2}\overline{\chi}, \tag{9·9}$$

$$\alpha_{4s} = -v_1^s v_1^r v_1^r + v_1^s \overline{\chi} - v_2^s \overline{\chi}. \tag{9·10}$$

### 10. *The third approximation*

The next approximation to $\gamma_{mn}$ is determined by solving the equations

$$\gamma^{(3)}_{mn|ss} = 2\Lambda^{(3)}_{mn}, \quad \gamma^{(3)}_{ms|s} = -\frac{c_1^{\prime\prime(m)}}{r_1},$$

where the quantity $2\Lambda^{(3)}_{mn}$ has the value given by the expression (15·2) in the paper by Einstein *et al.* On working out the divergence of $2\Lambda^{(3)}_{mn}$ we find that it vanishes, that is,

$$2\Lambda^{(3)}_{mn|n} = 0. \tag{10·1}$$

In order to find the principal deviation from the Newtonian laws of motion, all that essentially remains is to calculate the values of the quantities $c_1^{\prime\prime(m)}$. We denote the terms of $2\Lambda^{(3)}_{mn}$ which give rise to contributions to $c_1^{\prime\prime(m)}$ by $2\Lambda^*_{mn}$. We readily see that $2\Lambda^*_{mn}$ is of the form

$$\begin{aligned}2\Lambda^*_{mn} = {} & A_{mns}\frac{(x^s - x_1^s)}{r_1^3} + B_m\frac{(x^n - x_1^n)}{r_1^3} + B_n\frac{(x^m - x_1^m)}{r_1^3} \\ & + 6C_s\frac{(x^m - x_1^m)(x^n - x_1^n)(x^s - x_1^s)}{r_1^5} + 6D_{nsr}\frac{(x^m - x_1^m)(x^s - x_1^s)(x^r - x_1^r)}{r_1^5} \\ & + 6D_{msr}\frac{(x^n - x_1^n)(x^s - x_1^s)(x^r - x_1^r)}{r_1^5} + 6E_{srt}\delta_{mn}\frac{(x^s - x_1^s)(x^r - x_1^r)(x^t - x_1^t)}{r_1^5} \\ & + 30K_{srt}\frac{(x^m - x_1^m)(x^n - x_1^n)(x^r - x_1^r)(x^s - x_1^s)(x^t - x_1^t)}{r_1^7}.\end{aligned}$$

The equation

$$\gamma^*_{mn|ss} = 2\Lambda^*_{mn}$$

can be integrated in an elementary manner, and the coefficient $c_1^{\prime\prime(m)}$ of $-1/r_1$ in $\gamma^*_{mn|n}$ can then be written down. I find

$$\begin{aligned}c_1^{\prime\prime(m)} = {} & \tfrac{1}{2}A_{mnn} + \tfrac{3}{2}B_m + 2C_m + \tfrac{5}{2}D_{mss} + \tfrac{1}{2}D_{ssm} + \tfrac{1}{2}D_{sms} + \tfrac{1}{2}E_{mll} + \tfrac{1}{2}E_{lml} \\ & + \tfrac{1}{2}E_{llm} + 2K_{mll} + 2K_{lml} + 2K_{llm}.\end{aligned} \tag{10·2}$$

Now it is clear that $\Lambda^*_{mn}$ satisfies (10·1). Hence equating to zero the coefficients of $\frac{1}{r_1^3}$, $\frac{(x^m-x_1^m)(x^s-x_1^s)}{r_1^5}$, $\frac{(x^s-x_1^s)(x^r-x_1^r)}{r_1^5}$ in $2\Lambda^*_{mn|n}$ we find

$$A_{mll}+B_m=0,\quad D_{lsl}+D_{lls}=0,\quad E_{msr}+E_{smr}+E_{srm}+D_{msr}=0. \tag{10·3}$$

Putting $s=r$ in the latter equation we obtain

$$E_{mss}+E_{sms}+E_{ssm}+D_{mss}=0 \tag{10·4}$$

With the help of (10·3) and (10·4), the expression (10·2) becomes

$$c_1^{''(m)}=B_m+2C_m+2D_{mss}+2K_{mll}+2K_{lml}+2K_{llm} \tag{10·5}$$

On calculating the values of $B_m$, $C_s$, $D_{nsr}$ and $K_{srl}$ and substituting in (10·5) we arrive at the result

$$\begin{aligned} c_1^{''(m)} = 4m_1\bigg[ & -4m_2^2\frac{(x_1^m-x_2^m)}{r^4}-4m_2\frac{(x_1^s-x_2^s)}{r^3}v_1^m v_1^s \\ & +m_2\frac{(x_1^m-x_2^m)}{r^3}\left(v_1^s v_1^s+2v_2^s v_2^s-\tfrac{3}{2}\epsilon_2^2-\frac{5m_1}{r}\right)-\frac{3m_2}{r^2}(v_1^m-v_2^m)\,\epsilon_2 \\ & +4m_2\left\{\frac{(x_1^s-x_2^s)}{r^3}v_2^m-\frac{(x_1^m-x_2^m)}{r^3}v_2^s\right\}v_1^s\bigg]. \end{aligned}$$

The condition $$c_1^{(m)}=c_1^{'(m)}+c_1^{''(m)},$$

where the value of $c'^{(m)}$ is given by (9·1), then gives the equations of motion (8·4). The integration of the equations of motion has been carried out by Robertson (1938) and independently by Eddington and Clark (1938).

## THE LOSS OF GRAVITATIONAL ENERGY OF A ROTATING ROD

11. We now come to a problem of great interest. A spinning rod sets up a train of gravitational waves and the question arises whether these waves will carry away the energy of the rod so that it will gradually come to rest. It seems that the angular velocity of a rotating cohesive system, such as a rotating rod, is slowly decreasing. In the first investigations on the problem which were carried out by Einstein (1916, 1918) and Eddington (1922), the energy was represented by the pseudo-tensor $t^\nu_\mu$ and the outward flow of this pseudo-energy was calculated. Owing to the criticism directed against this method of attack, Eddington (1924) gave another discussion of the problem, the validity of which depends largely on the nature of cohesive forces. It is therefore a matter of some importance to show that

we can obtain the result as a condition of integrability of the equations for empty space.

We take a first-order solution for the external field of a rotating rod and try to build up a solution of the equations $G_{\mu\nu} = 0$ to a higher approximation. Consider a rod spinning with angular velocity $\omega$ in the plane of $x^2x^3$, and let $I$ be the moment of inertia. The field will consist of both periodic and non-periodic terms, and it is evident from § 7 that the first-order terms in the non-periodic part of the solution which give rise to the angular equations of motion are

$$h_{4n} = 2I\omega\left(\frac{x^2}{r^3}\delta_{n3} - \frac{x^3}{r^3}\delta_{n2}\right), \tag{11·1}$$

and the contribution to $M_{mn}$ is

$$M_{mn} = 6I\dot{\omega}\left\{\frac{x^3}{r^5}(x^m\delta_{n2} + x^n\delta_{m2}) - \frac{x^2}{r^5}(x^m\delta_{n3} + x^n\delta_{m3})\right\}. \tag{11·2}$$

A suitable solution for the periodic part is given in Eddington's first investigation; writing $p = 2\omega$ the solution he gives is

$$h_{\mu\nu} = \gamma_{\mu\nu} - \tfrac{1}{2}\eta_{\mu\nu}\eta^{\sigma\rho}\gamma_{\sigma\rho},$$

where

$$\gamma_{22} = -\gamma_{33} = \frac{Ip^2}{r}\cos p(t-r),$$

$$\gamma_{23} = \frac{Ip^2}{r}\sin p(t-r),$$

$$\gamma_{24} = Ip^2\left\{-\frac{x^2}{r^2}\cos p(t-r) - \frac{x^3}{r^2}\sin p(t-r)\right\} + Ip\left\{-\frac{x^2}{r^3}\sin p(t-r) + \frac{x^3}{r^3}\cos p(t-r)\right\},$$

$$\gamma_{34} = Ip^2\left\{-\frac{x^2}{r^2}\sin p(t-r) + \frac{x^3}{r^2}\cos p(t-r)\right\} + Ip\left\{\frac{x^2}{r^3}\cos p(t-r) + \frac{x^3}{r^3}\sin p(t-r)\right\},$$

$$\gamma_{44} = Ip^2\left\{\frac{{x^2}^2 - {x^3}^2}{r^3}\cos p(t-r) + \frac{2x^2x^3}{r^3}\sin p(t-r)\right\} + 3Ip\left\{\frac{{x^2}^2 - {x^3}^2}{r^4}\sin p(t-r) - \frac{2x^2x^3}{r^4}\cos p(t-r)\right\} - 3I\left\{\frac{{x^2}^2 - {x^3}^2}{r^5}\cos p(t-r) + \frac{2x^2x^3}{r^5}\sin p(t-r)\right\}.$$

Substituting these terms in $2L_{\mu\nu}$ we obtain terms with factors

$$\sin p(t-r)\cos p(t-r), \quad \cos^2 p(t-r) \quad \text{and} \quad \sin^2 p(t-r).$$

Now, we may write

$$\cos p(t-r)\sin p(t-r) = \tfrac{1}{2}\sin 2p(t-r), \quad \cos^2 p(t-r) = \tfrac{1}{2}(1+\cos 2p(t-r)),$$
$$\sin^2 p(t-r) = \tfrac{1}{2}(1-\cos 2p(t-r)),$$

and accordingly $2L_{\mu\nu}$ can be split up into periodic and non-periodic parts. From (11·2) it is clear that the angular equations of motion are obtained by picking out the terms of order $-3$ in $r$ from the non-periodic part of $2L_{\mu\nu}$, and we note that these terms are of the order $I^2p^5$. After some calculation we find

$$2L_{44} = 0,$$
$$2L_{mn} = I^2p^5\left(\frac{3}{4}+\frac{9}{4}\frac{x^{1^2}}{r^2}\right)\left\{\frac{x^2(x^n\delta_{m3}+x^m\delta_{n3})}{r^5}-\frac{x^3(x^m\delta_{n2}+x^n\delta_{m2})}{r^5}\right\}.$$

Take a solution of the form

$$h_{44} = 0, \quad h_{11} = 0, \qquad h_{12} = C\frac{x^1x^3}{r^3}+A\frac{x^{1^2}x^2}{r^5},$$
$$h_{22} = -2B\frac{x^2x^3}{r^3}+2A\frac{x^2x^3x^{1^2}}{r^5}, \quad h_{13} = -C\frac{x^1x^2}{r^3}-A\frac{x^{1^2}x^2}{r^5},$$
$$h_{33} = 2B\frac{x^2x^3}{r^3}-2A\frac{x^2x^3x^{1^2}}{r^5}, \qquad h_{23} = B\left(\frac{x^{2^2}-x^{3^2}}{r^3}\right)-A(x^{2^2}-x^{3^2})\frac{x^{1^2}}{r^5}.$$

Writing $2A+3B+3C = \lambda$ we find

$$M_{mn} = \lambda\left(\frac{5x^{1^2}}{r^2}-1\right)\left\{\frac{x^2}{r^5}(x^m\delta_{n3}+x^n\delta_{m3})-\frac{x^3}{r^5}(x^m\delta_{n2}+x^n\delta_{m2})\right\}.$$

Hence putting $\lambda = \frac{9}{20}I^2p^5$,

we have a solution such that

$$M_{mn}-2L_{mn} = \tfrac{6}{5}I^2p^5\left\{\frac{x^3}{r^5}(x^m\delta_{n2}+x^n\delta_{m2})-\frac{x^2}{r^5}(x^m\delta_{n3}+x^n\delta_{m3})\right\}.$$

Finally, writing $p = 2\omega$ and combining with (11·2), we obtain

$$M_{mn}-2L_{mn} = 6I(\dot{\omega}+\tfrac{32}{5}I\omega^5)\left\{\frac{x^3}{r^5}(x^m\delta_{n2}+x^n\delta_{m2})-\frac{x^2}{r^5}(x^m\delta_{n3}+x^n\delta_{m3})\right\}.$$

The condition for integrability is therefore

$$\dot{\omega} = -\tfrac{32}{5}I\omega^5,$$

and the rate of loss of energy

$$-\frac{d}{dt}(\tfrac{1}{2}I\omega^2) = \tfrac{32}{5}I^2\omega^6$$

is in agreement with the result obtained by other methods.

### ROTATING MASS OF LIQUID

12. In the preceding sections we have investigated solutions of the equations for empty space; we have taken a first order solution and by substituting this in expressions of the form (2·3) we have built up a solution to the next approximation. The method can be applied when we pass on to consider the interior of matter; and, as an example, I discuss the problem of a rotating mass of liquid of constant density and show that a possible form of the free surface is a spheroid.

Consider a weak field of the form

$$\left.\begin{aligned}\gamma_{11} &= \tfrac{1}{2}(p_1x^2+q_1y^2+r_1z^2)+\tfrac{1}{4}(a_1x^2+b_1y^2+c_1z^2)\,r^2; & \gamma_{23} &= \lambda_1 zyr^2+\mu_1 yz;\\ \gamma_{22} &= \tfrac{1}{2}(p_2x^2+q_2y^2+r_2z^2)+\tfrac{1}{4}(a_2x^2+b_2y^2+c_2z^2)\,r^2; & \gamma_{13} &= \lambda_2 xzr^2+\mu_2 xz;\\ \gamma_{33} &= \tfrac{1}{2}(p_3x^2+q_3y^2+r_3z^2)+\tfrac{1}{4}(a_3x^2+b_3y^2+c_3z^2)\,r^2, & \gamma_{12} &= \lambda_3 xyr^2+\mu_3 xy.\end{aligned}\right\} \tag{12·1}$$

On working out the components $T_{mn}$ of the energy tensor we find

$$\left.\begin{aligned}16\pi T_{11} &= Qy^2+(P'x^2+R'y^2+S'z^2), & 16\pi T_{12} &= -Qxy,\\ 16\pi T_{22} &= Qx^2+(P'x^2+R'y^2+S'z^2), & 16\pi T_{13} &= 16\pi T_{23} = 0,\\ 16\pi T_{33} &= \qquad\quad (P'x^2+R'y^2+S'z^2), & &\end{aligned}\right\} \tag{12·2}$$

provided certain conditions are satisfied Writing $Q = 16\pi\rho\omega^2$ we see that the part

$$16\pi T_{11} = Qy^2, \quad 16\pi T_{22} = Qx^2, \quad 16\pi T_{12} = -Qxy, \quad T_{33} = T_{13} = T_{23} = 0,$$

represents matter moving with constant angular velocity about the $z$-axis. The remainder

$$16\pi T_{11} = 16\pi T_{22} = 16\pi T_{33} = P'x^2+R'y^2+S'z^2, \quad T_{12}, T_{31}, T_{23} = 0,$$

represents a fluid under isotropic pressure.

It is found that the conditions mentioned above lead to the relations

$$P' = R' = \tfrac{1}{2}Q, \quad S' = 0,$$

that is, the pressure due to the rotation is

$$p = \text{const.} + \tfrac{1}{2}\rho\omega^2(x^2+y^2). \tag{12·3}$$

We now calculate the field due to a spheroid and hence deduce that this is a possible form of the free surface of the liquid. Taking the spheroid to be given by

$$\frac{x^2+y^2}{a^2}+\frac{z^2}{b^2} = 1, \tag{12·4}$$

the classical potential in the interior is given by

$$\tfrac{3}{4}M(-I+I_1x^2+I_1y^2+I_2z^2),$$

where $M$ is the mass of the spheroid and

$$I = \int_0^\infty \frac{du}{(a^2+u)(b^2+u)^{\frac{1}{2}}}; \quad I_1 = \int_0^\infty \frac{du}{(a^2+u)^2(b^2+u)^{\frac{1}{2}}}, \quad I_2 = \int_0^\infty \frac{du}{(a^2+u)(b^2+u)^{\frac{3}{2}}}.$$

Writing $a^2 = b^2(1+\lambda)$ we have

$$\frac{I_1}{I_1+\frac{1}{2}I_2} = \frac{(1+\lambda^2)\tan^{-1}\lambda-\lambda}{\lambda^3}, \quad \frac{I_2}{I_1+\frac{1}{2}I_2} = \frac{2(1+\lambda^2)(\lambda-\tan^{-1}\lambda)}{\lambda^3}. \tag{12·5}$$

We take as the first-order solution for the metric

$$\gamma_{44} = 3M\{-I+I_1(x^2+y^2)+I_2z^2\}, \quad \gamma_{mn}, \gamma_{4n} = 0. \tag{12·6}$$

The density is given by $16\pi T_{44} = \gamma_{44|ss}$, namely,

$$\pi\rho = \tfrac{3}{4}M(I_1+\tfrac{1}{2}I_2) \tag{12·7}$$

Now for a metric in which $h_{4n}$ is zero and $h_{mn}$, $h_{44}$ are independent of time, the value of $16\pi T_{mn}$ correct to the second order is

$$16\pi T_{mn} = \gamma_{mn|ss}-\gamma_{ms|sn}-\gamma_{ns|sm}+\delta_{mn}\gamma_{rs|sr}-2\Lambda'_{mn}+U_{mn}, \tag{12·8}$$

where $$U_{mn} = h_{mn}(G_{44}-G_{ll})+\delta_{mn}(h_{rs}G_{rs}+h_{44}G_{44}).$$

Now if $$h_{44} = V, \quad h_{mn} = V\delta_{mn}, \quad \text{and} \quad \gamma_{44} = 2V,$$

$$U_{mn} = 2VG_{44}\delta_{mn} = -VV_{|ss}\delta_{mn} = -\tfrac{1}{4}\gamma_{44}\gamma_{44|ss} \tag{12·9}$$

For the first-order solution (12·6)

$$2\Lambda'_{mn} = -\tfrac{1}{4}\gamma_{44|m}\gamma_{44|n}-\tfrac{1}{2}\gamma_{44}\gamma_{44|mn}+\tfrac{1}{4}\delta_{mn}\gamma_{44}\gamma_{44|rr}+\tfrac{3}{8}\delta_{mn}\gamma_{44|r}\gamma_{44|r}. \tag{12·10}$$

We take as the general form of the second approximation for $\gamma_{mn}$

$$\gamma_{11} = \tfrac{1}{4}(a_1x^2+b_1y^2+c_1z^2); \quad \gamma_{23} = d_1zyr^2; \quad \text{etc.} \tag{12·11}$$

Substituting in (12·8) we obtain the value of $16\pi T_{mn}$. For the pressure to be isotropic we require

$$\left.\begin{aligned} 16\pi T'_{11} = 16\pi T_{22} = 16\pi T_{33} = Px^2 + Ry^2 + Sz^2, \\ T_{12}, T_{23}, T_{13} = 0. \end{aligned}\right\} \tag{12·12}$$

It is found that the quantities $P$, $R$, $S$ are independent of $a_i$, $b_i$, $c_i$ and $d_i$; in fact

$$P = R = -9M^2 I_1(I_1 + \tfrac{1}{2}I_2); \quad S = -9M^2 I_2(I_1 + \tfrac{1}{2}I_2). \tag{12·13}$$

Using (12·5) and (12·7), these expressions become

$$P = R = -16\pi^2\rho^2 \frac{(1+\lambda^2)\tan^{-1}\lambda - \lambda}{\lambda^3}, \quad S = -16\pi^2\rho^2 \frac{2(1+\lambda^2)(\lambda - \tan^{-1}\lambda)}{\lambda^3}. \tag{12·14}$$

Adding the rotational terms (12·3) we have

$$p = \text{const.} + \tfrac{1}{2}\rho\omega^2(x^2+y^2) + \frac{P}{16\pi}(x^2+y^2) + \frac{S}{16\pi}z^2, \tag{12·15}$$

where $P$ and $S$ are given by (12·11).

Now if
$$\frac{\omega^2}{2\pi\rho} = \frac{(3+\lambda^2)\tan^{-1}\lambda - 3\lambda}{\lambda^3}, \tag{12·16}$$

the expression (12·15) becomes

$$p = \text{const.} + 2\pi\rho^2 \frac{(1+\lambda^2)}{\lambda^3}(\tan^{-1}\lambda - \lambda)\left\{\frac{x^2+y^2}{1+\lambda^2} + \frac{z^2}{1}\right\}. \tag{12·17}$$

The spheroid (12·4) is therefore a surface of equipressure.

It is with pleasure that I thank Sir Arthur Eddington for his advice in preparing the paper for publication.

## REFERENCES

Eddington, A. S. 1922 *Proc Roy. Soc.* A, **102**, 268–282
— 1924 *Mathematical theory of relativity*, 2nd ed. Camb. Univ. Press.
Eddington, A. S. and Clark, G L. 1938 *Proc. Roy. Soc.* A, **166**, 465–475.
Einstein, A. 1916 *S.B preuss. Akad. Wiss.* p. 688.
— 1918 *S.B. preuss Akad. Wiss.* p. 154.
Einstein, Infeld and Hoffmann 1938 *Ann. Math., Princeton, etc.*, **39**, 65–100.
Robertson, H. P. 1938 *Ann. Math., Princeton, etc.*, **39**, 101–104.

# The crystal structure of Rochelle salt (sodium potassium tartrate tetrahydrate $NaKC_4H_4O_6 . 4H_2O$)

By C. A. Beevers and W. Hughes

*(Communicated by W. L. Bragg, F.R.S.—Received 1 August 1940)*

The complete crystal structure of Rochelle salt (sodium potassium tartrate tetrahydrate) has been determined by Fourier and Patterson methods. Some of the difficulties in the application of these methods are discussed.

The tartrate molecule is found to lie approximately in three planes, the planes of each half of the molecule being inclined at 60° to the plane of the carbon atoms. The tartrate molecules are bonded to sodium and potassium atoms both directly and through the medium of water molecules. If the water molecules are to preserve their customary tetrahedral 'bonding' it is necessary to suppose that one of the carboxyl groups of the molecule is also a dipole. A reversal of the continuous chain of carboxyl-water-water dipoles is a possible explanation of the peculiar dielectric properties of the salt.

## INTRODUCTION

This work was undertaken primarily as a development of previous work on crystalline hydrates, and as an exercise in the X-ray analysis of a complex structure. As will be seen later the structure requires the determination of forty-seven parameters, has no centre of symmetry, and no features which permit any simplification of the direct methods of analysis which are now available. These methods are, however, so powerful, that in the authors' opinion they extend very greatly the complexity of structures which can be solved by X-ray analysis.

Rochelle salt is also of great interest as being optically active, and because of its somewhat remarkable electric properties. The potassium sodium salt has abnormally large values of the dielectric constant parallel to the $a$-axis between the temperatures $-10$ and $+25°$ C. This property has attracted much attention, a recent summary of the theoretical work being by Mueller (1940), but it seems clear that the theoretical work requires guidance by an accurate and complete X-ray analysis.

The present work also provides the first measurements on the configuration and size of the tartrate molecule.

## DESCRIPTION AND DISCUSSION OF THE STRUCTURE

Rochelle salt crystallizes in the orthorhombic bisphenoidal class and has been shown by many previous workers to possess the space group $P\,2_12_12$, having the absences ($h00$) when $h$ is odd, and ($0k0$) when $k$ is odd. We have verified this assignment of space group, and by measurements on high-order planes have deduced the following values of the cell edges for Rochelle salt itself, and for other members of the isomorphous series to which this salt belongs:

| | $a_0$<br>A | $b_0$<br>A | $c_0$<br>A |
|---|---|---|---|
| Potassium-sodium salt | 11·93 | 14·30 | 6·17* |
| Ammonium-sodium salt | 12·15 | 14·40 | 6·18* |
| Rubidium-sodium salt | 12·05 | 14·40 | 6·21* |

* By layer-line measurement only.

According to Groth the density of Rochelle salt is 1·790, and this requires four molecules of $KNaC_4H_4O_6.4H_2O$ in the unit cell.

The general positions of the space group $P\,2_12_12$ are the points

$$(xyz)\quad(\bar{x}\bar{y}z)\quad(\tfrac{1}{2}+x\ \tfrac{1}{2}-y\ \bar{z})\quad(\tfrac{1}{2}-x\ \tfrac{1}{2}+y\ \bar{z}),$$

while the special positions (on the twofold axes) are

$$(a)\quad(00z)\quad(\tfrac{1}{2}\tfrac{1}{2}\bar{z});\qquad(b)\quad(\tfrac{1}{2}0z)\quad(0\tfrac{1}{2}\bar{z}).$$

The different salts studied appear to be strictly isomorphous, but we have obtained accurate parameters only of the potassium salt. These parameters are probably very close to the true values for the other salts also.

The potassium atoms occupy the two sets of two-fold positions as shown in table 1, with $z$ parameters of 0·05 and 0·15 respectively. The sodium atoms occupy the general positions (0·23, $0{\cdot}\overline{01}$, 0·52), and (as shown in figure 1) this gives an arrangement of positive ions lying rather closely together in sheets perpendicular to the $b$-axis. The remaining atomic positions are listed in table 1, and the projection of the complete unit cell on the (001) plane is shown in figure 1 In this figure the atoms are numbered to correspond to table 1 and the $z$ co-ordinates are given alongside the circles representing the atoms.

The sodium atom has around it a co-ordination group of six, two oxygens and one hydroxyl from the tartrate groups, and three water molecules. The sodium-oxygen distances are given in figure 2, and average 2·39 A, which is sufficiently close to the accepted values. (Sum of Na and O radii

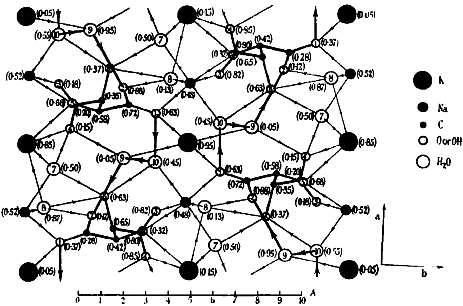

FIGURE 1 Projection on (001) plane, of the structure of Rochelle salt. The arrow heads on the bonds are drawn in a direction from positive atoms to negative atoms. The bonds involved in the 1–2 9–10 chains are drawn thick, so that the chains can be picked out.

TABLE 1

| | | | | |
|---|---|---|---|---|
| 2 K on (*a*) | | (0·00 | 0·00 | 0·05) |
| 2 K on (*b*) | | (0·00 | 0·50 | 0·15) |
| 4 Na on | | (0·23 | 0·99 | 0·52) |
| 4 O on | (1) | (0·12 | 0·10 | 0·37) |
| 4 O on | (2) | (0·22 | 0·20 | 0·12) |
| 4 O on | (3) | (0·23 | 0·40 | 0·82) |
| 4 O on | (4) | (0·06 | 0·37 | 0·85) |
| 4 OH on | (5) | (0·16 | 0·36 | 0·32) |
| 4 OH on | (6) | (0·29 | 0·24 | 0·63) |
| 4 $H_2O$ on | (7) | (0·40 | 0·08 | 0·50) |
| 4 $H_2O$ on | (8) | (0·25 | 0·05 | 0·87) |
| 4 $H_2O$ on | (9) | (0·44 | 0·30 | 0·05) |
| 4 $H_2O$ on | (10) | (0·42 | 0·40 | 0·45) |
| 4 C on | | (0·15 | 0·18 | 0·28) |
| 4 C on | | (0·12 | 0·28 | 0·42) |
| 4 C on | | (0·17 | 0·27 | 0·65) |
| 4 C on | | (0·15 | 0·35 | 0·80) |

from *Internationale Tabellen*, **2**, 611, is 2·32 A.) The potassium atom on (0, 0, 0·05) has a four-co-ordination group consisting of two oxygens from tartrate groups and two waters, while the other potassium atom touches two oxygens and two hydroxyls from tartrate groups, and four water molecules, thus having a co-ordination of eight. The interatomic distances in these groups are shown in figure 2.

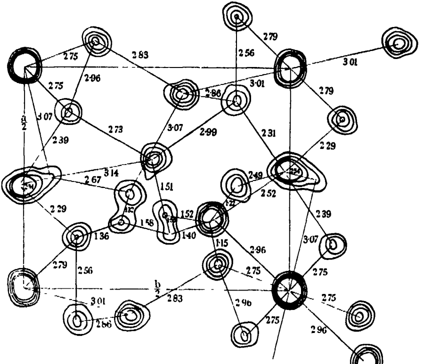

FIGURE 2. Final Fourier synthesis of one-quarter of the complete unit cell projected on (001), giving the positions chosen for the atoms and the interatomic distances in Angstrom units.

The potassium atom at (0, 0·05) has distances of 2·79 A to the two oxygens, and 3·01 to the two waters. Possibly it is also bonded to water molecule 8 (at 3·29 A) which would increase its co-ordination to six. If there are also residual forces to water molecule 10 (3·52 A) the co-ordination would go up to ten. These bonds above 3·2 A have not been included in figure 1, as they must be considerably weaker than the shorter bonds, but their possible existence suggests that the large K ion is readily polarizable, and has a somewhat indefinite co-ordination.

The tartrate molecule has its chain of carbon atoms almost exactly in a plane. Figure 3 is a perspective drawing of the molecule the carbon atoms being in the plane of the paper. The C(OH)—COOH groups constituting each half of the molecule are also practically plane groups inclined at 60° ± 2 to the plane of the carbon atoms. The C—C distances found are 1·58, 1·53 and 1·52 A, while the C—O distances are 1·36, 1·32, 1·22 and 1·15 A. The C—OH distances seem to be rather longer, viz. 1·40, 1·51 A. It must be stressed that all the final atomic positions have been chosen from the Fourier maps without manipulation with a view to obtaining good interatomic distances, so that the values may be taken as independent determinations. They are not regarded as being very accurate, but the mean of 1·54 A is good supporting evidence for the usually accepted separation of single bonded carbon atoms.

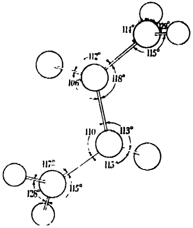

FIGURE 3. The tartrate molecule in parallel perspective viewed in a direction perpendicular to the plane of the carbon atoms, showing the angles between the various bonds. Each half of the molecule lies in a plane inclined at 60° to the plane of the carbon atoms.

The water molecule 7 (see figure 1) is 2·75 A from a potassium atom, 2·39 A from a sodium atom, 2·73 A from a hydroxyl group, and 2·96 A from an oxygen atom, and apart from neighbouring atoms in the same co-ordination group it makes no other close approaches. The four bonds described have an approximately tetrahedral distribution in agreement with the Bernal-Fowler model for the water molecule.

Water molecule 8 can also be given four bonds, although these are not so regular as in the previous case. These bonds are, to a potassium atom 3·07 A, to a sodium atom 2·34 A, to an oxygen atom 2·67 A, and to a hydroxyl group 3·14 A. If the latter distance be disregarded the water molecule may be regarded as of the planar type described by Beevers and Lipson (1934). It should be pointed out that this water molecule is not resolved from other atoms in any of the three Fourier projections considered, so that it is probably the least accurately located atom in the structure.

Water molecule 9 has a distance of 3·01 A to a potassium atom and distances of 2·83 and 3·07 A to oxygen atoms 4 and 2 respectively. It is distant 2·86 A from water molecule 10 and 3·20 A from the hydroxyl group 6 (in the unit cell $c_0$ removed) This final distance must be neglected if the molecule is to be fitted into the tetrahedral theory, and the bond between 10 and 9, regarded as a line of electrostatic force, may be taken as being directed from 10 to 9. The water molecule 10 has, in addition to the outgoing bond to 9, bonds to the sodium atom (2·31 A), to the oxygen atom 1 (2·56 A), and to the hydroxyl group 6 (2·99 A). The sodium bond must be regarded as incoming, so that one of the bonds to the tartrate molecule must also be regarded as incoming. If the bond from oxygen 1 be taken as incoming we obtain at once a simple explanation of the dielectric properties of Rochelle salt.

Oxygen 1 is behaving as a positive atom to water molecule 10, but as a negative atom to the potassium and sodium atoms with which it is also in contact. That is to say, the oxygen atom 1 in association with its carbon atom is strongly polarized perhaps because of a hydrogen nucleus from another part of the molecule. The positive direction of the bonds is thus 1 to 10, 10 to 9, 9 to 2. However, if the polarization of oxygen 1 can be transferred to oxygen 2 within the same molecule the positive bond direction may now go 2 to 9, 9 to 10, 10 to 1. Such a change requires the water molecules 9 and 10 to interchange a positive and negative bond, i.e. in each case one of the hydrogen nuclei within the molecule shifts to one of the tetrahedral negative areas. This chain of atoms 1–2–9–10–1–2–9–10, etc., extends along the direction of the $a$-axis, the direction in which the anomalies are observed. Thus, if a field is impressed on the crystal in this direction the chain of molecules will arrange themselves so that the direction of the bonds is the same as the direction of the field. This will involve, as has been pointed out by Jaffé (1937), a lowering of the symmetry to monoclinic, but since only the positions of hydrogen nuclei are involved the lowering of the symmetry will not be detectable by change in the X-ray intensities.

The facts that the anomaly disappears gradually as potassium is substituted by ammonium or rubidium or thallium and as the temperature is raised above 25° C are probably to be accounted for by an expansion of the structure so that some of the contacts 2–9, 9–10, 10–1, are broken. The bond 2–9 is already 3·07 A long and this is probably near the limit. There is also to be considered the possibility of the rotations of molecules or of chains of molecules above 25° C, by analogy with the change from ferro to paramagnetism. The lower Curie point might correspond to parameter changes which result in bonds being broken or made, or to the 'freezing' of the subatomic changes. Further accurate intensity work on Rochelle salt at different temperatures and with the potassium atoms substituted would enable these ideas to be tested rigorously. We think, however, that three-dimensional Fourier methods would be the best to adopt. We hope at some more favourable time to use a Fourier machine to do this work (Beevers 1939).

## METHOD OF ANALYSIS

Fourier and Patterson methods were used to supplement each other in the elucidation of the structure. The Fourier method used is a general one applicable whenever the crystal is a member of an isomorphous series. In the present case the ammonium, potassium, rubidium and thallium sodium tartrates were studied, Weissenberg photographs being taken about the $a$-, $b$-, and $c$-axes. From a knowledge of the position of the replaceable atoms in the lattice and observation of the changes of intensity between the different salts, the signs of the $F$'s can be obtained.

In the case of the thallium compound the position of the thallium atoms can be readily deduced, since to a first approximation the intensities depend only on these atoms. This deduction in the case of Rochelle salt was first made by Dr R. C. Evans, to whom we are indebted for access to his unpublished work If we next assume that atoms replacing thallium occupy the same positions, the sign of each $F$ may be taken to be the same as the sign of the thallium structure factor if there is an increase in the intensity as an atom is replaced by a heavier one. If there is a decrease in the intensity then the sign is opposite to the sign of the thallium contribution. In the actual carrying out of this process there are two difficulties, the first being due to the effect of the varying absorption coefficients on the intensities, which makes it impossible to compare photographs of different crystals directly. In this work crystals were used which had been ground to accurate cylinders parallel to the axis of rotation, thus enabling the absorption to be calculated (Bradley 1935). The substitution of potassium by rubidium is particularly useful since the copper $K\alpha$

radiation used has an absorption edge between this pair of alkali metals, and the change of absorption coefficient is not therefore so marked.

The second difficulty in the change of intensity method arises from the fact that many of the structure factors are small, and in the particular case of Rochelle salt rather a high proportion are actually zero. For example, in the $(h0l)$ set all planes with $l = 5$ have a thallium or potassium structure factor which happens to be zero. When the structure factor is small valuable information as to sign can be got by inspection of the thallium intensities, but when it is zero, of course, the sign cannot be derived by the method of substitution at all. In spite of these difficulties the projections obtained down the $a$- and $b$-axes were substantially correct and the three-dimensional structure could have been derived from them immediately had it not been for the fact that in each projection two molecules are superimposed. The resolving power is thus very low, and it was felt that more accurate positions were desirable. The lack of resolving power obtainable by Fourier methods is even more marked down the $c$-axis. The projection in this direction has a unit cell, as far as the potassium atoms are concerned, of one quarter of the true unit. This means that only the planes with $h$ and $k$ both even have a potassium contribution. Only these planes can therefore be used in a Fourier synthesis, and the resulting summation is a superposition of the four quarters of the unit cell.

The Patterson syntheses used in the work were:

(1) Sections at $z = 0$, $x = \frac{1}{2}$ and $y = \frac{1}{2}$ of the three-dimensional synthesis of the ammonium salt.

(2) Patterson synthesis of the $(hk0)$ planes excluding those having $h$ and $k$ both even.

The general intensities required for (1) were obtained mainly from layer-line Weissenberg photographs of the ammonium salt about the $a$-, $b$-, and $c$-axes. The use of the Weissenberg method rather than oscillation photographs requires a much greater total exposure time, but this is counterbalanced by the perfect resolution obtained, and the ease of analysis of the photographs. The experimental work throughout was performed on a Weissenberg camera of special design (having a vertical travel of 0·74 mm. per degree rotation of the crystal, and a radius of 5 cm.) and mounted alongside a Metropolitan-Vickers crystallographic X-ray set. The Weissenberg photographs gave all the intensities obtainable with Cu $K$ radiation except those within cusps having axes parallel to [111] in the reciprocal space. These remaining intensities were obtained from a set of oscillation photographs with [110] as rotation axis. In this case the layer-lines are so close together as to make the oscillation photograph the most advantageous method.

The derivation of the structure from the three sections of the general Patterson synthesis alone is not easy, and the Fourier syntheses previously described were found to be of great assistance in this work. The general Patterson synthesis is more symmetrical than the structure (it has the symmetry $P\ 2/m\ 2/m\ 2/m$ with a unit cell one-eighth of the unit of the structure) and provides a correspondingly large number of alternative atomic positions corresponding to each peak. A further difficulty in the interpretation is that in the section at $x = \frac{1}{2}$, for example, we obtain not only each peak due to a vector between corresponding atoms (related by the screw axis parallel to $a$) but also peaks of double weight due to different atoms having by chance the same value of $x$. In a structure as complex as Rochelle salt, with fifteen unique atoms in general positions within a $\frac{1}{2}a_0$ distance of 6 A there is almost certain to be a number of such coincidences, and they give rise to two pairs of atoms with the same interatomic vectors having $x$ components of $\frac{1}{2}a_0$. Similar considerations apply to the $y = \frac{1}{2}$ and $z = 0$ sections. There is no doubt that if the complete three-dimensional synthesis were available it would simplify a great deal the derivation of a complex structure. However, the labour of calculating the three-dimensional series with this size of unit cell is rather great.

The interpretation of the general Patterson sections and the Fourier projections together, enables rather accurate atomic sites to be found, the only remaining alternative being that a position may be $(xyz)$ or $(\frac{1}{2}-x\ \frac{1}{2}-y\bar{z})$, i.e. there is left a centre of symmetry at $(\frac{1}{4}, \frac{1}{4}, \frac{1}{2})$. If the first atom to be inserted is placed on one of these alternatives the Patterson synthesis of the $(hk0)$ planes (which is the projection parallel to the $c$-axis of the general Patterson) shows which alternatives are to be chosen for the other atomic positions. In this way two structures can be built up, related to each other by a centre of symmetry at $(\frac{1}{4}, \frac{1}{4}, \frac{1}{2})$ and these correspond to and $d$- and $l$-forms of the optically active compound. The X-ray evidence cannot of course distinguish between them.

*Note.* The calculated and observed intensities and other details of this work are to be deposited in the archives of the Royal Society.

### REFERENCES

Beevers 1939 *Proc. Phys. Soc.* **51**, 660.
Beevers and Lipson 1934 *Proc. Roy. Soc.* A, **146**, 570.
Bradley 1935 *Proc. Phys. Soc* **47**, 879.
Groth 1906 *Chem. Krist.* **3**, 332.
Jaffé 1937 *Phys. Rev.* **51**, 43.
Mueller 1940 *Phys. Rev.* **57**, 829.

# Application of the coincidence method for measurements of short life periods

By Józef Rotblat

*George Holt Physics Laboratory, University of Liverpool*

(*Communicated by J. Chadwick, F.R.S.—Received* 16 *September* 1940)

A method is described for the determination of short radioactive and nuclear life periods. It consists in varying the length of the electrical impulses produced in a coincidence arrangement of two Geiger-Müller counters. The method can be used for the measurement of life periods in the range $10^{-7}$ to $10^{-2}$ sec. The half-life period of radium C′ has been measured in this way and found to be $1{\cdot}45(\pm 0{\cdot}05) \times 10^{-4}$ sec. Experimental evidence has been obtained for the absence of γ-rays in the transition radium C′ →radium D, and some conclusions regarding the lifetimes of excitation states of radium C′ have been drawn. The determination of the intensity of weak sources and of the efficiency of Geiger counters for various types of radiation is described. The effect of a time lag in Geiger counters on the measurement of coincidences is discussed.

## Introduction

In recent years the Rossi coincidence set of two Geiger-Muller counters has been developed into an important instrument for investigations in nuclear physics. This method is based on the assumption that two particles simultaneously emitted from the source, each of which operates one counter, are recorded by the set as a coincidence. It is, however, obvious that the recording of coincidences is defined not only by the 'simultaneous' occurrence of two nuclear phenomena but rather by the ability of the circuit to select phenomena occurring in very short time intervals, i.e. by its resolving power. Two phenomena which occur in a time say $10^{-5}$ sec., one after the other, will be recorded as simultaneous by a coincidence set with a resolving time larger than $10^{-5}$ sec, while a circuit with a smaller resolving time will not record the 'coincidence'. The steady improvement in technique during recent years has resulted in the building of arrangements with very short resolving times, which, apart from other benefits, bring us nearer to the original idea of investigating true simultaneous phenomena or those which occur in extremely short time intervals (of the order of $10^{-12}$ sec ). On the other hand, the aforementioned dependence of the recording of coincidences on the resolving time suggests a new application of the coincidence method: by a deliberate variation of the resolving time, the time interval between two nuclear phenomena can be determined. Since the resolving time can be measured to a high degree of accuracy, this arrangement provides a valuable method of measuring radioactive or nuclear life periods which are so short that they cannot be measured by other methods. An application of this method to the measurement of the lifetime of radium C′ was published by the author (1939) and at the same time by Dunworth (1939), who measured also the lifetime of thorium C′. In the present paper the method is described in more detail.

## EXPERIMENTAL ARRANGEMENT AND RESULTS

*Variation of resolving time and calibration of circuit.* The use of the coincidence method for measurements of short time intervals requires an arrangement which permits the resolving time of the circuit to be varied conveniently within broad limits There are many possibilities of varying the coincidence resolving time A variation of the common anode resistance of the Rossi valves, $R_A$, or of the 'discriminator bias', $V_g$ (this is the grid bias at the mixer stage, figure 1), or of the electrical time constant of the mixer valve ($C_M R_M$) will affect the minimum time interval between the impulses in the two counters during which these are still recorded as a coincidence. These methods produce a change of the resolving time of the circuit as a whole. Another arrangement consists of the variation of the electrical time constants of the Rossi valves ($C_1 R_1$, $C_2 R_2$), and this can be done independently on either of the two valves. This method of variation of the duration of only one of the impulses produced by the entering of particles into the Geiger counters has some advantages which make it preferable to the others The rate of chance coincidences, which inevitably accompany all coincidence measurements, is proportional to the sum of the length of the electrical pulses on both Rossi valves. By keeping the length of one impulse constant and very small and varying only the length of the other impulse, the rate of chance coincidences is then reduced, this reduction amounts to nearly half, in the case of long resolving times, where the chance coincidences represent the dominating factor. If, as happens in most cases, the two particles which produce the coincidence can be distinguished, either because they are of different types or because of their different penetrating power, the method of changing the duration of only one impulse will also enable one to decide the order in which the particles are emitted. In the present work, the variation of the resolving time was accomplished by changing the grid resistance ($R_1$ or $R_2$, figure 1) in either of the two Rossi valves; this was found to be much more convenient than the variation of the capacities ($C$) which were consequently kept constant.

The determination of the length of the impulse for each value of the grid resistance was performed by means of counting chance coincidences. Two Geiger-Müller counters placed at a great distance one from the other, in order to exclude cosmic ray coincidences, were irradiated by two separate constant sources. Thus the recorded coincidences were only from uncorrelated particles The resolving time of the circuit was then determined from the formula

$$C_c = N_1 N_2(\tau_1 + \tau_2), \tag{1}$$

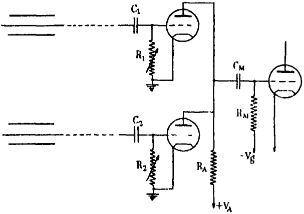

FIGURE 1

where $N_1$, $N_2$ are the rates of countings in each counter, $C_c$ the coincidence rate and $\tau_1$, $\tau_2$ the length of the impulses on each Rossi valve By choosing appropriate valves, the circuit was made completely symmetrical, as proved by the recording of identical coincidence rates when the resistances in both valves were interchanged. The validity of formula (1) and the symmetry of the circuit was checked many times by changing the values of $N_1$ and $N_2$, and by alternative variation of the resistances in each circuit After a proper adjustment of the other component values* it was found that the resolving time changes considerably when the resistances vary between 10,000 ohms and 10 megohms Figure 2 represents the calibration curve, this means the length of the impulse (on each Rossi valve) as a function of the grid resistance. Since both the resistance and resolving time vary by orders of magnitude, the ordinates and abscissae are both in a logarithmic scale. In the range of resistances 20,000 Ω–4 MΩ the calibration curve is linear and the relation between the length of impulse and resistance can be expressed by the formula

---

* The original coincidence set—with a constant resolving time—was built in this laboratory by Mr J. R. Holt, according to a scheme sent by Dr J. V. Dunworth. I wish to express here my gratitude to them.

$$\tau = 2{\cdot}5 \times 10^{-4} R^{0{\cdot}91},$$

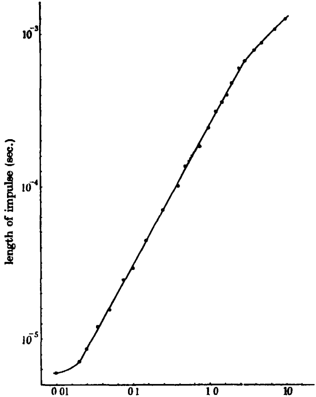

resistance (MΩ)

FIGURE 2

where $R$ is in megohms and $\tau$ in seconds. As seen from the curve, under the working conditions, the resolving time can be varied between $6 \times 10^{-6}$–$10^{-3}$ sec. This interval can be, if desired, shifted in either direction, by some changes in the values of other components.

*Determination of life period of radium C′ from α-β coincidences.* The first application of the method was the determination of the life period of radium C′. In this case, the emission of a β-ray from radium C is followed in a short time, which is on the average equal to the mean lifetime of radium C′, by the emission of an $\alpha$-particle. Since the $\alpha$-particles can be very easily distinguished from the $\beta$-particles and the efficiency of Geiger-Müller counters for both kinds of particles is relatively large, this process represents a most convenient case for testing the method.

In order to improve still further the working conditions, one of the counters—used for the detection of $\alpha$-particles—was operated in the proportional region, where it is sensitive only to $\alpha$-particles. The advantage of working in the proportional region is twofold· first, because by using a counter insensitive to $\beta$- and $\gamma$-rays the rate of counts in this counter, and hence the rate of chance coincidences is considerably reduced, which is of great importance, particularly in experiments with a long resolving time when chance coincidences usually predominate; secondly, because of the complete exclusion of cosmic ray coincidences, which is of importance at very short resolving times where the rate of coincidences is very small. Special tests were made in order to make sure that the operation of the counter in the proportional region does not influence the length of the impulses on the Rossi valve In spite of the fact that there is no flat part on the counter characteristic in the proportional region, it was found that the changes of the sensitivity of the counter with the potential applied to it are fairly small; by using as a high-tension source for the counter the customary neon stabilizer, the sensitivity of the $\alpha$-counter was found to remain practically constant (changes of 5%) during a period of over a week

The Geiger-Muller counters used for the detection of $\alpha$- and $\beta$-particles were of the same size. They were each made of a brass tube, 3 cm. in diameter and 7 cm. long, and provided with windows $2 \times 4$ cm , covered with mica of 1·5 cm. air equivalent. The counters were placed with their axes parallel and the windows facing each other, the distance between the axes was 4 cm. Between the counters was a shielding screen with a small aperture in which the source could be fixed. The source consisted of a thin-walled glass tube filled with radon. Measurements of the range of the $\alpha$-particles issuing from the tube showed that the walls of the tube had a thickness of 2·75 cm. air equivalent. Under these conditions the $\alpha$-particles from radium C′ only were registered, the total air equivalent in the path of the particles being larger than the range of the $\alpha$-particles from radon and radium A. An aluminium foil of 100 mg./cm.$^2$ thickness, interposed between the source and the $\beta$-counter, prevented the $\alpha$-particles from reaching that counter, and also cut off almost completely the $\beta$-rays from radium B.

The measurements consisted in counting the coincidence rate as a function of the length of the $\beta$-impulse, the length of the $\alpha$-impulse being kept constant at $6 \times 10^{-6}$ sec. However, in order to check the proper working of the circuit, the coincidence rate was also measured after each set of counting with reversed values of resistances, i e the length of the $\beta$-impulse $6 \times 10^{-6}$ sec. and of the $\alpha$-impulse variable. In this latter case, the recorded coincidences are practically only chance ones (there is also a very small rate of genuine coincidences, corresponding to the resolving time $6 \times 10^{-6}$ sec.). Since the total resolving time is in both cases the same, the difference between the two sets of counts gives at once the genuine rate of coincidences (with the mentioned correction). The difference in the coincidence rate in the two cases is very striking; for example, with a length of the $\beta$-impulse of $10^{-4}$ sec. and $\alpha$-impulse $6 \times 10^{-6}$ sec., the coincidence rate was 17 per minute, while with the resistances reversed it was only 1 per minute

TABLE 1

| Grid resistance $R$ | Length of $\beta$ impulse $\tau$ | Counting rate of $\alpha$-particles per min. $N_\alpha$ | Counting rate of $\beta$-particles per min $N_\beta$ | Total coincidence rate per min. $C$ | Chance coincidence rate $C_c$ | Genuine coincidence rate $C_g$ | $1500 \times C_g/N_\alpha$ | Mea valu |
|---|---|---|---|---|---|---|---|---|
| 5 MΩ | 85·5 | 1980 | 4045 | 257·9 ± 3·2 | 116·7 | 141·2 | 107·0 ± 2·4 | 107·2 ± 1·2 |
| | $\times 10^{-5}$ | 1451 | 3008 | 164·9 ± 2·8 | 63·8 | 101·1 | 104·6 ± 2·9 | |
| | sec. | 1260 | 2595 | 139·0 ± 2·0 | 47·9 | 91·1 | 108·5 ± 2·4 | |
| | | 884 | 1823 | 88·4 ± 1·7 | 24·1 | 64·3 | 109·2 ± 2·9 | |
| | | 546 | 1098 | 47·9 ± 1·0 | 9·2 | 38·7 | 106·3 ± 2·7 | |
| 0·5 MΩ | 13·2 | 2052 | 4325 | 83·6 ± 2·7 | 20·8 | 62·8 | 45·9 ± 2·0 | 48·6 ± 0·6 |
| | $\times 10^{-5}$ | 1846 | 3752 | 75·1 ± 1·4 | 16·2 | 58·9 | 47·8 ± 1·1 | |
| | sec. | 1550 | 3218 | 61·0 ± 1·4 | 11·8 | 49·2 | 47·5 ± 1·3 | |
| | | 1090 | 2235 | 41·6 ± 1·0 | 5·8 | 35·8 | 49·3 ± 1·3 | |
| | | 534 | 1108 | 18·5 ± 0·6 | 1·4 | 17·1 | 48·0 ± 1·7 | |

Owing to the relatively high efficiency of the counters for $\alpha$- and $\beta$-rays, the total coincidence rate was very high, and amounted sometimes to over 250 per minute. In order to ascertain that the recording circuit does not miss coincidences at such a high rate, the experiments were extended to a period of over a week, during which the intensity of the source had decreased to less than a quarter of its original value. Typical examples of the results are given in table 1 which contains the measurements obtained with two different values of the length of the $\beta$-impulse. The true coincidence rate $C_g$ is corrected for decay of the source by calculating its value for that intensity of the source which gave 1500 $\alpha$-particle counts per minute. It will be seen that for each set these corrected values $1500 \times C_g/N_\alpha$ are constant within the experimental error, showing that the behaviour of the circuit is satisfactory.

The final results are represented on figure 3, where the genuine coincidence rate—reduced to that intensity of the source which gave 1500 counts per minute in the $\alpha$-counter—are plotted against the length of the $\beta$-impulse on the Rossi valve. Except for the small distortion at the beginning, which can be seen more distinctly on the graph with the larger scale, the curve shows a pure exponential increase. As will be shown in the next chapter, this exponential increase is defined by the disintegration constant of radium C′. From the curve we obtain thus that $\lambda = (4{\cdot}78 \pm 0{\cdot}16) \times 10^3$ sec.$^{-1}$, or the half-life period of radium C′ is

$$T = (1{\cdot}45 \pm 0{\cdot}05) \times 10^{-4} \text{ sec.}$$

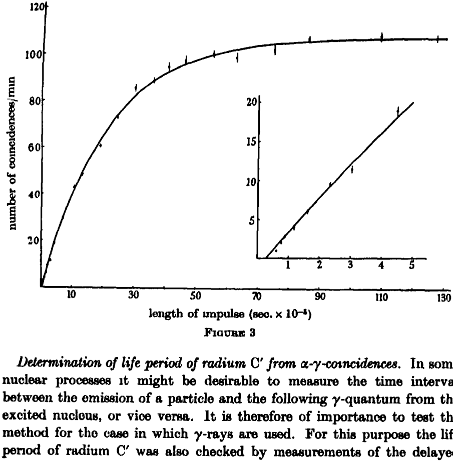

FIGURE 3

*Determination of life period of radium* C′ *from $\alpha$-$\gamma$-coincidences.* In some nuclear processes it might be desirable to measure the time interval between the emission of a particle and the following $\gamma$-quantum from the excited nucleus, or vice versa. It is therefore of importance to test the method for the case in which $\gamma$-rays are used. For this purpose the life period of radium C′ was also checked by measurements of the delayed coincidences between the $\gamma$-rays from the process RaC→RaC′ and the $\alpha$-particles. Apart from the technical aspect, this particular problem is also of interest for the investigation of the level scheme of radium C′.

The employed technique was much the same as in the case of $\alpha$-$\beta$-coincidences. Instead of the $\beta$-counter a $\gamma$-counter was used, consisting of a brass tube of the same dimensions and 1·1 mm. wall thickness; an additional aluminium screen of 4 mm. thickness was interposed between the counter and the source in order to absorb the hard $\beta$-rays from radium C. Owing to the smaller efficiency of the Geiger counter for $\gamma$-rays, the total coincidence rate was much reduced and the accuracy attained after the same period of experiment correspondingly less. The obtained results are represented in figure 4. From the curve we calculate the value for the half-life period of radium C′, $T = (1{\cdot}55 \pm 0{\cdot}20) \times 10^{-4}$ sec., which is in good agreement with that found from $\alpha$-$\beta$ coincidences.

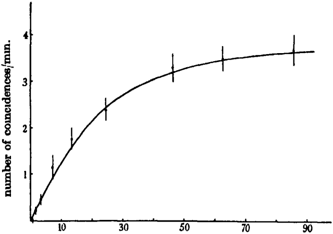

FIGURE 4

The agreement in the value of the half-life period indicates that the $\gamma$-rays arising in the process RaC→RaC′ are emitted immediately after the $\beta$-rays, or more strictly that none of the quantum levels of radium C′ of a high excitation has a life period longer than $10^{-5}$ sec. A further conclusion may also be drawn from these measurements. The curve of figure 4 goes through the zero of the co-ordinates; this means that no $\gamma$-rays of an appreciable amount are emitted simultaneously with the $\alpha$-particles. The experiments in which the length of the $\gamma$-ray impulse was constant and very short and the length of the $\alpha$-impulse varied, showed that under those conditions all recorded coincidences were only chance ones; this leads to the conclusion that no emission of $\gamma$-rays follows the emission of $\alpha$-particles within a period of $10^{-4}$ sec. We may therefore conclude that no $\gamma$-rays arise in the process RaC′→RaD, and consequently that the radium D nucleus is always formed in its ground state. This conclusion is in agreement with the scheme proposed by Ellis (1934).

## DISCUSSION

*Calculation of radioactive life period from coincidence measurements.* The determination of radioactive life periods from coincidence measurements is based on the following considerations. Suppose that the emission of a particle from a radioactive element results in the formation of a new radioactive element with a disintegration constant $\lambda$. The probability that the product will disintegrate in the time interval between $t$ and $t+dt$ (counting the time since the disintegration of the first element) is $\lambda e^{-\lambda t}dt$ Hence the probability for the emission of a particle from the product during a time $\tau$, or the rate of expected genuine coincidences when the duration of the first impulse is $\tau$, is given by

$$C_g = C_{\max}\int_0^{\tau}\lambda e^{-\lambda t}dt$$

where $C_{\max.}$ is the maximum rate of coincidences, which is theoretically obtained with an infinitely long resolving time.

However, for technical reasons, the integral cannot be taken from zero Theoretical considerations, as well as the experiments of Dunworth (1939), show that there exists a certain time lag between the moment when the particle enters the Geiger counter and the moment of occurrence of the drop of the potential of the wire, which marks the beginning of the electrical pulse. This time lag is obviously dependent upon the kind and size of the counter, the nature and pressure of the gas in it, and the value of the leak resistance. However, even with fixed conditions one may expect that the time lag will not be constant but will vary within certain limits. Thus if the duration of the electrical pulse is smaller than the difference in the duration of the time lags in the counters, it might happen that the impulse produced in the circuit of the first counter will be finished before the impulse in the second circuit has started. In such a case the emission of two particles simultaneously or in a very short time interval will not be recorded, the coincidence will be missed. Consequently, in the above integral the lower limit should be not zero, but a variable time dependent upon the occurrence of various differences in the time lags of the two counters. Without knowledge of the probability for the occurrence of various time lags, it is impossible to calculate this function. However, for practical purposes it will often be sufficient to assume a certain average difference in the duration of the time lags, $\tau_0$, which will be of the same order of magnitude as the time lag itself. We obtain then

$$C_g = C_{\text{max.}} e^{-\lambda\tau_0}[1 - e^{-\lambda(\tau-\tau_0)}]. \tag{2}$$

The rate of genuine coincidences is thus an increasing exponential function of the difference between the length of the first impulse and the average time lag. The exponential increase of $C_g$ is shown in figures 3 and 4, from which we have calculated the value of $\lambda$. The existence of the time lag is apparent on the first part of the curve in figure 3, which is given also in a larger scale. It can be seen that the curve is, at the beginning, distorted from its exponential character. Drawing the curve through the experimental points we obtain the value of $\tau_0$—the average time lag difference—as $3 \times 10^{-6}$ sec. This value is in fair agreement with the figure obtained by Dunworth and with those deduced from theoretical considerations (May 1939; Montgomery and Montgomery 1940).

*Determination of the absolute intensity of the source and the efficiencies of the counters.* The determination of the maximum rate of coincidences in the RaC→RaC′→RaD process permits also measurements of the absolute strength of the employed source and the efficiency of the Geiger counters for the detection of the radiations. We shall denote by $N$ the intensity of the source, i.e. the rate of disintegrations per unit of time, by $\epsilon_\alpha$, $\epsilon_\beta$, the efficiencies of the counters for $\alpha$- and $\beta$-rays ($\epsilon$ includes also the solid angle). The rate of counting in each counter is then given by

$$N_\alpha = N\epsilon_\alpha, \quad N_\beta = N\epsilon_\beta. \tag{3}$$

Since the emission of each $\beta$-ray from radium C is followed by the emission of one and only one $\alpha$-particle from radium C′, the maximum rate of coincidences will be

$$C_{\text{max}} = N\epsilon_\alpha\epsilon_\beta = N_\alpha N_\beta/N. \tag{4}$$

Measuring the values of $N_\alpha$, $N_\beta$, $C_{\text{max.}}$, we can from these equations calculate the other three values $N$, $\epsilon_\alpha$, $\epsilon_\beta$.

The experimental values are $C_{\text{max}} = 109$ per min., for $N_\alpha = 1500$ per min., and $N_\beta/N_\alpha = 2{\cdot}08$, we obtain therefore $N = 715$ particles per second, $\epsilon_\alpha = 3{\cdot}5 \times 10^{-2}$, $\epsilon_\beta = 7{\cdot}3 \times 10^{-2}$.

It must be remembered that at the time of experiment the $\beta$-counter was shielded with 100 mg./cm.$^2$ of aluminium, in order to absorb the $\beta$-rays from radium B. *By taking into account the absorption of the* $\beta$*-rays from radium C in that foil and the* $\gamma$*-rays recorded by the counter we calculate* the efficiency of the $\beta$-counter for $\beta$-rays with no absorber, $\epsilon_\beta = 15{\cdot}5 \times 10^{-2}$.

Analogous calculations for the case of $\alpha$-$\gamma$ coincidences, where $C_{\text{max.}} = 3{\cdot}7$ per min., give a value for the efficiency of the $\gamma$-counter $\epsilon_\gamma = 2{\cdot}5 \times 10^{-3}$. This is the average efficiency of the counter for the $\gamma$-rays emitted in the process Ra C $\rightarrow$ Ra C′.

The method of determination of the strength of the source from coincidence measurements represents a suitable and accurate method for measurements of the absolute intensity of weak sources. It is worth while mentioning that the use of the radium C process is the most appropriate for this purpose, since the assumption on which it is based, that each $\beta$-ray is followed by one $\alpha$-particle, is quite certain, this is not the case when other nuclear processes are used as a basis. It is also convenient and quick, owing to the high efficiency of the counter for $\alpha$- and $\beta$-rays. Once the efficiency of the $\beta$-counter is determined by means of the radium C process, the absolute intensity of other sources can be very easily found.

*Limits of application of the method.* The use of the coincidence method for measuring short life periods requires obviously that the resolving time of the circuit should be of the same order of magnitude as the measured time interval. The application of the method is limited however by factors other than the resolving time. As is evident from the preceding considerations coincidences are missed when the resolving time becomes smaller than the time lag of the counter The time lag will therefore define the lower limit of the life periods measurable by this method. With the counters used in the present work the time lag was about $10^{-6}$ sec., by some changes in the construction of the counters and circuits the time lag can be reduced by an order of magnitude. The lower limit may thus be set as $10^{-7}$ sec. The upper limit is defined only by the possibility of lengthening the impulse on the Rossi valve and could therefore be fairly high, here however the limit is defined by the rate of chance and cosmic-ray coincidences With increasing resolving time the rate of chance coincidences becomes relatively more and more important. If the experimental error has not to be too large, the rate of chance coincidences should not be greater than the rate of the genuine ones. From equations (1), (2) and (4), and by neglecting $\tau_2$, $\tau_0$ and the natural background of the counters, we find that $C_c$ will be of the same order as $C_g$ if $N \sim (1 - e^{-\lambda\tau})/\tau$. Therefore the strength $N$ of the source must not be larger than $\lambda$. But with a very weak source the absolute rate of coincidences is very small. For instance, for life periods of 0·1 sec. the intensity of the source must not be larger than

10 per sec. For a product of efficiencies $\epsilon_1\epsilon_2 \sim 10^{-3}$, this gives a maximum rate of genuine coincidences of only 0·6 per min. At smaller efficiencies of the counters this rate will be still smaller; if cosmic-ray coincidences are also recorded, they will represent the factor introducing the largest experimental error. The upper limit will therefore be about $10^{-1}$–$10^{-2}$ sec., according to the experimental arrangements. Some technical improvements which will increase the efficiencies of the counters may enable us to push the limit still higher, to the region where the life periods can be measured by ordinary methods.

It is a pleasure to the author to express his gratitude to Professor J Chadwick for the hospitality and kind interest and many valuable suggestions made during the work. The author is also greatly indebted to the Feliks Wiślicki Fund of Warsaw for the Fellowship which enabled him to come to England.

### REFERENCES

Dunworth, J V. 1939 *Nature, Lond.*, **144**, 152.
Ellis, C. D 1934 *Int. Conf. Physics.*
May, N. A. 1939 *Proc. Phys Soc.* **51**, 26.
Montgomery, C. G. and Montgomery, D. D. 1940 *Phys. Rev.* **57**, 1030.
Rotblat, J. 1939 *Nature, Lond.*, **144**, 248.

# Molecular anisotropy of urea, $CO(NH_2)_2$, and of related compounds

By Kathleen Lonsdale

*Davy Faraday Laboratory, Royal Institution, W.* 1

(*Communicated by Sir William Bragg, P.R.S.—Received* 4 *October* 1940)

[Plate 7]

The magnetic anisotropy of urea has been measured and compared with that of the carbonate and nitrate groups. It does not appear that the hydrogen bonds contribute appreciably to the anisotropy; the latter indicates about the same degree of resonance in all three groups. The anisotropy of the refractivities is greater in urea than in the carbonate group, showing that the $(NH_2)^-$ radical must be much more polarizable than the $O^-$ ion, allowance being made for the interionic distances. Urea nitrate, urea oxalate, cyanuric acid dihydrate and anhydrous cyanuric acid all crystallize in layer structures, as shown by cleavage, X-ray data, magnetic and optical observations. The magnetic anisotropy of urea nitrate and urea oxalate is approximately additive, but that of cyanuric acid dihydrate is considerably larger than the additive value for three urea molecules, being comparable with that of other cyanuric ring compounds. Although the molecules in each layer must be joined together by hydrogen bonds, it does not follow that hydrogen bonds form the links between successive layers, since the layer to layer distance of 3·05 ± 0·10 A is characteristic even of cyanuric triazide, which contains no hydrogen bonds.

## Urea

Urea or carbamide, $CO(NH_2)_2$, crystallizes from water in long colourless prisms, melting at 132°·7 C. These belong to the tetragonal scalenohedral class and the crystal structure has been investigated in detail (Mark and Weissenberg 1923; Hendricks 1928, Wyckoff 1931, 1933, Wyckoff and Corey 1934). The oxygen atom of one molecule approaches within 3 A of the amino-end of the next, the carbon-nitrogen distance (1·37 A) in the molecule is intermediate between the normal single-bond and the double-bond distances, and is comparable with those in the cyanuric ring (Knaggs 1935), while the carbon-oxygen distance (1·25 A) is the same as that in the carbonate group (Ewald and Hermann 1931, 1937). This is consistent with a structure in which molecules which are resonance hybrids of the forms

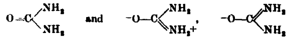

I    II

are linked together by hydrogen bonds. The tautomeric form

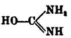

$$HO{-}C\begin{array}{l}\diagup NH_2\\ \diagdown\!\!\!\diagdown NH\end{array}$$

III

and the alternative zwitterion forms

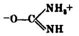

$$^{-}O{-}C\begin{array}{l}\diagup NH_2{}^{+}\\ \diagdown\!\!\!\diagdown NH\end{array}$$

IV

may also exist, although these would be expected to involve a rather larger carbon-oxygen distance than is actually found. It has been suggested by Clow (1937) that forms IV are more in accordance with the known mean diamagnetic susceptibility, but this argument is based on the applicability of the additive rule. In the case of resonance structures, however, the additive rule is not reliable, owing to the fact that 'molecular orbitals'—electrons whose probability density is distributed over the whole molecule—introduce a large extra susceptibility normal to the atomic plane, whose value depends on the nature of the resonance and the size of the molecule. A further unknown factor, not hitherto allowed for, is the possible contribution of the hydrogen bonds to the mean susceptibility (Angus and Hill 1940). Since these hydrogen bonds are highly directive, it does not seem probable that their individual magnetic susceptibility, if any, would be isotropic, although their joint contribution to the crystal susceptibilities might be In any case, the susceptibility of the molecule will not be isotropic and therefore measurements of the magnetic anisotropy of the crystal may be expected to provide further useful information on the subject of molecular structure.

### *Magnetic anisotropy of urea*

The mean susceptibility of urea has been independently measured by Pascal (1912), Devoto (1932) and Clow (1937). Their values agree closely, $-33{\cdot}60$. $-33{\cdot}40$ and $-33{\cdot}66$, giving a mean value $-33{\cdot}55$ ($\times 10^{-6}$).

The magnetic anisotropy of the crystals was qualitatively observed by V. v. Lang (1899), who stated that the diamagnetism was weakest along the principal axis (see also Bhagavantam 1929). This is correct, measurements on a number of good crystals (mass of largest 5·50 mg., density 1·333 g./c.c. at 21°/4° C) in a field of about 7000 oersted, using a quartz fibre long and fine enough to take a torsion of up to 6½ complete rotations for a 45° deflexion of the crystal, give the value

$$\chi_c - \chi_a = 2{\cdot}57 \times 10^{-6}.$$

Hence $$\chi_a = -34{\cdot}41 \times 10^{-6}, \quad \chi_c = -31{\cdot}84 \times 10^{-6}.$$

The molecular planes are parallel to the {110} crystal planes, and hence the susceptibilities of a single molecule in and perpendicular to the plane of the atoms are

$$K_\parallel = -31{\cdot}84 \times 10^{-6}, \quad K_\perp = -36{\cdot}98 \times 10^{-6},$$

giving an anisotropy of $5{\cdot}14 \times 10^{-6}$.

This value is comparable with the magnetic anisotropy of the carbonate and nitrate groups, which varies from 4·0 to 5·1 in different compounds (Krishnan, Guha and Banerjee 1933). In the carbonate and nitrate compounds investigated there were no hydrogen bonds, while the arrangement of hydrogen bonds in urea is such that it does not seem probable that they would contribute appreciably to the *crystal* anisotropy. The observed anisotropy in each case, therefore, is a consequence principally of the resonance in the molecule. It may be concluded that the resonance in $CO(NH_2)_2$ is of the same order as that in $CO_3^=$ or $NO_3^-$.

### *Optical anisotropy of urea*

The optical constants of crystalline urea have been measured a number of times, the results being given below in the form of a table (all data referred to Na 589):

| $\mu_\omega$ | $\mu_\epsilon$ | |
|---|---|---|
| 1·485 | 1·61 | Bolland (1908, 1910) |
| 1·484 | 1·602 | Whorry (1918) |
| 1·4743 | 1·6005 | Moore and Gatewood (1923) |
| 1·485 | 1·600 | Mayrhofer, Herzig and Lander (1926) |

The fact that the birefringence is positive is a direct consequence of the crystalline 'chain structure'. The optical anisotropy of the molecule itself is negative. In the following table the molecular refractivities,

$$R = \frac{M}{\rho}\frac{\mu^2-1}{\mu^2+2},$$

of the different groups are compared, allowance being made for the refractivities of the initial atoms in the carbonates and nitrate (Wasastjerna 1923; W. L. Bragg 1924; Pauling 1927) and for the crystal arrangement in urea.

| | | | | Crystal | | Group | | |
|---|---|---|---|---|---|---|---|---|
| | $\mu_\omega$ | $\mu_\epsilon$ | $\rho$ | $R_\omega$ | $R_\epsilon$ | $R_{\omega'}$ | $R_{\epsilon'}$ | |
| $CaCO_3$ (calcite) | 1·658 | 1·486 | 2·75 | 13·31 | 10·37 | 11·32 | 8·38 | $CO_3^=$ |
| $CaCO_3$ (aragonite) | 1·686<br>1·681 | 1·530 | 2·94 | 12·91 | 10·51 | 10·92 | 8·52 | |
| $NaNO_3$ | 1·585 | 1·336 | 2·256 | 12·62 | 7·81 | 12·16 | 7·35 | $NO_3^-$ |
| $CO(NH_2)_2$ | 1·482 | 1·604 | 1·335 | 12·82 | 15·47 | 15·47 | 10·17 | $CO(NH_2)_2$ |

The relatively large refractivity of the urea molecule, especially in its own plane, in spite of the increased distance between C and $NH_2$ as compared with the C-O distance in the carbonate group, clearly indicates that the $NH_2$ group is much more polarizable than the oxygen ion.

### UREA NITRATE

Urea nitrate, $CO(NH_2)_2.NO_3H$, forms monoclinic prismatic crystals from hot water. These are tabular on {001}, with {010} {110} {100} as side faces. There is a perfect cleavage parallel to the basal plane (001) and the crystals bend rather easily in this plane. They frequently twin by reflexion across (001), simulating orthorhombic symmetry. Barker (1911) has given the goniometric data $a:b:c = 0{\cdot}9965.1:0{\cdot}9142$, $\beta = 75°\,2\frac{1}{2}'$, but he has chosen a different $a$ axis, which makes the cleavage plane {101}. In view of the structural importance of the cleavage plane, it seems preferable to retain the earlier nomenclature (v. Lang 1862; Gaubert 1907), in which case the crystallographic constants given by Barker would become

$$a:b:c = 1{\cdot}1656:1:0{\cdot}9142, \quad \beta = 124°{\cdot}3.$$

X-ray photographs and magnetic and optical measurements all strongly indicate a layer structure, in which the molecules are parallel or nearly parallel to (001), the cleavage plane. Laue, rotation and Weissenberg photographs have been taken. The unit cell dimensions found are $a = 9{\cdot}50$, $b = 8{\cdot}20$, $c = 7{\cdot}54$ A, $\beta = 124°$. The density, determined by the suspension method in a mixture of ethyl iodide and alcohol, is 1·690 g /c.c. at 20°/4° C, and there are therefore four molecules in the unit cell. The following reflexions are missing: ($h0l$) if $l$ is odd, ($0kl$) if $k$ is odd, and in addition ($h0l$) reflexions are very weak when $h$ is odd. The space-group must be $P2_1/c$, the similarity in scattering power of $CO(NH_2)_2$ and $NO_3H$ probably accounting for the absence or weakening of reflexions whose absence would not be required from space-group considerations alone. The (002) plane, spacing

3·13 A, gives the most intense reflexion in the crystal, and in Laue photographs given a strong exposure the (00$l$) reflexion is accompanied by a very large intense diffuse spot in the (002) position (figure 1, plate 7). This is typical of layer structures, as may be seen by a comparison with the Laue photograph of hexamethylbenzene (figure 2, plate 7), in which the large diffuse spot corresponds to the (001) plane, parallel to which there are layers of flat molecules separated by the van der Waals' distance 3·66 A (Lonsdale 1929*a*, *b*; Brockway and Robertson 1939).

The fact that the (002) plane is not only a 'layer' plane, of moderately small spacing, but also grows as the main face on large crystals, and can in addition be bent to form a curved surface, makes this substance an excellent monochromator, giving an intense secondary beam well separated from the primary radiation. It has been used in this way in this laboratory and previously by Mr R. D. Preston (1939) at the National Physical Laboratory.

### *Magnetic anisotropy of urea nitrate*

Magnetically the crystals are nearly uniaxial, with the maximum diamagnetic susceptibility $\chi_2$ as nearly as can be measured normal to (001).

$$\chi_2 > \chi_1 > \chi_3 \quad (\chi_3 \text{ is along } b),$$

$$\chi_3 - \chi_2 = 8{\cdot}13 \times 10^{-6}, \quad \chi_1 - \chi_2 = 7{\cdot}05 \times 10^{-6}, \quad \chi_3 - \chi_1 = 1{\cdot}09 \times 10^{-6}.$$

A determination of absolute susceptibility was made by the Rabi-Krishnan method, using (ethyl iodide + alcohol) and (ethyl iodide + alcohol + $NiCl_2.6H_2O$) as the balancing liquids The value obtained for $\kappa_{\min}$ was $-0{\cdot}68_0 \times 10^{-6}$ ($\pm 0{\cdot}01_0$) at 20° C for crystals of density 1·690 g /c.c., so that

$$\chi_1 = -50{\cdot}6 \times 10^{-6}, \quad \chi_2 = -57{\cdot}6 \times 10^{-6}, \quad \chi_3 = -49{\cdot}5 \times 10^{-6}.$$

The mean susceptibility, $\bar{\chi} = -52{\cdot}6 \times 10^{-6}$. The sum of the mean susceptibilities of urea ($-33{\cdot}55$) and of $HNO_3$ ($-19{\cdot}2$; Pascal (1910) corrected to $\kappa_{H_2O} = -0{\cdot}72 \times 10^{-6}$) is $-52{\cdot}75$. The excellence of the agreement indicates that there is no resonance between the urea and nitrate groups, but only in the separate groups, and that the hydrogen bonds do not contribute appreciably to the mean susceptibility.

### *Optical anisotropy of urea nitrate*

V. v. Lang (1862) gives the following optical data: Strong negative double refraction, optic axial plane (010), acute bisectrix normal to (001). $2E = 21° 10'$ (red), $23° 10'$ (yellow), $24° 30'$ (green), $26° 30'$ (blue). These are easily verified qualitatively on cleavage slips. Hence $\alpha$ is perpendicular to (001), $\beta$ along $b$, $\gamma$ along $c$. Since $E = 11^\circ 35'$ (Na) and

$$\sin^2 E = \frac{\alpha(\gamma^2 - \beta^2)}{\gamma^2 - \alpha^2},$$

there can only be a very small difference between $\beta$ and $\gamma$.

## UREA OXALATE

Urea oxalate, $2CO(NH_2)_2 . C_2H_2O_4$, crystallizes from hot water in monoclinic prisms, platy on $\{010\}$, bounded by $\{110\}$ or $\{120\}$, $\{011\}$, $\{11\bar{1}\}$, $\{001\}$ and $\{20\bar{1}\}$ (Loschmidt 1865). There is a perfect cleavage parallel to $\{20\bar{1}\}$ which, however, is only a minor face on the crystals. The crystallographic data given by Loschmidt are $a:b:c = 0{\cdot}5642:1:0{\cdot}4106$, $\beta = 97^\circ 50'$. X-ray measurements of the unit cell give $a = 7{\cdot}02$, $b = 12{\cdot}42$, $c = 5{\cdot}08$ A.

The density, measured by the suspension method, is $1{\cdot}58_6$ g/c.c. at 21°/4° C, and hence there are two molecules of molecular weight 210·05 in the unit cell. [These X-ray data incidentally prove that there is no water of crystallization.] The absent reflexions are $(h0l)$, where $h$ is odd, and $(0k0)$, where $k$ is odd; the space-group, therefore, is $P\,2_1/a$. The reflexion from $(20\bar{1})$, spacing 3·10 A, is the most intense observed, and on Laue photographs taken with the crystal suitably placed there is a very large diffuse spot corresponding to the position of the $(20\bar{1})$ reflexion by monochromatic radiation (figure 3, plate 7). This crystal also, therefore, must possess a layer structure; the molecules lie parallel to $(20\bar{1})$ and are linked together by means of hydrogen bonds.

### *Magnetic anisotropy of urea oxalate*

The maximum diamagnetic susceptibility, $\chi_2$, is exactly normal to $(20\bar{1})$ Measurements on a large crystal weighing nearly 15 mg gave $\chi_2 > \chi_1 > \chi_3$, $\chi_1 - \chi_2 = 12{\cdot}54 \times 10^{-6}$, $\chi_3 - \chi_2 = 15{\cdot}80 \times 10^{-6}$, $\chi_3 - \chi_1 = 3{\cdot}27 \times 10^{-6}$.

The absolute susceptibility of urea oxalate was not determined; in every mixture of solutions tried, some chemical action was found to take place which changed the oxalate so that a gradually changing value of the susceptibility was found. A sufficient quantity of the material was not available for the powder method to be used.

The exact value of the magnetic anisotropy of a single molecule cannot be determined, either for urea nitrate or for urea oxalate, until the precise orientation of the molecules is known. If, however, we assume that the separate groups are magnetically uniaxial, an assumption known to be nearly true for $C_2H_2O_4$ (Lonsdale 1938) and probably true also for $CO(NH_2)_2$

and $HNO_3$, then it is possible to make a reasonable estimate of the anisotropy. The minimum molecule susceptibility must be either equal to, or less than, the minimum crystal susceptibility, and the molecule anisotropy will be equal to, or greater than, $[(\chi_3 - \chi_1) + (\chi_3 - \chi_2)]$. Thus for urea nitrate the molecule anisotropy will be at least 9·22, and for urea oxalate it will be at least 19·07( $\times 10^{-6}$). The tilt of the groups to the cleavage plane will be (for each substance) of the order of 20° to 25°. On the basis of existing measurements of the anisotropy of $CO(NH_2)_2$, $NO_3$ and $C_2H_2O_4$, the probable anisotropy of the urea nitrate molecule and the urea oxalate molecule respectively would be

$$5{\cdot}14 + 4{\cdot}89 = 10{\cdot}03\ (\times 10^{-6}) \quad \text{and} \quad 2(5{\cdot}14) + 9{\cdot}47 = 19{\cdot}75\ (\times 10^{-6}).$$

### *Optical anisotropy of urea oxalate*

Gaubert (1907, footnote on p. 380) reports that the optic axial plane is (010) and the acute bisectrix normal to $(20\bar{1})$. This has been verified on the crystals used; the birefringence is strongly negative, with $\beta$ along $b$, $\alpha$ normal to $(20\bar{1})$ and $\gamma$ parallel to $(20\bar{1})$ and (010). The optic picture seen in $(20\bar{1})$ is almost indistinguishable from that of urea nitrate in its cleavage plane, the optic axial angles having, as nearly as can be judged, almost the same value in the two substances.

## CYANURIC ACID DIHYDRATE

Cyanuric acid dihydrate, $C_3N_3O_3H_3 . 2H_2O$, may exist in two possible forms

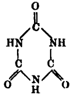

I

and

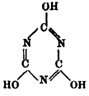

II

The first form can only involve a cyanuric ring in the zwitterion state

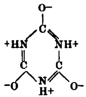

III

It forms monoclinic prismatic crystals from hot water, for which (Billows 1907*a*, *b*) $a : b : c = 1{\cdot}3694 : 1 : 1{\cdot}8502$, $\beta = 106° 4\tfrac{1}{2}'$. These are platy on {001}, elongated on *b*, and have side faces {101} {100} {10$\bar{1}$} {110} {011} {112}. There is a perfect cleavage on {101}, imperfect on {001}. X-ray measurements have not yet been made, on account of the instability of small crystals.

### *Magnetic anisotropy of cyanuric acid dihydrate*

The maximum diamagnetic susceptibility, $\chi_2$, is almost normal to (101). The crystals deteriorate rapidly in air, probably through the loss of some water of crystallization, and in breaking up they become more and more isotropic. The measurements of anisotropy are not, therefore, very accurate, but probably err on the side of being too small. The best measurements gave $\chi_1 - \chi_2 = 24{\cdot}2 \times 10^{-6}$, $\chi_3 - \chi_2 = 23{\cdot}9 \times 10^{-6}$. $\chi_1 - \chi_3$ was not measurable: $\chi_2 > \chi_3 \fallingdotseq \chi_1$. $\psi$ (angle $\chi_1 : c$, positive in obtuse $\beta$) $= -31^\circ{\cdot}1$. The angle $(101):(100) = 30^\circ{\cdot}5$.

The absolute susceptibility of cyanuric acid was not determined because in all the solutions tried the crystals quickly became cloudy, probably due to partial dehydration.

### *Optical anisotropy of cyanuric acid dihydrate*

Cleavage fragments show strong negative birefringence of the same order as that of urea nitrate or urea oxalate: $\beta$ is along *b*, $\alpha$ normal or almost normal to (101), $\gamma$ parallel to (101) and (010).

### *Discussion of structure*

The magnetic and optical observations again show that the structure is of a layer type, with the molecules parallel to the (101) planes The magnetic anisotropy is of the same order as that of other cyanuric ring compounds (cyanuric triazide $21{\cdot}9 \times 10^{-6}$, Lonsdale 1937, melamine, $C_3N_6H_6$, $21{\cdot}1_5 \times 10^{-6}$, Knaggs and Lonsdale 1940) and is larger than would be expected for molecules of form I alone. Cyanuric acid dihydrate can be synthesized from urea by strong heating, but the anisotropy is considerably larger than that of three molecules of urea, which would be $5\;14 \times 3 = 15{\cdot}4$ ($\times 10^{-6}$). The structure most strongly indicated by the magnetic data is therefore a resonance structure based on form II, the molecules being bound together in the crystal by hydrogen bonds

*Anhydrous cyanuric acid* has been examined by X-ray methods by Wiebenga and Moerman (1938), who found a pseudo-rhombic unit cell, the monoclinic angle being 90°. Here also the molecules are arranged in layers parallel to the (101) planes. There is a perfect cleavage and strong negative birefringence, the acute bisectrix being normal to (101). The cleavage planes (202) are 2·97 A apart. It is tempting to suppose, in view of this distance, that there are hydrogen bonds not only between molecules in one layer, but also between molecules in successive layers. That this is not necessarily the case, however, is shown by the fact that in cyanuric triazide the distance between successive layers of molecules is also 2·98 A (Knaggs 1935), although in this structure there are no hydrogen bonds. All cyanuric ring compounds so far examined possess layer structures.

I am very much indebted to Sir William Bragg and to the Managers of the Royal Institution, in whose laboratories this work was carried out; also to Dr I. E. Knaggs and Mr H. Smith who assisted with the X-ray experimental work, and to Professor A. Lowenbein, who synthesized the urea oxalate for me.

## REFERENCES

Angus and Hill 1940 *Trans. Faraday Soc.*, Hydrogen Bond Discussion **36**, **923**.
Barker 1911 *Min. Mag., Lond* . **16**, 207.
Billows 1907*a* *Riv. Min. ital.* **33**, 88.
— 1907*b* *Z. Kristallogr.* **46**, 481.
Bhagavantam 1929 *Indian J. Phys.* **4**, 1.
Bolland 1908 *Mh. Chem.* **27**, 965.
— 1910 *Mh. Chem* **31**, 387.
Bragg, W L. 1924 *Proc. Roy. Soc* A, **105**, 384.
Brockway and Robertson 1939 *J. Chem Soc.* p. 1324.
Clow 1937 *Trans. Faraday Soc* **33**, 384.
Devoto 1932 *R.C. Accad. Lincei*, **15**, 973.
Ewald and Hermann 1931 *Strukturbericht*, **1**, 617.
— — 1937 *Strukturbericht*, **3**, 660.
Gaubert 1907 *C.R. Acad Sci , Paris*, **145**, 378.
Hendricks 1928 *J. Amer. Chem Soc.* **50**, 2455.
Knaggs 1935 *Proc. Roy Soc.* A, **150**, 576
Knaggs and Lonsdale 1940 *Proc. Roy Soc* A, **177**, 140.
Krishnan, Guha and Banerjee 1933 *Phil. Trans.* A, **231**, 235.
v. Lang 1862 *S B. Akad. Wiss Wien*, **45**, 118
— 1899 *S.B. Akad. Wiss. Wien*, **108**, 557
Lonsdale 1929*a* *Proc Roy. Soc.* A, **123**, 494.
— 1929*b* *Trans. Faraday Soc* **25**, 352.
— 1937 *Proc. Roy. Soc.* A, **159**, 149.
— 1938 *J. Chem. Soc* p. 364.
Loschmidt 1865 *S.B. Akad. Wiss. Wien*, **51**, 9.
Mark and Weissenberg 1923 *Z Phys.* **16**, 1.
Mayrhofer, Herzig and Lander 1926 *Pharm. Mh* **4**, 7.
Moore and Gatewood 1923 *J. Amer. Chem. Soc.* **45**, 144.
Pascal 1910 *Bull. Soc. Chim. Fr.* **7**, 50.
— 1912 *Ann. Chim. (Phys.)*, **25**, 355.
Pauling 1927 *Proc. Roy Soc.* A, **114**, 181.
Preston 1939 *Proc. Roy Soc* A, **172**, 116.
Wasastjerna 1923 *Comment Phys. Math., Helsingf.* **1**, 37.
Wherry 1918 *J. Wash. Acad. Sci.* **8**, 277, 319.
Wiebenga and Moerman 1938 *Z. Kristallogr.* **99**, 217.
Wyckoff 1931 *Z. Kristallogr.* **81**, 102.
— 1933 *Z. Kristallogr.* **85**, 132.
— and Corey 1934 *Z. Kristallogr.* **89**, 462.

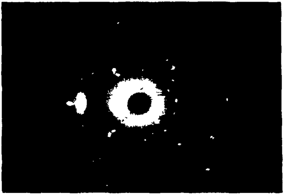

**Figure 1.** Urea nitrate. Laue photograph showing diffuse spot due to (002)

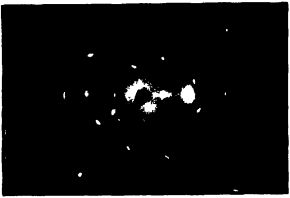

**Figure 2.** Hexamethylbenzene. Laue photograph showing diffuse spot due to (001).

**Figure 3** Urea oxalate. Laue photograph showing diffuse spot due to (201)

# The distribution of electricity in thunderclouds, II

By Sir George Simpson, K.C.B., D.Sc., F.R.S., and
G. D. Robinson, Ph.D.

(*Received* 10 *September* 1940)

The investigation of the distribution of electricity in thunderclouds described by Simpson and Scrase in 1937 has been continued at Kew Observatory. Alti-electrographs, which record the sign of the potential gradient, are sent up on small free balloons. Additional observations made during eight thunderstorms in the years 1937, 1938 and 1939 are discussed and the conclusions reached by Simpson and Scrase are confirmed. Each thundercloud has positive electricity in the upper half of the cloud, negative electricity in the lower half and in most storms if not in all there is a concentrated positive charge below the main negative charge. The generation of the positive and negative charges in the main body of the cloud is ascribed to the impact of ice crystals and that of the positive electricity in the base of the cloud to the breaking of rain drops in an ascending current of air.

Observations on the distribution of electricity in thunderclouds, in continuation of the work described by Simpson and Scrase in a paper published in these *Proceedings* in 1937 (referred to hereafter as S. and S.), have proceeded at Kew Observatory during the three years 1937–9.

These years proved to be very different in their production of thunderstorms at Kew and on the whole rather disappointing. In 1937 there were thunderstorms on eight days and thirty-five soundings were made, but the number of failures was unduly large; the records from five storms are available for discussion. The year 1938 was remarkably dry at Kew and only four storms were suitable for investigation; two of these were so slight that the records showed no measurable fields; thus only two storms from 1938 are available for discussion In 1939 there were only three suitable storms at Kew; two of these were very short, and sufficient data for useful discussion were not obtained. Table 1 gives the results of the three years' work.

Table 1

| | |
|---|---|
| Legible records | 38 |
| Records with fields too small to measure | 6 |
| Defective records | 14 |
| Records not recovered | 4 |
| Total number of soundings | 62 |

Before proceeding to describe the results of the soundings the following short recapitulation of the previous paper will help the reader to understand the new work. The alti-electrograph makes two records against time

(*a*) a record of the sign of the vertical electrical field, and

(*b*) a record of the atmospheric pressure, from which heights can be determined.

The electrical record is obtained by two electrodes about 3 mm. apart, resting on a disk of pole-finding paper which is rotated by a small clock. One electrode is connected to the case of the instrument and the other to an insulated wire about 25 m long trailing below the balloon. In a strong electric field a small current passes between the electrodes and a stain is produced on the disk below the positive electrode. When the field reverses the stain is produced under the other electrode. Thus at any time the direction of the field, if above a certain minimum value, can be read off from the disk. The width of the stain varies according to the strength of the current and therefore to some extent according to the strength of the electric field. A formula is given in S. and S. connecting the width of the stain with the strength of the field producing it.

The height of the balloon at any time could be determined from the pressure record if the temperature of the air were known. As temperatures at the balloon were not recorded this method was not available, and instead use was made of the known mean variation of pressure with height appropriate to the season. Dines meteorographs, which give records of both pressure and temperature, were attached to the alti-electrographs in two of the soundings, and a comparison of the heights determined by the two methods showed sufficiently good agreement.

The height having been determined in the way described, the approximate temperature at each height was found by assuming that below the cloud the lapse rate was the mean between the dry and saturated adiabatic lapse rates, while within the cloud the saturated adiabatic lapse rate was adopted.

The results of the soundings have been plotted on eight diagrams (figures 4–11). In the upper parts of the diagrams the ordinates are height and the abscissae time. In the first five diagrams each sounding is represented by a band erected vertically above the time at which the sounding commenced. The width of the band is proportional to the width of the trace on the original alti-electrograph record and to differentiate between positive and negative fields, the band is cross-hatched in the former case and left unhatched in the latter. The thickness of the trace is roughly proportional to the potential gradient, but the relationship between them is not simple, depending on a number of factors amongst which is the atmospheric pressure, so that the same thickness of trace represents a greater potential gradient near the ground than it does at greater elevations. The relationship between the thickness of the trace and the potential gradient was discussed at length in S. and S. and we have nothing to add to that discussion. At the same time the values of the potential gradient deduced in the manner there described cannot be accepted with confidence, and we have considered it best in this paper to use qualitative terms in describing the potential gradient and not to use actual values which might be quoted without the necessary reservations.

In the diagrams the base of the cloud, determined by observing the time the balloons entered the cloud, has been indicated by a line. Unfortunately, we have been unable to obtain data on which to locate the upper limits of the clouds as was done to some extent in S. and S. When, as the result of the analysis of the records, it has been possible to locate the position of charges in the clouds these have been indicated by groups of plus and minus signs. Most of these charges are located by the reversal of the field, in which case the volume charges are centred approximately about the point of reversal on the records; but in some cases, especially with the low positive charges, the exact position of the charge cannot be determined, and in these cases the group of plus signs has been enclosed in a dotted circle to indicate the indeterminate position of the charge.

In the last three diagrams (figures 9–11), the soundings have been plotted in a different way, which will be described when these storms are considered.

In the lower part of the diagrams there are two curves using the same time scale. The upper reproduces the potential gradient at the ground recorded at the Observatory. The potential gradient records generally start when the field at the ground exceeded 10 V/cm. and end after the storm has passed away. Most of the potential gradient records are much disturbed by the changes of field due to lightning discharges. A lightning flash usually causes an instantaneous change in the field, and then the field returns to its pre-discharge value at a relatively slow rate. It is difficult to say whether the mean potential gradient at the ground should be defined as the mean potential gradient taking the disturbed field due to the lightning "throws" into account or the mean value of the pre-discharge field. The difference may be very large, in some cases even changing the sign of the gradient (cf. the period 17.10–17.20 in figure 7 where the pre-discharge field is negative and the mean field positive). In this work the disturbed fields have been neglected and the potential gradient has been determined from the pre-discharge values.

The third and lowest curve in the diagrams gives the record of the electricity carried down by the rain. During most of the storms for which soundings are available records of the electricity of the rain were obtained at the Observatory. The instrument used, which was fully described by Scrase (1938), consists in principle of an insulated receptacle into which the rain falls. This receptacle is connected to an electrometer, the deflexion of which measures the charge received. After 3 c.c. of rain (representing a fall of 0·15 mm. of rain) have been collected the receptacle is automatically connected to earth and the electrometer discharged. During steady rain carrying a preponderance of charge of one sign the record consists of a sloping line, the amount and direction of the slope being a measure of the amount and sign of the electricity carried by the rain. Every time the receptacle is connected to earth after receiving 3 c.c. of rain the deflexion of the electrometer returns to zero and a mark is made on the photographic trace. The number of these marks in a given time is a measure of the average rate of rainfall during that time. Copies of the records have been reproduced for all the storms for which they are available, a scale being added which gives the total charge carried by each 3 c.c. of rain.

The results of the ascents made during 1934, 1935 and 1936, described in S. and S., led to the conclusion that a thundercloud has a positive charge in the upper layers, a negative charge in the lower layers and very frequently a region of positive charge in the base, below the negative charge. As the presence of a positive charge in the upper part of a thundercloud and of a negative charge in the lower part had already been deduced by C. T. R. Wilson and others from observations of the changes in the electrical field at ground level due to lightning discharges, the existence of these charges is now generally accepted, but several writers have questioned the reality of the low positive charge in the base of the cloud. The following quotation states the case:

> An interesting new attack on the problem has recently been made by Simpson and Scrase, who obtained records of the variation of potential gradient with height through a thundercloud by means of an apparatus attached to a sounding balloon. They confirmed in striking fashion that the upper part of a thundercloud is always positively charged and the main portion of the base negatively charged. They, however, also obtained a few records which were interpreted as indicating a positively charged region in the base of the cloud. The evidence consists essentially in the fact that in the few cases when a balloon was released beneath a storm in a region of positive potential gradient, the gradient never remained positive all the way up to the positive charge at the top of the cloud. While the existence of a positive charge near the base of the cloud is the most direct and perhaps the most natural interpretation of such a record, such a conclusion is by no means inevitable. In the first

> place, the balloon takes about 30 minutes to rise through the cloud and thus the temporal variations of the charges have not been eliminated. Secondly the path of the balloon in the cloud is unknown and may suffer considerable horizontal displacement relative to the cloud. It would seem, for example, that a balloon released in the region of positive gradient near the front of an advancing simple cloud of positive polarity would be carried horizontally by the air currents converging on the region of active separation of charge and might well reach a point where negative gradient existed and, indeed, extended right to the ground. In such a case the record would give all the effects interpreted as a positive charge in the base of the cloud....The regular occurrence of positive charge in the base of the cloud cannot therefore, be considered to be yet established with certainty (Wormell 1939, p. 300).

The difficulties met with in interpreting the records obtained by alti-electrographs, which give the potential gradient as a function of height and time only, was realized when S. and S. was written and they were discussed in detail on p. 324 of that paper. The authors were well aware of the complications produced by the temporal changes in the distribution of the electricity, which may be very large and rapid in a thunderstorm, and by the movement of the balloons in a horizontal direction; but they were convinced that the positive charge they found in the lower parts of the thunderclouds could not be explained in the way described in the above quotation, and a re-examination of all the records has confirmed this conclusion. It is possible that in the previous paper sufficient attention was not paid to the effects of the horizontal travel of the balloons and to changes of field due to distant charges of electricity, but in this paper, while retaining the previous method of presentation, an effort will be made to discuss in more detail the effects of these factors.

It will greatly help the reader if he has a clear image of the vertical electrical fields associated with the distribution of electric charges which the observations show to exist within a thunderstorm. We propose, therefore, to discuss in some detail the fields associated with a typical thunderstorm. It is hoped to confirm in this paper the conclusions reached in S. and S. that in most, if not in all, thunderstorms there is a positive charge in the upper half of the cloud, a negative charge in the lower half and a positive charge localized under the negative charge. We have therefore built up a model thunderstorm with this distribution of charge and calculated the vertical fields in its neighbourhood. Vertical fields are considered, as the alti-electrograph measures only this component.

In actual thunderstorms the vertical and horizontal extent of the regions containing the charges vary from storm to storm: if the vertical and horizontal dimensions of a charged volume are about equal, the charge may be conveniently represented as being contained within a sphere; but in some cases the two upper charges have a greater horizontal than vertica extent and would be more correctly represented by disks than spheres. As, however, the calculation of fields due to charged disks is very arduous, and as it will be seen that spheres represent sufficiently well the conditions in many storms, we have adopted spheres in our model storm. In figure 1 the vertical field associated with these charged spheres is represented.

To facilitate description the positive charge at the top of the cloud, the negative charge below it, and the positive charge in the base of the cloud will be designated by the letters $P$, $N$, and $Q$ respectively. In figure 1 $P$ is 24 coulombs of positive electricity uniformly distributed throughout a sphere of 2 km. radius centred at a height of 6 km., $N$ is a negative charge of 20 coulombs in a sphere of 1 km radius centred at a height of 3 km., and $Q$ is a positive charge of 4 coulombs in a sphere of $\frac{1}{2}$ km. radius centred at a height of $1\frac{1}{2}$ km. These heights are comparable with those which have been found in a typical thundercloud, and the quantities of electricity have been chosen to give a positive potential gradient of plus 40 V/cm. under the centre of the storm, a negative potential gradient of minus 60 V/cm. at 1·5 km. from the centre and positive potential gradient at all distances greater than 4·2 km. from the centre, potential gradients of this order are usually found near thunderstorms. The potential gradient at the ground at all distances from the central axis of the storm is shown by the curve at the bottom of figure 1.

The lines in the diagram represent lines of equal vertical potential gradient and are drawn at intervals of 100 V/cm., lines at multiples of 500 V/cm. being thickened. Table 2 contains the values of the vertical potential gradient at the points of maximum along the central axis—these values are also the values of the total electrical force at the points, as along the axis the direction of the total force is everywhere vertical

TABLE 2 *Vertical potential gradient at points on the axis*

| km. | | V/cm. |
|---|---|---|
| 8 | Top of $P$ | − 480 |
| 4 | Bottom of $P$ and top of $N$ | 2280 |
| 2 | Bottom of $N$ and top of $Q$ | −3110 |
| 1 | Bottom of $Q$ | 1070 |
| 0 | Surface | 40 |

Along the lines $AA$, $BB$, $CC$, of figure 1 the vertical force is zero, these lines therefore mark off the regions of positive from negative potential gradient. The gradient is positive below the line $CC$ and between the lines $AA$ and $BB$; it is negative between the lines $CC$ and $BB$ and above $AA$.

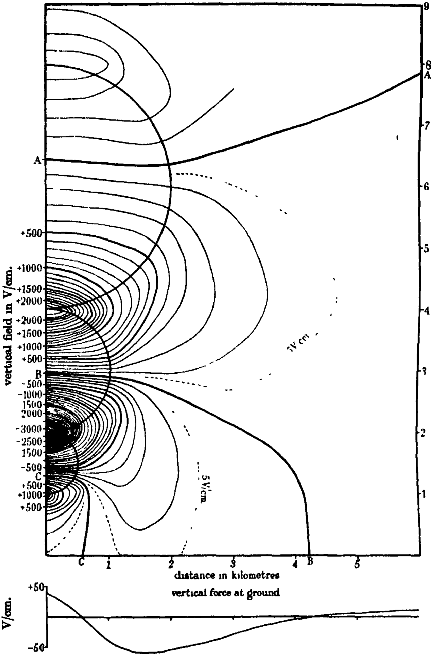

FIGURE 1. Isopleths of vertical field. Charges: 24, −20, and 4 coulombs in upper, middle, and lower spheres respectively.

It will be convenient to refer to the positive field between the lines *AA* and *BB* as the *P* field, the negative field between *BB* and *CC* as the *N* field and the positive field below *CC* as the *Q* field; while the negative field above the line *AA* will be referred to as the *U* field.

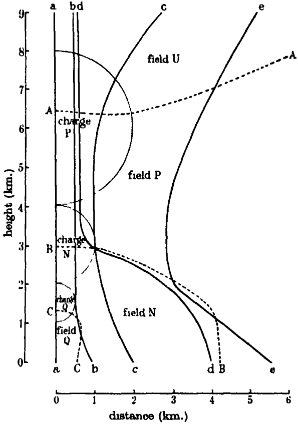

FIGURE 2. Representative tracks of balloons.

With such a symmetrical distribution of electricity the maximum field strength occurs on the axis where the spheres meet and these values are given in table 2. The greatest value is −3110 V/cm., which is less than the field necessary to produce an electrical discharge in air (taken to be 10,000 V/cm. as water or ice particles are present). Sparking values, however, would be reached with the same total charges by concentrating the charges instead of distributing them equally over the spheres. It is very probable that this is the actual way in which lightning discharges are initiated, irregularities in the air currents bringing oppositely charged masses of air or precipitation into close proximity, causing a local increase in the general high field and so producing locally a sufficiently high field for the discharge to commence.

We can now study the kind of alti-electrograph records which would be obtained in the neighbourhood of such a storm. The records will vary according to the positions of the starting points relative to the centre of the storm and according to the tracks of the balloons, whether they are vertical or lead towards or away from the axis. Figure 2 shows a number of typical tracks, and in figure 3 we have plotted the field along these tracks in the same way as the alti-electrograph records are plotted. Each record is represented by a vertical band of varying width, the width being proportional to the intensity of the vertical field and the sign of the field being indicated by shading the parts of the band representing positive field and leaving it unshaded where the field is negative.

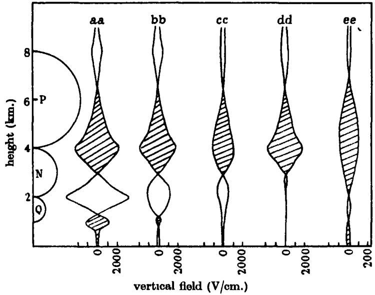

FIGURE 3. Alti-electrograph records from representative tracks.

The first record in figure 3 represents a sounding along the axis of the storm, i.e. an ascent starting at the centre of the storm and rising vertically (track *aa* of figure 2). In this case the record shows a small positive field near the ground which becomes rapidly greater as the region containing the positive *Q* charge is approached. The maximum positive field is reached on the boundary of the positive charge and then decreases towards the centre of the positive charge. The field changes sign near the centre of the positively charged sphere, but somewhat below the centre because of the strong action of the negative charge above the positive charge. The field then increases to a high negative value at 2 km. where the spheres containing the positive $Q$ charge and the negative $N$ charge meet. As the centre of the negative charge is reached the field again changes sign and becomes positive. The maximum value is again at the meeting point of the two charged spheres, above which the field decreases, changing sign some distance above the centre of the sphere containing the positive $P$ charge. From this point the field is negative, increasing to a maximum on the boundary of the sphere containing the $P$ charge and then decreasing rapidly to small values at greater heights.

The actual values of the field at the position of maximum intensity are of little importance, as these depend on the quantities of electricity which vary largely from storm to storm, but the shape of the curve representing the change of field with height (i.e. the shape of the boundary of the vertical band) is of importance. With charges spread over volumes more or less spherical, the maximum fields occur on the boundaries of the charged regions and decrease rapidly as one recedes from the boundary. This is clearly seen in the rapid decrease of the field below the $Q$ charge in the record we are considering. When therefore we see a rapid increase of field with height in the alti-electrograph records we may conclude that the balloon was then entering a charged region. This rapid change of field also explains why the field at the ground is never observed to attain anything like the intensity necessary to produce a lightning discharge.

Track *bb* of figure 2 represents the path of a balloon starting near the centre of the storm, but just outside the central region of positive potential gradient, then being drawn towards the axis of the storm. In this case the track starts in the $N$ field, but enters the $Q$ field which it traverses before entering the $N$ field again at a greater height. After this point the field changes are similar to those of track *aa* except that, as the balloon does not actually reach the axis, the fields are less intense. In S. and S. it was assumed that a reversal of the field indicated that the balloon had passed through or near a charged region, and in a record such as *bb* a negative charge would have been shown at 0·7 km. where the vertical field changes sign from negative to positive. That obviously would have been wrong, for the negative field near the ground is due to the negative charge centred at 3 km. and there is no negative charge at a height of 0·7 km.

Track *cc* is similar to track *bb* except that the balloon started at a greater distance from the centre of the storm. The track starts in the $N$ field and does not leave it until it enters the $P$ field at the level of the centre of the $N$ charge; the record, *cc*, therefore contains no positive field due to the $Q$ charge, the presence of which could not be inferred from this record.

In the model thunderstorm we are considering the potential gradient at the ground changes from negative to positive at a distance of 4·2 km. from the centre. At this distance the potential gradient is very small, and a balloon released here would record only very small negative fields as it traversed the $N$ field. If, however, after rising a certain distance the balloon is caught into a current of air blowing into the centre of the storm, it enters the strong fields near the axis. Such a track is *dd*, and the record shows little or no field until at a height of 3 km. a strong positive field is encountered. Unless one knew the path followed by the balloon this record might lead to quite erroneous conclusions, for at first sight it looks as though there were no strong fields in the lower atmosphere under the strong field at 3 km. and the presence of the $Q$ and $N$ charges might go unsuspected.

The final example, *ee*, is the track of a balloon starting in the outer positive field and being drawn into the storm at a lower level than in the previous case, but not penetrating so near to the axis The record *ee* in figure 3 (the scale of the field for this track has been increased 10 times) shows a positive field near the ground, then the usual sequence of negative, positive and negative potential gradients as the balloon traversed the $N$, $P$ and $U$ fields. In this case we have another example of a change of sign of the potential gradient without the local presence of a corresponding charge, for the positive field extending to 1·2 km. is directly due to the $P$ charge at the top of the cloud, and the change from positive to negative potential gradient is no evidence of a positive charge at 1·2 km. This track is the one visualized by Wormell in the quotation given above, and if all the records showing a low positive field were from tracks of this nature, he would be correct in saying that they gave no evidence of a low positive charge. In these examples the charges have been taken to be uniformly distributed throughout three spheres one above the other on the axis of the storm. There would have been no material change in the character of the records obtained along the tracks if the charge had been more spread out in the horizontal direction. The field due to a charged horizontal disk rapidly approaches that due to the same charge concentrated at the centre of the disk as one recedes from the edges of the disk in a horizonal direction. Thus the field due to a series of charged disks (representing in our case charged layers of cloud) is practically the same as the field we have found at 2 or 3 km. from the axis of the three spheres. At positions nearer the centre the boundaries between the vertical fields of different signs (*AA*, *BB* and *CC* in figure 1) are little changed by substituting charged disks for the charged spheres; but the maximum field on the axis is less intense and the fields do not change so rapidly in the vertical direction. Thus our discussion of the records obtained along typical tracks may be applied with very little change to a storm in which the charges are distributed in layers rather than in spheres.

In figure 1 the potential gradient at ground level is shown by a curve below the main diagram. The curve gives the potential gradient at all distances from the axis; it is therefore a potential gradient-distance diagram. If the storm represented in figure 1 passed centrally over a station and the value of the potential gradient at each instant were plotted on a diagram, the result would be a curve similar to the one at the bottom of figure 1, except that the abscissae would be time instead of distance. If the rate of travel of the storm were known, the times could be converted into distance and a curve exactly similar to that in figure 1 could be obtained. In each of the diagrams produced later in this paper a curve is given of the change of the potential gradient at the ground at Kew during the passage of each storm. By making the assumption that no large change took place in the structure of the storm as it passed over Kew, these potential gradient-time curves may be interpreted as giving the variations in potential gradient along a line through the storm. In some storms in which there are rapid developments this is by no means the case, large changes taking place during the period represented by the diagram, so that at no instant of time was the potential gradient along a line through the storm similar to the potential gradient shown in the diagram. Bearing this limitation in mind, the curves of potential gradient at the ground may be used to give a general idea of the electrical field at the ground under a storm considered stationary.

The shape of the potential gradient curve at a station over which the centre of the storm represented by figure 1 passed can easily be seen, for it would be a curve symmetrical about the centre, each half being similar to the curve at the bottom of figure 1. There would be at each end a positive portion due to the $P$ field, nearer the centre the curve would be below the base-line representing the negative $N$ field, then just before the centre is reached the curve would again cross the base-line and become positive in consequence of the $Q$ field. The low positive charge, $Q$, may not be large enough in all storms to cause the field in the centre of the storm to become positive, but a "hump" near the centre of the negative portion of the curve is a definite indication of the presence of a low positive charge; for in the absence of such a positive charge the negative portion of the curve would be at its lowest point in the centre of the storm. Typical examples of potential gradient curves having this form will be seen in figures 13, 15 and 19 of S. and S. and in figures 4, 5, 6, 7 and 10 of this paper.

## THE INDIVIDUAL STORMS

### 1. *Thundery shower*, 17 *September* 1937. *Soundings* 105 *and* 106. *Figure* 4

Thundery showers moving from the south occurred during the day 17 September 1937. One of these showers passed the Observatory between 14.45 and 16.00. During this period no lightning was seen, nor is there any trace of lightning discharges on the potential-gradient trace, but thunder was heard in the west.

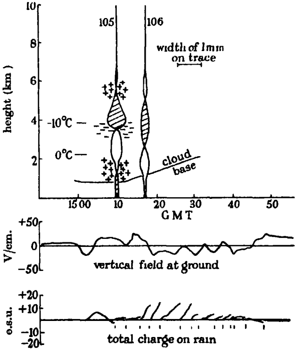

FIGURE 4. Thundery shower: 17 September 1937.

The first indication of the storm is seen on the potential gradient curve at 14.40, when positive fields greater than normal appeared. This potential gradient increased until it reached a flat maximum at about 14.54 and then decreased, passing to negative at 15.01. From this time until 15.45 the potential gradient was predominantly negative except for the period 15.03–15.17, when it became positive. After 15.45 the potential gradient remained positive, rising to a maximum at 15.49 and then slowly decreasing.

This course of the potential gradient is of the form shown in figure 1: there are two *P* fields at the beginning and end of the storm, one long *N* field divided into two parts by a *Q* field between 15.03 and 15.17; thus we should expect to find the distribution of the charge in the cloud similar to that shown in figure 1.

The first ascent, sounding 105, commenced at 15.10 when the field at the ground was positive. The record shows that the gradient was positive from the ground to 1·3 km, negative from 1·3 to 3·6 km., positive from 3·6 to 5·7 km. and then negative. Above 6 km the negative gradient rapidly decreased with height and was too small to be recorded above a height of 6·5 km.—the balloon rose to 13 km. This is exactly the sequence which we found for a balloon rising along the axis of our model storm, and record *aa* of figure 3 is similar to sounding 105. The fact that the lower positive field did not increase appreciably before changing to negative at 1·3 km. would indicate that the balloon did not actually pass through the positive charge *Q* but somewhat to the side; the height of the centre of the positive charge would therefore be somewhat higher than the point at which the field changed.

The second ascent, sounding 106, commenced at 15.17, 7 min. later than the previous one. The field at the ground was still positive but decreasing rapidly in strength. The sounding shows that the positive field extended only to a height of 0·2 km. and then gave place to a negative field which extended to a height of 2·6 km. Above this was a positive field to 5 km. and then a negative field which faded out at a height of about 6·6 km. This sequence is the same as in the previous sounding, but the fields are less strong, also in the second ascent the heights at which the field reversals took place are lower than in the previous ascent. This is what one would expect, for the first sounding was obviously nearer to the centre of the storm than the second, and the fields are stronger and the reversals higher in a track which is near the axis than in one some distance away.

There was not a great deal of rain from this storm at the Observatory; but what little fell carried a positive charge and it is difficult not to associate this positively charged rain with the positive electricity which the sounding revealed at a height of something over 1 km.

**The potential gradient at the ground and the fields within the cloud are all consistent with a distribution of electricity similar to that shown in figure 1, and the positively charged rain supports the view that the positive charge in the lower atmosphere was carried on the rain.**

2. *Thunderstorm*, 15 *July* 1937. *Soundings* 81 *and* 82. *Figure* 5

Thunder was first heard to the south-south-east and the storm moved north. Between 14.55 and 15.10 flashes of lightning were seen to the east of the Observatory. The balloons drifted east-south-east, i.e. towards the storm centre. The rain at Kew was not heavy.

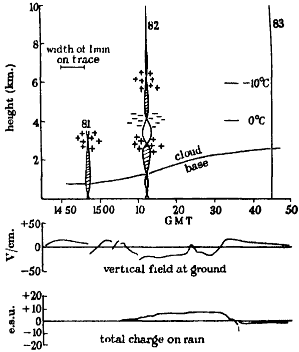

FIGURE 5. Thunderstorm 15 July 1937.

The potential gradient rose rapidly at 14.46 and remained positive, except for two reversals due to lightning discharges, until 15.06, when it became negative and remained negative until 15.30 when it changed to positive, rose to a maximum at 15.33 and then slowly decreased. From about 15.00 to the end the variation of the potential gradient reproduces the potential gradient curve shown in figure 1. There was, however, no negative potential gradient before this time. This would be explained if the positive $Q$ charge was somewhat ahead of the main negative charge, so that in front of the storm the field due to the $P$ charge and the $Q$ charge were together stronger than the field due to the $N$ charge.

Sounding 81 commenced at 14 58, half a minute after a violent lightning discharge had reversed the predominating positive field at the ground. The sounding showed a negative field just at the start; but the positive field was restored before the balloon had reached 200 m. The positive field extended to a height of 3 km. where it changed to negative. The balloon had only risen another 400 m. when it was forced down for about 1 km. after which it rose again. As there was no further electrical record after the balloon was forced down it is concluded that the trailing wire became entangled in the suspension cord or otherwise 'earthed'. The fact that the balloon was forced down indicates that it had either met heavy precipitation in the form of wet snow or had entered highly turbulent air with strong downward currents. In either case the balloon must have been near the axis of the storm, and therefore the height of the reversal of the field at 3 km. must have been near the height of the main lower positive charge. The potential gradient at the ground and the reversal of the field from positive to negative at 3 km. indicate the presence of a $Q$ charge over or near the station at that time.

Sounding 82 started at 15.14. The observers noted that the balloon moved towards the estimated centre of the storm. The potential gradient at the ground when the balloon was released was negative, and the record shows that the field met with by the balloon was predominantly negative and weak for the first 4 min. of the flight, then at a height of 1·2 km. the field changed to positive and became stronger as the ascent continued. At a height of 2·8 km. the field changed rapidly to high negative values and remained negative to 4 km., where it changed again to positive values which persisted to 6 km. Here the field finally changed to negative. The balloon rose to 16 km., but above 8 km. no measurable fields were recorded. The track of this balloon is similar to that of *bb* on figure 2, the record of which is shown on figure 3. The balloon started in the $N$ field, and drifted towards and entered the $Q$ field at a height of 1·2 km. This part of the track was near to the $N$–$Q$ boundary and therefore the field was small and occasionally reversed. On entering the $Q$ field the balloon moved nearer to the axis as it rose and so came into strong positive fields. It crossed the $Q$–$N$ boundary quite near to the centre, the height of the reversal being almost the same as that of the previous sounding. The $N$–$P$ boundary was crossed at 4 km. and the $P$–$U$ boundary at 6 km., and as the balloon was probably then not far from the axis of the storm, the heights at which the field was reversed may be taken as the heights of the centres of the charges, the heights of the $Q$, $N$ and $P$ charges in this storm may therefore be taken as 3, 4 and 6 km. respectively.

There was very little rain at the Observatory as the storm passed; but it will be noticed that positively charged rain commenced to fall, while the field at the ground was still positive and continued for a few minutes after the field had become negative. At the end of the storm there was a little negatively charged rain. This is consistent with the origin of the positive rain being connected with the formation of the $Q$ charge.

### 3. *Extensive thunderstorm* 21 *August* 1939.
### *Soundings* 127–132. *Figure* 6

The storm approached from the north-east, but owing to the available staff being wholly engaged in preparing and releasing the balloons very little detailed information about the characteristics of the storm was obtained. The balloons of the first three soundings were seen to enter smaller clouds on the advancing edge of the main cloud mass. The fourth balloon (sounding 130) was released in a rain squall which appeared to be moving from east to west, and about this time the electrical centre of the storm was estimated to be within 1 km. of the Observatory. This was the climax of the storm which then appeared to move away towards the east.

It will be seen from figure 6 that the potential gradient at the ground was highly disturbed owing to very frequent lightning discharges. On the approach of the storm the potential gradient was positive, but at about 16.00 it became negative, with lightning flashes causing positive throws. After 16.30 the trace is so disturbed by lightning discharges that it is impossible to determine whether the pre-discharge field was positive or negative. During this period the majority of the throws were positive, but there were a few throws to the negative. The pre-discharge field became definitely negative again at 17.00 and continued negative until 17.35 when it became positive, reaching its maximum at 17.39 and then decreasing in the usual way as the storm retreated. After 17.00, when the potential gradient was negative, the throws due to lightning were well over to the positive, some of the positive deflexions being very large. There was one single throw towards the negative at 17.37, just after the ground-potential gradient had become positive.

A glance at the records of the soundings is sufficient to show the presence of the $P$ and $N$ charges. It is interesting, however, to note that in successive ascents each of these charges was encountered at a lesser height. This may have been due either to a continuous lowering of the charges throughout the cloud with time or to the charges being in the form of layers which were higher in the cloud at the front of the storm than at the rear; there is no means of deciding which of these alternatives is correct.

Sounding 127 started some distance in front of the storm when the field was negative but small. A small negative field continued to a height of 6 km. when there were some reversals, but still of only small intensity. At 7 km. the field became suddenly positive and large. At 9 km. the balloon burst while still in a positive field. There can be little doubt that this balloon rose to about 6 km. in front of the storm and was then rapidly drawn into the active part of the storm. A track of this nature is shown at *dd* of figure 2, and the resulting record in figure 3 is very similar to that of sounding 127.

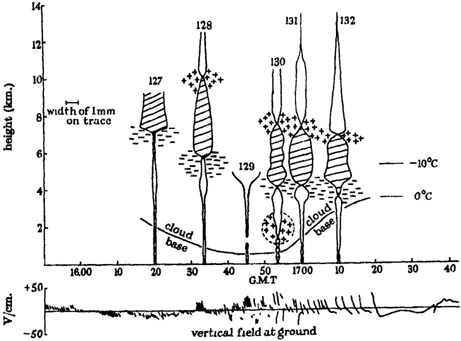

FIGURE 6. Extensive thunderstorm: 21 August 1939.

Sounding 128 probably followed a similar track, but being nearer the storm centre the fields were larger. This sounding pierced the upper positive charge and reached the *U* field at the top of the cloud.

Sounding 130 commenced in the heavy squall of rain marking the centre of the storm, and the field was continuously positive up to a height of

1·4 km. The field, however, was small and no doubt the charge was some distance away, so that the balloon rose rather near the boundary of the $Q$ field: in that case the centre of the charge would be higher than 1·4 km. at which height the field changed. This explanation is supported by the two following soundings, each of which recorded intermittent positive and negative fields up to heights of 0·9 and 0·6 km. respectively, showing that they were still further away from the centre of the positive charge.

There can be little doubt that in this storm the lightning discharges were taking place between the $N$ charge and the $P$ charge. With very few exceptions each discharge caused a positive throw, and this is the sign which a discharge between negative electricity at 5 km. and positive electricity at 8 km. would have at a point less than 8 km. away from the place of discharge. Also the last throw at 17.37 was negative, at which time the active centre of the storm was presumably more than 8 km. away—8 km. being the reversal distance for discharges between these heights.

The soundings during this storm again clearly reveal the presence of $Q$, $N$ and $P$ charges: the heights of these charges were greater than 1·4 km , between 3·6 and 7·0 km., and between 6·8 and 10·0 km. respectively.

### 4. *Thunderstorm,* 12 *August* 1938. *Soundings* 116–121. *Figure* 7

Thundery conditions set in at 16.30, but the storms were not at first near the Observatory, although the potential gradient was highly disturbed with occasional lightning throws. These conditions prevailed with much cloud until about 16.50 when a storm was seen to be approaching from the north-east. The centre passed north of the Observatory with flashes observed at a distance of 1–2 miles.

The potential had been consistently negative during the preliminary disturbed conditions, but with the approach of the storm the potential gradient became positive at 16.55. Just after this change the first balloon was released and it rose in a gap between the clouds so that it was seen for some considerable time against the blue sky until it was finally hidden by low cloud, thus confirming that at the time the potential gradient became positive the Observatory was outside the cloud mass of the approaching storm. The positive potential gradient from 16.55 to 17.04 was evidently that of the $P$ field surrounding the storm. The storm did not pass over the station, but from 17.04 to 17.39 the Observatory was under the influence of the $N$ field as the storm centre passed to the north The $P$ field was entered again in the rear of the storm at 17.39, the maximum being reached at 17.41, after which the field decreased in the usual way. This interpretation of the potential gradient at the ground is fully substantiated by the soundings.

As already stated the first sounding, no. 116, was made before the storm reached the Observatory, but just after the *P* field had given positive

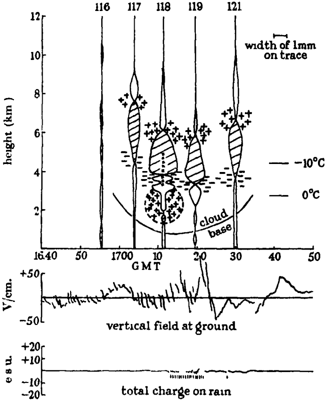

Figure 7. Thunderstorm: 12 August 1938.

potential gradient at the ground. The record of this sounding shows that large fields were not encountered in any part of its track. The field was positive from the ground to 1·3 km., then negative to 3·6 km.; then positive (but sometimes so weak as to leave no legible record) to 7·7 km., after which it became negative. There can be little doubt that the track followed by this balloon was similar to track *ee* of figure 2. It started in the *P* field, drifted through the *N* field, then, re-entering the *P* field again at 3·6 km., rose through the *P* field to a height of 7·7 km., when it finally entered the *U* field, thus reproducing in all essentials the record *ee* of figure 3. (It will be noticed that the potential-gradient scale used for record *ee* is ten times greater than that used for the other records on figure 3.)

The next sounding, no. 117, commenced when the field at the ground had become negative owing to the nearer approach of the storm. The field was negative from the ground to 4·4 km. where it became positive; it was positive from 4·4 to 7·5 km. and then changed to negative. This is the sequence one would expect for a balloon starting in the $N$ field some distance from the axis of the storm and rising vertically. The corresponding track on figure 2 is *cc*, and the record *cc* of figure 3 is the counterpart of the alti-electrograph record of sounding 117.

Sounding 118 commenced in a negative field at the ground; a positive field was entered for a short time, between 1·4 and 2·0 km. As the balloon rose the negative field increased, at first slowly and then very rapidly until at 3·0 km. sparking at the electrodes took place. At 3·8 km. the gradient changed almost instantaneously to positive, the field became even stronger and the sparking continued to a height of 5·0 km. The positive field decreased and changed to negative at 6·0 km., after which the field was negative to about 10·0 km., at which height it became too weak to leave a record. The track followed by this balloon was similar to track *bb* of figure 2, and the record of the sounding is similar in all respects to record *bb* of figure 3. The balloon left the ground in the $N$ field, but quite near to the $N$–$Q$ boundary. As the balloon rose it drifted into the $Q$ field giving the positive gradient between 1·4 and 2·0 km. On rising still further the balloon passed into the strong negative field between the $Q$ and $N$ charges and then into the still stronger positive field between the $N$ and $P$ charges. At 6·0 km. the field changed to negative as the balloon rose through the centre of the $P$ charge. From 3·0 to 5·0 km. there was sparking at the electrodes of the alti-electrograph; this was in the strong field above and below the centre of the $N$ charge. At this time the balloon must have been rising very near to the axis of the storm, and this is supported by the fact that the rate of ascent of the balloon was 230 m./min. between the ground and a height of 4·0 km. and 330 m./min. between 4·0 and 8·0 km., showing the presence of a strong vertical current. As the balloon rose so near to the axis of the storm the reversals of the field in this sounding fix with considerable certainty the heights of the centres of the charged regions.

Sounding 119 started probably somewhat nearer the centre of the storm than the previous one, but the balloon does not appear to have been drawn towards the centre. It started when the field was negative, but up to a height of 2·2 km. the field was so weak that only an intermittent trace was made on the alti-electrograph. Such weak fields, in the centre of a thunderstorm, could only occur near the boundary between positive and negative fields. This ascent, therefore, like the previous ascent, commenced near to, but outside, the *Q*–*N* boundary. That the balloon did not move towards the centre is shown by the absence of the positive field between the ground and 2·0 km. and by the lesser intensity of the *N* and *P* fields as compared with that of the previous sounding. This conclusion is also supported by the fact that the rate of ascent of the balloon did not change but remained at 250 m./min. throughout the flight. The balloon in sounding 119 therefore probably rose almost vertically and so passed farther away from the axis than in sounding 118, its track was therefore similar to *cc* of figure 2, except that it commenced nearer to the axis at the ground level, and it will be seen that the record along the track *cc* in figure 3 is very similar to the record of sounding 119.

Sounding 120 was lost. Sounding 121 commenced when the centre of the storm had passed to the north and the Observatory was in the same position relative to the centre as when sounding 117 commenced. The records of these two soundings are similar and are typical of ascents commencing in the *N* field at the ground some distance from the axis of the storm, and rising vertically.

The five soundings therefore are in complete accord with the passage of a storm of the *Q*, *N*, *P* type, the centre passing to the north of the Observatory at such a distance that the Observatory did not come within the *Q* field although it was very near to the boundary between the *Q* and *N* fields. The heights of the charge centres along the axis, as shown by sounding 118, were *Q* approximately 2·0 km., *N* 3·8 km., and *P* 6·0 km.

During the period 17.00–17.30 when the storm was nearest to the Observatory the changes of potential due to lightning strokes were all positive and therefore were probably due to discharges between the *P* and *N* charges. The largest positive throw was about 50 V/cm. at 17.22. At that time the observers estimated the centre of the storm to be between 1 and 2 miles to the north. Taking the distance to have been 2·0 km. and the discharge to have taken place between the *N* charge centred at 3·8 km. and the *P* charge centred at 6·0 km., we find that the discharge was one of 12 coulombs. This value can only be approximate; but it is of the right order of magnitude.

There was one short sharp shower of rain between 17.10 and 17.20, but there was very little charge on the rain. On the whole the little charge was negative; but towards the end there were one or two intervals with positively charged rain.

### 5. *Violent thunderstorm,* 10 *June* 1937. *Soundings* 75–78. *Figure* 8

There were widespread thunderstorms over south-east England on the evening of 10 June 1937. They appear to have commenced on the south coast soon after 18.00 and reached Kew at 19.00. At Kew the storm approached from the south, and at 19.20 a pronounced line squall passed over the Observatory. Lightning and thunder were first observed at 19.15, the active centre of the storm then being apparently 2 miles to the south-south-east and moving northwards. Accounts of the thunderstorm from Kew and other places will be found in the *Meteorological Magazine* for July 1937.

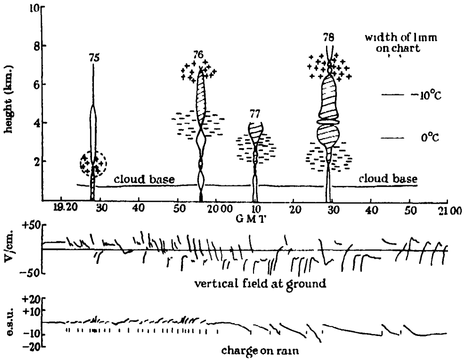

FIGURE 8. Violent thunderstorm: 10 June 1937.

Four balloons were released during the storm, the first at 19.28, a few minutes after the passage of the line squall. The next two balloons were forced down, the first after reaching a height of about 7·0 km. and the second at a height of 4·0 km.; both balloons subsequently rose again, but after the forced descent the electrical records became defective and cannot be used. The fourth balloon reached above 9·0 km.; but at that height the record becomes unreliable and there are some indications that this balloon also was temporarily forced down at a height of 10·0 km.

The records obtained during the storm are shown on figure 8. It has been found impossible to interpret the records so as to produce a simple consistent picture of the electrical structure of the storm. This is not surprising, for the wind was high and the balloons were carried far away from the Observatory, so that the potential gradient at the ground cannot be correlated with the fields registered at the balloons. No attempt will therefore be made to analyse the records as a whole, but a few remarks will be made on interesting features of the individual ascents.

As already stated the storm commenced with a violent squall which struck the Observatory at 19.20. For 15 min. after the squall the potential gradient at the ground was positive and fairly steady except for a few throws due to lightning discharges. The balloon which was released 8 min. after the passage of the squall rose at the normal rate to a height of 1·5 km., recording a small positive field all the way. At this height the rate of ascent was much reduced, indicating either a downward current of air or heavy precipitation. This continued for 2 or 3 min., during which the field changed sign three times: positive to negative, negative to positive, and positive to negative. The balloon then continued to rise at its original rate through a small negative field to a height of 5·0 km., where the field became too small to leave a record. The balloon reached 7·0 km. As the fields up to 7·0 km. immediately after the passage of the squall were so small it would appear that the squall itself was not the seat of the electrical separation. Electrical activity did not become pronounced until 17 min. after the squall had passed; then the potential gradient at the ground became negative and there was a great increase in the number and intensity of the throws due to lightning discharges.

The second ascent, sounding 76, commenced at 19.56. There were four major reversals of the field recorded by the alti-electrograph before the balloon reached 4·0 km What was the nature of these fields, whether they were due to the balloon passing through localities with different fields or due to time changes in the field as a whole cannot be determined from the record. At 4·0 km. the balloon entered a strong steady positive field which persisted to a height of 6·7 km., where a change to negative field occurred. There can be little doubt that whatever may have been the cause of the changing field below 4·0 km. the steady positive field between 4·0 and 6·7 km. was due to negative and positive charges centred at these heights.

There is little to say about sounding 77. The field was negative to a height of about 1·4 km , then alternating positive and negative to 2·7 km., after which to the height of 3·8 km., where the balloon was driven down, the field was positive, rising to high values at about 3·5 km. In this case it is not possible to fix with certainty the centre of the negative charge which produces the strong positive field above 2·7 km., but there are indications on the trace after the balloon had been driven down (not reproduced on the diagram) that it was in the neighbourhood of 2·4 km.

Sounding 78 has some remarkable features. The field was negative and small up to 2·0 km. There it became positive, but remained small up to 3·3 km. when it suddenly became strong. At 4·0 km. there was a sudden reversal to an equally strong negative field which persisted for 2 min., during which the balloon rose approximately 400 m.; then equally suddenly the field reverted to positive and was as strong as before the reversal. The field then remained positive to a height of 6·6 km. There were then two small reversals and at 7·2 km. the field became negative. After this point the record becomes unsatisfactory with indications of more positive field above 9·0 km.; but as the balloon was then drifting without rise and even with some descent it is considered best to neglect the record above 9·0 km.

The reversal at 4·0 km. is difficult to explain At first sight one thinks of a *lightning* discharge between the upper positive charge and the lower negative charge; but that would only destroy the field, it would not reverse it. The fact that the field after the reversal was practically the same as before seems to indicate that the upper and lower charges were not affected and that the reversal was due to some rearrangement of distant charges. It may be mentioned that according to the record the field changed at the balloon at 20.44, while there was a large positive throw on the potential gradient record at the ground at 20·43. The timing of the altielectrograph is not very accurate and the difference of 1 min. may not be significant. The throw and the reversal may therefore have been simultaneous, but even if they are related it is difficult to see what could have happened to produce a negative field change at 4·0 km. and a positive field change at the ground. It must be remembered that the balloon at that time may have been several miles away from the Observatory, as it had been in flight 15 min

The course of the potential gradient and the effects of the lightning discharges are so complicated in this storm that it is not possible to draw any useful conclusions from them. The rain-electricity record has some interesting features. In spite of the general complication of the storm, the course of the rain-electricity is unusually simple. Rain started at 19.21 just after the passage of the squall and was moderately heavy until 20 00. The rate of rainfall then changed and became very much less The sign of the electricity on the rain changed at this point also, so there seem to be two distinct masses of rain, probably of quite different origins. The first rain mass which fell at an average rate of 7·0 mm./hr. from 19.21 to 20.00 was positively charged throughout and there are no signs of a mixture of positively and negatively charged rain. Similarly, the light rain from 20.00 to 20.53 which fell at an average rate of 1·3 mm./hr. was negatively charged throughout.

It seems probable that the positively charged rain was associated with the positive charge at a height of about 2·0 km. shown by sounding 75, while the negatively charged rain originated in the negative electricity in the lower half of the cloud.

Although the storm was too complicated for its structure to be determined in detail it is clear that there was the usual *P* charge at the top of the cloud—indicated by sounding 76 at 6·8 km. and by sounding 78 at 6·6 km. The *N* charge was met with in sounding 76 at a height of 4·0 km., in sounding 77 at 2·4 km. and in sounding 78 at 2·0 km. Thus from sounding 76 to sounding 78 the height of the *N* charge had decreased by 2·0 km., which may have been due to a fall in time over the whole area or to a fall in distance from the front to the back of the storm. In either case there can be no doubt as to the presence of a negative charge below the upper positive charge. Sounding 75 reveals the presence of a positive charge in the base of the cloud probably carried by rain. This storm, therefore, in spite of its complicated nature and large extent, clearly reveals the presence of the *P*, *N* and *Q* charges.

In the diagrams representing the soundings in the five storms so far considered, the fields in the upper air have been plotted in bands vertically above the abscissae representing the times at which the balloons were released In the three storms which remain to be described a different method will be used. In these storms there was little wind and there is good evidence that during the early parts of the ascents, when records were being obtained, the balloons were for all practical purposes directly overhead. Thus the field at the balloon at any time during the ascent is directly comparable with the field at the ground at that time. To bring out this relationship, the alti-electrograph records are plotted against both time and height, with the result that the bands representing the fields at different heights are no longer vertical but slope towards the direction of increasing time. When this method is used one can see at once the rate of ascent of the balloons, for this is given by the slope of the alti-electrograph record.

### 6. *Very violent thunderstorm*, 13 *August* 1937.
### *Soundings* 88–99. *Figure* 9

On the afternoon of 13 August 1937 there was a very violent thunderstorm at Kew Observatory, particularly notable for the very heavy rain which fell, about 50 mm. being recorded in 2 hr. The course of the storm was as follows. Thunder was first heard at 14.45 and the first lightning was seen to the south, distance about 3 miles, at 14.50, rain having already begun. The storm developed very rapidly, with much lightning. At 15.23 there was a heavy downpour of rain which was followed by moderate to heavy rain for nearly an hour, after which the rain became light. A serious attempt was made during this storm to get as many records as possible,

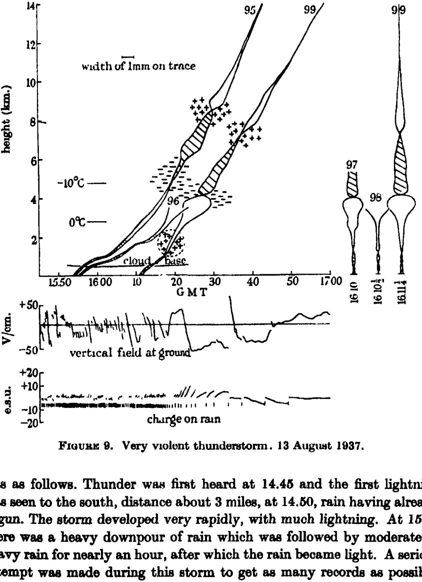

FIGURE 9. Very violent thunderstorm. 13 August 1937.

for its intensity and negligible motion made it very suitable for intensive investigation. Within an hour twelve balloons were launched in four batches, the balloons in each batch being released at intervals of about a minute. Unfortunately, the balloons were of defective quality and only two of the twelve penetrated the storm; seven either burst soon after release or remained quite near to the ground, so that their records are useless; the remaining three gave records only up to moderate heights. The soundings which gave useful records were nos. 95–99, the last five balloons which were released. They formed part of the last two batches, the individual balloons of the first batch being released at 15.53½ (not used), 15.54 and 15.54½, and those of the second batch at 16.10, 16.10½ and 16.11¼. The records have been plotted on figure 9. This diagram does not show the beginning of the storm, but starts at 15.50, more than an hour after the first thunder had been heard and 20 min. after the heavy downpour of rain between 15.20 and 15.30

The potential gradient during the first part of the storm, not reproduced in figure 9, began as usual with a positive field which changed to negative and then became very disturbed by lightning discharges, with many throws to positive. The potential gradient at the end of the storm can be seen from figure 9. The disturbed period continued until about 16.18, when, after 7 min. of positive potential gradient, the potential became negative with one large throw to the positive and several smaller ones. At 16 45 the gradient became positive, reached a maximum at 17.00, and then slowly returned to normal. During this period the storm was passing away, and the negative and positive potential gradients after 16.25 were clearly the $N$ and $P$ fields in the rear of the storm.

Soundings 95, 96 and 99 are plotted on figure 9 against their correct times. Sounding 99 was one of a batch of three all made within 2 min., too close together to be shown individually on the main diagram. These three soundings have therefore been plotted separately to the right of the main diagram, sounding 99 being repeated.

These five soundings represent the changes which took place in the electric field in the space of about 15 min. Comparing first soundings 95 and 99, which give the fields at the beginning and at the end of the interval, we see a remarkable difference. At the time of sounding 95 there was very little negative field between the heights of 3·0 and 4·0 km., while when sounding 99 was made through the same region 8 min. later (note that the balloon in sounding 99 rose more rapidly than that in sounding 95) there was a much larger negative field. The growth of the field can be followed by comparing soundings 96–99. Until we know more about the physical processes which cause the electrification within the clouds we cannot explain how this large field was generated.

Both soundings 95 and 99 show a reversal of the field between 7·0 and 9·0 km., revealing the presence of a positive charge in this part of the cloud. The centre of this charge appears to have fallen 1·2 km. in 8 min.; but this may have been partly due to lateral separation of the two balloons during their ascents.

The conditions revealed by the soundings near the ground are instructive. Soundings 95 and 96 showed a small negative field, which up to a height of 2·0 km. was subject to many reversals (represented by dots on the trace), probably coinciding with the reversals at the ground due to lightning flashes. Above 2·0 km. the reversals disappear and both soundings show steady negative fields Sounding 97 shows a positive field to a height of 1·0 km. and then a negative field above. The same positive field is shown by soundings 98 and 99 which were made within the next 2 min., but each shows the change from positive to negative field at a progressively lower level. It will be noticed that during the time covered by these flights positively charged rain was falling at the ground. It is therefore a natural conclusion that it was the volume charge of positive electricity carried on the rain which gave rise to the positive field shown in soundings 97–99. If this is correct then the bulk of the positive charge must have been above the 1·0 km. level, where the field changed from positive to negative. Further evidence on the height of this low positive charge is given by the reversals shown on soundings 95 and 96. There are only two or three of these above 2·0 km., and none at all above the freezing level. When the reversals were being recorded the balloon was ascending in a region influenced mainly by the negative charge between 4·0 and 6·0 km. and the lower positive charge. At each flash the field due to the former charge was reduced to a value numerically less than that due to the latter, and the field below the centre of the low positive charge became momentarily positive. Above this centre there was a reduction but no reversal of the field. The centre of the low positive charge must therefore have been located between 2·0 km. and the freezing level. In the storm we clearly have the *P*, *N* and *Q* charges and very strong evidence that the *Q* charge was carried on the rain.

### 7. *Thunderstorm*, 13 *September* 1937. *Soundings* 100, 101 *and* 102. *Figure* 10

This storm approached from the west. Rain commenced at 15.20 and for about 15 min. was fairly heavy, being at a rate of 25 mm./hr. for a few minutes after 15.30; the rain then decreased in intensity and light rain continued until the storm had passed. Thunder was first heard at about 15.30 and the first lightning was noticed a few minutes later. About 15.35, when the rain had decreased in intensity, the lightning became more intense, and between 15.40 and 16.00 there was a display of infrequent but spectacular flashes, apparently along the underside of the cloud, which was high and not particularly dense The storm moved very slowly and the balloons rose at a very high angle; all three instruments fell within 5·0 km. of the Observatory after rising to 14·0 km. or more.

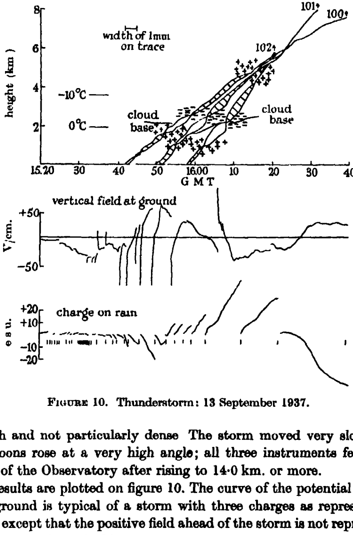

FIGURE 10. Thunderstorm: 13 September 1937.

The results are plotted on figure 10. The curve of the potential gradient at the ground is typical of a storm with three charges as represented in figure 1, except that the positive field ahead of the storm is not represented. The $N$ field is well marked between 15.24 and 15.44; the $Q$ field gave positive potential gradient from 15.44 to 16.08, and the $N$ field negative potential gradient from 16.08 to 16.28, after which the field became positive and remained positive as the storm passed away. The absence of the $P$ field in front of the storm and the presence of a strong $P$ field in the rear are explained by the development of the storm as it approached the Observatory. This is clear from the absence of lightning discharges until 15.33 when the Observatory was well within the boundary of the $N$ field.

From the record of the rain electricity it will be seen that there was very little charge associated with the moderately heavy rain at the commencement of the storm; what little there was appears to have been positive. At 15.35 the rain became lighter, and with this change in the character of the rain the sign of the electricity carried down changed to negative. The rate of rainfall continued to decrease, but the quantity of electricity carried by each c.c. of rain increased, reaching $-6{\cdot}8$ e.s.u./c.c. just before 15.50. At 15.53 the rate of rainfall increased again and the sign of the rain electricity also changed, becoming positive. From 15.53 to 16.22 the rain was very light and steadily decreasing in intensity, but it was very highly charged with positive electricity, the charge increasing on the whole as the rate of rainfall decreased. In successive buckets from 15.53 to 16.22 the charge was 2·8, 3·1, 2·5, 6·8, 15·5, and 9·9 e.s.u./c.c. The total rainfall during the period was 0·9 mm., i.e. an average rate of 1·8 mm./hr., a very small rate of rainfall.

Sounding 100 commenced at 15.43 just before the potential gradient at the ground changed from negative to positive. The balloon rose in the $N$ field to a height of 0·4 km. and then entered the $Q$ field. The positive gradient of the $Q$ field was traversed to a height of 1·6 km., where the field became negative, the boundary between the $Q$ and $N$ fields being crossed at this level. As the balloon continued its ascent the $N$–$P$, and $P$–$U$ boundaries were crossed at 2·2 and 4·4 km. respectively. The path of the balloon was similar to *bb* of figure 2, and the same sequence of field was met with as in record *bb* of figure 3.

Sounding 101 started at 15 51 when the $Q$ field at the ground was near its maximum. The first part of the ascent was consequently in a positive field. The $Q$–$N$ boundary was crossed at 1·0 km., the $N$–$P$ boundary at 2·4 km. and the $P$–$U$ at 4·6 km.

Sounding 102 also started in the $Q$ field and crossed the three boundaries at 0·8, 2·2 and 4·2 km. respectively.

Examining the upper parts of these three soundings we notice that the three traces come very close together near the top, all three coinciding at 16.20 at a common height of 5·4 km. This is a fortuitous result due to the fact that the three balloons had different rates of ascent. As the balloons rose almost vertically this means that above 4·0 km. they must have been very near together, and it is interesting to note that they all three recorded the same negative field when they were together at 16.20; this is further evidence of the reliability of the alti-electrograph records. All three soundings give the heights of the $P$ and $N$ charges as approximately 4·4 and 2·3 km. respectively.

The diagram shows the heights at which the balloons entered the cloud base. For soundings 100 and 102 this height was approximately 2·1 km. Sounding 101 gives the base of the cloud 0·5 km. lower; but this may have been due to the balloon during this sounding entering a local patch in which the level of the cloud was lower than the general base. There is no reason to believe that the cloud base as a whole fell 0·5 km. between 15.56 and 16.01 and then rose by the same amount during the next 6 min. We will now consider the $Q$ charge. The potential gradient at the ground was positive from 15.45 to 16 05 with a maximum of 60 V/cm. at 15.52, obviously due to the passage of the $Q$ charge either directly overhead or quite near to the Observatory. At the time of the maximum field at the ground the balloon of sounding 100 crossed the $Q$–$N$ boundary at a height of 1·6 km.; this therefore must have been the height of the centre of the $Q$ charge at that time. Soundings 101 and 102 showed the boundary at 1·0 and 0·8 km. respectively. The explanation of these changes appears to be straightforward. Positive electricity was being generated near the axis of the storm in a region which was over the Observatory at 15.52. Sounding 100 went through this region and fixed the centre of the positive charge at about 1·6 km. The charged region moved with the storm and soundings 101 and 102 did not go so near to the centre; therefore the boundary between the $Q$ and $N$ fields was crossed at a lower level. It is possible also that there had been some lowering of the charged region because the change from 1·6 to 1·0 km. in 3 min. is larger than one would expect from the movement of the storm alone; on the other hand, the effect of the $Q$ charge had almost ceased at the ground when sounding 102 crossed the $Q$–$N$ boundary, and therefore the centre of the storm was then some distance from the Observatory. Positively charged rain reached the ground just when the $Q$ charge was overhead, as judged by the positive potential gradient at the ground, and continued until 16.24, this falling rain must have lowered the centre of the charged region. The decrease in height of the reversal of the field from positive to negative shown in these three ascents must therefore be ascribed to both causes the movement of the centre of the charged region away from the Observatory and a lowering of the centre of the charged region by the transfer downwards of the positive electricity on the rain. It is important to notice that in this storm the positive charge was mainly, if not entirely, in the clear air below the cloud and therefore can only have been carried by the rain.

At 16.00 there were three balloons in the air, one above the other, and it will be seen from the diagram that at this time one was in a positive field at a height of 0·4 km., one was in a negative field at a height of 1·9 km., and the other was in a positive field at a height of 2·7 km. This is conclusive proof of the reality of three separate charges of electricity at different heights in the atmosphere and a complete answer to Wormell's criticism quoted above.

Between 15.41 and 15.55 there were six intense lightning flashes which caused large changes of the field at the ground as will be seen from the potential gradient record. As already stated these flashes were seen to be along the underside of the cloud. There can therefore be little doubt that they were between the positive charge below the cloud and the negative charge in the base of the cloud. At that time the former was at a height of 1·6 km. and the latter at a height of 2·2 km. Assuming that the discharges were equivalent to a transfer of $Q$ coulombs of electricity between these two heights directly above the Observatory, then we have for the change of field at the ground:

$$\Delta F = 1{\cdot}8\left(\frac{1}{(1{\cdot}6)^2}-\frac{1}{(2{\cdot}2)^2}\right)Q\times 10^2\,\mathrm{V/cm.}$$

The mean change of the field caused by the six flashes was −160 V/cm., hence the mean quantity of electricity discharged in each flash was 5 coulombs.

### 8. *Violent thunderstorm*, 11 *August* 1938. *Soundings* 108–115.
### *Figure* 11

The storm approached rather rapidly from the east. There was a sharp squall about 17.35, soon after the first sounding had commenced. With the squall heavy rain set in which continued to about 18 10, when the rain moderated and gave place to light rain which continued with some slight variations in intensity until the storm had passed away. The observers noted that there appeared to be two main active centres, one to the west and one to the south of the Observatory; in consequence the storm is complex and not easy to analyse.

The potential gradient at the ground was on the whole high and greatly disturbed by near lightning flashes. From 17.20, when the record commenced, to near the end of the storm the pre-flash potential gradient was

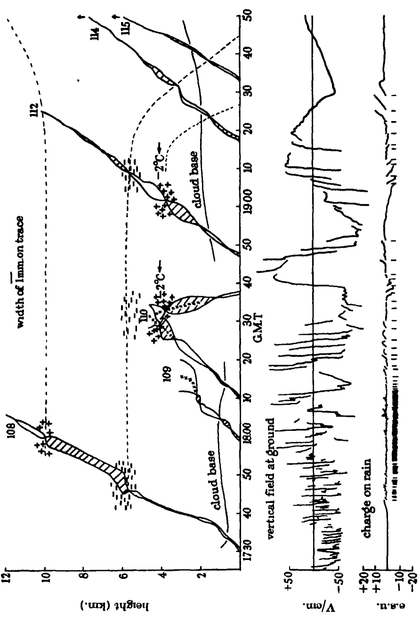

FIGURE 11. Violent thunderstorm: 11 August 1938.

negative and fairly steady, except for two periods of positive potential gradient with maxima at approximately 18.43 and 19.10. The usual final *N* and *P* fields were well developed as the storm passed away.

Eight soundings were made during the storm. One failed entirely, owing to stoppage of the clock, and one instrument has not been recovered. Two of the remaining balloons burst at moderate heights and the others reached 10 km. or more.

The first sounding, no. 108, commenced at 17.30. Five minutes later the squall struck the Observatory when the balloon was at a height of a little over 1 km. The rate of ascent of the balloon then changed from 3 (the normal rate of ascent in still air) to 8 m./sec., revealing an ascending current of 5 m./sec. The potential gradient at the ground when the ascent commenced was negative and the balloon record shows that it remained negative but small to a height of nearly 6·0 km. Here the field was reversed and a high positive field was recorded from 6·0 to 10·0 km. The field changed to negative at 10·0 km. and then slowly decreased with height, no clear record being left after a height of 10·5 km. There can be little doubt about the interpretation of this record. The ascent started in the *N* field in front of the storm. The balloon was drawn towards the active centre as it rose, remaining in the weak *N* field near the *N–P* boundary. It crossed the *N–P* boundary as it entered the active region and then traversed the *P* field where it was strong, near to the active centre. The track of the balloon was similar to *dd* of figure 2 and its record is similar to *dd* of figure 3. The reversals of the field at 5·8 and 10·0 km. give the levels of the *N* and *P* charges at the time of the ascent.

The second sounding, no. 109, commenced at 17.59 when very heavy rain, positively charged, and violent changes of potential gradient due to lightning, indicated that the active centre of the storm was very near. The rate of ascent was at first normal, then more rapid for a few minutes, after which it decreased quickly. For 3 min. the balloon hardly ascended at all, then it rose very rapidly for a minute and burst at a height of 3·0 km So far as one can measure from the record the balloon rose 700 m. in 40 sec just before it burst, giving a rate of ascent of 18 m./sec. With the rapid increase in the rate of ascent the field became negative, very strong, with much sparking at the electrode. There can be little doubt that this balloon entered the active centre of the storm and that the balloon was burst either by the turbulence of the air or by an electrical discharge—the strong sparking at the electrode makes the latter the more probable explanation. As there can be little doubt that above 2·2 km. the balloon and precipitation were being carried upwards in a strong ascending current the field recorded at the balloon cannot be used to determine the electrical charges at different heights. All that can be said is that the strong negative field indicates that at that time there was a great concentration of negative electricity above the balloon. As this accumulation may have been rising with the balloon no definite height can be assigned to it.

*Sounding 110 started 11 min. after no. 109; its rate of ascent was* normal and steady, showing that it did not experience the turbulent air met with in sounding 109. At a height of 4·3 km., when there was sparking at the electrodes, the balloon burst, probably again due to electrical discharge. The balloon did not fall very rapidly and the alti-electrograph record during the descent can be interpreted, although not with the same accuracy as on the ascent.

Although sounding 110 started 11 min. later than the previous sounding, the ascent was not retarded and the balloon reached 3·0 km. only 7 min. after the previous balloon had burst at that height. The later sounding experienced small to moderate negative fields from the ground to 3·2 km., thus the high field at 3·0 km. experienced by the previous balloon has largely decreased in 7 min. At 3·2 km. a strong positive field was met which lasted to 4·0 km., where it changed to an equally strong negative field; in both these high fields there was sparking at the electrodes. When the balloon burst at 4·3 km., it was still in the strong negative field and the falling balloon experienced the negative field for the first part of its fall. It left the negative field and entered the positive field at a height of 3·8 km., i.e. 0·2 km. lower than the change took place on the ascent, a difference which is not significant in view of the uncertainty in interpreting the trace during the descent. The positive field extended downwards to the 1·2 km. level, where the field changed to negative and remained negative to the ground. On the ascent the change from negative to positive occurred at a height of 3·4 km. at 18.26, on the descent at 1·2 km. at 18.35. Thus in 9 min. the boundary between the negative and positive fields had descended 2·3 km.

The interpretation of this sounding can best be given by considering the lower part of record *aa* of figure 3. This record it will be remembered was obtained by calculating the field due to a small positive charge at a height of 1·5 km., a larger negative charge centred at a height of 2·0 km. and a positive charge at 6·0 km. The positive charge centred at 1·5 km. produces a positive field which is strong near to the boundary of the charged region and then rapidly decreases towards the ground; but with the charges used in the calculations the field remains positive right to the ground. If, however, the positive charge had been smaller or the negative charge immediately above larger, the positive field would not have extended to the ground, but would have ended a certain height above the ground, this height being determined by the relative quantities of positive and negative electricity.

The positive field between the levels 3·4 and 4·0 km., with negative field below and above, revealed on the ascending branch of sounding 110, was due to a positive charge centred at 4·0 km. and a negative charge above, the exact position of which cannot be fixed as the balloon burst before the centre of the charge was reached. The positive charge was being generated and accumulated, and at 18.26 the positive field extended downwards to the 3·4 km. level, where it was met by the ascending balloon; 9 min. later, at 18.35, the positive field had reached the 1·2 km. level where it was passed by the descending balloon. With further accumulation of charge the positive field extended still lower and reached the ground just before 18.40, when the potential gradient at the ground changed from negative to positive. The positive field at the ground became stronger until 18.43 when it reached its maximum. If at this time we could have obtained an instantaneous sounding, we should have obtained a record similar to *aa* of figure 3. It will be noticed that at this time the charge brought down by the rain changed from negative to positive, so that not only the field, but also the positive electricity causing the field, extended to the ground, for there can be little doubt that the positive electricity was carried by the rain.

This conclusion is supported by considering the temperature in the region where the positive charge had appeared. Attached to the alti-electrograph on this sounding was a Dines meteorograph. It showed a remarkably small lapse rate between 2·0 and 4·0 km. At 2·0 km. the temperature was 4° C and at 4·0 km. −2° C, the freezing-point being at 3·0 km. The accumulation of charge was therefore taking place in the neighbourhood of the freezing-point.

After 18.43 the positive field at the ground was decreasing, probably due to the falling out of charge on the rain. Sounding 112 commenced while the field at the ground was still positive and the balloon registered a positive field for about a minute, then the field at the ground and at the balloon became negative. At 18 55 the balloon again entered the positive field at a height of 2·0 km., showing that there was still positive electricity above. The positive field continued to a height of 3·7 km. where it changed to negative, putting the centre of the positive charge just a little lower than it had been during the previous sounding 32 min. earlier. It will be noticed that during the time the balloon was traversing the positive field between the 2·0 km. and 3·7 km. levels the field at the ground was negative. The negative field at the ground commenced to decrease in intensity at 18.53 showing that the positive charge was again increasing. The field at the ground became positive at 19.05 and reached a maximum at 19.10 after which it decreased. It will be noticed that the decrease in the positive gradient was again accompanied by positively charged rain.

To return to sounding 112· after passing the positive charge (*Q* charge) at 3·7 km. the balloon passed through the *N* field into the *P* field at 5·6 km. The *P* field was not strong and at about 8·4 km., before the *P–U* boundary was reached, the trace became too faint to register.

Sounding 114 is typical of an ascent starting in the *Q* field, and sounding 115 of an ascent starting in the *N* field. By this time the active centre of the storm was some distance away so that the fields were not strong, and although both soundings exceeded 10·0 km. the field was too weak to register the *P–U* boundary.

Little of use can be said about the lightning discharge, as no records were made of the position or distance of the discharges. Until 18.20 practically all the discharges were positive and therefore most likely between the *N* and *P* charges. After the *Q* charge had formed at about 18.28 there were a number of negative discharges and some large positive ones. With the data available it is not possible to say between which charges these flashes passed; but from the obvious relationship between the flashes and the shape of the potential gradient curve, the low positive charge must have been involved.

In this storm, more than in any of the others, we can follow the formation and dissipation of the *Q* charge and there can be no doubt that it was associated with the rain. It formed near to the level in the atmosphere where the freezing-point occurred, and it can be recognized in the electricity carried down by the rain. It is clear also that this process takes place under a region with a heavy negative charge, and therefore it is quite independent of the positive charge at the top of the cloud.

## DISCUSSION OF THE RESULTS

### *Location of the electrical charges*

In S. and S. an attempt was made to locate the position in the cloud of the main electrical charges. This was done by considering that every change of sign of the vertical field indicated the presence of a local charge of electricity. The height of all such charges was then plotted on a diagram (figure 9, S. and S.). This method is now seen to be defective, because many of the changes in the sign of the vertical field are not due to local charges but to distant charges which may be at very different levels from those at which the change of field is registered by the alti-electrograph.

It is not always easy to say whether a reversal of the field indicates a local charge; but our analysis of the storms described in this paper has given many clear cases of the relation of the balloon to the charge, and in these cases the height of the charge can be fixed with some degree of certainty. In other cases, when the track of the balloon cannot be deduced, reversals of high field, especially if there is sparking at the electrodes, show that the balloon is near to the charged area, and the point of reversal can be accepted as giving the height of the centre of the charge. By applying these considerations to all the storms described in these two papers it has been possible to pick out twenty-seven soundings each of which gives with reasonable certainty the position of at least two charges and in some cases of three. These twenty-seven soundings are taken from thirteen storms and they have been tabulated in table 3. When there are two or more soundings in one storm they have, if possible, been combined, mean values being taken, the object being to give each storm an equal value. In two storms, 19 June (21.00) 1936, and 21 August 1939, this was not advisable, as in each case there was a sounding at the beginning of the storm which gave heights and temperatures for the charges entirely different from those given by the later soundings. In these two cases both sets of values have been used. The table contains for each storm, the temperatures at the levels of the lower positive charge ($Q$), the negative charge in the lower cloud ($N$), and the upper positive charge ($P$), and in addition the temperature at the ground during the storm. As readers may wish to examine the soundings which have been selected, reference is given in the table to the diagram on which each sounding will be found.

The data contained in table 3 have been plotted on figure 12. There are fifteen sets of data, which for convenience we will call 'soundings', although some of them are combinations of two or more original soundings in the same storm. These have been numbered in order of increasing temperature at the $N$ charge (column 7) and plotted on figure 12 in that order. For each sounding the signs $+$, $-$, $+$, have been entered at the temperature where the $P$, $N$ and $Q$ charges respectively were centred (i.e. where the field reversed), the two former being connected by a vertical line. A dot enclosed in a circle represents the temperature at the ground during the storm.

In every storm, and in every individual sounding, the temperature at the $P$ charge was below $-10°$ C. It will also be noticed that on the whole

TABLE 3

| Date | Sounding | Temperature °C Ground | Q | N | P | Order on figure 12 | Trace plotted on diagram |
|---|---|---|---|---|---|---|---|
| 25 June 1935 | 13 | 20 | — | + 8 } + 5 | — | 15 | Figure 18 (S. and S.) |
| | 14 | | — | + 5 | — | | |
| | 16 | | — | + 3 | — | | |
| | 18 | | — | + 3 | — | | |
| 19 June 1936 (13.00) | 49 | 21 | — | − 9 | −32 | 5 | Figure 15 (S. and S.) |
| 19 June 1936 (21.00) | 52 | 20 | +5 | −13 | — | 3 | |
| | 53 | | — | 0 } 0 | −14 } −14 | 13 | Figure 14 (S. and S.) |
| | 54 | | — | + 1 | — | | |
| 5 Sept. 1936 | 63 | 15 | +4 | − 6 | −17 | 8 | Figure 16 (S. and S.) |
| 15 Sept. 1936 | 68 | 13 | −9 | −19 | −28 | 1 | Figure 17 (S. and S.) |
| 10 June 1937 | 76 | 18 | — | − 3 } +1 | −16 } −17 | 14 | Figure 8 |
| | 77 | | — | 2 | — | | |
| | 78 | | — | 5 | −17 | | |
| 15 July 1937 | 82 | 18 | +6 | − 1 | −12 | 12 | Figure 5 |
| 13 Aug. 1937 | 95 | 18 | — | −10 } −9 | −29 } −26 | 6 | Figure 9 |
| | 99 | | — | − 8 | −23 | | |
| 13 Sept. 1937 | 100 | 11 | +1 | − 4 | −18 | 10 | Figure 10 |
| 17 Sept. 1937 | 105 | 14 | +6 | − 8 | −21 | 7 | Figure 4 |
| 11 Aug. 1938 | 108 | 17 | — } −2 | −18 } −16 | −35 } −35 | 2 | Figure 11 |
| | 112 | | −2 | −15 | — | | |
| 12 Aug. 1938 | 117 | 19 | — | −10 } −6 | −29 } −23 | 9 | Figure 7 |
| | 118 | | — | − 7 | −20 | | |
| | 119 | | — | − 4 | −18 | | |
| | 121 | | — | − 5 | −25 | | |
| 21 Aug. 1939 | 128 | 21 | — | −12 | −38 | 4 | |
| | 130 | 18 | — | − 3 } −2 | −23 } −21 | 11 | Figure 6 |
| | 132 | | — | 0 | −19 | | |

the temperature at the $P$ charge decreased with the temperature at the $N$ charge, although there are large variations in the differences, the average value of which is 15° C.

The temperature at the $N$ charge was 0° C or below in thirteen out of the fifteen soundings. The lowest temperature recorded at the $N$ charge was $-19$° C on 15 September 1936, and the highest 8° C on 25 June 1935, the mean of the fifteen soundings being $-7$° C.

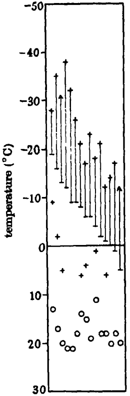

FIGURE 12. Temperatures at the centres of the $P$, $N$ and $Q$ charges and at the ground.

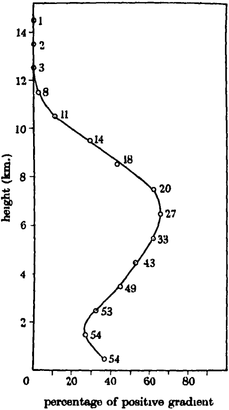

FIGURE 13. Frequency of positive fields according to height.

In five of the seven storms in which the position of the $Q$ charge could be fixed the temperature at the level of the charge was above the freezing-point; in one of the others it was $-2$° C and in the remaining storm $-9$° C.

There appears to be no relationship between the temperatures at the ground and the temperatures at the different charges.

### *The potential gradient in the clouds*

In S. and S. reasons were given for concluding that sparking occurred at the electrodes of the alti-electrograph when the field reached approximately 100 V/cm., and attention was drawn to the surprisingly large number of soundings in which no sparking occurred. This remarkable absence of large fields within a thunderstorm is even more strongly marked in the new records. Thirty-seven new soundings are discussed in this paper and sparking occurred only in three, nos. 118, 109 and 110. The balloons burst in three other soundings when in strong fields, nos. 129, 96 and 98, and these may have been destroyed by electrical discharge, although the instruments on recovery showed no signs of such a discharge. One is led to the conclusion that the fields in a thundercloud are of the order of 100 V/cm., except in relatively small regions where there is great electrical activity and in which lightning discharges originate. We find no evidence of large horizontal sheets of positive and negative electricity with fields approaching the discharge field (10,000 V/cm.) between them.

The percentage frequency with which positive and negative fields occurred at different heights was considered in S. and S. and the results were given in table 2 and figure 8 of that paper. The same method has been applied to all the soundings now available and the results are plotted on figure 13, in which the abscissae are percentage frequencies of positive potential gradient and the ordinates height above the ground; the number of soundings used in determining the percentage is shown against each point. It will be seen that this curve is of the same form as the one published in S. and S.; but as there are now many more high ascents the upper part is completed and we find, as suggested in S. and S., that positive fields entirely disappear at the greater heights, no positive fields being recorded at a greater height than 12·0 km.

In figure 14 the same data have been plotted against temperature instead of against height—the temperature being obtained in the way described on p. 282. As temperature is intimately related to height the form of the two curves is similar, but the lower point of inflexion is much sharper and occurs very near to 0° C. The implication of this will be discussed later.

### *The potential gradient at the ground*

In discussing the individual storms we have seen that many of them are associated with changes of potential gradient at the ground similar to the changes which would be experienced if a storm similar in structure to that used for calculating figure 1 passed over the station. Such a distribution of electricity gives at the ground a positive field when the storm is approaching and receding, and a negative field nearer the centre which is reversed or reduced in intensity when the most active part of the storm is overhead. This distribution of the field at the ground was recognized in the previous work and exhibited in figure 21 of S. and S.

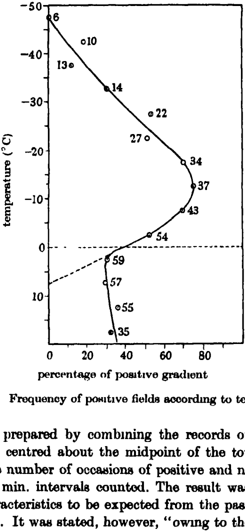

FIGURE 14 Frequency of positive fields according to temperature.

That figure was prepared by combining the records of twenty storms. Each record was centred about the midpoint of the total period of disturbance and the number of occasions of positive and negative gradients in each of the 5 min. intervals counted. The result was a curve clearly showing the characteristics to be expected from the passage of storms of the *Q*, *N*, *P* type. It was stated, however, "owing to the great difference in size, duration and rate of travel between one storm and another it is difficult to combine satisfactorily the records of different storms". This difficulty was experienced when the new records were treated in the same way; and the resulting curve, whilst showing the expected form, was irregular, especially near the ends, owing to the phases of storms of long duration not coinciding with those of storms of short duration. A slightly modified method was therefore employed. Records of twelve new storms were available. Each record, beginning and ending where the potential gradient exceeded 10 V/cm., was divided into twenty equal parts and the proportion of positive and negative fields in each part determined. The corresponding parts of the storms were then combined and the percentage frequency of positive potential gradient determined for each of the twenty parts. The results are plotted in figure 15, which clearly shows the predominance of positive fields as the storm approaches and recedes, the excess of negative fields nearer the centre and the increased frequency of positive fields in the immediate neighbourhood of the centre of the storms. A similar result has been obtained in a different way by Wormell (1939). In tables 4 and 5 of his paper Wormell gives the duration in minutes of positive and negative pre-discharge potential gradients according to the distance of the nearest active storms, from which the following values have been taken:

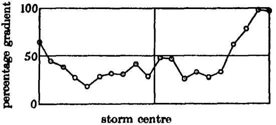

FIGURE 15. Frequency of positive fields at ground-level.

TABLE 4. DURATION OF POSITIVE AND NEGATIVE PRE-DISCHARGE POTENTIAL GRADIENTS (WORMELL)

| Distance of nearest active storm in km. | Percentage positive fields |
|---|---|
| <3 | 38 |
| 3–5 | 29 |
| 5–10 | 40 |
| 10–15 | 59 |
| >15 | 76 |

Thus we see exactly the same distribution of potential gradient as found in our work, and there can now be no doubt that the average distribution of potential gradient at the ground in the neighbourhood of a thunderstorm is consistent with the distribution of electricity shown in figure 1.

In S. and S. it was suggested that the $P$ and $N$ charges are associated with ice crystals, and the $Q$ charge with rain. These conclusions will now be examined in the light of all the soundings which are now available.

### *The P and N charges*

It has now been possible to analyse more or less completely the electrical field in fourteen storms, and diagrams have been published, six in S. and S., and eight in this paper, showing the distribution of charges which would account for the electrical field revealed by the soundings. In every one of these storms the presence of a positive charge near the top of the cloud and a negative charge in the lower half has been indicated. The presence of these two charges is responsible for the sequence of potential gradient changes near the ground as storms approach and recede. This is shown in figure 15, the high frequency of positive potential gradient on the fringe of the storm is due to the upper positive charge, while the large predominance of negative potential gradient under the main cloud is due to the negative charge in the lower half of the cloud. There can therefore now be no doubt that a positive charge at the top of the cloud with a negative charge below it is a normal feature of every thunderstorm.

### *The nature and origin of the P and N charges*

In figure 12 are plotted data from thirteen separate storms, in each of which there is reason to believe that the positions of two or three of the $P$, $N$ and $Q$ charges are fairly accurately fixed. The data used are the temperatures at the electrical centres of the charges, assuming that the reversal of the field approximately indicates the centre of the charge.

In every case the temperature at the centre of the $P$ charge was lower than $-10°$ C, and in thirteen out of fifteen cases considered the temperature at the centre of the $N$ charge was $0°$ C or lower. In other words, with two exceptions, which will be considered later, both $P$ and $N$ charges were within that part of the cloud which was below the freezing-point. There can be little doubt that the $P$ and $N$ charges are complementary, i.e. they are the results of some process which has separated the positive electricity in the upper part of the cloud from the negative electricity in the lower.

This process must therefore be one which can function in temperatures far below the freezing-point and within clouds which are known to be composed of ice crystals. We see no reason to change the opinion expressed in S. and S. that the cause of the separation of the electricity is the impact of ice crystal on ice crystal which leaves the ice negatively charged and the air positively charged. The general settling of the negatively charged ice crystals relatively to the positively charged air would then result in a separation of electricity with the positive charge above the negative.

On this theory the amount of electricity generated will depend on the turbulence of the air, which determines the frequency of the impacts, and on the number of ice crystals, for with a given turbulence the number of collisions will depend on the number of crystals. On the other hand, the size of the ice crystals will determine the rate of separation, and the velocity of the ascending currents the time during which a group of ice crystals will contribute to the whole process. In a thunderstorm we have violent ascending currents, producing much turbulence and large accumulation of ice crystals, just the factors which tend to increase the electrical effects. In non-thunderstorm clouds, with small ascending currents and relatively few ice crystals, the electrical separation is small and only small electrical fields, either in the clouds or below, are produced.

In the lower part of the cloud the negative charge is carried on the ice crystals which are falling relatively to the air. If there are no ascending currents the ice crystals approach the region of the cloud where the temperature is above the freezing-point and there melt. They continue their fall, however, as negatively charged rain carrying the negative charge into regions with temperatures above the freezing-point. This explains the two cases in which the temperature at the centre of the negative charge was above 0° C. The first of these was in the storm of 10 June 1937. From figure 8 it will be seen that sounding 78 showed the centre of the negative charge at 2·0 km. where the temperature was 5° C, and highly charged negative rain was falling as seen on the rain-electricity record. The progressive fall of the negative charge is seen by comparing the change from negative to positive field in soundings 76, 77 and 78. In sounding 76 the centre of the charge was at 4·0 km. with a temperature of $-3°$ C, in sounding 77 at 2·7 km. with a temperature of 2° C, and in sounding 78 at 2·0 km. with a temperature of 5° C. Here we clearly see the settling of the charge first on the ice crystals and then on the rain. The other cases of the centre of the negative charge being at a temperature above the freezing-point occurred on 25 June 1935 (figure 18, S. and S.). Here five soundings showed a change from negative to positive field at temperatures well above the freezing-point As there was no record of the rain-electricity it is impossible to say whether in this storm negative electricity was being carried down by the rain; but there is no reason to doubt that the explanation holds good in this case also.

### *The Q charge*

There can now be little doubt as to the frequent occurrence of a positive charge below the main negative charge in the lower part of the cloud. The analysis of the storms discussed in this paper has shown the presence of a $Q$ charge in every storm. The evidence is particularly conclusive in the storms of 13 September 1937 and 11 August 1938 (figures 10, 11). A re-examination of the storms discussed in S. and S., with the greater experience we now have, shows unmistakable evidence of a $Q$ charge in all the storms except the storm of 25 June 1935 (figure 18, S. and S.), and even in this storm there is a period of positive potential gradient at the ground between 13.18 and 13.26 which it would be difficult to explain except as the consequence of a positive charge below the negative charge revealed by all the soundings. It is probably too early to say that every thunderstorm has a low positive charge in addition to the main $P$ and $N$ charge; but there can be no doubt that the majority of thunderstorms have all three charges.

### *The nature and origin of the Q charge*

We have shown in the discussion of the individual soundings that the change of sign of the vertical field does not always indicate the true level of an electrical charge, and that in some cases it does not even indicate a separate charge at all. Thus a number of reversals of field which were interpreted in S. and S. as being due to a low positive charge cannot be used to determine the level of the $Q$ charge. Seven cases, however, have been included in figure 12 in each of which there was evidence that the balloon had been sufficiently near to the active centre to be quite sure that the change in field indicated the proximity of a charge and its approximate level. It should be noted that if the $N$ charge above the $Q$ charge is large the change of field occurs some distance below the centre of the $Q$ charge (see figure 1), also the boundary between the $N$ and $Q$ fields falls away rapidly from its highest point as one retreats from the axis of the storm. For these two reasons the centre of the $Q$ charge determined from the reversal of the field is likely to be too low. Figure 14, however, gives us further information regarding the location of the $Q$ charge. If every storm had been bipolar with the lower charge generally above, but occasionally a short distance below, the level at which the freezing-point occurs, the curve in figure 14 would have been unaltered from the highest point to 0° C, but from 0° C it would have rapidly approached the zero as indicated by the dotted line. Below this point all the fields would have been negative (neglecting one sounding which commenced in the $P$ field on the edge of the storm), and the percentage of positive fields would have been zero. The fact that the potential gradient in 30 % of the soundings from the ground to the level of the freezing-point was positive indicates the frequent presence of a positive charge below the negative charge on the ice crystals. As the frequency of the positive fields was practically constant from the 0° C level to the ground, the $Q$ charge must have been mainly in the neighbourhood of the freezing-point level. In two of the storms, 15 September 1936, sounding 68 (figure 17, S. and S.), and 11 August 1938 (soundings 110 and 112, figure 11), the centres of the positive charge as fixed by the change of field were at temperatures below the freezing-point. The case on 11 August can be easily explained as there were strong ascending currents, and the positively charged rain might well have been carried beyond the freezing-point level to a height where the temperature was $-2°$ C. The former case is more difficult to explain as the temperature at the centre of the positive charge was $-9°$ C; but there is nothing inherently improbable in positively charged precipitation being carried to great heights. In spite of these two cases the evidence is strong that the $Q$ charge is formed in temperatures above the freezing-point and that it is associated with heavy rainfall. We therefore see no reason to depart from the opinion expressed in S. and S. that the positive electricity which forms low down in the cloud is generated by the process of breaking drops as first suggested by Simpson in 1909.

## CONCLUSIONS

(*a*) In every thunderstorm there is a positive charge of electricity near the top of the cloud, where the temperature is below $-10°$ C.

(*b*) In every thunderstorm there is a negative charge below the upper positive charge, and in most cases this charge is in a part of the cloud where the temperature is below the freezing-point.

(*c*) The generation and separation of these charges occurs in the ice region, and the most probable cause is the collision of ice crystals in the turbulent air associated with the strong ascending currents in a thunderstorm. The collisions charge the ice negatively and the air positively, and it is the settling of the ice crystals relatively to the air which separates the positive and negative charges.

(*d*) Below the main negative charge in the lower half of the cloud there are in most, if not in all, thunderstorms regions containing positive charges.

With few exceptions the temperature where these positive charges occur is above the freezing-point.

(*e*) These low positive charges are associated with heavy rain and they are probably generated by the breaking of rain drops in ascending currents of air.

Our thanks are due to the Director of the Meteorological Office for permission to publish this paper which was undertaken as part of the scientific work of the Kew Observatory.

## REFERENCES

Scrase, F. J. 1938 *Geophys. Mem.* no. 75. London: Met. Office.
Simpson, G. C. 1927 *Proc. Roy. Soc.* A, **114**, 376–401.
Simpson, G. C. and Scrase, F. J. 1937 *Proc. Roy. Soc.* A, **161**, 309–352.
Wormell, T. W. 1939 *Phil. Trans.* A, **238**, 249–303.

---

# Exchange effects in the theory of the continuous absorption of light

## I. Ca and Ca$^+$

BY D. R. BATES, M.Sc. AND H. S. W. MASSEY, F.R.S.
*University College, London*

(*Received* 10 *September* 1940)

The continuous absorption coefficients of normal Ca and Ca$^+$ are calculated. Both the discrete and continuous wave functions used in the calculation include the effect of electron exchange. Comparison is effected with results obtained neglecting exchange and it is found that appreciable modifications are introduced by its inclusion. This is particularly true for Ca$^+$ which is a sensitive case owing to very strong interference in the integrand of the transition matrix element. The bearing of the results on the calculation of absorption coefficients in general is discussed, and it is pointed out that the discrepancy between theory and experiment for potassium arises because this also is a very sensitive case.

An application of the results for Ca is made to resolve a discrepancy between determinations of interstellar electron densities carried out using different methods by Stromgren and Struve.

A knowledge of the continuous absorption coefficients of various atoms is required for the theory of stellar atmospheres and of the ionized layers in the upper atmosphere of the earth. As it is difficult to obtain the required information by experiment except in a few cases, special importance attaches to the development of accurate theoretical methods. For atomic hydrogen an exact calculation can be made: but approximate methods, which often have little pretence to accuracy, must be resorted to in other cases. The problem is one of calculating the probability of an atomic electron making a transition from a discrete state to one of the continuum on absorption of the light quantum. This involves a knowledge of the corresponding atomic wave functions. In calculations which have been carried out previously the approximation used for the discrete wave function has usually been fairly satisfactory, but the same cannot be said about that representing the continuous state. In many cases this has been assumed to be of hydrogen-like form with an effective nuclear charge the same as that for the ground state function. This can lead to completely illusory results for absorption near the low-frequency limit, as has been pointed out by Bates (1939). A much better approximation is to take for the wave function the appropriate solution of the Schrödinger equation for the motion of the electron in the static average field of the atomic core. This procedure has been carried out for helium by Wheeler (1933), for the atoms of the first row in the periodic table from boron to neon by Bates (1939), for lithium by Hargreaves (1929) and for potassium by Phillips (1932). For the latter atom the theoretical results can be compared with the experimental results of Ditchburn and Braddick (1933) and the agreement is very poor indeed.† To attempt to remedy this situation it is necessary to carry the approximate determination of the continuous wave function a stage further, by including the possibility of electron exchange. This has been done for absorption by $H^-$ (Massey and Bates 1940). In this case the exchange effects were found to be unimportant, but it was pointed out that this is not likely to be a general result, particularly for heavier atoms. We have therefore chosen the case of absorption by Ca and $Ca^+$ in their ground states to investigate the matter further. A knowledge of the absorption of neutral and ionized calcium is important in astrophysics, and accurate ground state wave functions are obtainable from the calculations of D. R. Hartree and W. Hartree (1938) using the Fock method. The results obtained show that exchange can be very important and it is possible that its inclusion will clear up the discrepancy between theory and experiment for potassium. Calculations on the latter atom were begun by J. Ingham and

---

† For a summary of theoretical and experimental work see a review by Page (1939).

D. R. Hartree before our work was commenced, but these have been temporarily held up by the pressure of official duties. The possibility of bringing observed and calculated values into agreement for potassium by inclusion of exchange was first pointed out by D. R. Hartree, to whom we are indebted for several discussions on the matter.

From the calculated absorption coefficients it is possible to derive the coefficients of recombination for slow electrons into the ground states of Ca and Ca$^+$. The values we obtain may be utilized to resolve a discrepancy between the interstellar electron densities derived by Struve (1939) and by Strömgren (1939) using independent methods This aspect of the matter was first brought to our attention by Dr Strömgren of Copenhagen Observatory, and it was originally intended that he would carry out the astrophysical application of our results. The German occupation of Denmark has rendered this out of the question, so a brief analysis of the matter has been carried out by us and is described in the concluding section.

## GENERAL THEORY

The continuous absorption coefficient $k_\nu$ of an atom for light of frequency $\nu$ is given by

$$k_\nu = \frac{32\pi^4 m^2 e^2}{3h^3 c} \nu v \,|\, \mathbf{R} \,|^2, \tag{1}$$

where

$$\mathbf{R} = \int \Psi_i (\Sigma \mathbf{r}) \Psi_f^* \, d\tau. \tag{2}$$

$v$ is the velocity of the ejected electron, $\Psi_i$, $\Psi_f$ are the initial and final wave functions of the atom, suitably normalized,† and $\mathbf{r}$ is the displacement of a particular electron from the centre of the atom. If exact wave functions $\Psi$ are used this formula will give results of a high degree of accuracy so the theoretical problem is essentially one of obtaining accurate approximations for the wave functions.

For atoms such as Ca and Ca$^+$ we may write, with sufficient approximation,

$$\Psi_{i,f} = \phi_{i,f}(\mathbf{r}_c)\, \psi_{i,f}(\mathbf{r}), \tag{3}$$

where $\phi$ is a function of the co-ordinates $\mathbf{r}_c$ of the core electrons only and $\psi$ of the co-ordinates $\mathbf{r}$ of the outer shell electrons only Since the ground states of Ca$^+$ and Ca are $4s\,^2$S and $(4s)^2\,^1$S terms respectively, the excited states of the continuum, of energy $E$, to which the transitions take place, must be $(Ep)\,^2$P and $(Ep)(4s)\,^1$P terms respectively, in order that the selection rules be obeyed. We therefore have

---

† $\Psi_i$ is normalized to unit density and $\Psi_f$ to represent at infinity an incident wave of unit amplitude together with a core function of unit density. The case $v = 0$ requires special consideration for which see a preceding paper (Bates, Buckingham, Massey and Unwin 1939).

For Ca$^+$:

$$\Psi_i = \phi(\mathbf{r}_c)\,\psi^+(4s\,|\,\mathbf{r}), \quad \Psi_f = \phi(\mathbf{r}_c)\,\psi^+(Ep\,|\,\mathbf{r}). \tag{4}$$

For Ca:

$$\begin{aligned}\Psi_i &= \phi(\mathbf{r}_c)\,\psi(4s\,|\,\mathbf{r}_1)\,\psi(4s\,|\,\mathbf{r}_2),\\ \Psi_f &= 2^{-\frac{1}{2}}\phi(\mathbf{r}_c)\,[\psi^+(4s\,|\,\mathbf{r}_1)\,\psi(Ep\,|\,\mathbf{r}_2)+\psi(Ep\,|\,\mathbf{r}_1)\,\psi^+(4s\,|\,\mathbf{r}_2)].\end{aligned} \tag{5}$$

$\phi$ denotes the core function which is effectively the same for Ca, Ca$^+$ and Ca$^{++}$ respectively, $\psi^+(4s\,|\,\mathbf{r})$ is the wave function of the $4s$ electron of Ca$^+$, $\psi(4s\,|\,\mathbf{r})$ of Ca, while $\psi^+(Ep\,|\,\mathbf{r})$, $\psi(Ep\,|\,\mathbf{r})$ are the corresponding functions for an electron of positive energy $E$ moving in the field of normal Ca$^+$ and Ca respectively. Further, if $I$ is the ionization energy of Ca$^+$ or Ca then

$$E = h\nu - I.$$

Substituting these formulae in (2) we have

For Ca$^+$:

$$\mathbf{R} = \int \psi^+(4s\,|\,\mathbf{r})\,\mathbf{r}\,\psi^{+*}(Ep\,|\,\mathbf{r})\,d\mathbf{r}. \tag{6}$$

For Ca:

$$\mathbf{R} = \int \psi(4s\,|\,\mathbf{r})\,\psi^{+*}(4s\,|\,\mathbf{r})\,d\mathbf{r}\int \psi(4s\,|\,\mathbf{r})\,\mathbf{r}\,\psi^{*}(Ep\,|\,\mathbf{r})\,d\mathbf{r}, \tag{7}$$

since the individual electronic wave functions are supposed orthogonal.

Of the functions appearing in (6), (7), all but $\psi(Ep\,|\,\mathbf{r})$, $\psi^+(Ep\,|\,\mathbf{r})$ are given by the self-consistent field calculations carried out by D. R. and W. Hartree (1938) for Ca and Ca$^+$ The functions were calculated by the method due to Fock (1930) and include the effects of exchange. They must therefore be regarded as the most accurate which can be obtained at present if the wave function is written in the form (3).

Using these functions the left-hand integral of (7) may be evaluated numerically and we find

For Ca:

$$\mathbf{R} = 0{\cdot}98_5\int \psi(4s\,|\,\mathbf{r})\,\mathbf{r}\,\psi^{*}(Ep\,|\,\mathbf{r})\,d\mathbf{r}. \tag{8}$$

To complete the calculation it remains to determine the functions $\psi^+(Ep\,|\,\mathbf{r})$ and $\psi(Ep\,|\,\mathbf{r})$ with the same accuracy as the functions for the bound state.

## DETERMINATION OF CONTINUOUS WAVE FUNCTIONS

The Fock equations as developed by Hartree may be applied immediately to set up equations which must be satisfied by $\psi(Ep\,|\,\mathbf{r})$ and $\psi^+(Ep\,|\,\mathbf{r})$. For Ca$^+$ these equations will take the same form as for any excited $p$ electron, while for Ca they are of the same form as for the $p$ electron in a $(4s)\,(np)\,^1\mathrm{P}$ configuration. These equations have already been given by D. R. and W. Hartree (1938). Writing

$$\psi^+(Ep\,|\,\mathbf{r}) = 3(\epsilon v)^{-\frac{1}{2}}\,r^{-1}P(Ep\,|\,r)\begin{cases}\cos\theta\\ \sin\theta\cos\phi\\ \sin\theta\sin\phi,\end{cases}$$

then in atomic units

$$\left\{\frac{d^2}{dr^2}+(\epsilon+2Z_p^+/r-2/r^2)\right\}P(Ep\,|\,r)+Q/r=0, \tag{9}$$

where $\epsilon$ is the kinetic energy of the free electron in units 13·53 eV, $Z_p^+$ is the effective nuclear charge for potential of the Ca$^{++}$ core, and

$$Q=\sum_{n=1}^{3}\tfrac{2}{3}Y_1(ns,E\,|\,r)\,P(ns\,|\,r)$$
$$+\sum_{n=2}^{3}\{2Y_0(np,E\,|\,r)+\tfrac{4}{5}Y_2(np,E\,|\,r)-\eta_{npE}\}\,P(np\,|\,r),$$

where

$$Y_l(\alpha\beta,\gamma\delta\,|\,r)=\left\{\int_0^r P(\alpha\beta\,|\,r_1)\,P(\gamma\delta\,|\,r_1)\,(r_1\,|\,r)^l\,dr_1\right.$$
$$\left.+\int_r^\infty P(\alpha\beta\,|\,r_1)\,P(\gamma\delta\,|\,r_1)\,(r\,|\,r_1)^{l+1}\,dr_1\right\}.$$

$r\ ^1P(ns\,|\,r)$, $r^{-1}P(np\,|\,r)$ are the $s$ and $p$ self-consistent radial wave functions for Ca$^{++}$. The quantities $\eta_{npE}$ are Lagrange multipliers which are adjusted so the wave function $P(Ep\,|\,r)$ is orthogonal to the $P(np\,|\,r)$ functions appearing in $Q$.

For Ca the equation satisfied by $P(Ep\,|\,r)$ is of the same form as (9) but contains the additional term

$$-\tfrac{2}{3}Y_1(4s,E\,|\,r)\,P(4s\,|\,r)$$

in $Q$, and $Z_p^+$ is replaced by

$$Z_p=Z_p^+-Y_0(4s,4s\,|\,r).$$

In the equation (9), the terms represented by $Q$ arise from inclusion of exchange. If $Q$ is put equal to zero the equations are of the ordinary differential form and may be solved by standard numerical methods (Hartree 1927) using the function $Z_p^+$ given by D. R. and W. Hartree (1938). When exchange is included the equations become of integro-differential type as the unknown function $P(Ep\,|\,r)$ appears under integral signs in $Q$. No standard method exists for solving such equations, and a method of successive approximation was employed to obtain self-consistent solutions. The procedure adopted was to deal first with the case $\epsilon = 0$. Using the results of the Hartrees' investigations on the effect of exchange on the discrete wave functions of $Ca^+$ and Ca a reasonable first estimate was made of the solution. This was especially accurate for small distances $r$. The integrals appearing in $Q$ were evaluated by using this estimated function, and the equation (9) solved numerically with this form for $Q$. By comparison of the resulting solution with that first estimated it was then possible to improve the approximation. The process was repeated until the function used in evaluating $Q$ was sufficiently nearly the same as that resulting by solving (9) with this value of $Q$. It was found, as suggested by the Hartrees, that it was not necessary to take the undetermined multipliers $\eta$ into account until the final stages of the calculation. These multipliers were not important for $Ca^+$, but were more so for Ca.

Having obtained the solution for $\epsilon = 0$, results for other values of $\epsilon$ (up to $\epsilon = 0{\cdot}4$ for $Ca^+$ and $\epsilon = 0{\cdot}1$ for Ca) were obtained by taking for $Q$ the values given for $\epsilon = 0$ and then solving (9) directly. This is of sufficient accuracy owing to the slow variation of $Q$ with $\epsilon$.

In figure 1 the functions obtained for $\epsilon = 0$ for both $Ca^+$ and Ca are illustrated, those calculated with neglect of exchange† (i.e. with $Q = 0$) being included for comparison purposes.

It will be seen that for $Ca^+$ the effect of exchange is to pull in all the nodes of the function as if an additional attractive field were present. This is a general feature of exchange effects of a $p$ electron with a closed shell. For Ca again, exchange with the closed shell core pulls in the first two nodes, but the exchange repulsion due to the $4s$ electron, with opposite spin to the $Ep$ electron, cancels this effect for the higher nodes.

The normalization of the functions is somewhat laborious. The procedure has been described already by several authors. If $P(Ep\,|\,r)$ joins smoothly at large $r$ to

$$aG_1 + bH_1$$

where $G_1$, $H_1$ are the functions given by the authors in a previous paper (Bates, Buckingham, Massey and Unwin 1939), then the correct normalizing factor is

$$\{\tfrac{1}{2}\pi\,\epsilon^{\frac{1}{2}}(1+\epsilon)\}^{\frac{1}{2}}/(a^2+b^2)^{\frac{1}{2}}.$$

---

† It is to be noted that this means that exchange has been neglected in calculating the continuous but not the discrete wave function.

The difficulty is that the functions $G_1$, $H_1$ must be first evaluated numerically at two values of $r$ such that the function $Z_p/r$ has taken its asymptotic form ($2/r$ for Ca$^+$, $1/r$ for Ca), before this procedure can be applied. Some abbreviation of the work follows from the fact that functions used to normalize $P(Ep \mid r)$ for Ca at a particular value of $\epsilon$ may also be used to normalize $P(Ep \mid 2r)$ for Ca$^+$ at $4\epsilon$. In case the values calculated for $G_1$ and $H_1$ should be of use to other authors a table of them is included in the appendix.

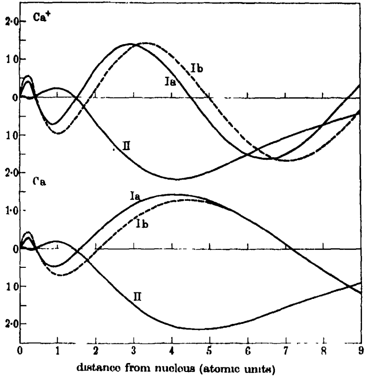

FIGURE 1. Wave functions concerned in the calculation of continuous absorption by Ca and Ca$^+$. Upper set of curves refer to Ca$^+$, lower to Ca. Curves I*a*: continuous wave function $P(op/r)$ including exchange ($\epsilon = 0$). Curves I*b*. continuous wave function $P(op/r)$ without inclusion of exchange ($\epsilon = 0$). Curves II: normalised discrete wave function $P(4s/r)$ multiplied by $r$ The continuous functions are normalised, apart from a factor $\epsilon^{-\frac{1}{2}}$.

## NUMERICAL RESULTS AND DISCUSSION

Having obtained the continuous wave functions, it is only necessary to complete the evaluation of the absorption coefficient by numerical integration. In obtaining the final numerical values the experimental value of the frequency $\nu$ was used rather than any theoretical value.

In table 1 the results obtained for Ca are given. It will be seen that the values do not depart much from the $\nu^3$ law either when exchange is introduced or not. The effect of exchange is, however, quite marked in leading to a larger value of the absorption coefficient at each frequency.

TABLE 1. CALCULATED ABSORPTION COEFFICIENTS FOR Ca AND Ca⁺

| | Energy of ejected electron in units 13·53 eV | Absorption coefficient | |
|---|---|---|---|
| | | Without exchange included | With exchange included |
| Calcium (spectral head 49,360 cm.$^{-1}$; 6·09 eV) | 0 | $1{\cdot}39 \times 10^{-17}$ cm.$^2$ | $2{\cdot}45 \times 10^{-17}$ cm.$^2$ |
| | 0·025 | 1·13 | 2·07 |
| | 0·050 | 0·93 | 1·77 |
| | 0·075 | 0·77 | 1·54 |
| | 0·100 | 0·65 | 1·35 |
| Calcium⁺ (spectral head 95,730 cm.$^{-1}$; 11·82 eV) | 0 | $7{\cdot}7_6 \times 10^{-19}$ cm.$^2$ | $2{\cdot}3_6 \times 10^{-19}$ cm.$^2$ |
| | 0·100 | $4{\cdot}8_3$ | $2{\cdot}4_4$ |
| | 0·200 | $2{\cdot}9_6$ | $2{\cdot}5_5$ |
| | 0·300 | $1{\cdot}9_3$ | — |
| | 0·400 | $1{\cdot}3_6$ | — |
| Hydrogen (spectral head 109,680 cm.$^{-1}$) | 0 | $6{\cdot}28 \times 10^{-18}$ cm.$^2$ | |

For Ca⁺, the results for which are also given in table 1, the effect of exchange is much more marked. This is a very sensitive case where the interference between the functions appearing in the integrand of the matrix element is very strong and small changes in either function make a great difference to the final answer. The extent of this interference may be judged by comparison of the absolute value of the absorption coefficient with that for Ca or for H (value given at the foot of the table). Actually the sign of the matrix element is changed by inclusion of exchange It is therefore by no means out of the question that cases should arise where the matrix element vanishes at some frequency near the limit giving a variation of absorption coefficient with frequency of the form observed by Ditchburn and Braddick (1933) for potassium.

In such cases as Ca⁺ where the results are so sensitive to small changes in the wave functions it is clearly out of the question to attain high accuracy in theoretical evaluation. Thus we have ignored the effect of polarization in the continuous wave function. Although its influence on the function may be small, the modification of the theoretical absorption coefficient may be considerable. It can always be said, however, that as the high sensitivity arises from strong cancellation in the integrand of the transition matrix element, in all cases where theoretical values are untrustworthy, the absorption coefficient will be small. This always assumes, of course, that the theory is not too crude. For example, it is necessary to determine the continuous wave function at least by numerical solution of the wave equation for the motion of the electron in the self-consistent field of the ion concerned. Empirical methods relying on the assignment of effective nuclear charge will not be adequate.

It is important to decide under what conditions we can expect high sensitivity to detail in theoretical absorption coefficients. This will occur almost exclusively in absorption by *s* electrons, for here only one final state of angular momentum is possible. In other cases two possible final states exist and it will be most unlikely that strong cancellation will occur in the matrix elements for transitions to both these states. It is unfortunate that the only cases where direct comparison of theory and experiment has proved possible should be of the sensitive type. The failure of theory to reproduce the exact form of the results for these cases should not be regarded as evidence of any fundamental failure, it is satisfactory that for potassium the theory agrees with observation in predicting a small absorption coefficient at the limit Summing up, we must expect that, where theory predicts a small absorption, this will really be small, though the magnitude and frequency variation may not be accurate. On the other hand, where the theoretical absorption coefficient is of normal order of magnitude ($10^{-17}$ cm.$^2$) it is probably reliable in both magnitude and frequency variation. We assume again of course that both wave functions involved in the theoretical determinations are derived from self-consistent field calculations as outlined above.

### *Astrophysical application—The electron density in interstellar space.*

Investigations on the electron density in interstellar space have been made by two distinct methods.

Strömgren (1939) considered the source of the electrons. He assumed that they were all derived from hydrogen, the electron density $N(e)$ being equal to the density of the hydrogen ions $N(\mathrm{H}^+)$ and much greater than the density of the hydrogen atoms $N(\mathrm{H})$. He examined in detail the rates of the various processes leading to the formation and destruction of excited atoms (of density $N(\mathrm{H}')$), and by using the results of quantal calculations (Cillié 1932, 1936), Bethe (1933), Menzel and Baker (1937, 1938) he was able to determine the equilibrium constant $K$ in the equation

$$N(e)\,N(\mathrm{H}^+)/N(\mathrm{H}') = K. \tag{10}$$

From the observed strength of $H_\alpha$, $N(H')$ may be determined as $3 \times 10^{-21}/\text{cm.}^3$, for the third excited state. By considering this case in detail an electron density of $3/\text{cm.}^3$, relatively insensitive to temperature, etc., was obtained.

Struve (1939) made use of measurements by Dunham (1937) in the interstellar absorption lines of calcium to determine the ratio of the density of singly ionized calcium ions, $N(\text{Ca}^+)$, to the density of calcium atoms, $N(\text{Ca})$. This was found to be 120. To obtain the electron density this result was substituted in the Saha equilibrium formula:

$$\frac{N(\text{Ca}^+)}{N(\text{Ca})} N(e) = \frac{(2\pi m)^{\frac{3}{2}}}{h^3} \frac{2q''}{q'} (kT_r)^{\frac{3}{2}} e^{-I/kT_r} (T_e/T_r)^{\frac{1}{2}} \beta, \tag{11}$$

where $I$ is the ionization potential of calcium, $q'$, $q''$ are the statistical weights of the atom and ion respectively, $T_r$, $T_e$ the temperatures respectively of the radiation and of the electrons and $\beta$ is the dilution factor. Taking $T_r = T_e = 15{,}000^\circ$ K and $\beta = 10^{-16}$ Struve finds $N(e) = 30/\text{cm.}^3$, ten times greater than the value found by Stromgren.

It was pointed out by Strömgren (1939) that the Saha formula (11) does not give the true equilibrium as it does not allow for electrons recombining to excited states and then cascading to the ground state. This process reduces the value of $N(e)$ given from (11) by a factor $\alpha_g/\alpha_t$ where $\alpha_g$ is the recombination coefficient to the ground state of Ca and $\alpha_t$ the total recombination coefficient. Now $\alpha_g$ may be determined from our calculated absorption coefficient $k_\nu$ by the relation

$$\alpha_g = \omega k_\nu (2h^2\nu^2/m^2c^2v),$$

where $\omega$ is the weighting factor $\frac{1}{8}$ and $v$ the velocity of the ejected electron. The recombination coefficients to the excited states may be obtained with sufficient accuracy by treating them as hydrogen-like (Bates *et al.* 1939). We then find for electrons at a temperature of 15,000° K,

$$\alpha_g = 10^{-14}/\text{cm.}^3/\text{sec}, \quad \alpha_t = 6 \times 10^{-14}/\text{cm.}^3/\text{sec.},$$

giving

$$\alpha_g/\alpha_t = \tfrac{1}{6}, \quad N(e) = 5/\text{cm.}^3.$$

This removes any disagreement between the two methods.

It should be noted that, while there is no marked discrepancy between quantal theory and experiment as regards recombination to the ground states of atoms, certain measurements by Kenty (1928) and Mohler (1937) point to a much greater total recombination coefficient than do the calculations we have just used. It is interesting to consider the effect of this difference. Taking $\alpha_g$ as before and using the experimental result

$\alpha_t = 4\times10^{-11}$/cm.$^3$/sec. gives $\alpha_g/\alpha_t = 2{\cdot}5\times10^{-4}$, $N(e) = 0{\cdot}008$/cm.$^3$. This is in very poor agreement with Strömgren's results. It thus appears that astrophysical evidence favours the view that the recombination observed by Kenty (1928) and Mohler (1937) was not due to a simple two-body radiative process—but it must be emphasized that this evidence is indecisive owing to the many uncertainties entering the astrophysical estimations.

Acknowledgement is due to the Ministry of Education for Northern Ireland for the award of a grant to one of us (D. R. B.).

## REFERENCES

Bates 1939 *Mon. Not. R. Astr. Soc.* **100**, 25.
Bates, Buckingham, Massey and Unwin 1939 *Proc. Roy. Soc.* A, **170**, 322.
Bethe 1933 *Handbuch der Physik*, **24**, 1.
Cillié 1932 *Mon. Not. R. Astr. Soc.* **92**, 820.
— 1936 *Mon. Not. R. Astr. Soc.* **96**, 771.
Ditchburn and Braddick 1933 *Proc. Roy. Soc.* A, **143**, 472.
Dunham 1937 *Publ. Astr. Soc. Pacif.* **49**, 26.
Fock 1930 *Z. Phys.* **61**, 126.
Gerasimović and Struve 1929 *Astrophys. J.* **69**, 19.
Hargreaves 1929 *Proc. Camb. Phil. Soc.* **25**, 75.
Hartree, D. R. 1927 *Proc. Camb. Phil. Soc.* **24**, 89.
Hartree, D. R. and Hartree, W. 1938 *Proc. Roy. Soc.* A, **164**, 167.
Kenty 1928 *Phys. Rev.* **32**, 624.
Massey and Bates 1940 *Astrophys. J.* **91**, 202.
Menzel and Baker 1937 *Astrophys. J.* **85**, 330; **86**, 70.
— — 1938 *Astrophys. J.* **88**, 52.
Mohler 1937 *Bur. Stand. J. Res., Wash.*, **19**, 447; 559.
Page 1939 *Mon. Not. R. Astr. Soc.* **99**, 385.
Phillips 1932 *Phys. Rev.* **39**. 905
Strömgren 1939 *Astrophys. J.* **89**, 526.
Struve 1939 *Proc. Nat. Acad. Sci., Wash.*, **25**, 36.
Struve and Elvey 1938 *Astrophys. J.* **88**, 364; **89**, 119.
Wheeler 1933 *Phys. Rev.* **43**, 258.

## APPENDIX

TABLE 2. FUNCTIONS USED IN NORMALIZING CONTINUOUS $p$ WAVE FUNCTIONS

| $r$ (atomic units) | $\epsilon = 0$† | $G_1$ | | | | $\epsilon = 0$† | $H_1$ | | | |
|---|---|---|---|---|---|---|---|---|---|---|
| | | 0·025 | 0·050 | 0·075 | 0·100 | | 0·025 | 0·050 | 0·075 | 0·100 |
| 2·0 | Identical with the function $(2r)^{\frac{1}{2}} J_3\{(8r)^{\frac{1}{2}}\}$ | $+0{\cdot}848_8$ | $+0{\cdot}837_4$ | $+0{\cdot}826_9$ | $+0{\cdot}814_8$ | Identical with the function $(2r)^{\frac{1}{2}} Y_3\{(8r)^{\frac{1}{2}}\}$ | $-0{\cdot}335_2$ | $-0{\cdot}307_8$ | $-0{\cdot}281_7$ | $-0{\cdot}256_9$ |
| 2·2 | | $0{\cdot}895_8$ | $0{\cdot}880_5$ | $0{\cdot}865_5$ | $0{\cdot}850_6$ | | $0{\cdot}208_9$ | $0{\cdot}179_4$ | $0{\cdot}152_3$ | $0{\cdot}126_3$ |
| 2·4 | | $0{\cdot}924_2$ | $0{\cdot}904_6$ | $0{\cdot}885_2$ | $0{\cdot}866_0$ | | $0{\cdot}076_2$ | $0{\cdot}047_1$ | $0{\cdot}019_6$ | $+0{\cdot}006_5$ |
| 2·6 | | $0{\cdot}933_8$ | $0{\cdot}909_3$ | $0{\cdot}885_1$ | $0{\cdot}861_2$ | | $+0{\cdot}057_1$ | $+0{\cdot}086_3$ | $+0{\cdot}113_7$ | $0{\cdot}139_5$ |
| 2·8 | | $0{\cdot}924_9$ | $0{\cdot}894_9$ | $0{\cdot}865_6$ | $0{\cdot}836_7$ | | $0{\cdot}189_4$ | $0{\cdot}217_6$ | $0{\cdot}244_5$ | $0{\cdot}269_4$ |
| 3·0 | | $0{\cdot}897_9$ | $0{\cdot}862_4$ | $0{\cdot}827_6$ | $0{\cdot}793_5$ | | $0{\cdot}317_9$ | $0{\cdot}345_6$ | $0{\cdot}370_1$ | $0{\cdot}393_3$ |
| 3·2 | | $0{\cdot}854_2$ | $0{\cdot}812_8$ | $0{\cdot}772_5$ | $0{\cdot}733_9$ | | $0{\cdot}440_5$ | $0{\cdot}466_9$ | $0{\cdot}488_9$ | $0{\cdot}508_5$ |
| 3·4 | | $0{\cdot}794_9$ | $0{\cdot}747_7$ | $0{\cdot}701_8$ | $0{\cdot}657_1$ | | $0{\cdot}555_1$ | $0{\cdot}576_8$ | $0{\cdot}596_1$ | $0{\cdot}613_2$ |
| 3·6 | | $0{\cdot}721_7$ | $0{\cdot}668_7$ | $0{\cdot}617_4$ | $0{\cdot}567_6$ | | $0{\cdot}660_1$ | $0{\cdot}677_5$ | $0{\cdot}692_5$ | $0{\cdot}705_3$ |
| 3·8 | | $0{\cdot}636_2$ | $0{\cdot}577_6$ | $0{\cdot}521_2$ | $0{\cdot}466_7$ | | $0{\cdot}753_7$ | $0{\cdot}766_1$ | $0{\cdot}775_6$ | $0{\cdot}783_1$ |
| 4·0 | | $0{\cdot}540_2$ | $0{\cdot}476_4$ | $0{\cdot}415_4$ | $0{\cdot}356_7$ | | $0{\cdot}834_6$ | $0{\cdot}841_2$ | $0{\cdot}844_7$ | $0{\cdot}845_7$ |
| 4·5 | | $0{\cdot}266_5$ | $0{\cdot}192_5$ | $0{\cdot}122_9$ | $0{\cdot}057_3$ | | $0{\cdot}978_1$ | $0{\cdot}965_4$ | $0{\cdot}949_7$ | $0{\cdot}931_1$ |
| 5·0 | | $-0{\cdot}032_6$ | $-0{\cdot}110_7$ | $-0{\cdot}182_8$ | $-0{\cdot}248_9$ | | $1{\cdot}031_7$ | $0{\cdot}994_9$ | $0{\cdot}955_4$ | $0{\cdot}931_9$ |
| 5·5 | | $0{\cdot}328_1$ | $0{\cdot}403_9$ | $0{\cdot}470_9$ | $0{\cdot}529_4$ | | $0{\cdot}996_8$ | $0{\cdot}933_6$ | $0{\cdot}867_8$ | $0{\cdot}801_3$ |
| 6·0 | | $0{\cdot}598_2$ | $0{\cdot}662_6$ | $0{\cdot}715_6$ | $0{\cdot}757_9$ | | $0{\cdot}881_9$ | $0{\cdot}790_7$ | $0{\cdot}699_5$ | $0{\cdot}609_7$ |
| 6·5 | | $0{\cdot}823_4$ | $0{\cdot}867_5$ | $0{\cdot}897_9$ | $0{\cdot}915_6$ | | $0{\cdot}700_5$ | $0{\cdot}583_7$ | $0{\cdot}469_9$ | $0{\cdot}360_7$ |
| 7·0 | | $0{\cdot}990_3$ | $1{\cdot}005_6$ | $1{\cdot}005_4$ | $0{\cdot}991_4$ | | $0{\cdot}469_3$ | $0{\cdot}331_6$ | $0{\cdot}201_9$ | $0{\cdot}079_3$ |
| 7·5 | | $1{\cdot}090_8$ | $1{\cdot}070_1$ | $1{\cdot}033_1$ | $0{\cdot}982_3$ | | $0{\cdot}206_3$ | $0{\cdot}055_9$ | $-0{\cdot}084_9$ | $-0{\cdot}209_1$ |
| 8·0 | | $1{\cdot}121_8$ | $1{\cdot}059_7$ | $0{\cdot}982_2$ | $0{\cdot}892_4$ | | $-0{\cdot}069_8$ | $-0{\cdot}225_6$ | $0{\cdot}362_9$ | $0{\cdot}480_4$ |
| 8·5 | | $1{\cdot}084_8$ | $0{\cdot}978_6$ | $0{\cdot}859_5$ | $0{\cdot}731_8$ | | $0{\cdot}341_9$ | $0{\cdot}491_2$ | $0{\cdot}615_3$ | $0{\cdot}713_9$ |
| 9·0 | | $0{\cdot}985_6$ | $0{\cdot}834_7$ | $0{\cdot}676_4$ | $0{\cdot}515_1$ | | $0{\cdot}594_3$ | $0{\cdot}725_6$ | $0{\cdot}824_5$ | $0{\cdot}892_9$ |
| 9·5 | | $0{\cdot}830_5$ | $0{\cdot}639_4$ | $0{\cdot}447_4$ | $0{\cdot}260_3$ | | $0{\cdot}814_9$ | $0{\cdot}915_2$ | $0{\cdot}978_1$ | $1{\cdot}005_9$ |
| 10·0 | | $0{\cdot}631_9$ | $0{\cdot}406_8$ | $0{\cdot}189_6$ | $+0{\cdot}013_3$ | | $0{\cdot}990_1$ | $1{\cdot}050_6$ | $1{\cdot}067_6$ | $1{\cdot}046_8$ |

$\epsilon$ is measured in units 13·53 eV.

† The Bessel functions arising in this case may be obtained from those tabulated in Jahnke-Emde, *Funktionentafeln*, by use of recurrence relations. It is convenient to choose the values of $r$ for the determination of the quantities $a$ and $b$ appearing in the normalization so that the tabulated values may be used directly.

# The polarization of electrons by double scattering

By H. S. W. Massey, F.R.S.

*Goldsmid Professor of Mathematics, University College, London*

and C. B. O. Mohr, Ph.D.

*Lecturer in Physics, University of Cape Town*

(*Received* 10 *September* 1940)

The scattering of electrons by gold, xenon and krypton atoms has been investigated using Dirac's equations. The polarization to be expected by double scattering at 90° has been studied for an energy range 100 to 150,000 eV. The results agree substantially in the energy range 10,000–150,000 eV with those obtained by Mott for an unscreened gold nucleus. It is found, however, that for lower energies the effect of screening is more important. In particular, at energies for which the intensity of single scattering at 90° is near a minimum, a large polarization is to be expected in the case of gold. For xenon the polarization never exceeds 4 % and for krypton 2 %.

Modifications of the interaction between a nucleus and electron which would reduce the polarization are considered.

As an example of a field as different as possible from the Coulomb type, the polarization produced in double scattering by a potential 'well' is investigated in detail.

The relativistic theory of the electron introduced by Dirac (1928) has been very successful in a number of directions. It led to the remarkable prediction of the existence and properties of positrons and, besides providing a quantitative theory of the scattering of short-wave radiation by free electrons (Klein and Nishina 1929), has given essentially correct formulae for the loss of energy by radiation experienced by the fast electrons occurring in cosmic-ray phenomena (Anderson and Neddermeyer 1936). In one direction, however, an outstanding discrepancy remains. In 1929 Mott developed the theory of the scattering of electrons by a scalar potential field using Dirac's equations and showed that polarization effects are to be expected on double scattering of electrons by a Coulomb field. Detailed calculation for a field with charge $79e$ (corresponding to scattering by gold nuclei) showed that in the second scattering a maximum asymmetry of 16 % was to be expected in the azimuthal distribution, about the direction of the first scattering, for electrons of energy 127 ekV. A number of experiments have been carried out to search for this effect but the maximum asymmetry which has been observed* is only 1·3 %, for 79 kV electrons, reported by Dymond (1932). This is to be compared with the theoretical value of 8 % for this energy. No basis for throwing the blame for the discrepancy on the failure of the experiments to reproduce the conditions assumed in the theory can be found (Richter 1937). Thus Rose and Bethe (1939) have recently shown that multiple scattering effects could not produce nearly sufficient depolarization, while inelastic collisions and electron exchange (Rose and Bethe 1939, Smith 1934) are quite incapable of modifying the expected results. Added interest is now attached to this difficulty by the steadily increasing body of experimental results relating to collisions of electrons of a few mV energy with nuclei which reveal striking discordance with theoretical expectations based on Dirac's theory (Champion 1939, Rose 1940).

In view of this unsatisfactory position we have carried out an investigation of the polarization effects to be expected in scattering by fields differing in form from the unscreened Coulomb type.† Detailed calculations have been made, over a wide energy range (100–150,000 eV), of the polarization to be expected in scattering by the self-consistent atomic fields of the gold, xenon and krypton atoms The results confirm the expectation that the introduction of screening does not modify the polarization to be expected at high energies (over 10,000 eV). At lower energies, however, it is found that for heavy atoms such as gold, large polarization may occur in narrow energy regions. An advantage of the use of screened fields in the calculations is that it is then necessary to evaluate separately the contributions from electrons with each quantized angular momentum, instead of using the summation method employed by Mott (1929) in dealing with unscreened fields. This separate analysis makes it easy to see what is effective in producing the polarization, and hence to suggest what alterations of field will effect given modifications therein In particular it is easy to show that reduction of the asymmetry to within the experimental limits would require most unlikely modifications of the field of force between electron and nucleus.

Finally, we have examined in detail the polarization to be expected in scattering by a field which is at the opposite extreme from the Coulomb type, the spherical potential 'well'. Exact solutions of Dirac's equations may be obtained in this case and they have been used to derive a number of results of interest.

---

* Kikuchi (1939) has observed an asymmetry for 75 okV electrons which agrees with the theoretical, but, as he used thick targets, multiple scattering effects would mask any real polarization, and his asymmetry must be ascribed to instrumental conditions.

† A summary of the results has been published in *Nature*, **146**, 264 (1940).

## §1. GENERAL THEORY

Consider a beam of electrons incident in the direction $LT_1$ on a target $T_1$ and scattered through an angle $\theta_1$, into the direction $T_1T_2$ so as to fall on a second target $T_2$. Then the number scattered by the second target in a direction making an angle $\theta_2$ with $T_1T_2$ depends not only on $\theta_2$ but also on $\phi_2$, the angle the plane containing $T_1T_2$ and the direction of scattering makes with the plane through $LT_1T_2$. If we confine our attention to the case where $\theta_1 = \theta_2$ the number scattered from $T_2$ is proportional to $1+\delta\cos\phi_2$, where

$$\delta = D(\theta_1)\,D(\theta_2)/F(\theta_1)\,F(\theta_2),$$

$$D(\theta) = f(\theta)\,g^*(\theta) - f^*(\theta)\,g(\theta); \quad F(\theta) = |f(\theta)|^2 + |g(\theta)|^2. \tag{1}$$

Here $f$, $g$ are certain functions of $\theta$ and the electron energy determined by the potential of the scattering field and are such that the effective cross-section for scattering of an unpolarized beam into the solid angle $d\omega$ about $\theta$ is

$$\{|f|^2 + |g|^2\}\,d\omega. \tag{2}$$

Mott (1929) has shown that $f$ and $g$ may be determined as follows. If $V$ is the potential of the scattering field, the radial parts $F_l$, $G_l$ of the Dirac wave function for an electron of energy $E$, rest mass $m$, and orbital and total angular momentum quantum numbers $l$ and $l+\frac{1}{2}$ respectively, satisfy the equations

$$\left.\begin{aligned} \frac{2\pi}{h}(mc + E/c - V/c)\,F_l + \frac{dG_l}{dr} - \frac{l}{r}\,G_l &= 0, \\ \frac{2\pi}{h}(mc - E/c + V/c)\,G_l + \frac{dF_l}{dr} + \frac{l+2}{r}\,F_l &= 0. \end{aligned}\right\} \tag{3}$$

The equations for the corresponding functions $F_{-l-1}$, $G_{-l-1}$ for an electron with angular momentum quantum numbers $l$, $l-\frac{1}{2}$ are obtained by replacing $l$ by $-l-1$ in (3).

If $V$ tends to zero for large $r$ faster than $r^{-2}$, $G_l$ must have the asymptotic form

$$G_l \sim \sin\left\{\frac{2\pi}{h}\left(\frac{E^2}{c^2} - m^2c^2\right)^{\frac{1}{2}} r - \tfrac{1}{2}l\pi + \eta_l\right\}, \tag{4}$$

where $\eta_l$ is a phase constant depending on $E$ and $V$. Then in terms of $\eta_l$, $\eta_{-l-1}$

$$\left.\begin{aligned} f(\theta) &= \frac{i}{2k}\Sigma\{(l+1)\,(1 - e^{2i\eta_l}) + l(1 - e^{2i\eta_{-l-1}})\}\,P_l(\cos\theta), \\ g(\theta) &= \frac{i}{2k}\Sigma\{e^{2i\eta_l} - e^{2i\eta_{-l-1}}\}\,P_l^1(\cos\theta), \end{aligned}\right\} \tag{5}$$

where
$$k^2 = \frac{4\pi^2}{h^2}(E^2/c^2 - m^2c^2).$$

Particular interest attaches to the case where $\theta = 90°$ as double scattering then gives the maximum asymmetry. In this case

$$P_l(\cos\theta) = 0, \quad l \text{ odd}; \qquad P_l^1(\cos\theta) = 0, \quad l \text{ even}$$

$$= (-1)^{l/2}\frac{1.3\ldots\ldots\overline{l-1}}{2.4\ldots\ldots l}, \quad l \text{ even.} \qquad = (-1)^{(l-1)/2}\frac{1.3\ldots\ldots l}{2.4\ldots\ldots l-1}, \quad l \text{ odd.}$$

Using the formulae (1) and (5)

$$|\delta|^{\frac{1}{2}} = 2\,|AD - BC|/(A^2 + B^2 + C^2 + D^2), \tag{6}$$

where $A$, $B$, $C$, $D$ are real numbers such that

$$\left.\begin{aligned} A + iB &= \Sigma_l \frac{P_l(0)}{2l+1}\{(l+1)(1 - e^{-2i\eta_l}) + l(1 - e^{-2i\eta_{-l-1}})\}, \\ C + iD &= i\,\Sigma_l P_l^1(0)\sin\chi_l e^{-2i\delta_l}, \\ \chi_l &= \eta_l - \eta_{-l-1}, \quad 2\delta_l = \eta_l + \eta_{-l-1}. \end{aligned}\right\} \tag{7}$$

We note that the maximum value of $|\delta|^{\frac{1}{2}}$ is unity, occurring when $A = \pm D$, $B = \pm C$. The percentage asymmetry $= 200\delta$ and can thus be as large as 200.

## §2. APPLICATION TO ATOMIC FIELDS

2·1. *The fields used.* We now consider in detail cases where the potential is that due to the neutral atoms of gold, xenon and krypton.

The self-consistent field for gold has not been worked out, but one is available for mercury (Hartree, D. R and Hartree, W. 1935), and it is possible to obtain a good approximation to that for gold from this. The procedure adopted was to suppose the wave functions of individual electrons effectively the same in both atoms and modify the $Z$ and $Z_p$ values for mercury by the removal of an outer electron and one unit of nuclear charge.

For krypton an approximate self-consistent field is available (Holtsmark 1930) and one for xenon was obtained by interpolation between fields available for the heavier atoms

2·2. *The differential equations.* Having obtained the fields the evaluation of the functions $f$ and $g$ can be carried out by numerical determination of the phases $\eta_l$, $\eta_{-l-1}$. To do this it was found convenient to transform the equations (3) as follows:

Eliminating $F_l$ gives

$$G_l'' + \left(\frac{2}{r} - \frac{\alpha'}{\alpha}\right) G_l' + \left\{\alpha\beta - \frac{l(l+1)}{r^2} + \frac{l}{r}\frac{\alpha'}{\alpha}\right\} G_l = 0,$$

where $$\alpha = \frac{1}{\hbar}(mc + E/c - V/c), \quad \beta = -\frac{1}{\hbar}(mc - E/c + V/c).$$

Putting $$G_l = \alpha^{\frac{1}{2}} \mathscr{G}_l / r,$$

$$\mathscr{G}_l'' + \phi_l(r)\, \mathscr{G}_l = 0, \tag{8}$$

where $$\phi_l = \alpha\beta - \frac{l(l+1)}{r^2} + \frac{l+1}{r}\frac{\alpha'}{\alpha} - \frac{3}{4}\frac{\alpha'^2}{\alpha^2} + \frac{1}{2}\frac{\alpha''}{\alpha}. \tag{9}$$

The asymptotic form of the solution of this equation which vanishes at $r = 0$ is

$$\sin(kr - \tfrac{1}{2}l\pi + \eta_l),$$

where $k^2 = (E^2/c^2 - m^2c^2)/\hbar^2$. Numerical solution of (8) thus gives $\eta_l$.

A similar procedure may be adopted for $\eta_{-l-1}$. The phase difference between the $\mathscr{G}_l$ and $\mathscr{G}_{-l-1}$ solutions arises from the fact that the functions $\phi_l$, $\phi_{-l-1}$ differ by $(2l+1)\,\alpha'/r\alpha$. The magnitude of the polarization therefore depends not only on the potential but also on the force and will be small when this force is small compared with $r$ times the total energy. This will be referred to in more detail in § 2·3.

In atomic units

$$\left.\begin{aligned} \alpha &= \gamma^{-1}(1+\epsilon) + \gamma Z_p/r, \quad \beta = \gamma^{-1}(\epsilon - 1) + \gamma Z_p/r; \\ \alpha' &= -\gamma Z/r^2, \quad \alpha'' = 2\gamma(Z - \tfrac{1}{2}rZ')/r^3, \end{aligned}\right\} \tag{10}$$

where $$\gamma = 2\pi e^2/hc = 137{\cdot}2, \quad \epsilon = E/mc^2.$$

Following the usual nomenclature of self-consistent field theory $Z$, $Z_p$ are the effective nuclear charges for field and potential respectively.

2·3. *Convergence of series*. The series $A$, $B$ converge very slowly. The condition that the phases $\eta_l$, $\eta_{-l-1}$ should be small for values of $l > l_0$ is that

$$\frac{2Z_p\epsilon}{r} \ll l_0(l_0+1)/r^2,$$

for such values of $r$ that $$kr \sim l_0 + \tfrac{1}{2}.$$

This is the usual criterion adopted in the calculation of collision cross-sections by the method of 'partial' cross-sections (Mott and Massey 1933*a*). Applied to gold it would indicate that for $k = 100$, the phases are small for $l > 10$. This does not mean, however, that the contribution to $A$ and $B$ from greater values of $l$ is unimportant, for there is a strong cancellation in sign between the successive terms of the series concerned and a large number of small phases make an important contribution. In fact for $k = 100$ at least 60 terms are required.

The convergence of the series for $C$ and $D$ is very much faster. The $l$th terms of these series contain $\sin(\eta_l - \eta_{-l-1})$ ($= \sin\chi_l$) as a factor and this becomes very small quite rapidly as $l$ increases. To examine the reason for this we return to equation (8). This may be written

$$\frac{d^2\mathcal{G}_l}{dr^2} + \{k^2 + v(r) - l(l+1)/r^2 - (l+1)\,w(r)\}\,\mathcal{G}_l = 0 \tag{11}$$

where

$$v(r) = 2Z_p\epsilon/r + \gamma^2 Z_p^2/r^2 - \frac{3}{4}\frac{\alpha'^2}{\alpha^2} + \frac{1}{2}\frac{\alpha''}{\alpha}, \quad w(r) = \gamma^2 Z/\{(1+\epsilon)\,r^3 + \gamma^2 r^2 Z_p\}. \tag{12}$$

Let $\overline{\mathcal{G}}$ be the proper solution of this equation with $w = 0$ and which has asymptotic form

$$\overline{\mathcal{G}} \sim \sin(kr - \tfrac{1}{2}l\pi + \overline{\eta}_l).$$

Then if $w$ is small we have

$$\mathcal{G}_l \sim \sin\{kr - \tfrac{1}{2}l\pi + \overline{\eta}_l - (l+1)\,\zeta_l\},$$

$$\mathcal{G}_{-l-1} \sim \sin\{kr - \tfrac{1}{2}l\pi + \overline{\eta}_l + l\zeta_l\},$$

where

$$\zeta_l = k^{-1}\int_0^\infty w\mathcal{G}_l^2\,dr \tag{13}$$

Hence to this approximation

$$\chi_l = \eta_l - \eta_{-l-1} = (2l+1)\,\zeta_l, \tag{14}$$

showing, as pointed out earlier, how strongly the $\chi_l$ and hence the polarization depend on the force $-Z/r^2$.

This will be valid if the right-hand side of (13) is small compared with unity, so that the size of $(2l+1)\,\zeta_l$ can be used as a criterion for the smallness of the $l$th term in the series for $C$ and $D$. Now $w$ is only large for small values of $r$ and with increasing $l$, $g_l$ becomes smaller and smaller in this region owing to the presence of the term $l(l+1)/r^2$ in the equation (11). Even for gold this term is always considerably greater than $(2l+1)\,w$ if $l$ is $> 1$, so we can expect $\chi_l$ to be always small for $l > 1$ and to become negligible rapidly as $l$ increases.

2·4. *Results and discussion*. The following procedure was adopted to calculate the percentage asymmetry $P = 200\delta$. The phases $\eta_0, \eta_1, \eta_{-2}$ and in certain cases $\eta_3, \eta_{-4}, \eta_5$, were calculated by accurate numerical integration of the equation (8) for a number of values of $\epsilon$. In this way the main contribution to the series for $C$ and $D$, which arises from $\eta_1$ and $\eta_{-2}$ was obtained without approximation. To complete the calculation a number of the higher phases in each case was calculated by Jeffreys' approximation (Mott and Massey 1933*b*) according to which

$$\eta_l = \tfrac{1}{2}(l+\tfrac{1}{2})\pi - kr_0 + \int_{r_0}^{\infty} \{\phi^{\frac{1}{2}} - k\}\, dr, \tag{15}$$

the lower limit of the integration being the outer zero $r_0$ of the integrand The accuracy of this approximation was confirmed by comparing results given by its use and by accurate numerical integration in a number of selected cases. Graphical interpolation was then used to obtain the remaining phases. Summation of the series for $A$ and $B$ was facilitated by observing that for large $l$ the terms fall off effectively as in a geometrical progression

This procedure gives results of sufficient accuracy for our purpose, as the quantities $A$ and $B$ of (7), containing so many terms, are not very sensitive to the exact values of the phases. The only further modification required is to estimate for gold the contribution from small terms involving $\chi_3$, $\chi_5$, etc., in $C$ and $D$. These were evaluated by use of (13) and (15), as high accuracy in the separate evaluation of $\eta_l$ and $\eta_{-l-1}$ would be necessary to obtain these small difference phases.

In figure 1 a number of the phases $\delta_l$ and $\chi_l$ are illustrated for gold. For xenon and krypton the phase diagram is very similar except that all $\chi$ except $\chi_1$ are completely negligible. For energies between 50 and 50,000 eV, $\chi_1$ is practically constant at 0·06 radian for krypton and 0·14 radian for xenon. To save space the other phases for these atoms are not illustrated but are available for communication to anyone who wishes to use them. For krypton the lower energy phases $\delta_l$ agree closely with those calculated by Holtsmark (1930).

The minimum which occurs in the phases for gold at energies in the neighbourhood of 50,000 eV arises from the presence of the factor $\epsilon$ multiplying the Coulomb potential term $2Z_p/r$ which appears in the equations for $\mathscr{G}_l$, $\mathscr{G}_{-l-1}$

Using these phases the percentage asymmetry $200\delta$ may be calculated. Comparison of the results for gold with those obtained by Mott (1932) neglecting screening is illustrated in figure 2, showing that any failure to observe appreciable polarization for 79 ekV electrons cannot be attributed to screening effects.

For energies lower than those considered by Mott the effect of screening becomes very marked. This may be seen by reference to table 1 which shows the variation with energy of the intensity $I, = (A^2+B^2+C^2+D^2)/k^2$, of single scattering at 90°. The highly irregular variations, due to diffraction, which do not occur for an unscreened Coulomb field have interesting consequences.

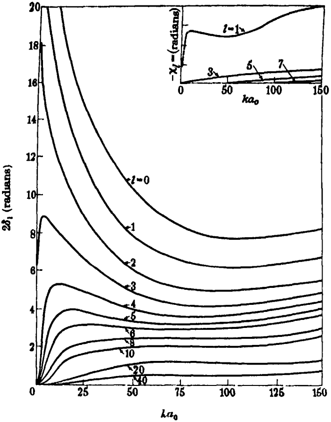

FIGURE 1. Phases for calculation of scattering of electrons by the atomic field of gold

Main figure illustrates values of $2\delta_l = \eta_l + \eta_{-l-1}$.
Inset figure illustrates values of $\chi_l = \eta_l - \eta_{-l-1}$.
Scale of inset figure is graduated in $\frac{1}{10}$th radians.

The percentage asymmetry can be written

$$200\delta = 200\,|\,AC - BD\,|\,k^2/I. \tag{16}$$

Where $I$ is small, as is the case for electrons with energies in the neighbourhood of 500 and 120 eV for gold, we can except large values of $200\delta$ if $C$ and $D$ are not too small, i.e. if $\chi_1$ is not too small. For gold, as $\chi_1$ is nearly

0·3 radian over a wide energy range, we can therefore expect large percentage asymmetries for electrons with energies at which $I$ is a minimum. Specimen values obtained by an approximate summation of the series concerned are given in table 1. Values obtained by more accurate summation, together with a detailed investigation of the angular distribution for single scattering, will be given by one of us (C. B. O. M.) in a later paper. In any case too much weight should not be attached to the exact numerical values obtained in the energy range concerned as they are very sensitive to the details of form and range of the atomic field. Nevertheless, the existence of the phenomenon follows simply from the fact that the function $I$ has deep minima and the quantities $C$ and $D$ are not both very small over the energy range concerned. The existence of the irregular variation of $I$ is in agreement with experiment as will be seen from table 1, where some experimental values of the scattering at 90° derived from Arnot's results for mercury (1930) are given. On the other hand, it does not always follow that the polarization is a maximum when the scattering is very small, as can be seen by reference to the case $k = 6{\cdot}25$ of table 1. Here, although $I$ is small, $AC - BD$ is much smaller still.

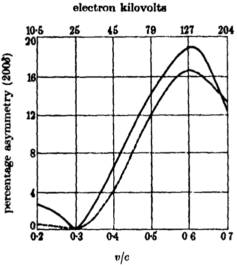

FIGURE 2. Percentage asymmetry in double scattering of electrons by gold. Full line, calculated with inclusion of screening. Dotted line, calculated for an unscreened gold nucleus.

Although the function $I$ for scattering by xenon and krypton also shows minima, the value of $\chi_1$ is not large enough in either case to give large

TABLE 1. ILLUSTRATING SCATTERING AND POLARIZATION PHENQMENA FOR THE GOLD ATOM

| Electron wave number $k$ (in atomic units) | Electron energy eV | Intensity of single scattering at 90° × $k^2$ | Percentage asymmetry $200\delta$ | Intensity of single scattering at 90° × $k^2$ for mercury observed by Arnot (1930) arbitrary units |
|---|---|---|---|---|
| 30 | 12,000 | 6·5 | 3·4 | — |
| 20 | 5,600 | 6·7 | 7·4 | — |
| 17 | 3,900 | 7·3 | 1·1 | — |
| 14 | 2,650 | 6·8 | 2·1 | — |
| 12 | 1,950 | 6·2 | 8·2 | — |
| 10 | 1,350 | 3·2 | 13 | — |
| 9·5 | 1,220 | 2·4 | 10 | — |
| 9 | 1,100 | 2·4 | 2 | — |
| 8·5 | 975 | 3·9 | 8 | — |
| 8 | 865 | 4·3 | 13 | — |
| — | 800 | — | — | 10 |
| 7·5 | 760 | 1·6 | 38 | — |
| 7 | 663 | 0·25 | 67 | — |
| — | 610 | — | — | 22 |
| 6·5 | 570 | 0·74 | 31 | — |
| 6·25 | 529 | 0·25 | 0 | — |
| 6 | 487 | 1·0 | 1 | 30 |
| 5·5 | 408 | 15·6 | 0 | — |
| — | 379 | — | — | 28 |
| 5 | 338 | 28 | 0·3 | — |
| 4·5 | 273 | 20 | 0 | — |
| 4 | 217 | 8 | 1·1 | — |
| — | 207 | — | — | 1·3 |
| — | 119 | — | — | 9·9 |

polarizations. The maximum value found is 4 % for xenon and 2 % for krypton for electrons with energies in the neighbourhood of 500 eV.

The possibility of detecting experimentally these low energy polarization effects for a heavy atom such as gold or mercury is of interest. Although it is an advantage to work with the lower energy electrons involved, the fact that large polarization is associated with small scattered intensity makes observation difficult.

## § 3. FIELD MODIFICATIONS NECESSARY TO REDUCE POLARIZATION

The most direct way of reducing the polarization is to decrease the relative importance of the term $w(r)$ involved in (11). This means a reduction of the gradient of the potential near the origin relative to the total potential.

For example, if, near the origin, the potential were changed from $Ze^2/r$ to $Ze^2(1-e^{-\lambda r})/r$ the value of $w$ would be much reduced for values of $r < 1/\lambda$. This, in turn, will greatly reduce the overlap integral (13) determining $\chi_l$ if

$$l(l+1)\,\lambda^2 \simeq k^2 + v\left(\frac{1}{\lambda}\right). \tag{17}$$

For when (17) is satisfied the function $w$ of (11) is small even at the maximum of $\overline{\mathscr{G}}_l$. As we have found that $\chi_1$ is by far the most important phase difference it follows that, for $k = 100$ (corresponding to 121 ekV electrons), $\lambda$ must be of the order 100 atomic units appreciably to reduce the polarization.

To make this more precise the case $\lambda = 100$ was investigated in detail using Jeffreys' approximation (15) A value of 0·12 radian was found for $\chi_1$. This would lead, apart from changes in the less sensitive quantities $A$ and $B$ of (6), to about one-tenth of the polarization given by the unmodified field. Even this is just within the experimentally determined limit of 1·0 % for 76 ekV electrons (Dymond 1934). Since $\lambda = 100$ involves field modifications at nuclear distances as great as $5 \times 10^{-11}$ cm., the departure from the Coulomb form would affect the orbits of $K$ electrons and would be apparent in various ways. It can therefore be regarded as out of the question.

An alternative possibility has been investigated by Rose (1940). He considers the effect of a very deep and very short range attraction This affects the $p_{\frac{1}{2}}$ but not the $p_{\frac{3}{2}}$ wave and the phase difference $\chi_1$ can be made to approximate to $\pi$. As $\sin\chi_1$ appears in the expressions for $C$ and $D$ this will greatly reduce the polarization. Rose found, however, that when the range and depth were adjusted to give small polarizations in this way, modifications of the scattered intensity were introduced which were not in agreement with experiment.

It seems difficult therefore to account, on any theoretical grounds, for the absence of observed polarization and it is very desirable that further experimental investigation of the matter be carried out.

## §4. POLARIZATION BY DOUBLE SCATTERING FROM A SPHERICAL POTENTIAL WELL

For a scattering potential $V$ defined by

$$V = -V_0,\ r < r_0;\ \ V = 0,\ r > r_0 \tag{18}$$

the behaviour of the phase differences $\chi_l$ is in marked contrast to the case of a Coulomb field, screened or unscreened. In the latter case only $\chi_1$ is really important but for the spherical well potential, which represents a field of force which is infinitely large at the point $r = r_0$ and zero elsewhere, the $\chi_l$ are all small except for such values of $l$ that the first maximum of $G_l$ or $G_{-l-1}$ falls near $r = r_0$. This follows from the fact that the $\chi_l$ depend more on the force than the potential (see § 2·2). In other words, for the spin orientation of the electron to be strongly affected its angular momentum must be such that it spends a relatively long time in the neighbourhood of the large force at $r = r_0$. The detailed analysis is as follows.

The general solutions of the equations

$$\left.\begin{aligned} \alpha F_l + dG_l/dr - \frac{l}{r} G_l &= 0, \\ -\beta G_l + dF_l/dr + \frac{l+2}{r} F_l &= 0, \end{aligned}\right\} \tag{19}$$

with $\alpha$, $\beta$ constants, may be written

$$\left.\begin{aligned} r^{\frac{1}{2}} G_l &= A_l J_{l+\frac{1}{2}}(r\sqrt{(\alpha\beta)}) + B_l J_{-l-\frac{1}{2}}(r\sqrt{(\alpha\beta)}), \\ r^{\frac{1}{2}} F_l &= (\beta/\alpha)^{\frac{1}{2}} [A_l J_{l+\frac{1}{2}}(r\sqrt{(\alpha\beta)}) - B_l J_{-l-\frac{1}{2}}(r\sqrt{(\alpha\beta)})]. \end{aligned}\right\} \tag{20}$$

This follows by use of the relation

$$x\frac{dJ_p}{dx} = pJ_p - xJ_{p+1}.$$

We may immediately use (20) to obtain the appropriate solutions for the potential (18)

For $r < r_0$ in order that the functions should be finite at the origin, we have

$$G_l = A_l J_{l+\frac{1}{2}}(k'r); \quad F_l = s' A_l J_{l+\frac{1}{2}}(k'r),$$

with

$$k'^2 = \{m^2c^4 + (E+V_0)^2\}/\hbar^2c^2, \quad s'^2 = (E+V_0-mc^2)/(E+V_0+mc^2).$$

For $r > r_0$,

$$G_l = C_l J_{l+\frac{1}{2}}(kr) + D_l J_{-l-\frac{1}{2}}(kr),$$

$$F_l = s[C_l J_{l+\frac{1}{2}}(kr) - D_l J_{-l-\frac{1}{2}}(kr)],$$

where

$$k^2 = (m^2c^4 + E^2)/\hbar^2c^2, \quad s^2 = (E-mc^2)/(E+mc^2). \tag{21}$$

The asymptotic form of $G_l$ is then given by

$$G_l \sim \sin(kr - \tfrac{1}{2}l\pi + \eta_l),$$

where

$$\tan\eta_l = (-1)^l D_l/C_l.$$

To determine $D_l/C_l$ use is made of the fact that $G_l$ and $F_l$ must be continuous at $r = r_0$, giving

$$\tan\eta_l = (-1)^l u_l/v_l,$$

where

$$\left.\begin{aligned} u_l &= sJ_{l+\frac{1}{2}}(k'r_0)\,J_{l+\frac{3}{2}}(kr_0) - s'J_{l+\frac{3}{2}}(k'r_0)\,J_{l+\frac{1}{2}}(kr_0), \\ v_l &= sJ_{l+\frac{1}{2}}(k'r_0)\,J_{-l-\frac{3}{2}}(kr_0) + s'J_{l+\frac{3}{2}}(k'r_0)\,J_{-l-\frac{1}{2}}(kr_0). \end{aligned}\right\} \tag{22}$$

An exactly similar procedure may be followed to obtain $\eta_{-l-1}$. The fundamental solutions for $G_{-l-1}$ are as for $G_l$ but are of the form $J_{\pm(l-\frac{1}{2})}$ for $F_{-l-1}$. We find

$$\tan\eta_{-l-1} = (-1)^l u_{-l-1}/v_{-l-1},$$

where $u_{-l-1}$, $v_{-l-1}$ are as for $u_l$, $v_l$ with $J_{\pm(l+\frac{1}{2})}$ replaced by $J_{\pm(l-\frac{1}{2})}$. By making use of the recurrence relation

$$J_{p-1}(x) + J_{p+1}(x) = \frac{2p}{x}J_p(x),$$

$\tan\eta_{-l-1}$ may be written in the alternative form

$$\tan\eta_{-l-1} = (-1)^l\{u_l - (2l+1)\,\sigma p_l\}/\{v_l + (2l+1)\,\sigma q_l\},$$

where

$$\sigma = \left(\frac{1}{kr_0} - \frac{s'}{sk'r_0}\right); \quad p_l = J_{l+\frac{1}{2}}(k'r_0)\,J_{l+\frac{1}{2}}(kr_0), \quad q_l = J_{l+\frac{1}{2}}(k'r_0)\,J_{-l\;\frac{1}{2}}(kr_0). \tag{23}$$

This brings out clearly the relation between the two sets of phases and shows that the quantity $\sigma$ is the parameter which is important in determining the polarization effects.

The phase differences $\chi_l$ can be expressed in the form

$$\tan\chi_l = \frac{2\sigma}{\pi}\frac{2l+1}{kr_0}\{J_{l+\frac{1}{2}}(k'r_0)\}^2/L,$$

where

$$\begin{aligned} L = \{J_{l+\frac{1}{2}}(k'r_0)\}^2\,(W_l + 2l + 1\sigma U_l) + \frac{s'}{s}\,(2l+1)(\sigma V_l + 2U_l)\,J_{l+\frac{3}{2}}(k'r_0)\,J_{l+\frac{1}{2}}(k'r_0) \\ + \left(\frac{s'}{s}\right)^2 V_l\{J_{l+\frac{3}{2}}(k'r_0)\}^2, \end{aligned}$$

$$U_l = J_{-l-\frac{3}{2}}(kr_0)\,J_{-l-\frac{1}{2}}(kr_0) - J_{l+\frac{3}{2}}(kr_0)\,J_{l+\frac{1}{2}}(kr_0), \quad V_l = \{J_{-l-\frac{1}{2}}(kr_0)\}^2 + \{J_{l+\frac{1}{2}}(kr_0)\}^2;$$

$$W_l = \{J_{-l-\frac{3}{2}}(kr_0)\}^2 + \{J_{l+\frac{3}{2}}(kr_0)\}^2. \tag{24}$$

In deriving this result use has been made of the relation

$$J_p(x)\,J_{-p+1}(x) + J_{p-1}(x)\,J_{-p}(x) = 2\sin p\pi/\pi x.$$

For values of $l \gg kr_0$ we find, on substitution of the series expansion of the Bessel functions

$$\tan \chi_l \simeq \pi(2l+1)\,\sigma(\tfrac{1}{2}kr_0)^{2l+2}\{\Gamma(l+\tfrac{3}{2})\}^{-2}. \tag{25}$$

This falls off rapidly as $l$ increases beyond $kr_0$.

Again, if $l \ll kr_0$ we may use the asymptotic expansions for the Bessel functions with argument $kr_0$ to give

$$\tan \chi_l = \frac{2\sigma}{\pi kr_0}(2l+1)\left\{1+\frac{s'^2}{s^2}\cot^2\theta_l-(2l+1)\frac{s'}{s}\sigma\cot\theta_l\right\}^{-1}, \tag{26}$$

where $\theta_l = k'r_0 - \frac{1}{2}l\pi$. If $\sigma$ is small this shows that $\chi_l$ is also small in the range $l < kr_0$.

Since we have shown that, if $\sigma$ is small, $\chi_l$ is small for $l \ll kr_0$ and also for $l \gg kr_0$, it follows that $\chi_l$ can only be large when $l \simeq kr_0$. The polarization is then mainly determined by $\chi_{l_0}$ where $l_0 \simeq kr_0$. From (24) it follows that $\chi_{l_0}$ will vanish if $J_{l_0+\frac{1}{2}}(k'r_0)$ vanishes. A necessary, but by no means sufficient, condition which must be satisfied in order that the polarization should not be very small is that $J_{l_0+\frac{1}{2}}(k'r_0)$ must not be nearly equal to 0, $l_0$ being the nearest odd integer to $kr_0$. If this condition is satisfied the polarization may still be small for other reasons, i.e. the series $A$ and $B$ may be large compared with $C$ and $D$.

In contrast to the atomic field calculations an additional variation is imposed on $C$ and $D$ due to rapid variation of the important phase difference $\chi_l$ with energy. The energy regions over which the polarization is large can therefore be expected to be more localized than for fields of Coulomb type.

*Numerical results and discussion.* It is difficult to decide which are the most appropriate values of $V_0$ and $r_0$ to choose for numerical investigation. To consider cases comparable with that of the gold atom calculations were carried out for such values of $V_0$ that

$$\int_0^{r_0} r^2 V_0\,dr = e^2\int_0^{\infty} rZ_p\,dr, \tag{27}$$

with $Z_p$ as for gold. This gives a relation between $r_0$ and $V_0$ such that the 'total potential' is the same as for the gold atom. The value of $r_0$ was then chosen, so the zero order phase $\eta_0$ was nearly the same as for scattering by gold atoms in the energy range of interest. Besides this particular choice of $V_0$ and $r_0$ other neighbouring values of $r_0$ were used and also a potential of depth three times that given by (27). The results are given in table 2. Cases (*d*), (*e*), (*f*) refer to values of $V_0$ satisfying (27), the others to values of $V_0$ one-third as large as given by (27).

TABLE 2. POLARIZATION BY SCATTERING FROM A SPHERICAL WELL POTENTIAL

| Electron wave number | Electron energy | Zero order phase | Asymmetry parameter | Critical Bessel functions | Percentage asymmetry |
|---|---|---|---|---|---|
| $ka_0$ | ekV | $\eta_0$ (radians) | $\sigma$ | $J_{kr_0+\frac12}$, $kr_0$ odd<br>$\left.\begin{matrix}J_{kr_0+1\frac12}\\ J_{kr_0-\frac12}\end{matrix}\right\}$, $kr_0$ even | $200\delta$ |
| Case (*a*). $V_0 = 2{\cdot}4\times10^6$ eV, $r_0 = 0{\cdot}05a_0$ | | | | | |
| 40 | 21 | 36·2 | 0·35 | −0·03 | Very small |
| 60 | 46 | 35·4 | 0·23 | $+0{\cdot}01_4$ | ,, |
| 80 | 81 | — | 0·17 | +0·06, −0·04 | ,, |
| 100 | 121 | 35·4 | $0{\cdot}13_5$ | +0·11 | 35 |
| 110 | 143 | — | — | +0·11 | 103 |
| 120 | 168 | 34·6 | 0·11 | +0·11 | 10 |
| Case (*b*). $V_0 = 3\times10^5$ eV, $r_0 = 0{\cdot}10a_0$ | | | | | |
| 30 | 12 | 14·8 | — | $+0{\cdot}08_5$ | 1 |
| 40 | 21 | — | — | −0·18, +0·14 | 24 |
| 50 | 33 | 13·3 | $0{\cdot}04_5$ | −0·19 | 104 |
| 60 | 46 | — | — | +0·08, −0·15 | 11 |
| 70 | 63 | 11·9 | $0{\cdot}03_0$ | $-0{\cdot}01_2$ | 8 |
| 80 | 81 | — | — | $+0{\cdot}17_5$, −0·12 | 112 |
| 90 | 100 | — | — | +0·17 | 53 |
| 100 | 121 | 11·1 | $0{\cdot}02_1$ | +0·10, +0·03 | 5 |
| Case (c) $V_0 = 3{\cdot}7\times10^4$ eV, $r_0 = 0{\cdot}20a_0$ | | | | | |
| 35 | 16 | — | $0{\cdot}005_1$ | −0·21 | 1·6 |
| 50 | 33 | 5·15 | $0{\cdot}003_3$ | +0·18, −0·17 | 2·3 |
| 70 | 63 | 4·16 | $0{\cdot}002_4$ | +0·26, +0·54 | 1·5 |
| 90 | 100 | 3·04 | $0{\cdot}001_6$ | +0·22, +0·19 | 1·0 |
| 110 | 143 | 3·02 | $0{\cdot}001_4$ | +0·21, +0·19 | 1·0 |
| Case (*d*). $V_0 = 1{\cdot}1\times10^5$ eV, $r_0 = 0{\cdot}20a_0$ | | | | | |
| 25 | 8·4 | 14·40 | 0·020 | 0·059 | 1·0 |
| 40 | 21 | $12{\cdot}9_5$ | 0·012 | 0·03, −0·13 | 0·3 |
| 50 | 33 | 12·0 | 0·010 | 0·15, −0·08 | 38 |
| Case (*e*). $V_0 = 3{\cdot}3\times10^4$ eV, $r_0 = 0{\cdot}30a_0$ | | | | | |
| $16\frac23$ | 3·6 | 11·2 | 0·006 | 0·067, −0·16 | Very small |
| $33\frac13$ | 15 | 8·3 | 0·005 | −0·21, +0·03 | ,, |
| $46\frac23$ | 28·5 | 7·2 | 0·004 | −0·06, −0·17 | 14·0 |
| Case (*f*). $V_0 = 1{\cdot}4\times10^4$ eV, $r_0 = 0{\cdot}40a_0$ | | | | | |
| 12·5 | 2 | 8·8 | 0·0026 | −0·18 | Very small |
| 22·5 | 4 | 6·9 | 0·0013 | −0·22 | 1·6 |
| 35 | 16 | 5·0 | 0·0009 | +0·20, −0·09 | 13 |
| 45 | 27 | 4·0 | 0·0007 | +0·23, +0·09 | 1 |

To indicate the factors which are important in determining the polarization for the spherical well potential we have included in the table values of the asymmetry parameter defined in (23) and of the 'critical' Bessel functions in each case. These are defined as follows. It was shown above that the only considerable phase differences which occur are those for which $l$ is close to $kr_0$. As we have restricted numerical calculations to integral values of $kr_0$ and as only odd $l$ values arise in considering asymmetry due to double scattering at 90°, the most important phase differences will be those for which $l = kr_0 \pm 1$ for $kr_0$ even and that for which $l = kr_0$ if $kr_0$ is odd. In order that these phase differences and hence the asymmetry should not be small, both $\sigma$ and the Bessel functions $J_{l+\frac{1}{2}}(k'r_0)$ (see (24)) for the appropriate $l$ values must not be too small. Hence, if $kr_0$, $= l_0$, is even the functions $J_{l_0+\frac{3}{2}}(k'r_0)$, $J_{l_0+\frac{1}{2}}(k'r_0)$ and, if $l_0$ is odd, $J_{l_0+\frac{1}{2}}(k'r_0)$ play a critical role. These are the functions given in the fifth column of table 2.

A study of the table now shows how strongly the asymmetry depends on $\sigma$ and the critical Bessel functions. In cases (*a*), (*b*) and (*d*), $\sigma$ is large enough to give almost complete polarization if the critical functions are near their maximum values. We find also rapid alternations of $200\delta$ as the electron energy changes, due to the alternations in the values of the functions. In cases (*c*), (*e*) and (*f*), on the other hand, $\sigma$ is so small that appreciable polarization only arises when the quantities $A$ and $B$ of (7) happen to be small together. This is so in case (*e*) for $k = 46\frac{2}{3}$. When $\sigma$ is very small as in (*c*), (*e*) and (*f*) the dependence on the critical Bessel functions is not very marked as the polarization is so small then under any conditions that the contribution from the regions of $l \simeq l_0$ does not dominate the quantities $C$ and $D$ so strongly.

It is of interest to note that, for values of $V_0$ and $r_0$ which give zero order phases $\eta_0$ comparable with those given by the atomic field (cases (*c*) and one intermediate between (*e*) and (*f*)), the polarization is rarely large, the maximum being of the same order (20%) as for gold in the energy range concerned.

## REFERENCES

Anderson and Neddermeyer 1936 *Phys. Rev.* **50**, 263.
Arnot 1930 *Proc. Roy. Soc.* A, **130**, 655.
Champion 1939 *Reports on Progress in Physics*, **5**, 348.
Dirac 1928 *Proc. Roy. Soc.* A, **117**, 610.
Dymond 1932 *Proc. Roy. Soc.* A, **136**, 638.
— 1934 *Proc. Roy. Soc.* A, **145**, 657.
Hartree, D. R. and Hartree, W. 1935 *Proc. Roy. Soc.* A, **149**, 210.
Holtsmark 1930 *Z. Phys.* **66**, 49.
Kikuchi 1939 *Proc. Phys-Math. Soc. Japan*, **12**, 524.
Klein and Nishina 1929 *Z. Phys.* **52**, 893.

Mott 1929 *Proc. Roy. Soc.* A, **124**, 425.
— 1932 *Proc. Roy. Soc.* A, **135**, 429.
Mott and Massey 1933*a* *Theory of atomic collisions*, p. 139. Oxford: Clarendon Press.
— — 1933*b* *Theory of atomic collisions*, p. 92. Oxford: Clarendon Press.
Richter 1937 *Ann. Phys., Lpz.*, **28**, 533.
Rose 1940 *Phys. Rev.* **57**, 280.
Rose and Bethe 1939 *Phys. Rev.* **55**, 277.
Smith, R. A. 1934 *Proc. Camb. Phil. Soc.* **30**, 520.

---

# $\beta$-ray spectra of light elements

By A. A. Townsend, M.Sc.[*]
*Emmanuel College, Cambridge*

(*Communicated by J. D. Cockcroft, F.R.S.—Received* 30 *June* 1940)

A magnetic spectrometer has been used to investigate the $\beta$-ray spectra of some elements of low atomic number. It is found that all the spectra follow the Fermi distribution law for a certain range from the high energy end-point, the range over which this is true is much greater if the maximum energy is large. The end-points found are: $C^{11}$ $0.981 \pm 0.005$ MeV, $N^{13}$ $1.218 \pm 0.004$ MeV, $Mn^{56}$ $2.88 \pm 0.01$ and $1.035 \pm 0.015$ MeV, $Cu^{64}$ (positrons) $0.649 \pm 0.004$ MeV, $Cu^{64}$ (negatrons) $0.574 \pm 0.004$ MeV, $Zn^{63}$ $2.320 \pm 0.005$ MeV.

## Introduction

The production of artificial radioactive elements in quantities of order 0·01 mC makes possible the use of a magnetic spectrometer for the investigation of $\beta$-ray energy spectra. The method has considerable advantages in speed and accuracy over cloud-chamber measurements, and spectrometers of good resolution can be used with sources of this magnitude. The present experiments have been carried out with a spectrometer of conventional design, intended for use with short period sources (of half-life greater than 5 min.). No extraordinary precautions have been taken to avoid scattering and absorption of those electrons whose energies lie below 100 ekV, but the spectra are thought to be accurate within twice the statistical error as shown on the diagrams

The elements which have been investigated are $C^{11}$, $N^{13}$, $Mn^{56}$, and the longer-lived products of the deuteron bombardment of copper, i.e. $Cu^{64}$ and $Zn^{63}$. These comprise four positron emitters and two negatron emitters.

---

[*] Exhibition of 1851 Scholar.

## APPARATUS

The spectrometer is shown in sketch in figure 1. The source and counter slits are each 2 cm. long and 2 mm. wide. With a radius of curvature of 8 cm. the total resolution is calculated to be 3·1 %, a value confirmed by measurements on conversion lines in the ThC″ spectrum.

The counter is cut from a solid brass block and is 1·6 cm. in diameter and 2·5 cm. long. The entry slit is covered by a mica window, 1·6 mg. cm.$^{-2}$ thick. It is filled with a mixture of argon and alcohol, and is of the self-extinguishing type. The natural effect is about eight counts per minute.

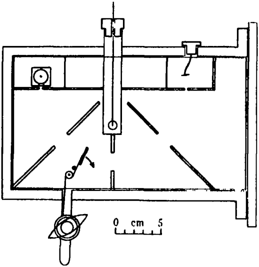

FIGURE 1

The counts were recorded on a fast counting meter whose resolution time was of order 0·004 sec. Measurements of loss due to finite resolution of the meter were made and corrections applied.

The pole-pieces of the electromagnet measure 24 by 16 cm., and the field is uniform within 2 % over the area employed in the spectrometer. The field strength is measured as a multiple of known $\gamma$-ray conversion lines, so that a slight non-uniformity of field does not affect the accuracy of the measurements. To measure the field a small flip coil between the pole-faces is reversed and the throw produced in a ballistic galvanometer is measured. This throw is compared with an approximately equal one made by reversing a known current flowing in the primary of a mutual inductance, the secondary of which is in series with the flip coil. In this way the linearity of the galvanometer deflexion need not be assumed. For fields of order 400 G the accuracy of reading is about 0·1 % and the error is estimated as under 0·3 %. The relative accuracy of field measurements is better.

The radioactive source is inserted by means of a plug in the vacuum box, after which the box can be exhausted. Apart from time taken in the preparation of the source, a count may be started 30 sec. after the start of the experiment. A shutter is used to obtain blank counts so that $\gamma$-ray effects can be eliminated.

With the exception of copper, all the sources were in the form of fine powder which was mounted on thin mica, using a weak solution of nail polish for adhesive. The copper was used in the form of foil.

## RESULTS

Corrections are applied to the counting rates for decay of the source and absorption of the $\beta$-rays in the counter window. The ordinates of the momentum distribution diagram are obtained by dividing these values by the corresponding $H\rho$ values. Momentum distributions for the elements listed above are plotted in figures 2–7. As insets on those diagrams are shown the Fermi (1934) plots of the distributions. Since the atomic numbers concerned are low, this can be done by plotting $(N/f)^{\frac{1}{2}}$ against $\sqrt{(1+\eta^2)}$, where

$N d\eta$ is the number of particles with momenta between $\eta$ and $\eta + d\eta$,

$$f = \eta^2 \frac{x}{1-e^{-x}},$$

$$x = \frac{2\pi Z}{137} \frac{\sqrt{(1+\eta^2)}}{\eta},$$

$Z$ = atomic number,

$\eta$ = momentum in units of $mC = \dfrac{H\rho}{1703}$.

No Konopinski-Uhlenbeck (1935) plots have been made, as they appear to have no significance for these elements.

*Carbon.* $C^{11}$, $T_{\frac{1}{2}} = 20{\cdot}6$ min.

This was prepared by the reaction $B^{10}(d; n)\,C^{11}$, using 950 kV deuterons. The boron powder was scraped off the copper target head and mounted as described above. Owing to the $N^{13}$ contamination, no counts were made for about 20 min. after irradiation, and measurements in the neighbourhood of the end-point were postponed longer. The end-point is $H\rho$ 4660 ± 20 (0·981 ± 0·005 MeV). As might be expected, this is considerably lower than the values obtained from cloud-chamber work, but is in reasonable agreement with a result obtained by Moore (1940) using the absorption method, i.e. 1·03 ± 0·03 MeV. The form of the spectrum appears simple, and the Fermi plot shows no sign of an intense second component. The plot is not straight but curved upwards slightly. This curvature appears to be due to failure of the Fermi distribution rather than to a weak softer component. This conclusion is confirmed by work on the annihilation radiation of $C^{11}$ carried out in this laboratory by Ward (1940). He finds no sign of any nuclear $\gamma$-rays.

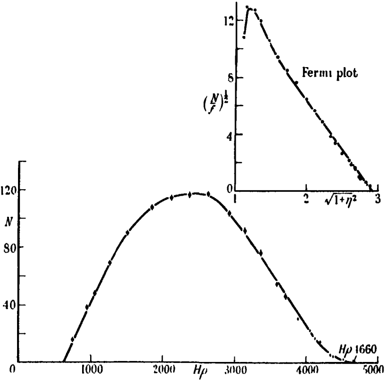

FIGURE 2 Positron spectrum of $C^{11}$.

*Nitrogen.* $N^{13}$, $T_{\frac{1}{2}} = 9{\cdot}95$ min.

This is prepared in a similar way, using the reaction $C^{12}(d, n)N^{13}$ on soot targets. The end-point is $H\rho$ 5500 ± 15 (1·218 ± 0·004 MeV). This figure may be compared with 1·198 ± 0·006 MeV obtained by Lyman (1939*a*) and 1·24 ± 0·03 MeV obtained by Moore (1940). The general form of the Fermi plot is similar to that of $C^{11}$, and the same conclusion could be drawn that there is only a single component. On the other hand, Richardson (1939) has reported the presence of a $\gamma$-ray of energy 280 ekV in intensity 0·4

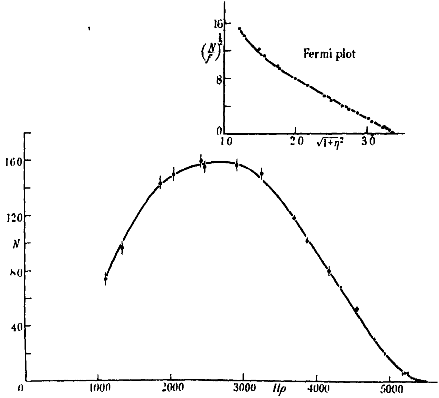

FIGURE 3 Positron spectrum of $N^{13}$.

quantum per disintegration, and Lyman (1939*b*) finds a $\gamma$-$\gamma$ coincidence rate for $N^{13}$, implying a $\gamma$-ray in intensity 0·25 quantum per disintegration. This does not agree with direct absorption measurements of Ward (1940), indicating that there is not more than 5 % of radiation of this energy. If it is assumed that the form of a $\beta$-ray spectrum does not vary erratically with nuclear constitution in this region, then it can be stated from the $\beta$-ray evidence that the contribution of a softer component to the observed spectrum is certainly less than 10 % and probably less than 5 %. It is true that the assumption that the Fermi distribution is correct will result in a larger intensity for the soft component, but no experimental support for this assumption exists in the present results.

*Manganese.* $Mn^{56}$, $T_{\frac{1}{2}} = 2{\cdot}55$ hr.

The radiomanganese is produced in the cyclotron, using the reaction $Mn^{55}$ (*d*; *p*) $Mn^{56}$, and both manganese and manganese dioxide were used as targets The spectrum is obviously complex, and it is easily possible to separate the components using the Fermi plot. This analysis is not critically dependent on the validity of the Fermi distribution, but internal evidence justifies its assumption for the range above $H\rho$ 4000. The two end-points come out at $H\rho$ $11170 \pm 35$ ($2{\cdot}88 \pm 0{\cdot}01$ MeV) and $H\rho$ $4850 \pm 50$ ($1{\cdot}035 \pm 0{\cdot}015$ MeV). Using a cloud chamber Brown and Mitchell (1936) obtained 2·9 and 1·2 MeV, while Dunworth (1939), using the absorption method,

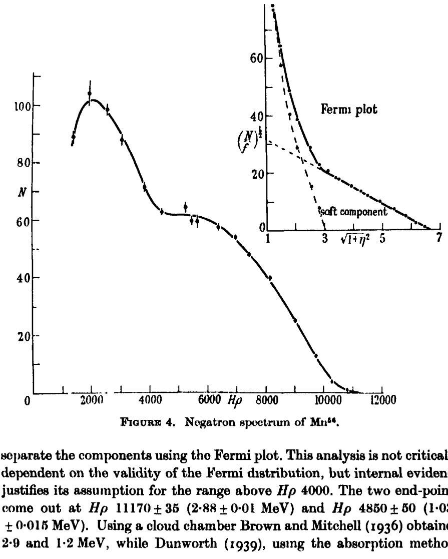

FIGURE 4. Negatron spectrum of $Mn^{56}$.

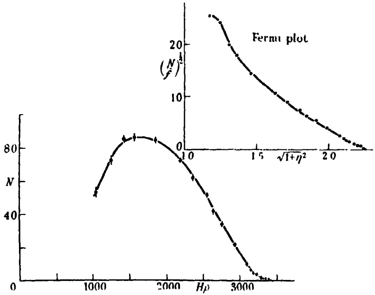

**FIGURE 5.** Positron spectrum of $Cu^{64}$.

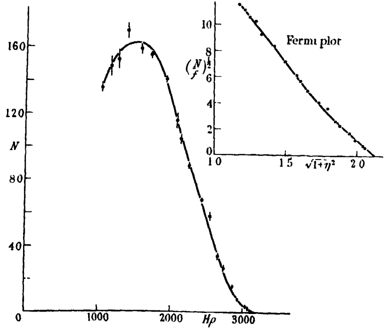

**FIGURE 6** Negatron spectrum of $Cu^{64}$.

obtained 2·8 and 1·1 MeV. A strong $\gamma$-ray of energy $1{\cdot}85 \pm 0{\cdot}025$ MeV is expected. Curran, Dee and Strothers (1940) have shown by direct measurement in a $\gamma$-ray spectrometer that $\gamma$-rays of energy 0·91 and 2·03 MeV are emitted.

*Copper.* $Cu^{64}$, $T_{\frac{1}{2}} = 10{\cdot}6$ hr.; $Zn^{63}$, $T_{\frac{1}{2}} = 39$ min.

$Cu^{64}$ is prepared by the reaction $Cu^{63}$ $(d, p)$ $Cu^{64}$ in the cyclotron. It is an example of $\beta$-ray branching and two spectra are plotted. The positron spectrum has an end-point at $H\rho$ $3480 \pm 15$ $(0{\cdot}649 \pm 0{\cdot}004$ MeV) and that of the negatron spectrum is $H\rho$ $3184 \pm 15$ $(0{\cdot}574 \pm 0{\cdot}004$ MeV). For the same spectra, Tyler (1939) has given the values $0{\cdot}659 \pm 0{\cdot}003$ and $0{\cdot}578 \pm 0{\cdot}003$ MeV in good agreement. In a detailed comparison the two spectra are seen to be of differing degrees of asymmetry, presumably due to the opposite effects of the atomic field on the two spectra.

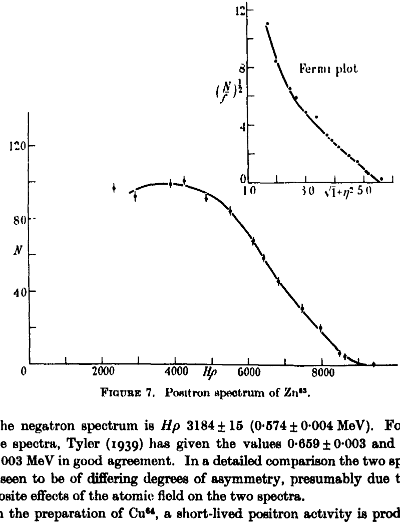

FIGURE 7. Positron spectrum of $Zn^{63}$.

In the preparation of $Cu^{64}$, a short-lived positron activity is produced, prepared by the reaction $Cu^{63}$ $(d; 2n)$ $Zn^{63}$. The spectrum was studied in the course of the experiment and the end-point is $H\rho$ 9260 ± 20 (2·320 ± 0·005 MeV). The Fermi plot is strongly curved and a $\gamma$-ray of energy around 1·5 MeV would be expected.

## DISCUSSION

Comparing these results with those obtained using natural radioactive elements, attention is drawn to the comparatively large range over which the Fermi distribution is correct. This is outstanding in the case of $Mn^{56}$ for which the Fermi plot is a straight line from $H\rho$ 11170 to 5000. Spectra of lower maximum energies show divergences from the theoretical distribution closer to the end-point, but still the range of validity of the Fermi expression is much greater than for elements such as RaE $N^{13}$ and RaE have approximately the same end-points, but whereas the spectrum of the latter deviates from theory below $H\rho$ 4500 (see for example, Flammersfeld 1939), that of the former shows no deviation at $H\rho$ 3500, though such a deviation would be expected if the reports of $\gamma$-rays from $N^{13}$ were correct. Among the elements investigated, it is also remarkable that these deviations are more serious if the end-point is low. In illustration, excepting $Zn^{63}$, the spectrum of which is probably complex, the Fermi plots of the two spectra of $Cu^{64}$ show by far the greatest deviation from the straight line, and it is just these spectra which have the lowest end-points It is unlikely that these features are incorrect, for they appear in most recent work on light elements (e.g. Tyler and Lyman) and the features of the $\beta$-ray spectrum of RaE are now known with reasonable precision. The conclusion is drawn that a positive deviation from the Fermi distribution exists at the low-energy end of the spectrum, becoming more serious as the atomic number is increased or the maximum energy reduced. In all cases there is a small region where the Fermi plot is a straight line.

A useful corollary of this result is that it is possible to make extrapolations of the end-points, provided that the range of energy considered is a small fraction of the total energy of the transition. This avoids troublesome and rather vague corrections to the observed curves in order to allow for the finite resolution of the spectrometer.

The radioactive sources used in these experiments were prepared in the Cavendish High Voltage and Cyclotron Laboratories, and I am indebted to the workers in these laboratories for their assistance. I also wish to thank Prof. J. D. Cockcroft and Mr P. I. Dee for their interest and advice.

For the duration of this work, I held an Overseas Scholarship of the Commissioners for the Exhibition of 1851, and an external research scholarship from Emmanuel College.

### REFERENCES

Brown and Mitchell 1936 *Phys. Rev.* **50**, 593
Curran, S. C., Dee, P. I. and Strothers, J. 1940 *Proc. Roy. Soc.* A, **174**, 546.
Dunworth, J. V. 1939 *Nature, Lond.*, **143**, 1065.
Fermi, E. 1934 *Z Phys.* **88**, 161.
Flammersfeld, A. 1939 *Z Phys.* **112**, 727.
Lyman, E. M. 1939*a* *Phys Rev.* **55**, 234.
— 1939*b* *Phys. Rev.* **55**, 1123.
Moore 1940 *Phys. Rev.* **57**, 355.
Richardson 1939 *Phys. Rev* **55**, 609.
Tyler 1939 *Phys. Rev* **56**, 125.
Ward 1940 In course of publication.

---

# Wind tunnel correction for a circular open jet tunnel with a reflexion plate

BY B DAVISON AND L. ROSENHEAD, D.SC.

(*Communicated by J Proudman, F.R.S —Received* 19 *July* 1940)

It is advantageous from many points of view to make test models as large as possible. One method of doing this is to measure the characteristics of half the model in existing wind tunnels One half of the aerofoil is mounted horizontally on a vertical reflexion plate and the plate is placed in a suitable position in an open jet which, in the undisturbed state, is of circular section. The contour of the jet is distorted, especially with models of large semi-span, but this distortion is neglected in the analysis The correcting factor associated with 'uniform' distribution of lift is worked out exactly and that associated with 'elliptic' distribution approximately. The effect of the induced downwash on the distribution of lift is ignored The results are given in suitable tables and figures.

Throughout the working range of normal experiments the correcting factor is of the same order of magnitude as that obtaining when a full model is tested in a jet of circular section.

## 1. THE CONFORMAL TRANSFORMATION

The characteristics of aerofoils are deduced from experiments made in wind tunnels. It is therefore necessary to calculate the amounts by which lift and drag, when measured in a tunnel, differ from their values when measured in free air at the same angle of incidence. Alternatively, it suffices to know the amount by which the incidence must be corrected in order to give the same value of the lift coefficient in free air. The basic theory for the calculation of this 'wind-tunnel correction' is well known. The original theory is due to Prandtl (1919), but it has been developed extensively by other investigators, notably Glauert (1930, 1933). Prandtl shows that the downwash at any point on the aerofoil is half that at a corresponding point far downstream, where the problem may be transformed into a two-dimensional one If $\phi$ and $\psi$ are the velocity potential and stream function in this region then Prandtl also shows that

(i) if the measurements are made in a tunnel of open working section, that is in a jet, then $\phi$ must be constant over the boundary of the cross-section of the jet;

(ii) if the measurements are made in a closed tunnel then $\psi$ must be constant over the boundary of the cross-section of the tunnel.

If the shape of the cross-section of the jet or tunnel is known, the above conditions can usually be satisfied by the introduction of appropriate image vortices. These image vortices, when taken together with the vortices existing in the wake behind the aerofoil, must satisfy the conditions prescribed by (i) and (ii). If the circulation round the aerofoil at a distance $x$ along the span from the middle of the aerofoil is $K(x)$, then the strength of the trailing vortex which extends downstream between $x$ and $x+\delta x$ is $-(dK/dx)\,\delta x$. The image vortices produce a downwash which varies along the span of the aerofoil in the tunnel and so change the effective angle of incidence of the aerofoil. This interference is the induced effect of the tunnel and produces the difference which necessitates the wind tunnel correction

In modern practice the test model is made as large as possible. It is fairly usual too, in such cases, to divide the aerofoil into two sections each of length equal to half the original span. One half of the aerofoil is then mounted horizontally on a vertical partition and the characteristics of half of the original aerofoil are measured in an open jet which in the undisturbed state is of circular section. The state of affairs is represented schematically in figure 1 *a*. The geometric centre of a cross-section of the jet is $C$. The radius of the undisturbed jet is $a$ The vertical partition is at a distance $c$ from $C$ where $a^2 = b^2+c^2$, so that the length $AB$ is equal to $2b$. $\psi$ must be constant along $AB$ and $\phi$ must be constant along the circular arc $AXB$. If we introduce the image of the system with respect to $AB$ we obtain the scheme shown in figure 1 *b*, and the condition $\psi$ is constant along $AB$ is satisfied automatically. We need, therefore, only seek a system which makes $\phi$ constant along the extended contour $AXBX'A$, which consists of two symmetrically situated circular arcs. The region within this contour can be mapped conformally on the region within the circle $|\zeta| = 1$ in a $\zeta$-plane by the transformation

$$\frac{\zeta-i}{\zeta+i} = \left(e^{-i(\pi-2\lambda)}\frac{z-ib}{z+ib}\right)^n, \tag{1}$$

or expressed in another form

$$\tan^{-1}\zeta = n\tan^{-1}\left(\frac{z}{a\sin\lambda}\right), \tag{1a}$$

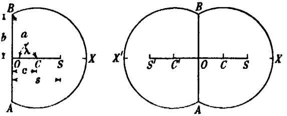

(a) z-plane (b) extended z-plane

FIGURE 1

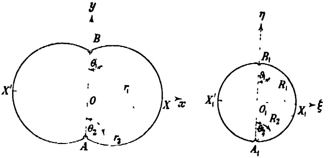

(a) extended z-plane (b) ζ-plane

FIGURE 2

where

$$n = \pi/2(\pi-\lambda)$$

$$\left.\begin{aligned} z &= x+iy, \quad \zeta = \xi+i\eta, \\ b &= a\sin\lambda, \quad c = a\cos\lambda. \end{aligned}\right\} \tag{2}$$

The axes of co-ordinate are defined in figure 2 and the transformation is defined by the relations

$$\begin{aligned} \zeta-i &= R_1 e^{i(\vartheta_1-\frac{1}{2}\pi)}, & \pi>\vartheta_1 &\geqslant -\pi, & R_1 &= \{\xi^2+(\eta-1)^2\}^{\frac{1}{2}}; \\ \zeta+i &= R_2 e^{i(\frac{1}{2}\pi-\vartheta_2)}, & \pi>\vartheta_2 &\geqslant -\pi, & R_2 &= \{\xi^2+(\eta+1)^2\}^{\frac{1}{2}}; \\ z-ib &= r_1 e^{i(\theta_1-\frac{1}{2}\pi)}, & \pi>\theta_1 &\geqslant -\pi, & r_1 &= \{x^2+(y-b)^2\}^{\frac{1}{2}}; \\ z+ib &= r_2 e^{i(\frac{1}{2}\pi-\theta_2)}, & \pi>\theta_2 &\geqslant -\pi, & r_2 &= \{x^2+(y+b)^2\}^{\frac{1}{2}}. \end{aligned}$$

## 2. UNIFORM DISTRIBUTION OF LIFT

A solution for uniform loading has been given by K. Kondo (1935). The following treatment is inserted principally because it leads up to the more important case of elliptic distribution of lift described in § 3, and secondarily because the treatment differs from that given by Kondo

The point in the $\zeta$-plane which corresponds to $(x, 0)$ of the $z$-plane is $(\xi, 0)$ where

$$\xi = \tan\{n \tan^{-1}(x/a \sin\lambda)\}, \tag{3}$$

and if there is a vortex of strength $K$ at $x_1$ there will be a vortex of equal strength at $\xi_1$. If we assume a uniform distribution of lift over an aerofoil of span $2s$ in the extended $z$-plane (see figure 2 *a*) then there are vortices of strength $\pm K$ springing downstream from the wing tips $x = \pm s$. There will therefore be vortices of strength $\pm K$ at the points $\xi = \pm s_1$, where

$$s_1 = \tan\{n \tan^{-1}(s/a \sin\lambda)\}. \tag{4}$$

In experiment the quantity $c/a$ $(= \cos\lambda)$ can be measured without much trouble, and for this reason $c/a$ is chosen as the parameter in table 1 instead of $\lambda$. In this table $\xi$ is given for different values of $x/a$ and $c/a$, and from it $s_1$ can be read off corresponding to different values of $s/a$ and $c/a$. The column $c/a = 1{\cdot}0$ needs a little explanation. It gives the value to which $\xi$ tends as $c/a$ tends to $1{\cdot}0$. For example, if $c/a = 1 - \frac{1}{2}\epsilon^2$, where $\epsilon$ is very small, then

$$\left.\begin{array}{ll} \text{(i) when } x/a \text{ is very small,} & \xi = \dfrac{x}{2a\epsilon}; \\[2ex] \text{(ii) when } x/a \text{ is `reasonably large', } & \xi = 1 - \dfrac{a\epsilon}{x}; \\[2ex] \text{(iii) when } x/a \text{ is equal to } 2 - \frac{1}{2}\epsilon^2, & \xi = 1. \end{array}\right\} \tag{3a}$$

The complex potential due to the vortices $\pm K$ at $\xi = \pm s_1$ is

$$W_1 = \frac{iK}{2\pi}\log\left(\frac{\zeta - s_1}{\zeta + s_1}\right). \tag{5}$$

The complex potential due to the image vortices which must be superposed on $W_1$ in order to make $\phi$ constant over the circle $|\zeta| = 1$ is

$$W_2 = \frac{iK}{2\pi}\log\left(\frac{\zeta^{-1} - s_1}{\zeta^{-1} + s_1}\right). \tag{6}$$

This can easily be verified for the singularities of $W_2$ lie outside the circle $\zeta| = 1$, and further, on putting $\zeta = e^{i\theta}$ it can be seen that $W_1$ and $W_2$ are

TABLE 1. VALUES OF $\xi$ FOR DIFFERENT VALUES OF $x/a$ AND $c/a$

(The column $c/a = 1·0$ must be interpreted as giving the limit to which $\xi$ tends as $c/a$ tends to 1·0.)

| $c/a$ ... | 0·0 | 0·1 | 0·2 | 0·3 | 0·4 | 0·5 | 0·6 | 0·7 | 0·8 | 0·9 | 1·0 |
|---|---|---|---|---|---|---|---|---|---|---|---|
| $x/a$ | $\xi$ | $\xi$ | $\xi$ | $\xi$ | $\xi$ | $\xi$ | $\xi$ | $\xi$ | $\xi$ | $\xi$ | $\xi$ |
| 0·0 | 0·000 | 0·000 | 0·000 | 0·000 | 0·000 | 0·000 | 0·000 | 0·000 | 0·000 | 0·000 | 0·000 |
| 0·1 | 0·100 | 0·095 | 0·091 | 0·088 | 0·086 | 0·086 | 0·088 | 0·093 | 0·104 | 0·133 | 1·000 |
| 0·2 | 0·200 | 0·189 | 0·180 | 0·175 | 0·172 | 0·172 | 0·176 | 0·185 | 0·205 | 0·256 | 1·000 |
| 0·3 | 0·300 | 0·282 | 0·270 | 0·261 | 0·256 | 0·255 | 0·260 | 0·273 | 0·300 | 0·368 | 1·000 |
| 0·4 | 0·400 | 0·376 | 0·358 | 0·345 | 0·338 | 0·336 | 0·341 | 0·356 | 0·388 | 0·463 | 1·000 |
| 0·5 | 0·500 | 0·468 | 0·445 | 0·428 | 0·418 | 0·414 | 0·419 | 0·433 | 0·470 | 0·544 | 1·000 |
| 0·6 | 0·600 | 0·559 | 0·530 | 0·508 | 0·494 | 0·489 | 0·491 | 0·505 | 0·538 | 0·613 | 1·000 |
| 0·7 | 0·700 | 0·650 | 0·613 | 0·586 | 0·568 | 0·559 | 0·559 | 0·571 | 0·603 | 0·673 | 1·000 |
| 0·8 | 0·800 | 0·739 | 0·695 | 0·662 | 0·639 | 0·626 | 0·623 | 0·632 | 0·660 | 0·723 | 1·000 |
| 0·9 | 0·900 | 0·827 | 0·774 | 0·735 | 0·707 | 0·689 | 0·682 | 0·688 | 0·711 | 0·766 | 1·000 |
| 1·0 | 1·000 | 0·914 | 0·851 | 0·805 | 0·771 | 0·749 | 0·738 | 0·740 | 0·757 | 0·804 | 1·000 |
| 1·1 | — | 1·000 | 0·927 | 0·872 | 0·832 | 0·805 | 0·790 | 0·785 | 0·799 | 0·837 | 1·000 |
| 1·2 | — | — | 1·000 | 0·938 | 0·891 | 0·858 | 0·838 | 0·829 | 0·836 | 0·866 | 1·000 |
| 1·3 | — | — | — | 1·000 | 0·947 | 0·908 | 0·883 | 0·869 | 0·870 | 0·892 | 1·000 |
| 1·4 |  | — | — | — | 1·000 | 0·956 | 0·923 | 0·905 | 0·901 | 0·914 | 1·000 |
| 1·5 |  | — | — | — | — | 1·000 | 0·963 | 0·939 | 0·929 | 0·935 | 1·000 |
| 1·6 | — | — | — | — | — | — | 1·000 | 0·971 | 0·955 | 0·954 | 1·000 |
| 1·7 | — | — | — | — | — | — | — | 1·000 | 0·978 | 0·971 | 1·000 |
| 1·8 | — | — | — | — | — | — |  |  | 1·000 | 0·986 | 1·000 |
| 1·9 | — | — | — | — | — | — |  | — | — | 1·000 | 1·000 |
| 2·0 | — | — |  | — | — | — |  | — |  | — | 1·000 |

conjugate complex numbers, so that the real part of $(W_1+W_2)$ is zero on the circle $|\zeta| = 1$. $(W_1+W_2)$ is the complex potential of the flow in the $z$-plane. If there had been no jet the disturbance would have been created by the two vortices of strengths $\pm K$ springing from the points $z = \pm s$, and the appropriate complex potential would have been

$$W_3 = \frac{iK}{2\pi}\log\left(\frac{z-s}{z+s}\right). \tag{7}$$

The disturbance induced by the boundaries of the jet is therefore the velocity field associated with the complex potential

$$W = W_1 + W_2 - W_3. \tag{8}$$

The downwash at $(x, 0)$ on the aerofoil due to the constraint of the jet boundary is

$$w = \tfrac{1}{2}i\left(\frac{dW}{dz}\right)_{z=x}. \tag{9}$$

If we assume as a first approximation that the downwash across the span is approximately the same as that at the centre of the complete aerofoil we can say that the downwash is everywhere equal to

$$\left[\frac{K}{2a}\operatorname{cosec}\left\{\frac{\pi}{\pi-\lambda}\tan^{-1}\left(\frac{s}{a\sin\lambda}\right)\right\}\Big/(\pi-\lambda)\sin\lambda\right]-\frac{K}{2\pi s}.$$

If $V$ is the speed of the undisturbed jet then the effect of the downwash is to tilt the stream downwards through an angle $w/V$ so as to diminish the angle of incidence and incline the lift force backwards through the same angle. If we make use of the equations

$$L = C_L \tfrac{1}{2}\rho V^2 S = 2s\rho V K, \tag{10}$$

where $L$ is the total lift, $\rho$ the density of the air and $S$ is the span multiplied by the mean chord, the existing theory can be summarized as follows. If $\alpha$, $C_L$ and $C_D$ are the measured values of the incidence, lift coefficient and drag coefficient in the wind tunnel, then the true values, in free air, of the incidence and drag coefficient at the measured value of $C_L$ are $\alpha+\Delta\alpha$ and $C_D+\Delta C_D$, where

$$\Delta\alpha = \delta\frac{S}{C}C_L, \quad \Delta C_D = \delta\frac{S}{C}C_L^2. \tag{11}$$

$C$ is equal to $\pi a^2$, the area of cross-section of the undisturbed jet, and $\delta$ is the correcting factor associated with the tunnel

For clarity we shall introduce two symbols, $\delta_U$ and $\delta_E$, which are the correcting factors based on the assumptions of 'uniform' and 'elliptic' distributions of lift over the complete aerofoil in the extended $z$-plane. If we make use of equations (9) and (11) we find that, with the approximations made,

$$\delta_U = -\frac{1}{8}\left[\frac{2na}{s\sin\lambda}\operatorname{cosec}\left(2n\tan^{-1}\frac{s}{a\sin\lambda}\right)-\frac{a^2}{s^2}\right] \tag{12}$$

It is clear from this formula that as $\lambda\to 0$, i.e. $c/a\to 1$, the value of $-\delta_U$ approaches infinity whatever the value of $s/a$. Further, at any fixed value of $\lambda$, the greatest value of $s/a$ is $1+\cos\lambda$ and the corresponding value of $\delta_U$ is

$$-\frac{1}{8\sin\lambda}\left[\frac{2n(1+\cos\lambda)-\sin\lambda}{(1+\cos\lambda)^2}\right].$$

Finally, when $\lambda = \frac{1}{2}\pi$ it can be seen that $\delta_U = -0{\cdot}125$ in agreement with the well-known approximate result for the correction associated with a circular jet.

We have approximated by assuming that the downwash is everywhere equal to that at $x = 0$. It is possible, however, to take account of the variation of induced downwash across the span. The correction then is

$$\Delta\alpha = -\frac{1}{L}\int \frac{w}{V}\,dL = \delta_U \frac{S}{C} C_L,$$

where $\qquad dL = \rho V K\,dx \quad \text{and} \quad L = 2s\rho V K.$

Hence

$$\begin{aligned}\delta_U &= -\frac{C}{LSC_L}\int_{x=-s}^{x=s} \frac{w}{V}\,dL,\\ &= -\frac{C}{LSC_L V}\int_{z=-s}^{z=s} \left(\tfrac{1}{2} i \frac{dW}{dz}\right)(\rho V K)\,dz,\end{aligned}$$

since $dz = dx$ along the $x$-axis. Hence

$$\delta_U = -i\frac{\rho K C}{2LSC_L}\int_{-s}^{s} \frac{dW}{dz}\,dz. \tag{13}$$

Now

$$\int_{-s}^{s} \frac{dW_2}{dz}\,dz = \int_{-s_1}^{s_1} \frac{dW_2}{d\zeta}\,d\zeta = -\frac{iK}{\pi}\log\left(\frac{1+s_1^2}{1-s_1^2}\right),$$

and

$$\begin{aligned}\int_{-s}^{s} \frac{d}{dz}(W_1 - W_3)\,dz &= \operatorname*{Lt}_{\epsilon\to 0}\int_{-(s-\epsilon)}^{(s-\epsilon)} \frac{d}{dz}(W_1 - W_3)\,dz\\ &= -\frac{iK}{\pi}\log\left\{\frac{s_1}{s}\left(\frac{dz}{d\zeta}\right)_s\right\}\end{aligned}$$

after some manipulation. Making use of the relation $W = W_1 + W_2 - W_3$ we obtain quite easily

$$-\delta_U = A + B = \frac{1}{16}\frac{a^2}{s^2}\log\left[\frac{1}{n}\frac{s_1}{1-s_1^2}\left(\frac{a\sin\lambda}{s} + \frac{s}{a\sin\lambda}\right)\right], \tag{14}$$

$$\left.\begin{aligned}&\text{where} & A &= \frac{1}{16}\frac{a^2}{s^2}\log\left(\frac{1+s_1^2}{1-s_1^2}\right),\\ &\text{and} & B &= \frac{1}{16}\frac{a^2}{s^2}\log\left[\frac{1}{n}\frac{s_1}{1+s_1^2}\left(\frac{a\sin\lambda}{s} + \frac{s}{a\sin\lambda}\right)\right].\end{aligned}\right\} \tag{15}$$

It should be noted that when $(s/a\sin\lambda)$ is small

$$\left.\begin{aligned}&s_1 \to \frac{ns}{a\sin\lambda}\left[1 - \tfrac{1}{3}(1-n^2)\left(\frac{s}{a\sin\lambda}\right)^2\right],\\ &A \to \frac{1}{8}\frac{n^2}{\sin^2\lambda}, \quad B \to \frac{1}{24}\frac{(1-n^2)}{\sin^2\lambda},\end{aligned}\right\} \tag{16}$$

and

$$-\delta_U = \frac{1+2n^2}{24\sin^2\lambda}. \tag{17}$$

Formula (17) holds, with good accuracy, over a wide range of the region in which experiments are usually made.

It is clear from (14) that as $c/a \to 1$ the value of $-\delta_U$ tends to infinity (see equation (3*a*)) whatever the value of $s/a$, and that for any fixed value of $\lambda$ the value of $-\delta_U$ tends to infinity as $s/a$ approaches its greatest value $(1+\cos\lambda)$. Further, when $\lambda = \frac{1}{2}\pi$ it can be seen that

$$-\delta_U = \frac{1}{8}\frac{a^2}{s^2}\tanh^{-1}\left(\frac{s^2}{a^2}\right),$$

$$= \frac{1}{8}\left\{1+\frac{1}{3}\frac{s^4}{a^4}+\frac{1}{5}\frac{s^8}{a^8}+\dots\right\}, \tag{18}$$

in agreement with the well-known result for a circular jet. Values of $-\delta_U$ are given in table 2 and are illustrated diagrammatically in figure 3.

TABLE 2. VALUES OF $-\delta_U$ FOR DIFFERENT VALUES OF $s/a$ AND $c/a$

| $s/a$ \ $c/a$ | 0·0 | 0·1 | 0·2 | 0·3 | 0·4 | 0·5 | 0·6 | 0·7 | 0·8 | 0·9 | 1·0 |
|---|---|---|---|---|---|---|---|---|---|---|---|
| $s/a \to 0$ | 0·125 | 0·117 | 0·111 | 0·110 | 0·111 | 0·118 | 0·129 | 0·155 | 0·207 | 0·368 | ∞ |
| 0·1 | 0·125 | 0·117 | 0·111 | 0·110 | 0·111 | 0·118 | 0·129 | 0·153 | 0·202 | 0·359 | ∞ |
| 0·2 | 0·125 | 0·117 | 0·111 | 0·109 | 0·110 | 0·117 | 0·128 | 0·150 | 0·198 | 0·334 | ∞ |
| 0·3 | 0·125 | 0·116 | 0·109 | 0·108 | 0·108 | 0·115 | 0·125 | 0·146 | 0·189 | 0·306 | ∞ |
| 0·4 | 0·126 | 0·115 | 0·109 | 0·107 | 0·107 | 0·111 | 0·120 | 0·140 | 0·180 | 0·274 | ∞ |
| 0·5 | 0·128 | 0·115 | 0·108 | 0·105 | 0·104 | 0·108 | 0·116 | 0·133 | 0·169 | 0·246 | ∞ |
| 0·6 | 0·131 | 0·116 | 0·108 | 0·104 | 0·102 | 0·106 | 0·111 | 0·127 | 0·157 | 0·219 | ∞ |
| 0·7 | 0·137 | 0·119 | 0·108 | 0·102 | 0·100 | 0·103 | 0·107 | 0·121 | 0·148 | 0·198 | ∞ |
| 0·8 | 0·148 | 0·124 | 0·110 | 0·102 | 0·099 | 0·100 | 0·103 | 0·116 | 0·138 | 0·178 | ∞ |
| 0·9 | 0·174 | 0·132 | 0·114 | 0·104 | 0·099 | 0·098 | 0·099 | 0·109 | 0·128 | 0·162 | ∞ |
| 1·0 | ∞ | 0·154 | 0·121 | 0·106 | 0·099 | 0·097 | 0·096 | 0·105 | 0·119 | 0·148 | ∞ |
| 1·1 | — | ∞ | 0·139 | 0·112 | 0·100 | 0·096 | 0·095 | 0·100 | 0·111 | 0·134 | ∞ |
| 1·2 | — | — | ∞ | 0·128 | 0·105 | 0·096 | 0·094 | 0·096 | 0·105 | 0·126 | ∞ |
| 1·3 | — | — | — | ∞ | 0·118 | 0·101 | 0·094 | 0·095 | 0·102 | 0·118 | ∞ |
| 1·4 | — | — | — | — | ∞ | 0·112 | 0·097 | 0·094 | 0·098 | 0·112 | ∞ |
| 1·5 |  | — | — |  | — | ∞ | 0·106 | 0·096 | 0·096 | 0·107 | ∞ |
| 1·6 | — | — | — | — | — | — | ∞ | 0·103 | 0·097 | 0·105 | ∞ |
| 1·7 | — | — | — | — | — | — | — | ∞ | 0·103 | 0·104 | ∞ |
| 1·8 | — |  |  | — | — | — | — | — | ∞ | 0·108 | ∞ |
| 1·9 | — | — | — | — | — | — | — | — | — | ∞ | ∞ |
| 2·0 | — | — | — | — | — | — | — | — |  | — | ∞ |

In tabulating $\delta_U$ separate tables were made of $A$ and $B$ in order to facilitate the numerical evaluation which has to be made in § 3. These tables are not here reproduced. The work involved was rather laborious and use was made of graphical interpolation.

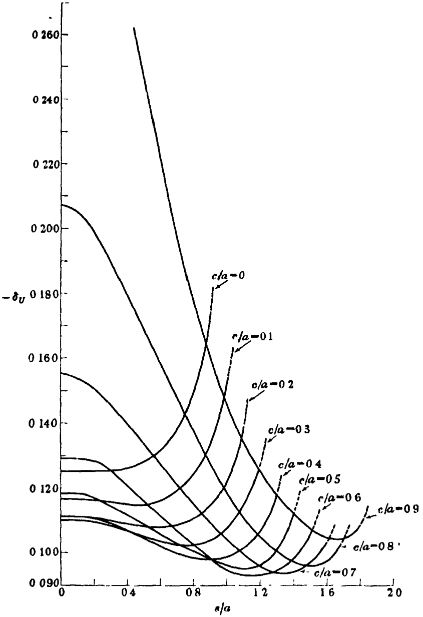

FIGURE 3. Graphs of $-\delta_U$

### 3. APPROXIMATION TO THE ELLIPTIC DISTRIBUTION OF LIFT

We here investigate the correcting factor $\delta_E$ when the distribution of circulation over the complete aerofoil in the extended $z$-plane is of the elliptic form, that is

$$K(x) = K_0\left\{1-\frac{x^2}{s^2}\right\}^{\frac{1}{2}}. \tag{19}$$

If in this formula we put

$$x = a\sin\lambda\tan\left(\frac{1}{n}\tan^{-1}\xi\right), \quad s = a\sin\lambda\tan\left(\frac{1}{n}\tan^{-1}s_1\right),$$

we see that the distribution of circulation in the $\zeta$-plane is

$$K(\xi) = K_0 F(\xi) \tag{20}$$

where

$$F(\xi) = \left\{1-\frac{\tan^2(n^{-1}\tan^{-1}\xi)}{\tan^2(n^{-1}\tan^{-1}s_1)}\right\}^{\frac{1}{2}},$$

$$= \left\{1-\frac{a^2\sin^2\lambda}{s^2}\tan^2\left(\frac{1}{n}\tan^{-1}\xi\right)\right\}^{\frac{1}{2}}. \tag{20a}$$

For small values of $s_1$ we can approximate by putting $\tan(n^{-1}\tan^{-1}s_1)$ equal to $s_1/n$, so that

$$F(\xi) = \left\{1-\frac{\xi^2}{s_1^2}\right\}^{\frac{1}{2}}, \tag{21}$$

and the distribution is also elliptic. The limiting case, $\lambda = \frac{1}{2}\pi$, corresponding to $n = 1$, is elliptic for all values of $s_1$. The other limiting case, $\lambda \to 0$, corresponding to $n \to \frac{1}{2}$, shows that $F(\xi) \to 1$, so that the circulation in the transformed plane tends towards the 'uniform distribution'. For intermediate values of $\lambda$ the form of $F(\xi)$ shows a systematic change from the elliptic to the uniform type. The distribution is symmetrical with respect to $\xi = 0$ and falls to zero at $\xi = \pm s_1$.

In a manner similar to that employed in § 2 the downwash, $w(x)$, at any point on the aerofoil can be split up into three parts by the relation

$$w = w_1 + w_2 - w_3, \tag{22}$$

where (i) $w_1$ is the component due to the trailing vortices in the $\zeta$-plane and is given by the relation

$$w_1(x) = -\frac{1}{2\pi}\frac{\partial\xi}{\partial x}\int_0^{s_1}\frac{\xi_1}{\xi_1^2-\xi^2}\frac{dK}{d\xi_1}\,d\xi_1. \tag{23}$$

(ii) $w_2$ is the component due to the image vortices in the $\zeta$-plane and is given by the relation

$$w_2(x) = -\frac{1}{2\pi}\frac{\partial\xi}{\partial x}\int_0^{s_1}\frac{\xi_1}{1-\xi^2\xi_1^2}\frac{dK}{d\xi_1}d\xi_1,$$

$$= +\frac{1}{2\pi}\frac{\partial\xi}{\partial x}\int_0^{s_1}\frac{1+\xi^2\xi_1^2}{(1-\xi^2\xi_1^2)^2}K(\xi_1)\,d\xi_1. \tag{24}$$

(iii) $w_3$ is the downwash which would have existed in the absence of the jet and is given by the equation

$$w_3(x) = -\frac{1}{2\pi}\int_0^{s}\frac{x_1}{x_1^2-x^2}\frac{dK}{dx}dx. \tag{25}$$

It should be noted that in these equations $K(x_1)$ is equal to $K(\xi_1)$, as these expressions denote the circulation round corresponding sections in the $z$- and $\zeta$-planes.

If the distribution in the $z$-plane is 'elliptic' it can be shown that $w_3(x)$ is constant along the span, and in fact that

$$w_3(x) = K_0/4s. \tag{26}$$

When $c/a = 0$, then, as might have been expected, $w_1(x) = w_3(x)$. At other values of $c/a$ the distribution in the $\zeta$-plane is also elliptic when $s/a$ is small. In this range it can be shown that

$$w_1(x) = K_0/4s \tag{26a}$$

to a first order of approximation. The contributions to $-\delta_U$ arising from terms corresponding to $w_2$ and $(w_1 - w_3)$ were $A$ and $B$. In the whole of the working range $B$ was found to be less than $A$. Only as $c/a$ became close to unity did $B$ increase to a non-negligible fraction of $A$. If the corresponding contributions to $-\delta_E$ are $A_1$ and $B_1$ then it is found, after some manipulation, that when $s/a$ is small

$$B_1 \to \frac{1}{24}\frac{1-n^2}{\sin^2\lambda}.$$

This limiting value is identical with the corresponding one associated with $B$ (cf. equation (16)). Crude numerical estimates lead one to believe that $B$ and $B_1$ are of the same order of magnitude throughout the whole working range, and we therefore approximate to the actual problem by assuming that $B_1$ can be put equal to $B$ in the analysis.

The total lift on the complete aerofoil is

$$L = \rho V\int_{-s}^{s}K(x)\,dx = \tfrac{1}{2}\pi s\rho V K_0. \tag{27}$$

The total increase in drag due to the induced downwash $w_2$ is

$$\begin{aligned}\int_{-s}^{s} \frac{w_2}{V} dL &= \frac{\rho}{2\pi}\int_{x=-s}^{x=s} K(x)\frac{\partial\xi}{\partial x}dx\int_0^{s_1}\frac{1+\xi^2\xi_1^2}{(1-\xi^2\xi_1^2)^2}K(\xi_1)\,d\xi_1 \\ &= \frac{\rho}{2\pi}\int_{\xi=-s_1}^{\xi=s_1} K(\xi)\,d\xi\int_0^{s_1}\frac{1+\xi^2\xi_1^2}{(1-\xi^2\xi_1^2)^2}K(\xi_1)\,d\xi_1 \\ &= \frac{\rho K_0^2}{\pi}\int_{\xi=0}^{\xi=s_1}\int_{\xi_1=0}^{\xi=s_1}\frac{1+\xi^2\xi_1^2}{(1-\xi^2\xi_1^2)^2}F(\xi)\,F(\xi_1)\,d\xi\,d\xi_1. \qquad (28)\end{aligned}$$

The effect of the downwash is therefore to decrease the effective angle of incidence by

$$\frac{1}{L}\int_{-s}^{s}\frac{w}{V}dL,$$

and the correction which must be applied to the wind-tunnel result is

$$\Delta\alpha = -\frac{1}{L}\int_{-s}^{s}\frac{w}{V}dL = \delta_E\frac{S}{C}C_L. \qquad (29)$$

It can be shown that
$$-\delta_E = \frac{2}{\pi^2}\frac{a^2}{s^2}I + B, \qquad (30)$$

where

$$\begin{aligned}I &= \int_0^{s_1}\int_0^{s_1}\frac{1+\xi^2\xi_1^2}{(1-\xi^2\xi_1^2)^2}F(\xi)\,F(\xi_1)\,d\xi\,d\xi_1 \\ &= \int_0^{s_1}\int_0^{s_1}(1+3\xi^2\xi_1^2+5\xi^4\xi_1^4+7\xi^6\xi_1^6+\ldots)\,F(\xi)\,F(\xi_1)\,d\xi\,d\xi_1 \\ &= I_0^2+3I_1^2+5I_2^2+\ldots(2p+1)\,I_p^2+\ldots, \qquad (31)\end{aligned}$$

and where
$$I_p = \int_0^{s_1}\xi^{2p}\,F(\xi)\,d\xi. \qquad (32)$$

Exact values of $I_p$ cannot be obtained except by lengthy and laborious numerical calculations. Approximate results can, however, be obtained fairly quickly. These results have been combined to produce table 3 and figure 4. The column headed $c/a = 0{\cdot}0$ is exact, as are also the rows up to about $s/a = 0{\cdot}5$. The remaining part of the table was deduced by making suitable approximations, by evaluating some special values exactly, and by graphical interpolation. It is hoped that accurate values of $I_p$ will soon be available, but it is not anticipated that the values will differ considerably from those given in table 3.

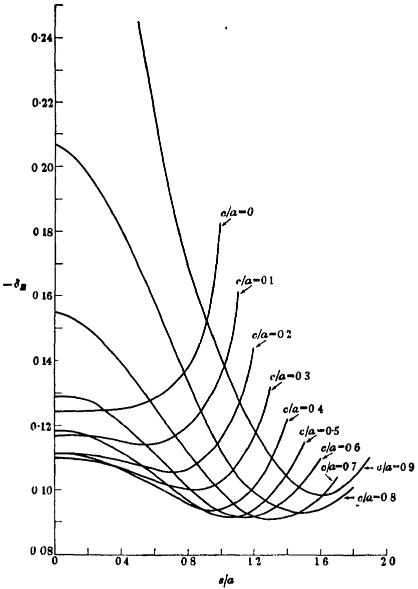

FIGURE 4. Graphs of $-\delta_E$

TABLE 3. VALUES OF $-\delta_E$ FOR DIFFERENT VALUES OF $s/a$ AND $c/a$

| $s/a$ \ $c/a$ | 0·0 | 0·1 | 0·2 | 0·3 | 0·4 | 0·5 | 0·6 | 0·7 | 0·8 | 0·9 | 1·0 |
|---|---|---|---|---|---|---|---|---|---|---|---|
| $s/a \to 0$ | 0·125 | 0·117 | 0·111 | 0·110 | 0·111 | 0·118 | 0·129 | 0·155 | 0·207 | 0·368 | ∞ |
| 0·1 | 0·125 | 0·117 | 0·111 | 0·110 | 0·111 | 0·118 | 0·129 | 0·153 | 0·202 | 0·359 | ∞ |
| 0·2 | 0·125 | 0·117 | 0·111 | 0·109 | 0·110 | 0·117 | 0·128 | 0·150 | 0·198 | 0·334 | ∞ |
| 0·3 | 0·125 | 0·116 | 0·109 | 0·108 | 0·108 | 0·115 | 0·125 | 0·146 | 0·189 | 0·306 | ∞ |
| 0·4 | 0·126 | 0·115 | 0·109 | 0·107 | 0·107 | 0·111 | 0·120 | 0·140 | 0·180 | 0·274 | ∞ |
| 0·5 | 0·127 | 0·114 | 0·108 | 0·105 | 0·104 | 0·108 | 0·116 | 0·133 | 0·169 | 0·245 | ∞ |
| 0·6 | 0·128 | 0·114 | 0·107 | 0·103 | 0·101 | 0·105 | 0·110 | 0·127 | 0·156 | 0·217 | ∞ |
| 0·7 | 0·131 | 0·116 | 0·105 | 0·101 | 0·098 | 0·101 | 0·106 | 0·119 | 0·145 | 0·194 | ∞ |
| 0·8 | 0·137 | 0·120 | 0·106 | 0·100 | 0·096 | 0·097 | 0·101 | 0·112 | 0·134 | 0·173 | ∞ |
| 0·9 | 0·151 | 0·126 | 0·110 | 0·100 | 0·094 | 0·094 | 0·096 | 0·105 | 0·122 | 0·155 | ∞ |
| 1·0 | 0·182 | 0·136 | 0·115 | 0·102 | 0·094 | 0·092 | 0·093 | 0·100 | 0·113 | 0·140 | ∞ |
| 1·1 | — | 0·161 | 0·124 | 0·107 | 0·096 | 0·092 | 0·092 | 0·095 | 0·106 | 0·129 | ∞ |
| 1·2 | — | — | 0·145 | 0·117 | 0·101 | 0·094 | 0·092 | 0·092 | 0·100 | 0·119 | ∞ |
| 1·3 | — | — | — | 0·132 | 0·110 | 0·099 | 0·094 | 0·091 | 0·096 | 0·111 | ∞ |
| 1·4 | — | — | — | — | 0·122 | 0·105 | 0·098 | 0·092 | 0·094 | 0·105 | ∞ |
| 1·5 | — | — | — | — | — | 0·115 | 0·104 | 0·094 | 0·093 | 0·100 | ∞ |
| 1·6 | — | — | — | — | — | — | 0·110 | 0·098 | 0·094 | 0·099 | ∞ |
| 1·7 | — | — | — | — | — | — | — | 0·106 | 0·097 | 0·100 | ∞ |
| 1·8 | — | — | — | — | — | — | — | — | 0·105 | 0·104 | ∞ |
| 1·9 | — | — | — | — | — | — | — | — | — | 0·110 | ∞ |
| 2·0 | — | — | — | — | — | — | — | — | — | — | ∞ |

Some of the more systematic considerations which gave rise to table 3 are the following: When $c/a = 0$, that is $\lambda = \frac{1}{2}\pi$ and $n = 1$,

$$F(\xi) = \left\{1-\frac{\xi^2}{s_1^2}\right\}^{\frac{1}{2}},$$

and $s_1 = s/a$. With this value of $F(\xi)$ we find

$$I_p = \tfrac{1}{2}\pi s_1^{2p+1}\frac{1}{2p+2}\,\frac{(2p-1)(2p-3)\ldots\ldots 1}{(2p)(2p-2)\ldots\ldots 2},$$

and that

$$-\delta_E = B+\frac{1}{2}\frac{a^2}{s^2}\left[\left(\frac{1}{2}\right)^2 s_1^2+\frac{1}{3}\left(\frac{1.3}{2.4}\right)^2 s_1^6+\frac{1}{5}\left(\frac{1.3.5}{2.4.6}\right)^2 s_1^{10}+\ldots\right], \tag{33}$$

$$= B+\left[\frac{1}{8}+\frac{3}{128}\frac{s^4}{a^4}+\frac{5}{512}\frac{s^8}{a^8}+\ldots\right], \tag{33a}$$

which is the well-known result for $\delta_E$ in a circular jet since $B = 0$ when $\lambda = \frac{1}{2}\pi$. The formula (33) is very useful for direct numerical evaluation for a wide range of $s/a$ as it converges very rapidly—for example, when $s/a = 0{\cdot}8$ the third term in the series is 0·0017. For higher values of $s/a$ direct evaluation becomes laborious, but another method is here available. The series in equation (33) can be expressed in a compact form, for if $E(k)$ is the complete elliptic integral of the second kind, with modulus $k$, then

$$E(k) = \int_0^{\frac{1}{2}\pi} (1-k^2\sin^2\phi)^{\frac{1}{2}}\,d\phi$$

$$= \tfrac{1}{2}\pi\left[1-\left(\frac{1}{2}\right)^2 k^2 - \frac{1}{3}\left(\frac{1.3}{2.4}\right)^2 k^4 - \frac{1}{5}\left(\frac{1.3.5}{2.4.6}\right)^2 k^6 - \ldots\right].$$

Hence equation (33) can be written as

$$-\delta_E = B + \frac{1}{2}\frac{a^2}{s^2 s_1^2}\left[1-\frac{2}{\pi}E(s_1^2)\right], \tag{34}$$

$$= B + \frac{1}{2}\frac{a^4}{s^4}\left[1-\frac{2}{\pi}E\left(\frac{s^2}{a^2}\right)\right]. \tag{34a}$$

The elliptic integral $E(k)$ is tabulated by Jahnke and Emde (1928) and in particular, when $s/a = 1$, the value of $-\delta_E$ is

$$-\delta_E = \frac{1}{2}\left[1-\frac{2}{\pi}\right] = 0{\cdot}1817.$$

This deals with $\lambda = \frac{1}{2}\pi$, but it should be noted that for other values of $\lambda$ the distribution is approximately elliptic in the $\zeta$-plane for small values of $s_1$ and so here again equation (33) is valid even though $s_1$ is not exactly equal to $s/a$. This consideration enables one to fill in the first six rows of table 3. Further, as $\lambda \to 0$, $F(\xi)$ tends to unity and $-\delta_E$ approaches infinity.

## 4. CONSIDERATION OF RESULTS

The working experimental range can be taken to be $c/a \leqslant 0{\cdot}75$ and $s/a \leqslant 0{\cdot}75(a+c)/a$. Within this range the correcting factors are of the same order of magnitude as those associated with the ordinary circular wind-tunnel arrangement. At greater values of $c/a$ and $s/a$ the distortion of the jet boundary will probably become serious and will invalidate the results obtained. In addition, the effect of the induced downwash on the distribution of lift has been ignored.

Up to the present, experimental checks are only available for the case $c/a = 0{\cdot}0$. Here, as $s/a$ changes from 0·0 to 1·0, $-\delta_U$ changes from 0·125 to infinity and $-\delta_E$ changes from 0·125 to 0·182. The values at $s/a = 1{\cdot}0$ are not to be taken too seriously but they give an indication of the way in which $\delta$ changes. Prandtl (1923) and Knight and Harris (1930) have confirmed that in experiments in a free jet the theoretical formula for the correction to the drag coefficient when the 'span to diameter' ratio is large, is less than that deduced from experiment. The theoretical formula for the correction to incidence shows marked discrepancies in the same direction, even at moderate values of $s/a$, but this is ascribed to other causes—principally to the influence of a general curvature of the jet The 'theoretical formula' mentioned here is that based on the assumption of elliptic distribution of lift. In particular Knight and Harris take a special case where $s/a = 0{\cdot}75$ The experimental correcting factor to the drag coefficient is found to be $-0{\cdot}142$. If we insert this value of $s/a$ in our formulae we find $\delta_E = -0{\cdot}133$ and $\delta_U = -0{\cdot}142$, and this suggests that even at this value of the span-to-diameter ratio the distribution of lift approaches more closely to the uniform type than to the elliptic type.

## 5. APPENDIX

### *List of symbols*

| | |
|---|---|
| $2a$ | diameter of the undisturbed jet; |
| $2b$ | length of the vertical reflexion plate or partition intercepted by the jet; |
| $c$ | displacement of the vertical partition from the centre of the jet, |
| $\lambda$ | the acute angle given by the relation $\lambda = \tan^{-1}(b/c)$; |
| $n$ | equal to $\pi/2(\pi-\lambda)$; |
| $x$ | co-ordinate along the span measured from the centre of the complete aerofoil, |
| $y$ | co-ordinate perpendicular to the aerofoil; |
| $z$ | equal to $x+iy$; |
| $\xi, \eta$ | co-ordinates corresponding to $x$ and $y$ in the transformed plane, |
| $\zeta$ | equal to $\xi+i\eta$; |
| $2s$ | span of the complete aerofoil in the extended $z$-plane, |
| $S$ | maximum area of projection of the wing, equal to the span multiplied by the mean chord, |
| $C$ | area of the undisturbed cross-section of the jet, equal to $\pi a^2$, |
| $\rho, V$ | density and speed of the air in the jet; |
| $\alpha, L, D$ | angle of incidence, lift and drag of the complete aerofoil; |
| $C_L, C_D$ | lift coefficient and drag coefficient, equal, respectively, to $L/\frac{1}{2}\rho V^2 S$ and $D/\frac{1}{2}\rho V^2 S$; |
| $\Delta\alpha, \Delta C_D$ | corrections to be applied to measured values of $\alpha$ and $C_D$ due to the wind-tunnel constraint; |
| $\delta_U, \delta_E$ | wind tunnel correcting factors based on assumptions of 'uniform' and 'elliptic' distributions of lift. |

REFERENCES

Glauert, H. 1930 *Aerofoil and airscrew theory*. Cambridge Univ. Press.
— 1933 *Rep. Memo. Aero. Res. Comm., Lond.*, no. 1566.
Jahnke, E. and Emde, F. 1928 *Funktionentafeln*. Leipzig: Teubner.
Knight, M. and Harris, T. A. 1930 *Rep. Nat. Adv. Comm. Aero., Wash.*, no. 361.
Kondo, K. 1935 *Rep. Aero. Res. Inst., Tokyo*, **10**, 8, no. 126.
Prandtl, L. 1919 *Tragflügeltheorie Nachr. Ges. Wiss. Göttingen.*
— 1923 *Ergebn. Aerodyn VersAnst. Göttingen*, **2**, *München and Berlin.*

---

# An investigation of the disintegration of boron by slow neutrons

By R. S. Wilson, B.A.

(*Communicated by J. Chadwick, F.R.S.—Received* 27 *September* 1940)

The disintegration of boron by slow neutrons has been investigated using an ionization chamber filled with boron trichloride in conjunction with a linear amplifier.

The magnitudes of the ionization impulses, measured by the oscillograph deflexions, should give under appropriate conditions a measure of the energy release in the disintegration process. The various factors which can affect the size of the oscillograph deflexion are discussed so as to define the appropriate conditions of experiment.

Evidence is found for two disintegration energies. Assuming that the greater energy release corresponds to the formation of the $Li^7$ nucleus in the ground state and is therefore 2·99 MeV, then the smaller energy, which is released in about 93–94% of the disintegrations, is 2·57 ± 0·05 MeV. An explanation is offered of the contradiction with the results of Maurer and Fisk. The $\gamma$-radiation associated with the reaction has been detected and a rough measurement of its quantum energy has been made.

The disintegration of boron by slow neutrons has been investigated by a number of workers (Rotblat 1936; Walen 1936; Fünfer 1937; Haxel 1937; O'Ceallaigh and Davies 1938; Bower, Bretscher and Gilbert 1938; Livingston and Hoffman 1938, Maurer and Fisk 1939). The earliest observations of this reaction left little doubt that the process is

$$_5B^{10} + {}_0n^1 = {}_3Li^7 + {}_2He^4.$$

Later experiments, while confirming the nature of the reaction, had for their object the measurement of the energy relations in the process. Most of them agree in indicating that the energy liberated in the reaction is about 2·5 MeV, whereas the value of the energy derived from the masses of the nuclei concerned is 2·99 MeV. The results of Bower *et al.*, obtained from observations of tracks in an expansion chamber containing boric acid methyl ester, are particularly clear in showing that the main reaction gives rise to the formation of a $Li^7$ nucleus in an excited state. Some observations (Haxel 1937; O'Ceallaigh and Davies 1938; Livingston and Hoffmann 1938) suggest, however, that in a small proportion of cases the $Li^7$ is formed in the ground state.

On the other hand Maurer and Fisk, using an ionization chamber filled with boron trichloride in conjunction with a linear amplifier, did not confirm this simple picture of the reaction but found evidence for the presence of four, probably five, definite disintegration energies, all of roughly the same probability. The method used by them has, in principle, some obvious advantages. Assuming that the energy required to produce a pair of ions is constant and that the amplifier does not distort the original impulse, then the amplitude of the recorded impulse gives directly a measure of the disintegration energy. Also a large number of disintegrations can be examined in a short time. In practice, however, the method must be used with care, for the ionization chamber and amplifier may introduce undesirable effects. In fact, the work described in the present paper, carried out by the same method, does not confirm the results of Maurer and Fisk, and analysis suggests that these were due to distortion in their amplifier coupled with an over-emphasis of detail which might more properly be attributed to statistical variations.

Before proceeding to the actual observations, a brief discussion is given of certain factors governing the form of distribution curve obtained with this method.

## FACTORS AFFECTING THE SHAPE OF THE DISTRIBUTION CURVE

### (a) *Geometry*

If disintegrations take place in the gas of an ionization chamber, then a number of the disintegration particles will strike the electrodes or pass out of the effective collecting volume, and the full number of ions will not be collected. For a parallel infinite pair of plates it can be shown that for an isotropic disintegration the distribution of the lengths of the paths is represented by a background of uniform height upon which is superimposed a peak of the same shape as the original but reduced in size. If the separation of the plates is $d$, and the length of the path of the disintegration particle is $l_0$, then the fraction of the total which is in the background is $l_0/2d$ ($l_0 \leqslant d$). The effect of using finite plates is to increase the number of particles with short path. Taking account of the variation of ionization along the track of the particles we can draw the expected number/ionization curve as shown in figure 1 *a*. Since the shape of the peak is unaltered, it is unnecessary to use a very large separation of the plates to avoid 'edge' effects, although it is an advantage to have the diameter of the plates large compared with their separation.

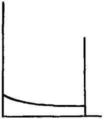

FIGURE 1*a* Edge effect.

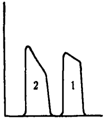

FIGURE 1*b* Effect of collecting time for (2) is longer than for (1).

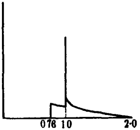

FIGURE 1*c*. Effect of counting rate.

### (*b*) *Collecting time*

Immediately a pair of ions is formed between the electrodes the potential of the collecting plate will rise approximately linearly in time to a maximum given by $V = q/C$, where $C$ is the capacity of the electrodes and associated circuits, and then decay exponentially to zero. The time taken to reach a maximum is that taken for the slowest ion to reach the plates (there is no sudden rise in potential as the ion touches the electrodes). The exponential decay is determined by the time constant of the collecting electrodes and associated circuits; the time constant is usually a matter of a few seconds. For a group of ions formed by an ionizing particle the impulse will not have quite this form (due to different collecting times of different ions), but the simple form given above will be a fair approximation. Such an impulse will be distorted on passing through the intervalve couplings of the linear amplifier, in particular its maximum will be reduced to a fraction

$$\{1 - \exp(-\tau_c/\tau_e)\}\,\tau_e/\tau_c$$

of its ideal value on passing through a single coupling stage; $\tau_c$ is the collecting time and $\tau_e$ the time constant of the intervalve coupling circuit. When disintegrations take place in a gas the collecting time will vary, according to the place where the disintegration occurs, and so also will the size of kick observed on the oscillograph. The form of distribution curve is shown in figure 1 *b*, broad at the peak but not extended at the skirts. This broadening is greatest for long collecting times. For short collecting times the curve is approximately rectangular as in (1), for longer collecting times it becomes definitely trapezoidal as in (2). For short collecting times $\tau_c \ll \tau_e$ the fractional reduction of voltage is $\frac{1}{2}\tau_c/\tau_e$: the effects of successive stages are additive, so that for $n$ similar coupling stages the reduction of voltage is $n\tau_c/2\tau_e$. Now the collecting time for plates of separation $d$ and collecting voltage $V$ varies between $d^2/V(K_+ + K_-)$ and $d^2/VK_+$ or $d^2/VK_-$, whichever is the larger, where $K_+$ and $K_-$ are the mobilities of positive and negative ions Thus the variation of collecting time is greater than a factor of two. If therefore we wish to have a spread of less than 10 % in the peak, the maximum collecting time must be less than $\tau_e/5n$.

### (c) *Effect of counting rate*

The shape of the pulse after the maximum has been reached is also determined by the intervalve couplings. For an amplifier with four similar coupling stages the impulse has the form shown in figure 2. If now a second pulse is received before the original one dies out, the recorded size of the second pulse is different from its ideal value. This causes a broadening of the curve, particularly at the skirts. The height of the skirts is proportional to the counting rate. It was found that with coupling circuits of 1/20 sec. time

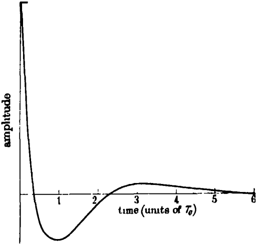

FIGURE 2. Form of impulse after passing through four similar coupling stages.

constant the broadening of the curve was appreciable at a counting rate of 120 per min. A maximum rate of 50 per min. was therefore preferred. Higher counting rates could be used with smaller time constants.

### DETAILS OF APPARATUS AND RESULTS OBTAINED

From the above considerations the conditions for obtaining a sharp peak are: short collecting time; an amplifier with coupling circuits of long time constant; and slow counting rate, with the edge effects subordinate to these.

If the gas pressure is $p$ and the separation of the plates is $d$, then the collecting time is proportional to $pd^2$ for a given collecting voltage. The edge effect is inversely proportional to $pd$. If we are limited, as in this case, by the total available voltage, then the small chamber at high pressure has the advantage over a large one at low pressure. If we are limited by the electrical field that can be applied, then the two chambers would have identical characteristics. The smaller chamber is more economical, and, moreover, experience with a chamber 30 cm. diameter and 30 cm. deep showed that it was difficult to screen such a chamber from electrical interference, as one point only would be effectively earthed. An external screen was necessary.

The chamber used had plates 8 cm. diameter separated by 9 mm., and was filled with boron trichloride to a pressure of 53 cm. at 20° C. A neutron source of polonium mixed with beryllium powder was separated from the chamber by 5 cm. of paraffin wax and the whole surrounded by a further 5 cm of paraffin wax. The counting rate was 48 per min. The five-valve amplifier had four coupling circuits of time constant 1/20 sec. each and the final stage was transformer coupled to the oscillograph. The latter was almost critically damped and could respond to a pulse in 1/2000 sec., so that little distortion of the pulse would be introduced by the oscillograph. The impulses were recorded photographically in the usual manner.

The distribution in size of the oscillograph kicks is given in figure 3, from which it will be seen that in addition to the main peak of 18·2 mm. deflexion there is a smaller peak of about 21·1 mm. deflexion. The main peak must clearly correspond to the reaction commonly observed, in which the energy release has been estimated by several observers to be about 2·5 MeV. On this assumption the energy release in the reaction indicated by the smaller peak will be about 2·92 MeV, thus strongly suggesting that this peak corresponds to a reaction in which the $Li^7$ nucleus is formed in the ground state, for which the calculated energy release is 2·99 MeV.* The magnitude of this peak shows that about 6–7 % of the disintegrations take place in this way.

---

* See the note at the end of this paper, and especially the reference to the work of E. Riddle Graves.

It should of course be possible to form directly, from the magnitude of the oscillograph deflexion, estimates of the energy release. The amplifier was calibrated by means of the $\alpha$-particles from a source of thorium active deposit, when the ionization chamber was filled with air. It was found in this way that 1 mm. deflexion corresponds to the release of 4800 ions The main peak thus corresponds to the release of about 87,000 ions and the smaller peak to about 102,000 ions. The ionization energy for boron trichloride is, however, not known, so that these values cannot be translated accurately, it is only possible from the existing data to state that the energy releases are approximately 2·4 MeV and 2·8 MeV respectively.

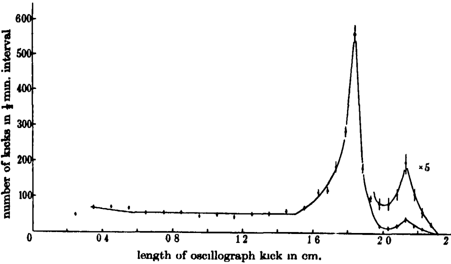

FIGURE 3

The collecting voltage used in these experiments was 1300 V. When this was reduced to half value the size of the impulses in the main peak was reduced by 8 %. The spread of the peak due to variations of collecting time must therefore have been less than 8 %. The number of particles in the background and the spread of the peak were greater than anticipated. These effects increased with time and were attributed to the deposition of boron or boric acid on the electrodes.

We are now in a position to put an alternative interpretation on the results of Maurer and Fisk. At one point in their amplifier they used a coupling circuit with a time constant of 1/200 sec. and as the *collecting time at higher pressures cannot have been less than 1/100 sec. we expect that variations of collecting time will be important in their* experiments.

Maurer and Fisk's interpretation of their curves suggests that peaks due to groups of particles differing in energy by a factor of 10 % would disappear in turn as the pressure of gas in the chamber is reduced. The analysis given above does not confirm this idea. The observations are consistent with the idea that the peak is broadened at higher pressures due to increased collecting time; the curves of figure 1 *b* can be nicely fitted to their experimental points. As the calibrating source was so situated that ions produced by it had the largest collecting time, the peak referred to this standard appears to move towards the high energy side at increased pressures.

As has been stated, the results obtained here suggest that in the greater number of boron disintegrations, 93–94 %, the $Li^7$ nucleus is formed in an excited state of energy about 0·4 MeV. This value is in good agreement with values obtained from the proton groups in the $Li^6$-$d$-$p$ reaction, which indicate a level at 0·45 MeV, and from the radioactivity of $Be^7$ which is accompanied by $\gamma$-radiation of energy $0{\cdot}425 \pm 0{\cdot}025$ MeV arising from a transition between the two levels in the resultant $Li^7$ (cf Livingston and Bethe 1937; Rumbaugh, Roberts and Hafstad 1938).

The ratio of the two groups is in good agreement with the experimental findings of Livingston and Hoffmann (1938), although not with their published values, which are in error owing to an oversight in their analysis. They have in fact quoted the square root of the ratio, and an inspection of their curves indicates that 92–93 % of the disintegrations lead to the excited state

## DETECTION OF THE $\gamma$-RADIATION

The $Li^7$ nuclei formed in the excited state will go to the ground state by the emission of a $\gamma$-ray. The detection of this $\gamma$-radiation would confirm the proposed disintegration scheme, but it is rendered difficult by the fact that the polonium-beryllium source emits a $\gamma$-radiation of much greater intensity. This difficulty was overcome in the following way. A boron-lined counter was operated in the proportional region so that it responded only to heavily ionizing particles such as are emitted in the $B^{10}(n, \alpha)\,Li^7$ reaction. This counter was connected to one line of a coincidence amplifier and an adjacent $\gamma$-ray counter was connected to the other line. The neutron source and both counters were embedded in blocks of paraffin wax. The resolving time of the coincidence circuit was rather less than $2 \times 10^{-6}$ sec. so that no coincidences between the γ-rays and neutrons emitted by the source could be recorded owing to the fact that the neutrons take a time of about $10^{-5}$ sec. to slow down to thermal velocities. The coincidences observed were therefore due to γ-rays associated in time with the α-particles from the boron disintegration, together with a small number of chance coincidences. The absorption coefficient of the radiation was measured by measuring the coincidence rates when different thicknesses of lead were placed between the two counters.

The number of coincidences obtained, after deduction of the chance coincidence rate of about 1 per hour, was $3 \cdot 6 \pm 0 \cdot 55$ per hour with no absorber, $3 \cdot 27 \pm 0 \cdot 33$ per hour with a lead absorber of 2·56 g./cm.$^2$, and $1 \cdot 08 \pm 0 \cdot 37$ with 6·13 g./cm.$^2$.

These results are not sufficiently accurate to give more than an indication that the energy of the radiation is about 0·5 MeV, but they offer some confirmation of the simple level scheme suggested by the ionization measurements.

*Note added by J. Chadwick.* In a private letter, Dr C. W. Gilbert informs me that he has extended the observations of Bower, Bretscher and Gilbert (1938) (measurements of track lengths in an expansion chamber containing a boron ester) and has obtained clear evidence of a group of tracks corresponding to an energy release about 0·5 MeV greater than that of the main group. The intensity of this group is about 9 % of the main group. His results thus agree well with those of Mr Wilson.

Mr Gilbert's measurements, combined with those of Bower, Bretscher and Gilbert, give values for the energy releases of 2·20 MeV and 2·72 MeV, if the energy-range relation for α-particles given by Livingston and Bethe (1937, p. 245) is adopted.

In a recent paper (1940, *Phys. Rev.*, **57**, 855) Miss E. Riddle Graves has discussed the energy release in the ($B^{10}$, n) reaction. On the basis of a chain of reactions she deduces a value for the maximum energy release which does not involve those nuclear masses which are in doubt. She obtains a value of 2·68 or 2·78 MeV, according as to whether Bainbridge's or Aston's result for the ($2H^2 - He^4$) doublet is taken.

The accord between this value for the maximum energy release and the energy release deduced from the higher of the two groups suggests that the higher group does in fact correspond to a process leading to the ground state of $Li^7$ and that the energy-range relation for α-particles is reliable.

## APPENDIX

### (1) *Edge effects*

Consider an element of volume $dx\,dy\,dz$ at a distance $x$ from an infinite plane electrode. If particles are emitted from this volume with path lengths, limited by impact with the electrode, lying between $l$ and $l+dl$, they will be emitted within a solid angle $2\pi x\,dl/l^2$. If there are $n$ such particles emitted per unit volume and they are isotropically distributed, then the number of particles lying within the given range is $nx\,dl\,dx\,dy\,dz/2l^2$. If we have two electrodes separated by a distance $d$, and consider particles emitted from a cylinder of unit cross-section limited by the electrodes, then the number of particles in the given range emitted from the cylinder is

$$N(l)\,dl = \frac{2n\,dl}{2l^2}\int_0^l x\,dx \qquad (1)$$
$$= \tfrac{1}{2}n\,dl,$$

which is a uniform distribution.

The total number of particles emitted from this cylinder is $N = nd$, whereas the number of particles in the background is

$$N_b = \int_0^{l_0} \tfrac{1}{2}n\,dl$$
$$= \tfrac{1}{2}nl_0, \quad l_0 \text{ is maximum range of particles.}$$

Hence $\quad N_b/N = l_0/2d, \quad l_0 < d \quad$ (otherwise limits of (1) are incorrect).

### (2) *Effect of coupling circuits*

The intervalve coupling circuit consists of a grid resistance $R$ in series with a grid condenser $C$. The voltage across them is $V$ and the voltage $V_g$ across the resistance is applied to the grid of the succeeding valve. We have

$$V_g = e^{-t/\tau_c}\left[\int e^{t/\tau_c}\frac{dV}{dt}\,dt + \text{constant}\right],$$

where $\tau_c = RC$, the constant being fixed by the initial conditions.

The form of pulse applied to the coupling is

$$\begin{aligned} V &= 0 & t &\leqslant 0,\\ V &= V_0 t/\tau_c & 0 \leqslant t &\leqslant \tau_c,\\ V &= V_0 e^{-k(t-\tau_c)} & t &\geqslant \tau_c, \end{aligned}$$

where $\tau_c$ is the collecting time of the ions and $k$, which is the time constant of the input circuit of the first valve, is less than 1 sec.$^{-1}$.

During the initial rise of the grid potential $V_g$ rises according to the law

$$V_g = V_0 \frac{\tau_e}{\tau_c}(1 - e^{-t/\tau_e}).$$

When $V$ reaches its maximum value $V_0$ and starts to decrease exponentially $V_g$ also starts to decrease; its maximum (at $t = \tau_c$) is

$$V_0 \frac{\tau_e}{\tau_c}(1 - e^{-\tau_c/\tau_e}).$$

In the arrangement used $\tau_e$ was chosen to be large compared with $\tau_c$; the peak value of $V_g$ is thus effectively $V_0$. In considering the subsequent behaviour of $V_g$ it is sufficient to consider $V$ as a constant, for $k$ is very much smaller than $1/\tau_e$. Thus $V_g$ falls off exponentially according to the law

$$V_g = V_0 e^{-t/\tau_e}.$$

In considering the form of the impulse at later stages of amplification it will be sufficient to treat it as rising instantaneously to a certain value and then decaying according to the law which is derived below.

After passing through the second coupling circuit

$$V_g' = V_0(1 - t/\tau_e)\, e^{-t/\tau_e}.$$

After passing through the third coupling circuit

$$V_g'' = V_0(1 - 2t/\tau_e + \tfrac{1}{2}t^2/\tau_e^2)\, e^{-t/\tau_e},$$

and after passing through the fourth coupling circuit

$$V_g''' = V_0(1 - 3t/\tau_e + \tfrac{3}{2}t^2/\tau_e^2 - \tfrac{1}{6}t^3/\tau_e^3)\, e^{-t/\tau_e}$$

which is depicted in figure 2.

A second impulse will have an apparent amplitude differing from that of the main group by more than 10 % if it arrives while the original impulse differs from zero by more than $1/10V_0$. The length of time during which this is so is $1{\cdot}6\tau_e$, so that for a counting rate $N$, a fraction $1{\cdot}6N\tau_e$ of the particles will have amplitudes differing from the ideal value by more than 10 %.

The author wishes to express his thanks to Professor J. Chadwick, F.R.S., who suggested the experiment and gave much encouragement and advice. Thanks are also due to Dr M. H. L. Pryce for interesting discussions. Finally, the author wishes to acknowledge the financial aid received from the Department of Scientific and Industrial Research during the period in which this work was carried out.

## REFERENCES

Bower, Bretscher and Gilbert 1938 *Proc. Camb. Phil. Soc.* **34**, 290.
Fünfer 1937 *Ann. Phys., Lpz.*, **29**, 1.
Haxel 1937 *Z. Phys.* **104**, 540.
Livingston and Bethe 1937 *Rev. Mod. Phys.* **9**, 325.
Livingston and Hoffman 1938 *Phys. Rev.* **53**, 227.
Maurer and Fisk 1939 *Z. Phys.* **112**, 436.
O'Ceallaigh and Davies 1938 *Proc. Roy. Soc.* A, **167**, 81.
Rotblat 1936 *Nature, Lond.*, **138**, 203.
Rumbaugh, Roberts and Hafstad 1938 *Phys. Rev.* **54**, 655.
Walen 1936 *C.R. Acad. Sci., Paris*, **203**, 1500.

# A study of sensitized explosions

# V. Some new experiments on the hydrogen-oxygen reaction sensitized by nitrogen peroxide

BY F. S. DAINTON AND R. G. W. NORRISH, F.R.S.
*Laboratory of Physical Chemistry, Cambridge*

(*Received* 21 *May* 1940)

The effect of pressure and temperature of reactants, of inert gases, of vessel diameter and of surface condition on the induction periods and explosion boundary of $2H_2+O_2$ mixtures containing nitrogen peroxide have been determined in the temperature range 350–410° C. The principal results may be summarized:

(*a*) Increase of pressure causes the separation of the upper and lower limiting concentration of sensitizer to increase from zero to a maximum value at the inversion pressure. Above this pressure the upper limit decreases and the lower limit increases linearly with increase of pressure. The induction periods of $H_2$-$O_2$-$NO_2$ mixtures of constant $NO_2$ content decrease rapidly with increase of pressure, approaching a small value asymptotically.

(*b*) All foreign gases lengthen the induction periods and eventually quench the ignition of an explosive mixture of $H_2$-$O_2$-$NO_2$ of constant composition. The order of efficiency of the non-reactant gases in lengthening the induction periods is $CO_2 > N_2 > A = He$, whereas the order of efficiency in quenching ignition is $CO_2 > He > N_2 > A$.

(*c*) The induction period at the upper limit always exceeds the induction period at the lower limit. The reverse is true of the rates of the slow reactions in the vicinity of the limits.

(*d*) At constant total pressure, rise of temperature causes the upper limit ($P_U$) to be raised according to the equation

$$\log P_U = -E/RT + \text{constant}.$$

$E$ is 19,500 cal. at a total pressure of 75 mm. and increases with pressure to 25,600 cal. at 472 mm.

(*e*) At constant pressure the upper limit decreases and the lower limit increases as the reciprocal of the square of the diameter.

Gaseous ignition processes, in common with other chain reactions, are highly susceptible to positive and negative catalysis by traces of foreign substances, and the introduction of controlled amounts of such catalysts and inhibitors simplifies the study of ignition. The reason for this lies in the fact, first demonstrated by Semenoff (1928), that in the simplest case,* the reaction velocity of a chain reaction under isothermal conditions increases slowly to a constant value when a quantity $\phi$ is negative, but when $\phi$ has positive values the reaction is continuously self-accelerating and may become explosively rapid.

---

* In this case, the only chain processes considered are *initiation* and *propagation* both independent of the number of centres present, and *branching* and *deactivation* processes which depend only on the first power of the concentration of the centres. Self neutralization of the centres, which proceeds at a rate proportional to the second power of the concentration, will be considered later.

This net branching factor $\phi$ is defined as the difference between the *probabilities of branching* and *deactivation in processes which are of the first order with respect to n, and for an uncatalysed reaction at constant temperature is a function of the total pressure of reactants only.* In a catalysed reaction, $\phi$ frequently changes with the partial pressure of the catalyst at about the same rate as it does with the pressure of reactants. If, in this latter case, the catalytic effect is also confined to very small amounts of the sensitizer, say 1 mm., then in a 1/100 molal mixture of catalyst to reactants the inaccuracy in $\phi$ due to error in measuring pressures is reduced one hundred fold. This precise control and ready reproduction of $\phi$ by adjustment of the concentration of sensitizer greatly facilitates the study of explosion. When a catalyst is, in addition, sufficiently effective to cause explosion at temperatures well below those at which the unsensitized reaction takes place with perceptible velocity the reactions responsible for chain branching in the unsensitized reaction will be almost entirely absent, and need not be considered when a reaction scheme is being devised. The hydrogen-oxygen reaction sensitized by nitrogen peroxide and nitrosyl chloride which will be described in this and the succeeding paper, are two examples of such sensitization of ignition.

The work on the $H_2$-$O_2$-$NO_2$ reaction described in the present paper, and of which a preliminary account has been given by the present authors (1939), was undertaken to determine which of the two following theories is correct The first theory, the so-called 'isothermal' or 'chain' theory, was developed by Hinshelwood and Williamson (1934) and von Elbe and Lewis (1937, 1939), and holds that the condition for ignition is merely that the branching exceeds the deactivation, i.e. that the boundary between ignition and slow reaction is merely the locus of all compositions for which $\phi = 0$. The second theory is the so-called 'thermal' theory, due to Foord and Norrish (1935), and this holds that owing to the recombination of centres in three-body collisions, a process dependent on the second power of the concentration of the centres, a positive value of $\phi$ does not ensure that the reaction rate is continuously self-accelerating under isothermal conditions. The operation of this factor would restrict the reaction velocity to a finite equilibrium value which is the larger the greater $\phi$. Ignition is considered to occur only when in some favourable volume element the rate of liberation of heat associated with this equilibrium velocity is greater than the rate of conduction away. The explosion boundary is then defined by equating $\phi$ to some finite positive value which depends on the thermal conductivity.

### EXPERIMENTAL METHOD

*Apparatus.* The apparatus differed only in detail from that used in the earlier investigations of Foord and Norrish (1935). It consisted of a pyrex or quartz cylindrical reaction vessel held horizontally in an electric furnace, the temperature of which was controlled to ± 0·5° C over 38 cm. of its length, either by hand regulation or by a 'Multelec' automatic regulator and recorder, operated by the e.m.f. from a chromel-alumel thermojunction. Gas mixtures of any desired composition and pressures up to 690 mm. Hg could be admitted to the reaction vessel through a wide-bore tap from a mixing vessel. In order to make up these mixtures and to follow pressure changes after admission of the gas, the reaction vessel and mixing vessel were connected by capillary tubing to a Bourdon gauge of the mirror type described by Foord (1934). The whole apparatus could be rapidly evacuated by a three-stage quartz mercury diffusion pump, backed by a Hyvac pump.

Measurements were made both in vessels with a clean surface and in vessels the surface of which was covered by a layer of potassium chloride. This layer was deposited by allowing the vessel to stand overnight full of a 10 % solution of potassium chloride in distilled water. After decanting the solution the vessel was attached to the apparatus through the ground joint and the water vapour pumped off at 300° C. This surface layer of potassium chloride could be removed by repeated washing with concentrated nitric acid and distilled water; and vessels cleaned in this manner gave the same results as before the treatment with potassium chloride.

*Preparation of gases. Hydrogen* and *oxygen* were prepared by the electrolysis between nickel electrodes of 10 % caustic soda solution saturated with baryta, and stored over water. Both gases were purified from traces of each other by passage over platinized asbestos heated electrically in pyrex tubes, and dried by passage over phosphorus pentoxide. The hydrogen was further dried before use by passing through a spiral cooled in liquid air. The oxygen was condensed in a trap cooled in liquid nitrogen, one-third pumped off to remove traces of nitrogen and the residue evaporated as required.

*Nitrogen peroxide* was obtained by gently warming a mixture of dry lead nitrate and clean dry sand in a slow stream of dry oxygen. The nitrogen peroxide was condensed to a red liquid in a trap cooled in an ice-salt freezing mixture and oxygen bubbled through until the solid obtained by cooling to liquid air temperatures was colourless. The final sample was obtained by fractional distillation in vacuo and was considered to be pure if it gave the right vapour pressure curve between −20 and +15° C (see Egerton 1914).

*Nitrogen* was taken from the cylinder and traces of combustible substances removed by passage over copper oxide heated electrically to a dull red heat in a pyrex tube, over solid caustic potash and through a glass spiral cooled in liquid air. *Argon* was also taken from a cylinder and purified in the same manner as the nitrogen, except that the spiral was cooled in solid carbon dioxide. Preliminary experiments with cylinder gases which had merely been dried gave very variable results, and it was not until combustible materials had been removed that the induction periods in the presence of foreign gases became reproducible.

*Helium* was obtained from the Royal Society Mond Laboratory and stored over water. Immediately before use it was purified by passage over phosphorus pentoxide and activated charcoal cooled in liquid air. *Carbon dioxide* was obtained from the solid after the air had been pumped off.

In view of the trace catalysis of chain processes, reproducibility of concentration limits and induction periods under standard conditions were taken as sufficient criteria of the purity of the gases.

*Practical methods.* For the preparation of gas mixtures containing accurately known small amounts of nitrogen peroxide between 1 and 4 mm. partial pressure, a mixture of oxygen with 10 % nitrogen peroxide was made up in a subsidiary mixing vessel of 3 l. capacity and allowed to attain uniform composition over a period of 12 hr. When mixtures containing less than 1 mm. nitrogen peroxide were required, this 10 % mixture was further diluted with oxygen to a convenient concentration in another mixing vessel. All the concentrations, foreign gas, nitrogen peroxide, hydrogen and oxygen, are expressed as the pressures associated with these concentrations at 364° C.

The procedure adopted in all the experiments was as follows. Requisite amounts of the appropriate nitrogen peroxide-oxygen mixture were drawn off into the main mixing vessel and extra oxygen and hydrogen added, in that order. This mixture was allowed to become homogeneous by diffusion for a minimum time, varying from 5 min. at total pressures of 100 mm. to 15 min. at total pressures of 600 mm. After this interval the gas was admitted to the reaction vessel and Bourdon gauge and observations made on the occurrence of slow reaction or ignition, and the length of the induction period. After each experiment, the mixing vessel, reaction vessel and gauge were pumped out for 15 min., previous measurements with a McLeod gauge having shown that a pressure of $6 \times 10^{-4}$ mm. Hg could be attained in this time.

To assist in the maintenance of constant surface conditions during a series of experiments lasting several days the furnace temperature was never allowed to fall below 320° C overnight.

## EXPERIMENTAL RESULTS

### 1. *Pressure of reactants*

It had previously been observed by Thompson and Hinshelwood (1929) that at a given temperature and mixture composition ($2H_2 + O_2$) in porcelain or silica vessels of unspecified diameter, the effect of increasing the total pressure of hydrogen and oxygen over the range 150-600 mm. is to lower the upper limiting concentration of nitrogen peroxide and slightly to raise the lower limit. In a quartz vessel of internal diameter 25 mm. at five temperatures between 351 and 409° C, this appears to be true only at pressures greater than a certain value. As the total pressure is reduced below this value the upper limit falls. This is illustrated by the isothermals of figure 1 from which it may be seen that the position of the maximum of the upper limit, which we shall call the inversion pressure, is about 300 mm. at 364° C, and increases slightly with temperature.

It later became apparent that it would be interesting to discover whether the lower limit passes through a minimum, as the total pressure increases Both upper and lower limits were therefore determined at 364° C in a pyrex reaction vessel of internal diameter 7·0 mm., which had been rinsed with a 10 % aqueous solution of potassium chloride before use. The results are given in table 1. These results are plotted in figure 2, from which it may be seen that there is a lower limiting pressure of reactants, in this case 127 mm., below which there is no ignition Above this pressure, the separation of the limits increases with pressure, passing through a maximum at 300 mm Above this inversion pressure the lower limit rises and the upper limit falls linearly with pressure until a second limiting pressure is reached, in this case about 690 mm., above which the ignition is replaced by slow reaction.

Thus at any given pressure of reactants there are two concentrations of nitrogen peroxide which mark the boundaries of the explosion region, and similarly at any given concentration of sensitizer there are two pressures of reactants enclosing an ignition region. Further, a given change in total pressure has almost three times the effect on the upper limit that it has on the lower limit.

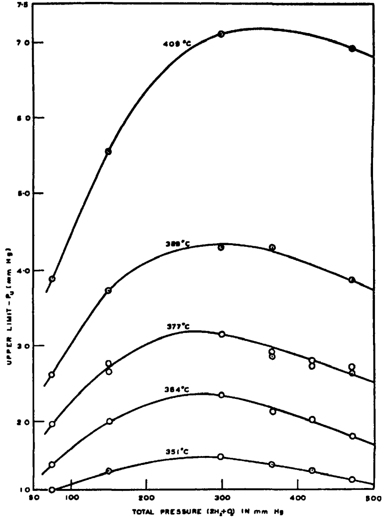

FIGURE 1 Variation of the upper limit ($P_U$) with total pressure of reactants ($2H_2 + O_2$) at different temperatures. Quartz reaction vessel, internal diameter 25 0 mm.

The induction period at a given concentration of nitrogen peroxide falls off very rapidly with increase of total pressure, as shown in figure 3. At pressures up to 400 mm. this decrease is more rapid than the reciprocal of the first power of $p$; whilst above these pressures $p\tau$ is roughly constant. This is illustrated in table 2. Although the induction period is so markedly

TABLE 1. EFFECT OF PRESSURE OF REACTANTS ($2H_2+O_2$) ON THE UPPER ($P_U$) AND LOWER ($P_L$) CRITICAL CONCENTRATIONS OF NITROGEN PEROXIDE AT 364° C. PYREX REACTION VESSEL, SURFACE COATED WITH KCl, INTERNAL DIAMETER 7·0 MM.

| Pressure in mm. Hg ($2H_2+O_2$) | 46·5 | 93·0 | 120·0 | 127·0 | 129·6 | 132·0 | 150·0 | 200·0 | 300·0 | 400·0 | 500·0 | 600·0 | 675·0 | 690 |
|---|---|---|---|---|---|---|---|---|---|---|---|---|---|---|
| $P_U$ in mm. Hg | | No ignition | | 0·585 | 0·71 | 0·84 | 1·07 | 1·29 | 1·47 | 1·31 | 1·06 | 0·89 | 0·74 | No ignition |
| $P_L$ in mm. Hg | | | | 0·585 | 0·54 | 0·476 | 0·40 | 0·35 | 0·31 | 0·39 | 0·46 | — | 0·60 | |

TABLE 2. VARIATION OF THE INDUCTION PERIOD ($\tau$) AND THE PRODUCT $p\tau$ WITH TOTAL PRESSURE $p$ ($2H_2+O_2$). PYREX REACTION VESSEL, 7·0 MM. INTERNAL DIAMETER, SURFACE POISONED WITH KCl. PRESSURE OF $NO_2$, 0·59 MM.

| Total pressure ($2H_2+O_2$) in mm. $p$ | 46·5 | 93 | 120 | 127 | 129·6 | 132 | 150 | 225 | 300 | 400 | 500 | 600 | 675 | 690 |
|---|---|---|---|---|---|---|---|---|---|---|---|---|---|---|
| Induction period in sec. $\tau$ | >300 | SR 200 | SR 40 | SR 29 | *27 | *25 | *16 | *7 | *4 | *2 | *1·2 | *1·0 | *0·9 | SR 0·9 |
| $p \times \tau$ | — | 18,600 | 4,800 | 3,683 | 3,560 | 3,300 | 2,400 | 1,575 | 1,200 | 800 | 600 | 600 | 607·5 | 621·0 |

The prefix SR indicates slow reaction and * indicates ignition.

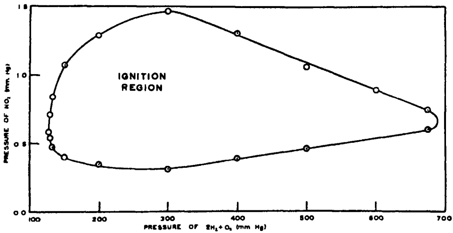

FIGURE 2. The ignition boundary at 364° C in pyrex reaction vessel, internal diameter 7·0 mm., surface poisoned with KCl.

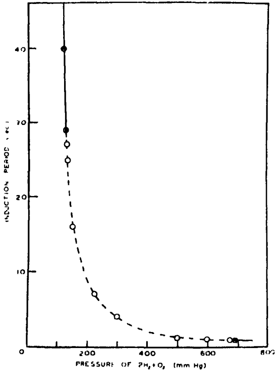

FIGURE 3. Variation of the induction period ($\tau$) with total pressure of reactants at 364° C. Pyrex reaction vessel, 7·0 mm. internal diameter, surface poisoned with KCl Pressure of $NO_2$, 0·59 mm. Broken line and ⊙ indicates ignition; full line and ⊗ indicates slow reaction.

affected by total pressure, the group of curves in figure 4 are all of the same type and show that the dependence on concentration of nitrogen peroxide is represented by the same form of equation, whatever the pressure of reactants, and that the induction period at the upper limit always exceeds that at the lower limit. Associated with this inequality of the induction periods at the limits is the fact that the rate just below the lower limit is always faster than just above the upper limit.

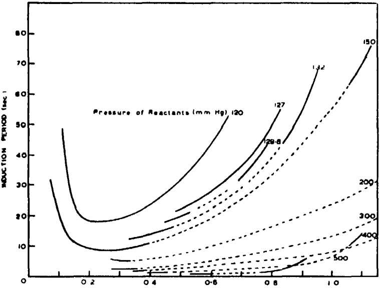

FIGURE 4. Variation of induction period ($\tau$) with concentration of nitrogen peroxide at different total pressures of reactants, at 364° C Pyrex reaction vessel, internal diameter 7 0 mm., surface poisoned with KCl. Broken line indicates ignition, full line indicates slow reaction.

### 2. *Temperature*

The explosion region is considerably expanded by increase in temperature. Thompson and Hinshelwood (1929) showed that whereas the lower limit is only slightly lowered, the upper limit increases exponentially with temperature. This has been confirmed, and the upper limits of ignition for a quartz reaction vessel of internal diameter 25 mm. are given in table 3 and plotted in figure 5 From figure 6 it is evident that, at a given pressure, the upper limit is raised according to the equation

$$\log_e P_U = -E/RT + \text{const.}$$

$E$ has values between 19,500 and 25,600 cal., depending on the pressure as is shown in table 4. The values of $E$ corresponding to the last three pressures in the table must be considered as approximate, since the logarithmic dependence of $P_U$ on $1/T$ is less valid, the higher the total pressure.

TABLE 3. UPPER LIMITS EXPRESSED AS PRESSURE OF $NO_2$ ($P_U$) IN MM. AT DIFFERENT TOTAL PRESSURES ($P_{2H_2+O_2}$) AND TEMPERATURES

| Total pressure in mm. Hg ... | 75 | 150 | 300 | 368 | 420 | 472 |
|---|---|---|---|---|---|---|
| 351° C | 1·10 | 1·34 | 1·52 | 1·42 | 1·34 | 1·21 |
| 364° C | 1·42 | 2·05 | 2·34 | 2·11 | 2·01 | 1·78 |
| 377° C | 1·97 | 2·75 | — | 2·90 | 2·78 | 2·68 |
| 377° C | 1·88 | 2·65 | 3·13 | 2·86 | 2·71 | 2·62 |
| 389° C | 2·62 | 3 71 | 4·28 | 4·28 | — | 3·84 |
| 409° C | 3·88 | 5·56 | 7·10 | — | — | 6·90 |

TABLE 4. VARIATION OF $E$ WITH TOTAL PRESSURE. QUARTZ VESSEL, DIAMETER 25 MM.

| Total pressure $P_{2H_2+O_2}$ in mm. Hg | 75 | 150 | 300 | 368 | 420 | 472 |
|---|---|---|---|---|---|---|
| $E$ in kcal. | 19·5 | 20·2 | 21·3 | 23·4 | 24·3 | 25·6 |

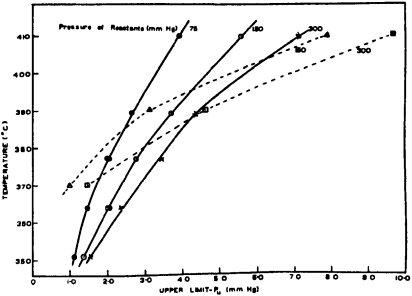

FIGURE 5. Variation of the upper limit ($P_U$) with temperature at different total pressures of reactants. Quartz reaction vessel, internal diameter 25·0 mm. Broken lines refer to the data of Thompson and Hinshelwood.

This result may be contrasted with the value of *ca.* 45 kcal. for $E$, which was deduced by Hinshelwood and Williamson (1934) from Thompson and Hinshelwood's data. In view of this large discrepancy it is interesting to find that the upper limits as determined by Gibson and Hinshelwood (1928) and expressed as pressures of nitric oxide in mm. for 400 mm. hydrogen and 200 mm. of oxygen in a porcelain reaction vessel of 200 c.c. capacity, at temperatures of 371, 390, 404 and 421° C lead to a value of $E$ of 27,000 cal. in close agreement with the values recorded here.

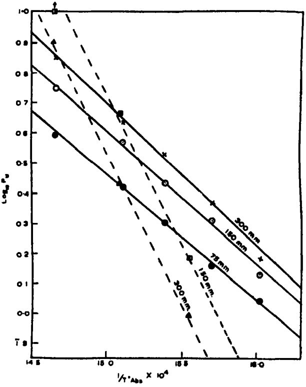

FIGURE 6. Variation of $\log_{10} P_U$ with $1/T°$ at different total pressures of reactants. Quartz reaction vessel, internal diameter 25·0 mm. The points △ and □ are taken from the data of Thompson and Hinshelwood.

Whilst seeking for a suitable temperature to study the effect of total pressure on the ignition limits, the variation of the induction period with concentration of sensitizer was obtained for 150 mm. $2H_2 + O_2$ at three temperatures, in pyrex reaction vessel of internal diameter 7·0 mm. These results are given in figure 7.

### 3. *Added foreign gases*

For a given explosive mixture of oxygen, hydrogen and nitrogen peroxide at a given temperature, addition of carbon dioxide, nitrogen, helium or argon lengthens the induction period and eventually quenches the ignition. In figure 8 the change in induction period ($\tau$) of 70 mm. hydrogen, 35 mm. of oxygen and 2·24 mm. nitrogen peroxide at 377° C is plotted against the amount of added gas, and it will be observed that the suppression pressures for the gases are in the ratio

$$A \cdot N_2 : He . CO_2 : \; 6{\cdot}0 . 3{\cdot}6 \cdot 3{\cdot}0 . 1{\cdot}0 .^{*}$$

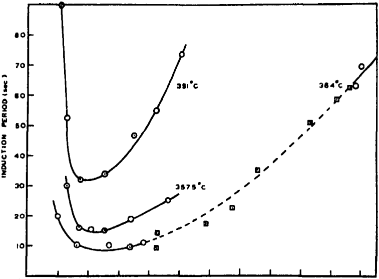

FIGURE 7 Variation of the induction period ($\tau$) with the concentration of nitrogen peroxide at 351, 357·5 and 364° C Constant pressure of reactants = 150 mm Hg. Pyrex vessel, internal diameter 7·0 mm, surface poisoned by KCl Broken line and ☐ indicates ignition, full line and ○ indicates slow reaction

In agreement with this result the upper limit is depressed by addition of foreign gases. In the case of nitrogen, as figure 9 shows, this lowering may be considered, to a first approximation, as linearly dependent on the amount of added nitrogen. The dependence of the limit on temperature is only affected by added nitrogen in so far as the constant in the equation

$$\log_e P_U = -E/RT + \text{constant}$$

---

* It should be noticed that the same order and magnitude of quenching pressures has been obtained for the $H_2$-$O_2$-NOCl system (see Part VI), and that the extinguishing action of these inert gases on hydrogen-air mixtures ignited by a spark has been shown by van Heiningen (1936) always to decrease in the order $CO_2$, He, $N_2$, A. Thus the amounts of these gases necessary to prevent flame in hydrogen-air-foreign gas mixtures containing 15 % hydrogen at atmospheric pressure are A, 64·5 %; $N_2$, 59·5 %; He, 57·5 %; and $CO_2$, 50 %

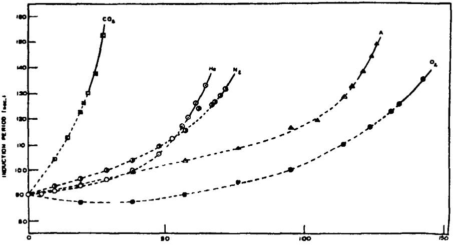

FIGURE 8. The effect of various gases on the induction period of a mixture containing 70 mm. $H_2$, 35 mm $O_2$, and 2·24 mm. $NO_2$ at 377° C in quartz reaction vessel, internal diameter 25·0 mm Broken line indicates ignition, full line slow reaction

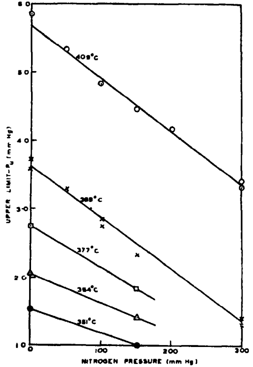

FIGURE 9. The effect of nitrogen on the upper limit ($P_U$) of 100 mm. $H_2$ + 50 mm. $O_2$ at various temperatures. Quartz reaction vessel, internal diameter 25 mm.

is lowered, for as figure 10 shows, only the intercept on the line

$$1/T = 14{\cdot}5 \times 10^{-4},$$

is altered, the slope of the $\log_e P_U : 1/T$ curve remaining the same.

The above results are all obtained in a quartz reaction vessel of large internal diameter (25 mm.), in which, at the pressures and temperatures employed, surface deactivation would be expected to be of minor importance.

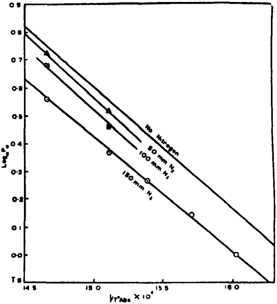

FIGURE 10. The effect of nitrogen on the temperature dependence of the upper limit of 100 mm. $H_2$ + 50 mm $O_2$. Quartz reaction vessel, internal diameter 25 mm

Under conditions where surface deactivation plays a large part in controlling the branching, as for example at a total gas pressure of 120 mm. at 377° C in a pyrex reaction vessel 7·0 mm. internal diameter, which had been rinsed out with 10% aqueous potassium chloride solution, rather different results were obtained which are summarized in figure 11. For the three gases, carbon dioxide, argon and nitrogen, if the pressure is sufficiently large the limit is depressed, the order of decreasing effectiveness of the gases being the order of decreasing atomicity. At low pressures in the case of nitrogen and argon, this decrease is preceded by an increase and the limit passes through a maximum value. This expansion of the explosion region does not occur when carbon dioxide is the foreign gas, but even in this case the initial falling off of the limit is only slight. Although no measurements have been carried out at constant concentrations of nitrogen peroxide for more than four pressures of foreign gas, those data which are available show that the induction period passes through a minimum value as the pressure of inert gas is increased.

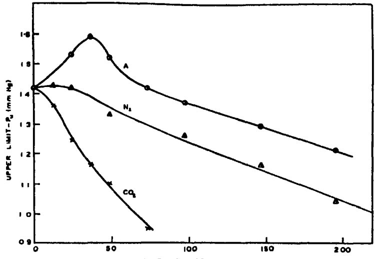

FIGURE 11. The effect of carbon dioxide, nitrogen and argon on the upper limit of 80 mm. $H_2$ and 40 mm. $O_2$ at 377° C. Pyrex reaction vessel 7·0 mm. internal diameter, surface poisoned with KCl. –⊙– argon, –△– nitrogen, –×– carbon dioxide.

### 4. *Vessel diameter, etc.*

That this reaction is subject to considerable surface deactivation is shown by the inert gas experiments for the small diameter vessel given above, and by the observation of Norrish and Griffiths that the slight increase of surface obtained by fitting the reaction vessel with an axial entry tube was sufficient to replace ignition by rapid reaction which rose to a maximum value and then decreased again as the concentration of $NO_2$ was increased. The nature of this deactivation has been investigated by determining the ignition limits for 80 mm hydrogen and 40 mm. oxygen at 377° C in cylindrical pyrex reaction vessels of different diameter, before and after treatment with a 10 % aqueous solution of potassium chloride. The results are given in table 5 and figure 12, and may be summarized:

(*a*) Above a certain critical diameter the upper limit increases and the lower limit decreases with diameter in a linear way, the effect being very small. Below this *critical* diameter (about 10·0 mm. in both poisoned and

TABLE 5. CRITICAL CONCENTRATIONS OF NITROGEN PEROXIDE, AND INDUCTION PERIODS OF 120 MM. $2H_2+O_2$ IN DIFFERENT VESSELS AT 377° C

| Internal diameter mm. | State of surface | Upper limit $P_U$ in mm. | Induction period in sec. at the upper limit | Lower limit $P_L$ in mm. | Induction period in sec. at the lower limit |
|---|---|---|---|---|---|
| 28·1 | Normal | 2·48 | 75 | — | — |
| 23·6 | Normal | 2·34 | 64 | — | — |
| 19·3 | Normal | 2·38 | 68 | — | — |
| 19·3 | KCl treated | 2·31 | 88 | 0·05 | 3 |
| 16·7 | Normal | 2·40 | 76 | 0·06 | 1–2 |
| 16·7 | KCl treated | 2·26 | 77 | 0·07 | 2 |
| 10·0 | Normal | 2·14 | 64 | — | — |
| 10·0 | Normal | 2·07 | 68 | — | — |
| 10·0 | KCl treated | 1·96 | 70 | 0·12 | 1·0 |
| 8·9 | Normal | 1·98 | 60 | 0·10 | 2·0 |
| 8·9 | KCl treated | 1·82 | 64 | 0·19 | 3·0 |
| 7·0 | Normal | 1·88 | 45 | — | — |
| 7·0 | Normalized by washing with conc. $HNO_3$ | 1·80 | 40 | 0·16 | 2·0 |
| 7·0 | KCl treated | 1·27 | 40 | 0·32 | 6·0 |
| 5·0 | Normal | | No ignition | | |
| 5·0 | Normal | | No ignition | | |
| 6·0* | Normal | 1·57 | 59 | 0·29 | 3·5 |

* Performed 12 weeks after measurements on other vessels.

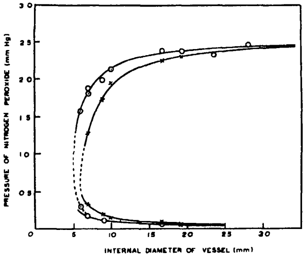

FIGURE 12. The effect of vessel diameter and surface condition on the ignition limits of 80 mm. $H_2$ and 40 mm. $O_2$ at 377° C. × are values of limits in vessels rinsed with 10 % aqueous KCl before use. ⊙ are values of limits in untreated vessels. The full lines were obtained theoretically by assigning arbitrary values to the equations on p. 441 of Part VII.

unpoisoned vessels) the explosion limits converge very rapidly and there is a *limiting* diameter below which explosion is replaced by a reaction of finite velocity whatever the concentration of sensitizer. The onset of this slow reaction is preceded by an induction period which varies with catalyst concentration in the normal manner. Qualitative observation indicates that the rate of slow reaction in this vessel varies with nitrogen peroxide concentration in such a way that it is at a maximum when the induction period is at a minimum. The shape of the curve is in agreement with the results of Norrish and Griffiths.

(*b*) The effect of poisoning the vessel surface by coating with potassium chloride, is slightly to lower the upper limit and to raise the lower limit, in the region where the diameter has little effect, i.e. above 10·0 mm. For diameters slightly less than the critical diameter, the influence of treatment with KCl is much greater and the limiting diameter is displaced towards larger values; in this case from 5·1 to 5·9 mm.

(*c*) Without exception the induction period was lengthened by poisoning and by a decrease in diameter, the effect being most marked at concentrations of nitrogen peroxide outside the ignition limits.

(*d*) Two experiments were carried out in cylindrical pyrex reaction vessels of internal diameter 25·1 mm. and the same length, both containing an axial tube of 7 mm. external diameter. When the gases were admitted through this tube the upper limit was found to be 2·10 mm., and when the gases were admitted at the other end of the reaction vessel the upper limit was 1·98 mm. It is evident from this result that the mode of entry of gases is not a factor appreciably affecting the ignition condition.

## CONCLUSION

The isothermal branched chain theory of this reaction as proposed by von Elbe and Lewis (1937, 1939) was based on the assumption that Thompson and Hinshelwood's results were a full description of the facts. Several differences between these results and those recorded above are, however, apparent, the differences being especially marked for the effect of temperature and pressure of the reactants on the explosion limits. As our results are more numerous and self-consistent and as they confirm the earlier measurements of Gibson and Hinshelwood (1928) we shall consider them to be reliable. In Part VII of the present series it will be shown that the theory of von Elbe and Lewis (1939) cannot be used to predict the experimental variation of the induction period and ignition limits with pressure of reactants and does not therefore 'furnish a complete description of the experimental data'. Further, the asymmetric influence which is apparent in the inequality $\tau_U > \tau_L$, is not inherent in the chain theory, but may be traced to the physical conditions which must be satisfied for the complete propagation of explosion. This physical condition is neglected in the isothermal theory but is a natural corollary of the thermal theory which will be presented in Part VII.

The authors wish to express their thanks to Messrs George Kent, Ltd., of Luton, for the gift of a 'Multelec' automatic temperature regulator and recorder, and to the Royal Society and Imperial Chemical Industries (Explosives Group) Ltd. for financial assistance which has made this work possible.

## REFERENCES

Egerton, A. C. 1914 *J. Chem. Soc.* p. 615.
von Elbe, G. and Lewis, B. 1937 *J. Amer. Chem. Soc.* **59**, 2022.
von Elbe, G. and Lewis, B. 1939 *J. Amer. Chem. Soc.* **61**, 1350.
Foord, S. G. 1934 *J. Sci. Instrum.* **11**, 126.
Foord, S. G. and Norrish, R. G. W. 1935 *Proc. Roy. Soc.* A, **152**, 196.
Gibson, C. H. and Hinshelwood, C. N. 1928 *Trans. Faraday Soc.* **24**, 559.
Heiningen, J. J. van 1936 *Rec. Trav. chim. Pays-Bas*, **55**, 65.
Hinshelwood, C. N. and Williamson, A. T. 1934 *The reaction between hydrogen and oxygen*, p. 85. Oxford Univ. Press.
Norrish, R. G. W. and Dainton, F. S. 1939 *Nature, Lond.*, **144**, 30.
Norrish, R. G. W. and Griffiths, J. G. A. 1933 *Proc. Roy. Soc.* A, **139**, 147.
Semenoff, N. 1928 *Z. Phys.* **48**, 571.
Thompson, H. W. and Hinshelwood, C. N. 1929 *Proc. Roy. Soc.* A, **124**, 219.

# A study of sensitized explosions

# VI. Experimental observations on the hydrogen-oxygen reaction sensitized by nitrosyl chloride

BY F. S. DAINTON AND R. G. W. NORRISH, F.R.S.

*Laboratory of Physical Chemistry, Cambridge*

(*Received* 21 *May* 1940)

Small amounts of nitrosyl chloride lower the ignition temperature of $2H_2+O_2$ mixtures by over 200° C, the efficiency of this substance in this respect being slightly greater than nitrogen peroxide. At a given temperature the ignition is confined between a lower and an upper concentration of catalyst, outside which only slow reaction occurs. Both the slow reaction and the ignition are preceded by an induction period, the length of which passes from large values through a minimum to further large values as the catalyst concentration is increased, and which, in contrast to the $H_2$-$O_2$-$NO_2$ system, is unaffected by irradiation with light from a mercury-vapour lamp.

The induction periods and limits depend on the pressure and temperature of reactants in a very similar way to the induction periods and limits of the $H_2$-$O_2$-$NO_2$ system described in Part V. The similarity of the two systems extends to the effect of non-reactant gases in quenching the ignition, the quenching pressures being of the same magnitude in both systems. A difference is, however, found in that these foreign gases shorten the induction period in this system whereas they lengthen it in the $H_2$-$O_2$-$NO_2$ system.

If small amounts of two different substances catalyse a given reaction to about the same extent in a given temperature range, the physical conditions which must be satisfied for ignition to occur should be identical in the two cases. It ought therefore to be possible to discover analogous phenomena in the two systems and so confirm any theory of ignition.

The sensitization of the hydrogen-oxygen reaction by nitrosyl chloride has now been investigated for the first time, and the results are presented in this paper. They indicate that the same type of sensitization is operative as when nitrogen peroxide is the catalyst, and that these two systems are equally suitable for studying the mechanism of ignition of $2H_2+O_2$ mixtures in the temperature region 350–400° C. There are strong similarities between the two systems, and in the following paper (Part VII) it will be shown that the phenomena associated with the addition of inert gases, and with change in concentration of reactants and sensitizer, point to a thermal ignition condition, which is the same in the two reactions. Such differences as do exist between the two reactions can be attributed to the different ways in which they adjust themselves to meet this thermal condition, i.e. they lie merely in the chemical reactions leading to explosion.

## EXPERIMENTAL METHOD

The apparatus and its use were identical with that already described by the present authors (1940).

*Nitrosyl chloride* was prepared in an all-glass apparatus by the action of a solution of nitrosyl bisulphate ($NOHSO_4$), obtained when the dried vapours from refluxed aqua regia were passed through absorption towers containing concentrated sulphuric acid, on half its weight of warm dry sodium chloride. Nitrosyl chloride (b.p. $-5\cdot5°$ C) was separated from hydrogen chloride (b.p. $-83°$ C) contained in the evolved gases by condensation in a trap cooled in a bath of melting chloroform (temperature $= -63°$ C), and was finally distilled twice in vacuo. In this way, a sample of 4 g. of nitrosyl chloride was obtained as a deep red liquid freezing to a lemon yellow solid at liquid-air temperatures, at which the sample was kept until required.

*Methane* was prepared by the reduction of methyl iodide by zinc copper couple in aqueous alcoholic solution at temperatures around 35° C. Methyl alcohol, hydrogen iodide and iodine were removed by bubbling the effluent vapours through strong alkali and acid. The remaining gas was condensed in liquid air and fractionated in vacuo. Combustion of a sample of the gas used showed it to be at least 99 % pure methane.

The *hydrogen*, *oxygen*, *carbon dioxide*, *nitrogen*, *helium* and *argon* were all obtained as described in the previous paper.

That the purification methods were adequate was shown by the ready reproducibility of induction periods and ignition limits.

In the irradiation experiments two sources of light were used: a high-pressure quartz mercury vapour lamp running hot on 220 V and 1·5 amp. which emitted strongly between 2300 and 7000 A, and a 220 V d.c. carbon arc, the intensity of the strong emission (visible and 2478 A line) of which could be maintained constant over long periods, by a clockwork mechanism which kept the separation of the electrodes constant. By means of a quartz lens fitted flush with the end of the furnace, the radiation from one of these sources was focused into a convergent beam passing into a plane-ended conical quartz reaction vessel 180 mm. long and tapering from 38 mm. outside diameter at one end to 10 mm. at the other. A diaphragm 38·5 mm. in diameter was placed about 50 mm. from the light source, and between the lens and this diaphragm water or chlorine filters could be interposed.

## EXPERIMENTAL RESULTS

*Critical concentration limits of sensitizer.* At any given temperature and pressure of hydrogen and oxygen the ignition is confined between two limiting pressures of nitrosyl chloride. For instance, at 367° C in the conical quartz reaction vessel the value of the lower limit ($P_L$) = 0·17 mm. and the upper limit ($P_U$) = 0·80 mm. for 150 mm. $2H_2 + O_2$. (It is of interest that at 357° C in the same vessel the critical limits of nitrogen peroxide for the same amount of hydrogen and oxygen were found by Norrish and Foord (1935, figure 3, p. 204) to be 0·17 and 0·52 mm. respectively, indicating that nitrogen peroxide and nitrosyl chloride are almost equivalent in catalytic and inhibiting power.) At concentrations outside these limits a slow reaction occurs, the rate of which is smaller the further the concentration from the appropriate critical value.

*Induction periods.* The onset of both ignition and slow reaction is preceded by an induction period during which no appreciable pressure change occurs, but which is terminated by a slight temporary rise of pressure. In this respect, and also in the fact that the plot of induction period against nitrosyl chloride concentration is continuous and shows a minimum value, this system strongly resembles the $H_2$-$O_2$-$NO_2$ system. Comparing figure 1 of this paper with figure 3 of the paper by Norrish and Foord, differences are apparent. First, the minimum induction period lies at sensitizer concentrations less than $P_L$, i.e. in the region of slow reaction and not in the ignition region, which is the region of maximum catalysis. This has also been found under certain conditions with nitrogen peroxide (see the curves of figure 4, p. 401 of the previous paper). Secondly, the transition from very long induction periods to measurable induction periods in the region of slow reaction below the lower limit occurs in a much narrower range of concentration than when nitrogen peroxide is used as a catalyst. In both cases these induction periods and concentration limits are reproducible and the induction period at the upper limit is always larger than that at the lower limit.

*The slow reaction.* Although no quantitative measurements were made of the pressure change which takes place during slow reaction, the reactions at concentrations immediately below the lower limit were considerably faster than those immediately above the upper limit.

*The effect of irradiation.* Measurements over two ranges of sensitizer concentration embracing the upper and lower limits showed that irradiation does not alter the induction periods or the explosion limits, either when the mercury-vapour lamp was used, or when an 18 mm. thick water filter was interposed between the carbon arc and the reaction vessel. When the carbon arc was used without the water filter the induction period was appreciably shortened. That this shortening was due to the heating effect of the infrared radiation from the arc was shown by the fact that it was only perceptible when the thermocouple recorded a rise in temperature during illumination. This photo-insensitivity is in striking contrast to the nitrogen peroxide system, where under similar conditions Norrish and Foord (1935) found the induction periods to be annihilated.

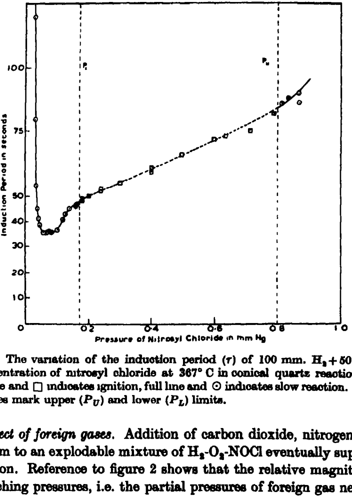

FIGURE 1. The variation of the induction period ($\tau$) of 100 mm. $H_2$ + 50 mm. $O_2$ with concentration of nitrosyl chloride at 367° C in conical quartz reaction vessel. Broken line and □ indicates ignition, full line and ⊙ indicates slow reaction. Vertical broken lines mark upper ($P_U$) and lower ($P_L$) limits.

*The effect of foreign gases.* Addition of carbon dioxide, nitrogen, argon and helium to an explodable mixture of $H_2$-$O_2$-NOCl eventually suppresses the ignition. Reference to figure 2 shows that the relative magnitudes of the quenching pressures, i.e. the partial pressures of foreign gas necessary to suppress ignition, are

$$CO_2 : He : N_2 : A :: 1 : 3{\cdot}1 : 3{\cdot}8 : 6{\cdot}3,$$

*almost identical with the* $H_2$-$O_2$-$NO_2$ *system.*[*] The induction periods, on the other hand, are shortened by these gases, not lengthened as is the case with nitrogen peroxide, and the order of effectiveness in shortening the induction period is not the same as that for quenching ignition. As is apparent in figure 2, for small amounts of foreign gas, i.e. up to 50 mm., carbon dioxide has most effect, nitrogen occupies second place, whilst argon and helium are almost equally effective and jointly take third place.

The effect of 50 mm. of these gases on the steady reaction rate of 150 mm. $2H_2+O_2$ at a concentration of sensitizer greater than the upper limit $P_U$ was also studied. The relative values of the velocity constants of mixtures containing 0·84 mm. NOCl in the conical vessel of 367° C are given in table 1. All these gases slow the reaction down, but their order of effectiveness in this respect should be contrasted with their relative efficiencies in quenching ignition. The most striking and important difference is that although within the limits of experimental accuracy argon and helium have the same effect on the slow reaction, helium is much more effective than argon in preventing explosion.

TABLE 1. THE EFFECT OF 50 MM. OF FOREIGN GAS ON THE VELOCITY CONSTANT OF THE SLOW REACTION

| Foreign gas | — | He | A | $CO_2$ | $N_2$ |
|---|---|---|---|---|---|
| Relative velocity constant | 1·0 | 0·89 | 0·86 | 0·65 | 0·58 |

*Methane*, which is itself combustible, behaves quite differently from the other gases. It is over a hundred times as efficient as carbon dioxide in quenching the ignition, and it causes the induction periods to be lengthened. *Oxygen* in excess of the stoichiometric proportion is much more effective

---

[*] The absolute magnitudes of the quenching pressures are of the same order in the two cases. Thus Dainton and Norrish (1941) found that for 105 mm. $2H_2+O_2+$ 2·25 mm. $NO_2$ in a quartz cylindrical reaction vessel at 377° C the amounts of the various gases required to quench explosion were

| $NO_2$ | $CO_2$ | He | $N_2$ | A | $O_2$ |
|---|---|---|---|---|---|
| 0·25 | 21 | 57 | 68·5 | 114 | 133 mm. Hg, |

whereas for 150 mm. $2H_2+O_2+0·596$ mm. NOCl in conical quartz reaction vessel at 367° C the quantities are

| NOCl | $CO_2$ | He | $N_2$ | A | $O_2$ |
|---|---|---|---|---|---|
| 0·21 | 16·5 | 49 | 60 | 100 | 116·5 |

When the figures for the NOCl system are multiplied by the factor $[NO_2]/[NOCl]$ given in the first column we obtain

0·25 19·5 58·5 71·5 119 130

which compare favourably with the $NO_2$ system.

than any of the other gases in shortening the induction period, but is the least effective in quenching ignition. This extreme effect is doubtless due to the fact that, in addition to its physical effect on chain development and the ignition condition, oxygen, as a reactant, plays a part in the propagation of chains.

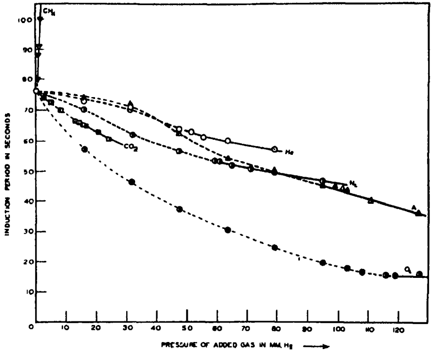

Figure 2. The effect of various gases on the induction period of a mixture containing 100 mm. $H_2$, 50 mm. $O_2$ and 0·596 mm. NOCl at 367° C in conical quartz reaction vessel. Broken line indicates ignition, full line slow reaction. ⊙ helium, ◑ nitrogen, △ argon, □ carbon dioxide, ⊗ excess oxygen.

*Effect of total pressure of reactants.* At a given temperature $P_U$ passes through a maximum value and then declines as the pressure increases. This is illustrated for four temperatures in figure 3, from which it will be seen that the maximum value of $P_U$ occurs at a total pressure in the neighbourhood of 150 mm. In the $H_2$-$O_2$-$NO_2$ system a similar dependence of $P_U$ on total pressure is found, but the value of the "inversion pressure" is 300 mm. (see figures 1 and 2 of Part V; and Norrish and Dainton 1939).

The similarity between the two systems extends to the effect of total pressure on the induction period at constant concentrations of sensitizer. In both cases the induction period falls off continuously from very high

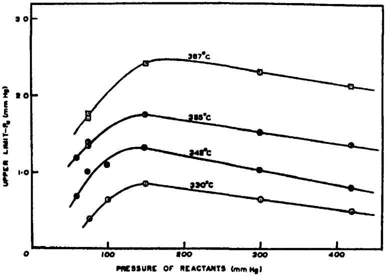

Figure 3. Variation of the upper limit ($P_U$) with total pressure of reactants ($2H_2+O_2$) at different temperatures. Quartz reaction vessel, internal diameter 25·0 mm.

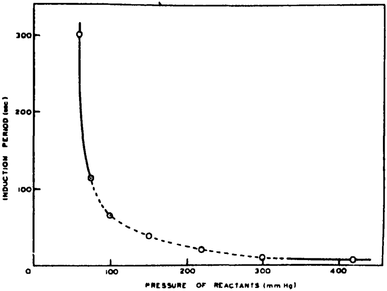

Figure 4. Variation of the induction period ($\tau$) with total pressure of reactants at 355° C. Quartz reaction vessel, internal diameter 25·0 mm. Pressure of NOCl 1·47 mm. Hg. Broken line indicates ignition, full line indicates slow reaction.

values at low pressures to an almost constant steady value at high pressures. As figure 4 and table 2 illustrate, the curve of induction period against total pressure is asymptotic with lines parallel to both axes and does not satisfy the equation

$$p\tau = \text{constant},$$

the deviations from this equation being most marked at low pressures.

Table 2. The variation of the induction period ($\tau$) and the product ($p\tau$) of $2H_2+O_2$ mixtures containing 1·47 mm. NOCl, with total pressure ($p$) of reactants. Temperature = 355° C. Cylindrical quartz reaction vessel, 25·0 mm. diameter

| Total pressure $p$ in mm. Hg | 60 | 75 | 100 | 150 | 220 | 300 | 420 |
|---|---|---|---|---|---|---|---|
| Induction period in sec. | SR 300 | SR 114 | *66 | *38 | *20 | *10 | SR 7 |
| Product $p\tau$ | 18,000 | 8,550 | 6,600 | 5,700 | 4,400 | 3,000 | 2,940 |

SR indicates slow reaction. * indicates ignition.

*Effect of temperature.* Rise in temperature facilitates both the branching and propagation of reaction chains and hence causes the upper limit ($P_U$) to rise and the induction period ($\tau$) to fall. In figure 5, $\log_{10} P_U$ is plotted against $1/T°$ K, and it is seen that except at the lowest temperature and low total pressures these two quantities are related by an equation of the form

$$\log_e P_U = -E/RT + \text{constant}.$$

Both the constant of this equation and $E$ increase with pressure, the actual magnitudes being given in table 3 below.

Table 3

| Total pressure in mm. Hg | 75 | 150 | 300 | 420 |
|---|---|---|---|---|
| $E$ in kcal. | 13·8 | 18·8 | 24·1 | 31·3 |
| Value of the constant (to third place only) | 12·0 | 16·1 | 20·1 | 25·4 |

## Conclusion

Since at a given temperature and pressure of reactants, the ignition is confined between two concentrations of nitrosyl chloride, this compound, like nitrogen peroxide, can play the dual role of catalyst and anticatalyst for the combustion of hydrogen. The efficiency of nitrosyl chloride in these respects is about the same as nitrogen peroxide, and the similarity also extends to the dependence of the induction period on catalyst concentration. In both cases the plot of the induction period against catalyst concentration is a smooth curve showing a minimum, and the induction period at the upper limit ($\tau_U$) always exceeds that at the lower limit ($\tau_L$). The upper limit ($P_U$), and the induction period at constant nitrosyl chloride content, vary with total pressure of hydrogen and oxygen in a precisely similar fashion as when nitrogen peroxide is used. Although addition of foreign non-reactant gases to explosive $H_2$-$O_2$-NOCl mixtures of constant composition lowers the induction period, addition of sufficient of these gases quenches the explosion, the relative amounts necessary to achieve this being

$$A:N_2:He:CO_2::6{\cdot}3:3{\cdot}8:3{\cdot}1\cdot 1,$$

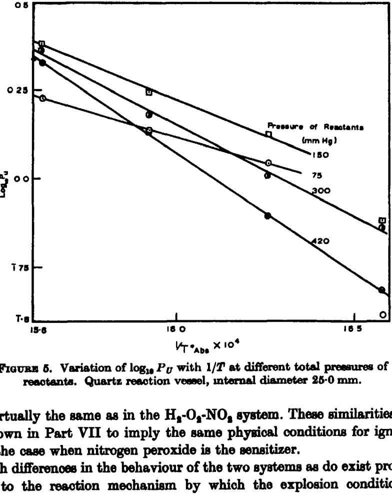

FIGURE 5. Variation of $\log_{10} P_U$ with $1/T$ at different total pressures of reactants. Quartz reaction vessel, internal diameter 25·0 mm.

i.e. virtually the same as in the $H_2$-$O_2$-$NO_2$ system. These similarities will be shown in Part VII to imply the same physical conditions for ignition as is the case when nitrogen peroxide is the sensitizer.

Such differences in the behaviour of the two systems as do exist provide clues to the reaction mechanism by which the explosion condition is attained. Thus since light capable of dissociating nitrogen peroxide has no effect on induction periods of nitrosyl chloride mixtures it is obviously not possible to explain the sensitizing power of this compound as due to nitric oxide and nitrogen peroxide to which it may give rise. Further nitrosyl chloride is a slightly more powerful sensitizer than nitrogen peroxide, a fact which indicates that the latter compound is not the real catalyst in this case. In Part VII these and other facts are further discussed and correlated with the conclusion that the effective initial centres are chlorine atoms.

The authors wish to express their gratitude to the Chemical Society and the Royal Society for grants which have made this work possible, and one of us (F. S. D.) is indebted to the Goldsmiths' Company for the award of a Senior Studentship and to Imperial Chemical Industries (Explosives Group) for a maintenance grant.

## REFERENCES

Foord, S. G. and Norrish, R. G. W. 1935 *Proc. Roy. Soc.* A, **152**, **196**.
Norrish, R. G. W. and Dainton, F. S. 1939 *Nature, Lond.*, **144**, **30**.
Norrish, R. G. W. and Dainton, F. S. 1940 *Proc. Roy. Soc.* A, **177**, **393**.

# A study of sensitized explosions

## VII. A chain-thermal theory of the reaction between hydrogen and oxygen sensitized by nitrogen peroxide or nitrosyl chloride

By F. S. Dainton and R. G. W. Norrish, F.R.S.
*Laboratory of Physical Chemistry, Free School Lane, Cambridge*

(*Received* 21 *May* 1940)

Both these reactions are chain processes for which the net branching factor $\phi$ is inversely proportional to the induction period. By applying this relation to the experimental results described in Parts V and VI, it is shown that ignition only occurs when the net branching factor attains a value determined by the sum of two quantities, one proportional to the thermal capacity and the other proportional to the thermal conductivity. It is pointed out that this ignition condition cannot be accounted for by any isothermal theory of ignition, but that it may readily be deduced from a thermal theory in which explosion is visualized as occurring only when the initial reaction rate, in a favourable volume element, is large enough to ensure that a critical temperature $T_e$ is reached in a critical time $t_e$.

Theories of reaction kinetics are developed from these two systems which give $\phi$ in terms of the experimental variables. The expressions so deduced lead to a dependence of the induction period on these variables identical with that found experimentally. The effects of vessel diameter, surface condition, temperature, and concentrations of sensitizer, reactants and foreign gases on the explosion are satisfactorily accounted for by substituting these expressions in the ignition condition of the chain-thermal theory.

The existence of critical pressure limits of sensitizer and reactants bounding an explosion region, and of induction periods preceding both slow reaction and ignition, in the catalysis of the combustion of hydrogen by traces of nitrogen peroxide and nitrosyl chloride which is described in detail in the two previous papers, is unmistakable evidence of the chain character of these reactions. Hinshelwood and Williamson (1934) and later von Elbe and Lewis (1937) have given theoretical treatments of the first of these reactions, based on the results of Thompson and Hinshelwood (1929). In these treatments, reaction schemes are developed which, in the notation used in this paper, give the branching factor $\phi$ in terms of the experimental variables, such as temperature and concentration of reactants and sensitizer. Self-neutralization of the centres is neglected, and the concentration of centres, $n$, is supposed to increase with time $t$, when $\phi$ is positive, according to the equation

$$n = \frac{\theta}{\phi}(e^{\phi t} - 1), \tag{1}$$

where $\theta$ is the rate of production of centres in primary processes, whereas when $\phi$ is negative, $n$ approaches a steady value of $\theta/\phi$ asymptotically. The boundary between ignition and slow reaction, i.e. the dependence of the upper and lower limits on the other parameters, is obtained by equating the expression for $\phi$ to zero. Since these experiments of Thompson and Hinshelwood however, Norrish and Griffiths (1933) and Foord and Norrish (1935) discovered the light sensitivity and induction periods of this reaction, and on the basis of their results propounded a chain-thermal theory of explosion, in contrast to the chain-isothermal theories of Hinshelwood and his co-workers. To include these data von Elbe and Lewis later, (1939), modified the details of their earlier reaction mechanism, but retained the isothermal condition of explosion. This theory was claimed to furnish 'a complete description of the experimental data'.

There are several reasons why this claim may not be admitted. First, in conceding that the sudden increase in pressure which occurs at the end of the induction period of the slow reaction is due to the local failure of isothermal conditions in the centre of the vessel, they imply that a similar state of affairs precedes ignition, and hence that the explosion does *not* take place isothermally. This point had already been made by Foord and Norrish (1935, p. 211). Secondly, in order to explain Foord and Norrish's observation that the induction period at the lower limit is shorter than at the upper limit the authors are compelled to make the artificial assumption that the true lower limit is lower than the experimental one, a tacit admission that a positive value of $\phi$ governs the ignition at this point. Thirdly, as pointed out in the present paper, the effect of an increase in pressure of reactants or of addition of foriegn non-reactant gases which would be predicted by their theory is in conflict with the facts described in Part V.

According to the theory of branching chain reactions, a discernible reaction rate is only attained when $n$ reaches a critical value $n_c$, i.e. after an induction period $\tau$ given by

$$\tau = \frac{1}{\phi}\log\left(1 + \frac{n_c\phi}{\theta}\right). \tag{2}$$

Variations in the logarithmic term of this equation will not be important in determining the value of $\tau$ when $\phi$ has finite positive values, and hence an *increasing induction period* may be taken as diagnostic of a *decreasing* $\phi$. This fact is the basis of a general test of all isothermal theories of explosion. In the particular case of the $H_2$-$O_2$-$NO_2$ system, Thompson and Hinshelwood have shown, and we have confirmed, that at pressures above 300 mm. the upper limit decreases and the lower limit increases, i.e. the explosion region shrinks, as the total pressure of reactants increases. According to "isothermal" theories, $\phi$ at constant concentration of nitrogen peroxide correspondingly decreases from positive values in the explosion region through zero at the explosion boundary to negative values in the region of slow reaction. The induction period ($\tau$) at constant concentration of nitrogen peroxide ought therefore to increase with pressure of reactants. Actually, both in this system and in the $H_2$-$O_2$-NOCl system the induction periods decrease with total pressure to almost constant values. This discrepancy will be found in all isothermal theories which define the explosion boundary as the locus of all compositions for which $\phi$ is zero.

Since at any given sensitizer concentration the explosion is confined between upper and lower pressure limits, and the induction period is much greater at the lower than the upper pressure limit, it follows that $\phi$ at each of these bounding pressures must be different, being higher at the upper limit and vice versa. Now any chain theory of ignition, thermal or isothermal, assumes that $\phi$ has positive values within the explosion region, and hence since there is slow reaction above the upper total pressure limit we are faced with the corollary that slow reaction can occur when $\phi$ has positive values, but that for explosion to occur, $\phi$ must attain a finite positive value which increases with total pressure.

Foord and Norrish, who, for different reasons than those given here, had already arrived at the conclusion that $\phi$ was positive in the $H_2$-$O_2$-$NO_2$ system, pointed out that this might be so, if the reaction centres can recombine at a rate proportional to the square of their instantaneous concentration. Under isothermal conditions, the number of centres is then restricted to an equilibrium value $n_e$ given by

$$n_e = \frac{\phi \pm \sqrt{(\phi^2 + 4\delta\theta)}}{2\delta}, \tag{3}$$

and their growth with time given by

$$\frac{dn}{dt} = \theta + \phi n - \delta n^2, \tag{4}$$

where $\delta$ is the velocity constant of the self-neutralization process.

The end of the induction period both for slow reaction and ignition is marked by a slight temporary pressure increase, which since the formation of water from its elements involves a pressure decrease, must be attributed to a rise in temperature caused by the exothermicity of the reaction. Foord and Norrish visualized explosion as occurring when the evolution of heat associated with this equilibrium concentration of centres, and of which the temporary pressure increase is a manifestation, occurs in a favourable volume element at a rate exceeding the rate of removal by conduction. If $\delta$ and $\theta$ are constant this means that before explosion can ensue, $\phi$ must attain a certain critical value dependent on the thermal conductivity of the system. The present paper deals with a refinement of this idea and with its application to both the $H_2$-$O_2$-$NO_2$ and $H_2$-$O_2$-NOCl systems. Schemes of reaction kinetics for both systems are suggested, which give $\theta$ and $\phi$ in terms of the experimental variables, and which are in accord with the experimental data.

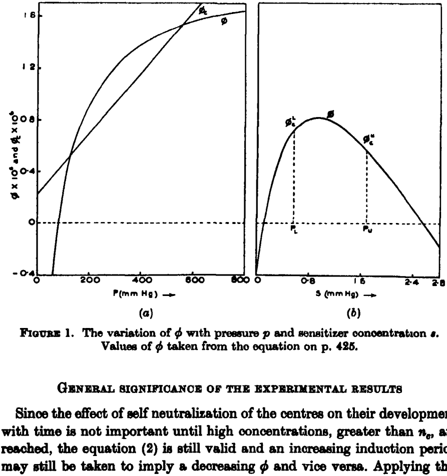

(a) (b)

FIGURE 1. The variation of $\phi$ with pressure $p$ and sensitizer concentration $s$. Values of $\phi$ taken from the equation on p. 425.

## GENERAL SIGNIFICANCE OF THE EXPERIMENTAL RESULTS

Since the effect of self neutralization of the centres on their development with time is not important until high concentrations, greater than $n_c$, are reached, the equation (2) is still valid and an increasing induction period may still be taken to imply a decreasing $\phi$ and vice versa. Applying this method to the experimental data given in Parts V and VI the following conclusions may be summarized:

(1) From the variation of the induction period with sensitizer concentration (Part V, figure 4, and Part VI, figure 1), $\phi$ is clearly a quadratic function of the sensitizer concentration $s$. A function of the type

$$\phi = \frac{As}{1+Bs} - Ds, \tag{5}$$

where $A$, $B$ and $D$ are arbitrary constants, would give the required dependence of $\tau$ on $s$ for both systems. This function is plotted in figure 1 (*b*).

(2) Since $\tau_U > \tau_L$ (Part V, figure 4, and Part VI, figure 1), it is clear that for both systems $\phi_L > \phi_U$. This conclusion is also consistent with the observed higher reaction velocities in the neighbourhood of the lower limit as compared with those just above the upper limit.

(3) At constant sensitizer concentration the induction period for both these systems, when plotted against reactant ($2H_2 + O_2$) pressure, lies on a smooth curve convex to both axes and apparently asymptotic to lines drawn close and parallel to both axes (see Part V, figure 3, and Part VI, figure 4). At low pressures $\phi$ clearly has very small values, but increases with pressure to a value which is independent of pressure. The equation

$$\phi = \frac{Ep}{1+Fp} - G/p \tag{6}$$

would satisfy these requirements ,and the curve of $\phi$ against $p$ of figure 1 (*a*) has been obtained by assigning arbitrary values to the constants of this equation. For the purposes of figure 1 and hence also equations (5) and (6) the expression

$$\phi = \frac{5 \times 10^{-6} ps}{200s + p} - 10^{-6} s - \frac{10^4}{2p}$$

has been used, where $p$ and $s$ are respectively the pressures in mm. of reactants and nitrogen peroxide, and the numerical constants are reasonably selected in view of the results and the known velocity constants of certain of the chain processes at 600° abs. A similar expression would apply to the nitrosyl chloride case, but this has not been evaluated.

(4) The value of $\phi$ which must be attained before explosion can take place increases with pressure. It will be shown later that if $\phi_c$ is this critical value of the net branching factor then

$$\phi_c = A'p + B', \tag{7}$$

where $B'$ is usually the more important term and is proportional to the thermal conductivity of the system, whilst the coefficient $A'$ depends on the thermal capacity of the system.

(5) Irradiation with wave-lengths adequate to dissociate $NO_2 = NO + O$ and $NOCl = NO + Cl$ has no effect on the limits of ignition in either case. As the condition for ignition, whether the thermal or isothermal theory be adopted, is not altered by irradiation it must be concluded that neither is $\phi$ altered. When nitrosyl chloride is used as a sensitizer the induction periods are unaltered by irradiation, and hence $\theta$ is also unaltered. On the other hand, when nitrogen peroxide is used, the induction periods were found by Foord and Norrish to be shortened by light capable of liberating an oxygen atom from the sensitizer, this shortening being the greater the more intense the incident light. It can only be concluded that in this case $\theta$ is greatly increased by irradiation.

(6) Rise of temperature affects both reactions in the same way, causing the induction periods to be shortened, and the upper limit ($P_U$) to be raised, $\log_e P_U$ being approximately proportional to the reciprocal of the absolute temperature (see Part V, figure 6, and Part VI, figure 5). This may be interpreted by assuming the constants $A$ and $B$ of equation (5) to be exponentially dependent on temperature in the same manner as velocity constants.

(7) In a given vessel at constant temperature the induction periods of $H_2$-$O_2$-$NO_2$ mixtures of constant composition are raised by sufficient of any added gas, being very markedly affected by methane in this respect (see Part V, figure 8). At the same temperature in the same vessel, A, He, $N_2$ and $CO_2$ and $O_2$ in excess of the stoichiometric proportion, lower the induction period of mixtures of $H_2$-$O_2$-$NOCl$ of constant composition, whilst methane has the same effect on both systems (see Part VI, figure 2). Clearly $\phi$ is lowered by non-reactant gases in the $NO_2$ sensitized reactions under the same conditions that it is raised in the NOCl sensitized reaction. The ultimate quantitative effect of these gases on the *explosibility* of the two systems, as measured by the quenching pressures, is, however, substantially the same (see p. 404 of Part V and footnote, p. 415, of Part VI). This fact indicates that in each case the critical value of $\phi$ which must be attained for explosion to occur ($\phi_c$), is altered to the same extent in each system, and that the alteration in $\phi_c$ is much larger than the change in $\phi$.

(8) The fact that the slow reaction of given $H_2$-$O_2$-$NOCl$ mixtures is retarded by inert gases although the induction period is shortened (see table 1, Part VI), is clear evidence that the steady reaction rate does not depend on $\phi$ alone, and receives ready interpretation if it is conceded that centres may recombine in three-body collisions.

(9) The results summarized in table 5 of Part V show that the effect of decreasing vessel diameter is to decrease $P_U$ and increase $P_L$. The induction periods at these limits do not show any progressive variation with vessel diameter over the range 5–30 mm. and hence the explosion condition is the same. The dependence of $P_U$ and $P_L$ on $d$ is therefore to be attributed to change of surface deactivation as it affects $\phi$. This point of view is confirmed by the fact that the induction period of mixtures of constant composition is always increased by decreasing the vessel diameter or by coating the surface with KCl. If $G$ of equation (6) is a function of the surface condition and proportional to $1/d^2$ the observed results can be accounted for.

The effect of surface has not been so closely examined in the NOCl catalysed reaction, but from the fact that inert gases shorten the induction period, i.e. raise $\phi$, a surface deactivation term must clearly be included in the expression for $\phi$.

These facts must be accommodated by any comprehensive theory of reaction kinetics and the ignition conditions in these two systems.

## THE CHAIN-THERMAL THEORY

*The ignition condition.* It has been argued (p. 423) that in the $H_2$-$O_2$-$NO_2$ system, the self-neutralization of the centres must be considered. This argument was based on the contrast between the observed dependence of the induction period on total pressure and concentration of nitrogen peroxide, and the effect of pressure on the ignition limits; and will therefore also be valid for the $H_2$-$O_2$-NOCl system where similar phenomena are encountered. In both cases, as soon as the induction period is over, the reaction will proceed at a rate proportional to $pn_e$, $n_e$ being defined by equation (3) and $\delta$ is a quantity which to a first approximation is proportional to $[M]$, the sum of the concentrations of all the molecules present. Since $\delta$ is the velocity constant of a ternary collision process it will be small and $4\delta\theta$ can probably be neglected in comparison with $\phi^2$. The potential equilibrium reaction rate ($\omega_e$) at the end of the induction period will be given by the simplified expression

$$\omega_e = kpn_e = \frac{\phi p}{\delta'[M]},$$

where $\delta' = \dfrac{\delta}{[M]\,k}$, and $k$ is the velocity constant of the propagation reaction.

Now both of these sensitized reactions are exothermic (57,000 cal./gmol. of water formed), and as they develop their temperature will rise, but also reactants will be consumed. Rise of temperature is known to cause $\phi$ to increase; and consumption of reactants may cause $\phi$ either to decrease continuously (in the region of the lower limit), or to decrease only after an initial increase (in the region of the upper limit). Depending on the magnitude of the initial rate, the precise dependence of $\phi$ on temperature and mixture composition, and the thermal capacity and conductivity of the system, so will the temperature either rise very rapidly (both $dT/dt$ and $d^2T/dt^2$ being positive) to a high maximum value, most of the reactants being consumed before this temperature maximum is attained, or rise slowly ($dT/dt$ positive but $d^2T/dt^2$ negative) to a low maximum value, only a fraction of the reactants being consumed. The physical conditions remaining constant, there will thus be a minimum initial reaction velocity which will ensure the first state of affairs. Owing to the concentration gradients of reaction centres within the reaction vessel, which are imposed by the deactivating influence of the wall, this critical reaction velocity will be attained most easily in the elements of volume lying at the centre of the reaction vessel. When this velocity is attained, neighbouring less favourable volume elements will be heated to ignition, which will therefore spread throughout the whole vessel.

If $C_v$ is the thermal capacity, assumed constant, of the most favourable volume element at unit pressure, $K$ is a constant proportional to the thermal conductivity of the gaseous medium round it, $T_0$ the initial temperature, $T$ the temperature after time $t$, and $Q$ the heat liberated for every gram molecule of water formed, then

$$\frac{Q}{N}\frac{p\phi_0}{\delta'[M]}f_1(T)f_2(t)\,dt = pC_v\,dT + K(T-T_0)\,dt, \tag{8}$$

where $N$ is Avogadro's number and $\phi = \phi_0 f_1(T) f_2(t)$, $f_1(T)$ expressing the temperature dependence of $\phi$ and $f_2(t)$ the time dependence. Even if these functions $f_1$ and $f_2$ were precisely known, which they are not, equation (8) could not be integrated analytically.* It is known, however, that $\phi$ increases with $T$ and must eventually decrease with $t$. In this case by assuming constant arbitrary values for $pC_v$, $K$ and $Qp/N\delta'[M]$ a family of curves would be obtained for $T$ plotted against $t$, each curve corresponding to a given value of $\phi_0$, and all showing a maximum value for $T$ as in the diagram of figure 2*a*. Associated with each of these curves in 2*a* is one in 2*b* showing the fractional amount of combustion after a certain time. This family would be split into two groups, the transition from one group to the other occurring continuously, but very rapidly, over a very small range of values of $\phi_0$. In one group the maximum temperature is high, $d^2T/dt^2$ is positive and this corresponds to explosively rapid luminescent reaction in which most of the reactants are consumed. In the other the maximum temperature is only slightly above $T_0$, $d^2T/dt^2$ is never positive, and this corresponds to slow

---

* Numerical integration of this equation, after selecting the functions $f_1(T)$ and $f_2(t)$ appropriate to the particular explosion under consideration, has already been carried out by several authors. Thus Rice, Allen and Campbell (1935), and later Rice and Campbell (1939), assuming an exponential increase with temperature and an exponential decay with time of the non-chain but explosive decomposition of ethyl azide in the presence and absence of diethyl ether, have obtained the first part of a family of curves similar to that described here. Appin, Chariton and Todes (1936), assuming almost identical functions to Rice *et al.* for the decomposition of methyl nitrate, have also calculated $T/t$ and percentage decomposition/time curves which are in accord with the qualitative ideas described here. In both these cases, however, the induction periods are very short, of the same order of magnitude as the time of admittance of the reactants to the reaction vessel. It is questionable therefore whether a theory, the basic

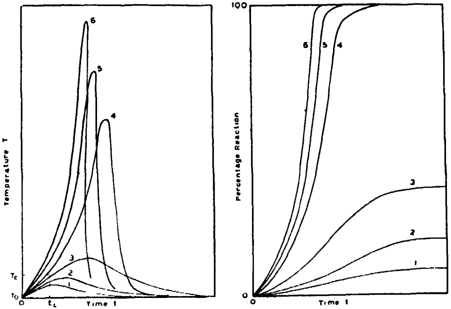

(*a*) (*b*)

FIGURE 2. (*a*) The temperature $T$ after time $t$. (*b*) The percentage of reaction which has taken place after time $t$. The numbers 1, 2, 3, 4, 5, 6 represent the values of $\phi_0$ on an arbitrary scale In this case the critical value of $\phi_0$ bounding the ignition is 3·5.

premise of which is that the gases are initially at a uniform temperature and pressure, can be applied to these reactions in which there is scarcely time for hydrodynamic and thermal equilibrium to be attained before an appreciable amount of reaction has occurred. This criticism clearly does not apply to the application of this theory to the $H_2$-$O_2$-$NO_2$ and $H_2$-$O_2$-NOCl systems, which are characterized by long induction periods during which no pressure change occurs.

non-luminescent reaction. In both cases a temperature rise does occur, which will be evidenced by an increase of pressure such as is found to mark the end of the induction period.

The bounding conditions for the two types of curve may be visualized as the attainment by the volume element of a critical temperature $T_c$ in a short critical time $t_c$ during the first "burst" of reaction, whilst the rate may still be regarded as $\omega_c$. Mathematically

$$\frac{Q}{N}\frac{p\phi}{\delta' M}t_c = p\int_{T_0}^{T_c} C_v\,dT + K\int_0^{t_c}(T-T_0)\,dt.$$

The increase in temperature of the volume element during the short time $t_c$ is probably almost linear, and hence we may write

$$\phi\frac{p}{[M]} = \delta'(AC_v p + BK).$$

For ignition to occur in this system $\phi$ must exceed a value $\phi_c$ such that

$$\phi_c = \frac{\delta'[M]}{p}(AC_v p + BK), \tag{9}$$

where $A$ and $B$ are constants. This is the condition for ignition which will be adopted.

### THEORY OF REACTION KINETICS

(1) *The* $H_2$-$O_2$-$NO_2$ *system*. Two reaction mechanisms have been advanced by Foord and Norrish (1935) and von Elbe and Lewis (1939), which give $\phi$ in terms of the concentrations of reactants. The latter scheme was devised to account on an isothermal basis for the decrease of $P_U$ and the increase of $P_L$ with total pressure, and as already pointed out, automatically yields an expression for $\phi$ in conflict with the observed trend of induction periods with pressure (see Part V, figure 3). It may also be objected, on similar grounds, that since this theory is capable of predicting a correct order of effectiveness of foreign gases in lengthening the induction period (this order should be the same as the order of efficiency of these substances as third bodies in the association process

$$HO + NO_2 + M = HNO_3 + M$$

and would be predicted as $CO_2 > N_2 > A > He$, since this order applies to these gases, when, as third bodies, they facilitate the recombination of iodine atoms (Rabinowitch and Wood 1936), bromine atoms (Rabinowitch and Wood 1936; Smith, Ritchie and Ludlam 1937) and the formation of complexes such as $HO_2$ (Ritchie 1937) and $NCl_4$ (Griffiths and Norrish 1934)) it automatically predicts the same order for the explosion-quenching efficiencies and is incorrect in that respect. Since, in addition, the experimental relations for the effects of vessel diameter and surface condition on the explosion limits cannot readily be deduced from this scheme of reaction kinetics, it will be rejected.

The scheme of Foord and Norrish on the other hand leads to an expression for $\phi$ which when substituted in the explosion condition ($\phi = \phi_c$, $\phi_c$ being defined by equation (9)) satisfies, with one exception, all the facts summarized in the preceding section. The exception is, that whereas the theory allows for a decrease of the induction periods as foreign non-reactant gases are added, in fact, the induction periods are lengthened (Part V, figure 8). This fact coupled with the variation of the induction period with total pressure (Part V, figure 3) indicates that $\phi$ may be decreased in a specific manner by foreign gases, but may not be decreased by an increase in the pressure of reactants. This is possible if the fraction of the total number of centres which are sufficiently highly energized to effect dissociation of a molecule of nitrogen peroxide on collision and thus cause branching, is unaffected at high pressures by a change in the amount of reactants but is reduced by an increase in the pressure of foreign gas. This suggests that these "hot" centres are occasionally formed by interaction of ordinary centres with molecules of one or other reactant in a highly exothermic process. Their rate of formation is thus proportional to the total pressure of the reactants. Such "hot" centres may be deactivated and thus revert to normal centres by collision with any molecular species present. Their rate of removal is thus proportional to the total pressure of the system, including that of the foreign gas. Other factors remaining constant, $\phi$ is proportional to the concentration of hot centres, and hence would be expected on these grounds to be decreased by foreign gases.

Introducing this concept into the mechanism of Foord and Norrish (1935), we may distinguish two types of chain carrier: (1) ordinary centres $X$ the concentration of which is denoted by $n$, which are capable of propagating chains and which are subject to removal by wall destruction and by nitrogen peroxide, and (2) 'hot' centres $Y$ described above, the concentration of which is denoted by $n^*$ and which are occasionally produced by the exothermic reaction of a normal centre $X$ with one of the reactants, and which revert to ordinary centres by collision with any molecule. When that molecule is nitrogen peroxide they cause it to be disrupted into nitric oxide and an oxygen atom. It must be emphasized that the removal of a hot centre does not terminate a chain, as it always implies the production of a fresh centre.

It is generally agreed (Foord and Norrish 1935; von Elbe and Lewis 1939) that chains are initiated by the reaction of hydrogen with oxygen atoms produced by the dissociation of $NO_2$. There have also been suggestions (Norrish and Griffiths 1933) that since this dissociation is endothermic to the extent of 71·5 kcal. the reaction

$$NO + O_2 = NO_2 + O$$

which only required 45·9 kcal. is the predominating source of oxygen atoms in the unirradiated reaction, the nitric oxide concentration being controlled by the equilibrium

$$2NO_2 = 2NO + O_2 - 26 \text{ kcal.}$$

The equilibrium constant of this reaction has been measured by Bodenstein and Ramstetter (1922) and calculated by Zeise (1936) from spectroscopic data. The results agree and lead to a value for

$$K_p^{385^\circ \text{C}} = \frac{[NO]^2[O_2]}{[NO_2]^2} = ca.\ 0{\cdot}02 \text{ atmosphere.}$$

A typical equilibrium mixture at this temperature would be 76 mm. $O_2$, 0·76 mm. $NO_2$, and 0·24 mm. NO. Taking 5550 gmol. c.c.$^{-1}$ sec.$^{-1}$ as the velocity constant of the dissociation at this temperature (deduced from the value $2\sqrt{2}\,\pi\sigma^2_{NO_2}\bar{u}e^{-E/RT}$, $\sigma_{NO_2}$ being taken as $3{\cdot}3 \times 10^{-8}$ cm. and $E$ as 30,000 cal.), the time for the attainment of equilibrium of a mixture which contains initially 1·0 mm. $NO_2$ is greater than 2500 sec. This is about one hundred times the order of magnitude of the induction periods under these conditions and hence the reaction $NO + O_2 = NO_2 + O$ is an unimportant source of oxygen atoms. The reaction scheme now takes the form

Initiation ($k_1$) $NO_2 = NO + O$
($k_2$) $O + NO_2 = NO + O_2$
($k_3$) $O + H_2 = X$.
Branching ($\alpha$) $Y + NO_2 = X + NO + [O \rightarrow X]$.
Termination ($\beta$) $X + NO_2$ = destruction
($\gamma$) $X$ + wall = destruction.

The hot centres $Y$ are produced by

($k_5$) $X + H_2$ or $O_2 = Y$

and deactivated by ($k_6$) $Y + M = X + M$.

The figures in brackets are the velocity constants. The wall removal of the hot centres $Y$ and of oxygen atoms (process (4) of Foord and Norrish's mechanism) are here neglected, since in their passage to the wall the oxygen atoms are unlikely to survive repeated collisions with hydrogen molecules, and the hot centres will not outlive more than one or two collisions of type $k_6$. Moreover, the experimental results do not demand incorporation of such reactions into the scheme.

If $S$ is the concentration of nitrogen peroxide and $p = \frac{2}{3}[H_2]$, then the above mechanism leads to the following equation for the development of the centres with time under isothermal conditions:

$$\frac{dn}{dt} = \theta_{NO_2} + \phi_{NO_2} n - \delta n^2,$$

$$\left.\begin{aligned} &\text{where} \qquad \theta_{NO_2} = \frac{k_1 k_3 [H_2] s}{k_2 s + k_3 [H_2]} \\ &\text{and} \qquad \phi_{NO_2} = \frac{\alpha k_3 k_5 s [H_2] p}{(k_2 s + k_3 [H_2])(\alpha s + k_6 [M])} - \beta s - \gamma. \end{aligned}\right\} \qquad (10)$$

(2) *The* $H_2$-$O_2$-NOCl *system*. Numerous measurements of the velocity constant of the dissociation of nitrosyl chloride have been made but the most reliable are those of Waddington and Tolman (1935) which lead to a value of $6{\cdot}127 \times 10^6$ gmol. c.c.$^{-1}$ sec.$^{-1}$ at 368° C. If the fate of nitrosyl chloride were determined solely by the equilibrium

$$2NOCl \underset{k_2}{\overset{k_1}{\rightleftharpoons}} 2NO + Cl_2 - 18{\cdot}6 \text{ kcal.},$$

then appreciable amounts of nitric oxide would be formed in a minute from 1 mm. NOCl. By the reactions

$$2NO + O_2 = 2NO_2 + 25{\cdot}9 \text{ kcal.}$$

and $$NO + O_2 = NO_2 + O - 45{\cdot}9 \text{ kcal.}$$

amounts of nitrogen peroxide would be formed during the induction period, which, though small, would be large enough to be catalytically active. That nitrogen peroxide, so formed, is not the catalyst in this system is shown by the experimental observations (*a*) that ignition occurs in this system at lower temperatures than in the $H_2$-$O_2$-$NO_2$ system, and (*b*) that the induction period is unaffected by irradiation with light of wave-length and intensity sufficient to annihilate the induction periods in the $H_2$-$O_2$-$NO_2$ system.

Although nitrogen peroxide is excluded as a source of oxygen atoms, it is still possible to construct reaction schemes, in which the same centres are playing corresponding parts in the chain development of each system. Such schemes are however artificial, and demand the participation of intermediates such as nitroxyl chloride ($NO_2Cl$) the individuality of which is by no means certain, and hence also of unknown equilibria such as

$$2NO_2Cl \rightleftharpoons 2NOCl + O_2$$

to define the concentration of such intermediates. If it is admitted that chlorine atoms can give rise to reaction centres by the almost thermoneutral reaction

$$Cl + H_2 = HCl + H - 700 \text{ cal.}$$

then the principal criticisms which can be brought against these reaction schemes and which centre round the fact that the most likely effect of binary collisions involving one molecule of nitrosyl chloride, would from energy considerations, be the dissociation into nitric oxide and a chlorine atom, are avoided. We may construct the reaction scheme

$$\begin{array}{llll}
\text{Initiation} & (k_1') & NOCl & = NO + Cl - 38{,}500 \text{ cal.} \\
 & (k_2') & Cl + NOCl & = NO + Cl_2 + 19{,}500 \text{ cal.} \\
 & (k_3') & Cl + H_2 & = HCl + [H \rightarrow X]. \\
\text{Branching} & (\alpha') & NOCl + X & = NO + X + [Cl \rightarrow X]. \\
\text{Termination} & (\beta') & X + NOCl & = \text{destruction} \\
 & (\gamma') & X + \text{wall} & = \text{destruction}
\end{array}$$

which leads to values of $\theta_{NOCl}$ and $\phi_{NOCl}$

$$\left.\begin{aligned}
\theta_{NOCl} &= \frac{k_1' k_3'[H_2] s'}{k_2' s' + k_3'[H_2]} \\
\text{and} \qquad \phi_{NOCl} &= \frac{\alpha' k_3'[H_2] s'}{k_2' s' + k_3'[H_2]} - \beta' s' - \gamma'
\end{aligned}\right\} \qquad (11)$$

where $s'$ is the concentration of nitrosyl chloride. The effect of foreign noncombustible gases in shortening the induction period shows that there is no need to assume that hot centres are formed, and as will be shown later there is good reason for this.

At first sight the fact that irradiation with light 2000–7000 A has no effect on the induction period would appear to invalidate this mechanism, because it would be anticipated that by increasing the number of chlorine atoms by

$$NOCl + h\nu = NO + Cl$$

the term $k_1'$ and hence also $\theta$ would be increased and the induction period shortened. In the $H_2$-$O_2$-$NO_2$ system the thermal dissociation of nitrogen peroxide due to the high endothermicity of the reaction is a very rare occurrence, and consequently the photochemical reaction may be more frequent under the experimental conditions. Foord and Norrish suggest that $k_1$ photo/$k_1$ thermal may have to be as large as $10^6$ to produce the observed effect on the induction period. Now the thermal dissociation of nitrosyl chloride may be considered at 368° C as approximately

$$e\,71{,}500-38{,}500/(R\times 691)=10^{8\cdot 14}$$

times as rapid as the thermal dissociation of nitrogen peroxide. Hence the photochemical dissociation of nitrosyl chloride would have to be very much faster than the photolysis of nitrogen peroxide under the same conditions. Actually the quantum yields of

$$NO_2+h\nu=NO+O,$$
$$NOCl+h\nu=NO+Cl,$$

are the same, and although the threshold wave-length for nitrosyl chloride (*ca.* 7600 A, Goodeve and Katz 1939) is much larger than for nitrogen peroxide (*ca.* 4360 A, Norrish 1929) yet the absorption coefficients appear to be lower over the frequency ranges for which measurements have been made for both of them (see Leermakers and Ramsperger 1932; Goodeve and Katz 1939; Holmes and Daniels 1934). It is therefore very likely that although light would cause a very large percentage increase in the rate of production of oxygen atoms from nitrogen peroxide, only a very slight percentage increase in the rate of production of chlorine atoms would be caused by irradiation of nitrosyl chloride. This would appear to dispose of the only criticism which can be brought against this mechanism, which will therefore be tentatively adopted.

## APPLICATION OF THE CHAIN-THERMAL THEORY TO THE EXPERIMENTAL RESULTS

Comparison of the expressions for $\phi_{NO_2}$ (10), $\phi_{NOCl}$ (11) and $\phi_c$ (9) with equations (5), (6) and (7) shows that the theory from which the former were deduced gives a satisfactory account of the experimental results summarized in the latter. In the following paragraphs this theory will be shown to be satisfactory even with respect to details.

### (1) *Sensitizer concentration*

At constant total pressure and in the absence of foreign gases $\phi_{NO_2}$ and $\phi_{NOCl}$ are dependent on sensitizer concentration in a similar way which is shown in figure 1. So are $\theta_{NO_2}$ and $\theta_{NOCl}$. $\phi_{NO_2}$ and $\theta_{NO_2}$ are substantially the same as was obtained by Foord and Norrish (1935), and since these authors obtained the trend of induction periods with sensitizer concentration correctly, this theory will also be satisfactory. A similar trend would be predicted for the $H_2$-$O_2$-NOCl system, and reference to Part VI, figure 1 will show that it has been found.

Reference to figure 1 shows that at constant temperature, decrease of $p$ alone ($s$ constant) would cause $\phi$ to decrease continuously. For initial concentrations of sensitizer greater than that necessary to give the maximum value of $\phi$, decrease of $s$ alone ($p$ constant) would cause $\phi$ to increase to a maximum value before decreasing. Hence, the decrease of $p$ and $s$ together, such as occurs during reaction, would lead to a time dependence of $\phi$ as shown in the curve $\phi_U$ of figure 3. This is the state of affairs for reaction mixtures of composition in the neighbourhood of the upper limit. On the other hand, at the lower limit the decrease of $p$ and $s$ during reaction may be deduced from figure 1 as giving a time dependence ($f_2(t)$ of equation 8, p. 428) of the form without a maximum as given by curve $\phi_L$ of figure 3.

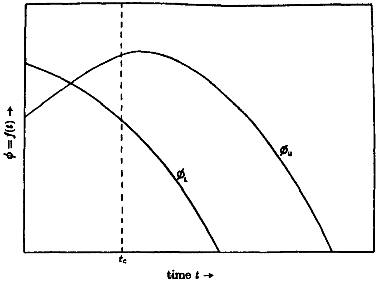

FIGURE 3. The isothermal variation of $\phi$ with time, i.e. $f_2(t)$. Curve $\phi_U$ refers to initial concentrations of sensitizer in the region of the upper limit, and curve $\phi_L$ to initial concentrations of sensitizer in the region of the lower limit.

Because of this difference in $f_2(t)$, in a system in which $pC_v$ and $K$ are constant, the *initial* value of $\phi_L$ necessary to cause the volume element to generate the heat which brings the temperature to the critical value $T_c$ in the short time $t_c$ and so ensure ignition, will be larger than the *initial* value of $\phi_V$ necessary for the same purpose. There are two consequences of this. First, $\tau_V$ should always exceed $\tau_L$; and from Part V, figure 4 and Part VI, figure 1 this is seen to be the case. Secondly, if the reaction rate is correctly given as $(kp\phi)/\delta$, the rate of the slow reaction in the immediate vicinity of the lower limit should be greater than in the vicinity of the upper limit. This phenomenon has repeatedly been observed, but as its significance was not fully realized at the time, unfortunately no measurements were made.

### (2) *Irradiation*

The great difference in the responses made by these two systems to illumination has already been discussed.

### (3) *The effect of pressure*

#### (*a*) *On the induction period.*

At constant concentration of sensitizer both $\phi_{\text{NOCl}}$ and $\phi_{\text{NO}_2}$ increase steadily with total pressure $p = \frac{3}{2}[\text{H}_2]$, in the manner shown in figure 1. At high total pressures $k_3[\text{H}_2] > k_2 s$, $k_3'[\text{H}_2] > k_2' s'$ and thus $\theta_{\text{NO}_2}$, $\phi_{\text{NO}_2}$, $\theta_{\text{NOCl}}$ and $\phi_{\text{NOCl}}$ are all independent of pressure. Hence at high pressures the induction periods should tend to steady values, as has been found. At lower pressures $k_2 s > k_3[\text{H}_2]$ and $k_2' s' > k_3'[\text{H}_2]$, and neglecting the variation of the coefficients $\gamma$ and $\gamma'$ with pressure, reference to equations (10) and (11) shows that the four quantities $\theta_{\text{NO}_2}$, $\phi_{\text{NO}_2}$, $\theta_{\text{NOCl}}$ and $\phi_{\text{NOCl}}$, are all proportional to $p$. Substitution in equation (2) shows that the relation $\tau p =$ constant should express the dependence of the induction period on pressure. The fact that the terms $\gamma$ and $\gamma'$ are inversely proportional to $p$, however, makes this relation the less valid the lower the pressure, and makes $\tau \propto 1/p^n$ where $n$ is always greater than unity, but decreases with pressure.

#### (*b*) *On the explosion boundary.*

The ignition areas will be bounded by two curves, the equations for which are obtained by equating the values for $\phi$ under these conditions to the value of $\phi_c$ given in equation (9). The expressions so deduced are

For $\text{NO}_2$-$\text{H}_2$-$\text{O}_2$

$$\frac{2\alpha k_2 k_5 ps}{3k_6(k_2 s + \frac{2}{3}k_3 p)} - \beta s - \gamma = \delta'(ApC_v + BK).$$

For $\text{NOCl}$-$\text{H}_2$-$\text{O}_2$

$$\frac{2\alpha' k_3' ps'}{3(k_2' s' + \frac{2}{3}k_3' p)} - \beta' s' - \gamma' = \delta'(ApC_v + BK).$$

$\gamma$ and $\gamma'$ are the probabilities that the centres will be removed at the wall and are proportional to the diffusion coefficients of the centres through the particular gaseous mixture. Writing $\gamma = \Gamma/p$ and $\gamma' = \Gamma' p$, and allowing for the fact that the thermal capacity $pC_v$ increases with pressure, whereas the thermal conductivity of a mixture of constant composition may be taken as independent of pressure over the range covered by experiment, the equations of the ignition boundaries become

For $NO_2$
$$\frac{\dfrac{2\alpha k_3 k_5}{3k_6} s}{k_2 s + \frac{2}{3} k_3 p} - \beta s - \Gamma/p = A'p + B'.$$

For NOCl
$$\frac{\frac{2}{3}\alpha' k_3' s'}{k_2' s' + \frac{2}{3} k_3' p} - \beta' s' - \Gamma'/p = A'p + B'.$$

For convenience we may distinguish two special cases, and for brevity only one of the above equations will be developed, since these equations differ only in the magnitude of the constants and the same behaviour will be found in the $H_2$-$O_2$-NOCl as in the $H_2$-$O_2$-$NO_2$ system.

($\alpha$) *Low sensitizer concentrations.* $s = P_L$ and at all pressures $\frac{2}{3}k_3 > k_2 s$ and the equation for the dependence of the lower limit ($P_L$) on pressure ($p$) is

$$A'p^2 - \left\{P_L\left(\frac{\alpha k_5}{k_6} - \beta\right) - B'\right\} p + \Gamma = 0,$$

and there are clearly two positive values of the pressure for certain low concentrations of sensitizer. If $P_L$ has values such that the coefficient of $p$ is positive, the variation of $P_L$ with total pressure is of the form shown by that part of the curve lying between 130 and 700 mm. in Part V, figure 2.

($\beta$) *High sensitizer concentration.* $s = P_U$ and *at low total pressures* $k_2 s > \frac{2}{3}k_3 p$ and the upper limit ($P_U$) will be given by

$$\beta P_U = \left(\frac{2\alpha k_3 k_5}{3k_6 k_2} - A'\right) p - \frac{\Gamma}{p} - B',$$

implying that the upper limit falls off rapidly with decrease in total pressure, principally due to the reduction in $\phi$ caused by increased loss of centres by diffusion to the wall, i.e. the $\Gamma/p$ term. *At higher total pressures* this term is small and almost constant, but neither $k_2 s$ nor $\frac{2}{3}k_3 p$ predominates over the other and

$$P_U = \frac{2\alpha k_3 k_5}{3k_6\left(\dfrac{k_2}{p} + \dfrac{2}{3}\dfrac{k_3}{s}\right)} - A'p - B' - \gamma,$$

indicating a decrease of $P_U$ with $p$. The upper limit should thus increase with $p$ initially due to the fact that $\phi$ is increasing with pressure more rapidly than $\phi_c$. The lower limit decreases for the same reason. At higher pressures the loss of oxygen (or chlorine) atoms in $k_3$ (or $k_3'$) counterbalances to some extent the production of centres in that reaction, and $\phi$, as is shown by the trend of the inductions period with pressure tends to a constant value. On the other hand, due to the increase of self-neutralization and increasing thermal capacity of the system, $\phi_c$ continues to increase linearly with pressure. The quantity $\phi - \phi_c$ passes through a maximum value and declines to zero, and causes the critical concentrations of sensitizer to converge at high pressures. In the $H_2$-$O_2$-$NO_2$ case the whole closed ignition region which was predicted was also obtained experimentally (Part V, figure 2). In the $H_2$-$O_2$-NOCl case only the upper limits were studied, but they were found to conform to type. It will be noticed from Part V, figure 1, and Part VI, figure 3, that the 'inversion pressure', i.e. the pressure at which $P_U$ has its maximum value, is about 300 mm. when nitrogen peroxide is sensitizer, and about 150 mm. when nitrosyl chloride is used. This difference is readily interpreted when it is considered that, ceteris paribus, the larger $k_3$ the smaller the value of this inversion pressure. Schumacher (1930) has shown that $\left(\frac{k_3}{k_3}\right)^{300^\circ\,\mathrm{K}} = 10^{-4}$, from which it may be argued that the energy of activation of

$$O + H_2 = HO + H \rightarrow \text{centres}$$

is at least 6 kcal., whereas the reaction

$$Cl + H_2 = HCl + H \rightarrow \text{centres} - 0{\cdot}7\ \text{kcal.}$$

probably has a lower value. In other words $k_3' > k_3$, and the inversion pressure should be smaller in the NOCl sensitized reaction.

### (4) *The effect of temperature on the ignition limits*

As the initial temperature $T_0$ rises there will be some change in the explosion condition, but the variation of $\phi$ with temperature will be principally responsible for the alteration of the explosion limits. Neglecting the variation of collision and diffusion rates with temperature the dependence of the limits on temperature will be given approximately by putting the left-hand sides of equations (10) and (11) equal to constants. By definitions, $\alpha$, $k_6$, $k_7$, $\beta$, $\gamma$ and $\alpha'$, $\beta'$, $\gamma'$ will contain no temperature dependent term. The rate of formation of hot centres in the nitrogen peroxide reaction will however be increased by temperature, and so will the branching reaction in the nitrosyl-chloride reaction. Let $k_5 = k_5^0 e^{-E/RT}$ and $\alpha' = \alpha_0' e^{-E'/RT}$.

There is no simple relationship expressing the lowering of the lower limit with temperature but for low total pressures and high concentration of sensitizer we obtain by approximating as before

for $NO_2$
$$\beta P_U = \frac{2\alpha k_5^0}{k_6}\frac{k_3}{k_2} e^{-E/RT} p - \left(\frac{\Gamma}{p} + \text{constant}\right)$$

and NOCl
$$\beta' P_U = 2\alpha_0' \frac{k_3'}{k_2'} - e^{-E'/RT} p - \left(\frac{\Gamma'}{p} + \text{constant}\right).$$

From Schumacher's data $k_3/k_2$ is known to be proportional to $e^{-6000/RT}$. $k_3'/k_2'$ is probably less dependent on temperature; $e^{-1000/RT}$ would be deduced from the energies of the bonds which are involved*. If both the terms $(\Gamma/p + \text{constant})$ and $(\Gamma'/p + \text{constant})$ are small the relations

for $NO_2$
$$\log_e P_U = \frac{-(E+6)\,\text{kcal.}}{RT} + \log_e \frac{2\alpha k_5^0}{3\beta k_6} p,$$

and NOCl
$$\log_e P_U = \frac{-(E'+1)\,\text{kcal.}}{RT} + \log_e \frac{2\alpha_0'}{3\beta'} p$$

should hold. Relations of this type have been obtained experimentally and comparison with experiment for pressures less than the inversion values indicates that $E$ is about 15,000 cal. and $E'$ about 12,000 cal.

At high total pressures a linear relation between $\log_{10} P_U$ and $1/T$ is not rigidly obeyed, nor can it be deduced from the expression (9), (10) and (11).

### (5) *The effect of surface*

The discussion in this paragraph is confined to the nitrogen peroxide system.

Bursian and Sorokin (1931) have shown that in cases of branching chain reactions with deactivation at the wall, coefficients of the type $\gamma$ may be set proportional to $D/d^2$ over a wide range of conditions, where $D$ is the diffusion coefficient of the centres through the gas and $d$ is the vessel diameter.

The favourable volume element from which ignition spreads is of very small dimensions and it is unlikely that the heat transfer conditions will be affected by variation of the diameter over the experimental range of diameters. In confirmation of this point of view is the fact that the induction period at the upper limit, which is an indirect measure of $\phi$ at the upper limit, does not show any progressive variation with diameter but has a value lying between 60 and 77 sec. for all diameters except one, between 8 and 30 mm., both in vessels which have been treated with potassium chloride and in vessels which have not been so treated. At constant total pressure therefore the effect of vessel diameter on the ignition limits will be given by

---

* $k_3'$ refers to the exothermic reaction $Cl + NOCl = Cl_2 + NO$ which probably proceeds at every collision. $k_2'$ refers to $Cl + H_2 = HCl + H$ reaction which, from the heats of dissociation of the $H_2$ and HCl molecules, 103·4 and 102·7 kcal. respectively, is endothermic to the extent of about 1000 cal.

$$\frac{\frac{2\alpha k_3 k_5}{3k_6} ps}{k_2 s + \frac{2}{3} k_3} - \beta s - \frac{\epsilon D}{d^2} = A'p + B',$$

where $\epsilon$ is a constant of proportionality. This equation may be simplified to meet two special cases, both concerned with a constant low total pressure and both of which have been realized:

(*a*) At high concentrations of nitrogen peroxide $s = P_U$, $k_2 s > \frac{2}{3} k_3 p$ and

$$P_U = \frac{1}{\beta}\left\{\left(\frac{2\alpha k_3 k_5}{3k_2 k_6} - A'\right)p - B'\right\} - \frac{\epsilon D}{d^2}$$
$$= \text{a constant} - \frac{\epsilon D}{d^2}.$$

(*b*) At low concentrations of nitrogen peroxide $s = P_L$, $\frac{2}{3} k_3 p > k_2 s$ and

$$P_L = \frac{1}{\left(\frac{\alpha k_5}{k_6} - \beta\right)}\left\{A'p + B' + \frac{\epsilon D}{d^2}\right\}$$
$$= \text{a constant} + \frac{\epsilon D}{\left(\frac{\alpha k_5}{k_6} - \beta\right) d^2}.$$

Arbitrary values may be assigned to the constants in these equations such that the full lines of Part V, figure 12 are obtained. The two equations appropriate to the limits in the vessels treated with KCl may be obtained from the corresponding equations appropriate to vessels with normal surface, by multiplying the coefficients of $1/d^2$ in the latter by 1·87. An interpretation of this factor would be that the effect of coating the walls with potassium chloride is to increase the efficiency of the surface in adsorbing those centres which strike it, by 87 %.

### (6) *The effect of foreign gases*

Addition of a foreign gas alters both the critical value of $\phi$ which must be attained for ignition ($\phi_c$) and the ability of the system to meet this condition, i.e. $\phi$ itself.

(*a*) *Induction periods.*

The branching factor $\phi$ will be affected through the alteration of the diffusion coefficient and hence also of $\gamma$ and $\gamma'$. All the gases will hinder the diffusion to the wall, but from the coefficients of self-diffusion it would be anticipated that $CO_2$ and $N_2$ would be more efficient than the inert gases. $\phi$ is thus increased, and if this were the only factor the induction periods would be shortened; carbon dioxide being very effective, nitrogen less so and the inert gases least. Such is the case with nitrosyl chloride as sensitizer, but in the nitrogen peroxide system this catalytic effect is opposed by the reduction in the stationary concentration of the hot centres by increase of the composite term $k_6[M]$, representing an increase in the gas deactivation. In vessels of large diameter where surface deactivation is of negligible magnitude over the ranges of pressure concerned, addition of foreign gases would be expected to lengthen the induction period. This is the case illustrated in Part V, figure 8, from which it is seen that for small amounts of added gas the efficiency in lengthening the induction period depends, as might have been expected, primarily on the atomicity of the gas. At higher pressures this order is disturbed by the influence of the $\gamma$ term. Under conditions where high surface deactivation obtains and only the reactants are present, $\phi$ could pass through a maximum value as the foreign gas is added. This has been realized in the 7·0 mm. diameter vessel which had been rinsed with aqueous potassium chloride, where the induction periods of a given mixture pass through a minimum as the gas is added.

The expression for the temperature dependence of the upper limit in the presence of a fixed amount of inert gas may be deduced by the methods given as

$$\log_e P_U = \frac{-(E+6)\,\text{kcal.}}{RT} + \log_e \frac{2\alpha p^3 k_3^0}{3\beta k_6[M]}.$$

This equation implies that the addition of foreign gas merely causes the second term, which is independent of $T$ to be reduced. Reference to Part V, figure 10, shows that this has been verified for the case of addition of nitrogen.

(*b*) *Slow reaction.*

Although non-reactant foreign gases bring about a decrease in the induction period in the NOCl system, the same gases also retard the slow reaction, so indicating that the value of $\phi$ is not the only factor determining the reaction rate. This fact can readily be interpreted by the chain-thermal theory which leads to the expression

$$\omega = \frac{\phi}{\delta'}\frac{p}{[M]} = \frac{p}{\delta'[M]}\left\{\frac{\frac{1}{2}\alpha' k'_3 p s'}{k'_2 s' + \frac{1}{2}k'_3 s'} - \beta' s' - \gamma'\right\}.$$

The reaction rate is reduced by added gases because the retarding effect of the increase in self neutralization of centres ($\delta'[M]$ term) outweighs the accelerating influence of the decreased wall removal term ($\gamma'$). For small amounts of added gas the order of efficiency of the gases in increasing $\phi$ is known from Part VI, figure 2, to be $CO_2 > N_2 > A = He$ and the order of efficiency in retarding the reaction by increasing the self-neutralization of the centres is probably the same. Depending on the relative magnitudes of these effects any order of overall inhibitive efficiency might be produced, provided argon and helium were equivalent. The experimental order of $N_2 > CO_2 > A = He$ therefore is in agreement with the chain-thermal theory.

(*c*) *The quenching pressures.*

Although non-reactant gases increase the net branching factor $\phi$, in the NOCl catalysed reaction and decrease it in the $NO_2$ catalysed reaction, their ultimate quantitative effects on the explosion, as measured by the magnitudes and order of the quenching pressures, are the same in each system (see Part VI). It can only be concluded that the effect of these gases on the ignition condition, i.e. the critical value of $\phi$ which must be attained for explosion, is much more profound than their effect on the ability of the systems to meet this condition, i.e. $\phi$. $\phi_c$ will be altered by three factors:

(*a*) The increased probability of self neutralization of centres will cause $\phi_c$ to be raised, and the order of increasing efficiency of the gases would be expected to be the order of increasing atomicity. This order,

$$He < A < N_2 < CO_2,$$

receives confirmation from the fact that it has also been shown to apply to the cases where the gases facilitate the recombination of iodine and bromine atoms, and the formation of complexes such as $HO_2$ and $NCl_4$ (see p. 431).

(*b*) Addition of equal pressures of these gases will cause the thermal capacity of the system to be increased by amounts proportional to their individual molal capacities. These are, at 15° C and constant volume: $CO_2$, 6·67; $N_2$, 4·9; A, 3·0; and He, 3·0, and hence the increase in $\phi_c$ associated with this property alone would be greater for carbon dioxide than for nitrogen, and greater for nitrogen than for argon and helium, the two last named having the same effect.

(c) The gaseous thermal conductivity will be changed. Although this cannot be evaluated, it is probably true to say that the addition of a gas of lower thermal conductivity than $2H_2 + O_2$ mixtures will lower the thermal conductivity and vice versa. The values of the coefficients of thermal conductivity in kilo-erg cm.$^{-2}$ sec.$^{-1}$ (° C cm.$^{-1}$) taken from the *International Critical Tables* are $H_2$, 15·9; $O_2$, 2·33; He, 13·9; $N_2$, 2·28; A, 1·58; $CO_2$, 1·37. Although the values refer to 273° K the correction for 650° K will not alter the order. The thermal conductivity of $2H_2 + O_2$ mixtures at pressures where it is independent of pressure has been found by Wassiljewa (1904) to be about 10 units. To a first approximation therefore the conductivity of a $2H_2 + O_2$ mixture may be said to be lowered by oxygen and nitrogen to an equal degree, argon and carbon dioxide being a little more effective in this respect, whereas *helium will raise* the thermal conductivity. $\phi_c$ will be affected accordingly.

If $\phi_c$ depended merely on the factors (*a*) and (*b*) the quenching pressures would be expected to fall in the order

$$CO_2 \ll N_2 \ll A < He.$$

If $\phi_c$ also depended on factor (*c*) it would be expected that the first three of these gases would still fall in this order, but that less helium would be required to quench ignition than this order indicates. The experimental order of

$$CO_2 \ll He < N_2 \ll A$$

is in excellent agreement with this point of view.

### (7) *The effect of methane*

Small quantities of methane cause a pronounced increase in the induction period in both these systems and it is clear that this gas affects the branching and development of the chains in a profoundly different manner from the other gases. As a combustible it would be anticipated that it would react very readily with the chain propagating particles. An example of such a chain-ending reaction in the $H_2$-$O_2$-$NO_2$ system might be

$$CH_4 + O = CH_2 + H_2O$$

and in the $H_2$-$O_2$-NOCl system

$$CH_4 + Cl = CH_3 + HCl.$$

### THE NATURE OF THE CHAIN MECHANISM

In attempting to assign chemical identity to normal centres $X$ and hot centres $Y$ we can make use of the fact that in the $NO_2$-sensitized reaction the variation of the upper limit with temperature indicates that an energy of activation of the order 15,000 cal. is to be associated with reaction $k_3$ for the production of hot centres by the reaction of an ordinary centre with a reactant. It follows that if the hot centre is the only product of reaction $k_3$, the sum of its heat of formation and 15,000 cal. must be at least equal to the heat of dissociation of nitrogen peroxide, viz. 71·5 kcal. It is further desirable that the hot centre should possess a sufficiently long life to be subject to deactivation by other molecules in the system.

Both these requirements are satisfied by regarding the association complex $HO_2$ when endowed with its energy of formation (*ca.* 54 kcal.) + 15 kcal. as a hot centre, i.e. $HO_2^*$; and $HO_2$ without this energy as one of the ordinary centres. The $HO_2$ complex is also inevitable in the NOCl sensitized reaction, since it is the only possible product of the interaction of hydrogen atoms and oxygen molecules at temperatures as low as 330° C.

In both reactions $HO_2$ would be capable of propagating the chain by

$$HO_2 + H_2 = H_2O + OH,$$

$$HO + H_2 = H_2O + [H \xrightarrow{+O_2+M} HO_2].$$

The removal of centres by catalyst ($\beta$ and $\beta'$ terms) might be

$$HO + NOCl = NO_2 + HCl,$$

$$HO + NO_2 = HNO_3.$$

These reactions are merely suggested as providing a possible mechanism and no claim is advanced that they are established by the present work.

### CONCLUSION

The present work establishes the fact that the explosive combustion of hydrogen, sensitized by either nitrogen peroxide or nitrosyl chloride, is of the 'chain-thermal' type, and it draws attention to the discrepancy between the chain-isothermal theory proposed by von Elbe and Lewis (1939) and the experimental results presented in Part V. It is concluded that, owing to the influence of self-neutralization of the reaction centres, which has been shown to be operative, explosion does not occur when the branching just exceeds the deactivation, i.e. when the net branching factor $\phi$ is positive, but only when the branching exceeds the deactivation by an amount equal to the sum of two quantities, one of which is proportional to the thermal capacity and the other proportional to the thermal conductivity, and both of which are proportional to the velocity constant of the self-neutralization process.

The net branching factor $\phi$ may be defined in terms of the experimental variables: concentration of reactants and of sensitizer, amount and nature of foreign gas, temperature, vessel diameter and surface condition; and may be regarded as a measure of the ability of the system to meet the condition for ignition. The differences which are observed between the $H_2$-$O_2$-NOCl and $H_2$-$O_2$-$NO_2$ systems in respect of the effect of foreign gases and pressure of reactants may be explained if it is assumed that nitrogen peroxide starts chains by virtue of the oxygen atoms which it yields on dissociation,

$$NO_2 = NO + O,$$

whilst nitrosyl chloride starts chains by virtue of the chlorine atom it yields in

$$NOCl = NO + Cl.$$

Both these dissociations may be effected either thermally, photochemically or by collisions of a molecule of sensitizer with a highly energized centre.

The authors desire to express their thanks to the Chemical Society and the Royal Society for grants for apparatus, and one of us (F. S. D.) is indebted to the Goldsmiths' Company for the award of a Senior Studentship.

## REFERENCES

Appin, A., Chariton, J. B. and Todes, O. M. 1936 *Acta Phys.-chim. U.R.S.S.* **5**, 655.
Bodenstein, M. and Ramstetter 1922 *Z. phys. Chem.* **100**, 68.
Bursian, V. and Sorokin, V. 1931 *Z. phys. Chem.* B, **12**, 247.
Dainton, F. S. and Norrish, R. G. W. 1941 *Proc. Roy. Soc.* A, **177**, 393.
Dainton, F. S. and Norrish, R. G. W. 1941 *Proc. Roy. Soc.* A, **177**, 411.
von Elbe, G. and Lewis, B. 1937 *J. Amer. Chem. Soc.* **59**, 2022.
von Elbe, G. and Lewis, B. 1939 *J. Amer. Chem. Soc.* **61**, 1350.
Foord, S. G. and Norrish, R. G. W. 1935 *Proc. Roy. Soc.* A, **152**, 196.
Goodeve, C. F. and Katz, S. 1939 *Proc. Roy. Soc.* A, **172**, 432.
Griffiths, J. G. A. and Norrish, R. G. W. 1931 *Trans. Faraday Soc.* **27**, 455.
Hinshelwood, C. N. and Williamson, A. T. 1934 *The reaction between hydrogen and oxygen*, p. 82.
Holmes, H. H. and Daniels, F. 1934 *J. Amer. Chem. Soc.* **56**, 632.
Leermakers, J. A. and Ramsperger, H. C. 1932 *J. Amer. Chem. Soc.* **54**, 1837.
Norrish, R. G. W. 1929 *J. Chem. Soc.* p. 1158

**Norrish, R. G. W. and Griffiths, J. G. A.** 1933 *Proc. Roy. Soc.* A, **139**, 147.
**Rabinowitch, E. and Wood, W. C.** 1936 *J. Chem. Phys.* **4**, 497.
**Rice, O. K., Allen, A. O. and Campbell, H. C.** 1935 *J. Amer. Chem. Soc.* **57**, 2212.
**Rice, O. K. and Campbell, H. C.** 1939 *J. Chem. Phys.* **7**, 700.
**Ritchie, M.** 1937 *J. Chem. Soc.* p. 857.
**Schumacher, H. J.** 1930 *J. Amer. Chem. Soc.* **52**, 2584.
**Smith, W., Ritchie, M. and Ludlam, E. B.** 1937 *J. Chem. Soc.* p. 1680.
**Thompson, H. W. and Hinshelwood, C. N.** 1929 *Proc. Roy. Soc.* A, **124**, 219.
**Waddington, G. and Tolman, R. C.** 1935 *J. Amer. Chem. Soc.* **57**, 689.
**Wassiljewa, A.** 1904 *Phys. Z.* **5**, 737.
**Zeise, H.** 1936 *Z. Elektrochem.* **42**, 785.

---

# Infra-red absorption spectra of some amino compounds

BY LOTTE KELLNER

(*Communicated by W. T. Astbury, F.R.S.*—
*Received* 25 *June* 1940—*Revised* 21 *November* 1940)

An investigation of the infra-red absorption spectra of five amino compounds (glycine, diketopiperazine, tetramethyl-diketopiperazine, glycyl-glycine and urea) has been made in the region 2·8–3·6 $\mu$. The substances were used in the form of thin crystalline layers deposited on quartz windows.

The spectra are discussed with regard to the molecular structure of the compounds under consideration. The number and position of the N—H frequencies in glycine and glycyl-glycine are in agreement with the assumption that these two molecules are in the zwitterion form in the crystal. The close similarity between the spectra of diketopiperazine and tetramethyl-diketopiperazine on the one hand, and the amino acids and urea on the other, proves that no lactam-lactim interchange occurs in diketopiperazine and its derivative. Both compounds are shown to possess a centre of symmetry. It follows from the experimental evidence that in all the substances investigated resonance between the C—N and C=O bonds takes place.

## 1. INTRODUCTION

The infra-red absorption spectra of five amino compounds (glycine, diketopiperazine, tetramethyl-diketopiperazine, glycyl-glycine and urea) have been studied between 2·8 and 3·6 $\mu$. Though the Raman spectra of glycine and urea are known (Kahovec and Kohlrausch 1936; Kohlrausch and Pongratz 1934), the infra-red spectra of none of the five substances have been observed in this region. It was the object of these investigations to determine the N—H frequencies near 3 μ and the presence or absence of O—H bands, and to apply this knowledge to the elucidation of the molecular structure.

## 2. Experimental methods

The quartz spectrometer used for these experiments has been described previously (Kellner 1936). As quartz shows considerable absorption in the spectral region under consideration, the spectrometer slits had to be opened to approximately 0·7 mm. width, corresponding to a spectral range of 0·022 μ. The wave-length calibration was carried out in the same way as formerly described, but above 3·18 μ Drummond's data (1934) for the refractive index of quartz were substituted for Rubens's values. Readings were taken at intervals of 0·01 μ. As the substances used are soluble, if at all, only in water or alcohol, both of which liquids have very intense absorption bands in this region, it was necessary to study these compounds in the form of thin crystalline deposits on quartz windows. The two diketopiperazines, which are nearly insoluble, were deposited from a suspension of the finely ground powder in absolute alcohol, while in the case of the other three substances a solution in alcohol or water was left to crystallize in a thin layer on the window. The thickness of this crystalline deposit was approximately 0·1 mm. Part of the window was left free from the deposit. The window was then set in a holder before the spectrometer slit, and the light beam allowed to pass alternately through the uncovered and covered half of the window. The ratio of the two galvanometer deflexions obtained for the two positions of the quartz window gave the transmission of the compounds under investigation. Though the amount of scattered light in these layers is considerable, the absorption bands stand out distinctly from the general background. In the case of glycine and urea, two deposits were studied; one had been obtained from a solution in water and one from a solution in alcohol. The observed spectra were identical.

## 3. Experimental results

The results of the experiments are given in figure 1, curves I–V, and in table 1. Figure 1 shows the absorption of the five compounds as function of the wave-lengths. Each curve shows the mean results of five sets of measurements. In all cases, a band at 3300 cm.$^{-1}$ was found in addition to those shown in the diagrams and the table, indicating the presence of O—H bonds. This band disappeared entirely when the substance was subjected to prolonged drying. It must be ascribed, therefore, to traces of adsorbed water in the crystals.

The observed bands are grouped round 3400 and 2900 cm.$^{-1}$ respectively. The latter group indicates the presence of C—H linkages and is absent from the urea spectrum, while the 3400 group lies in the region of the N—H frequencies. No selective absorption could be detected in the region between 3170 and 3030 cm.$^{-1}$.

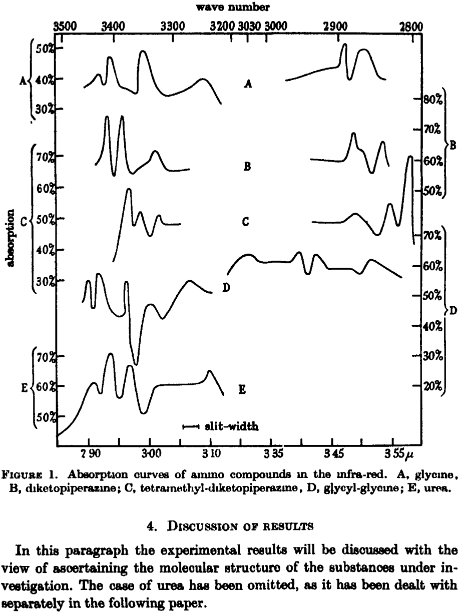

FIGURE 1. Absorption curves of amino compounds in the infra-red. A, glycine, B, diketopiperazine; C, tetramethyl-diketopiperazine, D, glycyl-glycine; E, urea.

## 4. DISCUSSION OF RESULTS

In this paragraph the experimental results will be discussed with the view of ascertaining the molecular structure of the substances under investigation. The case of urea has been omitted, as it has been dealt with separately in the following paper.

TABLE 1. WAVE NUMBERS OF ABSORPTION BANDS

| Glycine $\nu$ | Diketo-piperasine $\nu$ | Tetramethyl-diketopiper-asine $\nu$ | Glycyl-glycine $\nu$ | Urea $\nu$ |
|---|---|---|---|---|
| — | — | — | 2800 | — |
| 2860 | 2840 | 2830 | 2860 | — |
| 2890 | 2880 | 2880 | 2920 | — |
| — | — | — | 2950 | — |
| — | — | — | 3020 | — |
| 3235 | — | — | — | 3218 |
| — | 3320 | 3315 | 3280 | — |
| 3340 | — | 3340 | 3330 | — |
| — | 3390 | 3373 | 3380 | 3376 |
| 3410 | 3420 | — | — | 3410 |
| 3440 | — | — | 3430 | 3434 |
| — | — | — | 3450 | — |

### (a) *Glycine*, $NH_2 . CH_2 . COOH$

Glycine shows three bands between 3450 and 3330, in addition to a weak band at 3235 and two bands near 2860 due to the valence vibrations of the $CH_2$ group. If the classical formula $NH_2 . CH_2 . COOH$ is correct, two N—H bands and one O—H band can be expected near 3330, as well as two C—H bands between 2950 and 2860. The O—H band should be very broad, but figure 1 shows that the three observed bands between 3450 and 3330 are all equally sharp. They are therefore all to be assigned to N—H vibrations, in agreement with the X-ray analysis of glycine (Albrecht and Corey 1939), which indicates a zwitterion molecule of the form $NH_3^+ . CH_2 . COO^-$ in the solid state.

The nuclear distances in the crystal are C—N = 1·39 A, C—C = 1·52 A, and the two C=O distances are 1·25 and 1·27 A, i.e. practically identical. The C—N distance of 1·39 A is considerably shorter than the ordinary single bond distance of 1·47 A, and Albrecht and Corey conclude that resonance occurs in glycine between the C—N and C=O linkages. The results of the infra-red absorption measurements confirm this conclusion, as the N—H frequencies of C—N single bond compounds lie between 3330 and 3220 (Bell 1927), while the N—H frequencies in aromatic compounds appear near 3450 (Bell 1925). In the case of glycine, these vibrations have a position between these limits. Gaseous ammonia shows a doubly degenerate frequency, $\nu$ 3407, and a single frequency, $\nu$ 3336 (Howard 1935). In glycine the doubly degenerate vibration splits into the two oscillations, 3440 and 3410, in consequence of the lower symmetry of the molecule. The position of the C—H frequencies, $\nu$ 2890 and $\nu$ 2860, corresponds to the presence of a C—C single bond, in agreement with the C—C distance of 1·52 A. The band $\nu$ 3235 has also been observed for urea, and may be assigned to the first overtone of the C=O vibration near 1660 cm.$^{-1}$.

The Raman spectrum of glycine has been observed by Wright and Lee (1935), Kahovec and Kohlrausch (1936) and Edsall (1936). No trace of the N—H oscillations was found by these investigators, while Kahovec and Kohlrausch showed that they are present in the glycine esters which possess an ordinary $NH_2$ group and no zwitterion structure. These results are in accordance with the assumption of ionic bonds in the $NH_3^+$ group, as the Raman lines of ionic linkages are expected to have vanishing intensity. On the other hand, the infra-red bands will be very intense, as the dipole moment changes rapidly with the nuclear distance in heteropolar linkages.

If it is assumed that the resonance in glycine confers the same amount of double bond character on the C—N bond as in the case of urea, and correspondingly decreases the C=O double bond, the same force constants for the C—N and C=O valence forces should apply in both cases (see the following paper). If valence forces only are taken into account and the $NH_3^+$ and $CH_2$ groups are treated as mass points, the following equations for the four valence vibrations of the $NH_3^+ . CH_2 . COO^-$ molecule are obtained:

$$\begin{aligned}
\lambda_{1,2,3}^3 - \lambda_{1,2,3}^2 \Big\{ & f_{C-N}\left(\frac{1}{m_{CH_2}}+\frac{1}{m_{NH_3}}\right)+f_{C-C}\left(\frac{1}{m_{CH_2}}+\frac{1}{m_C}\right)+f_{C-O}\left(\frac{1}{m_O}+\frac{2\cos^2\frac{1}{2}\omega}{m_C}\right)\Big\} \\
+\lambda_{1,2,3}\Big\{ & f_{C-N}f_{C-C}\left[\frac{1}{m_{CH_2}}\left(\frac{1}{m_{NH_3}}+\frac{\sin^2\gamma}{m_{CH_2}}\right)+\frac{1}{m_C}\left(\frac{1}{m_{CH_2}}+\frac{1}{m_{NH_3}}\right)\right] \\
& +f_{C-C}f_{C-O}\left[\frac{1}{m_O m_C}+\frac{1}{m_{CH_2}}\left(\frac{1}{m_O}+\frac{2\cos^2\frac{1}{2}\omega}{m_C}\right)\right] \\
& +f_{C-N}f_{C-O}\left(\frac{1}{m_{CH_2}}+\frac{1}{m_{NH_3}}\right)\left(\frac{1}{m_O}+\frac{2\cos^2\frac{1}{2}\omega}{m_C}\right)\Big\} \\
& -f_{C-C}f_{C-N}f_{C-O}\Big\{\frac{1}{m_C m_O}\left(\frac{1}{m_{CH_2}}+\frac{1}{m_{NH_3}}\right) \\
& +\frac{1}{m_{CH_2}}\left(\frac{1}{m_O}+\frac{2\cos^2\frac{1}{2}\omega}{m_C}\right)\left(\frac{1}{m_{NH_3}}+\frac{\sin^2\gamma}{m_{CH_2}}\right)\Big\} = 0,
\end{aligned}$$

$$\lambda_4 = f_{C-O}\left(\frac{1}{m_O}+\frac{2\sin^2\frac{1}{2}\omega}{m_C}\right).$$

The $\lambda_i$ stand for $4\pi^2\nu_i^2$. The $f_{C-C}$, $f_{C-N}$ and $f_{C-O}$ refer to the C—C, C—N and C=O valence force constants, respectively; $\gamma$ is the angle N—C—C = 112° (Albrecht and Corey), and $\omega$ the angle O—C—O = 122°.

If the force constants, $f_{C-N} = 6\cdot6\times10^5$ dynes/cm. and $f_{C=O} = 9\cdot7\times10^5$ dynes/cm., evaluated from the urea spectrum (see the following paper), are used, together with the commonly accepted value, $f_{C-C} = 5\cdot0\times10^5$ dynes/cm., the following valence vibrations are computed:

$$\nu_1 = 840, \quad \nu_2 = 1322, \quad \nu_3 = 1420, \quad \nu_4 = 1778.$$

The calculated frequencies agree very well with the observed data, 870, 1320, 1400 and 1650, when it is taken into consideration that the angular forces, which contribute considerably to the oscillations in this spectral region, have been neglected. It is permissible to leave the N—H and C—H frequencies out of the calculations, as they lie so far away from the chain vibrations. Further confirmation of the resonance between the C—N and C=O bonds in glycine comes from the fact that the C=O frequency in the glycine esters and in the hydrochloride is considerably higher than in glycine itself (approximately 1720 as compared with 1650).

### (b) 2, 5-*diketopiperazine* (*glycine anhydride*) $(NH.CO.CH_2)_2$

A short discussion of the spectrum of this substance has previously been given (Kellner 1937), but the new evidence on the crystalline structure (Corey 1938) and the near infra-red spectrum (Ellis and Bath 1939) demands certain modifications of the former interpretation. The analysis of the crystal structure of glycine anhydride makes it evident that a type of resonance similar to that in glycine occurs between the C—N and C=O bonds. The nuclear distances are OC—N = 1·33 A, C—O = 1·25 A, OC—$CH_2$ = 1·47 A and N—$CH_2$ = 1·41 A. The carbon, oxygen and nitrogen atoms lie in one plane; the molecule has a centre of symmetry and belongs to the symmetry group $S_2$(i). The hydrogen atoms are arranged symmetrically with respect to the symmetry plane. The relatively short carbon-carbon and nitrogen-methylene carbon distances seem to indicate that the C—C bonds are involved in the resonance, but this assumption is not borne out by the evidence of the infra-red bands. The two C—H frequencies, 2880 and 2840, are typical for $CH_2$ groups attached to C—C single bonds. As the glycine anhydride molecule possesses two $CH_2$ groups, four C—H frequencies may be expected, two of which, belonging to the symmetry classes $A_g$ and $B_g$, will be forbidden in the infra-red spectrum. The presence of only two C—H bands confirms, therefore, the existence of a centre of symmetry in the molecule. The two missing C—H vibrations should appear in the Raman spectrum. It follows from the symmetry requirements of the oscillations that the C—H frequencies of the classes $A_g$ and $B_u$ will be of the form

$4\pi^2\nu^2 = f_{\mathrm{C-H}}\left(\frac{1}{m_{\mathrm{H}}}+\frac{2\cos^2\frac{1}{2}\theta}{m_{\mathrm{C}}}\right)$, where $f_{\mathrm{C-H}}$ is the C—H valence force constant and $\theta$ the tetrahedral angle; and the two oscillations of $A_u$ and $B_g$ will be of the form $4\pi^2\nu^2 = f_{\mathrm{C-H}}\left(\frac{1}{m_{\mathrm{H}}}+\frac{2\sin^2\frac{1}{2}\theta}{m_{\mathrm{C}}}\right)$. It will be seen that for the two infra-red active bands, $\nu_{A_u} > \nu_{B_u}$. Therefore $\nu$ 2880 is assigned to the symmetry class $A_u$, and $\nu$ 2840 to the class $B_u$.

Ellis and Bath (1939), who have observed the absorption bands of diketopiperazine in the region of the first overtone, find two parallel bands at $1{\cdot}703\,\mu$ and $1{\cdot}754\,\mu$ and a perpendicular band at $1{\cdot}745\,\mu$. They assign $1{\cdot}703\,\mu$ to the first overtone of the parallel C—H valence frequency, $\nu_\pi$; $1{\cdot}745\,\mu$ to the first overtone of the perpendicular C—H valence frequency, $\nu_\sigma$; and $1{\cdot}754\,\mu$ to the third overtone of the parallel deformation frequency of the $CH_2$ group, $\delta_\pi$. This classification takes no account of the selection rules which apply to the symmetry group $S_2$ (i). Only those overtones and combination tones have non-vanishing intensity in the infra-red or Raman spectrum which belong to the permitted symmetry type (Tisza 1933). The symmetry types to which the binary overtones and combination tones of the group $S_2$ (i) conform have been calculated by group theoretical methods and are set out in table 2, together with the infra-red and Raman activity and the band type.

TABLE 2

| Infra-red active | | Raman active | |
|---|---|---|---|
| Parallel band of type $A_u$ | Perpendicular band of type $B_u$ | Type $A_g$ | Type $B_g$ |
| $A_g + A_u$ | $A_u + B_g$ | $[A_g^n]$ | $A_u + B_u$ |
| $B_g + B_u$ | $A_g + B_u$ | $[B_g^n]$ | $A_g + B_g$ |
| | | $[A_u^n]$ $n$ even | $[B_g^n]$ $n$ odd |
| | | $[B_u^n]$ $n$ even | |

The symbols $A_g + B_u$, etc. stand for the summation frequency of $\nu_{A_g}$ and $\nu_{B_u}$, etc., $[A_g^n]$ means the $(n-1)$th overtone of the fundamental $\nu_{A_g}$. It follows from the table that all overtones for which $n$ is even are forbidden in the infra-red spectrum; but four binary combination tones of the four C—H valence vibrations could be expected, namely, the parallel bands $\nu_{A_g} + \nu_{A_u}$ and $\nu_{B_g} + \nu_{B_u}$, and the perpendicular bands $\nu_{A_u} + \nu_{B_g}$ and $\nu_{A_g} + \nu_{B_u}$.

Three bands only have been observed by Ellis and Bath. If we assume that they correspond to the combination tones $\nu_{A_g} + \nu_{A_u}$, $\nu_{B_g} + \nu_{B_u}$ and $\nu_{A_g} + \nu_{B_u}$, they enable us, in connexion with the two fundamentals here observed, to evaluate the two inactive oscillations $\nu_{A_g}$ and $\nu_{B_g}$, taking into consideration that $\nu_{A_g} < \nu_{B_g}$. It is found that $\nu_{A_g} = 2856$ and $\nu_{B_g} = 3032$ furnish the parallel combination tones $\nu_{A_g} + \nu_{A_u} = 5736$ (5701 observed) and $\nu_{B_g} + \nu_{B_u} = 5872$ (5872 observed), and the perpendicular bands $\nu_{B_g} + \nu_{A_u} = 5912$ (not observed) and $\nu_{A_g} + \nu_{B_u} = 5696$ (5731 observed). Fox and Martin (1940) point out that in Ellis and Bath's interpretation the parallel combination tone is larger than the perpendicular, contrary to what is usually found. This objection would apply to the present classification as well, but the terms 'parallel' and 'perpendicular' refer here to the symmetry axis of the whole molecule, which is inclined to the symmetry axis of the single $CH_2$ group which Fox and Martin have in mind.

Three more bands have been observed for diketopiperazine in the region of the N—H frequencies. The molecule should possess two N—H valence vibrations of the types $A_g$ and $B_u$ respectively. In $\nu_{A_g}^{NH}$ the two N—H bonds stretch in phase; in $\nu_{B_u}^{NH}$ they move out of phase. Only $\nu_{B_u}^{NH}$ should be infra-red active, and may be identified with $\nu$ 3420. $\nu$ 3320 is assigned to the permitted summation frequency of the two C═O vibrations $\nu_{A_g}^{C=O} + \nu_{B_u}^{C=O}$, as it can be inferred from the Raman spectrum of glycine that these oscillations will be near 1650 cm.$^{-1}$. This leaves $\nu$ 3390 still unaccounted for. It seems indicated from its proximity to 3420 that it is identical with the forbidden N—H frequency $\nu_{A_g}^{N-H}$. It is known that in the case of liquid benzene a few forbidden bands appear in the infra-red spectrum. The proximity of the N—H bands to those of glycine confirms the evidence of the crystal analysis (Corey 1938), that in 2, 5-diketopiperazine resonance occurs between the C—N and C═O bonds, and that the molecule does not possess any O—H linkages as had formerly been suggested (Sanborn 1932). It follows that neither keto-enol nor lactam-lactim transformation occurs in the molecule.

### (c) *Tetramethyl-diketopiperazine* $[NH.CO.C(CH_3)_2]_2$

The spectrum of tetramethyl-diketopiperazine is very similar to that of 2, 5-diketopiperazine. The interpretation follows the same lines: $\nu$ 3373 is identified with the asymmetric N—H frequency and $\nu$ 3340 with the symmetric N—H frequency. The two N—H vibrations are shifted to smaller frequencies as compared with glycine anhydride. The shift is practically the same for both bands. $\nu$ 3315 can again be assigned to the combination tone of the two C═O vibrations. The similarity of the positions of the N—H and C═O oscillations to those of diketopiperazine leads to the conclusion that the same type of resonance between the C—N and C═O bonds takes place in tetramethyl-diketopiperazine. The number of C—H oscillations has increased to three. As the molecule possesses four $CH_3$ groups, six C—H frequencies would be expected in the case of central symmetry, but they might overlap to such an extent that a smaller number is observed. The similarity between the spectra of diketopiperazine and its derivative makes it feasible to assume that these substances have the same symmetry.

### (*d*) *Glycyl-glycine* $NH_2.CH_2.CO.NH.CH_2.COOH$

Glycyl-glycine exhibits four bands in the region of the N—H frequencies, ν 3450, 3430, 3380 and 3330; and four C—H frequencies, ν 3020, 2950, 2920 and 2860, in addition to a band at ν 3280. The appearance of four C—H vibrations is in agreement with the existence of four C—H linkages in the molecule, and the four N—H frequencies show that glycyl-glycine in the crystal is in the zwitterion form $NH_3^+.CH_2.CO.CH_2.NH.COO^-$. The position of the N—H vibrations between 2·9 and 3·0 μ again points to the probability that resonance occurs between the C—N and C=O bonds. Correspondingly, ν 3280 may be assigned to the first overtone or a binary combination tone of the oscillations of the C=O linkages involved in the resonance. The infra-red absorption spectrum of glycyl-glycine ethyl ester dissolved in $CCl_4$ has been observed by Buswell, Downing and Rodebush (1939). They report absorption bands at 3720, 3390, 3090, 2990 and 2960, and a band at 3280 which vanishes for a concentration of 0·008 mol. No ionic structure is to be expected in the glycyl-glycine ester, and 3390 therefore represents the N—H frequencies. The C—H frequencies are surprisingly high for C—C single bond compounds, even for very low concentrations. In the crystal their frequencies are reduced by 40–70 cm.$^{-1}$. In the case of the ethyl ester, the absorption bands include the C—H oscillations of the ethyl group as well, so that a comparison between the two observations is not possible.

I wish to express my gratitude to Professor H. Dingle for putting the laboratory facilities of the Imperial College of Science and Technology, London, S.W. 7, at my disposal. I am furthermore very much indebted to Professor A. C. Chibnall and Dr W. T. Astbury for providing me with the five compounds.

## REFERENCES

Albrecht and Corey 1939 *J. Amer. Chem. Soc.* **61**, 1087.
Bell 1925 *J. Amer. Chem. Soc.* **47**, 3039.
Bell 1927 *J. Amer. Chem. Soc.* **49**, 1837.
Buswell, Downing and Rodebush 1939 *J. Amer. Chem. Soc.* **61**, 3252.
Corey 1938 *J. Amer. Chem. Soc.* **60**, 1598.
Drummond 1934 *Nature, Lond.*, **134**, 937.

Edsall 1936 *J. Chem. Phys.* **4**, 1.
Ellis and Bath 1939 *Phys. Rev.* **55**, 1098.
Ellis and Bath 1939 *J. Chem. Phys.* **7**, 862.
Fox and Martin 1940 *Proc. Roy. Soc.* A, **175**, 208.
Howard 1935 *J. Chem. Phys.* **3**, 207.
Kahovec and Kohlrausch 1936 *S.B. Akad. Wiss. Wien*, IIb, **145**, 579.
Kellner 1936 *Proc. Roy. Soc.* A, **157**, 100.
Kellner 1937 *Nature, Lond.*, **140**, 123.
Kohlrausch and Pongratz 1934 *Z. phys. Chem.* B, **27**, 176.
Sanborn 1932 *J. Phys. Chem.* **36**, 1799.
Tisza 1933 *Z. Phys.* **82**, 48.
Wright and Lee 1935 *Nature, Lond.*, **136**, 300.

---

# The vibrations and the molecular structure of urea and guanidonium

BY LOTTE KELLNER

(*Communicated by W. T. Astbury, F.R.S.*—
*Received* 25 *June* 1940—*Revised* 21 *November* 1940)

The vibrations of urea and guanidonium have been calculated for a field containing valence and angle forces. The assumption is made that urea has the symmtery $C_{2v}$ and guanidonium $C_{3h}$.

It is shown that it is possible to assign every observed frequency of these two substances to definite modes of vibration under these assumptions. The force constants have been evaluated and have been found to be $f_{C-N} = 7{\cdot}1 \times 10^5$ dynes/cm. for guanidonium, and $f_{C-N} = 6{\cdot}6 \times 10^5$ dynes/cm. and $f_{C=O} = 9{\cdot}7 \times 10^5$ dynes/cm. for urea. These values are compatible with the hypothesis that quantum mechanical resonance occurs in both molecules, with the result that the C—N bond in urea has approximately 28 % double-bond character and the C=O linkage a corresponding single-bond character. The guanidonium ion shows complete resonance; each C—N bond has $\frac{1}{3}$ double-bond character. Curves have been drawn to illustrate the relation between the valence force constants and the bond character.

## 1. INTRODUCTION

It has been evident for some time, from the study of the chemical behaviour as well as from the X-ray investigation of the crystalline structure of urea and guanidonium, that these two molecules show quantum mechanical resonance between several possible configurations. Pauling (1935) suggests resonance between a homopolar (figure 1, I) and two ionic (figure 1, II, III) structures for urea, $CO(NH_2)_2$, and ascribes 28 % double-bond character to the C—N linkages and a corresponding single-bond character to the C=O bond, in agreement with the X-ray measurements of the nuclear distances of $d_{C-O} = 1{\cdot}25$ A and $d_{C-N} = 1{\cdot}37$ A (Wyckoff and Corey 1934). In the guanidonium ion, $C^+(NH_2)_3$, all three structures (figure 2, I, II, III) should have equal probability, which means that resonance is complete and each C—N bond has ⅓ double-bond character. The nuclear distances in organic compounds are known to be very accurately constant for linkages of the same type in different molecules, and these distances have been used up to now as the only criteria for the bond character. The force constants measuring the valence forces remain constant in the same way, and provide further means of determining the occurrence of quantum mechanical resonance between different configurations. It has been found in the case of the C—C bond, which is best known, that ethane, with a typical single bond, furnishes $f_{C-C} = 4{\cdot}96 \times 10^5$ dynes/cm. (Sutherland and Dennison 1935), while the

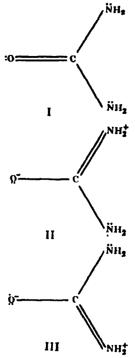

FIGURE 1. Electronic structure of urea.

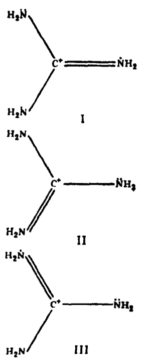

FIGURE 2. Electronic structure of guanidonium

values $f_{\text{C=C}} = 9{\cdot}79 \times 10^5$ (Sutherland and Dennison 1935), $f_{\text{-C-}} = 7{\cdot}56 \times 10^5$ (Kohlrausch 1936) and $f_{\text{C}\equiv\text{C}} = 15{\cdot}71 \times 10^5$ (Sutherland and Dennison 1935) are obtained from ethylene, benzene and acetylene, respectively. It will be seen that in a molecule with alternating double bonds (so far, benzene is the only molecule for which this has been worked out) the force constant is nearly $\frac{1}{2}(f_{\text{C-C}}+f_{\text{C=C}})$. In the present paper the vibrations of urea and guanidonium have been computed theoretically and the force constants calculated from the observed vibration spectra.

## 2. METHOD OF COMPUTATION OF VIBRATIONS

The vibrations of urea and guanidonium have been calculated as functions of the force constants in the usual way. A harmonic potential function was chosen, and the molecule assumed to be held together by valence and angle forces only. The resulting secular equation was factorized, by means of group theoretical methods, into determinants of lower orders corresponding to the symmetry type of the molecule under consideration.

## 3. VIBRATIONS OF UREA

The potential function has the form.

$$\begin{aligned}2V = {} & f_{\text{C=O}}\,\xi^2_{\text{C=O}} + f_{\text{C-N}}(\xi^2_{\text{C-N}_1} + \xi^2_{\text{C-N}_2}) + f_{\text{N-H}}(\xi^2_{\text{N}_1\text{-H}_1'} + \xi^2_{\text{N}_1\text{-H}_1''} \\ & + \xi^2_{\text{N}_2\text{-H}_2'} + \xi^2_{\text{N}_2\text{-H}_2''}) + d' s_{\text{C=O}} s_{\text{C-N}} \{(\Delta\alpha_1)^2 + (\Delta\alpha_2)^2\} + d s^2_{\text{C-N}} \{\Delta(2\beta)\}^2 \\ & + \delta_1 s_{\text{C-N}} s_{\text{N-H}} \{(\Delta\gamma_1)^2 + (\Delta\gamma_2)^2 + (\Delta\gamma_3)^2 + (\Delta\gamma_4)^2\} + \delta_2 s^2_{\text{N-H}} \{(\Delta\gamma_6)^2 + (\Delta\gamma_7)^2\} \\ & + 4\tau s^2_{\text{N-H}} \sin^2 \tfrac{1}{2}\Theta \{(\Delta\Theta_1)^2 + (\Delta\Theta_2)^2\} \\ & + \kappa s_{\text{C=O}} \sin\beta \sin 2\beta \{(\Delta\Phi_1)^2 + (\Delta\Phi_2)^2 + (\Delta\Phi_3)^2\}. \qquad (1)\end{aligned}$$

The $\xi_i$ are the elongations of the valence links under the influence of the valence forces, the $\Delta\alpha_i$ and $\Delta\gamma_i$ refer to the deviations of the valence angles from the equilibrium position and will be understood by reference to figure 3. $\Delta\Theta_i$ measures the twist of the C—N bonds, and $\Delta\Phi_i$ the angle between the planes $\text{OCN}_i$ and $\text{OCN}_{i+1}$. $\Delta\Phi_i$ occurs only when the atoms C, O and N move out of the plane originally containing them. $2\beta$ is the angle between the two C—N valencies, and the angle between the N—H bonds has been taken to be the tetrahedral angle 109° 28'. $f_{\text{C-N}}$, $f_{\text{C-O}}$ and $f_{\text{N-H}}$ are the valence force constants, and $d'$, $d$, $\delta_1$ and $\delta_2$ the angle force constants $\tau$ measures the torsion of the C—N bonds and $\kappa$ the force with which the C, O and N atoms are held in one plane. The co-ordinates are simple linear functions of the displacements of the vibrating atoms from their equilibrium positions. In calculating these functions the procedure of Lechner (1932) has been followed; his method has been extended to include oscillations in which the atoms move out of the molecular plane.

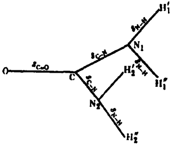

$OCN_1 = \alpha_1$
$OCN_2 = \alpha_2$
$N_1CN_2 = 2\beta$
$CN_1H_1' = \gamma_1$
$CN_1H_1'' = \gamma_2$
$H_1'N_1H_1'' = \gamma_6$
$CN_2H_2' = \gamma_3$
$CN_2H_2'' = \gamma_4$
$H_1'N_2H_2'' = \gamma_7$

FIGURE 3. The urea molecule

It is known from the investigation of the crystalline structure of urea (Wyckoff and Corey 1934) that the molecule has the symmetry $C_{2v}$ and that the carbon, oxygen and nitrogen atoms lie in one plane. The twofold symmetry axis $C_2$ passes through the C=O line. It follows from group theoretical considerations that the vibrations of urea split up into four symmetry types. Table 1 shows their behaviour with respect to the symmetry elements of $C_{2v}$, their activity in the infra-red and Raman spectra and the number of vibrations in each symmetry class.

TABLE 1

| Symmetry class | Symmetry properties | | Infra-red spectrum | | Raman spectrum | | |
|---|---|---|---|---|---|---|---|
| | Symmetric | Anti-symmetric | Activity | Band type | Activity | Degree of depolarization | No. of vibrations |
| $A_1$ | $C_2, \sigma_x, \sigma_y$ | — | Active | Perpendicular | Active | $\rho < \frac{6}{7}$ | 6 |
| $A_2$ | $C_2$ | $\sigma_x, \sigma_y$ | Inactive | — | ,, | $\rho = \frac{6}{7}$ | 3 |
| $B_1$ | $\sigma_y$ | $C_2, \sigma_x$ | Active | Perpendicular | ,, | $\rho = \frac{6}{7}$ | 4 |
| $B_2$ | $\sigma_x$ | $C_2, \sigma_y$ | Active | Parallel | ,, | $\rho = \frac{6}{7}$ | 5 |

$C_2$, $\sigma_x$ and $\sigma_y$ refer to the symmetry elements of the group $C_{2v}$. There are $3 \times 8 - 6 = 18$ vibrations altogether. The equation connecting the six vibrations of the class $A_1$ is given by the determinant (2), where $\lambda = 4\pi^2\nu^2$. The vibrations of the type $A_2$ are found by solving the equation (3). The symmetry type $B_1$ furnishes the fourth-order determinant (4), and the five vibrations belonging to the class $B_2$ are connected by the secular equation (5).

$$\begin{vmatrix} \lambda - f_{C=O}\left(\frac{1}{m_O}+\frac{1}{m_C}\right) & \frac{2\cos\beta f_{C-N}}{m_C} & 0 & \frac{2\sin\beta}{m_C}(d' s_{C=O}+2d\, s_{C-N}) & -\frac{2\delta_1 \sin\beta\, s_{N-H}}{m_C} & 0 \\ \frac{\cos\beta f_{C=O}}{m_C} & \lambda - f_{C-N}\left(\frac{1}{m_N}+\frac{2\cos^2\beta}{m_C}\right) & \frac{2f_{N-H}}{3m_N} & -\frac{\sin 2\beta}{m_C}(d' s_{C=O}+2d\, s_{C-N}) & 2\delta_1\left(\frac{2\sqrt{2}\, s_{C-N}}{3m_N} + \frac{\sin 2\beta\, s_{N-H}}{2m_C}\right) & -\frac{2\sqrt{2}\,\delta_2 s_{N-H}}{3m_N} \\ 0 & \frac{f_{C-N}}{3m_N} & \lambda - f_{N-H}\left(\frac{1}{m_H}+\frac{2}{3m_N}\right) & -\frac{\sqrt{2}}{3m_N}(d' s_{C=O}+2d\, s_{C-N}) & -2\delta_1\left\{\frac{\sqrt{2}}{12}\frac{s_{C-N}}{m_H}+\frac{1}{m_N} \times\left(\frac{\sqrt{2}}{6}s_{C-N}-\frac{\sqrt{2}}{6}s_{N-H}\right)\right\} & \frac{2\sqrt{2}\,\delta_2 s_{N-H}}{3m_N} \\ \frac{\sin\beta f_{C=O}}{m_C s_{C-N}} & -\frac{\sin 2\beta f_{C-N}}{m_C s_{C-N}} & -\frac{2\sqrt{2} f_{N-H}}{3m_N s_{C-N}} & \lambda - \left(\frac{d' s_{C=O}}{s_{C-N}}+2d\right) \times\left(\frac{1}{m_N}+\frac{2\sin^2\beta}{m_C}\right) & \frac{\delta_1}{s_{C-N}}\left\{\frac{\sin^2\beta\, s_{N-H}}{m_C} + \frac{1}{2m_N}\left(s_{N-H}+\frac{s_{C-N}}{3}\right)\right\} & \frac{4\delta_2 s_{N-H}}{3m_N s_{C-N}} \\ -\frac{\sin\beta f_{C=O}}{2m_C s_{C-N}} & f_{C-N}\left(\frac{\sin 2\beta}{4m_C s_{C-N}} + \frac{2\sqrt{2}}{3m_N s_{N-H}}\right) & -\frac{\sqrt{2} f_{N-H}}{3m_N} \times\left(\frac{1}{s_{N-H}}-\frac{1}{s_{C-N}}\right) & (d' s_{C=O}+2d\, s_{C-N})\left(\frac{\sin^2\beta}{m_C s_{C-N}} + \frac{1}{2m_N s_{C-N}}+\frac{1}{6m_N s_{N-H}}\right) & \lambda - \delta_1\left\{\frac{\sin^2\beta\, s_{N-H}}{m_C s_{C-N}}+\frac{1}{m_N} \times\left(\frac{11 s_{C-N}}{6 s_{N-H}}+\frac{1}{3}-\frac{s_{N-H}}{2 s_{C-N}}\right)\right\} & -\delta_2\left\{\frac{1}{2m_H}+\frac{2}{3m_N} \times\left(1+\frac{s_{N-H}}{s_{C-N}}\right)\right\} \\ 0 & -\frac{2\sqrt{2} f_{C-N}}{3m_N s_{N-H}} & \frac{4\sqrt{2} f_{N-H}}{3m_N s_{N-H}} & \frac{4}{3m_N s_{N-H}}(d' s_{C=O}+2d\, s_{C-N}) & 2\delta_1\left\{\frac{s_{C-N}}{2m_H s_{N-H}} - \frac{2}{3m_N}\left(\frac{s_{N-H}}{s_{C-N}}-1\right)\right\} & \lambda - \frac{8\delta_2}{3m_N} \end{vmatrix} = 0. \tag{2}$$

$$\begin{aligned}\lambda^3-\lambda^2\left\{f_{\mathrm{N-H}}\left(\frac{1}{m_{\mathrm{H}}}+\frac{4}{3m_{\mathrm{N}}}\right)+\frac{s_{\mathrm{C-N}}}{s_{\mathrm{N-H}}}\delta_1\left(\frac{1}{m_{\mathrm{H}}}+\frac{s_{\mathrm{N-H}}}{s_{\mathrm{C-N}}m_{\mathrm{N}}}+\frac{3s^2_{\mathrm{N-H}}}{2m_{\mathrm{N}}s^2_{\mathrm{C-N}}}+\frac{1}{6m_{\mathrm{N}}}\right)+\frac{2\tau}{m_{\mathrm{H}}}\right\}+\lambda\left\{\frac{s_{\mathrm{C-N}}}{m_{\mathrm{H}}s_{\mathrm{N-H}}}f_{\mathrm{N-H}}\delta_1\left[\frac{1}{m_{\mathrm{H}}}+\frac{1}{m_{\mathrm{N}}}\left(\frac{s_{\mathrm{N-H}}}{s_{\mathrm{C-N}}}+\frac{3s^2_{\mathrm{N-H}}}{2s^2_{\mathrm{C-N}}}+\frac{3}{2}\right)\right]\right.\\ \left.+\frac{2\tau f_{\mathrm{N-H}}}{m_{\mathrm{H}}}\left(\frac{8}{9m_{\mathrm{H}}}+\frac{4}{3m_{\mathrm{N}}}\right)+\frac{2s_{\mathrm{C-N}}\delta_1\tau}{m_{\mathrm{H}}s_{\mathrm{N-H}}}\left[\frac{1}{9m_{\mathrm{H}}}+\frac{1}{m_{\mathrm{N}}}\left(\frac{s_{\mathrm{N-H}}}{s_{\mathrm{C-N}}}+\frac{3s^2_{\mathrm{N-H}}}{2s^2_{\mathrm{C-N}}}+\frac{1}{6}\right)\right]\right\}-\frac{8s_{\mathrm{N-H}}}{3m^2_{\mathrm{H}}m_{\mathrm{N}}s_{\mathrm{C-N}}}f_{\mathrm{N-H}}\delta_1\tau=0. \quad (3)\end{aligned}$$

$$\begin{vmatrix} \lambda-f_{\mathrm{N-H}}\left(\frac{1}{m_{\mathrm{H}}}+\frac{4}{3m_{\mathrm{N}}}\right) & \frac{\sqrt{2}\,\delta_1}{m_{\mathrm{N}}}(s_{\mathrm{C-N}}+s_{\mathrm{N-H}}) & -\frac{2\sqrt{6}}{3m_{\mathrm{N}}}\kappa s_{\mathrm{C-O}}\sin\beta(1+2\cos^2\beta) & \frac{2\sqrt{2}\,s_{\mathrm{N-H}}}{3\sqrt{3}\,m_{\mathrm{H}}}\tau \\ \frac{\sqrt{2}}{m_{\mathrm{N}}}f_{\mathrm{N-H}}\left(\frac{1}{s_{\mathrm{C-N}}}+\frac{1}{3s_{\mathrm{N-H}}}\right) & \begin{array}{l}\lambda-\frac{\delta_1}{s_{\mathrm{C-N}}s_{\mathrm{N-H}}}\left\{\frac{3s^2_{\mathrm{N-H}}}{m_{\mathrm{C}}}+\frac{s^2_{\mathrm{C-N}}}{m_{\mathrm{H}}}\right.\\ \quad\left.+\frac{1}{2m_{\mathrm{N}}}\left(\sqrt{3}\,s_{\mathrm{N-H}}+\frac{s_{\mathrm{C-N}}}{\sqrt{3}}\right)^2\right\}\end{array} & \begin{array}{l}\sqrt{3}\,(1+2\cos^2\beta)\kappa\left\{\frac{4\sin\beta}{m_{\mathrm{C}}s_{\mathrm{C-N}}}\right.\\ \quad\times(s_{\mathrm{C-O}}+\cos\beta\, s_{\mathrm{C-N}})\\ \quad\left.+\frac{\sin\beta\, s_{\mathrm{C-O}}}{m_{\mathrm{N}}}\left(\frac{1}{s_{\mathrm{C-N}}}+\frac{1}{3s_{\mathrm{N-H}}}\right)\right\}\end{array} & \frac{8\sqrt{3}}{9m_{\mathrm{H}}}\tau \\ -\frac{4\sqrt{6}\,f_{\mathrm{N-H}}}{3\sin 2\beta\, m_{\mathrm{N}}s_{\mathrm{C-N}}} & \begin{array}{l}\frac{2\sqrt{3}\,\delta_1}{\sin 2\beta}\left\{\frac{2}{m_{\mathrm{C}}}\left(\frac{s_{\mathrm{N-H}}}{s_{\mathrm{C-N}}}+\frac{s_{\mathrm{N-H}}\cos\beta}{s_{\mathrm{C-O}}}\right)\right.\\ \quad\left.+\frac{1}{m_{\mathrm{N}}}\left(\frac{s_{\mathrm{N-H}}}{s_{\mathrm{C-N}}}+\frac{1}{3}\right)\right\}\end{array} & \begin{array}{l}\lambda-\frac{2(1+2\cos^2\beta)}{\cos\beta\, s_{\mathrm{C-O}}s_{\mathrm{C-N}}}\\ \quad\times\kappa\left\{\frac{s^2_{\mathrm{C-O}}}{m_{\mathrm{N}}}+\frac{2\cos^2\beta\, s^2_{\mathrm{C-N}}}{m_{\mathrm{O}}}+\frac{4}{m_{\mathrm{C}}}\right.\\ \quad\left.\times(s_{\mathrm{C-O}}+\cos\beta\, s_{\mathrm{C-N}})^2\right\}\end{array} & 0 \\ \frac{\sqrt{6}\,f_{\mathrm{N-H}}}{6m_{\mathrm{H}}s_{\mathrm{N-H}}} & \frac{2\sqrt{3}\,s_{\mathrm{C-N}}\delta_1}{3m_{\mathrm{H}}s_{\mathrm{N-H}}} & 0 & \lambda-\frac{2\tau}{m_{\mathrm{H}}} \end{vmatrix}=0. \quad (4)$$

$$\begin{vmatrix}
\lambda-f_{C-N}\left(\frac{1}{m_N}+\frac{2\sin^2\beta}{m_C}\right) & \frac{2f_{N-H}}{3m_N} & \frac{2\sin\beta d'}{m_C}(\cos\beta\, s_{C=O}+s_{C-N}) & 2\delta_1\left(\frac{2\sqrt{2}\,s_{C-N}}{3m_N}-\frac{\sin 2\beta\, s_{N-H}}{2m_C}\right) & -\frac{2\sqrt{2}\,s_{N-H}}{3m_N}\delta_2 \\
\frac{f_{C-N}}{3m_N}. & \lambda-f_{N-H}\left(\frac{1}{m_H}+\frac{2}{3m_N}\right) & -\frac{\sqrt{2}\,s_{C=O}\,d'}{3m_N} & -\frac{\sqrt{2}}{3m_N}\delta_1(s_{C-N}-s_{N-H}) & \frac{2\sqrt{2}\,s_{N-H}}{3m_N}\delta_2 \\
\frac{2\sin\beta f_{C-N}}{m_C}\left(\frac{\cos\beta}{s_{C-N}}+\frac{1}{s_{C=O}}\right) & -\frac{2\sqrt{2}f_{N-H}}{3m_N s_{C-N}} & \begin{array}{l}\lambda-\frac{s_{C-N}}{s_{C=O}}d'\left\{\frac{s^2_{C=O}}{s^2_{C-N}}+\frac{2}{m_O}\right.\\ \qquad\left.\times\left(1+\frac{s_{C=O}}{s_{C-N}}\cos\beta\right)^2\right\}\end{array} & \begin{array}{l}s_{N-H}\delta_1\left\{\frac{1}{m_N}\left(\frac{1}{s_{C-N}}+\frac{1}{3s_{N-H}}\right)\right.\\ \qquad\left.+\frac{2\cos\beta}{m_C}\left(\frac{\cos\beta}{s_{C-N}}+\frac{1}{s_{C=O}}\right)\right\}\end{array} & \frac{4s_{N-H}}{3m_N s_{C-N}}\delta_2 \\
\begin{array}{l}f_{C-N}\left(\frac{2\sqrt{2}}{3m_N s_{N-H}}\right.\\ \qquad\left.-\frac{\sin 2\beta}{2m_C s_{C-N}}\right)\end{array} & -\frac{\sqrt{2}f_{N-H}}{3m_N}\left(\frac{1}{s_{N-H}}-\frac{1}{s_{C-N}}\right) & \begin{array}{l}d'\left\{\frac{\cos\beta}{m_C s_{C-N}}\right.\\ \qquad\times(\cos\beta\, s_{C=O}+s_{C-N})\\ \qquad\left.+\frac{s_{C=O}}{2m_N}\left(\frac{1}{s_{C-N}}+\frac{1}{3s_{N-H}}\right)\right\}\end{array} & \begin{array}{l}\lambda-\delta_1\left\{\frac{1}{3m_N}\right.\\ \qquad+\frac{s_{N-H}}{s_{C-N}}\left(\frac{\cos^2\beta}{m_C}+\frac{1}{2m_N}\right)\\ \qquad\left.+\frac{s_{C-N}}{s_{N-H}}\left(\frac{1}{m_H}+\frac{11}{6m_N}\right)\right\}\end{array} & \begin{array}{l}\delta_2\left\{\frac{2}{3m_N}\left(1-\frac{s_{N-H}}{s_{C-N}}\right)\right.\\ \qquad\left.+\frac{1}{2m_H}\right\}\end{array} \\
-\frac{2\sqrt{2}f_{C-N}}{3m_N s_{N-H}} & \frac{4\sqrt{2}f_{N-H}}{3m_N s_{N-H}} & \frac{4s_{C=O}}{3m_N s_{N-H}}d' & \begin{array}{l}-2\delta_1\left\{\frac{2}{3m_N}\right.\\ \qquad\left.-\frac{2s_{C-N}}{3s_{N-H}}\left(\frac{1}{m_H}+\frac{1}{m_N}\right)\right\}\end{array} & \lambda-2\delta_2\left(\frac{1}{m_H}+\frac{4}{3m_N}\right)
\end{vmatrix}=0. \qquad (5)$$

## 4. INTERPRETATION OF THE $CO(NH_2)_2$ AND $CO(ND_2)_2$ SPECTRA AND EVALUATION OF FORCE CONSTANTS

The Raman spectrum of $CO(NH_2)_2$ and $CO(ND_2)_2$ has been investigated by Kohlrausch and Pongratz (1934) and by Otvos and Edsall (1939). Their data are given in table 2, together with the results of the study of the infra-red spectrum (see preceding paper). The letters *P* and *D* mean 'Polarized' and 'Depolarized' respectively. It follows from table 1 that the polarized bands belong to the symmetry type $A_1$ and that there are six vibrations of this class, three of which are principally valence vibrations and three deformation frequencies The N—H valence vibration is known to lie in the region 3300–3500 cm.$^{-1}$, so that the 3235 band cannot be interpreted as a fundamental as there is only one N—H valence oscillation of the type $A_1$. All the other strongly polarized bands can be assigned to fundamental vibrations (table 3).

TABLE 2

| Infra-red spectrum Kellner (see preceding paper) | $CO(NH_2)_2$ Raman spectrum | | $CO(ND_2)_2$ Raman spectrum |
|---|---|---|---|
| | Kohlrausch and Pongratz | Otvos and Edsall | Otvos and Edsall |
| — | 525 (2*b*) | 534 (2) *D* | 458 (1) *D* |
| — | — | | 548 (1) *P* |
| — | 685 (1*b*) | 601 (2) *D* | — |
| | 1000 (8) | 1008 (10) *P* | 997 (6) *P* |
| | 1157 (1*b*) | 1167 (4) *P* | 890 (5) *P* |
| | 1350 (½) | Not observed | 1049 (1) ? |
| | 1458 (0) | 1478 (2*b*) *D* | Not observed |
| — | — | — | 1201 (1*b*) ? |
| — | 1593 (2*b*) | 1604 (4*b*) *P*? | 1247 (3) *P* |
| — | 1665 (0) | 1680 (3*b*) *P* | 1613 (3*b*) *P* |
| 3218 | 3218 (1*b*) | 3235 (5*b*) *P* | — |
| 3376<br>3410 | 3383 (3*vb*) | 3385 (6*vb*) *P* | 2421 (5*vb*) *P* |
| — | — | – | 2506 (3) *P*? |
| 3434 | — | — | — |
| Not observed | 3462 (2*vb*) | 3496 (5*b*) *D* | 2603 (3) *D* |

TABLE 3. FUNDAMENTAL VIBRATIONS OF UREA OF CLASS $A_1$

| $\nu_1$ | $\nu_2$ | $\nu_3$ | $\nu_4$ | $\nu_5$ | $\nu_6$ | Molecule |
|---|---|---|---|---|---|---|
| Not observed | 1008 | 1167 | 1604 | 1680 | 3385 | $CO(NH_2)_2$ |
| 548 | 997 | 890 | 1247 | 1613 | 2421 | $CO(ND_2)_2$ |

If the determinant (2) is evaluated under the assumption that the angle forces can be neglected as compared with the valence forces, the following third-order equation is obtained:

$$\begin{aligned}\lambda^3-\lambda^2\Big\{&f_{\mathrm{C-O}}\Big(\frac{1}{m_{\mathrm{C}}}+\frac{1}{m_{\mathrm{O}}}\Big)+f_{\mathrm{C-N}}\Big(\frac{1}{m_{\mathrm{N}}}+\frac{2\cos^2\beta}{m_{\mathrm{C}}}\Big)+f_{\mathrm{N-H}}\Big(\frac{1}{m_{\mathrm{H}}}+\frac{2}{3m_{\mathrm{N}}}\Big)\Big\}\\ &+\lambda\Big\{f_{\mathrm{C-O}}f_{\mathrm{C-N}}\Big[\frac{2\cos^2\beta}{m_{\mathrm{C}}m_{\mathrm{O}}}+\frac{1}{m_{\mathrm{N}}}\Big(\frac{1}{m_{\mathrm{O}}}+\frac{1}{m_{\mathrm{O}}}\Big)\Big]\\ &+f_{\mathrm{C-O}}f_{\mathrm{N-H}}\Big(\frac{1}{m_{\mathrm{C}}}+\frac{1}{m_{\mathrm{O}}}\Big)\Big(\frac{1}{m_{\mathrm{H}}}+\frac{2}{3m_{\mathrm{N}}}\Big)\\ &+f_{\mathrm{C-N}}f_{\mathrm{N-H}}\Big[\Big(\frac{1}{m_{\mathrm{N}}}+\frac{2\cos^2\beta}{m_{\mathrm{C}}}\Big)\Big(\frac{1}{m_{\mathrm{H}}}+\frac{2}{3m_{\mathrm{N}}}\Big)-\frac{2}{9m_{\mathrm{N}}^2}\Big]\Big\}\\ &-f_{\mathrm{C-O}}f_{\mathrm{C-N}}f_{\mathrm{N-H}}\Big\{\frac{1}{m_{\mathrm{N}}}\Big(\frac{1}{m_{\mathrm{C}}}+\frac{1}{m_{\mathrm{O}}}\Big)\Big(\frac{4}{9m_{\mathrm{N}}}+\frac{1}{m_{\mathrm{H}}}\Big)\\ &+\frac{2\cos^2\beta}{m_{\mathrm{C}}m_{\mathrm{O}}}\Big(\frac{1}{m_{\mathrm{H}}}+\frac{2}{3m_{\mathrm{N}}}\Big)\Big\}=0.\end{aligned}\qquad(6)$$

It is known that the C—N valence vibration, which is not very different from the C—C vibration, lies between approximately 800 and 1000 cm.$^{-1}$, while the C=O oscillation in aldehydes, ketones and fatty acids occurs at 1700 cm.$^{-1}$. The frequency 1008 may therefore be assigned to the C—N valence vibration, and 1680 to the C=O oscillation. The fact that this latter value is lower than in ordinary C=O bonds indicates that the C=O linkage in urea is weakened in accordance with the conception of resonance in the molecule. As the symmetrical N—H valence vibration in ammonia is 3336, the band 3385 is assigned to the symmetrical N—H oscillation in urea. Using these frequencies, and putting $2\beta = 114^\circ 44'$ (Wyckoff and Corey 1934), the following figures for the valence force constants are obtained:

$$\left.\begin{aligned}f_{\mathrm{C-O}}&=9{\cdot}7\times10^5\ \text{dynes/cm.},\\ f_{\mathrm{C-N}}&=6{\cdot}6\times10^5\ \text{dynes/cm.},\\ f_{\mathrm{N-H}}&=6{\cdot}3\times10^5\ \text{dynes/cm.}\end{aligned}\right\}\qquad(7)$$

If $m_{\mathrm{D}}$ is substituted for $m_{\mathrm{H}}$ in equation (6) and the above force constants are used, the following frequencies (table 4) are computed for $\mathrm{CO(ND_2)_2}$ from (6):

TABLE 4. VALENCE VIBRATIONS OF CLASS $A_1$ FOR $CO(ND_2)_2$

| | $\nu_2$ | $\nu_5$ | $\nu_6$ |
|---|---|---|---|
| Observed | 997 | 1613 | 2421 |
| Calculated | 909 | 1727 | 2440 |

The agreement between observed and calculated values is satisfactory, as the contribution of the angle forces to the vibrations has not been taken into account. The frequencies 1167 and 1604 for $CO(NH_2)_2$ (if 1604 is polarized, which still seems doubtful) and 548, 890 and 1247 for $CO(ND_2)_2$ are to be interpreted as deformation vibrations.

It follows from (3) and (4) that the symmetry classes $A_2$ and $B_1$ contain one N—H valence vibration each, in which the two N—H bonds of each $NH_2$ group perform an asymmetric vibration. The other frequencies of these types are bending frequencies. If the angle forces are again neglected, the asymmetric N—H frequency is found to be $\nu = 3460$, taking $f_{N-H} = 6 \cdot 3 \times 10^5$ dynes/cm., so that the observed band $\nu = 3496$ may be identified with this oscillation. In the case of the N—D linkage, the corresponding vibration is obtained at $\nu$ 2550 ($\nu$ 2603 observed). The infra-red spectrum shows a band at 3434 and no band at 3496. As the bands of the type $A_2$ are forbidden in the infra-red spectrum, $\nu$ 3496 is therefore to be assigned to the class $A_2$ while $\nu$ 3434 belongs to the symmetry type $B_1$.

The vibrations of $B_2$ (5) contain one C—N valence frequency in addition to a symmetric N—H oscillation. This C—N frequency represents an asymmetric oscillation of the two C—N bonds. If the angle forces are left out of consideration and the above values (7) used for $f_{C-N}$ and $f_{N-H}$, the frequency 1456 is obtained for $CO(NH_2)_2$ and 1470 for $CO(ND_2)_2$. In the latter case no corresponding band has been observed, while the observed $\nu$ 1478($CO(NH_2)_2$) agrees very well with the calculated value.

Equation (3) shows that a bending frequency and a torsional vibration of the $NH_2$ groups fulfils the symmetry requirements of the class $A_2$. The nitrogen and hydrogen atoms move in such a way in this bending frequency that the valence angles H—N—H remain unchanged while the angles H—N—C are deformed. A comparison with the corresponding frequencies of guanidonium (12) shows that the secular equation has the same form, and the assignment of the vibrations can therefore be taken over with the only alteration that the distance $s_{C-N}$ is slightly different in the case of urea. The band 1164 is correspondingly assigned to the bending frequency of class $A_2$ for $CO(ND_2)_2$. The torsional vibration is probably too low for observation. It seems that the analogous oscillation of $CO(NH_2)_2$ is obscured by the relatively intense band $\nu$ 1680. If the same values of $\delta_1$, $\tau$ and $f_{N-H}$

are used as for guanidonium (13), the computation leads to the following results (table 5):

TABLE 5. VIBRATIONS OF UREA OF CLASS $A_2$

| | $CO(NH_2)_2$ | $CO(ND_2)_2$ | $CO(NH_2)_2$ | $CO(ND_2)_2$ | $CO(NH_2)_2$ | $CO(ND_2)_2$ |
|---|---|---|---|---|---|---|
| | N—H valence vibration | | Bending vibration | | Torsional vibration | |
| Calculated | 3420 | 2544 | 1563 | 1110 | 113 | 107 |
| Observed | 3496 | 2603 | Obscured by 1680? | 1164 | Not observed | Not observed |

As the oscillations of the type $B_1$ (5) are forbidden in the $C^+(NH_2)_3$ spectrum (10), they are tentatively assigned to $CO(NH_2)_2$ frequencies which have no analogues in the guanidonium spectrum. The remaining lines, which occur in both spectra in approximately the same positions, have been placed in class $B_2$.

The intense polarized lines $\nu$ 3235 and $\nu$ 2506 have been classified as the first overtones of the fundamentals 1680 and 1247 respectively. These overtones have the symmetry properties of vibrations belonging to the class $A_1$ (this follows from group theoretical considerations) and are therefore polarized Their high intensities can be explained by resonance with the intense fundamentals 3380 and 2421. The possibility that these frequencies (2506 and 3235) might be due to a weakening of the N—H bonds, by the formation of hydrogen bonds with the oxygen atom of a neighbouring molecule, is ruled out by the fact that $\nu$ 2506 is of higher frequency than the N—D vibration 2421, while it should be considerably lower in the case of hydrogen bonding

The proposed interpretation is set out in table 6, but it must be pointed out here that it is by no means definite Unfortunately, no use could be made of Teller's product theorem (Angus, Bailey, Hale, Ingold, Leckie, Raisin, Thomson and Wilson 1936) which would permit a final decision of the assignment to the symmetry classes, as this theorem presupposes the complete knowledge of the spectrum of two isotopic molecules.

## 5. VIBRATIONS OF GUANIDONIUM

It is assumed that the C=N double bond oscillates in the guanidonium ion $C^+(NH_2)_3$ between the three equivalent C—N linkages. In this case the C—N distances will be equal and each bond will have ⅓ double-bond character. The molecule has then the symmetry $C_{3h}$, i.e. a threefold axis $C_3$ through the carbon atom and perpendicular to the plane through the nitrogen and carbon atoms (the resonance forces these atoms into one plane), and a symmetry plane $\sigma_h$ perpendicular to this axis. The hydrogen atoms of each $NH_2$ group are symmetrically arranged with regard to $\sigma_h$. As $C_{3h}$ has a threefold symmetry axis, it gives rise to degenerate vibrations. The vibrations belong to four classes, of which the oscillations of the last two are doubly degenerate. The symmetry properties and numbers of frequencies are shown in table 7.

TABLE 6

| Symmetry type | $CO(NH_2)_2$ | $CO(ND_2)_2$ | Mode of vibration |
|---|---|---|---|
| $A_1$ $\nu_1$ | — | 548 | Bending vibration |
| $\nu_2$ | 1008 | 997 | Symmetrical valence vibration of C—N linkages |
| $\nu_3$ | 1167 | 890 | Bending vibration |
| $\nu_4$ | 1604 | 1247 | Bending vibration |
| $\nu_5$ | 1680 | 1613 | Valence vibration of C—O linkage |
| $2\nu_5$ | 3235 | — | — |
| $2\nu_4$ | — | 2506 | — |
| $\nu_6$ | 3385<br>3410 infra-red | 2421 | Symmetrical valence vibration of N—H (N—D) linkages |
| $A_2$ $\nu_7$ | Not observed | Not observed | Torsional vibration of $NH_2$ groups |
| $\nu_8$ | Obscured by 1680? | 1164 | Bending vibrations of $NH_2$ groups |
| $\nu_9$ | 3496 | 2603 | Asymmetrical valence vibration of N—H (N—D) linkages |
| $B_1$ $\nu_{10}$ | Not observed | Not observed | Bending vibration |
| $\nu_{11}$ | Not observed | 1201? | Folding of 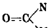 $O{=}C\langle{}^{N}_{N}$ plane |
| $\nu_{12}$ | 1350 | 1049 | Bending vibration |
| $\nu_{13}$ | 3434 infra-red | 2603 | Asymmetrical valence vibration of N—H (N—D) linkages |
| $B_2$ $\nu_{14}$ | Not observed | Not observed | Bending vibration |
| $\nu_{15}$ | 534 | 458 | Bending vibration |
| $\nu_{16}$ | 601 | Not observed | Bending vibration |
| $\nu_{17}$ | 1478 | Not observed | Asymmetrical valence vibration of C—N linkages |
| $\nu_{18}$ | 3376 infra-red | Obscured by 2421? | Symmetrical valence vibration of N—H (N—D) linkages |

TABLE 7

| | Symmetry properties | | | Infra-red spectrum | | Raman spectrum | | |
|---|---|---|---|---|---|---|---|---|
| Symmetry class | Symmetric | Anti-symmetric | Degeneracy | Activity | Band type | Activity | Degree of depolarization | No. of vibrations |
| $A_1$ | $C_3$, $\sigma_h$ | — | — | Inactive | — | Active | $\rho < \frac{6}{7}$ | 4 |
| $A_2$ | $C_3$ | $\sigma_h$ | — | Inactive | — | Inactive | $\rho = \frac{6}{7}$ | 4 |
| B′ | $\sigma_h$ | — | $C_3$ | Active | Perpendicular | Active | $\rho = \frac{6}{7}$ | 5 |
| B″ | — | $\sigma_h$ | $C_3$ | Inactive | — | Active | $\rho = \frac{6}{7}$ | 3 |

There are $3 \times 10 - 6 = 24$ vibrations altogether, of which only 12 will be observed in the Raman spectrum (the vibrations of the classes B′ and B″ have to be counted double), and four of these should be polarized and relatively stronger than the others. The infra-red spectrum will show only five bands.

The potential function $V$ of $C^+(NH_2)_3$ has been chosen in the same way as for urea.

$$
\begin{aligned}
2V = {} & f_{C-N}\{\xi^2_{C-N_1} + \xi^2_{C-N_2} + \xi^2_{C-N_3}\} \\
& + f_{N-H}\{\xi^2_{N_1-H_1'} + \xi^2_{N_1-H_1''} + \xi^2_{N_2-H_2} + \xi^2_{N_2-H_2''} + \xi^2_{N_3-H_3'} + \xi^2_{N_3-H_3'}\} \\
& + d s^2_{C-N}\{(\Delta\alpha_1)^2 + (\Delta\alpha_2)^2 + (\Delta\alpha_3)^2\} + \delta_2 s^2_{N-H}\{(\Delta\gamma_1)^2 + (\Delta\gamma_2)^2 + (\Delta\gamma_3)^2\} \\
& + \delta_1 s_{C-N} s_{N-H}\{(\Delta\Theta_{11})^2 + (\Delta\Theta_{12})^2 + (\Delta\Theta_{21})^2 + (\Delta\Theta_{22})^2 + (\Delta\Theta_{31})^2 + (\Delta\Theta_{32})^2\} \\
& + \kappa \sin^2 120^\circ\, s^2_{C-N}\{(\Delta\Phi_1)^2 + (\Delta\Phi_2)^2 + (\Delta\Phi_3)^2\} \\
& + 4\tau \sin^2 \tfrac{1}{2}\Theta\, s^2_{N-H}\{(\Delta\Theta_1)^2 + (\Delta\Theta_2)^2 + (\Delta\Theta_3)^2\}. \qquad (8)
\end{aligned}
$$

The symbols have the same meaning as in the case of urea. The arrangement of the angles will be understood by reference to figure 4 which represents a molecule distorted by a vibration. The C—N linkages form a valence angle of 120° with each other in the equilibrium position.

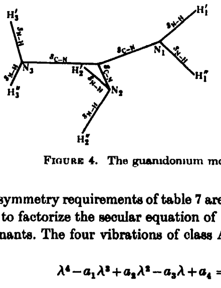

$H_i'N_iH_i'' = \gamma_i$
$H_i'N^iC = \theta_{i1}$
$H_i''N_iC = \theta_{i2}$
$N_1CN_2 = \alpha_1$
$N_2CN_3 = \alpha_2$
$N_3CN_1 = \alpha_3$

FIGURE 4. The guanidonium molecule.

When the symmetry requirements of table 7 are taken into consideration, it is possible to factorize the secular equation of 16 rows and columns into four determinants. The four vibrations of class $A_1$ are represented by the equation (9)·

$$\lambda^4 - a_1\lambda^3 + a_2\lambda^2 - a_3\lambda + a_4 = 0, \qquad (9)$$

where

$$a_1 = \frac{f_{\text{C-N}}}{m_{\text{N}}} + f_{\text{N-H}}\left(\frac{1}{m_{\text{H}}} + \frac{2}{3m_{\text{N}}}\right) + \delta_2\left(\frac{2}{m_{\text{H}}} + \frac{8}{3m_{\text{N}}}\right) + \delta_1\left(\frac{11s_{\text{C-N}}}{3m_{\text{N}}s_{\text{N-H}}} + \frac{s_{\text{N-H}}}{2m_{\text{N}}s_{\text{C-N}}} + \frac{1}{3m_{\text{N}}} + \frac{s_{\text{C-N}}}{m_{\text{H}}s_{\text{N-H}}}\right);$$

$$\begin{aligned}a_2 = {} & \frac{f_{\text{C-N}}f_{\text{N-H}}}{3m_{\text{N}}}\left(\frac{3}{m_{\text{H}}} + \frac{4}{3m_{\text{N}}}\right) + \frac{2f_{\text{C-N}}\delta_2}{3m_{\text{N}}}\left(\frac{3}{m_{\text{H}}} + \frac{8}{3m_{\text{N}}}\right) + \frac{2f_{\text{N-H}}\delta_2}{m_{\text{H}}}\left(\frac{1}{m_{\text{H}}} + \frac{2}{m_{\text{N}}}\right) \\ & + \frac{f_{\text{C-N}}\delta_1}{3m_{\text{N}}}\left(\frac{65s_{\text{C-N}}}{6m_{\text{N}}s_{\text{N-H}}} + \frac{3s_{\text{N-H}}}{2m_{\text{N}}s_{\text{C-N}}} + \frac{1}{3m_{\text{N}}} + \frac{3s_{\text{C-N}}}{m_{\text{H}}s_{\text{N-H}}}\right) \\ & + f_{\text{N-H}}\delta_1\left(\frac{5s_{\text{C-N}}}{2m_{\text{H}}m_{\text{N}}s_{\text{N-H}}} + \frac{s_{\text{N-H}}}{2m_{\text{H}}m_{\text{N}}s_{\text{C-N}}} + \frac{1}{3m_{\text{H}}m_{\text{N}}} + \frac{s_{\text{C-N}}}{m_{\text{H}}^2 s_{\text{N-H}}} + \frac{s_{\text{N-H}}}{9m_{\text{N}}^2 s_{\text{C-N}}} + \frac{2}{3m_{\text{N}}^2} + \frac{s_{\text{C-N}}}{m_{\text{N}}^2 s_{\text{N-H}}}\right) \\ & + \delta_1\delta_2\left(\frac{5s_{\text{C-N}}}{m_{\text{H}}m_{\text{N}}s_{\text{N-H}}} + \frac{4s_{\text{C-N}}}{m_{\text{N}}^2 s_{\text{N-H}}} + \frac{s_{\text{N-H}}}{m_{\text{H}}m_{\text{N}}s_{\text{C-N}}} + \frac{4s_{\text{N-H}}}{9m_{\text{N}}^2 s_{\text{C-N}}} + \frac{2}{m_{\text{H}}m_{\text{N}}} + \frac{8}{3m_{\text{N}}^2} + \frac{3s_{\text{C-N}}}{2m_{\text{H}}^2 s_{\text{N-H}}}\right);\end{aligned}$$

$$\begin{aligned}a_3 = {} & \frac{f_{\text{C-N}}f_{\text{N-H}}\delta_1}{3m_{\text{N}}}\left(\frac{73s_{\text{C-N}}}{6m_{\text{H}}m_{\text{N}}s_{\text{N-H}}} + \frac{3s_{\text{N-H}}}{2m_{\text{H}}m_{\text{N}}s_{\text{C-N}}} + \frac{1}{m_{\text{H}}m_{\text{N}}} + \frac{3s_{\text{C-N}}}{m_{\text{H}}^2 s_{\text{N-H}}}\right) \\ & + \frac{2f_{\text{C-N}}f_{\text{N-H}}\delta_2}{m_{\text{H}}m_{\text{N}}}\left(\frac{1}{m_{\text{H}}} + \frac{4}{3m_{\text{N}}}\right) \\ & + \frac{f_{\text{C-N}}\delta_1\delta_2}{3m_{\text{N}}}\left(\frac{6}{m_{\text{H}}m_{\text{N}}} + \frac{23s_{\text{C-N}}}{m_{\text{H}}m_{\text{N}}s_{\text{N-H}}} + \frac{9s_{\text{C-N}}}{2m_{\text{H}}^2 s_{\text{N-H}}} + \frac{64}{m_{\text{N}}^2} + \frac{64s_{\text{C-N}}}{3m_{\text{N}}^2 s_{\text{N-H}}} + \frac{3s_{\text{N-H}}}{m_{\text{H}}m_{\text{N}}s_{\text{C-N}}}\right) \\ & + \frac{f_{\text{N-H}}\delta_1\delta_2}{m_{\text{H}}}\left(\frac{6s_{\text{C-N}}}{m_{\text{H}}m_{\text{N}}s_{\text{N-H}}} + \frac{s_{\text{N-H}}}{m_{\text{H}}m_{\text{N}}s_{\text{C-N}}} + \frac{3s_{\text{C-N}}}{2m_{\text{H}}^2 s_{\text{N-H}}} + \frac{6s_{\text{C-N}}}{m_{\text{N}}^2 s_{\text{N-H}}} + \frac{2s_{\text{N-H}}}{3m_{\text{N}}^2 s_{\text{C-N}}} + \frac{2}{m_{\text{H}}m_{\text{N}}} + \frac{4}{m_{\text{N}}^2}\right);\end{aligned}$$

$$a_4 = \frac{f_{\text{C-N}}f_{\text{N-H}}\delta_1\delta_2}{3m_{\text{H}}m_{\text{N}}}\left(\frac{6}{m_{\text{H}}m_{\text{N}}} + \frac{25s_{\text{C-N}}}{m_{\text{H}}m_{\text{N}}s_{\text{N-H}}} + \frac{3s_{\text{N-H}}}{m_{\text{H}}m_{\text{N}}s_{\text{C-N}}} + \frac{16}{9m_{\text{N}}^2} + \frac{9s_{\text{C-N}}}{2m_{\text{H}}^2 s_{\text{N-H}}} + \frac{64s_{\text{C-N}}}{3m_{\text{N}}^2 s_{\text{N-H}}}\right)$$

$\Theta$ has been taken to be the tetrahedral angle, 109° 28′. The carbon atom does not take part in the totally symmetric vibrations but remains at rest.

The inactive vibrations of the type $A_2$ are represented by the determinant (10). The oscillations of the type B′ follow from equation (11). This is the only active type of vibrations in which the carbon atom takes part. The remaining three vibrations of the class B″ are obtained from equation (12):

$$\begin{aligned}\lambda^3 - \lambda^2 & \left\{ f_{\text{N-H}}\left(\frac{1}{m_{\text{H}}} + \frac{2\sin^2\frac{1}{2}\Theta}{m_{\text{N}}}\right) + \delta_1\left[\frac{s_{\text{C-N}}}{m_{\text{H}}s_{\text{N-H}}} + \frac{(\cos\Theta\, s_{\text{C-N}} - s_{\text{N-H}})^2}{2\cos^2\frac{1}{2}\Theta\, m_{\text{N}}s_{\text{C-N}}s_{\text{N-H}}}\right] + \frac{2\tau}{m_{\text{H}}}\right\} \\ & + \lambda\left\{\frac{f_{\text{N-H}}\delta_1}{m_{\text{H}}s_{\text{N-H}}}\left(\frac{s_{\text{C-N}}}{m_{\text{H}}} + \frac{s_{\text{C-N}}^2 + s_{\text{N-H}}^2 - 2\cos\Theta s_{\text{C-N}}s_{\text{N-H}}}{2\cos^2\frac{1}{2}\Theta\, s_{\text{C-N}}m_{\text{N}}}\right) + \frac{4\sin^2\frac{1}{2}\Theta f_{\text{N-H}}\tau}{m_{\text{H}}}\left(\frac{1}{m_{\text{N}}} + \frac{2\cos^2\frac{1}{2}\Theta}{m_{\text{H}}}\right)\right. \\ & \left. + \frac{2\delta_1\tau}{m_{\text{H}}}\left[\frac{\cos^2\Theta\, s_{\text{C-N}}}{m_{\text{H}}s_{\text{N-H}}} + \frac{(\cos\Theta\, s_{\text{C-N}} - s_{\text{N-H}})^2}{2\cos^2\frac{1}{2}\Theta\, m_{\text{N}}s_{\text{C-N}}s_{\text{N-H}}}\right]\right\} - \frac{4\sin^2\frac{1}{2}\Theta\, s_{\text{N-H}}f_{\text{N-H}}\delta_1\tau}{m_{\text{H}}^2 m_{\text{N}}s_{\text{C-N}}} = 0. \qquad (12)\end{aligned}$$

$$\begin{vmatrix}
\lambda - f_{\text{N-H}}\left(\dfrac{1}{m_{\text{H}}} + \dfrac{2\sin^2\frac{1}{2}\Theta}{m_{\text{N}}}\right) & \dfrac{\tan\frac{1}{2}\Theta}{m_{\text{N}}}\delta_1(\cos\Theta\, s_{\text{C-N}} - s_{\text{N-H}}) & \dfrac{3\sqrt{3}\, s_{\text{C-N}}}{2m_{\text{N}}}\kappa & -\dfrac{2\sin\frac{1}{2}\Theta\cos\Theta\, s_{\text{N-H}}}{m_{\text{H}}}\tau \\
\dfrac{\tan\frac{1}{2}\Theta f_{\text{N-H}}}{m_{\text{N}}\, s_{\text{C-N}}\, s_{\text{N-H}}}(\cos\Theta\, s_{\text{C-N}} - s_{\text{N-H}}) & \begin{aligned}\lambda - \dfrac{\delta_1}{2s_{\text{C-N}}\, s_{\text{N-H}}}\Bigg\{&\dfrac{2s^2_{\text{C-N}}}{m_{\text{H}}} \\ &+ \dfrac{(\cos\Theta\, s_{\text{C-N}} - s_{\text{N-H}})^2}{\cos^2\frac{1}{2}\Theta\, m_{\text{N}}} \\ &+ \dfrac{3s^2_{\text{N-H}}}{\cos^2\frac{1}{2}\Theta\, m_{\text{C}}}\Bigg\}\end{aligned} & \begin{aligned}\dfrac{3\sqrt{3}}{4\cos\frac{1}{2}\Theta\, s_{\text{N-H}}}\kappa\Bigg\{&\dfrac{3s_{\text{N-H}}}{m_{\text{C}}} \\ &+ \dfrac{(\cos\Theta\, s_{\text{C-N}} - s_{\text{N-H}})}{m_{\text{N}}}\Bigg\}\end{aligned} & -\dfrac{2\sin\frac{1}{2}\Theta\sin\Theta}{m_{\text{H}}}\tau \\
\dfrac{4\sqrt{3}\sin\frac{1}{2}\Theta}{m_{\text{N}}\, s_{\text{C-N}}}f_{\text{N-H}} & \begin{aligned}\dfrac{2\sqrt{3}}{\cos\frac{1}{2}\Theta\, s_{\text{C-N}}}\delta_1\Bigg\{&\dfrac{3s_{\text{N-H}}}{m_{\text{C}}} \\ &- \dfrac{(\cos\Theta\, s_{\text{C-N}} - s_{\text{N-H}})}{m_{\text{N}}}\Bigg\}\end{aligned} & \lambda - 9\kappa\left(\dfrac{1}{m_{\text{N}}} + \dfrac{3}{m_{\text{C}}}\right) & 0 \\
-\dfrac{\cos\Theta}{\sin\frac{1}{2}\Theta\, m_{\text{H}}\, s_{\text{N-H}}}f_{\text{N-H}} & -\dfrac{2\cos\Theta\, s_{\text{C-N}}}{m_{\text{H}}\, s_{\text{N-H}}}\delta_1 & 0 & \lambda - \dfrac{2\tau}{m_{\text{H}}}
\end{vmatrix} = 0. \qquad (10)$$

$$\begin{vmatrix}
\lambda-f_{\mathrm{C-N}}\left(\frac{1}{m_{\mathrm{N}}}+\frac{3}{2m_{\mathrm{C}}}\right) & \frac{2}{3m_{\mathrm{N}}}f_{\mathrm{N-H}} & -\frac{3id\,s_{\mathrm{C-N}}}{2m_{\mathrm{C}}} & 2\delta_1\left(\frac{3i\,s_{\mathrm{N-H}}}{4m_{\mathrm{C}}}-\frac{2\sqrt{2}\,s_{\mathrm{C-N}}}{3m_{\mathrm{N}}}\right) & -\frac{2\sqrt{2}\,s_{\mathrm{N-H}}}{3m_{\mathrm{N}}}\delta_2 \\
\frac{f_{\mathrm{C-N}}}{3m_{\mathrm{N}}} & \lambda-f_{\mathrm{N-H}}\left(\frac{1}{m_{\mathrm{H}}}+\frac{2}{3m_{\mathrm{N}}}\right) & -\frac{\sqrt{2}\,d\,s_{\mathrm{C-N}}}{3m_{\mathrm{N}}} & \frac{\sqrt{2}}{3m_{\mathrm{N}}}\delta_1(s_{\mathrm{C-N}}-s_{\mathrm{N-H}}) & \frac{2\sqrt{2}\,s_{\mathrm{N-H}}}{3m_{\mathrm{N}}}\delta_2 \\
\frac{9i\,f_{\mathrm{C-N}}}{2m_{\mathrm{C}}s_{\mathrm{C-N}}} & -\frac{2\sqrt{2}}{m_{\mathrm{N}}s_{\mathrm{C-N}}}f_{\mathrm{N-H}} & \lambda-3d\left(\frac{1}{m_{\mathrm{N}}}+\frac{3}{2m_{\mathrm{C}}}\right) & -3\delta_1\left(\frac{1}{3m_{\mathrm{N}}}+\frac{3s_{\mathrm{N-H}}}{2m_{\mathrm{C}}s_{\mathrm{C-N}}}+\frac{s_{\mathrm{N-H}}}{m_{\mathrm{N}}s_{\mathrm{O-N}}}\right) & \frac{4s_{\mathrm{N-H}}}{m_{\mathrm{N}}s_{\mathrm{C-N}}}\delta_2 \\
f_{\mathrm{C-N}}\left(\frac{3i}{4m_{\mathrm{C}}s_{\mathrm{C-N}}}-\frac{2\sqrt{2}}{3m_{\mathrm{N}}s_{\mathrm{N-H}}}\right) & \frac{\sqrt{2}}{3m_{\mathrm{N}}}f_{\mathrm{N-H}}\times\left(\frac{1}{s_{\mathrm{N-H}}}-\frac{1}{s_{\mathrm{C-N}}}\right) & -\frac{d}{2}\left(\frac{1}{m_{\mathrm{N}}}+\frac{s_{\mathrm{C-N}}}{3m_{\mathrm{N}}s_{\mathrm{N-H}}}-\frac{3}{2m_{\mathrm{C}}}\right) & \lambda-\delta_1\left\{\frac{1}{m_{\mathrm{N}}}\left(\frac{s_{\mathrm{N-H}}}{2s_{\mathrm{C-N}}}+\frac{1}{3}+\frac{11s_{\mathrm{C-N}}}{6s_{\mathrm{N-H}}}\right)+\frac{s_{\mathrm{C-N}}}{m_{\mathrm{H}}s_{\mathrm{N-H}}}+\frac{3s_{\mathrm{N-H}}}{4m_{\mathrm{C}}s_{\mathrm{C-N}}}\right\} & \delta_2\left\{\frac{1}{3m_{\mathrm{N}}}\left(\frac{s_{\mathrm{N-H}}}{s_{\mathrm{O-N}}}-1\right)-\frac{1}{2m_{\mathrm{H}}}\right\} \\
-\frac{2\sqrt{2}}{3m_{\mathrm{N}}s_{\mathrm{N-H}}}f_{\mathrm{C-N}} & \frac{4\sqrt{2}}{3m_{\mathrm{N}}s_{\mathrm{N-H}}}f_{\mathrm{N-H}} & \frac{4d\,s_{\mathrm{C-N}}}{3m_{\mathrm{N}}s_{\mathrm{N-H}}} & \delta_1\left\{\frac{4}{3m_{\mathrm{N}}}\left(1-\frac{s_{\mathrm{C-N}}}{s_{\mathrm{N-H}}}\right)-\frac{s_{\mathrm{C-N}}}{m_{\mathrm{H}}s_{\mathrm{N-H}}}\right\} & \lambda-2\delta_2\left(\frac{1}{m_{\mathrm{H}}}+\frac{4}{3m_{\mathrm{N}}}\right)
\end{vmatrix}=0. \qquad (11)$$

This equation is exactly the same in form as equation (3) of urea, as mentioned above. It would therefore be expected that these three modes of vibration would be alike in both molecules.

Class $A_1$ contains two valence vibrations, of which one is principally a symmetric oscillation of the nitrogen atom towards and away from the static carbon atom (breathing frequency), while the second is a symmetric vibration of the N—H bonds. The remaining two are bending frequencies, in which the valence angles H—N—C and H—N—H are distorted.

In the symmetry type B′ the nitrogen and hydrogen atoms execute a two-dimensional motion round their equilibrium positions; there are two valence vibrations, one corresponding roughly to an asymmetric oscillation of the C—N bonds and one to a symmetric stretching of the N—H linkages. Three bending frequencies belong to the same symmetry type, deforming all the valence angles of the molecule.

The class B″ is represented by an asymmetric N—H valence vibration, a torsional vibration of the three $NH_2$ groups in phase with each other, and a deformation frequency in which the angles H—N—C are distorted.

## 6. INTERPRETATION OF THE $C^+(NH_2)_3$ AND $C^+(ND_2)_3$ SPECTRA AND EVALUATION OF FORCE CONSTANTS

The Raman spectra of solutions of $C^+(NH_2)_3$ in $H_2O$ and of $C^+(ND_2)_3$ in $D_2O$ respectively have been observed by Otvos and Edsall (1939). The results of their experiments are shown in table 8 together with the assignment of the bands proposed here. The assignment has been chosen in analogy with the urea spectrum. As it is well known that the breathing frequency is the most intense line in the Raman spectrum, the frequencies 1008 and 921 are interpreted as $\nu_1$. The choice of the four $A_1$ vibrations is determined by the fact that they have to be strongly polarized. The upper index, in brackets, indicates the twofold degeneracy. It is not possible to include $\nu$ 2374 in the assignment, as $C^+(ND_2)_3$ has only one polarized N—D vibration. Otvos and Edsall themselves suggest that the line belongs to the $D_2O$ spectrum. On the other hand, if the lines 3360–3471 and 2496–2591 are really caused by the molecules of the solvent, it seems justifiable to conclude that the intense frequencies of $C^+(NH_2)_3$ and $C^+(ND_2)_3$, which are to be expected in this region, are overlapped by the strong water bands.

The force constant $f_{C-N}$ of $C^+(NH_2)_3$ will be very near to the value for urea, and $f_{N-H}$ may be taken to be the same in both cases. It is assumed that the nuclear distances in the isotopic molecules $C^+(NH_2)_3$ and $C^+(ND_2)_3$

are alike, namely $s_{\mathrm{N-H}} = 1{\cdot}02$ A and $s_{\mathrm{C-N}} = 1{\cdot}33$ A. The latter value requires some explanation. The only hitherto observed C—N distance in guanidonium, viz. 1·18 A (Theilacker 1935), is obviously too small, as the triple C≡N bond in HCN has a length of 1·15 A. The above figure for $s_{\mathrm{C-N}}$ was therefore assumed as likely on the ground that in urea $s_{\mathrm{C-N}}$ is 1·27 A (in urea the C—N bonds have less than $\frac{1}{3}$ double-bond character). Using these values, it is possible to compute all vibrations of $C^+(NH_2)_3$ and $C^+(ND_2)_3$ with one set of force constants (13):

TABLE 8. CLASSIFICATION OF THE RAMAN SPECTRUM OF $C^+(NH_2)_3$ AND $C^+(ND_2)_3$

| $C^+(NH_2)_3$ | $C^+(ND_2)_3$ | Denotation | Symmetry type | Mode of vibration |
|---|---|---|---|---|
| 536 (4*b*) *D* | 459 (3) *D* | $\nu_5^{(2)}$ | B′ | Bending frequency |
| 1015 (8) *P* | 921 (8) *P* | $\nu_1$ | $A_1$ | Breathing frequency |
| 1462 (0*vb*) | — | $\nu_6^{(2)}$ | B′ | Asymmetric C—N valence frequency |
| 1565 (2*vb*) *D* | 1193 (1*b*) *D* | $\nu_7^{(2)}$ | B′ | Bending frequency |
| — | 1278 (1) *P* | $\nu_2$ | $A_1$ | Bending frequency |
| 1670 (1*vb*)? | — | $\nu_{10}^{(2)}$ | B″ | Bending frequency |
| — | 2127 (0?) | $2\nu_{10}^{(2)}$ | B′ | — |
| Resonance: | | | | |
| 3212 (3*b*) | — | $2\nu_{10}^{(2)}$ | B′ | — |
| — | 2374 (6) *P* $D_2O$? | — | — | — |
| 3290 (3*b*) | 2433 (6) *P* | $\nu_3$ | $A_1$ | Symmetric valence frequencies of N—H |
| 3360–3471 $H_2O$? | Obscured by 2433 | $\nu_8^{(2)}$ | B′ | N—D linkages |
| 3360–3471 | 2496–2591 (6) $D_2O$? | $\nu_{11}^{(2)}$ | B″ | Asymmetric valence frequency of N—H (N—D) linkages |

$$\left.\begin{aligned} f_{\mathrm{C-N}} &= 7{\cdot}1\times10^5 \text{ dynes/cm.}, & f_{\mathrm{N-H}} &= 6{\cdot}3\times10^5 \text{ dynes/cm.},\\ \delta_1 &= 0{\cdot}80\times10^5 \text{ dynes/cm.}, & \delta_2 &= 0{\cdot}14\times10^5 \text{ dynes/cm.},\\ 3d &= 0{\cdot}70\times10^5 \text{ dynes/cm.}, & \tau &= 0{\cdot}10\times10^5 \text{ dynes/cm.} \end{aligned}\right\} \quad (13)$$

The constants $\delta_2$ and $3d$ are suspiciously small, and no great reliance can be placed upon them. Nevertheless, table 9, in which the observed and calculated frequencies are compared, shows that the accuracy of the calculations (roughly ± 10 %) is quite reasonable.

TABLE 9. FREQUENCIES OF $C^+(NH_2)_3$ AND $C^+(ND_2)_3$

| Symmetry and vibration | | $C^+(NH_2)_3$ | | $C^+(ND_2)_3$ | |
|---|---|---|---|---|---|
| | | Calculated | Observed | Calculated | Observed |
| $A_1$ | $\nu_1$ | 1020 | 1015 | 924 | 921 |
| | $\nu_2$ | 1410 | Not observed | 1113 | 1278 |
| | $\nu_3$ | 3354 | 3290 | 2432 | 2433 |
| | $\nu_4$ | 622 | Not observed | 501 | Not observed |
| B′ | $\nu_5^{(2)}$ | 651 | 536 | 483 | 459 |
| | $\nu_6^{(2)}$ | 1501 | 1462 | 1360 | Not observed |
| | $\nu_7^{(2)}$ | 1534 | 1565 | 1320 | 1193 |
| | $\nu_8^{(2)}$ | 3370 | 3360–3471? | 2470 | 2496–2591? |
| | $\nu_9^{(2)}$ | 360 | Not observed | 342 | Not observed |
| B″ | $\nu_{10}^{(2)}$ | 1510 | 1670 | 1116 | $1063 = \frac{1}{2} \times 2127$ |
| | $\nu_{11}^{(2)}$ | 3445 | 3360–3471? | 2544 | 2496–2591? |
| | $\nu_{12}^{(2)}$ | 112 | Not observed | 108 | Not observed |

### 7. FORCE CONSTANTS AND MOLECULAR STRUCTURE OF UREA AND GUANIDONIUM

The interpretation given above of the guanidonium spectrum agrees very well with the assumption of complete resonance between the three C—N bonds. Urea would belong to the symmetry group $C_{2v}$ even if no resonance occurred in the molecule between the C=O and C—N linkages, but here confirmation of the resonance hypothesis comes from the values of the valence force constants, $f_{C-N}$ and $f_{C=O}$. It was mentioned in § 1 of the present paper that the force constants of the C—C valence bond are roughly proportional to the strength of the bond (single, double, triple, partial bond). The C—N single bond furnishes a force constant $f_{C-N}$ of $4{\cdot}86 \times 10^5$ dynes/cm. for methylamine according to Kohlrausch (1931) and of $4{\cdot}95 \times 10^5$ dynes/cm. according to Bailey, Carson and Daly (1939), while Kohlrausch (1931) obtained a value of $f_{C\equiv N} = 17{\cdot}9 \times 10^5$ for the C≡N triple bond. The study of the formaldehyde spectrum leads Sutherland and Dennison (1935) to a force constant $f_{C=O} = 13{\cdot}45 \times 10^5$ for the C=O double bond. The values obtained here for urea (7), $f_{C=O} = 9{\cdot}7 \times 10^5$ and $f_{C-N} = 6{\cdot}6 \times 10^5$, are considerably different from the above figures. As is to be expected in the case of resonance, the C—N force constant is greater for urea than for ordinary C—N single bonds (by 35 %), while the C=O force constant in urea is weakened by 39 % as compared with formaldehyde. It can therefore be concluded that in urea the C—N valence bond has partial double-bond character, while the C=O linkage is weakened by approximately the same amount. The spectrum of guanidonium furnishes $f_{C-N} = 7\cdot1 \times 10^5$ (13) in agreement with the assumption that each C—N bond has $\frac{1}{3}$ double-bond character. The force constants of the C—C, C—N and C—O valence linkages have been plotted as functions of the bond strengths in figure 5 as far as they are known. While these curves are not very far removed from straight lines for the C—C and C—N linkages, the C—O curve is irregular.

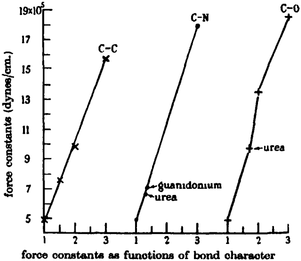

FIGURE 5. Force constants of the C—C, C—N bonds as functions of the bond character.

## REFERENCES

Angus, Bailey, Hale, Ingold, Leckie, Raisin, Thomson and Wilson 1936 *J. Chem. Soc.* p. 971.

Bailey, Carson and Daly 1939 *Proc. Roy. Soc* A, **173**, 339.

Kohlrausch 1931 *Der Smekal-Raman Effekt.*

Kohlrausch 1936 *Phys. Z.* **37**, 58.

Kohlrausch and Pongratz 1934 *Z. phys. Chem.* B, **27**, 176.

Lechner 1932 *S.B. Akad. Wiss. Wien*, IIa, **141**, 291.

Otvos and Edsall 1939 *J chem Phys* **7**, 634

Pauling, Brockway and Beach 1935 *J. Amer. Chem Soc* **57**, 2705.

Sutherland and Dennison 1935 *Proc. Roy Soc* A, **148**, 250

Theilacker 1935 *Z. Kristallogr.* **90**, 51 and 256.

Wyckoff and Corey 1934 *Z. Kristallogr.* **89**, 462.

# Submarine seismic investigations

By E. C. Bullard and T. F. Gaskell
*Department of Geodesy and Geophysics, Cambridge*

(*Communicated by Sir Gerald P. Lenox-Conyngham, F.R.S.—
Received 7 October* 1940)

The refraction seismic method has been used to investigate the form of the surface of the hard rocks underlying the sediments on the continental shelf to the west of the English Channel. This surface is found to slope steadily downwards on receding from the land, and to reach a depth of over 8000 ft. at the 100 fm. line. The velocity of elastic waves in the sediments is about 6000 ft./sec. near the surface and up to 9700 ft./sec. lower down, compared to 16,000—22,000 ft./sec. in the basement. The bearing of these results on the structure and history of the shelf is discussed.

## 1. Introduction

At the meeting of the International Union of Geodesy and Geophysics held at Edinburgh in 1936 Professor R. M. Field described some experiments that had been made by M. Ewing the year before (Ewing, Crary and Rutherford 1937). In these experiments the refraction seismic method had been used to determine the thickness of the sediments on the Continental Shelf on the eastern side of the United States. Part of the area studied was dry land and the measurements there presented no special technical difficulty, but part was submerged, and the novel feature of the work was that it had been found possible to use the method at sea. Professor Field suggested that similar work should be undertaken on this side of the Atlantic. In 1937 Dr Bullard visited the United States on the invitation of Professor Field and learnt in detail from Professor Ewing how his work had been carried out.

On returning to England application was made through the National Committee on Seismology to the Royal Society for funds, and to the Hydrographer, Vice-Admiral Edgell, for a ship. These requests were granted, the Admiralty allowed the use of H.M.S. *Jason*, an 850 ton surveying ship, for a week in July 1938, and the Royal Society appointed a committee under the chairmanship of Admiral Edgell to administer the funds and to direct the work. Preliminary experiments were made in Lake Windermere with the co-operation of the Fresh Water Biological

Station; in the Wash with a ship lent by the Great Ouse Catchment Board, and in Plymouth Sound in the *Salpa*, a trawler lent by the Marine Biological Station. These experiments were valuable and enabled various difficulties to be overcome which might have seriously hindered the work in the *Jason*; the thanks of the authors are due to the directors of the Fresh Water and Marine Biological Stations and to the Engineers of the Ouse Catchment Board for their co-operation.

The experiments on board the *Jason* were carried out by the authors assisted by Mr L. H. Flavill. A preliminary account has been published (Bullard and Gaskell 1938), but it was thought desirable to make further measurements in 1939 to supplement those of 1938. For this purpose two Brixham trawlers, the *Arthur Rogers* and the *Renown*, were hired. These ships were constructed of wood and were of 60 tons displacement and 60 ft. long, and both were provided with sails and with auxiliary engines The former was in charge of her owner Mr Byng and was manned by an amateur crew, the latter had a professional skipper and cook and an amateur crew. Experiments were made with these ships for a fortnight in June 1939. Mr T. F. Gaskell and Mr B. C. Browne were in the *Arthur Rogers* and Dr Bullard and Mr Flavill in the *Renown*.

From the above account it will be clear that the work could not have been carried out without the co-operation of those controlling the ships. Success would also have been impossible without the assistance and advice of the captains, officers and crews of the *Jason*, the *Arthur Rogers* and the *Renown*. Our special gratitude is due to Vice-Admiral Edgell, to Captain Hardy and Lieutenant Griffiths of the *Jason*, and to Mr Byng, owner of the *Arthur Rogers*.

## 2. APPARATUS AND TECHNIQUE

The technique employed was similar to that described by Ewing, Crary and Rutherford (1937). A geophone was lowered to the bottom of the sea from an anchored ship, and charges of explosive were fired from a second vessel which was not anchored. In 1938 the geophones employed for work on land were used. These instruments, which have been described by Bullard and Kerr-Grant (1938), were enclosed in watertight cases (figure 1) with heavy bases. In the preliminary work a method was devised for laying three of these instruments, the right way up, in a line on the sea bottom. This worked satisfactorily in 20 fm. in Plymouth Sound, but when it was tried in 40 fm. off the Lizard it resulted in the loss of two instruments and 3000 ft. of cable. After this it was decided to use only one geophone. The instrument was lowered by the steel wire of the Lucas sounding machine of the *Jason*; the wire being attached to the top, and the electric cable being paid out with some slack so that the strain came on the steel wire. The instrument was suspended about 2 fm. from the bottom until just before firing a shot, and was then lowered to the bottom. The steel and the electric cables were then slowly paid out till the shot had been fired. After the shot had been fired the instrument was again raised off the bottom and the slack in the electric cable pulled in. In this way when the ship swung round the geophone was free to come with it, and the cable did not become twisted round the anchor chain, as sometimes occurs if the geophone is left on the bottom. To prevent pulls on the cable, due to the ship's motion and to currents, from disturbing the geophone a 30 lb. weight was attached to both cables about 6 ft. from the geophone. When a shot was fired this weight rested on the bottom near the geophone.

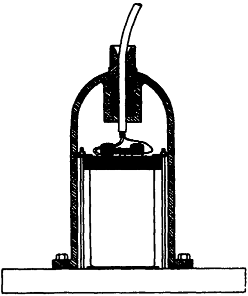

FIGURE 1. Geophone used in 1938 (overall diameter 10 in.).

The experience in 1938 showed that it was desirable to design a special geophone for use at sea. It was desirable that the instrument should be robust and that it should work in either the erect or inverted position. The instrument used in 1939 is shown in figure 2 *a* and *b*. It consisted of a horseshoe magnet lying in a horizontal plane and constrained by springs so that it could only move in a vertical direction. Above and below the magnet were a pair of armatures carrying coils connected in opposition. The instrument was damped by filling the case with oil. The gaps were about 2 mm. wide and the natural period about 0·03 sec. The sensitivity and its variation with frequency were similar to those of the instrument used in 1938. The steadiness of the records from this instrument before the explosion occurred was better than that of those used in 1938 and about twice the amplification could be employed. If the precautions are taken of paying out slack whilst a record is being taken and of providing a weight near the geophone, the steadiness of the instrument is as good as or better than that usually found on land.

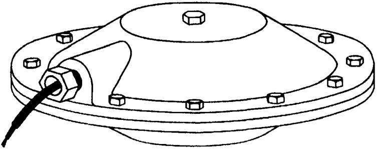

FIGURE 2*a*. Exterior of geophone used in 1939 (overall diameter 10 in.).

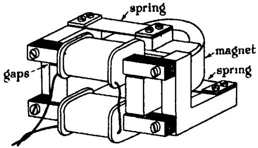

FIGURE 2*b*. Mechanism of geophone used in 1939.

The output from the geophone was amplified by a three-valve amplifier, resistance-capacity coupled (two H 2 valves and one PM 2A), and fed through a transformer to two of the strings of a six-string galvanometer. One of these strings was shunted to give a record of about a fifth of the amplitude of the other; in this way the record was not lost when the amplitude became so large that the shadow of the string recording at full sensitivity was not recorded. The galvanometer was one of the type used in sound ranging in the 1914–18 war and was presented to us by the Royal Air Force Experimental Station. The harp was modified to allow the strings to pass each other. A time scale was provided by a reed, driven by a 100-cycle valve-maintained tuning fork.

In 1938 the explosive used was T.N.T. in 1¼ lb. blocks; a number of these blocks were tied together, a primer was provided for every four blocks, and the central block carried an electric detonator. In 1939 blasting gelatine in 10 lb. sticks was used. These were placed in open tin cans which were tied together and weighted with clay; one 160 lb. charge was packed in a dust bin. The blasting gelatine is much cheaper than T.N.T. and seems to give a bigger ground motion. In 1938 the explosive was lowered from one of the *Jason*'s boats. It was only safe to launch the boat on fairly calm days and in consequence measurements could only be made on five days. It was thought that this difficulty could be avoided by using two small ships in place of a large ship and a boat. It was this that led to the hire of the two trawlers for the 1939 work. It was found that the proportion of days on which it was possible to work was not much increased as the *Renown* could not safely be anchored in deep water except on fairly calm days. The anchor employed was a 1 cwt. CQR designed by Professor G. I. Taylor; with this anchor and 150 fm. of cable on a hand winch it was found possible to anchor in a depth of 100 fm. It was not possible to handle charges greater than 60 lb. from the *Jason*'s boat, and it is an advantage of the use of two trawlers that it allows charges of any size to be used. The largest charge (160 lb. of blasting gelatine in 100 fm.) did not damage the ships, though the *Arthur Rogers* received a very noticeable blow from the sound wave. Some care would be necessary if larger charges were to be used in shallow water.

The instant of explosion was recorded by the breaking of a wire wrapped round the charge. This wire was included in the modulator circuit of a wireless transmitter. The signal was received on the recording ship and fed to one string of the galvanometer. In preliminary experiments in 1938 40 megacycle transmitters and receivers were used, but considerable trouble was experienced with variations in wave-length when the boat with the explosives rolled. A 7 megacycle transmitter and 40 megacycle receiver were finally used on the boat and a 40 megacycle transmitter and 7 megacycle receiver on the *Jason*. In 1939 transmitters working on 7·0 and 7·3 megacycles, stabilized with crystal oscillators, were used. These transmitters radiated about ¼ watt and permitted duplex telephony, which is a great convenience. Some trouble was caused by loose rigging; the transmitter induced currents into various wires on the ship, and sudden variations in these currents due to changes in resistance at loose joints caused clicks in the receiver. These clicks sometimes appeared on the records and are difficult to distinguish from the marks showing the instant of explosion.

The distance from geophone to explosion was measured roughly by taking the mast-head angle of the recording ship from the explosives boat. Preliminary trials showed, in agreement with Ewing's experience, that the wave travelling through the water from the explosion to the geophone was clearly recorded and enabled the distance to be determined from the known velocity of sound in sea water. The records taken on the *Jason* did not always show this wave as clearly as could be wished, and in 1939 a hydrophone was hung over the ship's side at a depth of about 20 ft. and connected through an amplifier to one of the strings of the galvanometer. This always showed the sound through the water very clearly and usually enabled it to be identified with certainty on the geophone record. The distance from the explosion to the geophone is not exactly equal to that to the hydrophone, and it is therefore preferable to use the wave on the geophone record when it can be identified.

## 3. Account of the operations

The *Jason* sailed from Portsmouth on Sunday, 10 July 1938. The weather next day was too rough for the boat with the explosives to be lowered, but by the 12th it had improved sufficiently for measurements to be made at station no. 1, 3·8 miles south of the Lizard (figure 3). Three instruments were laid on the sea bottom, but the swinging of the ship with the tide caused two of them to be lost, after which it was decided to use only one instrument at a time and to attach a steel cable to it. During the night the *Jason* moved 112 miles west-south-west to station 5, on the 13th measurements were made at this station, but only a lower limit was obtained for the thickness of the sediments. The *Jason* then moved 53 miles further west-south-west to station 7; on the 14th, measurements were made at this station; again no bottom could be found to the sediments with the amount of explosive that it was possible to handle from the boat. The sea next day was too rough to allow the boat to be launched and the *Jason* moved east-north-east again to station 2, and on the 16th a good set of records was obtained. On the 17th, measurements were made at station 3. The *Jason* sailed homewards that evening and arrived at Swanage on Monday, 18 July.

The *Arthur Rogers* and the *Renown* sailed from Plymouth on Saturday, 3 June 1939; next day both ships put into St Mary's in the Scilly Isles On the 5th, two shots were fired in the anchorage to determine the velocity of elastic waves in the granite there. Both ships then sailed to station 4 and the *Renown* anchored. Next day measurements were made at this station, and during the night both ships sailed to station 6, where measurements were made on the 7th. It was intended to make the next measurements near station 7, which had been visited in 1938, but the next two days were

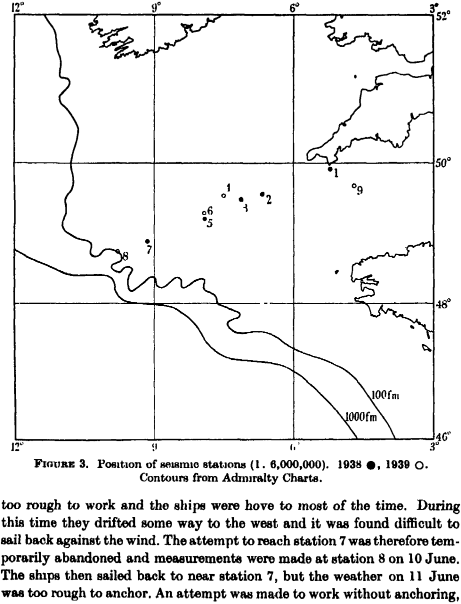

FIGURE 3. Position of seismic stations (1 : 6,000,000). 1938 ●, 1939 ○. Contours from Admiralty Charts.

too rough to work and the ships were hove to most of the time. During this time they drifted some way to the west and it was found difficult to sail back against the wind. The attempt to reach station 7 was therefore temporarily abandoned and measurements were made at station 8 on 10 June. The ships then sailed back to near station 7, but the weather on 11 June was too rough to anchor. An attempt was made to work without anchoring, but it was found impracticable to prevent the ship from pulling on the cables and disturbing the geophone. As the weather appeared to be getting worse it was decided to return to Helford. The *Arthur Rogers* arrived there on the evening of the 12th and the *Renown* on the 13th. On 14 June measurements were made at station 9 in mid-channel, and on Thursday, 15 June, both ships returned to Plymouth.

## 4. RESULTS

A typical record is illustrated diagrammatically in figure 4. The first event to be recorded is the wireless signal indicating that the explosion has occurred (*A*, figure 4); next a wave travels through the water to the boat carrying the explosive, modulates the wireless transmitter by shaking it, and is therefore recorded by the string connected to the wireless receiver (*B*, figure 4). The separation of the two records is the time taken for the wave to travel from the explosion to the boat; this is the time taken to travel through a distance rather greater than the depth of the water. At short distances the next event to be recorded is the arrival at the geophone of the wave through the sediments, but at greater distances this is preceded by the refracted wave which has travelled down through the sediments, along in the rocks below, and up again, the arrival of such a wave is illustrated at *C* in figure 4. This first arrival may be succeeded by waves through the sediments (*D*, figure 4) Before the latter have subsided, the sound through the water will arrive at the hydrophone, which has until then been steady (*E*, figure 4). The same wave may or may not be apparent on the geophone record (*F*, figure 4).

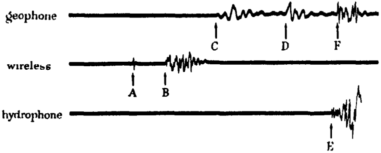

FIGURE 4. Diagrammatic illustration of a record

Figure 5 is a reproduction of a record taken at station 6 with 20 lb of blasting gelatine at a distance of 22,210 ft. Only the geophone trace is reproduced, but the points at which the wireless records the instant of explosion and the hydrophone records the arrival of the sound are marked. At 4·2 sec. the trace recorded at full sensitivity becomes illegible owing to its great amplitude, but the low sensitivity trace (reproduced above the other) prevents the record being lost.

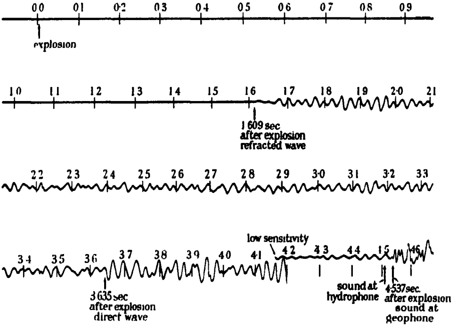

FIGURE 5. Reproduction of the geophone trace at station 6 at 22,210 ft. The record is half full size.

The positions of the stations are shown in figure 3 and in table 3. The times and distances are summarized in table 1 and the deduced thicknesses and velocities for the various layers in table 2. The geophone was kept at a fixed point and a number of explosions were fired along a line passing through the geophone. When sufficient shots had been fired on one side of the geophone the explosives boat usually sailed to a suitable distance on the other side and a further shot was fired. The record from this shot enabled any slope of the surface separating the sediments from the underlying rock to be detected, and the error produced by it in the measured velocities to be allowed for.

The methods used in reducing such observations have recently been discussed by the authors in some detail (Bullard, Gaskell, Harland and Kerr-Grant 1940) and this discussion will not be repeated here. Straight lines were fitted by least squares to the observed times of arrival of the

TABLE 1. TIMES AND DISTANCES

| Station no. | Wt. of explosive lb.† | Distance ft. | Time sec. | | | Residuals $10^{-3}$ sec. | | |
|---|---|---|---|---|---|---|---|---|
| 1 | T.N.T. | 430 | — | — | 0·045 | — | — | — |
| | ,, | 790 | — | — | 0·082 | — | — | — |
| | ,, | 1,870 | — | 0·190 | — | — | +4 | — |
| | ,, | 2,605 | — | 0·243 | — | — | −3 | — |
| | ,, | 4,210 | 0·377 | 0·377 | — | +1 | −3 | — |
| | ,, | 5,230* | 0·435 | — | — | (+12)* | — | — |
| | ,, | 6,890 | 0·497 | 0·605 | — | −2 | +2 | — |
| | ,, | 8,540 | 0·576 | — | — | +1 | — | — |
| 2 | 1½ T.N.T. | 700 | — | 0·112 | — | — | 0 | — |
| | 5 ,, | 1,980 | — | 0·288 | — | — | −28 | — |
| | 12½ ,, | 3,370 | 0·380 | — | — | −19 | — | — |
| | 12½ ,, | 4,480 | 0 460 | 0·709 | — | −6 | −6 | — |
| | 23¾ ,, | 5,900* | 0·620 | 0·940 | — | (+68)* | 0 | — |
| | 17½ ,, | 6,080 | 0·590 | 0·980 | — | +27 | +11 | — |
| | 20 ,, | 8,400 | 0·720 | — | — | +16 | — | — |
| | 37½ ,, | 9,040 | 0·746 | — | — | +3 | — | — |
| | 50 ,, | 11,320 | 0·860 | — | — | −21 | — | — |
| | 25 ,, | 12,130 | 1·03? | Record too feeble to use | | | | |
| 3 | 2½ T.N.T. | 660 | — | 0·096 | — | — | +6 | — |
| | 5 ,, | 2,270 | — | 0·298 | — | — | −12 | — |
| | 10 ,, | 3,260 | 0·380 | 0·440 | — | −4 | −6 | — |
| | 15 ,, | 3,970 | 0·420 | 0·560 | — | +6 | +17 | — |
| | 25 ,, | 5,040* | 0·560 | 0·700 | — | (+102)* | +11 | — |
| | 20 ,, | 5,270 | 0·470 | 0·740 | — | +3 | +19 | — |
| | 62½ ,, | 6,990 | 0·530 | 0·930 | — | −8 | −26 | — |
| | 30 ,, | 8,930 | 0 620 | — | — | +2 | — | — |
| 4 | 1½ B.G. | 1,610 | — | 0 244 | — | — | +7 | — |
| | 2½ ,, | 2,230 | — | 0·342 | — | — | −5 | — |
| | 5 ,, | 6,270 | 0·628 | 0·968 | — | −4 | −8 | — |
| | 10 ,, | 8,210 | 0·727 | 1·30 | — | +8 | +20 | — |
| | 15 ,, | 10,540 | 0 820 | 1·63 | — | −4 | −10 | — |
| 5 | 1¼ T.N.T. | 940 | 0 172 | — | — | — | — | — |
| | 3¾ ,, | 2,740 | 0 450 | — | — | — | — | — |
| | 5 ,, | 3,638 | 0·546 | — | — | — | — | — |
| | 6¼ ,, | 4,932 | 0·73 | — | — | — | — | — |
| | 7½ ,, | 6,510 | 1·224 | — | — | — | — | — |
| | 10 ,, | 8,100 | 1·44 | — | — | — | — | — |
| 6 | 1 B G | 420 | — | 0·073 | — | — | +5 | — |
| | 2 ,, | 3,250 | — | 0 492 | — | — | −36 | — |
| | 10 ,, | 8,730 | 0 929 | 1·37 | — | +39 | −48 | — |
| | 18 ,, | 9,780* | 0·831 | 1·538 | — | (−113)* | — | — |
| | 8 ,, | 9,840 | 0·948 | 1·605 | — | 0 | +6 | — |
| | 15 ,, | 13,490 | 1·076 | 2·182 | — | −62 | −10 | — |
| | 20 ,, | 22,210 | 1 609 | 3 635 | — | +21 | +27 | — |
| | 40 ,, | 38,530 | 2 528 | — | — | (+68) | (explosion marker ambiguous) | |

* Shot on other side of recording ship.

† T.N.T. = Trinitrotoluene, B G. = Blasting gelatine.

Table 1 (*continued*)

| Station no. | Wt. of explosive lb. | Distance ft. | Time sec. | | | Residuals $10^{-3}$ sec. | | |
|---|---|---|---|---|---|---|---|---|
| 7 | 1¼ T.N.T. | 280 | — | — | 0·048 | — | — | −1 |
| | 2½ „ | 600 | — | — | 0·113 | — | — | +9 |
| | 1¼ „ | 1,110 | — | — | 0·200 | — | — | +7 |
| | 5 „ | 3,530 | — | — | 0·596 | — | — | −17 |
| | 8¾ „ | 4,260 | — | — | 0·766 | — | — | +26 |
| | 12½ „ | 4,900 | — | 0·774 | — | — | −11 | — |
| | 15 „ | 6,260 | — | 0·951 | 1·146 | — | +25 | +58 |
| | 20 „ | 8,040 | — | 1·128 | — | — | +18 | — |
| | 25 „ | 10,940 | — | 1·421 | — | — | +10 | — |
| 8 | 5 B G. | 4,780 | — | 0·742 | — | — | −30 | — |
| | 10 „ | 13,370 | — | 1·667 | 2·23 | — | +4 | −90 |
| | 10 „ | 17,630 | — | 2·091 | 3·05 | — | −14 | −10 |
| | 20 „ | 24,350 | 2·722 | — | 4·13 | +7 | — | −100 |
| | 40 „ | 31,870 | 3·028 | — | 5·52 | −5 | — | −20 |
| | 70 „ | 39,080 | 3·397 | — | 6·85 | +57 | — | +60 |
| | 80 „ | 43,170 | 3·497 | — | 7·46 | −16 | — | −40 |
| | 160 „ | 50,560 | 3·748 | — | 8·87 | −80 | — | +80 |
| | 140 „ | 59,710 | 4·248 | — | — | +33 | — | — |
| 9 | 1 B G. | 500 | — | 0·051 | — | — | −1 | — |
| | 2 „ | 2,460 | — | 0·212 | — | — | −42 | — |
| | 4 „ | 4,410 | — | 0·460 | — | — | +4 | — |
| | 6 „ | 6,770 | 0·712 | 0·712 | — | +2 | +12 | — |
| | 20 „ | 8,230 | 0·814 | — | — | −11 | — | — |
| | 28 „ | 12,390 | 1·186 | — | — | +34 | — | — |
| | 40 „ | 14,000 | 1·252 | — | — | −26 | — | — |
| | 70 „ | 16,480 | 1·474 | — | — | +1 | — | — |

waves. The velocities and intercepts obtained, together with their standard errors, are given in table 2. In computing the standard errors of the velocities no allowance has been made for the possible effect of undetected slope. In table 1 the observed times and the residuals from the adopted lines are arranged in columns so that at any station the points lying on one line are in the same column. It was found that the line corresponding to the direct wave usually went through the origin within the uncertainty of measurement, in the least squares reduction of such lines the intercept was forced to be exactly zero.

*Station* 1. This station is 3·8 miles south of the Lizard. The first two points on the time-distance curve (figure 6) give a velocity of 9000 ft./sec. The next three points and a second arrival on the shot at 6890 ft. give 12,000 ft /sec. Shots at 4210, 6890 and 8540 ft. give a velocity of 21,760 ft./sec. The time-distance graph indicates an increase in velocity from 9000 to 12,000 ft./sec. in the first 200 ft., followed by a sudden change to

TABLE 2. SUMMARY OF VELOCITIES AND INTERCEPTS

| Station no. | Velocity ft./sec. | Intercept sec. | Thickness ft. |
|---|---|---|---|
| 1 | 9,000 | 0·000 | 200 |
| | 12,000 ± 150 | 0·029 ± 0·005 | 1020 |
| | 21,760 ± 380 | 0·183 ± 0·006 | |
| | | | Total 1220 |
| 2 | 6,270 ± 60 | 0·000 | 650 |
| | 16,490 ± 890 | 0·194 ± 0·025 | |
| 3 | 7,310 ± 80 | 0·000 | 960 |
| | *24,350 ± 830 | 0·251 ± 0·008 | |
| 4 | 6,420 ± 50 | 0·000 | 1170 |
| | 22,200 ± 1600 | 0·350 ± 0·025 | |
| 5 | Combined with station 6 | | |
| 6 | 6,160 ± 50 | 0·000 | 1420 |
| | †19,290 ± 2040 | 0·437 ± 0·071 | |
| 7 | Combined with station 8 | | |
| 8 | 5,750 ± 20 | 0·000 | 990 |
| | 9,640 ± 170 | 0·276 ± 0·019 | 7120 |
| | 23,550 ± 1140 | 1·680 ± 0·089 | |
| | | | Total 8110 |
| 9 | 9,680 ± 270 | 0·000 | 1320 |
| | 12,730 ± 520 | 0·178 ± 0·039 | |

* 19,000 ft./sec. if allowance is made for slope.

† 21,000 ft./sec. if allowance is made for slope.

TABLE 3. SUMMARY OF RESULTS

| Station no. | Lat. N | Long. W | Depth of sea (ft.) | Depth to hard rock: Below sea bottom (ft.) | Depth to hard rock: Below sea level (ft.) |
|---|---|---|---|---|---|
| 1 | 49° 55′ | 5° 12′ | 270 | 0 | 270 |
| 2 | 49 34 | 6 40 | 360 | 650 | 1010 |
| 3 | 49 30 | 7 09 | 360 | 1010 | 1320 |
| 4 | 49 33 | 7 30 | 410 | 1170 | 1580 |
| 5 | 49 13 | 7 55 | 450 | > 1400 | > 1850 |
| 6 | 49 18 | 7 55 | 440 | 1420 | 1860 |
| 7 | 48 54 | 9 10 | 520 | > 3570 | > 4090 |
| 8 | 48 45 | 9 48 | 590 | 8110 | 8700 |
| 9 | 49 41 | 4 42 | 280 | 0 | 280 |

21,760 at a depth of 1220 ft. It is quite possible that the increase from 9000 to 12,000 is gradual, although two layers have been assumed for convenience of calculation.

The rock with a velocity of 21,760 ft./sec. is presumably similar to the igneous rocks exposed on the neighbouring land, where the velocity in a gabbro has been determined by Gaskell and Harland to be 20,500 ft./sec. It is surprising to find that this rock is so deeply buried at a point only 3·8 miles from its outcrop. The wave from a shot at 5230 ft. on the opposite side of the recording ship arrived 0·011 sec. later than was expected from the straight line through the other points. This would indicate that the interface was sloping at 1 in 90 along the line away from the land, but with so few shots this cannot be regarded as certain. The velocity found for the overlying material is much too great for recent sediments near the surface (compare the velocities found at the other stations or in the Mesozoic clays of East England), and is that to be expected for a hard shale or a sandstone. This result is discussed below.

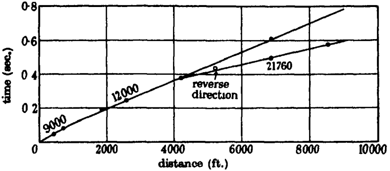

FIGURE 6. Time-distance graph for station 1.

*Station* 2. Eleven shots were fired at distances up to 12,130 ft. Insufficient explosive was used for the furthest shot and the results were not used in the calculation. The time-distance graph is shown in figure 7. A layer giving a velocity of 6270 ft./sec. and a thickness of 650 ft. is indicated, overlying rock giving a velocity of 16,490 ft./sec. A shot in the reverse direction indicates a slope of 2° along the line. If this persists all along the line the true velocity would be 14,900 ft./sec. The velocity in the top layer indicates a fairly well consolidated sediment. The rock below may well be granite similar to that in the Scilly Isles 20 miles to the north-east, where a velocity of 15,390 ± 130 ft./sec. was obtained in 1939. The velocity here is definitely lower than that at most of the other stations.

*Station* 3. Eight satisfactory records were taken between 665 and 8934 ft. Two records at 11,300 and 12,620 ft. were too feeble to be used. The time-distance graph is shown in figure 8. The results indicate a thickness of 980 ft. of material with a velocity of 7500 ft./sec., overlying material with a velocity of 24,350 ft./sec. A shot in the reverse direction gives a point above the 24,350 ft./sec. line, indicating a slope of 4°, the sediment being thickest to the south-east. If this slope exists all along the line the velocity below the sediment would be 19,000 ft /sec

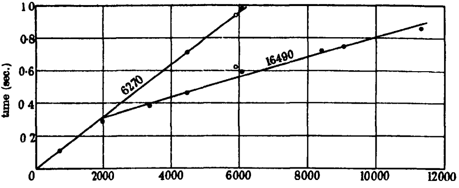

FIGURE 7. Time-distance graph for station 2.

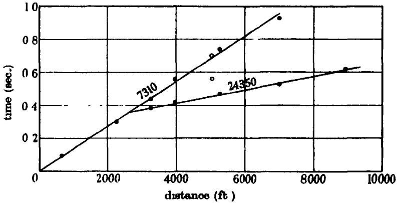

FIGURE 8. Time-distance graph for station 3.

*Station* 4. This was the first station visited in 1939. It was intended to be midway between stations 3 and 4, but owing to an error in navigation it is 10 miles to the north of the intended position A transition from 6420 to 22,200 ft./sec. is found at a depth of 1170 ft. Unfortunately the instant of explosion is not recorded on two records taken at about 4000 and 5000 ft.; these records show the direct and refracted waves and the sound very clearly, but in the absence of an explosion mark neither the distances nor the times are known exactly. The failure of these two records greatly increases the uncertainty of the velocity in the lower layer and of the calculated depth, but in a general way there is no doubt about the result. The time-distance graph is shown in figure 9.

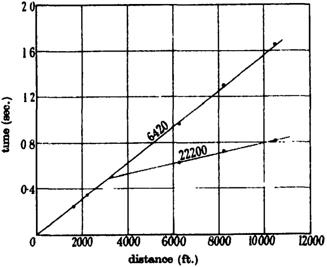

FIGURE 9. Time-distance graph for station 4.

*Station* 5. Nine records were taken at distances up to 14,000 ft, but insufficient explosive was used for the longer shots. The results merely show that there is no rock giving a velocity as great as 20,000 ft./sec. within 1400 ft. of the surface. The measurements are plotted on figure 10 with those at the neighbouring 1939 station no. 6.

*Station* 6. This was the second station visited in 1939. It was intended to be at the same point as the 1938 station, but is 5 miles to the north. The observations at the shorter distances agree with those at station 5 (see figure 10). At greater distances a refracted wave with a velocity of about 19,000 ft./sec. is observed. A shot in the reverse direction indicates a slope of 2°. If this extends all along the line the true velocity would be 21,000 ft./sec.

*Station* 7. Too little explosive was used for the shots beyond 11,000 ft. and the records are too weak to use. The nine nearer records give times that do not give a straight line on a time-distance graph. The first three records give a straight line, which is continued by second arrivals on some of the later records. This probably indicates a layer giving a velocity of about 5750 ft./sec. and with a more or less definite lower boundary. Below this the velocity increases to about 9640 ft./sec. It is clear from the records that no branch of the time-distance curve giving a velocity as great as 20,000 ft./sec. can have an intercept less than 0·80 sec. This sets a lower limit of 3570 ft. to the thickness of the sediments and indicates that no rocks with this velocity lie at less than 4000 ft. below sea level. The unsuccessful attempts to extend the measurements at this station in 1939 have been described above.

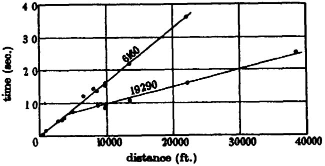

FIGURE 10. Time-distance graph for stations 5 and 6. ⊕ station 5, ● station 6.

*Station* 8. This station is about a mile inside the 100 fm. line and very near the edge of the Continental Shelf (the edge being taken as the line where the slope of the sea floor changes from about 1 in 3000 to 1 in 30). The results obtained in 1938 at station 7 had suggested that sediments of a thickness approaching 10,000 ft. might exist at this station and that a long line would therefore be necessary. Nine records were taken at distances between 4780 and 59,710 ft. The records at the shorter distances agreed with those taken at station 7. A pulse lying near the low velocity line observed at station 7 is recorded on nearly all the records. The records out of 20,000 ft. give points lying on the higher velocity line found at station 7. The results from station 7 have therefore been combined with those at this station, and the combined time-distance graph is shown in figure 11. A branch of the time-distance curve giving a velocity of 23,550 ft./sec. is observed on six records taken at distances between 24,000 and 60,000 ft. The sound, besides being recorded by the microphone, is also visible on the geophone records, its sharp onset occurring on the more distant records over 1 sec. after the rather gradual onset of the 5750 ft./sec. wave. There is therefore little doubt that the latter really is a wave through the sediments and not a wave through the water.

The fast wave from the rock below the sediments is particularly well observed at this station, and the calculated value of the depth should be more accurate than at most of the other stations.

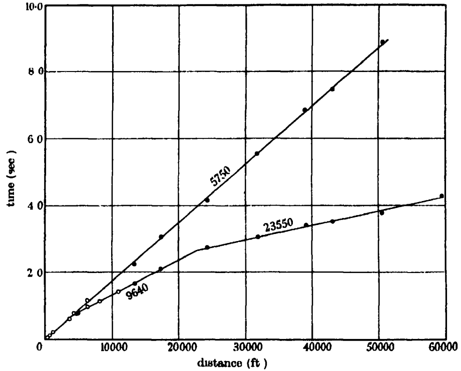

FIGURE 11 Time-distance graph for stations 7 and 8. ○ station 7, ● station 8.

*Station* 9. The object of the measurements at this station was to determine whether the material giving a velocity of 9000–12,000 ft./sec. found at station 1 near the Lizard extended to the middle of the Channel The results show that there is no unconsolidated sediment, the velocity being about 9700 ft./sec near the surface and increasing to about 12,700 ft /sec at a depth of about 1300 ft. The increase may well be continuous, although it has been treated as discontinuous for purposes of calculation. There is no sign of a wave with a velocity of about 20,000 ft./sec.; such a wave would have been observed if its time-distance line had an intercept of more than 0·5 sec From this it may be shown that rock giving a velocity of 20,000 ft./sec. cannot be present at a depth of less than 3400 ft. below the bottom of the sea. The considerable thickness of rocks with a velocity of 9000–12,000 ft./sec. found at these two stations indicates that the igneous and metamorphic rocks that form the southernmost points of Cornwall (Land's End, the Lizard, the Eddystone Rock, etc.) do not form the floor of the Channel.

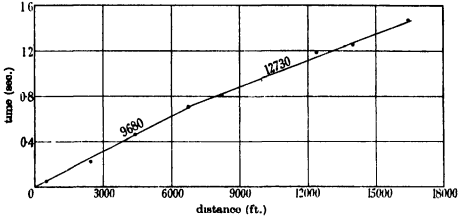

FIGURE 12. Time-distance graph for station 9

## 5. ERRORS

The residuals in the last three columns of table 1 have been used to calculate the standard error of one observation. For this purpose the waves that arrive first were treated separately from those arriving when the ground was already in motion, and each group was divided into those with transmission times of less than and greater than 0·7 sec. The results were

30 first arrivals taking less than 0·7 sec.,
standard error = $16 \times 10^{-3}$ sec.
28 first arrivals taking more than 0·7 sec.,
standard error = $34 \times 10^{-3}$ sec.
4 second arrivals taking less than 0·7 sec.,
standard error = $12 \times 10^{-3}$ sec.
21 second arrivals taking more than 0·7 sec.,
standard error = $52 \times 10^{-3}$ sec.

Allowance has been made for the 24 velocities and intercepts that have been determined before the residuals were calculated. These figures may be compared with the $3 \times 10^{-3}$ sec. obtained in work on land with very similar apparatus (Bullard *et al.* 1940). The impression gained from measuring the records is that the uncertainty for the shorter shots is two or three thousandths of a second and for the more distant ones about fifteen thousandths, rising to perhaps twenty-five thousandths for some of the very distant second arrivals. The considerable excess of the observed errors over these values might be accounted for by departures of the rocks from uniformity, but we are not satisfied that this conclusion is justified. On the 1939 cruise the disturbances caused to the wireless by loose rigging occasionally made the record of the instant of explosion a little indefinite, also the record of the sound on the microphone is often preceded by a small disturbance which can cause some ambiguity when the sound is not discernible on the geophone record. These causes may have produced a few large residuals which have increased the standard error. If further work were done it would be desirable to arrange that the breaking of the wire round the charge caused the transmitter to send a 500 cycle note instead of a pulse as at present.

## 6. NATURE OF THE SEDIMENTS

The velocities found for the waves travelling in the top 1000 ft. of sediments vary from 5750 to 7310 ft./sec. This may be compared with 4900–6300 ft./sec. found in the coastal plain of Virginia (Ewing *et al.* 1937), and with 5900 in the Gault, 5000–7000 in the Oxford Clay, and 7600–8700 ft./sec. in the Lower Lias of East England. The velocities found are therefore what might reasonably be expected for marine sediments that have undergone no very extreme degree of consolidation.

Stations 7 and 8 where the depth of the floor is greatest show that the velocity increases to about 9600 ft./sec. It is a matter of great importance to the subsequent argument to determine whether the rock giving this velocity is similar to the sediments above, only more thoroughly consolidated by the weight of the overlying rocks, or whether it is separated from them by a major unconformity. In the former case there is at the edge of the shelf a thickness of over 8000 ft. of more or less continuous sediments laid on a basement of rocks giving a velocity of about 20,000 ft./sec. In the latter case we have two separate sedimentary series of possibly widely differing ages; there might for instance be a Palaeozoic series giving the 9600 ft./sec., overlain by recent sediments.

The evidence on which this matter has to be decided is not entirely conclusive, but as there is little prospect of collecting more for some time to come, it seems worth while to discuss it. Measurements of velocity in thick sedimentary series in other parts of the world have given comparable velocities at similar depths. For instance, data quoted by Ewing and Leet (1932) give the velocities shown in table 4 for the sediments of Louisiana.

TABLE 4

| Depth ft. | Velocity ft./sec. |
|---|---|
| 0 | 4500 |
| 2000 | 6680 |
| 4000 | 7890 |
| 6000 | 8870 |
| 8000 | 9720 |

There is therefore nothing in the velocity of 9600 ft./sec. to suggest that the rocks are not unmetamorphosed sediments. Further the velocity is exceptionally low for the English Palaeozoic or Pre-Cambrian; Bullard *et al.* (1940) measured twenty-six velocities all lying between 11,260 and 19,600 ft./sec. A few measurements of velocities in the Palaeozoic and Pre-Cambrian rocks of West England have been made without finding any with a velocity as low as 9600. It would therefore be somewhat surprising if the 9600 ft./sec. rock were Palaeozoic. It is desirable that further measurements should be made, since some types of rock, in particular the Old Red Sandstone and the Coal Measure shales, have not been studied. It may, however, be assumed tentatively that these rocks are unmetamorphosed but fairly well consolidated sediments, similar to those found in bore holes on the Atlantic coastal plain of the U.S.A.

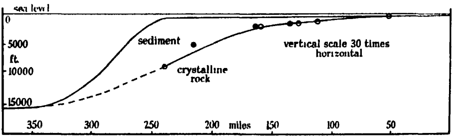

FIGURE 13. Section along the line of measurements. The two stations marked ● give only an upper limit to the level of the crystalline rocks.

## 7. THE FORM OF THE FLOOR

Figure 13 shows a section along the line of measurements; the results used are summarized in table 3. It shows that the floor slopes gradually seawards, and that if this slope were extrapolated it would pass over smoothly into the floor of the deep ocean beyond. Whether the floor is in fact continuous across the edge of the shelf it is impossible to say, and further investigation of the matter on the eastern side of the Atlantic is for the present impossible. If the floor is continuous then the edge of the shelf cannot mark the site of a fault, and must represent merely the edge of a pile of sediments growing seaward. There is good evidence from the presence of erratics on the sea floor that sedimentation is not at present going on in the western approaches to the English Channel. It may therefore be supposed that a particle of sediment falling on the sea floor is not able to rest there, but is carried hither and thither by wave and current action until it comes to rest in deeper and quieter water on the slope beyond the 100 fm. line. The surface of the shelf would consist of material having a grain size that could just not be moved by wave motion and currents. Such a process would result in the shelf gradually growing forward on the downward sloping surface of the floor, whilst the sea bottom on the shelf was covered throughout by relatively coarse sand (Shepard and Cohee 1936). At the edge landslips would occur and maintain the slope at the angle of repose. In this way great thicknesses of "slumped" sediments of the kind described by Jones (1939) and others would be produced. The weight of the superincumbent sediments would drive out some of the water and to some extent consolidate the lower part of the sediments, and would produce the observed increase in velocity. The sediments would lie in lens-shaped masses, as shown in figure 14, the older rocks lying below and to the west of the younger. The progress of sedimentation may be interrupted by vertical movements or by changes of currents, and the succession is not necessarily continuous. How long the total time required may be we have no means of estimating. In the Atlantic coastal plain of the United States most systems from Cretaceous to recent are represented, and analogy suggests that the European continental shelf is not likely to be entirely of recent origin.

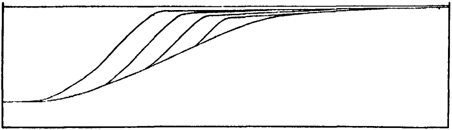

FIGURE 14. Hypothetical arrangement of sediments Vertical scale 30 times horizontal

Some doubt is thrown on the correctness of this view of the structure of the shelf by the results of dredging carried out by Stetson in the Georges Bank canyons (Stetson 1936, Stephenson 1936, Bassler 1936, Cushman 1936). From points 10 miles from the mouth of one canyon and 4 miles from the mouth of another he obtained Cretaceous sandstone, which he gives strong reason to suppose was in place. Such an occurrence is difficult to reconcile with the structure shown in figure 14, which allows the older sediments to be exposed some way on the landward side of the edge of the shelf but not just at the edge. It is most desirable that further dredging and core sampling should be carried out, particularly in canyons further south where there is no possibility of the material being broken from large erratics. While this paper was passing through the press, a letter from Professor Shepard has appeared (1940) criticising the view suggested above. Some comments on this letter have been made by one of the authors (Bullard, 1940).

## 8. THE ROCKS BENEATH THE CHANNEL

The two stations 1 south of the Lizard, and 9 in mid-Channel show no surface low-velocity layer. A rock giving a velocity of 9680 ft./sec. is directly on the surface, underlain by a rock giving a velocity of 12,700 ft./sec. Dredging near the Lizard has shown that the bottom of the sea is covered with a red sandstone which is probably *in situ* (Crawshay, 1907, Worth 1907). Specimens of what is said to be this rock are to be seen in the fish storage tank at the back of the Marine Biological Station at Plymouth. The layer 200 ft. thick giving a velocity of 9000 ft./sec. at station 1 is presumably this rock and possibly also the 1320 ft. of 8690 ft./sec. at station 9. The failure to find any really high velocity rock at either station is somewhat surprising, as igneous and metamorphic rocks occur on the south coast of Cornwall at Land's End, the Lizard, and the Eddystone Rock, and also in Brittany. It was thus natural to suppose that they would have been continuous under the Channel at no great depth. It appears from this and from the dredging results that the Channel is not merely a place where the sea has broken through, but is also the site of a basin of Mesozoic rocks softer than those on either side.

It is conceivable that the rock giving 9600 ft./sec. at these stations is to be correlated with that giving 9640 ft./sec. at station 8, but the absence of such a velocity at intermediate stations makes this unlikely.

## 9. Possible methods of working in deeper water

It is clearly desirable that measurements similar to those described in this paper should be extended beyond the edge of the shelf into water over 1000 fm. deep. The difficulties of handling long lengths of electric cable would make this a prohibitively expensive undertaking if a technique similar to that employed in the present work were used. To reduce the length of the electric cables Ewing tried lowering the apparatus and charges to the bottom on a steel cable; the charges, geophones, and recorder being all on the bottom, and interconnected by electric cable. The disturbances produced by the ship pulling on the cable were so great as to render this method impracticable. He then tried lowering the instruments separately, attached to petrol-filled balloons which caused them to rise again at the conclusion of the measurements (Ewing 1938). As far as is known, no deep water results have yet been obtained by this method, but there seems no reason why it should not work.

A few preliminary experiments were made with an alternative method in the late summer of 1939, but had to be abandoned before it was certain that it would work. As it is uncertain when it will be possible to resume the work it is thought worth while to describe the method briefly here. It was proposed to let a line of charges sink freely to the bottom, attached to clocks or other devices to ensure that they fired some time after reaching the bottom. It was hoped that the elastic waves through the bottom could be detected by a microphone at the surface of the sea. The distance and time of explosion can be determined if the direct and reflected waves through the sea from the explosion to the microphone can be observed.

Whilst investigating this method a very curious phenomenon was observed When a detonator was exploded in water two separate pulses were observed. The cause of the second one is unknown, but it is possible that it is due to collapse of the bubble of gas formed by the explosion. This phenomenon, and indeed the whole question of the propagation of a wave from an explosion in water deserves further investigation.

## References

Bassler, R. S. 1936 *Bull. Geol. Soc. Amer.* **47**, 411–412.

Bullard, E. C. 1940 *Nature, Lond.*, **146**, 432.

Bullard, E. C. and Gaskell, T. F. 1938 *Nature, Lond.*, **142**, 916.

Bullard, E. C., Gaskell, T. F., Harland, W. B. and Kerr-Grant, C. 1940 *Phil. Trans.* **239**, 29–94.

Bullard, E. C. and Kerr-Grant, C. 1938 *Mon. Not. R. Astr. Soc., Geophys. Suppl.* **4**, 341–350.

Crawshay, L. R. 1907 *J. Marine Biol. Assn*, **8**, 99–117.
Cushman, J. A. 1936 *Bull. Geol. Soc. Amer.* **47**, 413–440.
Ewing, M. 1938 *Trans. Amer. Geophys. Union*, 19th Annual Meeting, pp. 248–251.
Ewing, M., Crary, A. P. and Rutherford, H. M. 1937 *Bull. Geol. Soc. Amer.* **48**, 753–802.
Ewing, M. and Leet, L. D. 1932 *Trans. Amer. Inst. Min. Metall. Eng.* "Geophysical Prospecting", pp. 263–270.
Jones, O. T. 1939 *Quart. J. Geol. Soc., Lond.*, **95**, 335–382.
Shepard, F. P. 1940 *Nature, Lond.*, **146**, 431–432.
Shepard, F. P. and Cohee, G. V. 1936 *Bull. Geol. Soc. Amer.* **47**, 441–458.
Stephenson, L. W. 1936 *Bull. Geol. Soc. Amer.* **47**, 367–410.
Stetson, H. C. 1936 *Bull. Geol. Soc. Amer.* **47**, 339–366.
Worth, R. H. 1907 *J. Marine Biol. Assn.* **8**, 118–188.

# The dissociation constants of the methylammonium ions and the basic strengths of the methylamines in water

BY D. H. EVERETT AND W. F. K. WYNNE-JONES

(*Communicated by Sir Harold Hartley, F.R.S.—Received* 4 *November* 1940)

The dissociation constants of the three substituted methylammonium ions have been determined in water at 10° intervals from 0 to 50° C. From these results values have been derived and tabulated for the free energies of dissociation, heats of dissociation, entropies of dissociation and the heat capacity changes for these ions, as well as the corresponding quantities for the ionization of the amines. The heat capacity changes are discussed and it is shown that they cannot be interpreted by simple electrostatic theory. It is shown that the anomalous order of the basic strengths of the amines probably disappears at low temperatures.

**We have shown recently that the dissociation constants of positively charged acids may be determined accurately by measurements of the e.m.f.s of cells of the following composition (Everett and Wynne-Jones 1938):**

$$H_2 \left| \begin{array}{c|c|l} \mathrm{HCl} & \mathrm{KCl} & \text{amine} \\ & & \text{amine hydrochloride} \\ \mathrm{KCl} & 3{\cdot}5\,\mathrm{N} & \mathrm{KCl} \end{array} \right| H_2$$

**The liquid junction potential may be eliminated by an extrapolation method, and by carrying out measurements at different ionic strengths the thermodynamic dissociation constants may be evaluated.**

This work has now been extended to the primary, secondary and tertiary methylammonium ions whose dissociation constants have been determined at 10° intervals over the range 0–50° C.

## EXPERIMENTAL

The experimental method was essentially the same as in the earlier work but several refinements were introduced.

For the measurement of the e.m.f. we used a Tinsley Vernier potentiometer, reading directly to 0·01 mV, in conjunction with a Cambridge D'Arsonval galvanometer and a Weston standard cell. The 20, 30, 40 and 50° C thermostats were similar to those previously employed. The 0 and 10° baths were cooled by standing in a Frigidaire refrigerator containing calcium chloride solution. The rate of cooling could be adjusted by varying the depth of immersion of the baths in the refrigerator liquid. Sunvic hot-wire vacuum switches were used for the two low-temperature thermostats in conjunction with all-mercury thermoregulators. The temperature control was to within 0·01 at 0, 20, 30 and 40° C, and to 0·02 at 10 and 50° C.

The cells were the same as those used for the ammonia work, apart for slight modifications mentioned below for use with trimethylamine. In the later experiments transfer of the solutions to the cells was carried out in a closed $CO_2$-free system so that contact with the atmosphere was avoided. All solutions were made up from conductivity water and used immediately after preparation The amine hydrochlorides, purified as described below, were kept in vacuum desiccators. The e.m.f. of the cells remained constant to 0·01 mV; the reproducibility was usually 0·05 mV although deviations of 0·10 mV occurred occasionally

In working with trimethylamine buffers the high partial vapour pressure of the amine caused some difficulty. After 1–2 hr. bubbling at 20° C the e.m.f. of the cells fell off very rapidly. This was traced to the removal of trimethylamine from the cell solution by the hydrogen stream; the contents of the bubblers were found to be over one-half depleted in amine after 4 hr. bubbling. Eventually a train of six bubblers with a total capacity of 30 c.c. was found sufficient to produce efficient saturation of the hydrogen stream for the duration of a run. We note in this connexion that Harned and Robinson (1928) found that cells containing ammonia and trimethylamine were less reproducible than those containing mono- or dimethylamine.

The high partial vapour pressure of trimethylamine does not make it necessary, however, to apply any correction to the e.m.f. of the cells since the extrapolation to zero concentration of buffer, the buffer ratios remaining approximately constant, eliminates not only the liquid junction potentials but vapour pressure effects also.

The bases examined are much stronger than ammonia so it is necessary to apply a correction for the removal of amine by the reaction.

$$\text{amine} + H_2O = \text{amine } H^+ + OH'.$$

Since the activity coefficients of the hydrogen ions are the same in the two cell compartments, we have, neglecting for the evaluation of this correction the liquid junction potential,

$$E = (RT/F)\ln(c_{HCl}/c_{H^+}\text{ buffer}),$$

from which $c_{H^+}$ in the buffer may be evaluated. The ionic product of water at different ionic strengths of KCl is known from the work of Harned and Hamer (1933) so that the OH′ concentration in the buffer solution may be calculated. The true buffer ratio is then given by

$$r = (c_{\text{amine}\,H^+} + c_{OH'})/(c_{\text{amine}} - c_{OH'}),$$

where $c_{\text{amine}}$ and $c_{\text{amine}\,H^+}$ refer to analytical values.

## PURIFICATION OF MATERIALS

### *Monomethylamine hydrochloride*

Three samples of monomethylamine hydrochloride were used. The first had been purified in 1932 by Mr K. T. B. Scott; this was dried for 2 hr in an oven at 100° C and at 50 mm pressure and had m.p. 223–227° C. The other samples were obtained by purification of B.D.H. chemical which was first washed with pure chloroform to remove traces of dimethylamine hydrochloride, the presence of which had been detected in the commercial product by the benzene sulphonyl chloride test. The product was recrystallized from *n*-butyl alcohol in two portions. Six to eight extractions were carried out with each portion using 4–6 parts of fresh solvent for each extraction. The crystals were drained on a centrifuge, and after heating 2–3 hr. at 100° C 50 mm. pressure they had m.p. 224–226° C; but they still had a strong odour of *n*-butyl alcohol. One portion was washed with chloroform, filtered and dried as before and had m.p. 227–231° C. The second portion, which was recrystallized from water, centrifuged and dried, had m.p. 229–233° C (Beilstein Hw, 225–228° C, EgB. I, no definite m.p.). The various samples gave identical results in the e.m.f. measurements

### *Dimethylamine hydrochloride*

This salt was obtained by purification of the B.D.H. product. It was recrystallized twice, with centrifuging, from absolute alcohol, then from absolute alcohol with a few drops of concentrated hydrochloric acid, and finally from absolute alcohol. After drying under reduced pressure the product melted sharply at 170–171° C (Beilstein quotes 171° C). A large number of recrystallizations were necessary owing to difficulty in removing an unidentified impurity which coloured the hot solutions bright green, changing to a brownish colour on cooling. A similar impurity which could neither be isolated nor identified appeared to be present in one sample of trimethylamine hydrochloride but in this case was more easily removed.

### *Trimethylamine hydrochloride*

An old sample of the hydrochloride (B.D.H. 1932) was recrystallized from pure chloroform and then from water, m.p. 278–281° C. A freshly supplied sample (B.D.H.) was recrystallized from chloroform and had m.p. 282–284° C (Beilstein quotes 277° C). Owing to the wastefulness of recrystallizing from water, this second sample was not purified further.

## RESULTS

In tables 1–3 the experimental results for cells containing mono-, di- and trimethylamine respectively are summarized. Readings were not always made exactly at round temperatures, and the figures given are interpolated values. The interpolation was, however, not usually over more than a few tenths of a degree corresponding to a change of not more than 0·1 mV in the e.m.f.

The concentrations are expressed in g.mol./1000 c.c. of solution at 15° C, and the factor $RT/F$ has been taken as $0^{\circ}\cdot0019836\,T$ with $T = t^{\circ}\,\mathrm{C} + 273\cdot1$.

Tables 4–6 contain the values of $-\log K'$ at various concentrations of amine ion and at various ionic strengths; the extrapolated values to zero buffer concentration are given, and at the foot of each table are the logarithms of the thermodynamic dissociation constants at the different temperatures.

In these tables the concentrations of the amine ions have been corrected by taking into account the ionisation of the amines.

## SUMMARY OF EXPERIMENTAL RESULTS

### TABLE 1. CELLS CONTAINING MONOMETHYLAMINE

| $I$ | $c_{\mathrm{CH_3NH_2}}$ | $c_{\mathrm{CH_3NH_3^+}}$ | $c_{\mathrm{HCl}}$ | $E_{0°}$ | $E_{10°}$ | $E_{20°}$ | $E_{30°}$ | $E_{40°}$ | $E_{50°}$ |
|---|---|---|---|---|---|---|---|---|---|
| 0·20 | 0·04176 | 0 04109 | 0·02048 | — | — | 0·53295 | 0·53142 | 0·52980 | — |
| | 0·02581 | 0·02373 | 0·01287 | — | — | 0·52232 | 0·52042 | 0·51847 | 0·51644 |
| | 0·02543 | 0·02543 | 0·01269 | 0·52336 | 0·52172 | 0·51995 | 0·51801 | 0·51595 | 0·51385 |
| | 0·03803 | 0·03802 | 0·01903 | 0·53338 | 0·53214 | 0·53074 | 0·52920 | 0 52748 | 0·52559 |
| | 0·01590 | 0·01589 | 0·00794 | 0·51156 | 0·50959 | 0·50733 | 0·50490 | 0·50244 | 0·49995 |
| | 0·01589 | 0·01577 | 0·00797 | 0·51183 | 0·50963 | 0·50738 | 0·50499 | — | — |
| | 0·04200 | 0·03965 | 0·02050 | 0·53641 | 0·53514 | 0·53382 | 0·53245 | 0·53094 | — |
| | 0·03323 | 0·03295 | 0·01600 | — | — | 0·52636 | 0·52466 | 0·52281 | — |
| 0·15 | 0·04248 | 0·04165 | 0·02050 | 0·53460 | 0·53337 | 0·53200 | 0·53058 | 0·52906 | 0·52745 |
| | 0 02124 | 0·02083 | 0·01025 | 0·51721 | 0·51530 | 0·51324 | 0·51112 | 0·50888 | 0·50660 |
| | 0·03212 | 0·03175 | 0·01600 | 0·52789 | 0·52641 | 0·52481 | 0·52311 | 0·52135 | — |
| | 0·03094 | 0 03094 | 0·01550 | 0·52756 | 0·52641 | 0·52448 | 0·52280 | 0·52100 | 0·51901 |
| | 0·01547 | 0·01547 | 0·00775 | 0·51012 | 0·50791 | 0·50559 | 0·50313 | 0·50057 | 0·49783 |
| | 0 02080 | 0·02070 | 0 01040 | — | — | 0·51363 | 0·51160 | 0·50948 | 0·50716 |
| 0·10 | 0·04130 | 0·04118 | 0·02050 | 0·53314 | 0·53195 | 0·53058 | 0·52915 | 0·52761 | 0·52595 |
| | 0·02065 | 0·02059 | 0·01025 | 0·51604 | 0·51420 | 0·51211 | 0·51000 | 0·50780 | 0·50550 |
| | 0·03152 | 0·03083 | 0·01560 | 0·52716 | 0·52575 | 0·52419 | 0·52250 | 0·52066 | 0·51875 |
| | 0·01463 | 0·01471 | 0·00735 | 0·50780 | 0·50555 | 0·50316 | 0·50073 | 0·49826 | 0·49574 |
| 0·05 | 0·02496 | 0·02505 | 0·01250 | 0·51981 | 0·51817 | 0·51643 | 0·51460 | 0·51263 | 0·51055 |
| | 0·01659 | 0·01666 | 0·00830 | 0·50986 | 0·50772 | 0·50545 | 0·50317 | 0·50091 | 0·49852 |

### TABLE 2. CELLS CONTAINING DIMETHYLAMINE

| $I$ | $c_{\mathrm{(CH_3)_2NH}}$ | $c_{\mathrm{(CH_3)_2NH_2^+}}$ | $c_{\mathrm{HCl}}$ | $E_{0°}$ | $E_{10°}$ | $E_{20°}$ | $E_{30°}$ | $E_{40°}$ | $E_{50°}$ |
|---|---|---|---|---|---|---|---|---|---|
| 0·20 | 0·03008 | 0·02999 | 0·01500 | 0·53003 | 0·53077 | 0·53118 | 0·53134 | 0·53129 | 0 53095 |
| | 0·02040 | 0 02038 | 0 01020 | 0·52058 | 0·52083 | 0·52078 | 0·52045 | 0·51989 | 0·51907 |
| | 0 04298 | 0 04291 | 0·02150 | 0·53910 | 0·54028 | 0·54104 | 0·54152 | 0·54176 | 0·54160 |
| | 0·01603 | 0·01600 | 0·00800 | 0·51456 | 0·51454 | 0·51420 | 0·51365 | 0·51289 | 0·51180 |
| | 0·03677 | 0·03856 | 0·01839 | 0·53404 | 0·53495 | 0·53558 | 0·53591 | 0·53606 | 0·53589 |
| 0·15 | 0 04612 | 0·04598 | 0·02300 | 0·53940 | 0·54060 | 0·54152 | 0·54215 | 0·54258 | 0·54273 |
| | 0·02493 | 0·02487 | 0·01250 | 0·52486 | 0·52540 | 0·52570 | 0·52570 | 0·52550 | 0·52498 |
| | 0·04113 | 0·04101 | 0 02050 | 0·53666 | 0·53778 | 0·53860 | 0·53911 | 0·53940 | 0·53935 |
| | 0 01677 | 0·01669 | 0·00840 | 0·51484 | 0·51494 | 0 51473 | 0·51430 | 0·51358 | 0·51265 |
| 0·10 | 0·03662 | 0·03660 | 0·01830 | 0·53270 | 0·53367 | 0·53435 | 0·53476 | 0·53495 | 0 53500 |
| | 0·00650 | 0·03726 | 0·01096 | 0·47981 | 0·47904 | 0·47788 | 0·47630 | 0·47445 | 0·47225 |
| | 0 01911 | 0 01903 | 0 00950 | 0 51677 | 0·51706 | 0·51706 | 0·51679 | 0 51630 | 0·51560 |
| | 0·01600 | 0 01600 | 0 00800 | 0·51260 | 0 51269 | 0·51249 | 0 51203 | 0·51136 | 0·51050 |
| 0·05 | 0·02476 | 0·02462 | 0 01235 | 0·52231 | 0 52293 | 0·52331 | 0·52338 | 0·52326 | 0·52281 |
| | 0·01589 | 0·01572 | 0·00790 | 0·51164 | 0·51171 | 0 51158 | 0 51112 | 0·51051 | 0·50972 |

TABLE 3. CELLS CONTAINING TRIMETHYLAMINE

| $I$ | $c_{(CH_3)_3N}$ | $c_{(CH_3)_3NH^+}$ | $c_{HCl}$ | $E_{0^\circ}$ | $E_{10^\circ}$ | $E_{20^\circ}$ | $E_{30^\circ}$ | $E_{40^\circ}$ | $E_{50^\circ}$ |
|---|---|---|---|---|---|---|---|---|---|
| 0·20 | 0·03027 | 0·03031 | 0·01514 | 0·46743 | 0·47154 | 0·47513 | 0·4779 | — | — |
| | 0·04605 | 0·04594 | 0·02290 | 0·47697 | 0·48143 | 0·48524 | 0·4883 | | — |
| | 0·03640 | 0·03643 | 0·01820 | 0·47179 | 0·47580 | 0·4793 | — | — | - |
| | 0·02199 | 0·02193 | 0·01103 | — | — | 0·46710 | — | — | — |
| | 0·01809 | 0·01809 | 0·00905 | — | — | 0·46240 | — | — | — |
| | 0·02749 | 0·01605 | 0·01093 | 0·47282 | 0·47680 | 0·48020 | 0·48304 | 0·48517 | 0·4867 |
| | 0·01346 | 0·05374 | 0·01681 | 0·43760 | 0·44040 | 0·44252 | 0·44404 | 0·4450 | 0·4455 |
| | 0·02344 | 0·02334 | 0·01171 | 0·4638 | 0·4664 | 0·46900 | 0·47092 | 0·47235 | 0·4733 |
| | 0·03996 | 0·03997 | 0·01997 | 0·47395 | 0·47765 | 0·48186 | 0·48472 | 0·48685 | 0·4885 |
| 0·15 | 0·03245 | 0·03251 | 0·01624 | 0·46995 | 0·47394 | 0·47739 | 0·48021 | 0·48234 | 0·4838 |
| | 0·03990 | 0·03994 | 0·01995 | 0·47280 | 0·47725 | 0·48089 | 0·48385 | 0·48600 | 0·48748 |
| | 0·01858 | 0·01857 | 0·00929 | 0·45550 | 0·45905 | 0·46190 | 0·46415 | 0·46570 | 0·4666 |
| | 0·02859 | 0·02861 | 0·01430 | 0·46550 | 0·46951 | 0·47278 | 0·4754 | 0·4773 | 0·4786 |
| | 0·04568 | 0·04636 | 0·02302 | 0·47568 | 0·48008 | 0·48372 | 0·48685 | 0·48930 | 0·4909 |
| 0·10 | 0·02666 | 0·02448 | 0·01254 | 0·46331 | 0·40740 | 0·47080 | 0·47335 | — | — |
| | 0·01738 | 0·01737 | 0·00869 | 0·45216 | 0·45560 | 0·45842 | 0·46074 | 0·46265 | 0·46411 |
| | 0·02596 | 0·02597 | 0·01298 | — | — | 0·46839 | 0·47080 | 0·47290 | 0·4746 |
| | 0·01819 | 0·01821 | 0·00910 | 0·45370 | 0·45715 | 0·45995 | 0·46225 | 0·46385 | 0·46483 |
| | 0·03925 | 0·03923 | 0·01963 | 0·47080 | 0·47503 | 0·47875 | 0·48190 | 0·48445 | 0·48620 |
| 0·05 | 0·02503 | 0·02503 | 0·01252 | 0·45864 | 0·46261 | 0·46596 | 0·46865 | 0·47061 | 0·47190 |
| | 0·01701 | 0·01702 | 0·00851 | 0·45023 | 0·45386 | 0·45685 | 0·45925 | 0·46090 | 0·46194 |

TABLE 4. MONOMETHYLAMINE

| $I$ | $c_{CH_3NH_3^+}$ | $-\log K'_{0^\circ}$ | $-\log K'_{10^\circ}$ | $-\log K'_{20^\circ}$ | $-\log K'_{30^\circ}$ | $-\log K'_{40^\circ}$ | $-\log K'_{50^\circ}$ |
|---|---|---|---|---|---|---|---|
| 0·20 | 0·0420 | — | — | 10·8665 | 10·5387 | 10·2302 | — |
| | 0·0405 | 11·5818 | 11·2107 | 10·8637 | 10·5383 | 10·2311 | 9·9406 |
| | 0·0388 | 11·5838 | 11·2147 | 10·8684 | 10·5421 | 10·2332 | 9·9399 |
| | 0·0338 | — | 11·2120 | 10·8676 | 10·5411 | 10·2324 | 9·9398 |
| | 0·0262 | 11·5823 | 11·2139 | 10·8675 | 10·5409 | 10·2322 | 9·9417 |
| | 0·0246 | — | — | 10·8687 | 10·5414 | 10·2333 | 9·9426 |
| | 0·0166 | 11·5812 | 11·2163 | 10·8695 | 10·5416 | 10·2335 | 9·9435 |
| | 0·0165 | 11·5820 | 11·2118 | 10·8666 | 10·5383 | 10·2285 | 9·9351 |
| | 0·0000 | $11·584_5$ | $11·217_0$ | $10·870_3$ | $10·544_0$ | $10·236_8$ | $9·945_8$ |
| 0·15 | 0·0424 | 11·5627 | 11·1933 | 10·8466 | 10·5214 | 10·2150 | 9·9258 |
| | 0·0325 | 11·5537 | 11·1846 | 10·8385 | 10·5129 | 10·2066 | |
| | 0·0317 | 11·5675 | 11·2049 | 10·8526 | 10·5275 | 10·2206 | 9·9296 |
| | 0·0216 | 11·5567 | 11·1879 | 10·8400 | 10·5151 | 10·2071 | 9·9169 |
| | 0·0214 | 11·5675 | — | 10·8469 | 10·5225 | 10·2162 | 9·9253 |
| | 0·0162 | 11·5635 | 11·1949 | 10·8481 | 10·5214 | 10·2118 | 9·9185 |
| | 0·0000 | $11·568_5$ | $11·200_5$ | $10·852_0$ | $10·526_5$ | $10·220_8$ | $9·932_0$ |
| 0·10 | 0·0419 | 11·5418 | 11·1740 | 10·8280 | 10·5034 | 10·1975 | 9·9083 |
| | 0·0316 | 11·5465 | 11·1804 | 10·8350 | 10·5100 | 10·2026 | 9·9127 |
| | 0·0212 | 11·5395 | 11·1722 | 10·8251 | 10·5001 | 10·1935 | 9·9041 |
| | 0·0153 | 11·5438 | 11·1763 | 10·8301 | 10·5046 | 10·1990 | 9·9101 |
| | 0·0000 | $11·546_0$ | $11·179_0$ | $10·833_0$ | $10·508_8$ | $10·201_3$ | $9·914_5$ |
| 0·05 | 0·0256 | 11·5188 | 11·1523 | 10·8086 | 10·4858 | 10·1805 | 9·8921 |
| | 0·0172 | 11·5200 | 11·1539 | 10·8075 | 10·4837 | 10·1797 | 9·8922 |
| | 0·0000 | $11·522_5$ | $11·155_0$ | $10·810_0$ | $10·487_5$ | $10·182_8$ | $9·895_8$ |
| 0·00 | 0·0000 | $11·496_8$ | $11·130_0$ | $10·787_0$ | $10·466_0$ | $10·160_5$ | $9·876_8$ |

### TABLE 5. DIMETHYLAMINE

| $I$ | $c_{(\mathrm{CH_3})_2\mathrm{NH_2^+}}$ | $-\log K'_{0^\circ}$ | $-\log K'_{10^\circ}$ | $-\log K'_{20^\circ}$ | $-\log K'_{30^\circ}$ | $-\log K'_{40^\circ}$ | $-\log K'_{50^\circ}$ |
|---|---|---|---|---|---|---|---|
| 0·20 | 0 0440 | 11·6355 | 11·3080 | 10·9956 | 10·6984 | 10·4157 | 10·1435 |
| | 0 0395 | 11·6324 | 11·3036 | 10·9922 | 10 6961 | 10 4153 | 10·1459 |
| | 0·0310 | 11 6301 | 11·3019 | 10·9904 | 10·6940 | 10·4129 | 10·1437 |
| | 0 0210 | 11 6346 | 11·3054 | 10·9934 | 10 6956 | 10·4125 | 10·1418 |
| | 0·0170 | 11·6373 | 11·3088 | 10·9965 | 10·6998 | 10·4176 | 10·1460 |
| | 0 0000 | 11·641$_{\text{[illegible]}}$ | 11·311$_{\text{[illegible]}}$ | 10 998$_5$ | 10·703$_{\text{[illegible]}}$ | 10 417$_0$ | 10·146$_{\text{[illegible]}}$ |
| 0·15 | 0 0470 | 11·6085 | 11 2808 | 10·9706 | 10 6756 | 10·3957 | 10 1282 |
| | 0 0420 | 11 6095 | 11·2827 | 10 9727 | 10 6775 | 10 3969 | 10·1279 |
| | 0·0260 | 11·6172 | 11·2893 | 10·9792 | 10·6843 | 10·4037 | 10·1347 |
| | 0 0175 | 11·6155 | 11·2881 | 10 9776 | 10 6829 | 10 4001 | 10 1309 |
| | 0·0000 | 11 623$_0$ | 11·296$_0$ | 10·985$_{\text{[illegible]}}$ | 10·689$_0$ | 10 405$_0$ | 10·136$_0$ |
| 0·10 | 0 0375 | 11·5870 | 11·2600 | 10·9501 | 10·6559 | 10·3762 | 10·1109 |
| | 0 0375 | 11·5853 | 11 2602 | 10·9510 | 10·6551 | 10·3732 | 10 1024 |
| | 0·0200 | 11 5901 | 11·2641 | 10·9547 | 10 6608 | 10·3804 | 10·1134 |
| | 0·0170 | 11·5954 | 11·2692 | 10·9603 | 10·6657 | 10 3856 | 10·1189 |
| | 0·0000 | 11 600$_0$ | 11·274$_0$ | 10 963$_0$ | 10·668$_5$ | 10·387$_{\text{[illegible]}}$ | 10·120$_{\text{[illegible]}}$ |
| 0·05 | 0 0255 | 11·5688 | 11·2430 | 10·9355 | 10 6424 | 10·3637 | 10 0964 |
| | 0 0165 | 11 5751 | 11·2486 | 10·9411 | 10·6469 | 10·3679 | 10·1022 |
| | 0 0000 | 11·580$_0$ | 11 253$_0$ | 10 946$_0$ | 10 652$_0$ | 10·371$_5$ | 10·105$_{\text{[illegible]}}$ |
| 0·00 | 0 0000 | 11·553$_0$ | 11·228$_5$ | 10·922$_0$ | 10 630$_{\text{[illegible]}}$ | 10·352$_0$ | 10 087$_5$ |

### TABLE 6. TRIMETHYLAMINE

| $I$ | $c_{(\mathrm{CH_3})_3\mathrm{NH^+}}$ | $-\log K'_{0^\circ}$ | $-\log K'_{10^\circ}$ | $-\log K'_{20^\circ}$ | $-\log K'_{3}\,.$ | $-\log K'_{40^\circ}$ | $-\log K'_{50^\circ}$ |
|---|---|---|---|---|---|---|---|
| 0·20 | 0·0538 | 10 4542 | 10·2191 | 9 9885 | 9·7629 | 9·5426 | 9 3290 |
| | 0 0460 | 10 4455 | 10·2142 | 9 9880 | 9·7650 | — | — |
| | 0 0401 | 10·4502 | 10·2077 | 9·9904 | 9·7652 | 9·5427 | 9·3265 |
| | 0·0365 | 10·4510 | 10·2152 | 9·9871 | — | — | — |
| | 0·0304 | 10 4510 | 10 2198 | 9·9964 | — | — | — |
| | 0·0235 | 10·4929 | 10·2385 | 10·0009 | 9·7678 | 9·5420 | 9 3220 |
| | 0·0221 | — | — | 9·9953 | — | — | — |
| | 0·0182 | — | — | 10·0026 | — | — | — |
| | 0 0162 | 10 4603 | 10·2244 | 9·9960 | 9·7727 | 9·5527 | 9 3367 |
| | 0·0000 | 10·468$_0$ | 10·231$_0$ | 10·005$_{\text{[illegible]}}$ | 9·775$_{\text{[illegible]}}$ | 9·551$_0$ | 9·332$_{\text{[illegible]}}$ |
| 0·15 | 0·0465 | 10·4263 | 10·1964 | 9·9664 | 9·7444 | 9·5260 | 9·3076 |
| | 0·0400 | 10·4296 | 10·2011 | 9·9744 | 9·7514 | 9 5297 | 9 3107 |
| | 0 0287 | 10·4398 | 10·2084 | 9 9805 | 9·7565 | 9·5356 | 9·3185 |
| | 0·0187 | 10·4427 | 10·2102 | 9·9819 | 9·7584 | 9·5383 | 9 3211 |
| | 0 0000 | 10·452$_{\text{[illegible]}}$ | 10·217$_{\text{[illegible]}}$ | 9·987$_{\text{[illegible]}}$ | 9·761$_{\text{[illegible]}}$ | 9·539$_{\text{[illegible]}}$ | 9·319$_0$ |
| 0·10 | 0 0393 | 10·3990 | 10·1676 | 9·9435 | 9·7248 | 9·5107 | 9 2971 |
| | 0·0261 | — | — | 9·9467 | 9 7216 | 9 5063 | 9·2981 |
| | 0·0246 | 10·4190 | 10·1909 | 9 9665 | 9·7426 | — | — |
| | 0·0183 | 10·4192 | 10·1856 | 0·9578 | 9·7362 | 9 5175 | 9·3030 |
| | 0 0175 | 10·4099 | 10·1775 | 9 9508 | 9·7301 | 9 5178 | 9·3113 |
| | 0·0000 | 10·424$_{\text{[illegible]}}$ | 10·191$_{\text{[illegible]}}$ | 9 961$_{\text{[illegible]}}$ | 9·740$_{\text{[illegible]}}$ | 9 520$_0$ | 9·306$_0$ |
| 0·05 | 0·0251 | 10·3702 | 10·1425 | 9·9199 | 9 7012 | 9·4846 | 9·2708 |
| | 0·0171 | 10·3826 | 10·1555 | 9·9324 | 9·7145 | 9·4982 | 9·2863 |
| | 0·0000 | 10·390$_5$ | 10·161$_0$ | 9 935$_0$ | 9·717$_0$ | 9·499$_{\text{[illegible]}}$ | 9·287$_0$ |
| 0·00 | 0 0000 | 10·354$_5$ | 10·128$_0$ | 9·906$_5$ | 9·692$_{\text{[illegible]}}$ | 9·476$_5$ | 9·270$_{\text{[illegible]}}$ |

### METHODS OF EXTRAPOLATION

#### *Extrapolation to zero buffer concentration*

In figure 1 are shown several typical extrapolations for results at 20° C. For monomethylamine the extrapolation is of about the same magnitude as in the case of ammonia, but the effect increases markedly on passing to di- and trimethylamine. Furthermore, in the latter cases, the slope of the lines shows a definite tendency to vary both with ionic strength and with temperature. In making these extrapolations therefore, we have allowed the slope to increase regularly both with decreasing ionic strength and decreasing temperature. For trimethylamine at 0° C and at an ionic strength of 0·05 N $\log K'$ changes by about 0·012 (i.e. 3 % in $K$) between 0·01 N buffer concentration and zero, while at 50° C and 0·20 N ionic strength the corresponding change is about 0·002 (i.e. ½ % in $K$). We estimate the accuracy of these extrapolations to be roughly ± 0·0010 for monomethylammonium

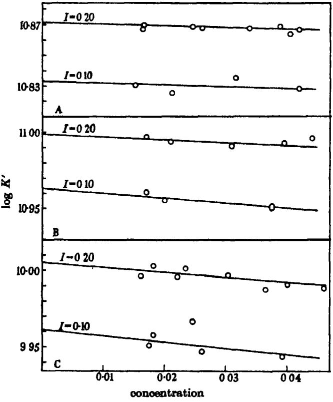

FIGURE 1. Extrapolation to zero buffer concentration.

± 0·0020 for dimethylammonium, and ± 0·0030 for trimethylammonium ions.

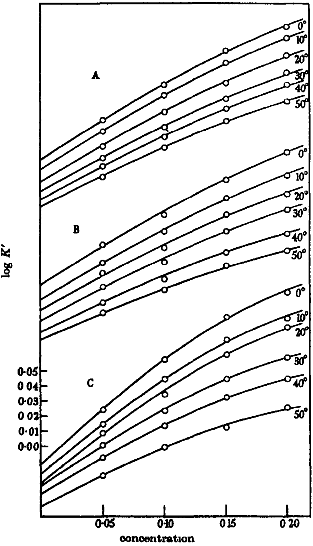

Figure 2. Extrapolation to zero ionic strength.

### *Extrapolation to zero ionic strength*

Figure 2*a*, *b* and *c* shows the extrapolations of log $K'$ to zero ionic strength. Here again we notice a steady deviation from the simple behaviour of the ammonium ion for which log $K'$ is a linear function of the ionic strength to within the accuracy of our measurements. For the methylamines a marked curvature of this plot is observed and the limiting slope of the line is found to vary approximately linearly with temperature, i.e.

$$\frac{\partial}{\partial T}\left(\frac{\partial \ln K}{\partial I}\right)_{I\to 0} = \text{constant.}$$

By reversing the order of differentiation this leads to

$$\frac{\partial}{\partial I}\left(\frac{\Delta H}{RT^2}\right) = \text{constant,}$$

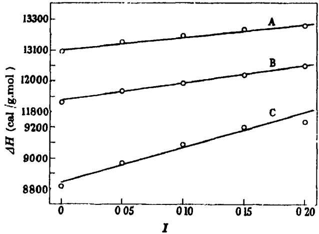

FIGURE 3 $\Delta H_{298\cdot 1}$ as a function of ionic strength.

i.e. at any given temperature $\Delta H$ becomes a linear function of ionic strength at low ionic strengths. In figure 3 the values of $\Delta H$ obtained from analysis of the results at various ionic strengths are plotted against $I$. The relation predicted from the extrapolation graphs is seen to be verified, thus confirming the consistency of the analysis of the results.

### ANALYSIS OF RESULTS AND COMPARISON WITH OTHER WORK

The three amines we have now examined differ markedly from the ammonium ion in that for them the relation between $\log K$ and $1/T$ is not linear, indicating that the ionization of the methylammonium ions is accompanied by a change in heat capacity. It should be noted that the inconstancy of the heats of dissociation of these ions implies that the relation

$$dE/dT = \frac{2{\cdot}303R}{F}(B + \log c_{H^+} + \log c_{NH_3} - \log c_{NH_4^+}),$$

employed in our treatment of the temperature coefficients of the cells containing ammonia and ammonium chloride, is inapplicable to cells containing buffer solutions of the other amines.

We have analysed our results in terms of the equation

$$\log K = \frac{A}{T} + \frac{\Delta C_p}{R} \log T + B \tag{1}$$

by the same procedure as we have previously employed (Everett and Wynne-Jones 1939). The slopes of the lines determining $\Delta C_p$ and $A$ were evaluated analytically by the method of least squares. The results were analysed at different ionic strengths to obtain data on the influence of ionic strength on the various thermodynamic functions. The results of this analysis are contained in table 7.

TABLE 7

| | $\Delta C_p$ | $\Delta S^\circ_{298\cdot1}$ | $\Delta G^\circ_{298\cdot1}$ | $\Delta H_{298\cdot1}$ | $\Delta H_0$ | $A$ | $B$ | $\Sigma\|\nu$ |
|---|---|---|---|---|---|---|---|---|
| | | | | Monomethylammonium ion | | | | |
| 0·20 | 8·0 | −4·5 | 14595 | 13247 | 10879 | −2378·9 | −12·6212 | 0·0013 |
| 0·15 | | −4·5 | 14568 | 13229 | 10861 | −2375·0 | −12·6178 | 8 |
| 0·10 | | −4·5 | 14542 | 13188 | 10820 | −2366·0 | −12·6280 | 7 |
| 0·05 | | −4·6 | 14512 | 13146 | 10778 | −2356·8 | −12·6377 | 3 |
| 0·00 | | −4·7 | 14484 | 13088 | 10720 | −2344·2 | −12·6576 | 6 |
| | | | | Dimethylammonium ion | | | | |
| 0·20 | 23·1 | −9·0 | 14789 | 12093 | 5225 | −1142·6 | −35·7187 | 0·0007 |
| 0·15 | | −9·2 | 14770 | 12037 | 5169 | −1130·3 | −35·7459 | 5 |
| 0·10 | | −9·3 | 14743 | 11981 | 5113 | −1118·1 | −35·7667 | 7 |
| 0·05 | | −9·4 | 14719 | 11933 | 5065 | −1107·5 | −35·7848 | 9 |
| 0·00 | | −9·5 | 14687 | 11859 | 4991 | −1091·5 | −35·8162 | 9 |
| | | | | Trimethylammonium ion | | | | |
| 0·20 | 43·8 | −14·3 | 13479 | 9227 | −3798 | +830·6 | −67·1096 | 0·0013 |
| 0·15 | | −14·3 | 13459 | 9202 | −3823 | +836·0 | −67·1133 | 8 |
| 0·10 | | −14·6 | 13429 | 9083 | −3942 | +861·9 | −67·1783 | 9 |
| 0·05 | | −14·9 | 13394 | 8965 | −4060 | +887·9 | −67·2402 | 7 |
| 0·00 | | −15·2 | 13358 | 8815 | −4210 | +920·6 | −67·3233 | 10 |

The values of $\Delta C_p$ given above are the means of those for the different ionic strengths, the variation with ionic strength being less than the experimental error In calculating $A$ and $B$, $\Delta C_p/R$ was taken to the nearest 0·2, so that in utilizing the table to obtain the constants in equation (1), the tabulated value of $\Delta C_p$ should be divided by 1·986 and the result taken to the nearest 0·2

It should also be noted that the same observation regarding $\Delta C_p/R$ applies to table 1 of our previous paper (1939).

The values of $\log K_{\mathrm{AmH^+}}$ have also been combined with Harned and Hamer's (1933) data for the ionization of water in potassium chloride solutions to obtain figures for the equilibrium constants for the basic functions of the amines, e.g.

$$CH_3NH_2 + H_2O = CH_3NH_3^+ + OH'.$$

Table 8 contains a summary of these values ($K_b$), and in table 9 we give the other thermodynamic functions for these ionizations at zero ionic strength

TABLE 8

$-\log K_b$

| | $I \rightarrow 0{\cdot}200$ | 0·150 | 0·100 | 0·050 | 0·000 |
|---|---|---|---|---|---|
| | | | Monomethylamine | | |
| °C | | | | | |
| 0 | 3·1182 | 3·1504 | 3·1940 | 3·2531 | $3{\cdot}449_0$ |
| 10 | 3·0795 | 3·1108 | 3·1537 | 3·2132 | $3{\cdot}405_8$ |
| 20 | 3·0583 | 3·0916 | 3 1319 | 3·1907 | $3{\cdot}380_8$ |
| 30 | 3·0496 | 3·0798 | 3·1210 | 3·1774 | $3{\cdot}367_8$ |
| 40 | 3·0535 | 3·0846 | 3·1247 | 3·1831 | $3{\cdot}374_5$ |
| 50 | 3·0647 | 3·0922 | 3·1323 | 3·1913 | $3{\cdot}386_8$ |
| | | | Dimethylamine | | |
| 0 | 3·0617 | 3·0959 | 3·1400 | 3·1956 | $3{\cdot}392_8$ |
| 10 | 2·9855 | 3·0153 | 3·0587 | 3·1152 | $3{\cdot}306_5$ |
| 20 | 2·9303 | 2·9586 | 3·0019 | 3·0547 | $3{\cdot}245_8$ |
| 30 | 2·8906 | 2·9172 | 2·9605 | 3·0129 | $3{\cdot}203_8$ |
| 40 | 2·8695 | 2·8996 | 2·9392 | 2·9936 | $3{\cdot}183_8$ |
| 50 | 2 8637 | 2·8882 | 2·9268 | 2·9813 | $3{\cdot}174_5$ |
| | | | Trimethylamine | | |
| 0 | 4·2347 | 4·2669 | 4·3160 | 4·3851 | $4\ 590_5$ |
| 10 | 4·0655 | 4·0933 | 4·1417 | 4·2072 | $4{\cdot}407_8$ |
| 20 | 3·9238 | 3·9566 | 4·0039 | 4·0657 | $4{\cdot}260_5$ |
| 30 | 3·8186 | 3 8452 | 3·8890 | 3·9479 | $4{\cdot}141_8$ |
| 40 | 3·7385 | 3·7656 | 3·8062 | 3·8661 | $4{\cdot}058_5$ |
| 50 | 3 6777 | 3·7052 | 3·7408 | 3 7993 | $3\ 992_8$ |

TABLE 9

| $\Delta C_p$ | $\Delta S^\circ_{298\cdot1}$ | $\Delta G^\circ_{298\cdot1}$ | $\Delta H_{298\cdot1}$ | $A$ | $B$ | $T_m$ |
|---|---|---|---|---|---|---|
| | | | Monomethylamine | | | |
| 59·0 | −14·2 | 4638 | 402 | −3929 8 | 83·1516 | 31·8 |
| | | | Dimethylamine | | | |
| 74·1 | −9·4 | 4435 | 1631 | −5182·5 | 106·3102 | 47·0 |
| | | | Trimethylamine | | | |
| 94·8 | −3·7 | 5764 | 4675 | −7194·6 | 137·8173 | 74·3 |

The early determinations of the basic strength of the methylamines carried out by conductivity methods, giving classical dissociation constants, show on the whole very little agreement with one another. The only determinations which seem to have been carried out carefully with purified materials are those of Moore and Winmill (1912) and Somerville (1931), and these are in good agreement with one another. In table 10 these values are compared with our work interpolated to 25° C. We see that the conductivity method gives high values of $K$ as is to be expected if allowance is not made for interionic attraction forces. The dissociation constants of the methylamines have also been determined by an e.m.f. method by Harned and Robinson (1928), and their results recalculated by Harned and Owen (1930). While the value of the dissociation constant of monomethylamine obtained by these workers is only slightly greater than that now reported, their figures for the other two amines are very much lower. It is our experience that errors in the potentiometric method tend to give low values of $K$. Furthermore, Harned and Owen's calculations involve a rather uncertain extrapolation, and no mention is made of the purity of the amines employed.

TABLE 10. VALUES OF $K_b \times 10^4$ AT 25° C

| | Moore and Winmill | Somerville | Harned and Owen | This work |
|---|---|---|---|---|
| $CH_3NH_2$ | 4·74 | 4·69 | 4·38 | 4·246 |
| $(CH_3)_2NH$ | 6·35 | 6·44 | 5·20 | 5·994 |
| $(CH_3)_3N$ | 0·647 | 0·638 | 0 545 | 0·631$_{8}$ |

### DISCUSSION OF RESULTS

The most interesting outcome of this work is the discovery that there are appreciable and even large heat capacity changes accompanying the dissociation of the substituted ammonium ions. These dissociations involve no change in the number of charges and, on electrostatic grounds, it is to be expected that for such isoelectric processes the heat capacity change should be small, nevertheless, our value of $\Delta C_p$ for the dissociation of the trimethylammonium ion is almost as great as any observed for the dissociation of an uncharged acid. It is significant that with increasing substitution of methyl groups in the ammonium ion the values of $\Delta C_p$ steadily rise from approximately zero to 43·8 cal /deg. It is difficult to explain these results either on simple electrostatic grounds or by taking into account the orientation of solvent molecules by the ions and it seems probable that we must also consider the properties of the amine molecules. Examination of the partial pressures of aqueous solutions of ammonia and of the methylamines (Felsing and Phillips 1936) shows a steady transition from a strongly concave partial pressure curve for ammonia to a markedly convex curve for trimethylamine; this is also brought out by comparison of the vapour pressures of the pure amines with the Henry's law constants for their dilute aqueous solutions:

| | $NH_3$ | $CH_3NH_2$ | $(CH_3)_2NH$ | $(CH_3)_3N$ |
|---|---|---|---|---|
| Vapour pressure at 25° C | 7520 | 2681 | 1763 | 2299 |
| Henry's law constant at 25° C | 750 | 428 | 610 | 3600 |

This behaviour shows clearly that, whereas there is strong attraction between ammonia and water molecules, the substitution of methyl groups for hydrogen atoms reduces this attraction until for trimethylamine the attraction of the amine molecules for one another becomes dominant. This effect is seen very strikingly in the substituted ethylamines, where, as is well known, triethylamine with water shows a lower critical solution temperature at 20°. We believe that the strongly hydrophobic character of the alkyl groups in the substituted amines is responsible for the large positive values of $\Delta C_p$ in the dissociation of their ions.

We have discussed elsewhere the possibility of interpreting values of $\Delta C_p$ for ionization processes on a simple electrostatic basis and we have arrived at the conclusion that such an explanation is not plausible. We revert to the matter because in a recent publication Baughan (1939) has claimed the validity of just such a treatment based on the simple electrostatic theory originally advanced by Born (1920). Baughan has followed essentially the separation into electrostatic and non-electrostatic effects suggested by Gurney (1938), but, whereas Gurney assumed that the entropy of ionization is a purely electrostatic quantity, Baughan assumes the heat capacity change to be the quantity calculable by the use of Born's equation. In consequence of this difference between the two methods the validity of Baughan's assumption, while essential to Gurney's treatment, does not establish the latter which requires independent verification. There are, however, three reasons for disputing Baughan's claim that the values of the heat capacity changes can be calculated electrostatically:

(1) The values he uses for the heats of ionization are those given by Harned and his coworkers and our recalculated values do not usually agree with these.

(2) The dielectric constant data used by Baughan are those of Åkerlöf (1932) which differ from the more recent data of Wyman and Ingalls (1938).

(3) The ionic radii required to make the theory fit the results are very small

We find that when we use what are, in our opinion, better values of the heats of ionization and of the dielectric constant, the ionic radii are still further reduced and it is not possible to account for the data for any single equilibrium without making the ionic radii vary with temperature.

The data presented in this paper strain the electrostatic interpretation even more. If we combine the dissociation of the trimethylammonium ion with the ionization of formic acid, we obtain the ionic equilibrium

$$N(CH_3)_3 + HCOOH = NH(CH_3)_3^+ + HCOO^-,$$

for which $\Delta C_p = -85{\cdot}2$ cal./deg. and $\Delta S^\circ_{298{\cdot}1} = -2{\cdot}0$ cal./deg. From the thermodynamic relation $\Delta C_p = T\,.\,d(\Delta S)/dT$ it is evident that $\Delta S^\circ$ will become positive below a temperature of about 17° C and, consequently, Gurney's treatment fails completely. On the other hand, the mean ionic radius required to account for the value of $\Delta C_p$ is less than 0·3 A.

The present position with regard to the interpretation of the temperature coefficients of ionic equilibrium constants can be stated briefly as follows. The simple electrostatic theory fails to account for the entropy changes and, on any reasonable assumptions, can account for only a fraction of the change in heat capacity. Orientation effects have been shown by Eley and Evans (1938) to be responsible for a large part of the entropy of solution of an ion, and Everett and Coulson (1940) have shown that orientation of solvent molecules also contributes substantially to the heat capacity of an ion. Our results show that, for equilibria involving neutral molecules as well as ions, the heat capacities of the neutral molecules cannot be ignored.

## BASIC STRENGTH OF THE AMINES

A problem which has often excited interest is that of the relative strengths of ammonia and the various alkylamines It is well known that the introduction of successive alkyl groups into ammonia increases the basic strength, but the trialkylamines are always weaker than the dialkylamines Examination of the data in methyl and ethyl alcoholic solvents showed that the order of acid and basic strength depends upon the solvent (Wynne-Jones 1933), and it was suggested that a measure of the intrinsic strengths of acids and bases could be obtained by extrapolating the relative strengths to infinite dielectric constant It appeared likely that the order of intrinsic strengths of ammonia and the methylamines might then become

$$NH_3 < NH_2(CH_3) < NH(CH_3)_2 < N(CH_3)_3.$$

In our discussion of the thermodynamics of acid-base equilibria we considered the relative strengths of various related acids and tentatively suggested that, whereas $\Delta H_0$ could have no fundamental significance, the relative values might be regarded as measure of the intrinsic strengths of the acids involved. In figure 4 we show the values of the thermodynamic functions for the dissociation of the ammonium and methylammonium ions and it is clear that only the heat and free energy changes at room temperature are anomalous. Furthermore, by plotting ($\log K_{\text{mono.}} - \log K_{\text{di.}}$) against temperature as shown in figure 5, the relative acid strength of mono- and dimethylammonium ions is seen to be reversed at only $-10°$ C. From the values of $\Delta H_0$ the acid strengths of the various ammonium

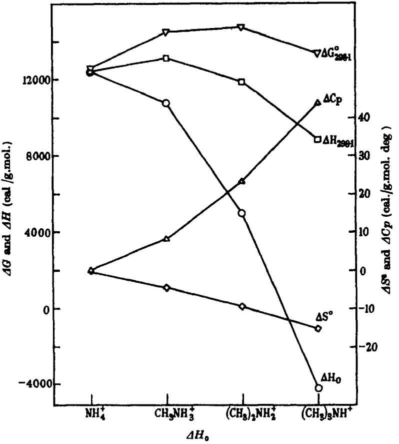

FIGURE 4. The thermodynamic functions for the dissociation of the ammonium and methylammonium ions.

ions, and hence also the basic strengths of the amines, are seen to vary continuously from ammonia to trimethylamine, but the order is the reverse of that given above.

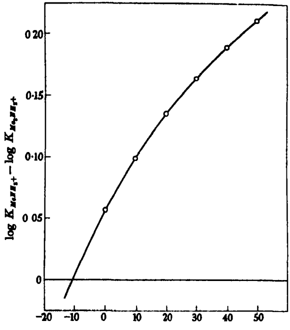

FIGURE 5. Relative acid strengths of mono- and dimethylammonium ions

The discrepancy between the two methods of estimating intrinsic strength cannot be resolved until we have temperature coefficient data for other solvents and clearer understanding of the meaning of $\Delta H_0$.

We acknowledge our indebtedness to Imperial Chemical Industries Ltd. for the loan of a potentiometer and of a refrigerator, and to the Council of University College, Dundee, for a Research Grant which enabled one of us (D.H.E.) to carry out this work.

## REFERENCES

Åkerlof 1932 *J. Amer. Chem Soc* **54**, 4125.
Baughan 1939 *J. Chem. Phys* **7**, 951.
Born 1920 *Z. Phys.* **1**, 45.
Eley and Evans 1938 *Trans. Faraday Soc.* **34**, 1093.

Everett and Coulson 1940 *Trans. Faraday Soc.* **36**, 633.
Everett and Wynne-Jones 1938 *Proc. Roy. Soc.* A, **169**, 190.
Everett and Wynne-Jones 1939 *Trans. Faraday Soc.* **35**, 1380.
Felsing and Phillips 1936 *J. Amer. Chem. Soc.* **58**, 1973.
Gurney 1938 *J. Chem. Phys.* **6**, 499.
Harned and Hamer 1933 *J. Amer. Chem. Soc.* **55**, 2194.
Harned and Owen 1930 *J. Amer. Chem. Soc.* **52**, 5079.
Harned and Robinson 1928 *J. Amer. Chem Soc.* **50**, 3157.
Moore and Winmill 1912 *J. Chem. Soc.* **101**, 1635.
Somerville 1931 *J. Phys. Chem.* **35**, 2412.
Wyman and Ingalls 1938 *J. Amer. Chem. Soc.* **60**, 1182.
Wynne Jones 1933 *Proc. Roy. Soc.* A, **140**, 440.

# INDEX TO VOLUME 177 (A)

Amino compounds, infra-red absorption spectra (Kellner), 447.
Andrews, K. W., Davies, H. E., Hume-Rothery, W. and Oswin, C. R. The equilibrium diagram of the system silver-zinc, 149.
Anniversary address (Bragg), 1.
Apparent sizes of atoms in metallic crystals (Hume-Rothery and Raynor), 27

Bates, D. R. and Massey, H S. W. Exchange effects in the theory of the continuous absorption of light, I, 329.
Beeck, O., Givens, J. W., Smith, A E and Williams, E. C On the mechanism of boundary lubrication, I, II, 90, 103.
Beeck, O., Smith, A. E., Wheeler, A. Catalytic activity, crystal structure and adsorptive properties of evaporated metal films, 62.
Beevers, C. A. and Hughes, W. The crystal structure of Rochelle salt, 251
$\beta$-ray spectra of light elements (Townsend), 357.
Blackett, P. M. S. and Lovell, A. C B. Radio echoes and cosmic ray showers, 183.
Boron, disintegration by slow neutrons (Wilson), 382.
Bragg, Sir William. Anniversary address, 1
Bullard, E. C. and Gaskell, T. F. Submarine seismic investigations, 476.

Catalytic activity, crystal structure and adsorptive properties of evaporated metal films (Beeck, Smith and Wheeler), 62.
Chapman, S The characteristics of thermal diffusion, 38.
Clark, G. L The derivation of mechanics from the law of gravitation in relativity theory, 227.
Coincidence method for measurements of short life periods (Rotblat), 260
Cosmic-ray intensity, seasonal variations (Duperier), 204

Dainton, F. S. and Norrish, R. G. W. A study of sensitized explosions, V, VI, VII, 393, 411, 421.
David, H. G and Munson, R. J. The mobility of alkali ions in gases, 192
Davies, H. E. *See* Andrews and others.
Davison, B. and Rosenhead, L. Wind tunnel correction for a circular open jet tunnel with a reflexion plate, 366.
Derivation of mechanics from the law of gravitation in relativity theory (Clark), 227.
Duperier, A. The seasonal variations of cosmic-ray intensity and temperature of the atmosphere, 204.

Electromagnetic two-body problem (Synge), 118
Everett, D. H and Wynne-Jones, W. F K. The dissociation constants of the methylammonium ions and the basic strengths of the methylamines in water, 498
Exchange effects in the theory of the continuous absorption of light (Bates and Massey), 329.
Explosions, sensitized (Dainton and Norrish), 393, 411, 421.

Fürth, R. A thermodynamical theory of the tensile strength of isotropic bodies, 217.

Ganguli, N. and Krishnan, K. S. The magnetic and other properties of the free electrons in graphite, 168.
Gaskell, T. F. *See* Bullard and Gaskell.
Givens, J. W. *See* Beeck and others.
Graphite, properties of free electrons (Ganguli and Krishnan), 168.

Hoselitz, K. The mobility of alkali ions in gases, 200.
Hughes, W. *See* Beevers and Hughes.
Hume-Rothery, W. and Raynor, G. V. The apparent sizes of atoms in metallic crystals with special reference to aluminium and indium, and the electronic state of magnesium, 27.
Hume-Rothery, W. *See* Andrews and others.

Isotropic bodies, thermodynamical theory (Fürth), 217.

Kellner, L. Infra-red absorption spectra of some amino compounds, 447.
Kellner, L. The vibrations and the molecular structure of urea and guanidonium, 456.
Knaggs, I. E., Lonsdale, K., Williams, G. and Wood, R G. The structure of melamine, $C_3N_6H_6$, 140.
Krishnan, K. S. *See* Ganguli and Krishnan.

Lonsdale, K. Molecular anisotropy of urea, 272.
Lonsdale, K. *See* Knaggs and others.
Lovell, A. C. B. *See* Blackett and Lovell.

Massey, H. S. W. and Mohr, C. B. O. The polarization of electrons by double scattering, 341.
Massey, H. S. W. *See* Bates and Massey.
Mechanism of boundary lubrication (Beeck, Givens, Smith and Williams), 90, 103.
Melamine, structure and optical properties (Knaggs, Lonsdale, Williams and Wood), 140.
Methylammonium ions, dissociation constants, and the basic strengths of the methylamines in water (Everett and Wynne-Jones), 499.
Mobility of alkali ions in gases, IV (David and Munson), 192, V (Hoselitz), 200.
Mobility of positive ions in their own gas (Munson and Tyndall), 187.
Mohr, C. B. O. *See* Massey and Mohr.
Munson, R. J. and Tyndall, A. M. The mobility of positive ions in their own gas, 187.
Munson, R. J. *See* David and Munson.

Norrish, R G. W. *See* Dainton and Norrish.

Oswin, C. R. *See* Andrews and others.

**Polarization of electrons by double scattering (Massey and Mohr), 341.**

**Radio echoes and cosmic ray showers (Blackett and Lovell), 183**
**Raynor, G. V. *See* Hume-Rothery and Raynor.**
**Robinson, G. D. *See* Simpson and Robinson.**
**Rochelle salt, crystal structure (Beevers and Hughes), 251**
**Rosenhead, L. *See* Davison and Rosenhead.**
**Rotblat, J. Application of the coincidence method for measurements of short life periods, 260.**

**Silver-zinc equilibrium diagram (Andrews, Davies, Hume-Rothery and Oswin), 149.**
**Simpson, Sir George and Robinson, G. D. The distribution of electricity in thundercloud, II, 281.**
**Smith, A. E. *See* Beeck and others.**
**Submarine seismic investigations (Bullard and Gaskell), 476.**
**Synge, J. L. On the electromagnetic two-body problem, 118.**

**Thermal diffusion, characteristics (Chapman), 38.**
**Thundercloud, distribution of electricity (Simpson and Robinson), 281.**
**Townsend, A. A. $\beta$-ray spectra of light elements, 357.**
**Tyndall, A. M. *See* Munson and Tyndall.**

**Urea, molecular anisotropy (Lonsdale), 272.**
**Urea and guanidonium, vibrations and molecular structure (Kellner), 456.**

**Wheeler, A. *See* Beeck and others.**
**Williams, E. C. *See* Beeck and others.**
**Williams, G. *See* Knaggs and others.**
**Wilson, R. S. An investigation of the disintegration of boron by slow neutrons, 382.**
**Wind tunnel correction for a circular open jet tunnel with a reflexion plate (Davison and Rosenhead), 366.**
**Wood, R. C. *See* Knaggs and others.**
**Wynne-Jones, W. F. K. *See* Everett and Wynne-Jones.**

END OF THE ONE HUNDRED AND SEVENTY-SEVENTH VOLUME (SERIES A)

# ABSTRACTS

# OF PAPERS COMMUNICATED TO THE ROYAL SOCIETY OF LONDON

**In accordance with a resolution of Council, summaries or abstracts of papers are to be published as soon as practicable. The publication of such abstracts in no way indicates that the papers have been accepted for publication in any fuller form. These abstracts are issued for convenience with the "Proceedings of the Royal Society of London" but do not form a part of the "Proceedings".**

NOTE—The pagination of the 'Abstracts' will be consecutive through the year and independent of the 'Proceedings'. To avoid any confusion with the 'Proceedings', the page numbers will be preceded by the letter S (*i.e.* Summary).

---

24 FEBRUARY 1941

---

## Anatomical and histological changes during the oestrous cycle in the mare.

By J. HAMMOND, F.R.S. and K. WODZICKI. (*Received* 18 *November* 1940.)

The mares chosen for the investigation of the changes in the reproductive organs during the oestrous cycle were kept under observation for some time before they were killed. The duration of the heat period in these animals was 7 days and the length of the dioestrus was 16 days. Ovulation takes place at about a day before the end of oestrus. The size of the ovary during the oestrous cycle is chiefly influenced by the growing Graafian follicle. The number of follicles present at different stages varies greatly. The numerous small follicles present at the beginning of oestrus disappear later in the cycle; it is suggested that this may be due to the lack of follicle-stimulating hormone.

The colour of the corpus luteum varies greatly at different stages of the cycle. The rupture of the follicle is associated with some bleeding. The active stage of the corpus luteum is very short and the maximum diameter of the corpus luteum seems to be always below that of the Graafian follicle. The greater development of the Graafian follicle, with its secretion of oestrin, in the mare leads to its playing a more important rôle than in the cow and the sow, in which species the corpus luteum takes a more dominant part in the cycle. It appears that the much longer oestrus in the mare than in the cow is due to the longer time required by the follicle to come to the surface and to break through. This is probably due to the peculiar structure of the ovary in the mare, since the ovulation, which is spontaneous, can only occur in the small ovulation fossa. No pronounced secretion stage occurs during oestrus in the Fallopian tubes.

The anatomical and histological changes in the uterus of the mare during the cycle are slight as compared with those in species which have a specialized placentation, such as the rabbit, ferret and cat; they are similar to those changes which occur in a species with a simple placentation such as the pig.

Cyclic changes are described in the epithelial cells of the cervix, which acts as a large mucous gland. It is probable that ejaculation takes place directly through the cervix into the uterus.

The changes in the vagina proper and the vestibulum vaginae are described; they are less pronounced in the mare than in the cow, but some cornification and leucocytosis, similar to that found in some rodents, occurs.

## The sun's magnetic field and the diurnal and seasonal variations in cosmic ray intensity.

By L. Jánossy and P. Lockett. (*Communicated by P. M S. Blackett, F.R.S.—Received* 18 *November* 1940.)

The diurnal and seasonal variations in the vertical cosmic ray intensity, produced by an extending solar magnetic dipole field, are calculated at latitudes 0 and 45° and compared with experimental data.

It appears that the diurnal variation at latitude 45° can be largely accounted for by assuming the existence of a solar dipole of moment $1 \cdot 1 \times 10^{34}$ gauss : cm.$^3$, a value which is consistent with experimental evidence. The diurnal variation at the equator, however, cannot be explained by the hypothesis of a solar magnetic dipole field.

The seasonal variation in intensity obtained, assuming the above value for the solar dipole moment, is of the same order of magnitude as the experimental variation but shows a two month phase discrepancy.

## Precise measurements of the energies of $\beta$-rays from radium (B + C).

By A. F. A. Harper and N. F. Roberts (*Communicated by C. D Ellis, F.R.S.—Received* 20 *November* 1940.)

Precise measurements of the $H\rho$ values of $\beta$-rays from radium B have been made by Ellis and Skinner (1924), Ellis (1934), Scott (1934) and Rogers (1936, 1937). Except for Rogers and Scott, who used the same methods, the results have differed from one another by amounts considerably in excess of the estimated probable errors.

Measurements have been made by the authors of the $H\rho$ of eleven $\beta$-rays of radium B and of one of radium C. The values are based on eleven photographs of the spectra taken with a spectrograph of the type used by Ellis and ten photographs with a spectrograph of the type introduced by Scott, the field strengths used ranging from 190 to 1050 gauss. The values obtained agree closely with those of Rogers for the lines measured by him; Rogers's values being 1931·7 gauss cm., 1671·3 gauss cm., and 1406·2 gauss cm., and our values 1931·9, 1671·6 and 1406·2 gauss cm. These values are considered correct to 1 part in $10^4$.

The energies corresponding to the $H\rho$ values have been calculated using weighted mean values of $e/m$ and $c$ given respectively by Bearden and von Friesen. The error in the energies is approximately 1 part in $10^3$.

Measurement of the $H\rho$ of the same line for a number of widely differing values of $H$ was a valuable check on the presence of systematic errors which had not been made by previous workers. An appreciable apparent increase of $H\rho$ with $H$ was found, and a comparison of the calculated and observed line forms showed that this apparent increase was to be attributed to scattering of electrons in the emulsion. This effect appears to be one of the most important now limiting the accuracy obtainable by the present methods.

## **Photosynthesis in intermittent illumination.** By G. E. Briggs, F.R.S. (*Received* 29 *November* 1940.)

The reduction of one molecule of carbon dioxide per two thousand molecules of chlorophyll for each intense flash of light of very short duration while three hundred or more are reduced when the duration of the flash is greatly increased can be explained by assuming that chlorophyll sensitizes the activation of a substance $A$ which, by handing its energy, causes the reduction of carbon dioxide in combination with a substance $S$. The decay of activated $A$ is a relatively rapid process while that of the activated compound of carbon dioxide and $S$ is relatively slow. The yield for short flashes is determined by $A$, that for long flashes by $S$. The ratio of $S$ to $A$ is of the order of 100.

## **The γ-ray transition of radio-bromine.** By R. E. Siday. (*Communicated by P. M. S. Blackett, F.R.S.—Received* 4 *December* 1940.)

The disintegration by the emission of $\gamma$-rays of the metastable isotope of radio-bromine was investigated by the method of cloud chamber The principal $\gamma$-ray was found to have an energy of 47 kV and a coefficient of internal conversion in the $K$ shell of 0·38. A much weaker $\gamma$-ray reported ambiguously to have an energy of either 25 or 37 kV was confirmed and shown to have, in fact, an energy of 37 kV.

## **Cones of extinct Cycadales from the Jurassic rocks of Yorkshire.** By T. M. Harris. (*Communicated by Sir Albert Seward, F.R S.—Received* 13 *December* 1940.)

Very few fossils representing reproductive organs of the Cycadales in the strict sense are known. Two new species of male cones, *Androstrobus manis* and *A. wonnacotti* are described, these being the first male cones in which agreement with those of the Cycads has been proved to exist in structure as well as in general appearance. The little known female cone *Beania gracilis* Carruthers is also described and new information is given about its development, its finer structure and in particular about the anatomy of the seed.

Reasons are put forward for attributing *Androstrobus manis* and *Beania gracilis* to the same plant as *Nilssonia compta*. This is an important step, as *Nilssonia* is one of the most abundant and widespread genera of leaves in the Mesozoic rocks.

## The determination of the vapour pressure curve of liquid helium below 1·6° K using a magnetic thermometer. By B. Bleaney and R. A. Hull.

(*Communicated by F. A. Lindemann, F.R.S.—Received* 17 *December* 1940.)

The vapour pressure curve of liquid helium below 1·6° K has been determined using the susceptibility of various paramagnetic salts as the thermometer. It is found that the results agree with the theoretical curve recently calculated by Bleaney and Simon to within the experimental error of 0·004° down to 1° K and differ from the 'scale 1937' of Schmidt and Keesom, e.g. by 0·03° at 1° K.

## The effective susceptibility of a paramagnetic powder. By B. Bleaney and R. A. Hull.

(*Communicated by F. A. Lindemann, F.R.S.—Received* 17 *December* 1940.)

The effective susceptibility (that is, the magnetic moment divided by the external magnetic field) of a paramagnetic powder loosely packed into an ellipsoidal container has been measured against the vapour pressure of liquid helium, and hence, using the results of the preceding paper, against the susceptibility of the compact salt. The definition of the 'Curie' temperature scale is based on the latter, and it is found that the correction to be applied in calculating the 'Curie' temperature from the effective susceptibility of the powder agrees with that given by a theoretical expression derived from Breit's calculation of the demagnetizing field of a powder. This is of importance both in experiments using a loosely packed powder and in experiments using a paramagnetic powder mixed with a non-magnetic material.

# ABSTRACTS

# OF PAPERS COMMUNICATED TO THE ROYAL SOCIETY OF LONDON

**In accordance with a resolution of Council, summaries or abstracts of papers are to be published as soon as practicable. The publication of such abstracts in no way indicates that the papers have been accepted for publication in any fuller form. These abstracts are issued for convenience with the "Proceedings of the Royal Society of London" but do not form a part of the "Proceedings".**

---

18 MARCH 1941

---

## A self-consistent field for methane and its applications.

By R. A BUCKINGHAM, H. S. W. MASSEY, F R S., and S. R. TIBBS

(*Received* 6 *November* 1940.)

An approximate self-consistent field for methane has been obtained by first averaging the proton distribution over all orientations so as to obtain a spherically symmetrical field due to all the nuclei. The eight-electron problem then presented was solved by the usual self-consistent field method without exchange. Rapid convergence to self-consistency was found by using as initial approximations the charge distributions given by Coulson for the two-quantum orbitals of the tetrahedral system, averaged over all orientations.

The self-consistent wave functions are used to calculate the charge distribution, energy, diamagnetic susceptibility and polarizability of the molecule and also the van der Waals forces between two molecules. The scattering of slow electrons by the self-consistent field obtained is also investigated in detail and compared with observations of total collision areas and angular distributions for methane. The observed similarity of behaviour between argon and methane in scattering slow electrons is reproduced by the theory, provided the same approximation of using the self-consistent field without exchange is employed for each. Comparison of observed and calculated values of the quantities investigated indicates that the methane field is little less satisfactory than the corresponding field for atoms.

## The low temperature properties of gaseous helium. II. By R. A. Buckingham, J. Hamilton and H. S. W. Massey, F.R.S. (*Received 6 November* 1940.)

Some earlier calculations of the second virial and viscosity coefficients of gaseous helium have been extended, using as before the exact quantum formulae. A brief discussion of the atomic interaction, which is expressed in the form

$$V(\sigma) = \epsilon f(\sigma),$$

where $\sigma = r/r_0$, $r_0$ is the atomic separation when $V$ is a minimum, and $f(1) = -1$, is followed by the results of the new calculations and their interpretation. Several interactions, with widely varying values of $\epsilon r_0^3$, have been employed, and inferences about the actual interaction are made by interpolating the available experimental data, a method particularly suitable for interpreting future results. The results of some calculations by de Boer and Michels have been incorporated. It is found that the present data for the second virial coefficient, between 2 and 4·3° K, indicate for $\epsilon r_0^3$ a value about $122 \times 10^{-16}$ erg A$^3$. Though the separate determination of $r_0$ and $\epsilon$ is not likely to be very precise unless calculations are extended to temperatures much beyond the present limit (11° K), the assumption of a probable value for the first van der Waals coefficient leads to the values

$$r_0 = 2{\cdot}93\ \text{A}, \quad \epsilon = 14{\cdot}2 \times 10^{-16}\ \text{erg}.$$

The influence of possible variations in the function $f(\sigma)$ are discussed and shown to be of secondary importance, and these results are based on a reasonable form for $f(\sigma)$ with two parameters.

Comparisons are also made with two viscosity measurements below 5° K, but the inferences from these are not at all in agreement with the evidence from the equation of state.

## The flame spectrum of carbon monoxide. II. Application to 'after-burning'. By A. G. Gaydon. (*Communicated by A. C. G. Egerton, F.R.S.—Received* 29 *November* 1940.)

In a previous paper it has been shown, from a study of the spectrum of the carbon monoxide flame, that the molecules of $CO_2$ formed by the combustion are initially in a highly excited state of internal vibration. An attempt is made here to derive approximate values for the lifetimes of those vibrationally activated molecules.

The orders of magnitude of the radiative lifetime for the three types of vibration are derived. From data obtained from supersonic dispersion in $CO_2$ the relaxation times, or collision lifetimes, are discussed with especial emphasis on the effect of moisture on the collision life of the activated molecules. A section is also devoted to the possibility of the close resonance between the vibrations $\nu_1$ and $\nu_2$ of $CO_2$ resulting in a high percentage of dissociation after the combustion of the dry gas.

The results give a good interpretation of the experiments of Garner and colleagues on the marked effect of moisture and other catalysts on the infra-red emission of the flame, and the general failure to observe a strong emission band at 14·9$\mu$. The results of the theory go far towards explaining the latent energy of the combustion observed by David and colleagues.

The lifetime of the activated molecules is calculated to be not more than a few tenths of a second, but dissociation and recombination processes might lengthen this time. For moist gases the lifetime will be very much less, and the infra-red radiation from the flame and the latent energy of the products should similarly be much reduced, in agreement with experiment. The vibrationally activated molecules are to be regarded as essentially normal molecules of $CO_2$ in which the vibrational energy has not had time to reach equipartition with the energy in other degrees of freedom; spectroscopically there is no evidence to show that they are electronically excited or peculiar in any other way.

Experiments on the absorption spectrum of a long length of burning gas show strong absorption due to hot oxygen, this being particularly marked when the gases are dry. This is interpreted as being due to transfer of the vibrational energy from the $CO_2$ to the $O_2$ molecules, the absorption spectrum of which is thereby shifted to longer wave-lengths

## The electron diffraction of multilayers of esters of fatty acids. I. By A. Cameron and G. Coumoulos. (*Communicated by E. K Rideal, F.R S.—Received* 9 *December* 1940.)

The arrangement of the long axis of the long-chain organic molecules is revealed by electron diffraction patterns of inclined specimens. The side spacings are estimated by a superimposed pattern of kaolin which has a known 'standard' structure and lattice constants. A 3 cm. vacuum valve was designed to isolate the apparatus from the oil-diffusion pumps.

## On the electron diffraction of multilayers of esters of fatty acids. By G. Coumoulos and E. K. Rideal, F.R S (*Received* 9 *December* 1940 )

Electron diffraction results for the arrangement and the orientation of the molecules and the side spacings of the two-dimensional crystals of thin multilayers of methyl and ethyl stearate, and octadecyl acetate are given A state similar to the $\alpha$ modification in crystals is a stable form for thin multilayers of long-chain esters. The 'multilayer' state is transient and is replaced by an aggregation of micro-crystals with 'fibre' orientation.

## On transition from laminar to turbulent flow in the boundary layer. By A. Fage and J. H. Preston. (*Communicated by E. F. Relf, F.R.S.—Received* 10 *December* 1940.)

Information on transition from laminar to turbulent flow in boundary layers on streamline bodies of revolution in a water stream is obtained from visual and photographic observation of the movements of small particles and filament bands. The cases considered are transition caused by isotropic turbulence in the free stream, by a falling velocity in a stream substantially free from turbulence, and by flow disturbances from surface wires.

A non-dimensional number, specified in terms of the intensity and scale of turbulence, the boundary-layer thickness, and the mean velocity just outside the layer, is found to be representative of the conditions of flow in the boundary layer of a body in a turbulent stream: and values of this number at transition obtained from observations made for a body of revolution have the same order of magnitude as those calculated for a flat plate from measurements taken by Hall and Hislop.

Transition in a region of falling velocity in a steady stream arises from a separation of the laminar boundary layer from the surface; and after separation, the flow in the layer becomes turbulent and then rejoins the surface. The observed position of transition is near the position of separation given by a solution of the momentum equation for laminar flow and for the observed distribution of velocity just outside the layer.

Flow disturbances from a surface wire placed in a laminar boundary layer cause fully-developed turbulent flow to be established at the wire when $u_1 d/\nu > 400$, where $d$ is the wire diameter, $u_1$ is the velocity in the laminar layer at a distance $d$ from the surface, and $\nu$ is the kinematic viscosity.

The measured maximum value of the downstream component of turbulent velocity in the stream behind a grid is about 3·3 times the root-mean-square value.

## **General classical theory of spinning particles in a Maxwell field.** By H. J. Bhabha and H. C. Corben. (*Communicated by P. A. M. Dirac, F.R.S —Received* 18 *December* 1940)

The purpose of this paper is to give the complete classical theory of a spinning particle moving in a Maxwell field. The particle is assumed to be a point, and its interaction with the field is described by a point charge $g_1$ and a point dipole $g_2$. The Maxwell equations are assumed to hold right up to the point representing the particle. Exact equations are then derived for the motion of the particle in a given external field which are strictly consistent with the conservation of energy, momentum and angular momentum, and hence contain the effects of radiation reaction on the motion of the particle. The mass, the angular momentum of the spin, etc, appear in the equations as arbitrary mechanical constants. It is shown that in the presence of a point dipole the energy tensor of the field can and must be redefined so as to make the total field energy finite In the general theory there is no relation between the electric and magnetic dipole moments of the particle and the state of its translational motion. A procedure is given for deriving from the general equations specialized equations consistent with the condition that the dipole is always a purely magnetic or electric one in the system in which the particle is instantaneously at rest The radiation reaction terms are very much simpler in either of these specialized cases than in the general case. The effect of radiation reaction is to make the scattering of light by a rotating dipole *decrease* inversely as the square of the frequency for high frequencies just as for scattering by a point charge.

## General classical theory of spinning particles in a meson field.

By H. J. BHABHA. (*Communicated by P. A. M. Dirac, F.R.S.—Received* 18 *December* 1940.)

An exact classical theory of the motion of a point dipole in a meson field is given which takes into account the effects of the reaction of the emitted meson field. The meson field is characterized by a constant $\chi = \mu/\hbar$ of the dimensions of a reciprocal length, $\mu$ being the meson mass, and as $\chi \to 0$ the theory of this paper goes over continuously into the theory of the preceding paper for the motion of a spinning particle in a Maxwell field. The mass of the particle and the spin angular momentum are arbitrary mechanical constants. The field contributes a small finite addition to the mass, and a negative moment of inertia about an axis perpendicular to the spin axis.

A cross-section (formula 88*a*) is given for the scattering of *transversely* polarized neutral mesons by the rotation of the spin of the neutron or proton which should be valid up to energies of $10^9$ eV. For low energies $E$ it agrees completely with the old quantum mechanical cross-section, having the same dependence on energy proportional to $p^4/E^2$ ($p$ being the meson momentum). At higher energies it deviates completely from the quantum mechanical cross-section, which it supersedes by taking into account the effects of radiation reaction on the rotation of the spin. The quantum theory of the interaction of neutrons with mesons goes wrong for $E > 3\mu$ The cross-section is a maximum at $E \sim 3{\cdot}5\mu$, its value at this point being $3 \times 10^{-26}$ cm$^2$, after which it decreases rapidly, becoming proportional to $E^{-2}$ at high energies. The scattering of longitudinally polarized mesons is due to the translational but not the rotational motion of the dipole and is at least twenty thousand times smaller

With the assumption previously made by the present author that the heavy particles may exist in states of any integral charge, and in particular that protons of charges $2e$ and $-e$ may occur in nature, the above results can be applied to *charged* mesons. Thus transversely polarized mesons should undergo a very big scattering and consequent absorption at energies near $3{\cdot}5\mu$ Hence the energy spectrum of mesons should fall off rapidly for energies below about $3\mu$, as is observed Scattering plays a relatively unimportant part in the absorption of longitudinally polarized mesons, and they are therefore much more penetrating.

## A stress-strain curve for the atomic lattice of iron.

By S L SMITH and W. A. WOOD. (*Communicated by G. W C Kaye, F.R S.—Received* 23 *December* 1940.)

Measurements have been made on the stress-strain relationship for the atomic lattice of iron (purity 99·95 %). The changes in dimensions of the atomic lattice of tensile specimens have been determined in the direction perpendicular to the applied stress and compared with the contraction in external dimensions which occurs in the same direction. It has been shown that the lattice stress-strain curve, obtained by plotting the lateral change in lattice spacing against the tensile stress, exhibits three main characteristics. Up to the external yield point, the lattice contraction is directly proportional to the applied stress. Beyond the yield point, the lattice contraction slows down as the stress increases. Finally, at still higher stresses, the lattice tends to expand. A further set of experiments, in which cycles of stress are employed, show that when a stress greater than the yield stress is applied and then removed from a specimen, the lattice is left with a permanent expansion which depends in a regular manner upon the value of the stress applied. It is concluded that beyond the external yield point, the iron lattice undergoes two distinct modifications. First, the lattice spacing tends to contract elastically, in conformity with the external elastic contraction exhibited by the specimen in the same direction (perpendicular to the applied stress). Second, the lattice tends to deform in a manner which leads to a superposed expansion of lattice spacing. The actual change of spacing at a particular stress is then the resultant of the two effects; a process which explains the unexpected shape of the lattice stress-strain curve, and affords systematic information on the problem of internal strains in metals. Further experiments indicate that the permanent expansion of the lattice after loading occurs not only in the direction perpendicular to the applied stress, but also in the direction of the stress; the permanent lattice deformation thus represents a decrease in density of the test specimen. Finally, the results of some experiments are recorded on the effect of temperature on the lattice expansion effect, and it is shown that recovery of the lattice can be produced by mild heat treatment at a temperature much lower than that required to renew the properties of the metal by recrystallization.

## Relaxation methods applied to engineering problems. VII. Problems relating to the percolation of fluids through porous materials. By F. S. Shaw and R. V. Southwell, F.R.S. (*Received* 3 *January* 1941.)

The accepted theory of percolation of fluids through porous materials (which is based on Darcy's law of resistance) indicates that the velocities can be calculated from a velocity potential which, in two-dimensional motion, is plane harmonic within the fluid field. The associated stream function, and the fluid pressure, are also plane harmonic, so in cases where all boundaries are known their determination is an ordinary problem in plane-potential theory. But in cases where a free surface exists (as in the percolation of water through earth dams), its shape is not known a priori, consequently orthodox methods cannot be applied.

Here the relaxation method developed in earlier papers is shown to be applicable without special assumption, and to yield results of more than sufficient accuracy. Three typical examples are treated, the third involving 'refraction' of the lines of flow and pressure at the junction of two materials of different porosity.

## Critical and co-operative phenomena. VI. The neighbour distribution function in monatomic liquids and dense gases. By J. Corner and J. E. Lennard-Jones, F.R.S. (*Received* 9 *January* 1941.)

The methods of dealing with liquids developed in preceding papers are applied to the calculation of the distribution of atoms in liquids and dense gases. It is shown that when the motion of the atoms resembles that of linear oscillators this distribution function takes a particularly simple form. The theoretical formulae are compared with recent experimental results for potassium.

The inverse problem of determining intermolecular forces from known distribution functions is considered and a mathematical method of deriving this information is given.

### Further investigations of solid $n$-paraffins; repulsion potential and compressibility. By A. MÜLLER. (*Communicated by Sir William Bragg, F.R.S.—Received* 30 *January* 1941.)

Experiments are made on the compressibilities of solid $n$-paraffins. The lattice deformations due to pressure are measured with the aid of X-rays, the pressures ranging between 700 and 1500 atmospheres. It is found that the linear compressibilities in a plane normal to the chain axes are of the order of 3 to $12 \times 10^{-12}$ cm $^2$/dyne. The compressibility in the direction of the chain is less than $3 \times 10^{-13}$ cm.$^2$/dyne.

Numerical estimates show that the repulsive forces between paraffin chains have their origin essentially in the hydrogen shells that surround the carbon chain. The forces are of the same order as those existing between helium atoms.

### Deuteron-induced fission in uranium and thorium. By D. H. T. GANT and R. S. KRISHNAN. (*Communicated by J. D. Cockcroft, F.R.S.—Received* 3 *February* 1941.)

Nuclear fission of uranium and thorium under bombardment by deuterons of about 9 MeV has been investigated both qualitatively and quantitatively by the use of the 'active deposit' technique

The following results have been obtained: (i) the range of the fission fragments from both uranium and thorium is about 2·3 cm. in air; (ii) the decay curve agrees in scale and shape with that which would be expected from a complex mixture of radioactive bodies; (iii) the active deposit has been examined for emission of $\beta$-rays, positrons, $\gamma$- and X-rays, $\alpha$-particles and neutrons; the radiations are found to bear a general similarity to those resulting from neutron-induced fission; (iv) some of the radioactive bodies have been isolated by chemical methods, some correspondence with the products of neutron-induced fission is shown, (v) the ratio of the fission cross-sections for 9 MeV deuterons and (Li + D) neutrons has been measured; (vi) the excitation function has been studied.

The experimental results from (v) and (vi) are compared with calculations based on Bohr and Wheeler's treatment of the mechanism of the process.

### A survey of anthocyanins, VII. By G. H. BEALE, J. R. PRICE and V. C. STURGESS. (*Communicated by Sir Robert Robinson, F.R.S.—Received* 3 *February* 1941.)

The anthocyanins have been identified in the flowers, fruits and leaves of approximately 200 species of plants. The results have been combined with earlier data, to ascertain the frequency with which derivatives of the three main anthocyanidin types occur as flower pigments among the species so far examined.

Classification of the natural habitats of the species examined shows that pelargonidin derivatives predominate in the flowers of tropical and sub-tropical species, whereas delphinidin derivatives are the commonest in temperate and alpine plants.

The colours of tropical and sub-tropical flowers containing cyanidin or delphinidin derivatives are generally redder than those of temperate species containing the same anthocyanin. It is concluded that red-flowered forms have a greater survival value than blue in most tropical plants. On the basis of the anthocyanin present in the flowers of 32 species of *Tulipa*, the genus falls into two groups in accordance with the morphological classification.

# ABSTRACTS

# OF PAPERS COMMUNICATED TO THE ROYAL SOCIETY OF LONDON

**In accordance with a resolution of Council, summaries or abstracts of papers are to be published as soon as practicable. The publication of such abstracts in no way indicates that the papers have been accepted for publication in any fuller form. These abstracts are issued for convenience with the "Proceedings of the Royal Society of London" but do not form a part of the "Proceedings".**

---

31 December 1940

---

**The seasonal variations of cosmic-ray intensity and temperature of the atmosphere.** By A. Duperier. *(Communicated by P. M. S. Blackett, F.R.S.—Received 4 March 1940.)*

A careful examination of the upper atmospheric data for Europe and the United States indicates that the mean temperature of the upper atmosphere in spring differs from that of summer more than from that of winter. The magnitude of the second difference, as defined, depends on the height of the atmosphere which is considered and is a maximum at a height of about 6 km. and changes sign at heights above 12 km. (figure) This lag in the warming of the atmosphere in spring is found to be paralleled by a lag in the diminution of intensity of the cosmic rays. A similar phenomenon is found in autumn. The cooling of the atmosphere as a whole is found to be less between summer and autumn than between autumn and winter, though the effect is markedly less definite than in spring

The cosmic ray variation is found to be correlated more closely with the mean temperature of the atmosphere up to 16 km than with the temperature near the ground. This provided additional support for the theory of Blackett that the temperature variation of penetrating cosmic rays is related to the instability of the mesotron. The temperature coefficient of the cosmic rays as deduced from the seasonal data is found to be 0·18 % per ° C, and this is in rough agreement with the prediction of the theory.

## The production of waves by the sudden release of a spherical distribution of compressed air in the atmosphere.

By J. J. Unwin, M.Sc. (*Communicated by G. I. Taylor, F.R.S.—Received 27 June* 1940.)

An attempt has been made to develop a method for dealing with solutions of problems connected with the production of waves by spherical concentrations of compressed air. Starting from the general equations for three-dimensional spherically symmetrical flow in a homogeneous compressible medium having constant entropy everywhere, a process has been devised to apply step-by-step calculations over small intervals of time to investigate the general features of such a motion. A complete solution has been worked out in one particular case for a not very intense initial distribution of pressure, and various indirect checks have indicated that the results are reasonably accurate. These results show many features of distinct interest. As distinct from plane or spherical sound wave theory, it is found that a train of waves passes away from the centre of disturbance, the amplitudes and wave lengths falling off from wave to wave. Furthermore, as distinct from finite amplitude plane wave theory which shows that any wave must eventually become a shock wave, the waves obtained in the finite amplitude spherical wave case show no indication of becoming shock waves, and indeed show towards the closing stages of the calculation a similarity to sound wave propagation. The method is applicable to any spherically symmetrical motion up to such a time as the formation of a shock wave takes place and then fails owing to the assumption of constant entropy.

## Short period fluctuations in the characteristics of wireless echoes from the ionosphere.

By T. L. Eckersley, F.R.S. and F. T. Farmer. (*Received* 6 *August* 1940.)

This paper deals with the effect of irregularities in the ionosphere on reflected radio waves. Such irregularities occur mainly in the *E* layer. These irregularities vary rapidly and cause e.m.f.s on two spaced aerials to be incorrelated with a consequent apparent spread in direction. Manual methods are not sufficiently rapid to resolve these variations. These rapid fluctuations are studied by recording the ellipses on a cathode-ray tube produced by the e.m f.s on two spaced frames. This is done by taking photographs at intervals of $\frac{1}{25}$ sec., and the technique is made applicable to impulses by a device which desensitizes the apparatus for all but a small fraction of the time base period, so that observations can be confined to a single pulse of the echo pattern. The same apparatus can be used both for directional and polarization measurements by appropriate connexion of the aerials.

The results show that for normal *E* and *F* reflexions the relative e.m.f. in the two aerials, and in consequence the directions and polarizations, remain constant over many seconds.

Reflexions from scattering clouds are however entirely different. The apparent ray directions and the polarizations only remain constant over a fraction of a second (between $\frac{1}{25}$ and $\frac{1}{4}$ sec.) and the difficulty of balancing by manual methods the electric force in one frame against that in another is entirely explained. The results show that the abnormal *E* region is also irregular in time and space.

### The dissociation constants of the methylammonium ions and the basic strengths of the methylamines in water. By D. H. EVERETT and W. F. K. WYNNE-JONES. (*Communicated by Sir Harold Hartley, F.R.S.—Received 4 November* 1940.)

The dissociation constants of the ions $CH_3NH_3^+$, $(CH_3)_2NH_2^+$ and $(CH_3)_3NH^+$ have been determined at intervals of 10° from 0 to 50° by a method involving the measurement of the potential of a hydrogen electrode placed in buffer solutions of each amine and its hydrochloride.

By combining these results with the known values for the ionic product of water, values have been obtained for the ionic equilibria of the type

$$CH_3NH_2 + H_2O = CH_3NH_3^+ + OH^-$$

conventionally referred to as the ionization constants of the amines.

The heats, entropies and heat capacities of these reactions have been calculated and the results compared with the simple electrostatic theory of the ionization process: it is found that the heat capacity changes are too large to be explained on this basis.

### The kinetics of the polymerization of isoprene on sodium surfaces. By J. L. BOLLAND. (*Communicated by E. K. Rideal, F.R.S.—Received 4 November* 1940.)

The kinetics of the polymerization of isoprene liquid and vapour occurring on sodium surfaces have been investigated at 60 and 25° C. In the case of the liquid phase, polymerization diffusion of monomer to the catalytic surface is shown to be the rate controlling factor, except when the sodium surface is in the form of a sphere of sufficiently small dimensions.

The kinetics of the polymerization in presence of toluene are consistent with the view that polymeric chains are initiated by formation of free radicles on the sodium surface, the subsequent propagation occurring while the polymer is still attached to the sodium termination occurs exclusively by interaction with toluene. In absence of toluene an alternative termination reaction, leading to cross linking and requiring 4·6 kcal. more activation energy than the process involving toluene, comes into play.

### On the salinity of the surface waters of the Irish Sea. By J. PROUDMAN, F.R.S. (*Received 4 November* 1940.)

This paper gives a statistical treatment of most of the observations of the salinity of the surface waters of the Irish Sea which were taken up to the end of the year 1939. Its objects are: (1) To put on record the chief variations of the salinity in the central part of the sea during the whole period of observation. (2) To calculate grand mean values of the characteristics of the salinity and of its seasonal variation for stations distributed over the whole area of the sea. (3) To investigate the degree of correlation between the salinities at pairs of stations, and to find for what time differences the coefficients of correlation attain maximum values. (4) To investigate the degrees of correlation between the salinities at different stations and the rainfall and barometric gradients; and to find the time lags which correspond to maximum correlation coefficients. (5) To obtain from the correlation coefficients such indications as they may afford of the mean currents of the sea.

## The heart of the salamander (*Salamandra salamandra*), with special reference to the conducting (connecting) system and its bearing on the phylogeny of the conducting systems of mammalian and avian hearts.

By F. Davies and E. T. B. Francis. (*Communicated by W. E. Le Gros Clark, F.R.S.—Received* 8 *November* 1940.)

The study of nine salamander hearts by means of serial sections cut in three planes has demonstrated muscular continuity between the several cardiac chambers, and the entire absence of any specialized muscle or 'nodal tissue' at the junctional sites, or in any other part of the heart. The heart muscle forms a continuum. The cardiac muscle fibres are characterized by their large size (i.e. breadth) and they have the same general histological characters in all parts of the heart.

In each of the chambers the musculature is arranged in a basket-work fashion, but at each of the junctional sites the muscle suddenly changes to a regular circular arrangement. The sinus, at its junction with the right atrium, contains striated muscle only in its ventral wall, and it is this wall only of the sinus which thus establishes muscular continuity with the ring of muscle (S.-A. ring) around the sinu-atrial opening. The musculature of both atria is continuous with that of the ventricle in two ways. From the ring of muscle (A.-V. ring) surrounding the common opening of the atria into the ventricle, the atrio-ventricular funnel dips down into the ventricle, and the caudal border of this funnel is continuous with an invaginated part of the base of the ventricle, and more extensively with ventricular papillary muscles, which are continued into the inner ventricular trabeculae about the middle level of the ventricle. The A.-V. funnel is homogeneous in structure. The ventricular muscle is directly continued into that of the bulbus cordis.

The course which the wave of contraction takes during its transmission from the sinus throughout the heart and many of the details of the phases of the cardiac cycle are described.

The delay in the transmission of the wave of contraction from one cardiac chamber to the next is accounted for by the relatively long path which the impulse has to traverse at the junctional sites, without postulating the existence of specialized 'block fibres' at these sites. The branching of the muscle fibres has the effect of converting the morphological circular arrangement of the fibres at these junctions into a physiological spiral.

The glycogen content of the various parts of the frog's heart is found to increase in the order sinus, atria, ventricle and bulbus cordis. This is correlated with a similar increasing order of density of musculature and work done, the glycogen being a reserve potency for the energy of muscular contraction. The fact that the intrinsic rhythmic rates of the several chambers decrease in the same order as the glycogen content increases may or may not be coincidental.

Cutting and ligature experiments, with cinephotographic and kymographic records, reveal the intrinsic rhythmic rates of the various cardiac chambers of the salamander heart.

No satisfactory reason has yet been adduced to account for the different intrinsic rhythmic rates of the several parts of the heart when these are isolated from each other.

The dorsal mesocardium has been traced in its entirety The sinu-ventricular fold is a part of the continuous dorsal mesocardium and does not constitute a direct muscular sinu-ventricular connexion.

The distribution of the intracardiac nerve cells has been noted and the probable pathway of migration of these nerve cells in the embryo has been suggested

The significance of the results of this investigation in relation to the phylogeny of the specialized conducting system of the hearts of homoiothermal vertebrates (mammals and birds) is discussed. The view is expressed that the cardiac conducting systems of homoiothermal vertebrates constitute a neomorphic development, correlated with functional requirements, and are not remnants of more extensive tissues of similar structure in the lower vertebrate heart. Variations in this newly evolved formation probably account for the different descriptions of such elements in various mammalian and avian hearts.

## Anatomical and histological changes during the oestrous cycle in the mare.

By J. HAMMOND, F.R.S. and K WODZICKI (*Received* 18 *November* 1940.)

The mares chosen for the investigation of the changes in the reproductive organs during the oestrous cycle were kept under observation for some time before they were killed. The duration of the heat period in these animals was 7 days and the length of the dioestrus was 16 days. Ovulation takes place at about a day before the end of oestrus. The growth of the follicle is very rapid during the period of oestrus. The size of the ovary during the oestrous cycle is chiefly influenced by the growing Graafian follicle The number of follicles present at different stages varies greatly. The numerous small follicles present at the beginning of oestrus disappear later in the cycle; it is suggested that this may be due to the lack of follicle-stimulating hormone.

The colour of the corpus luteum varies greatly at different stages of the cycle. The rupture of the follicle is associated with some bleeding The active stage of the corpus luteum is very short and the maximum diameter of the corpus luteum seems to be always below that of the Graafian follicle. The greater development of the Graafian follicle, with its secretion of oestrin, in the mare leads to its playing a more important role than in the cow and the sow, in which species the corpus luteum takes a more dominant part in the cycle. It appears that the much longer oestrus in the mare than in the cow is due to the longer time required by the follicle to come to the surface and to break through. This is probably due to the peculiar structure of the ovary in the mare, since the ovulation, which is spontaneous, can only occur in the small ovulation fossa. No pronounced secretion stage occurs during oestrus in the Fallopian tubes.

The anatomical and histological changes in the uterus of the mare during the cycle are slight as compared with those in species which have a specialized placentation, such as the rabbit, ferret and cat; they are similar to those changes which occur in a species with a simple placentation such as the pig.

Cyclic changes are described in the epithelial cells of the cervix, which acts as a large mucous gland. It is probable that ejaculation takes place directly through the cervix into the uterus.

The changes in the vagina proper and the vestibulum vaginae are described; they are less pronounced in the mare than in the cow, but some cornification and leucocytosis, similar to that found in some rodents, occurs.

## Structure and molecular anisotropy of sorbic acid, $CH_3.CH:CH.CH:CH.COOH$.

By K. Lonsdale, J. M. Robertson and I Woodward. (*Communicated by Sir William Bragg, P R S.—Received* 18 *November* 1940.)

A preliminary study of sorbic acid has shown that the monoclinic unit cell contains eight molecules, these being linked in pairs by hydrogen bonds about the symmetry centres of the crystal, with the long chain axis of the molecule in or near to the (010) plane and inclined at between 10 and 15° to the *a* axis in the obtuse angle $\beta$. The molecular chains must be rotated so as to bring some of the atoms out of the (010) plane, and an approximate measure of this rotation is provided by measurements of optical and magnetic anisotropy, which give $\pm 35°$ as the angle between the *b* axis and the normal to the molecular plane. The magnetic anisotropy due to resonance in the conjugated chain is about half as large as that in the benzene ring and falls into line with previous observations on non-cyclic conjugated compounds. The orientation of the molecules has been confirmed by observation of the size and shape of the diffuse spots occurring on well-exposed Laue photographs taken with radiation from a copper target, and the usefulness of these photographs as a secondary method of structure determination has been emphasized.

# INDEX TO AUTHORS

**Note.**—The letter S is to be understood with all page references

Andrade, E. N. da C. and Chow, Y. S. 24
Andrews, K. W., Davies, H E., Hume-Rothery, W. and Oswin, C. R. 67
Astbury, W T. and Dickinson, S. 46
Astbury, W. T. and Preston, R. D 22
Austen, A. E. W. and Whitehead, S. 21

Badger, G. M, Cook, J. W, Hewett, C L, Kennaway, E. L., Kennaway, N. M, Martin, R. H. and Robinson, A. M. 72
Baldwin, E and Bell, D J 79
Bates, D. R. and Massey, H. S. W. 76
Beeck, O, Givens, J. W. and Smith, A E 58
Beeck, O, Givens, J W and Williams, E C 58
Beeck, O., Smith, A E and Wheeler, A 57
Beevers, C A. and Hughes, W 72
Bell, D. J, *see* Baldwin
Bell, R P. and Lidwell, O M 34, 38
Benjamin, M and Jenkins, R. O. 38
Berg, W. F 4
Binnie, A. M and Squire, H. B 61
Birse, E. A. B and Melville, H W 6
Blackett, P M S and Lovell, A C B 80
Bolland, J L 83
Booth, F. and Wilson, A H. 27
Browne, B C and Bullard, E C. 8
Bullard, E C and Gaskoin, T F. 79
Bullard, E. C, *see also* Browne
Bunn, C W. 37
Burgoyne, J. H 2, 36, 51
Burgoyne, J H, Newitt, D M and Tang, T L 1
Burrows, M G T and Stockmayer, W. H 39

Campbell, N. R. 73
Catcheside, D G 18
Chalmers, B. 9
Chang, M-Ch. and Walton, A. 72
Chao, S. H. and Taylor, W. H 34
Chapman, S. 77
Chen, H. K., Nicol, H. and Thornton, H. G. 52
Chen, H. K. and Thornton, H G. 32
Chow, Y. S, *see* Andrade
Clark, G. L. 66
Clews, C. J. B. and Robinson, H R. 48
Conn, G. K. T, Lee, E, Sutherland, G B B M and Wu, C. K. 41
Cook, J. W., *see* Badger
Cooper, J. A. and Garner, W. E 11
Corkan, R. H, Doodson, A T and Proudman, J. 5
Cowan, S. L. 52, 53
Crawford, B. H. 26, 31

Dainton, F S and Norrish, R. G. W. 45, 46
David, H G and Munson, R J 75
Davies, F and Francis, E T B 84
Davies, H E, *see* Andrews
Davison, B and Rosenhead, L 70
Dickinson, S, *see* Astbury
Dingle, H and Pryce, A. W. 51
Doodson, A. T 3
Doodson, A. T, *see also* Corkan
Duperier, A 81

Eckersley, T L and Farmer, F T 82
Edwards, J 4
Ehrenhaft, F 16
Elder, J S, Hodges, D B, Phillips, W F., Schonland, B F J and van Wyk, J. W. 29
Everett, D H and Wynne-Jones, W. F K 83
Ewer, R F and Fox, H M 22

Farmer, F T, *see* Eckersley
Fertel, G E F, Gibbs, D F, Moon, P B, Thompson, G P and Wynn-Williams, C. E. 27
Fox, D L and Pantin, C F A 47
Fox, H M, *see* Ewer
Fox, J J and Martin, A E. 11
Fraenckel, G and Rudall, K. M 13
Francis, E T B, *see* Davies, F
Fröhlich, H and Nabarro, F R N. 23
Fuchs, K 30
Fürth, F 35

Ganguli, N and Krishnan, K S 68
Garner, W E, *see* Cooper
Gaskoin, T. F, *see* Bullard
Gatty, O 61
Gaydon, A G 59
Gibbs, D F, *see* Fertel
Givens, J W, *see* Beeck
Goldsbrough, G. R 79
Green, A E. 35
Grüneberg, H, Hallpike, C S and Ledoux, A 21
Guter, M, Newitt, D. M and Ruhemann, M. 41

Haddon, A. C 35
Hallpike, C S, *see* Grüneberg
Hammond, J and Wodzicki, K 85
Hanes, C S 30
Harris, E. J. 18
Hartree, E. F and Keilin, D 44

Havelock, T. H. 31
Heitler, W. and Ma, S. T. 43
Hewett, C. L., *see* Badger
Hill, A. V. 5
Hill, R. and Scarisbrick, R. 39
Hinshelwood, C. N. and Smith, R. E. 17, 65
Hodges, D. B., *see* Elder
Hollick, F. S. J. 55
Hoselitz, K. 75
Hughes, W., *see* Beevers
Hume-Rothery, W. and Raynor, G. V. 2, 74
Hume-Rothery, W., *see also* Andrews

Jánossy, L. and Rossi, B. 1
Jenkins, R. O., *see* Benjamin
Johnson, M. L. 77
Johnson, P. and Moelwyn-Hughes, E. A 8
Jones, J. W. 10
Jones, J. W and Orton, J. H. 9
Jones, T. T. and Melville, H W. 23

Keilin, D., *see* Hartree
Kellerman, E W. 56
Kellner, L 60, 61
Kendrew, J C. and Moelwyn-Hughes, E. A. 42
Kennaway, E. L, *see* Badger
Kennaway, N. M, *see* Badger
Knaggs, I. E, Lonsdale, K, Williams, G. and Wood, R G 74
Knott, G, Schulman, J. H and Wells, A F. 65
Kothari, D S and Singh, B N 44
Krishnan, K. S., *see* Ganguli
Kundu, B. C. and Preston, R D. 33

Lawrence, A. S. C. and Robinson, J. R. 47
Ledoux, A, *see* Grüneberg
Lee, E, Sutherland, G. B. B. M and Wu, C K. 42
Lee, E., *see also* Conn
Lidwell, O M, *see* Bell
London, H. 64
Lonsdale, K. 78
Lonsdale, K., Robertson, J. M. and Woodward, I 86
Lonsdale, K., *see also* Knaggs
Lovell, A. C B, *see* Blackett
Löwenstein, O and Sand, A. 36
Lunt, R W 69
Lunt, R. W, Meek, C A. and Swindell, G. E. 70

Ma, S. T., *see* Heitler
Macfadyen, W. A. 43
Mackenzie, K and Muller, H J. 63
Martin, A. E, *see* Fox, J J.
Mason, A W. and Shutt, W. J. 15
Massey, H. S. W. and Mohr, C. B. O. 76
Massey, H. S. W, *see also* Bates
Medawar, P. B. 25
Meek, C. A., *see* Lunt
Meldrum, F. R. 3, 4
Melville, H. W., *see* Birse, Jones
Millott, N. 19
Moelwyn-Hughes, E. A., *see* Johnson, Kendrew
Mohr, C. B. O., *see* Massey
Moon, P. B., *see* Fertel
Moy-Thomas, J. A. 66
Muller, H. J., *see* Mackenzie
Munson, R. J. and Tyndall, A. M. 74
Munson, R. J., *see also* David

Nabarro, F R. N. 33
Nabarro, F R N, *see also* Fröhlich
Newitt, D. M., *see* Burgoyne, Guter
Nicol, H., *see* Chen
Norrish, R. G. W. and W. MacF. Smith 56
Norrish, R. G. W. and Reagh, J. D. 50
Norrish, R. G. W., *see also* Dainton

O'Bryan, H. M and Skinner, H. W. B. 33
Oldham, J W. H. and Ubbelohde, A R 37
Oswin, C R, *see* Andrews

Pantin, C F A, *see* Fox, D. L.
Payman, W. and Shepherd, W C F. 27
Pellew, A and Southwell, R. 14, 62
Pelmore, D. R. and Simons, E L. 17, 18
Phillips, W F, *see* Elder
Picken, L E R. 26, 73
Pickles, A. T and Sucksmith, W. 27
Powell, H M., *see* Sidgwick
Preston, R D 80
Preston, R. D, *see also* Astbury, Kundu
Proudman, J. 54, 83
Proudman, J., *see also* Corkan
Pryce, A. W, *see* Dingle

Randall, J T and Wilkins, M. H. F 7
Rayleigh, Lord, 40
Raynor, G. V., *see* Hume-Rothery
Robertson, J M, *see* Lonsdale
Robinson, G. D. and Simpson, G C. 75
Robinson, H R, *see* Clews
Robinson, J R., *see* Lawrence
Rosenhead, L, *see* Davison
Rossi, B., *see* Jánossy
Rotblat, J. 76
Rudall, K M, *see* Fraenckel
Ruhemann, M., *see* Guter

Sand, A., *see* Löwenstein
Scarisbrick, R., *see* Hill, R
Schnurrmann, R. 50, 51
Schonland, B. F. J., *see* Elder
Schulman, J. H., *see* Knott
Shutt, W. J., *see* Mason
Sidgwick, N. V. and Powell, H. M. 61
Simons, E. L, *see* Pelmore
Simpson, G. C., *see* Robinson, G. D.
Singh, B. N., *see* Kothari
Skinner, H. W. B. 16

Skinner, H. W. B., *see also* O'Bryan
Smith, A. E., *see* Beeck
Smith, R. E., *see* Hinshelwood
Smith, S. L. and Wood, W A. 60
Smith, W. MacF., *see* Norrish
Southwell, R., *see* Pellew
Squire, H. B., *see* Binnie
Srivastava, B. N. 25
Stockmayer, W. H., *see* Burrows
Sucksmith, W., *see* Pickles
Sutherland, G B. B M., *see* Conn, Lee
Swindell, G. E , *see* Lunt
Synge, J. L. 65

Tang, T. L , *see* Burgoyne
Taylor, T. W. J. 34
Taylor, W. H., *see* Chao
Thompson, G. P , *see* Fertel
Thornton, H. G , *see* Chen
Townsend, A. A. 48
Tyndall, A M , *see* Munson

Ubbelohde, A. R., *see* Oldham
Unwin, J. J. 82

Vaidya, W. M. 49

Walker, M. G. 28
Walton, A , *see* Chang
Ward, A. F H. 64
Watson, M. A. 20
Webb, D. A 31
Wells, A F., *see* Knott
Wheeler, A., *see* Beeck
Whitehead, S , *see* Austen
Wilkins, M H F , *see* Randall
Williams, E. C., *see* Beeck
Williams, G , *see* Knaggs
Wilson, A H , *see* Booth
Wilson, R S. 78
Wodzicki, K , *see* Hammond
Wood, R G , *see* Knaggs
Wood, W. A , *see* Smith, S L
Woodward, I , *see* Lonsdale
Wright, E M 71
Wu, C K , *see* Conn, Lee
van Wyk, J. W , *see* Elder
Wynne-Jones, W F K , *see* Everett
Wynn-Williams, C E , *see* Fertel

I.A.R.I. 75

INDIAN AGRICULTURAL RESEARCH
INSTITUTE LIBRARY, NEW DELHI.

| Date of Issue | Date of Issue | Date of Issue |
|---|---|---|
| | | |
| | | |
| | | |
| | | |
| | | |
| | | |
| | | |
| | | |
| | | |
| | | |
| | | |
| | | |
| | | |
| | | |
| | | |

GIPNLK—H-40 I.A.R.I.—29-4-55—15,000